(2)

CONTRACTOR'S MEETING IN PROPULSION

Sponsored by

AIR FORCE OFFICE OF SCIENTIFIC RESEARCH

15–19 June 1992

THE UNIVERSITY OF CALIFORNIA, SAN DIEGO

CENTER FOR ENERGY AND COMBUSTION RESEARCH

DEPARTMENT OF APPLIED MECHANICS AND ENGINEERING SCIENCES

LA JOLLA, CALIFORNIA 92093

REPORT DOCUMENTATION PAGE

Form Approved
OMB No. 0704-0188

1. AGENCY USE ONLY (Leave blank)	2. REPORT DATE	3. REPORT TYPE AND DATES COVERED
	7 July 1992	Technical

4. TITLE AND SUBTITLE
(U) AFOSR Contractors Meeting in Propulsion

5. FUNDING NUMBERS
PE - 61102F
PR - 2308
AFOSR-91-0162

6. AUTHOR(S)
M A Birkan and J M Tishkoff

7. PERFORMING ORGANIZATION NAME(S) AND ADDRESS(ES)
Air Force Office of Scientific Research
Building 410
Bolling AFB DC 20332-6448

8. PERFORMING ORGANIZATION REPORT NUMBER

9. SPONSORING/MONITORING AGENCY NAME(S) AND ADDRESS(ES)
AFOSR/NA
Building 410
Bolling AFB DC 20332-6448

10. SPONSORING/MONITORING AGENCY REPORT NUMBER

11. SUPPLEMENTARY NOTES

12a. DISTRIBUTION/AVAILABILITY STATEMENT
Approved for public release; distribution is unlimited

12b. DISTRIBUTION CODE

13. ABSTRACT (Maximum 200 words)

Abstracts are given for research in airbreathing combustion, rocket propulsion, and diagnostics in reacting media supported by the Air Force Office of Scientific Research.

14. SUBJECT TERMS
Instability, Flames, Propulsion, Gas Turbines, Combustion, Shear Layer, Supersonic, Soot, Sprays, Lasers, Fluorescence, Spectroscopy, Rocket, Plasma, Scrmajets

15. NUMBER OF PAGES
298

16. PRICE CODE

17. SECURITY CLASSIFICATION OF REPORT	18. SECURITY CLASSIFICATION OF THIS PAGE	19. SECURITY CLASSIFICATION OF ABSTRACT	20. LIMITATION OF ABSTRACT
Unclassified	Unclassified	Unclassified	UL

AGENDA

AFOSR CONTRACTORS MEETING ON PROPULSION
15-19 JUNE 1992

MONDAY, 15 JUNE 1992

Session Topic: Plasma Propulsion
Chairman: Chris Andrews, Phillips Laboratory

9:00 - 9:30 Plasma Instabilities and Transport in the MPD Thrusters
A J Kelly, Princeton University

9:30-10:00 Performance Characteristics of Plasma Thrusters
M Martinez-Sanchez, MIT

10:00-10:30 Laser Sustained Plasmas in Non-Local Thermal Equilibrium Conditions
H Krier, University of Illinois at Urbana

10:30-11:00 BREAK

11:00-11:30 LIF Diagnostics for Arcjet Thrusters
D Keefer, UTSI

11:30-12:00 Recovery of Frozen Flow Losses in Arcjets
V Subramaniam, Ohio State University

12:00-12:30 Plasma Propulsion Diagnostics
R A Spores, Phillips Laboratory

12:30-2:00 LUNCH

2:00-2:30 Arcing Phenomena on High Voltage Power Systems
D E Hastings, MIT

2:30-3:00 ICRF Plasma Heating in the Tandem Mirror Rocket
T F Yang, MIT

3:00-3:30 Ionized Cluster Beams for Space Propulsion
W S Williamson, Hughes Aircraft Co.

3:30-4:00 BREAK

Session Topic: Propellants
Chairman: D Weaver, Phillips Laboratory

4:00-4:30 Studies of Broad-Band Optical absorbers for Solar Powered Rocket Propulsion Systems
P W Langhoff, Indiana University

4:30-5:00 Thermal Decomposition Mechanisms of New Polycyclic Nitramines
T B Brill, University of Delaware

5:00-5:30 Gas Phase Kinetics of Nitramine Combustion
M Branch, University of Colorado

5:30-7:30 DINNER RECESS

7:30-9:30 WORKSHOP
Cluster Ion Propulsion
R Spores, Phillips Laboratory

TUESDAY, 16 JUNE 1992

Topic: Liquid Fuelled Propulsion Systems
Chairman: D Talley, Phillips Laboratory

9:00-9:30 Fundamentals of Acoustic Instability in Liquid-Fuelled Rockets
F A Williams, University of California-SD

9:30-10:00 Acoustic Waves in Complicated Geometries
V Yang, Penn State

10:00-10:30 Role of Unsteady Atomization on Liquid Rocket Instability
J W Daily, University of Colorado

10:30-11:00 BREAK

11:00-11:30 Combustion Instability with Impinging Jet Injectors
R J Santoro, Penn State

11:30-12:00 Combustion Instability with Coaxial Injectors
M Micci, Penn State

12:00-12:30 Droplet Collisions
C K Law, Princeton University

12:30-2:00 LUNCH

Session Topic: Solid-Fuelled Propulsion Systems
Chairman: Thomas Hawkins, Phillips Laboratory

2:00-2:30 Distributed Combustion in Solid-Fuelled Rockets
M Beckstead, Brigham Young University

2:30-3:00 Oscillatory Internal Flow Studies
R S Brown, United Technologies-CSD

3:00-3:30 Solid Rocket Combustion Phenomena
D R Kassoy, University of Colorado

3:30-4:00 BREAK

4:00-4:30 Flame Driving and Flow Turning Loss in Solid Rockets
B T Zinn, Georgia Tech

4:30-5:00 Combustion and Plumes
D Weaver, Phillips Laboratory

WEDNESDAY, 17 JUNE 1992

9:30-11:30 WORKSHOP
Propellants/Chamber Dynamics/Plumes
Complex problems requiring multidisciplinary approaches
D Weaver/D Talley, Phillips Laboratory
M Birkan, AFOSR

WEDNESDAY, 17 JUNE 1992

Session Topic: Sprays
Chairman: Dr David Mann, Army Research Office

1:00 - 1:30 Particle Dispersion In Turbulent Shear Flows
I M Kennedy and W Kollmann, University of California, Davis

1:30 - 2:00 Breakup and Turbulence Generation in Dense Sprays
G M Faeth,University of Michigan

2:00 - 2:30 Ramjet Research
A S Nejad, WL/POPT

2:30 - 3:00 Fuels Combustion Research
W M Roquemore, WL/POSF

3:00 - 3:30 BREAK

3:30 - 4:00 Fundamental Studies of Droplet Interactions in Dense Sprays
W A Sirignano and S E Elghobashi, University of California, Irvine

4:00 - 4:30 Numerical Analysis of Time-Dependent Two-Phase Non-Reacting Flows
S K Aggarwal, University of Illinois, Chicago

4:30 - 5:00 Atomization of Viscous Liquid Sheets
E A Ibrahim, Tuskegee University

5:00 - 7:00 DINNER RECESS

7:00 - 9:00 WORKSHOP

Application of Combustion Research to Propulsion
S M Correa, General Electric Corporate Research and Development

THURSDAY, 18 JUNE 1992

Session Topic:Diagnostics
Chairman:G S Roy, Office of Naval Research

8:00 - 8:45 Advanced Diagnostics for Reacting Flows
R K Hanson, Stanford University

8:45 - 9:15 Novel Nonlinear Laser Diagnostic Techniques
D Huestis, G Faris, and J Jeffries, SRI International

9:15 - 9:45 Rapid Concentration Measurements by Picosecond Time-Resolved Laser-Induced Fluorescence
G B King and N M Laurendeau, Purdue University

9:45 - 10:15 Energy Conversion Device Diagnostics
B N Ganguly, WL/POOC-3

10:15 - 10:45 BREAK

10:45 - 11:15 CATCARS: Two-Dimensional Coherent Anti-Stokes Raman Scattering With Application To The Hydrogen Arcjet
E J Beiting, Aerospace Corporation

11:15 - 11:45 Development and Application of Fluorescent Diagnostics to Fundamental Droplet and Spray Processes
L A Melton, University of Texas at Dallas and M Winter, United Technologies Research Center

11:45 - 12:15 Nonlinear Spectroscopy of Multicomponent Droplets and Two- and Three-Dimensional Measurements in Flames
R K Chang, M B Long, and R Kuc, Yale University

12:15 - 2:00 LUNCH

Session Topic: Physciochemical Processes
Chairman:A S Nejad, WL/POPT

2:00 - 2:30 High Temperature Reaction Kinetics of Boron Oxides and Hydroxides
A J Twarowski and T A Seder, Rockwell International Science Center

2:30 - 3:00 Initiation and Modification of Reaction by Energy Additions: Kinetic and Transport Phenomena
M-S Chou, TRW Space and Technology Group

3:00 - 3:30 Transport Phenomena and Interfacial Kinetics in Multiphase Combustion Systems
D E Rosner, Yale University

3:30 - 4:00 BREAK

4:00 - 5:00 BUSINESS SESSION

Contractors and grantees supported in Dr Tishkoff's AFOSR programs only

5:00 - 7:00 DINNER

7:00 - 9:00 WORKSHOPS

Supercritical Sprays
T Edwards, WL/POSF and D Talley, OL-AC PL/MKRP

Soot
H F Calcote, AeroChem Research Laboratories, Inc

FRIDAY, 19 JUNE

Session Topic:Soot
Chairman:B Ganguly, WL/POOC-3

8:30 - 9:00 Proposal for Mechanistic Models of Soot Formation
M B Colket, United Technologies Research Center

9:00 - 9:30 Detailed Studies of Soot Formation in Laminar Diffusion Flames for Application to Modeling Studies
R J Santoro, Pennsylvania State University

9:30 - 10:00 Computer Modeling of Soot Formation Comparing Free Radical and Ionic Mechanisms
H F Calcote, AeroChem Research Laboratories, Inc

10:00 - 10:30 BREAK

10:30 - 11:00	Development of Predictive Reaction Models of Soot Formation M Frenklach, Pennsylvania State University
11:00 - 11:30	Fuels Combustion Research I Glassman, Princeton University
11:30	ADJOURN

PLASMA INSTABILITIES AND TRANSPORT IN THE MPD THRUSTER

AFOSR Contract No. AFOSR-91-0162

Edgar Y. Choueiri, Arnold J. Kelly an Robert G. Jahn

Electric Propulsion and Plasma Dynamics Lab.
Princeton University
Princeton, NJ. 08544

1 Summary

The current study aims at developing and testing transport coefficient models that include the effects of plasma turbulence and that can be used in more realistic numerical simulations of MPD thruster[1] flows. Computer models of the MPD thruster rely on the numerical solution of the magnetohydrodynamics (MHD) equations to predict the performance and aid in the design of higher efficiency thrusters. Current MHD models of the accelerator include only classical transport[2] (i.e. transport due to collisions between particles) and overpredict the performance of the experimental prototypes. The inclusion of anomalous transport (i.e. transport due to "collisions" of particles with the oscillating fields of unstable waves in the plasma) is expected to greatly enhance the validity and applicability of such models. During the past year our reserach has produced a first generation of transport coefficient models that can be readily included in any MHD computer code. This abstract describes these models and some of the numerical simulation results obtained through their inclusion in working codes.

[1]Throughout this abstract the term MPD thruster refers to the coaxial, self-field, high-current, gas-fed MagnetoPlasmaDynamic thruster.

[2]Throughout this abstract, "transport" refers to the following processes: electrical conductivity, particle diffusion, viscosity and thermal conductivity.

2 Technical Discussion

During the past year we have derived anomalous ion heating and electron momentum exchange rate models that are ready for inclusion in any code intended for the numerical simulation of MPD thrusters. In order to facilitate this inclusion we aimed to reduce the complicated physics inherent in such models to a straightforward mathematical expression (ideally in a polynomial form) that can be used in numerical codes to calculate the flow fields *self-consistently* with the calculation of microinstability-induced transport. Recent theoretical and experimental evidence of the existence of such turbulence has motivated this modelling activity. The hope is to better represent the microscopic physics in numerical plasma fluid codes and to investigate the extent of turbulence effects on the performance of MPD thrusters.

The anomalous ion heating and electron momentum exchange rate models discussed here are derived in ref. [1] from a second-order weak turbulence theory. The theory is based on a generalized fully electromagnetic dispersion tensor that can represent various microinstabilities which may be sustained by a magnetoactive, collisional, finite-beta, flowing and transverse-current carrying plasma. The interested reader is referred to that work for more details.

In general the microstability (and hence microturburlence) description depends on the following set of eight independent macroscopic parameters

$$kr_{ce}, \quad \Psi, \quad \frac{m_i}{m_e}, \quad \frac{\omega_{pe}}{\omega_{ce}}, \quad \beta_e, \quad \frac{u_{de}}{v_{ti}}, \quad \frac{T_i}{T_e}, \quad \frac{\nu_{ei}}{\omega_{lh}}. \tag{1}$$

The first two parameters kr_{ce} (r_{ce} being the electron cyclotron radius) and Ψ represent the normalized wavenumber and propagation angle (with respect to the magnetic field) of the oscillations respectively and are varied to growth-maximize the solutions. Since all anomalous transport rates used here were calculated at maximum growth these two parameters drop out of the final models. The mass ratio m_i/m_e is that of argon. All solutions reported below for the case of the MPD thruster plasma were found to be very insensitive to the fourth parameter, namely the ratio of electron plasma frequency to the electron cyclotron frequency ω_{pe}/ω_{ce}, as long as that ratio exceeded 10 which was the case for all the simulations that have been so far conducted at EPPDyL[2]. Similarly, the solutions were weakly dependent on β_e (the ratio of electron thermal pressure to magnetic pressure) as long as the electron Hall parameter did not exceed 10. Although that was the case for the numerical simulations conducted so far, it is expected that the simulation of more realistic geometries at high total currents might raise the electron Hall parameter enough to require the full inclusion of finite-beta effects.

The last three parameters are the most important for our problem. First, u_{de}/v_{ti} (the ratio of the current velocity to the ion thermal velocity) must reach a threshold for the instability to be excited and hence for anomalous transport to be operative. For the entire region of parameter-space considered in

the simulations that threshold was very near 1.5. Second, the ion to electron temperature ratio plays a role in scaling the level of turbulence. Invariably for our parameter-space, it was found that increasing T_i/T_e causes a devaluation of anomalous transport. The most important of all the macroscopic parameters turned out to be the last one namely ν_{ei}/ω_{lh} where ν_{ei} is the effective electron collision frequency and ω_{lh} is the lower hybrid frequency. Indeed this parameter can be replaced by the electron Hall parameter Ω since

$$\Omega \equiv \frac{\omega_{ce}}{\nu_{ei}} = \frac{(m_i/m_e)^{1/2}}{\nu_{ei}/\omega_{lh}}. \tag{2}$$

The weak turbulence theory calculations of the anomalous rates required the knowledge of the saturation energy density of the fluctuations. A model based on saturation by ion trapping was used. Accurate description of the saturation mechanism is still pending particle simulation of the relevant instabilities. For a detailed discussion of other possible saturation mechanisms such as electron trapping, resonance broadening and wave-wave coupling as well as a description of the adopted ion trapping saturation model see ref. [1].

The anomalous resistivity calculated from the above mentioned theories is

$$\eta_{AN} \equiv \frac{m_e(\nu_e^P)_{AN}}{e^2 n_e} \tag{3}$$

and is usually normalized by its classic counterpart $\eta_{Cl} \equiv m_e\nu_{ei}/e^2n_e$. We found that an increase in the electron Hall parameter for typical values of T_i/T_e leads to a very significant increase in the anomalous resistivity *if* the parameter u_{de}/v_{ti} is above the stability threshold. It is interesting to note that the scaling of this ratio with the Hall parameter is in general agreement with that recently inferred experimentally in ref. [3] from measurements in the anode region.

The frequency $(\nu_e^P)_{AN}$ contributes to the anomalous resistivity which in turn, through the Joule heating term in the fluid energy equation, enhances the electron heating rate. The anomalous ion heating rate represents the time rate of ion bulk heating due to turbulence.

A two-parameter, variable cross-term, least square fit was made to the calculated rates in order to facilitate their inclusion and use in the flow code.

The resulting two-parameter interpolating polynomial for $(\nu_i^T)_{AN}/\nu_{ei}$ has an average accuracy of 15% and reads

$$\begin{aligned}\frac{(\nu_i^T)_{AN}}{\nu_{ei}} &= 5.36 \times 10^{-5} + 1.29 \times 10^{-5}\ \Omega \\ &+ 6.03 \times 10^{-6}\ \Omega^2 + 9.44 \times 10^{-8}\ \Omega^3 \\ &+ \frac{T_h}{T_e}(-7.55 \times 10^{-7} - 5.41 \times 10^{-6}\ \Omega \\ &- 3.93 \times 10^{-6}\ \Omega^2).\end{aligned} \tag{4}$$

The ions are heated by the turbulent fluctuations at a rate $(Q_i)_{AN} = \frac{3}{2}(\nu_i^T)_{AN} T_h$

The effective conductivity introducing the anomalous resistivity effect to the flow code has the form

$$\sigma_{eff} = \frac{e^2 n_e}{m_e(\nu_{ei} + (\nu_e^P)_{AN})}, \tag{5}$$

where $(\nu_e^P)_{AN}$ is the electron-wave momentum exchange frequency, which is again computed through an interpolating polynomial of average accuracy of 10%

$$\begin{aligned} \frac{(\nu_e^P)_{AN}}{\nu_{ei}} &= 0.192 + 3.33 \times 10^{-2}\ \Omega + .212\Omega^2 \\ &\quad - 8.27 \times 10^{-5}\ \Omega^3 + \frac{T_h}{T_e}(1.23 \times 10^{-3} \\ &\quad - 1.58 \times 10^{-2}\ \Omega \\ &\quad - 7.89 \times 10^{-3}\ \Omega^2). \end{aligned} \tag{6}$$

At all the grid points of a the simulation mesh where $u_{de}/v_{ti} < 1.5$ both, $(\nu_e^P)_{AN}$ and $(\nu_i^T)_{AN}$ must be set to zero and all transport is assumed purely classical. Otherwise, the anomalous rates are computed from the above polynomials using the instantaneous macroscopic parameters and folded back into the flow equations at every time step thus insuring self-consistency.

These transport rate models are currently being tested and used in working codes. A sample of results from the code currently in use at EPPDyL[2] is shown in the appended color figures. The figures show the role of plasma turbulence in increasing anomalous resistivity and bulk heating in some critical regions of the thruster. Various such studies have pointed out that the cathode root and tip as well as the anode region are critical regions from the point of view of anomalous dissipation.

References

[1] E.Y. Choueiri. *Electron-Ion Streaming Instabilities of an Electromagnetically Accelerated Plasma.* PhD thesis, Princeton University, Princeton, NJ, USA, 1991.

[2] G. Caldo, E.Y. Choueiri, A. J. Kelly, and R. G. Jahn. An MPD code with anomalous transport. In 22^{nd} *International Electric Propulsion Conference*, Viareggio, Italy, 1991. IEPC-91-101.

[3] A.D. Gallimore, A. J. Kelly, and R. G. Jahn. Anode power deposition in MPD thrusters. In 22^{nd} *International Electric Propulsion Conference*, Viareggio, Italy, 1991. IEPC-91-125.

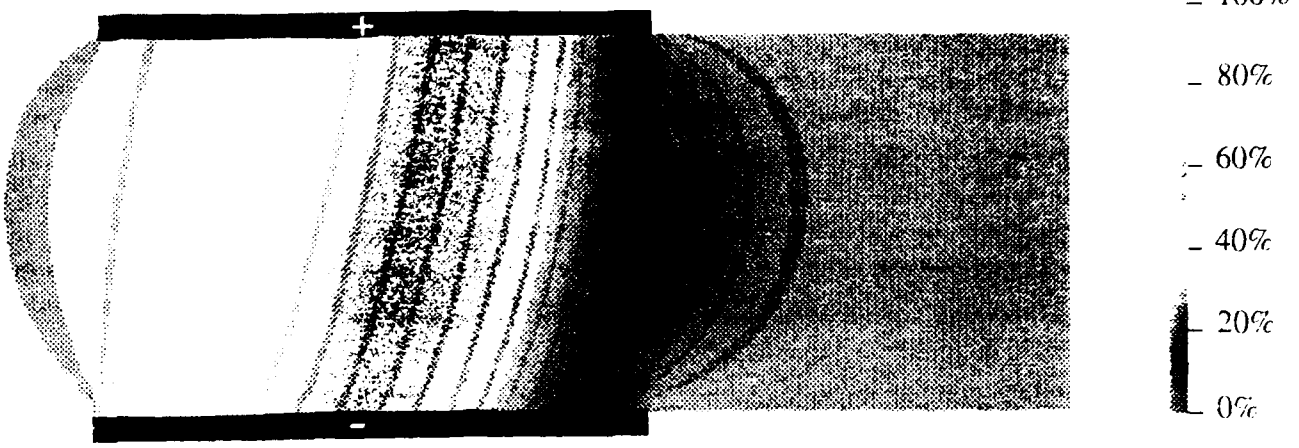

Enclosed current lines.

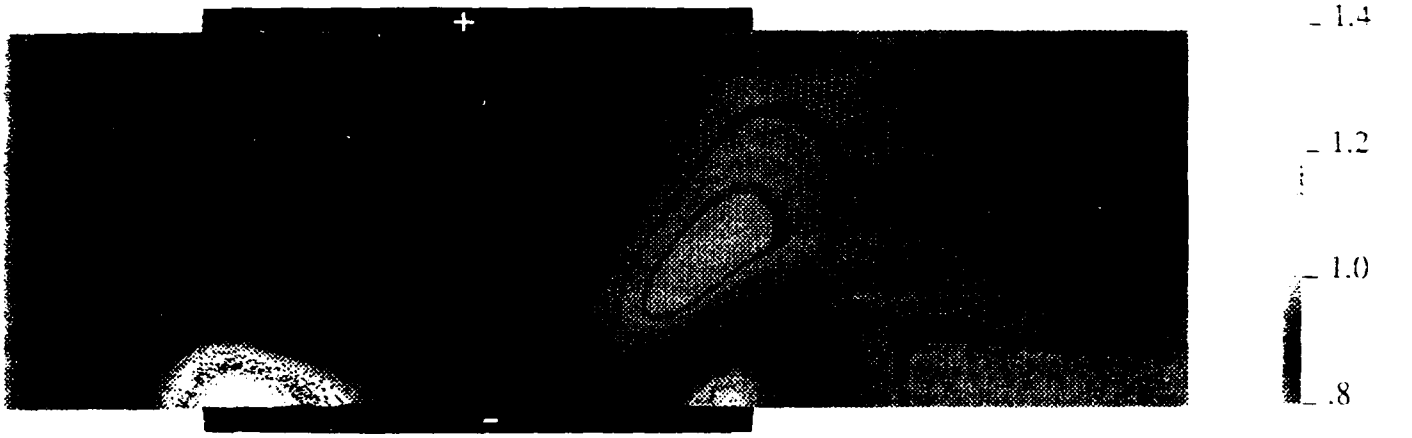

Ratio of classical to anomalous conductivity.

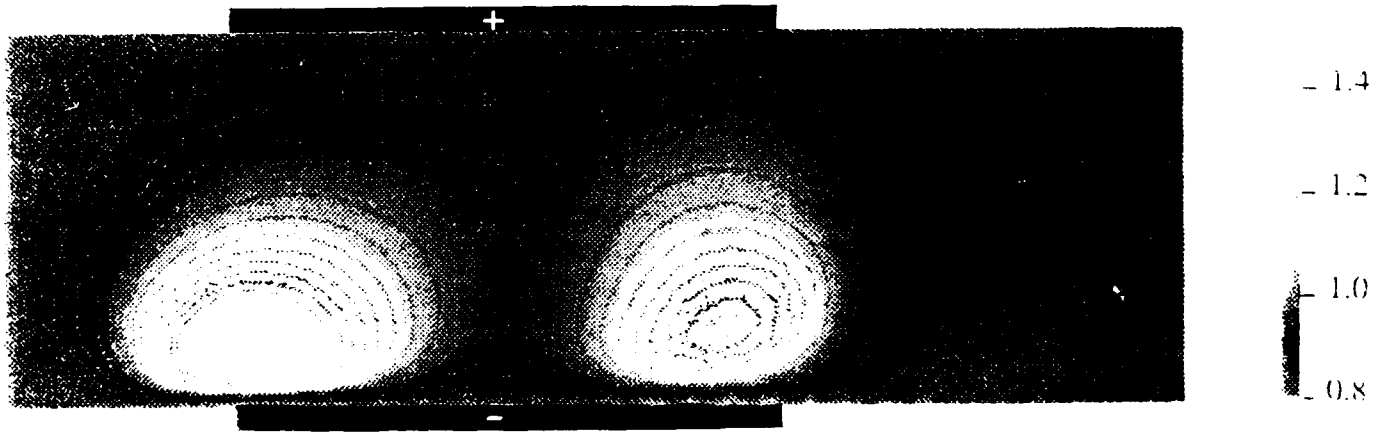

Ratio of anomalous to classical ion temperature.

PERFORMANCE CHARACTERISTICS OF PLASMA THRUSTERS

AFSOR Grant Contract No. 91-0256

Principal Investigator: Manuel Martinez-Sanchez

MIT, Dept of Aeronautics/Astronautics
Cambridge, MA 02139

OVERVIEW

The general goal of our research is to narrow down the uncertainty currently associated with predictions or extrapolations of performance for space plasma thrusters. The initial focus is on the arcjet for which two models are under development, one a fully numerical 2 1/2 dimensional code, and one a semi-analytical simplified model. An extension is planned to cover the moderate/low power Applied Field MPD and Hall devices, and work has begun on the latter. In addition to these topics, our group has ongoing theoretical research in the area of self-field MPD, with particular emphasis on anode effects and on inlet ionization and non equilibrium effects, and also on the effects of using carbon cluster propellants in ion engines.

TECHNICAL DISCUSSION

As noted, we have focused our in the 1st year of the Grant on modeling the arcjet. The work is not yet completed, but significant progress has been made. Two graduate students, (a Ph.D. candidate and a MS. candidate) are each developing a different modeling approach.

The more detailed model assumes a realistic axisymmetric arcjet geometry, with flow swirl included. In terms of the plasma physics, this is a two-fluid model, with electrons being allowed to develop velocities and temperatures different from those of the heavy species. The heavy species include molecular gas (H_2 and N_2 currently), atomic neutral gas and positive first ions. The dissociation and ionization are followed kinetically, thus allowing non-equilibrium to develop. Interdiffusion of species is also allowed (ambipolar in the case of the ions), as an important energy transfer mechanism. For the power levels (under 100 KW) considered, radiation loss is neglected.

Since the arc is controlled by a balance between Ohmic dissipation, heat convection and heat diffusion, especial emphasis has been put in correctly modeling the fluid transport properties of the multi-component gas. Figures 1 and 2 show hydrogen viscosity and thermal conductivity from out results, compared to data and more detailed kinetic theory solutions.

The numerical solution uses the McCormack time-marching method, on a body-fitted grid. The walls are made equipotential, and the potential of field points is cal. lated by overrelaxation between fluid steps. For the early part of a computation, the current is artificially constrained to attach to the cathode tip and to the nozzle part of the anode only, and the conductivity is made uniform. As Ohmic heating develops, the arc channel constricts and the attachment restrictions can be relaxed. Solutions for the constricted state are not yet reliable due to excessive error in mans conservation. Fig. 3 shows the initial current pattern (note the distorted vertical scale).

Once the numerical problems are overcome, we plan to conduct detailed calculations for the parameters of the German TT1 thruster [1]. These will also serve as check points for the simplified model described below.

The simplified model is patterned after that of Ref. 2,. it is a two-stream formulation which explicitly recognizes the role of heat diffusion in controlling arc radius, and the acceleration to a sonic condition at the constrictor exit. The basic constitutive properties (heat conduction potential, specific enthalpy and P/ρ are all represented as linear functions of electric conductivity, and the temperature outside the arc is taken equal to the wall temperature. because of the diffusion-inhibiting effect of convection by the flow ingested by the arc. Preliminary comparisons to the data of Ref. 1 indicate fair agreement as to the chamber pressure for given flow and current (see Fig. 3), but underprediction of the arc voltage by 30-50 volts, which could be related to unmodelled electrode drops on to viscous loss. Work is continuing on this task.

With the complete opening of communications with former Soviet scientists, the technology of Hall thrusters has become of immediate interest to the U.S. Consistent with out plans to investigate AF plasma thruster performance, we have started work on this closely related area. A review of Russian work and other research in Germany and Japan has been conducted. The literature did not provide a criterion to judge the device's thrust density limitations, and one has been constructed, based on the need to avoid collisions of accelerated ions with the abundant background neutrals. This has the form

$$\frac{F}{A} \leq (gIsp)\sqrt{\gamma m_i k T_n}\left(\frac{1}{Q_{in}L}\right)\frac{\eta_u}{1-\eta_u}$$

where F/A is the thrust per unit area, mi is the ion mass, $\gamma = 5/3$ Qin is the ion-neutral collision cross-section, L is the channel length and η_u is the utilization efficiency. For Xe, with $T_n = 400K$, $\eta_u = 0.75$, $I_{sp} = 2000sec.$, $Qin = 10^{-18}m^2$ and L = 0.1 m, we obtain $F/A = 53\frac{W}{m^2}$ about 90 times higher than for a gridded Xe ion engine of the same Isp. The electron density (4×10^{17} m^{-3}) implied by Eq. (1) is of the same order as reported [3,4] for partially optimized Hall thrusters.

In addition to this work, a linear stability theory of Hall thrusters has been developed, confirming and extending the earlier Russian work in this important area [5].

Progress will also be reported at the meeting on out continuing work in Self-Field MPD thrusters. This has centered on two phenomena: (a) The complex physics of the depleted anode layer, which is responsible for the larger part of the ions in high power MPD thrusters, and which we are modeling in detail. (b) The processes responsible for ignition of the plasma near the thruster inlet, with particular emphasis recently on photoionization and other radiative effects.

REFERENCES

1. Glocker, B. et al, "Medium Power Arcjet Thruster Experiments" AIAA Paper 90-2531, July 1990.

2. Martinez-Sanchez, M., "Electric Propulsion", contribution to an upcoming AIAA Propulsion Handbook, Ch.3.

3. A.I. Bugrova et al. "Physical Problems and Characteristics of Stationary Plasma Thrusters with Closed Electron Drift" IEPC-91-079, 22nd Intnl. Electric Prop. Conference, Italy, Oct. 1991.

4. K. Komurasaki et al. "Plasma acceleration Process in a Hall Current Thruster". IEPC-91-078 (loc cit.)

5. Ya. V. Esipchuk and G. N. Tilinin "Drift Instability in a Hall-current Plasma Accelerator. Zh. Tek Fiz., 46, 718-729 (April 1976).

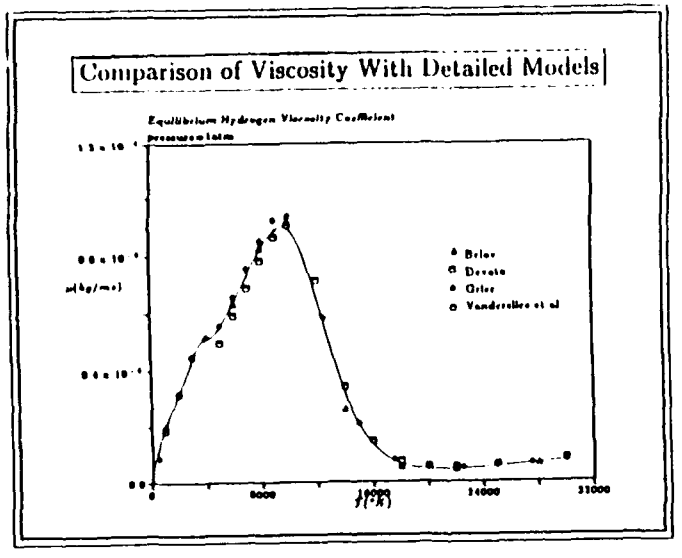

Figure 1

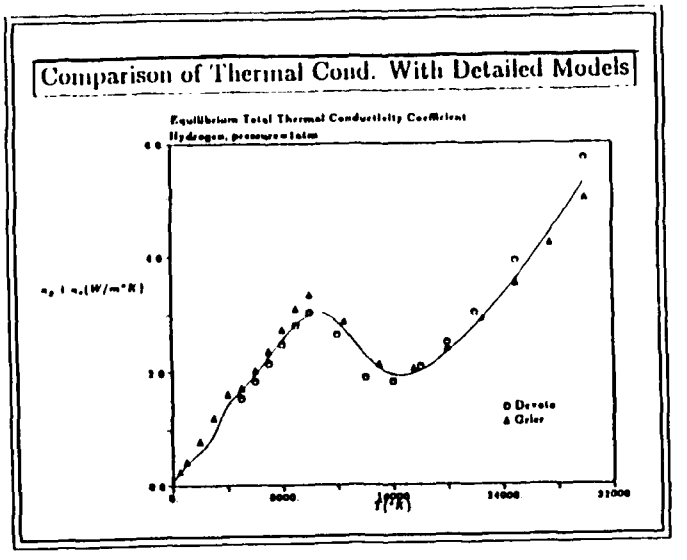

Figure 2

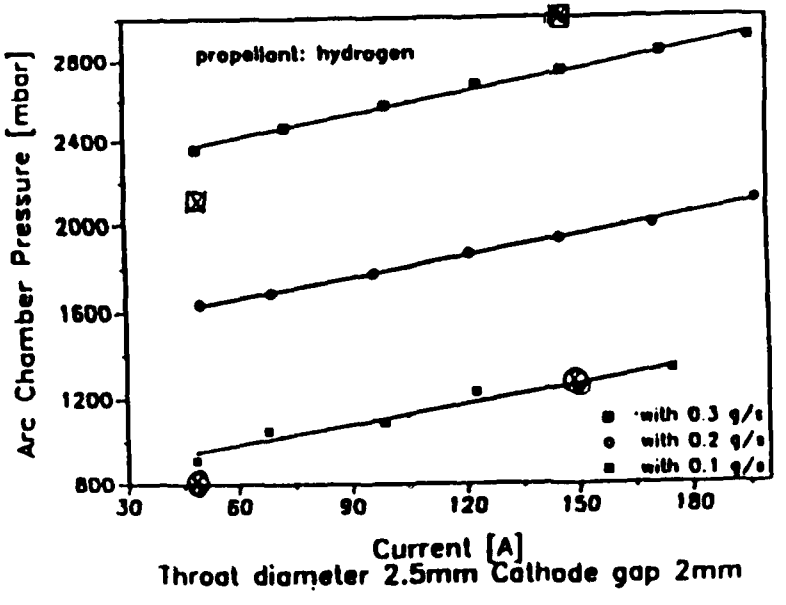

⊠, ⊗
FROM MODEL

Figure 3

Fig. 20: Current - Arc Chamber Pressure Characteristic with Hydrogen as Propellant

PERFORMANCE CHARACTERISTICS OF PLASMA THRUSTERS

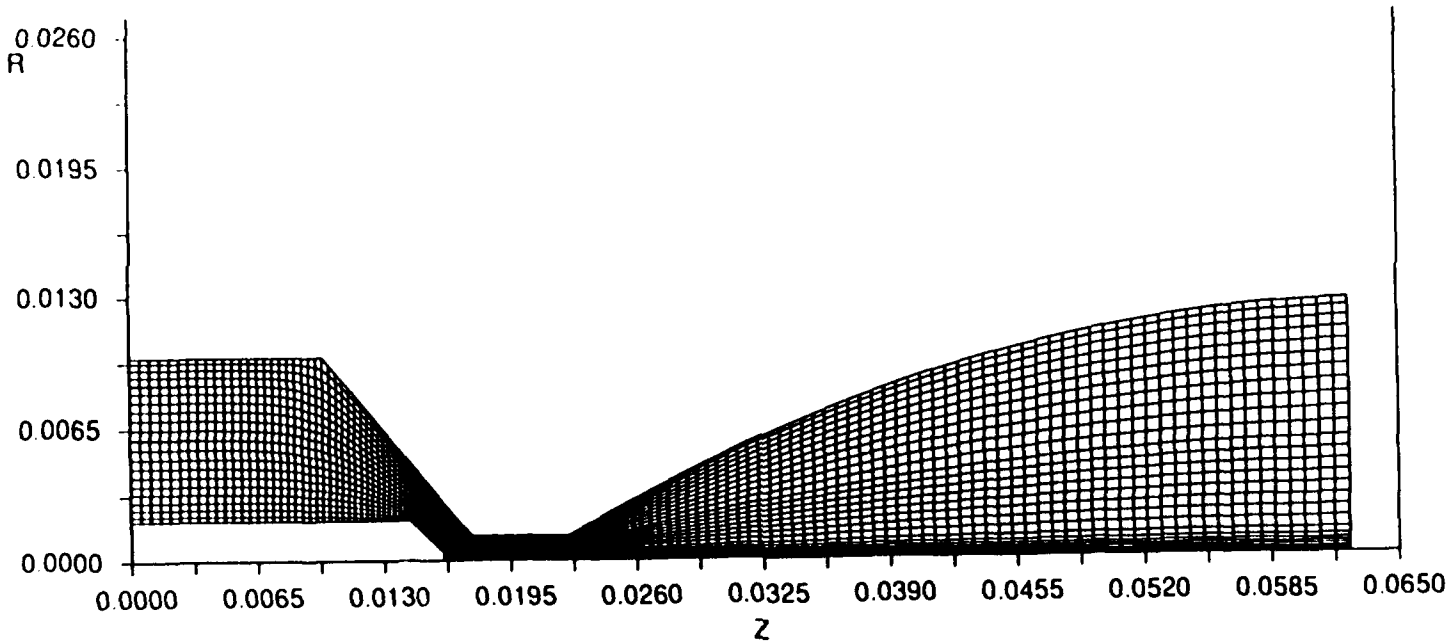

LASER SUSTAINED PLASMAS IN NON-LOCAL THERMAL EQUILIBRIUM CONDITIONS

AFOSR Grant No. 89-0274

Principal Investigators: Herman Krier and Jyoti Mazumder
Post Doctoral Fellow: David K. Zerkle
Ph.D. Candidate: Ayhan E. Mertogul

Department of Mechanical and Industrial Engineering
University of Illinois at Urbana-Champaign

SUMMARY/OVERVIEW:

This research is aimed at understanding the fundamental energy transfer mechanisms in laser sustained plasmas (LSP's) for application to rocket propulsion. The fraction of incident laser power absorbed by gases in the plasma and the fraction converted to useful enthalpy are considered the key performance parameters. The usual assumption of local thermodynamic equilibrium (LTE) is not used in this research; thus the thermodynamic state of the plasma is determined more accurately. Non-LTE based values for emission and absorption coefficients, as well as for the transport properties are used. The laser absorption coefficient is closely related to the plasma electrical conductivity. The investigation includes both experiments and detailed modeling. For comparison to the analyses global laser absorption is measured using cone calorimetry and the thermal conversion efficiency is determined by measurements of the gas temperature. Emission spectroscopy is used to determine electron number density and atomic level populations, which are used for determining non-LTE parameters such as electron and heavy particle kinetic temperatures and heavy particle number density. This work shows that kinetic nonequilibrium is the dominant non-LTE effect in laboratory LSP's.

Generalized non-LTE calculations are being performed which rely on collisional-radiative modeling to provide source terms in the gas flow conservation equations. The spectroscopic results reproduce the global absorption measured directly, and it is expected that the generalized model will be able to match those results as well as the spectroscopically determined electron number density and atomic level populations. The generalized model could then be used with confidence to predict the performance of LSP's as laser power approaches one megawatt. The ultimate goal of this research is the accurate prediction of LSP performance at the pressure, mass fluxes, and megawatt laser powers likely to be found in a full scale laser propulsion system.

TECHNICAL DISCUSSION:

Introduction

The central issue in the study of laser sustained plasmas for thermal rocket propulsion is the accurate prediction of plasma performance at operating conditions likely to be required in practice. That is, laser power of one to ten megawatts or higher, chamber pressures of two to five atmospheres or higher, and propellant (hydrogen) mass flux to achieve optimum performance. High laser power will be required to produce a practical thrust level, and the performance advantages of elevated pressure (above one atm.) and mass flux are well documented [1-4]. Predictions can be made by the application of an appropriate numerical model, and through the measurement of plasma properties at conditions available in the laboratory from which trends are identified.

Before reliable predictions can be made, the fundamental energy transfer mechanisms within the laser sustained plasma must be clearly understood. The absorption of laser power by the electrons via inverse bremsstrahlung (and other minor absorption mechanisms), the subsequent transfer of energy to the surrounding heavy particles, the convection and conduction of energy out

of the plasma,the diffusion of particles within and out of the plasma, and the radiation of energy within and out of the plasma must all be included in this understanding. The performance of an LSP as defined by its global absorption (percentage of incident laser power absorbed on the whole) and thermal conversion efficiency (percentage retained as thermal energy in the plasma exhaust gas) must be related to the internal plasma processes and understood on those terms.

As outlined in the summary, this investigation relies on several independent diagnostic techniques in order to characterize the LSP. The primary tools have been calorimeter measurements of transmitted laser power and (thermocouple) temperature measurements of plasma exhaust gas. The transmitted power is related to the absorbed power and the bulk gas temperature increase through the plasma is related to the thermal conversion efficiency. These techniques have been used to experimentally map the performance of argon LSP's as functions of laser power, gas pressure and mass flux, beam focusing geometry, and multiple plasma separation [1-3]. In recent experiments hydrogen plasmas have exhibited similar performance trends, but with much improved thermal conversion efficiency [4,5].

Non-LTE Emission Spectroscopy

In determining the thermodynamic state of the plasma, it is important to understand the concept of plasma temperature and the partitioning of energy. The energy content of the plasma gas is taken up by various modes. These include the kinetic energy of the free electrons and the heavy particles (neutral atoms and ions), the ionization energy of the ions, and the electronic excitation of the heavy particles. To a good approximation, the distribution of the energy in each of these modes can be characterized by a temperature parameter associated with Maxwell-Boltzmann statistics. The degree of ionization in the plasma can be similarly characterized by temperature (through the Saha equation). If the plasma is in LTE then the thermodynamic state of plasma matter is completely determined by the values of any two properties such as pressure and temperature. In LTE Boltzmann's law for the distribution of excited electronic states, Maxwell's law for the distribution of particles velocities (energies), and Saha's law describing the plasma composition are all associated with the same temperature parameter.

Past LSP research has been directed toward measuring performance in terms of global laser absorption and thermal conversion efficiency. In order to better understand these results on a physical level it is important to be able to measure temperature and particle number densities within the plasma. It is a goal of this research to measure or calculate correct values for plasma particle number densities and temperatures without reliance on an assumption of LTE. It is expected that this will lead to a better understanding of the laser energy conversion process.

A 10 kW continuous wave CO_2 laser is used to sustain argon plasmas in this work. Argon is important because it is inert, with sufficient studies in laser sustained plasmas (and arcjets) already performed under the assumption of local thermodynamic equilibrium. Hydrogen and argon LSP's are being studied numerically with hydrogen being the propellant of choice for laser propulsion missions. Defining the plasma state entails measuring or calculating the plasma constituent particle number densities and kinetic temperatures, as well as several atomic excitation temperatures [6].

The experimental portion of this work involves emission spectroscopy. Using an optical multichannel analyzer, both spectral and spatial information can be obtained simultaneously. The emission profile of the hydrogen Balmer series alpha line is measured for the determination of electron number density through Stark broadening theory. In argon plasmas a small amount of hydrogen is added for this purpose. In addition other spectral lines are measured and their integrated intensities used to determine upper atomic level population densities, which are used to determine excitation temperature. All data must be Abel inverted in order to back out volumetric emission from the measured line-of-sight integrated emission.

The measured quantities, electron number density and atomic level population densities from both neutral and ionic argon, are used to determine electron and heavy particle kinetic temperature. A multitemperature ideal gas equation of state and a non-LTE ionization equation are used to solve for these two quantities. Argon neutral number density is determined from the Boltzmann factors relating the measured neutral particle upper level population to the ground level. Argon ion number density is assumed equal to the measured electron number density.

The ideal gas equation of state is given by equation (1), the non-LTE ionization equation is after Potapov [7] and is given by equation (2), and the Boltzmann factors for argon neutral number density ar given by equation (3). The Boltzmann factors result in good values for neutral number

density due to the relatively low temperatures found in this LSP, and the high electron number densities, which exceed the critical densities set out by Drawin [8], and modified by Griem [9] to account for trapped resonance radiation. Therefore the neutral and ionic excitation temperatures, T_{exa} and T_{exi}, can be approximated by the temperature found by an LTE analysis of the upper level population densities. Figure 1 incorporates contour plots of calculated electron and heavy particle kinetic temperatures. *It is found that kinetic nonequilibrium is a dominant non-LTE effect in atmospheric argon LSP's.*

The laser beam profile is imposed on the field of measured and calculated values. As the laser profile interacts with the plasma flowfield the power absorbed at every spectroscopic measurement location can be calculated. This results in a determination of global laser absorption available for comparison to the calorimetrically determined value. The values determined are 85% ± 6% and 75 ± 4% from non-LTE spectroscopy and calorimetry, respectively.

Generalized Non-LTE LSP Model

The goal of a generalized non-LTE model is to predict results for global absorption and thermal efficiency of high pressure hydrogen laser sustained plasmas (LSP's) at very high powers. If it is known that the LSP is in LTE, then only *one* temperature is necessary for a complete thermodynamic description. In this case the solution algorithm also becomes somewhat simplified. However, in general LSP's cannot be assumed to be in LTE. In the non-LTE case a separate temperature could be assigned to each energy mode of each species, for example the translational temperature of the electrons could be different than that of the neutrals or any of the ions, or the neutral excitation temperature. The non-LTE case greatly complicates the solution process with the introduction of several new variables (the new temperatures). In addition, radiation can play an important role in the production and destruction of species in a non-LTE LSP which is not collisionally dominated. A new technique must be introduced to account for the coupling of the particles and radiation.

The prediction of global absorption and thermal efficiency can be considered to be a macroscopic prediction that requires the accurate prediction of LSP thermodynamic and transport properties including the species number densities of H_2, H, H^+, e^-, H^-, H_2^+, and H_3^+ at each point within the LSP. In addition, for a non-LTE LSP some method of accounting for the coupling between radiation and particles must be applied to each point in the LSP as well as across the LSP from one point to another. Finally, the macroscopic velocity, pressure and temperature fields for the entire LSP must be solved via the conservation equations using an iterative algorithm.

The calculation of species number densities is well documented for hydrogen plasmas in LTE [10]. The basic method is to first identify the reactants and products for each equilibrium reaction taking place. Then, setting the chemical potential of the reactants equal to that of the products, equations can be arrived at relating particle number densities to particle partition functions. These equations involve the equilibrium temperature, and are relatively easy to solve using an iterative process. The case of non-LTE species number densities requires a modification of the basic equilibrium solution algorithm and necessitates the introduction of additional species continuity equations. These equations are solved simultaneously with the plasma momentum and energy equations. In addition, a scheme to account for the production or destruction of species through the interaction with radiation (a collisional-radiative model) must be included in these calculations to provide source terms for the species continuity equations.

Specific heat, enthalpy, viscosity, thermal conductivity and electric conductivity can be calculated once the species fractions are known . In addition, the absorption of the incident laser beam can be calculated through the calculation and combination of several absorption coefficients including the electron-ion, electron-neutral and electron-molecular inverse bremsstrahlung coefficients. Most of the relations that determine these quantities are applicable to both LTE and non-LTE cases with only a slight modification of the input quantities.

Current plasma models used to predict results for hydrogen are limited to LTE LSP's with peak temperatures below 30000 K [11,12]. These models use tabulated thermodynamic and transport coefficient data. The logical approach to a generalized non-LTE model is to calculate all necessary properties as they are needed, thereby eliminating the need for tabulated data. This is an important feature of our ongoing research.

$$P = k_b[n_e T_e + (n_a + n_i) T_g] \left(1 - P_c^{DH}\right) \qquad (1)$$

$$n_e\left(\frac{n_i}{n_a}\right)\frac{T_g}{T_e} = 2\frac{Z_{exi}\left(\frac{T_{exi}}{T_e}\right)}{Z_{exa}\left(\frac{T_{exa}}{T_e}\right)}\left(\frac{2\pi m_e k_b T_e}{h^2}\right)^{(3/2)}\exp\left(\frac{-E_{Ia}}{k_b T_e}\right) \qquad (2)$$

$$n_a = \left(\frac{n_m}{g_m}\right)Z_{exa}(T_{exa})\ \exp\left[\frac{E_m}{k_b T_{exa}}\right] \qquad (3)$$

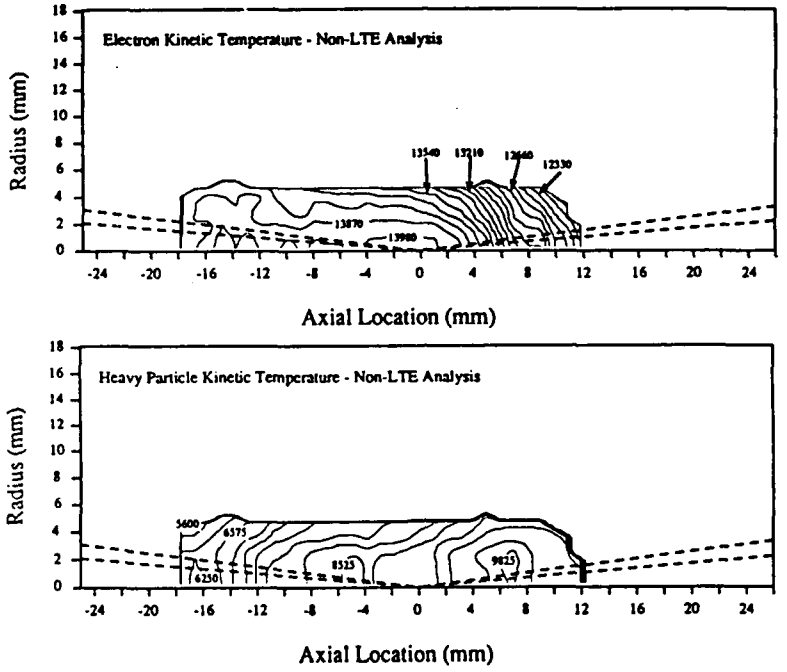

Figure 1 Plasma kinetic temperatures

References

1. Zerkle, D.K., Schwartz, S., Mertogul, A., Chen, X., Krier, H., Mazumder, J., "Laser-Sustained Argon Plasmas for Thermal Rocket Propulsion," *J. Propulsion and Power*, Vol. 6, No. 1, pp. 38-45, Jan.-Feb. 1990.
2. Mazumder, J., Krier, H., "Experimental and Numerical Studies of Laser Sustained Gas Plasmas," Final Technical Report under Grant No. AFOSR-88-0129, April 1989.
3. Schwartz, S., Mertogul, A., Eguiguren, J., Zerkle, D., Chen, X., Krier, H., Mazumder, J., "Laser-Sustained Gas Plasmas for Application to Rocket Propulsion," AIAA paper 89-2631 presented at the 25th Joint Propulsion Conference, Monterey, CA, July 10-12, 1989.
4. Krier, H., Mazumder, J., "Experimental Studies of Laser-Sustained Argon and Hydrogen Plasmas," Annual Technical Report under Grant No. AFOSR-89-0274, March 1990.
5. Mertogul, A., Zerkle, D.K., Krier, H., Mazumder, J., "CW Laser Sustained Hydrogen Plasmas for Thermal Rocket Propulsion," AIAA paper 90-2637 to be presented at the 21st International Electric Propulsion Conference, Orlando, FL, July 18-20, 1990.
6. Eddy, T.L., "Low Pressure Plasma Diagnostics Methods," AIAA paper 89-2830, presented at the 25th Joint Propulsion Conference, Monterey, CA, July 10-12, 1989.
7. Potapov, A.V., "Chemical Equilibrium of Multitemperature Systems," *High Temperature*, Vol. 4, pp. 48-51, 1966.
8. Drawin, H.W., *Z. Physik*, Vol. 228, p. 99, 1969.
9. Griem, H. R., Plasma Spectroscopy, McGraw-Hill, New York, 1964.
10. Patch, R. W., "Components of Hydrogen Plasma including Minor Species," NASA TN-D-4993, 1969.
11. Eguiguren, J.V., M.S. Thesis, University of Illinois at Urbana-Champaign, 1989.
12. Jeng S.-M., Keefer, D.R., "Effect of Finite Rate Chemistry on a Realistic Laser Thermal Rocket Performance," AIAA paper 88-2774, June 27-29, 1988.

LIF DIAGNOSTICS FOR ARCJET THRUSTERS

AFOSR Grant Contract No. AFOSR-91-0200

Principal Investigator: Dennis Keefer

Center for Laser Applications
University of Tennessee Space Institute
Tullahoma, TN 37388
(615) 455-0631

SUMMARY/OVERVIEW

Detailed measurements of the nozzle exit flow are needed to verify the applicability of various physical models incorporated in arcjet computational codes. Laser Induced Fluorescence (LIF) measurements can be utilized to accurately measure one or more components of the velocity distribution function of excited atoms in the exhaust flow. We have developed an accurate LIF method which simultaneously obtains two components of this distribution function. Once the distribution function has been measured, it is possible to obtain the mean velocity and the velocity fluctuations of the exhaust flow from moments of the distribution function. Measurements of the exhaust flow from an argon arcjet have been obtained and will be compared with predictions from the UTSI arcjet computational code.

TECHNICAL DISCUSSION

Computational codes for arcjets include physical models for several important plasma and chemical processes. These physical models describe radiation transfer, non-equilibrium reaction and recombination chemistry and various transport properties, such as electrical conductivity and viscosity. The geometry of the arcjet makes it difficult to measure the plasma properties within the constrictor and nozzle, but measurements are needed to assess the validity of the physical models used in the code. Since the physical models used in the code influence the entire flow field, it is possible to gain some insight into their validity by making detailed measurements of the nozzle exit flow. We have developed a LIF method which can obtain accurate and precise measurements of two or more components of the velocity distribution function for an excited neutral species. Computation of the first and second moments of this distribution yield accurate values for the vector components of the mean flow velocity and the variance of the velocity. These detailed measurements can then be compared with the code predictions to assess the validity of the physical models used in the code.

The LIF technique utilizes the very narrow, tunable light from a single-frequency dye laser to sample the Doppler shifted velocity distribution from an excited atomic state in the nozzle flow. The linewidth from these lasers is sufficiently narrow (< 1 MHz) to provide an ultimate sample resolution of approximately 1 m/s. In practice, the accuracy

and resolution of the mean velocity measurement in an arcjet plume is approximately 20 m/s. In our implementation of the LIF technique we utilize the optogalvanic effect in a hollow cathode lamp to provide the basic accuracy of the measurement. Simultaneous measurements of two or more velocity components are provided by multiplex methods using multiple crossed beams and chopping frequencies. A schematic of the experimental layout is shown in Figure 1. The beam from the dye laser is split into two parallel beams which pass through a dual frequency chopper and then through a lens to form the measurement volume. One of the beams passes through a beam splitter to provide a sample for the optogalvanic measurement. A single photodiode detector focuses the measurement volume and limits its spatial extent. The output from this detector is sent to a pair of lock-in amplifiers to separate the signal by chopper frequency. The output from these two lock-in amplifiers and a third lock-in amplifier, which provides the signal from the hollow cathode lamp, are recorded by a computer data acquisition system.

Data from a typical frequency scan of the argon (1s4-2p2) transition at a wavelength of 727.3 nm is shown in Figure 2. This data was obtained at the nozzle exit of a small argon arcjet operating with a power input of 320 W. One beam was oriented at 90 degrees to the nozzle axis to measure the radial component of the velocity distribution, and the second beam was oriented at 76 degrees to measure a component of the axial velocity. The measured mean velocity obtained from a scan taken 1 mm downstream of the nozzle exit is shown in Figure 3. The axial component of velocity peaks at approximately 3 km/s near the centerline, and the radial component of velocity reaches its maximum value of approximately 300 m/s at a distance of approximately 2.5 mm from the axis. Axial scans of the axial and radial components of the mean velocity together with the full width at half maximum (FWHM) of the distribution is shown in Figure 4.

The variance of the velocity distribution can be computed from the measurements, and it is tempting to relate this to the flow temperature. However, the variance includes contributions due to turbulence and to fluctuations of the mean velocity with time scales smaller than the measurement time constant (approximately 1 s). Furthermore, in these experiments it was found that the distribution function was not isotropic with a larger FWHM in the axial direction. These effects preclude using these measurements for a simple measurement of flow temperature. A detailed analysis and discussion of this experiment is given by Ruyten and Keefer [1].

The UTSI computational code is being modified to use argon as a propellent and will be used to predict the conditions measured in the experiments. At the same time, an arcjet supplied to us by NASA Lewis Research Center (LeRC) will be installed in our test facility and operated with an ammonia analog mixture of hydrogen and nitrogen. The laser will be converted in wavelength to use the hydrogen alpha line as a diagnostic, and additional measurements will be made to compare with the UTSI code.

REFERENCE

Ruyten, Wilhelmus M. and Keefer, Dennis, "Laser Fluorescence Velocimetry of an Arcjet Exhaust Plume," Paper No. IEPC-91-093, AIDAA/AIAA/DGLR/JSASS 22nd International Electric Propulsion Conference, Viareggio, Italy, October, 1991.

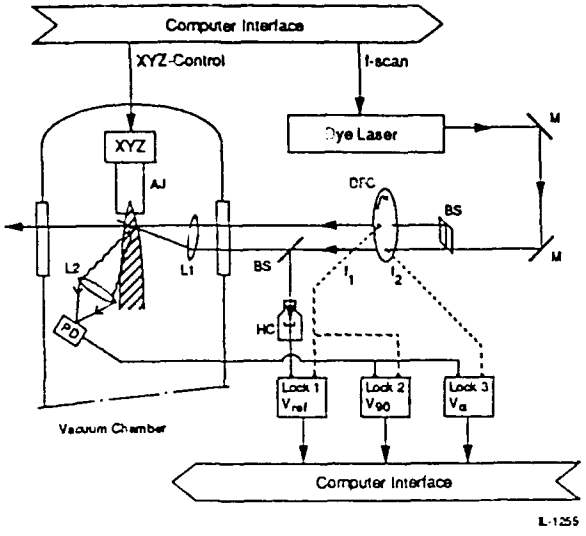

Fig. 1: Schematic of the complete LIF setup: M=mirror; BS=beam splitter; DFC=dual frequency chopper; HC=hollow cathode lamp; L1=focusing lens; L2=collection lens; PD=photo diode (with pinhole aperture); AJ=arcjet; LOCK=phase-locked amplifier. Not shown is a wavemeter that is used to tune the laser to the desired absorption line.

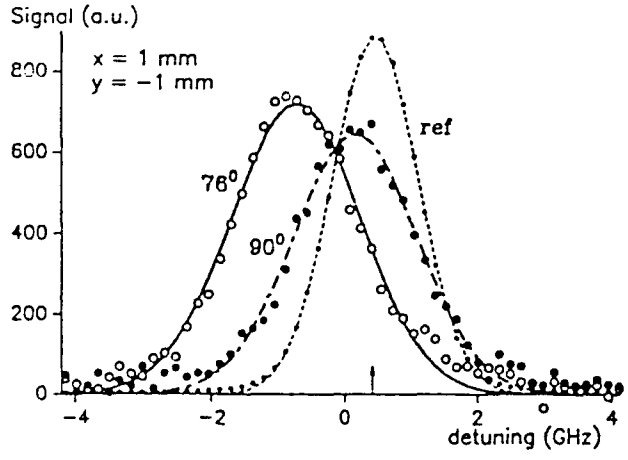

Fig. 2: Typical LIF Doppler profiles at 90° and 76°, recorded 1 mm downstream from the exit plane, 1 mm off centerline (on "upstream" side of laser beam). Gaussian curve fits are shown as well. The arrow indicates linecenter, as determined from the optogalvanic reference signal (rightmost curve).

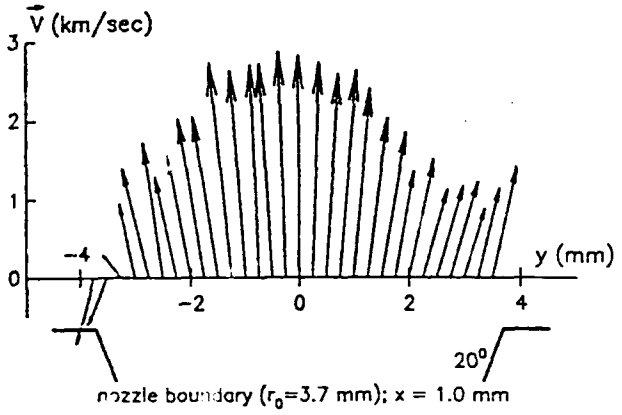

Fig. 3: Vector velocity diagram. The nozzle boundary is indicated. Aspect ratios for velocity and length scales are chosen such that all angles are shown correctly.

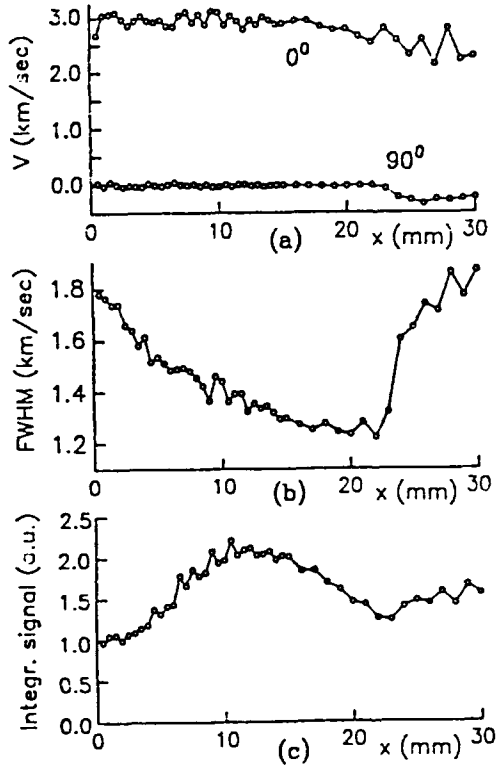

Fig. 4: Axial profiles of radial and axial velocity (a), average velocity spread (b), and average integrated signal (c) on centerline. All data reflect clearly the shock behavior that is observed visually as the crossing of two shock lines, 22 mm downstream from the exit plane.

RECOVERY OF FROZEN FLOW LOSSES IN ARCJETS

AFOSR Grant No. 91-0318

Principal Investigator: V. V. Subramaniam

Department of Mechanical Engineering
The Ohio State University
206 West 18th Avenue
Columbus, Ohio 43210

SUMMARY/OVERVIEW:

The performance of arcjet thrusters especially operating on molecular propellants such as ammonia (NH_3) or hydrazine (H_4N_2) is limited by frozen flow losses. In fact, as much as one-third of the input electrical energy into the device can be lost in various internal modes of the propellant molecules (vibration, electronic excitation, dissociation, and ionization). Scale-up of existing designs to higher powers requires a fundamental understanding of the various mechanisms of frozen flow losses, and the ability to accurately quantify them. This is our primary objective. Additionally, addition of simple monatomic species into the propellant stream to V-T (vibration-translation) relax the gas is being explored. This has the potential to extend the present limits on specific impulse for the ammonia and hydrazine arcjets.

TECHNICAL DISCUSSION:

The arcjet thruster is one in a class of devices known as electrothermal thrusters. Electrothermal thrusters derive their thrust by conversion of electrical energy (transmitted by a current on the order of a hundred amperes) into directed kinetic energy. This is achieved primarily by ohmic heating of the propellant, followed by expansion through a nozzle. The typical arcjet geometry consists of a plenum (subsonic flow), a constrictor (subsonic or sonic flow), and a diverging nozzle (supersonic flow). The propellant (typically hydrogen, ammonia, or hydrazine) is introduced via injection ports in a boron nitride backplate with a swirling (azimuthal) component of velocity. This swirl is typically required to stabilize arcs operating above atmospheric pressure. The arc itself consists of a region of high temperature gas confined to dimensions smaller than the constrictor diameter, but then expands to attach downstream on the nozzle walls. Despite the apparent simplicity of the device and its operation, current understanding of the processes of mass, momentum, energy, and species transport in such flows is poor. Efforts are under way to examine these transport processes using overall kinetics[1].

The nozzle region of the arcjet serves essentially as an energy conversion device to convert the input electrical energy into directed kinetic energy or thrust. The gas in the nozzle region undergoes a rapid expansion wherein the translational temperature decreases rapidly in the flow direction. This can be seen in the quasi 1-D cold air flow simulation of the 30 KW thruster, shown in Fig. 2. The geometry used for this case is shown in Fig. 1. While the translational temperature decreases in real flows however, internal processes such as vibrational and electronic energy transfer require times much longer than the characteristic flow time in order to equilibrate. Therefore, a substantial portion of the input electrical energy (30%-50% by simple estimates) remains "frozen" in these internal modes. This has dramatic implications for performance characteristics, and will influence the choice of propellant for a given mission. The focus of this proposed research is to (1) utilize existing and our own on-going state-resolved measurements of chemical rates in order to accurately calculate the amount of frozen flow losses in

ammonia and nitrogen arcjets, and to (2) explore the possibility of reducing these losses either by premixing a fast VT (vibration-translation) relaxing monatomic gas (such as He, Ne, Ar, etc.) in the propellant stream, or by injecting into the downstream nozzle section.

Frozen flow losses in the nozzle region are due to vibrational, rotational, and electroni non-equilibrium. This type of non-equilibrium is not unique to arcjets. Such high speed non-equilibrium flows are common in the study of various gas dynamic lasers[2]. Extensive experimental and numerical work has been performed at The Ohio State University[3,4]. A distinct feature of the arcjet however, is the presence of the arc in the plenum, constrictor, and nozzle regions. This arc is confined to only some regions of the flow and therefore, necessitates the inclusion of charged particles in the simulation of these regions. By contrast, the cooler regions of the flow are free of charged particles. This means that the chemical kinetics together with finite rate ionization and recombination will render the numerical solution stiff. Consequently, a 2-D, axisymmetric, viscous, cold-flow (no reactions) model of the arcjet fluid mechanics is being developed. This is an important step before including multiple species (electrons, ions, atoms, and molecules), multiple temperatures, and electromagnetics, but without including vibrational and electronic non-equilibrium. This pathological case is useful for model verification and to ensure that boundary conditions are adequately satisfied. Finally, the full chemical kinetics and state-resolved molecular energy transfer kinetics will be incorporated in a fully 3-D model.

The numerical methods for highly non-equilibrium high speed reacting *internal* flows is not by any means trivial. Although the numerical techniques of MacCormack[5-7] and Beam and Warming[8] are well developed for supersonic *external* compressible flows, the incorporation of finite rate kinetics and the problem of *internal* flow complicates the schemes substantially. Stringent demands must therefore be placed on computational speed, stability, and accuracy especially if a 3-D simulation is the ultimate goal. The chosen numerical scheme known as the Linear Block Implicit (LBI) method first developed by Briley and McDonald[9] shows tremendous promise. The calculation displayed for the quasi 1-D problem in Fig. 2 was obtained by running the code on the Ohio Supercomputer Center Cray Y-MP. Noteworthy are the ***convergence to machine accuracy (14 decimal places) in remarkably few time steps (200 steps) taking 1 second of CPU time on the Cray Y-MP***. Also of importance is the fact that this rapid convergence was obtained ***starting from zero initial guesses for almost all variables*** (obviously density was given a non-zero starting value). This method has also been tested on a converging nozzle whose dimensions are identical to the converging portion of the 30 KW arcjet geometry. Fig. 3 shows the axial Mach number profile along the nozzle center line. Note that this nozzle is choked. Corresponding transverse (radial) distributions of the axial velocity are displayed in Fig. 4 at the inlet and exit stations, showing the development of the boundary layers. Again, convergence to machine accuracy was obtained after 2000 time steps taking about 2 minutes of CPU time on the Cray Y-MP, starting from zero initial guesses. The convergence behavior is dramatically improved when starting values specified either by linear distributions or the quasi 1-D solutions themselves, are used. This method shows tremendous promise for 3-D simulations of supersonic, reacting, internal flows.

As part of any good computational effort, there must be a parallel theoretical component. This is to ensure the accuracy and correctness of the numerical model, as well as to provide physical insight into any numerically generated solutions. Although analytical models of the arcjet flow with chemistry are impossible, simple models with *judicious* approximations can simulate and explain *some* of the phenomena in the arcjet[10,11].

REFERENCES:

(1) R. P. Rhodes, and D. Keefer, "Numerical Modeling of an Arcjet Thruster", paper AIAA-90-2614, presented at the 21st International Electric Propulsion Conference, July 18-20, 1990, Orlando, Florida

(2) J. D. Anderson, Jr., *Gasdynamic Lasers: An Introduction*, Academic Press, New York, 1976

(3) W. Urban, J. X. Lin, V. V. Subramaniam, M. Havenith, and J. W. Rich, **Chem. Phys.** 130 , p. 389, 1989.

(4) A. Chiroux de Gavelle de Roany, C. Flament, J. W. Rich, V. V. Subramaniam, and W. R. Warren, "Kinetic Modelling of Gas Dynamic Flows with Nonequilibrium Vibrational Excitation", **AIAA J.**, accepted for publication.

(5) R. W. MacCormack, "The Effect of Viscosity in Hypervelocity Impact Cratering", paper AIAA-69-354, presented at the AIAA Hypervelocity Impact Conference, April 30-May 2, 1969, Cincinnati, Ohio.

(6) R. W. MacCormack, "A Numerical Method for Solving the Equations of Compressible Viscous Flow", paper AIAA-81-0110, presented at the AIAA 19th Aerospace Sciences Meeting, January 12-15, 1981, St. Louis, Missouri.

(7) R. W. MacCormack, Lecture Notes on "Numerical Methods for Compressible Viscous Flow", presented during a short course on Advances in Computational Fluid Dynamics, December 6-10, 1982, The University of Tennessee Space Institute, Tullahoma, Tennessee.

(8) R. M. Beam, and R. F. Warming, "An Implicit Factored Scheme for the Compressible Navier-Stokes Equations II: The Numerical ODE Connection", paper AIAA-79-1446, presented at the AIAA 4th Computational Fluid Dynamics Conference, July 23-24, 1979, Williamsburg, Virginia.

(9) W. R. Briley, and H. McDonald, "Solution of the Multidimensional Compressible Navier-Stokes Equations by a Generalized Implicit Method", **J. Comp. Phys. 24**, pp. 372-397, 1977.

(10) B. Glocker, H. O. Schrade, and P. C. Sleziona, "Numerical Prediction of Arcjet Performance", paper AIAA-90-2612, presented at the 21st International Electric Propulsion Conference, July 18-20, 1990, Orlando, Florida.

(11) M. Auweter-Kurtz, H. L. Kurtz, H. O. Schrade, and P. C. Sleziona, **J. Propulsion & Power**, Vol. 5, No. 1, Jan.-Feb. 1989.

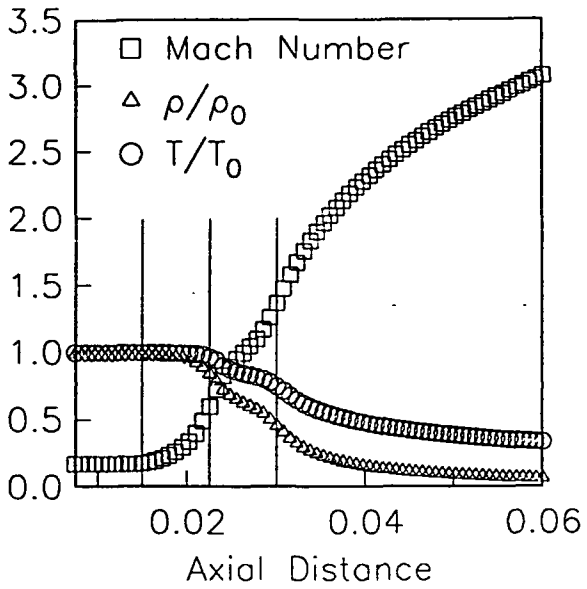

Fig. 2: Quasi 1-D cold flow solutions. The vertical demarcations show the locations where area changes occur (see Fig. 1).

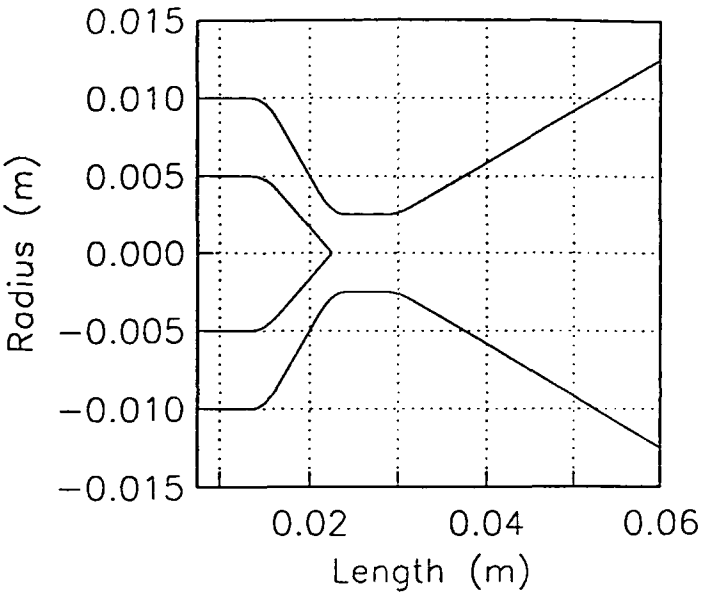

Fig. 1: Geometry of the 30 KW arcjet

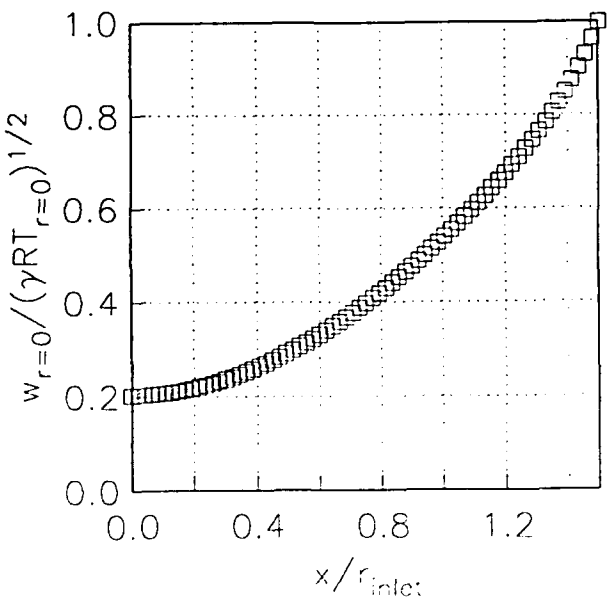

Fig. 3: The axial variation of the centerline Mach number is shown here for the fully viscous (Re=100), 2-D, axisymmetric, choked flow in a converging nozzle of the same dimensions as the converging section in the 30 KW arcjet is shown here (see Fig. 1).

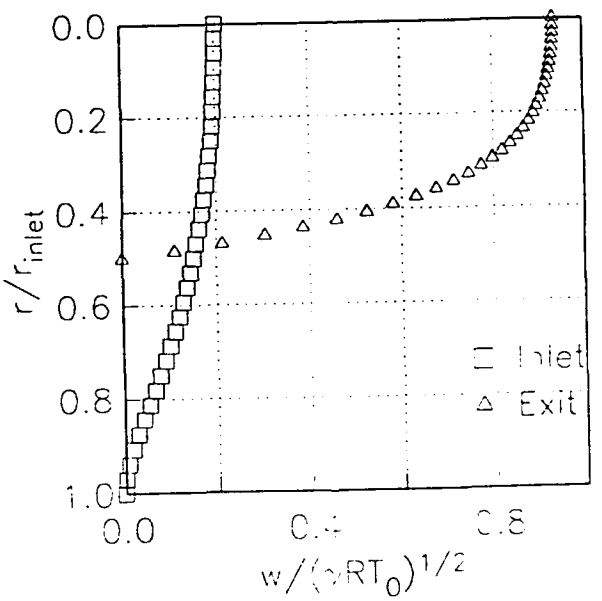

Fig. 4: The radial profiles of the axial velocity at the inlet and exit stations are shown here for the converging nozzle (same case as in Fig. 3).

Investigation of Arcjet-Power Processing Unit Interaction

Dr. Ronald Spores, OL-AC Phillips Laboratory
Prof. Daniel Erwin, University of Southern California

Objective:

Determine to what extent the power fluctuations of a high frequency switching Power Processing Unit (PPU) affects the operation of an arcjet propulsion system

Issues Currently Being Addressed:

- Momentum Flux (Velocity) Fluctuations of the plume throughout the PPU switching cycle
- Temperature Fluctuations throughout the switching cycle

Investigation of the Arcjet- Power Processing Unit Interaction

Dr. Ronald Spores, Phillips Lab and Prof. Daniel Erwin, USC

Relevance

The low overall efficiency of present arcjet propulsion systems (29% for a 30 kW arcjet) is one of the principal limiting parameters preventing an arcjet electric orbit transfer vehicle (EOTV) from becoming a reality. A great deal of effort has been directed toward developing a high efficiency power processing unit (PPU) and a large amount of research and development has been conducted over the years on improving the arcjet while the interaction effects of these critical propulsion components has been virtually ignored. Basic research into the PPU/arcjet interaction is of great importance to the Air Force and the Aerospace community who wish to integrate arcjets into satellite propulsion systems.

This research project is investigating how the plume temperature and momentum flux of a 1 kW arcjet is affected by the transient behavior of the PPU due to voltage fluctuations throughout its switching cycle. Due to weight and efficiency considerations on board a spacecraft, operational arcjet propulsion systems must use high frequency switching power supplies which are above 93% efficient. The switching power supply takes the DC current from the solar arrays and chops the current into a series of width modulated square wave pulses which are feedback regulated to maintain the output current to a predetermined value. As the input current across the electrodes of an arcjet fluctuates due to PPU switching, the power dissipation to the propellant is subsequently varied. These voltage variations likely result in small fluctuations in the anode arc attachment which affects gas expansion in the nozzle, propellant heating patterns, and boundary layer development. Thus, it is believed that both the propellant temperature and exit velocity are affected by power supply ripple. In order to investigate these phenomena, transient measurements of both the velocity and kinetic temperature in the plume of a 1 kW arcjet are taken synchronized with the master clock of the high frequency PPU which operates at 16kMz. Time dependent emission measurements of the of the hydrogen Balmer α line in the arcjet plume indicate an intensity variation of 30% during each switching cycle.

Arcjet Plume Velocity Measurements using Emission Spectroscopy

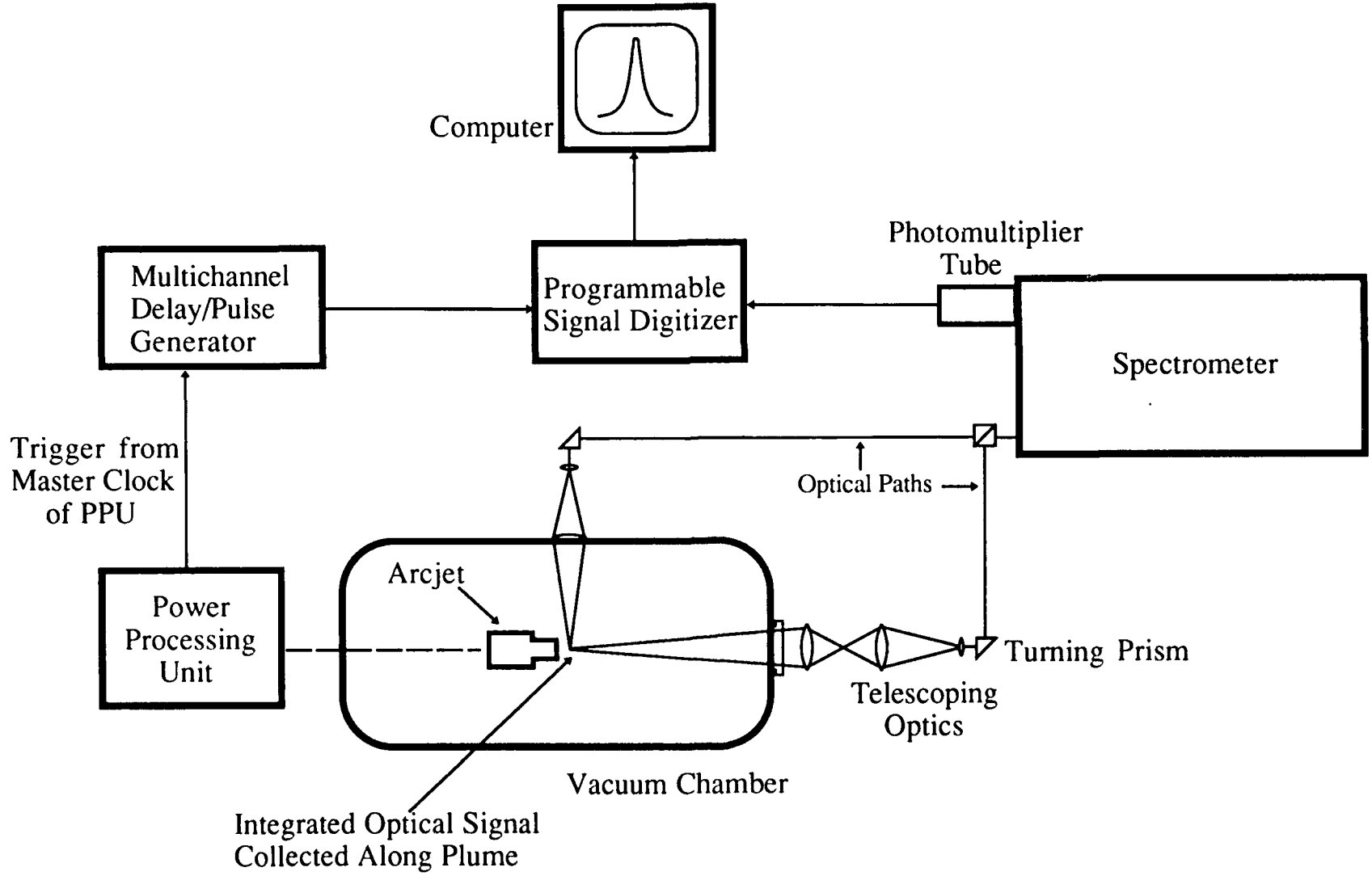

Scientific Approach

Both laser induced fluorescence and emission spectroscopy measurements of an arcjet's external plume are being investigated. Both non-intrusive techniques indirectly measure the velocity and temperature of the arcjet plume throughout the PPU switching cycle by time delaying measurements with the PPU Master clock. The figure shown is only of the emission spectroscopy experiment.

For emission spectroscopy, intensity measurements are taken throughout the PPU switching cycle at a series of wavelengths so that the complete hydrogen Balmer α transition lineshape profile is mapped out as a function of time. The emission data is of an integrated signal taken along the axis of the arcjet and looking back up into the constrictor region. This viewing angle collects light from both the internal arc of the arcjet and the external plume gas flow. Since it is the plume that is of primary concern here, the majority of the light from the arc core is intentionally blocked off at the image plane of the first lens. This does not eliminate the arc core emission but it does allow one to obtain data from the much weaker plume emission which can be seen is the Progress figure at a wavelength of 6565.05 Angstroms. Due to the velocity of the arcjet plume there is a wavelength doppler shift of the plume emission which is directly proportional to the gas velocity. Emission intensity is obtained in two dimensions: wavelength and time. By curve fitting the data at each phase throughout the PPU switching cycle, the velocity and translational temperature fluctuations of the plume can be obtained.

For Laser Induced Fluorescence, although the goal of obtaining temperature and velocity fluctuation measurements is the same, the technique is quite different and provides pointwise measurements unlike the spatially integrated signal of emission spectroscopy. The output wavelength of a tunable dye laser is scanned over the spectral region of an atomic transition line of the propellant (in this situation the Hydrogen Balmer α line is used). The control volume is defined by the intersection of the focussed laser beam and the focal region of the photomultiplier tube (PMT) collection optics which are positioned for 90^{o} collection of the incident laser light. Due to the velocity of the hydrogen atoms there is a Doppler shift of the laser light absorption wavelength. The light is then reemitted and the PMT determines the absorption wavelength profile with the width corresponding to temperature and the shift of the peak wavelength equating to velocity.

Emission Intensity Fluctuations

Throughout PPU Switching Cycle

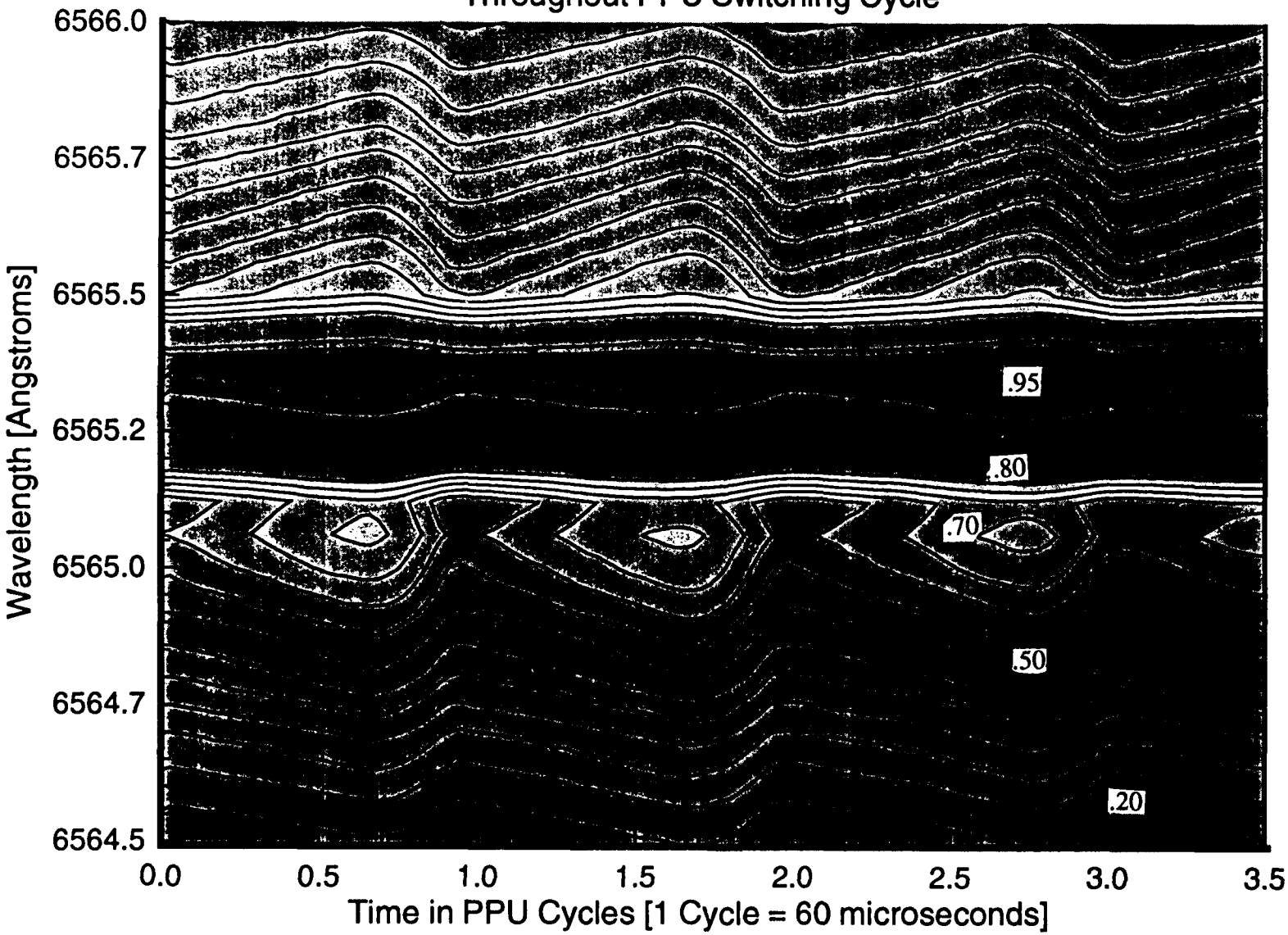

Progress

The color contour plot represents time resolved emission intensity data for a 1 kW hydrogen arcjet where the emission is solely the hydrogen Balmer α transition. In the plot, wavelength is expressed along the ordinate and time along the abscissa. The emission data is in arbitrary units with the color red representing the highest intesity and dark blue indicating the lowest. [Please note that the Progress figure indicates relative wavelengths, all values should have 2.55 Angstroms subtracted for the spectrometer calibration adjustment, this in no way affects any of the conclusions discussed here] As one marches in time along the abscissa of the plot, (note that the wavelength of peak intensity can be thought of as representing velocity of the plume- due to the Doppler shift), one notes that the peak intensity (red region, .95 normalized intensity) remains at exactly the same wavelength throughout all three and a half switching cycles of the PPU. This same lack of wavelength variation can also be said for the side maxima intensity that can be seen at 6565.05 A (.70 normalized intensity). This side peak is thought to represent the velocity of gas in the plume while the central red peak (6565.35 A) represents the low velocity arc core of the arcjet. The side peak has a wavelength shift of 0.3 A which equates to a plume velocity of 13.6 km/sec, this agrees well with other researchers. Thus, this preliminary data seems to indicate that the velocity of the arcjet does not fluctuate during a PPU switching cycle to within experimental resolution.

Note however that all contours bulge outward (away) from the central high intensity (red) region during each cycle with the maximum occurring about 2/3 through the cycle. This emission intensity fluctuation (of about 30%) throughout the PPU cycle indicates that the number density of atoms in the N=3 excited state level of hydrogen fluctuates. Thus, it seems to follow that the excited state frozen flow appears to vary throughout the switching cycle. This emission variation also corresponds to a temperature variation during the cycle even though it appears that velocity does not vary. One plausible explanation is that the time scales for momentum flux (velocity) variations are simply too long for the overall flow to react and thus the peak energy deposition per cycle simply goes into frozen flow losses instead of added thrust.

This study helps to validate the assumption of steady state flow velocity in the plume employed by other investigators but it brings into some question the assumption of using the steady state linewidth of an atomic transition for the measurement of translational temperature in the plume.

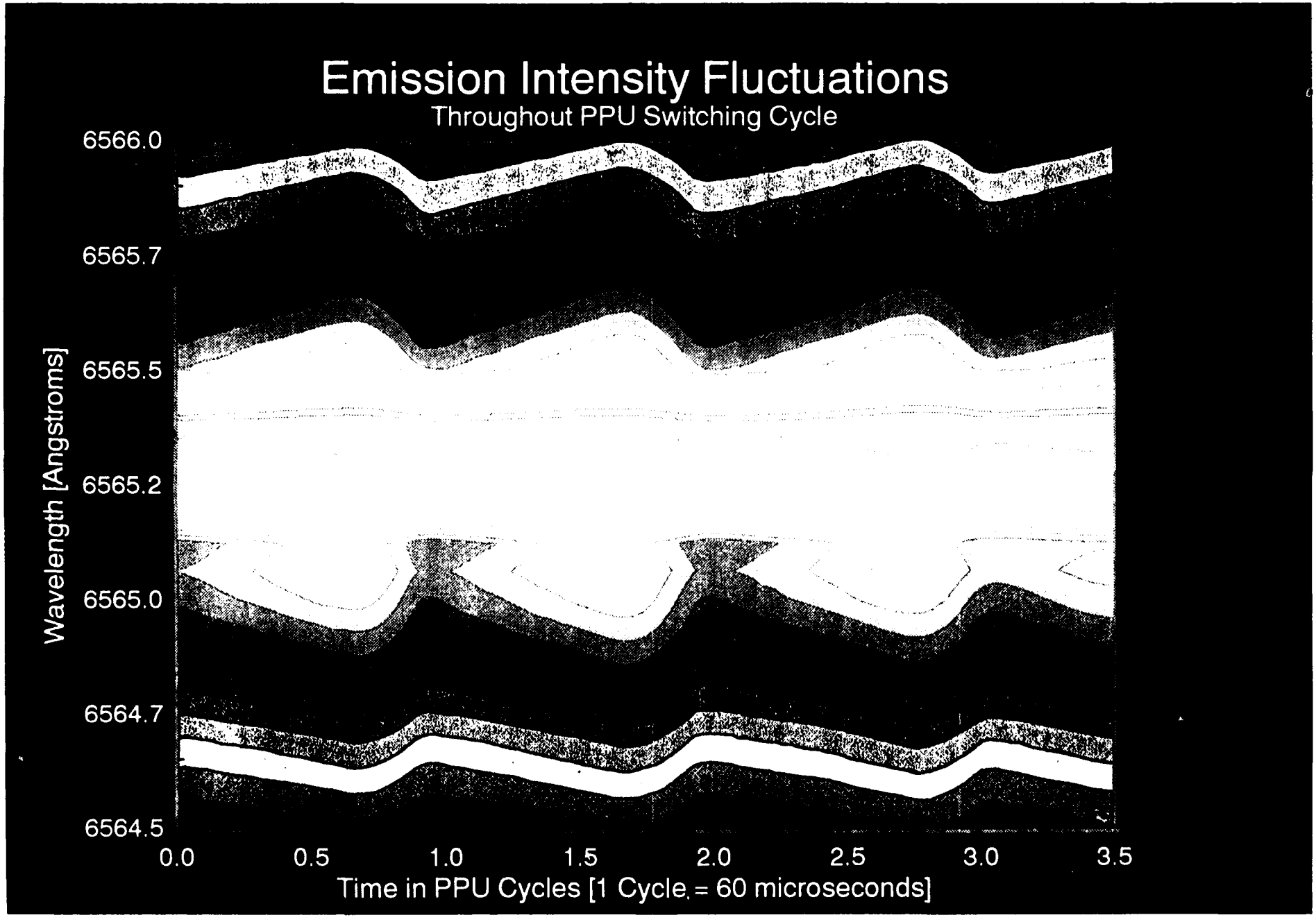
Emission Intensity Fluctuations
Throughout PPU Switching Cycle
6566.0
6565.7
6565.5
6565.2
6565.0
6564.7
6564.5
Wavelength [Angstroms]
0.0
0.5
1.0
1.5
2.0
2.5
3.0
3.5
Time in PPU Cycles [1 Cycle = 60 microseconds]

Future Research

- Internal Optically Accessible Arcjet to Investigate how Power Dissipation Fluctuations affect:
  - Heat Transfer to the Surrounding Walls
  - Thermionic Electron Emission from the Cathode
  - Propellant Turbulence in the Cathode Region
  - Energy Transport between the Arc and Propellant
- Development of a Numerical Model to Investigate Energy Transport Timescales of an Arcjet
- Employ a Variable Frequency Switching Power Processing Unit to investigate the possibilities of Resonance Heating Effects and Instability Frequencies

Future Research

Future research on this project will be in three areas.: 1) Investigation of the internal fluctuations in an arcjet via an internal optically accessible thruster, 2) the development of a one dimensional plasma model of the arcjet to investigate energy transport timescales and 3) construction of a variable switching frequency power supply.

By constructing an internal optically accessible thruster many of the transient phenomena taking place inside of the arcjet can be investigated. Internal fluctuations due to the PPU switching cycle are likely to affect a wide range of phenomena inside the arcjet including: thermionic electron emission from the cathode tip, propellant turbulence near the cathode, energy transport between the central arc and the surrounding propellant, heat transfer to the walls, and some researchers have suggested that power supply ripple affects cathode erosion. Due to spatial resolution, this type of research is best done on a larger size arcjet (30 kW).

It was originally expected that the energy transport would propagate through the arcjet and into the plume on a timescale that was a fraction of the switching cycle. However since velocity fluctuations were not observed our assumptions of energy propagation time are questionable and it is currently believed that further investigation in this area would prove fruitful. Thus, a one-dimensional numerical model is being developed to better understand the transient phenomena taking place in an arcjet. This model will be used to investigate the timescales of heat addition to the propellant via an electric arc and what is the expected response time of energy perturbations into the downstream flow expansion nozzle and into the arcjet plume. After the one-dimensional model has been developed it is anticipated that a full three dimensional numerical code will then be pursued.

The construction of a variable switching frequency power supply and its operation with an arcjet are being considered as part of the follow on research. It is anticipated that there is some upper bound frequency above which the energy deposition fluctuations no longer affect the flow, knowledge of this upper bound frequency would be helpful for systems integration onboard satellites. It is also possible that certain resonant frequencies exist for enhanced energy deposition or instability frequencies in an arcjet will be discovered by using a variable frequency power supply.

COMPARSION BETWEEN EXPERIMENTAL DATA AND THEORETICAL MODELS FOR HIGH VOLTAGE SOLAR ARRAY ARCING

AFOSR Grant Contract No. AFOSR-87-0340

Principal Investigator: Daniel Hastings

37-451, Dept of Aeronautics and Astronautics
MIT, Cambridge MA 02139

SUMMARY/OVERVIEW:
Solar arrays biased to high voltages are observed to undergo arc discharges in the space environment. A model has been developed on the basis of detailed Particle in Cell plasma simulations of a solar cell triple junction. This model is compared in detail to experimental data and shown to give a reasonable explanation for the data. On the basis of this model, it is possible to develop mitigation strategies to alleviate the high voltage arcing.

TECHNICAL DISCUSSION:

The model system studied consists of dielectric material placed on a negatively biased conductor in a plasma environment. For a solar array, the dielectric material corresponds to the coverglass and adhesive and the conductor corresponds to the interconnect. The solar cell itself is neglected because it's thickness is small compared to the coverglass and adhesive and because it is a semiconductor with a voltage drop across it of at most a volt or two.

Two types of charging mechanisms are considered. One is the charging due to ions from outside the electric sheath surrounding the solar arrays. Another is the charging due to electrons emitted from the conductor surface by enhanced field electron emission (EFEE). These charging processes are calculated by numerically integrating the particle orbits around the solar cell under the electric field which was consistent with the charging state of the dielectric material.

The numerical integration is done by a particle in cell simulation code. There are three major results.

(1) The ambient ions charge the dielectric front surface to the steady state potential $\simeq 5$ V, where 5 (eV is the kinetic energy of the incoming ions with the orbital velocity in LEO. Therefore, at the steady state given by the ion charging, a strong electric field of $E \simeq V/d$ is created at the triple junction where V is the bias potential on the conductor and d is the thickness of the dielectric.

(2) After the electric field reaches the value of $E = V/d$ at the triple junction, if there is an emission site with a high field enhancement factor β on the conductor surface near the triple junction, then

electrons can be emitted profusely and can charge the side surface. The functional dependence of the current density on the electric field at the emission site (E_e) is

$$j_{ec} = A(\beta^2 E_e^2) \exp(-\frac{B}{\beta E_e}), \tag{1}$$

where A, B are constants determined by work function of the surface ϕ_w. This charging due to enhanced field electron emission (EFEE) charges the side of the dielectric positive and can therefore enhance the electric field at the triple junction. It can develop very rapidly because of the strong exponential dependence of the current on the electric field. When the electric field doubles, the emission current increases by ten orders of magnitude. This incident current can desorb a significant amount of neutral gas from the surface and create a dense neutral cloud as high as 10^{21} m^{-3} over the surface. The electron current flowing through the neutral cloud can lead to a discharge like a surface flashover. Even if there is not a dense neutral cloud created over the dielectric, the electric field just over the surface may increase to the point where dielectric breakdown occurs of a thin layer along the side of the dielectric. For an initial conductor voltage of 500 Volts across a coverglass of 150 microns, the initial electric field imposed along the edge of the coverglass is 3.3×10^6 V/m. Typically, the coverglasses are held on with an adhesive which can have a dielectric breakdown strength as low as 2×10^7 V/m. Hence the electric field along the side of the coverglass only needs to be enhanced by an order of magnitude for dielectric breakdown of the adhesive or surface flashover of desorbed neutral gases to occur.

(3) Once the charging time of the dielectric coverglass is known, the arcing rate for a given solar array can be calculated assuming that it takes a negligible amount of time for the ionization of neutral gases or for dielectric breakdown to occur relative to the field buildup time. The arcing rate is then defined as the inverse of the time which is necessary to build up the electric field and charge the surface with ions. The time between arcs is therefore given by

$$\tau_{arc} = \tau_{efee} + \tau_{ion}, \tag{2}$$

where τ_{efee} is the charging time due to enhanced field emission electrons, and τ_{ion} is the charging time due to ions.

We have used the Particle in Cell simulation to calculate the arc rate numerically for the PIX II flight and show the results in Fig. 1. The PIX II experiment was conducted with 456 2 cm $\times$ 2cm solar cells. We divide the PIX II array surface into sections of area 0.01 m^2 and assume that arcs in the same section are all correlated but uncorrelated between different sections. Since the power supply was often shut down for more than 2 seconds in the flight experiment, it can be assumed that ions charge up the front surface while the power supply recovers. Therefore, the parameter ΔQ (the charge lost in an arc event from the front surface) for the flight data is assumed to be very small from $\Delta Q = 10^{-12}$ to $10^{-11}(C)$. For the ground data, the experiment time of 1500 sec is chosen. Since there was no problem of power supply recovery reported in the ground experiment, ΔQ is assumed to be from $\Delta Q = 10^{-9}$ to $10^{-11}(C)$. The emission site density is chosen as $n_{es} = 1 \times 10^5$ m^{-2} with an exponential distribution of field enhancement factors with average value $\beta_o = 150$ for the flight data and $n_{es} = 1 \times 10^6$ m^{-2}, $\beta_o = 120$ for the ground data. Since the

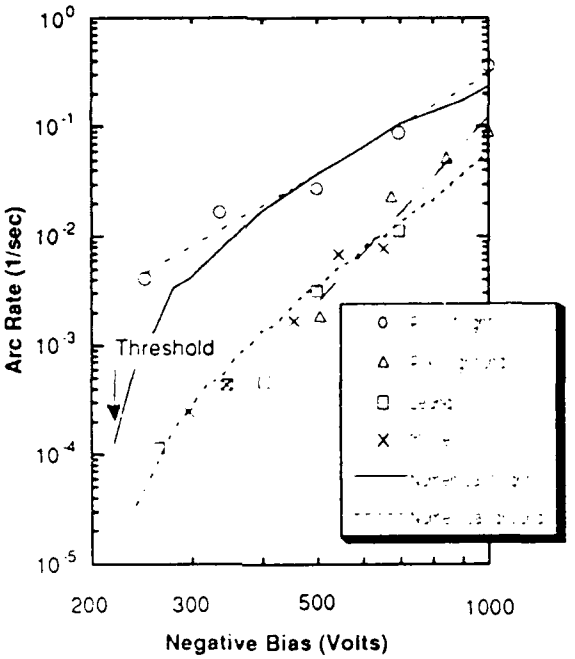

Figure 1: Experimental data for ground and flight experiments

samples used in the ground experiment and the flight experiment were different, it is possible that at the microscopic level the number of emission sites might be different. The plasma conditions were chosen as $n_e = 6.3 \times 10^9$ m^{-3} and $v_{ion} = 7.7 \times 10^3 (m/s)$ of oxygen for the flight data and as $n_e = 2 \times 10^{10}$ m^{-3} and $T_i = 1(eV)$ of argon for the ground data. The ground data and ground numerical curve shown in Fig. 1 have been normalized to the values at $n_e = 6.3 \times 10^9 (m^{-3})$ and $v_{ion} = 7.7 \times 10^3 (m/s)$ assuming that the arc rate is proportional to the ion flux $n_e v_{ion}$.

The results are shown in Fig. 1 with the experimental data. They show very good agreement with the data over the range the data exists. They predict a threshold when the charging process is exponentially slow and also predicts a saturation for high voltages. The lower parts of the curves occur when the enhanced field electron emission charging is the slowest charging process in the system. The arc rate dependence on voltage here is exponential and enables a threshold voltage to be defined with a small uncertainty. The threshold voltage therefore can be defined as the voltage at which the arc rate is decaying very rapidly. The upper parts of the arc rate curves are dominated by the ion recharging time. This leads to the decrease in the rate of change of the arc frequency as can be clearly seen in the data. The fact that the arc rate scales with the density for the higher voltages can also be explained from the dominance of the ion recharging time since

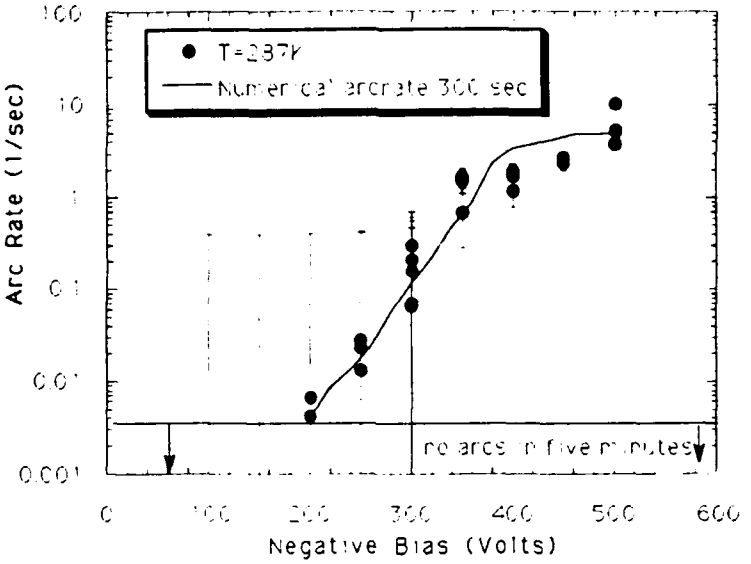

Figure 2: Arc rate against voltage for nominal density of $n_e = 1.1 \times 10^{12}$ m^{-3} and cell temperature of 287 K

this scales directly with the density. Finally, the two theory curves show clearly the difference between the ground and flight data and provide an explanation of the difference. The difference between the two experiments occured because the charge lost per event was different as well as the microscopic emission parameters. The difference in the charge lost affects the ion recharging time. The difference in the microscopic emission parameters effects the time to build up the electric field along the side surface.

In addition we have calculated the arc rate for the Japanese high voltage solar array (HVSA) experiment. In Fig. 2 we show the results for the ground experiments.

From this good agreement between the theory and the experiment we can deduce that the important elements of the arc formation are the presence of a triple junction, the geometry and secondary electron emission properties of the side surface, the preparation and work functions of imperfections on the interconnector or other biased surfaces, the physical size of the solar cell module and the plasma density.

ICRF Plasma Heating Experiment in the Tandem Mirror Rocket

Grant No. AFOSR-90-NA-001

Principal Investigators: F. R. Chang-Díaz*, T. F. Yang

MIT Plasma Fusion Center
Cambridge, Massachusetts 02139

Summary

Research activities in the past year have encompassed both the theoretical and experimental aspects of plasma heating, as well as a variety of engineering issues associated with a flight system. A key objective has been the calculation of rf-to-plasma power coupling efficiency. This quantity was recently found to be 68% from direct measurements of plasma properties. In addition, the measured plasma parameters for the 9.4 kW power level fit well with earlier performance predictions. Theoretical analyses of ICRF heating show that efficiency improves as plasma radius increases and the magnetic field becomes uniform. These effects will be examined experimentally in the future. Moreover, the proposed use of power generators at high voltage and high frequency promises significant weight and size savings for space applications.

Technical Discussion

Variable I_{sp}propulsion hinges on the reliable production and controlled exhaust of plasma from an rf heated tandem mirror device. To this general end, an experimental research program was initiated at MIT in 1988 [1]. These experiments have shed new light on the dynamics of these high-power devices and their application to multimegawatt space propulsion. As reported previously, the successful ICRF heating of a mirror plasma has been demonstrated both theoretically and experimentally [2]. Two types, I and II, of plasma discharges can be produced, with greater stability being obtained in type II at high magnetic fields. Plasma parameters nearly equivalent to those of large fusion devices have been obtained. These are shown in Table I. We are currently investigating a wide array of propulsion properties (power coupling, thrust and mass flow rate) in order to assess the overall benefit of this propulsion system.

1.0 Experimental Study

The experimental setup is shown in Figure 1. The ICRF wave is launched from a double-half-loop antenna located at the high field region of the central cell. The wave propagates radially inwards and toward the resonance mid-plane where the diagnostics are currently located. In order to determine a range of stable operating conditions, a series of experiments at various magnetic fields was performed. By varying the field intensity, it was found that plasma stability increases in direct proportion to the magnetic field intensity. A 172 eV ion temperature, a 21.6 eV electron temperature and a $1.98 \times 10^{17}\mathrm{m}^{-3}$ plasma density are obtained from probe measurements. In addition, the absence of pronounced H_α lines in the Doppler broadening spectrometer confirms the expectation of a high degree of ionization and hence a relatively low power loss due to atomic excitation. Other important parameters can be extracted from these data and are included in Table I. This operating point is shown in the performance graph of Figure 2 at the power level. From these data, the rf-to-plasma coupling efficiency is 68%.

---

* Astronaut Office, NASA Johnson Space Center, Houston, Texas

TABLE I. PLASMA PARAMETERS

T_i	Measured ion temperature	172 eV
T_e	Measured electron temperature	21.6 eV
n_e	Measured plasma density	1.98×10^{17} m^{-3}
τ	Extracted energy confinement time	50 μ s
P_{in}(rf)	Extracted input rf power	9.4 kW
P_{in}(microwave)	Extracted input microwave power	0.3 kW
P_{absorb}(ion)	Power absorbed by the ions n_ek $T_i V_p$	5.2 kW
P_{absorb}(electron)	Power absorbed by the electrons n_ek $T_e V_p$	0.69 kW
$P_{exhaust}$	Power flows into the exhaust chambers	0.5 kW
ξ	Coupling efficiency	68%
I_{sp}	Extracted specific impulse	12,852 s

Resource limitations have prevented us from operating in the streaming-plasma mode. This capability requires the manufacturing of a vacuum interface to the large vacuum tank in our laboratory. Also, two additional magnet power supplies are required to run the system asymmetrically. The future system enhancements are highly desirable.

Nevertheless, rapid progress has been made in the understanding of both the plasma and neutral components in the exhaust. The tandem mirror is operated at a mirror ratio of 10 and the plasma is well confined. Any exhaust plasma is the results of the loss-cone effect and is only 10% of the central density. However, this axial loss plasma shows no drop in temperature from that of the central cell. Radially, both density and temperature profiles are nearly flat suggesting no loss of efficiency due to profile effects. A laser fluorescence system is now operational to measure neutral density. The system utilizes a new two-optical-path fluorescence signal reduction method developed by our group. The radial profile of the neutral density in the exhaust has been measured. The results show a hollow profile, peaking near the edge and dropping to negligible values on axis. This phenomena agrees with our earlier prediction that the wall is insulated by neutrals. The density in the exhaust will match that of the central cell when the device is operated in the streaming-plasma mode. Both plasma temperature and density measurements are shown in Fig 3.

Two independent thrust measurement methods are being developed: a grid energy analyzer to measure ion axial energy and hence plasma velocity and thrust, and a very sensitive ballistic balance to measure total thrust. This later system has now been installed and is undergoing calibration tests.

2.0 Theoretical Analyses

A theoretical investigation of ICRF wave propagation in an axially inhomogeneous cylindrical plasma has been undertaken. The main result of this work has been the development of the code CYLWAVE. A parameter scan using this new tool reveals two important points: first, the behavior of the plasma impedance as a function of the mirror ratio is in good agreement with the resonance volume theory. This theory simply states that the dissipation is proportional to the volume of plasma that is close to the resonance; and second, optimum power coupling to the plasma is obtained with the resonance located directly underneath the rf antenna or at the machine midplane. These findings provide appropriate design guidelines which favor machines providing a large plasma volume in a

uniform magnetic field at the ion cyclotron resonance. These machines tend to be tandem mirrors with large plasma radius which also scale favorably in terms of kilograms per kilowatt.

3.0 Flight System Studies

A flight system design study has been undertaken assuming a 10 MW nuclear electric system at 60% rf-to-plasma coupling efficiency. I_{sp}variations between 2,000 and 30,000 s can be obtained while the thrust available varies between 1,000 and 60 N. This capability leads to throttling at constant power and allows for the continuous optimization of propulsive efficiency. Initial calculations performed recently for our group by NASA/Lewis indicate attractive 100-200 days transits for delivering a 1000 MT payload to Mars orbit. Thrust system design refinement using state-of-the-art superconducting technology as well as a more careful evaluation of the structural requirements in a space-borne system, have led to a much more compact and lightweight device. A conceptual picture of a 0.04 kg/kW rocket is shown in Figure 4. The design uses an existing space nuclear electric system from Rocketdyne [3] which brings the total specific mass to 8.04 kg/kW.

4.0 Conclusion

Experimental results continue to show good agreement with earlier theoretical predictions for this propulsion concept. Efficiency values of 68% appear to be viable and design guidelines based on these results are being implemented in overall system designs. Initial system and mission analyses show attractive scalings and competitive performance. Exploration of the system in the streaming plasma, asymmetric mode is highly desirable.

References

[1] F.R. Chang-Díaz, T.F. Yang, et. al. , DGLR/AIAA/JSASS 20th Intl. Elect. Propul. Conf., DGLRA-88-126, Garmisch-Partenkirschen, W. Germany(1988).

[2] F.R. Chang-Díaz, T.F. Yang, AFOSR Contract Meeting, Boulder, Co(1991)

[3] "Ultra-High Power Space Nuclear Power System Design", Rocketdyne Division, Rockwell International(1989)

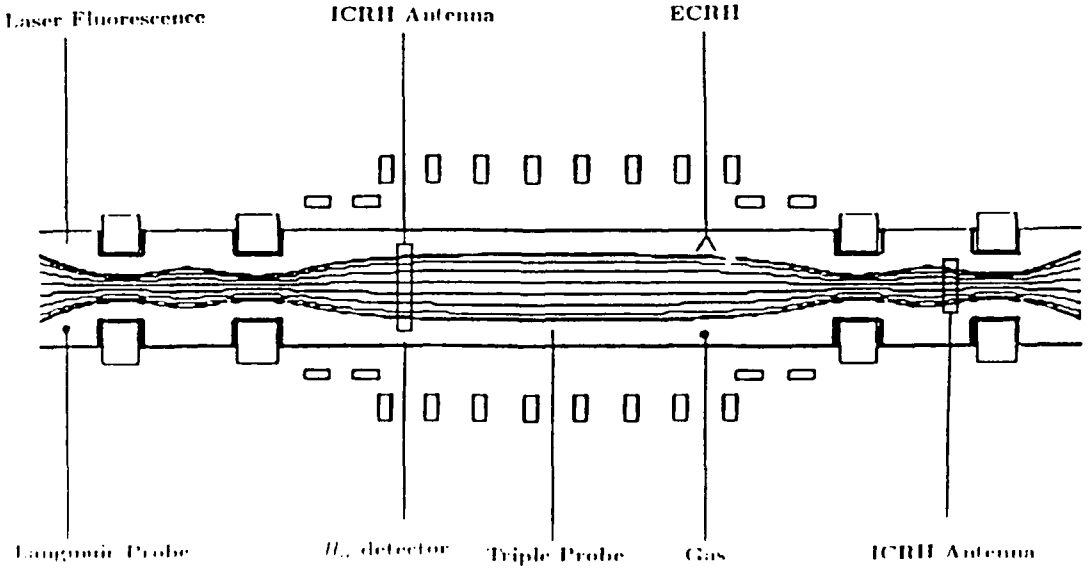

Figure 1. Experimental set-up

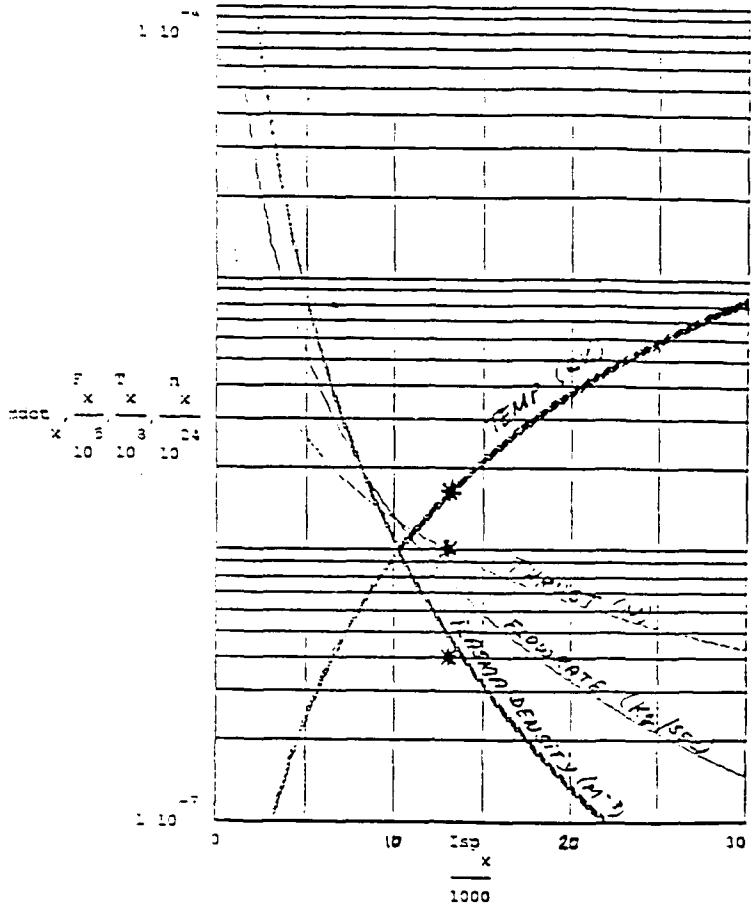

Figure 2. Performance parameters for 9.4 kW at 68% efficiency, hydrogen.

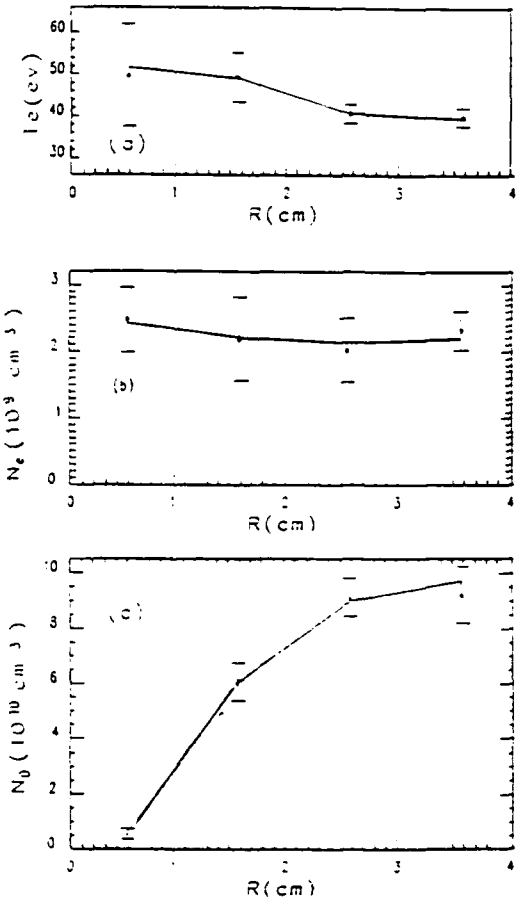

Figure 3. T_e, n_e, $N_o$in the exhaust.

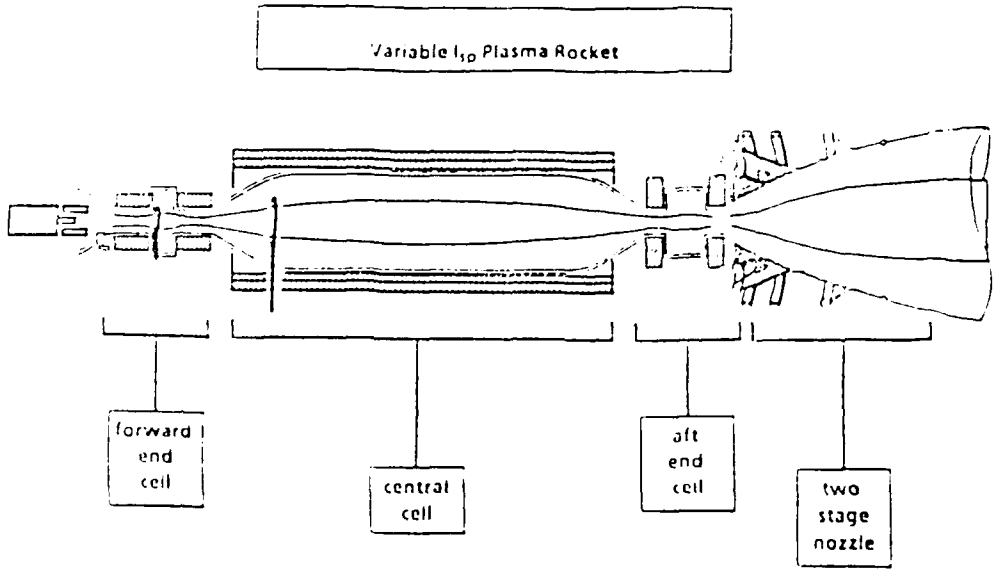

Figure 4. Conceptual picture of Tandem Mirror Rocket

IONIZED CLUSTER BEAMS FOR SPACE PROPULSION

AFOSR Contract No. F496-90-C-0085

W.S. Williamson and W. Knauer

Hughes Research Laboratories, Malibu, CA 90265

SUMMARY/OVERVIEW

In electric propulsion, electrical power is used to accelerate charged particles to high velocities to provide thrust at a higher specific impulse (≥3000 s) that can be obtained by chemical propellants (≤300 s). As specific impulse is increased, propellant mass decreases, but electrical power requirements increase. For many presently envisioned missions, the optimal specific impulse is in the range of 1000 to 2000 s, a range in which state-of-the-art ion thrusters exhibit poor efficiency. This efficiency could be increased substantially if a propellant with higher mass that xenon (mass 131 amu, presently used in ion thrusters) existed. We have investigated the promise of cluster ions (masses up to 105 amu) in satisfying that need. We have succeeded in condensing over 90% of the input thrust gas (carbon dioxide) into clusters of around 250 molecules, ionizing over 90% of these clusters, and acclerating them to provide thrust. However, more work is needed before engineering development could begin, to resolve efficiency losses in several areas.

TECHNICAL DISCUSSION

Figure 1 shows our concept for ion propulsion using ionized clusters. The basic idea is that atomic or molecular species introduced into the nozzle shown on the left will, under appropriate conditions, condense into clusters ranging from a few hundred to a few thousand atomsor molecules. These clusters can be readily ionized and accelerated to high energy, just as if they were heavy monoatomic inert gases.

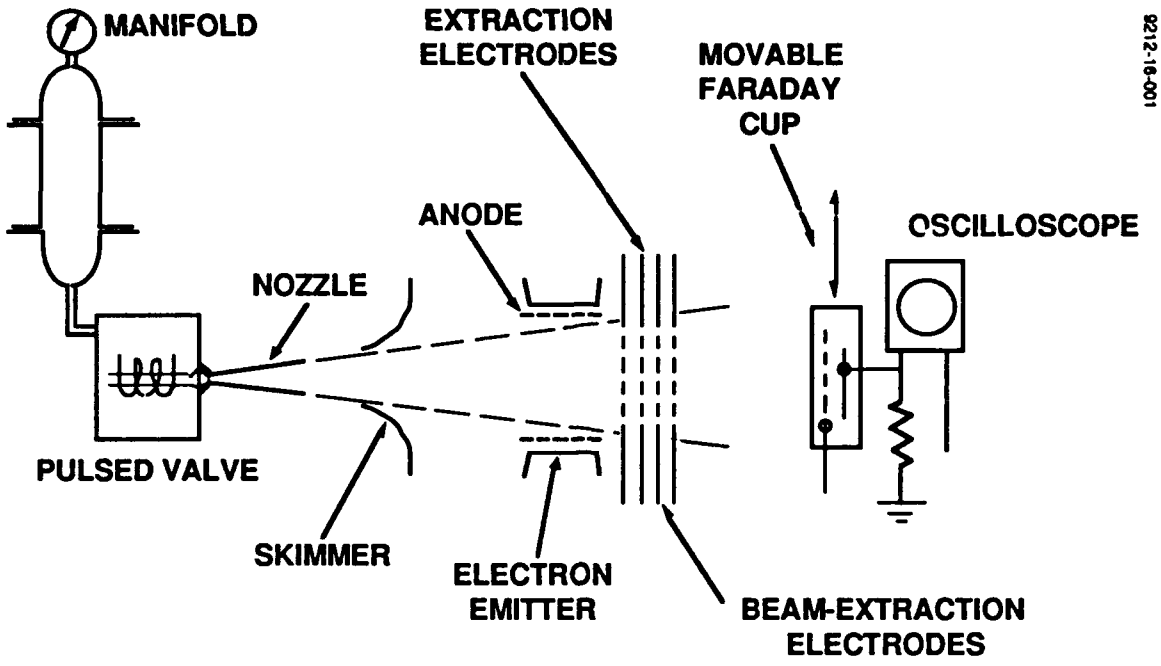

Figure 1. Schematic of the ionized-cluster apparatus used for this study.

Under this contract, we have made use of an apparatus constructed under a previous effort[1] to test the idea of using clusters to form a heavy propellant ion for space-propulsion applications. Basically, we have been successful in this attempt, although a great deal of additional work remains to be done to bring the concept to application. We have been able to demonstrate thrust levels above 10 mN in our relatively primitive laboratory apparatus, and we have achieved near-complete clusterization of carbon-dioxide gas, when supplied with hydrogen carrier gas to aid in the cluster-condensation process. Our work builds upon earlier studies[2] in achieving high clusterization with molecular gases; molecular gases form smaller clusters with masses around 15,000 amu, compared to inert-gas clusters, which typically have masses of the order of 250,000 amu. The smaller-mass clusters allow beam formation with lower voltages, which may be a practical advantage.

The key processes that appear to impede the path of ionized-cluster beams as a means of space propulsion are the need for excessive amounts of carrier gas (which degrades the propellant-utilization efficiency), the poor performance of the ionizer (which requires excessive power and produces excessively wide distributions of mass-to-charge

---

1. W. Knauer and R.L. Poeschel, "Cluster Beam Studies" AFOSR Final Report F49620-85-C-0125.

2. D.S. Goldin, AIAA Paper 67-85, (1967).

ratio) and the beam-extraction system, which accelerates only a small fraction of the incident ionized-cluster current. We believe that all of these difficulties may yield to further investigation, and the preliminary accomplishments that we have made in this study may lead to a viable space-propulsion system.

Studies of Broad-Band Optical Absorbers for Solar-Powered Rocket Propulsion Systems

Peter W. Langhoff
Department of Chemistry
Indiana Universiy
Bloomington, IN 47405

1. Introduction

Studies are reported in support of the AF Solar Rocket Propulsion Program (SRPP) [1], and of related programs pertaining more generally to aspects of radiant power conversion devices. The principle objective of the SRPP is the design, construction and operation of a high kW to low MW propulsion system employing concentrated solar radiation for the production of high-temperature, high-pressure gas propellant in the absence of chemical fuel combustion [2].

Strategies under investigation for achieving high specific impulse from concentrated radiation have centered on use of H_2 propellant gas and (i) black-body metal (Rh) surface absorbers with appropriate heat-exchanger configurations [3] or (ii) trace amounts of solar absorbers seeded in the propellant gas in a suitable windowed configuration [4]. Fluid absorption systems (ii) studied to date include halogens [5] and alkali metals in H_2 or inert buffer gas flows [4]. Optical absorbance characteristics, and hence local heating, in the flow stream in such high-temperature, high-pressure situations are sensitive functions of propellant gas temperature and density conditions, which conditions are conversely strong functions of local heating. Accordingly, this circumstance generally necessitates adoption of a self-consistent approach to the absorbance and propellant flow-field combination to obtain a satifactory device design, for which purpose precise values of state-to-state absorbance cross sections are required.

In furtherance of these requirements, attention is focused in the present study on theoretical modelling and computational interpretation of recently performed optical absorbance measurements in Li/Li_2 vapor seeded in H_2 and inert gas mixtures employing a high-temperature spectroscopy cell [4]. The calculations employing detailed Li/Li_2 state-to-state absorbance cross sections are found to account satisfactorally for the measured transmission spectra in all cases considered, suggesting the theoretical quantitative spectroscopy approach can be adopted with confidence for design studies of solar energy conversion and related power devices employing alkali metal and other absorbers over a broad range of physical conditions.

2. High-Temperature Spectroscopy Cell

The Larson spectroscopy cell is design for the study of metal vapors at temperatures up to 3,000°K and 100 atmospheres pressure [4]. The flow apparatus operates under well-characterized conditions of thermal equilibrium, and is fitted with optical ports for emission and absorbance spectroscopy measurements. An optical multi-channel analyzer

has been employed in obtaining a first set of transmission spectra in the wavelength interval of 440 to 740 nanometers (nm) at a resolution of $\approx$ 0.5 nm over the measured spectral interval. Approximately twenty data sets have been taken at 1 atmosphere pressure and cell temperatures up to 1,800°K employing varing concentrations of Li(v) seeded into $He/Ar/H_2$ entrainment gas flows.

In Figure 1 are show typical data taken at $\approx$ 1,600°K employing He/Ar entrainment gas and a Li(v) concentration of $\approx 10^{17}$ cm^{-3}. A number of aspects of Figure 1 are noteworthy. The saturated broad absorption feature at $\approx$ 670 nm is the Li 2s $\rightarrow$ 2p resonance absorption line [6], the bands centered at 490 and 680 nm are the molecular Li_2 X $\rightarrow$ B and A transitions, respectively [7], and the absorption feature at $\approx$ 580 nm is due to the 3s $\rightarrow$ 3p resonance line of impurity Na(v). These features and the quanititative nature of the spectrum are interpreted on basis of the state-to-state theoretical model and computations described immediately below.

3. Theory and Computations of Li/Li_2 Absorbance Spectra

The calculated transmission function for atomic Li and molecular Li_2 absorption is written in the familiar form [8]

$$T_{\Delta x}(h\nu) \equiv I_{\Delta x}(h\nu)/I_0(h\nu)$$

$$= exp\{-\sigma_{Li}(h\nu)(N_{Li}/V)\Delta x - \sigma_{Li_2}(h\nu)(N_{Li_2}/V)\Delta x\},$$

where the column densities $(N_{Li}/V)\Delta x$ and $(N_{Li_2}/V)\Delta x$ are measured in cm^{-2}, and the cross sections $\sigma_{Li}(h\nu)$ and $\sigma_{Li_2}(h\nu)$, measured in cm^2, are given by sums over products of unity normalized Voigt lineshape functions, transition-strengths, thermal-population factors for the individual lines considered, and a numerical conversion factor between cross section (cm^2) and oscillator strength density (eV^{-1}) [9]. Illustrative calculations are reported here in the case of a cell temperature of $\approx$ 1,600°K, a total pressure of 1 atmosphere, a total He/Ar buffer gas number density of $\approx 5.0 \times 10^{18}$ cm^{-3}, and a Li(v) seeding mole fraction of $\approx$ 0.15.

In Figure 2 is shown a transmission function in vibrational resolution in the absence of lineshapes, constructed employing vibrational energies and Franck-Condon factors only for the X $\rightarrow$ A and B band systems [10,11]. These calculated results are qualitative, and indicate the extent to which the known bands coincide with strong features in the experimental data of Figure 1.

In Figure 3 is shown the rotational structure of an individual X $\rightarrow$ A band (v" = 0 $\rightarrow$ v' = 3), constructed in the presence of instrument broadening employing a Lorentzian pressure width of $\approx$ 1 cm^{-1} [12,13], a Doppler width of $\approx$ 0.1 cm^{-1} [8], and a Gaussian instrument width of $\approx$ 0.5 nm $\approx$ 15 cm^{-1}.

In Figure 4 is shown a calculated transmission spectrum employing values of parameters appropriate to the measured data of Figure 1. Evidently, the calculations are in good

accord with the measured transmission spectrum. The numerical values of all parameters are consistent with the temperature/pressure conditions in the observation zone, with the estimated temperature (T $\approx$ 1,300 °K) in the Li evaporator in this case, with Li atom resonance pressure broadening data [12,13], and with values of the Li/Li_2 concentration ratio based on partition function estimates.

4. Concluding Remarks

The calculations reported here are designed to provide support for and clarify the nature of measured Li/Li_2 transmission spectra obtained from the Larson spectroscopy cell employing an optical multi-channel analyser. Comparison of the experimental data of Figure 1 with the calculations of Figure 4 indicates the extent to which theoretically-based quantitative spectroscopic calculations employing appropriate parameter values for the Li/Li_2 system are in accord with the measured data.

5. References

[1] K.K. Laug, "The Solar Propulsion Concept is alive and Well at the Astronautics Laboratory," JANNAF Propulsion Meeting, Cleveland, OH, May 1989.

[2] C.W. Larson, "Specifications for Solar-Powered Rocket Engine," Department of the Air Force Solicitation F04611-90-R-001, AF Flight Test Center, Edwards AFB, CA, April 1990.

[3] J.M. Shoji, "Solar Rocket Component Study," AFRPL Final Report TR-84-257, Rockwell International, Rocketdyne Divison, Canoga Park, CA, February 1985

[4] C.W. Larson, "The Spectroscopy of Hydrogen/Metal-Vapor Mixtures at High Temperatures and Pressures," AL-TR-88-080, August 1990.

[5] E.J. Bair, D. Antolovic, and P.W. Langhoff, "Radiation Augmented Fluid Technology, WPAFB Final Report WRDC-TR-89-2036, Wright Patterson AFB, OH 45433, June 1989.

[6] C.E. Moore, "Atomic Energy Levels," National Bureau of Standards Circular 467, Vol. 1, 1949.

[7] K.P. Huber and G. Herzberg, *Molecular Spectra and Molecular Structure: IV. Constants of Diatomic Molecules*, (Van Nostrand Reinhold, New York, 1979), pp. 374-5.

[8] A.C.G. Mitchell and M.W. Zemansky, *Resonance Radiation and Excited Atoms*, (Cambridge Press, Cambridge, 1971), chapts. 3-4.

[9] J.I. Steinfeld, *Molecules and Radiation*, 2nd Ed.,(MIT Press, Cambridge, MA, 1986), pp. 31-6, 295-6.

[10] P.Kusch and M.M. Hessel, J. Chem. Phys. **67**, 586 (1977).

[11] M.M. Hessel and C.R. Vidal, J. Chem. Phys. **70**, 4439 (1979).

[12] N. Allard and J. Kielkopf, Rev. Mod. Phy. **54**, 1103 (1982).

[13] K. Niemax and G. Pichler, J. Phys. **B8**, 179 (1975).

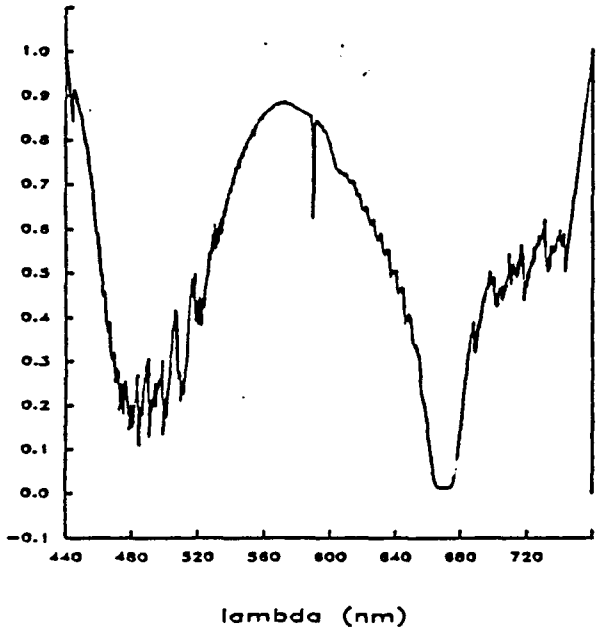

Figure 1. Experimentally determined Li/Li_2 transmission spectrum taken at an instrument resolution of $\Delta\lambda \approx 0.5$ nm and T ≈ 1,600°K in the presence of He/Ar buffer gas. Additional description of the experimental circumstances is provided elsewhere [4].

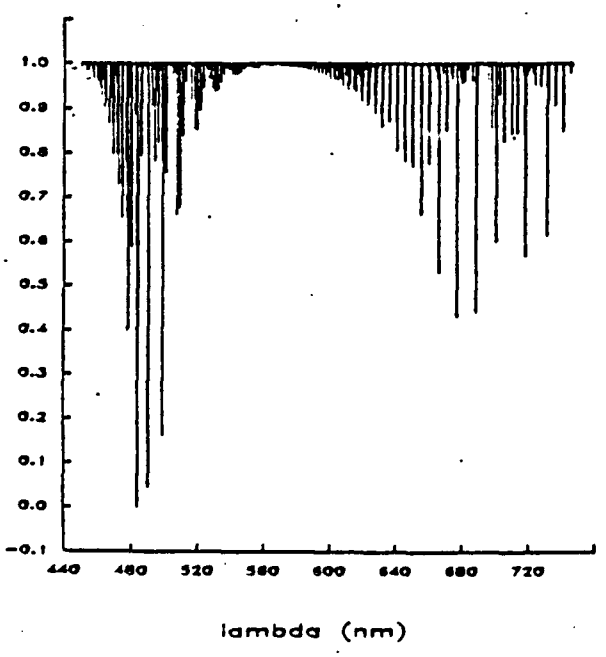

Figure 2. Calculated qualitative transmission spectra for Li_2 X → A, B bands constructed employing vibrational energies and Franck-Condon factors [10,11] in the absence of lineshape functions.

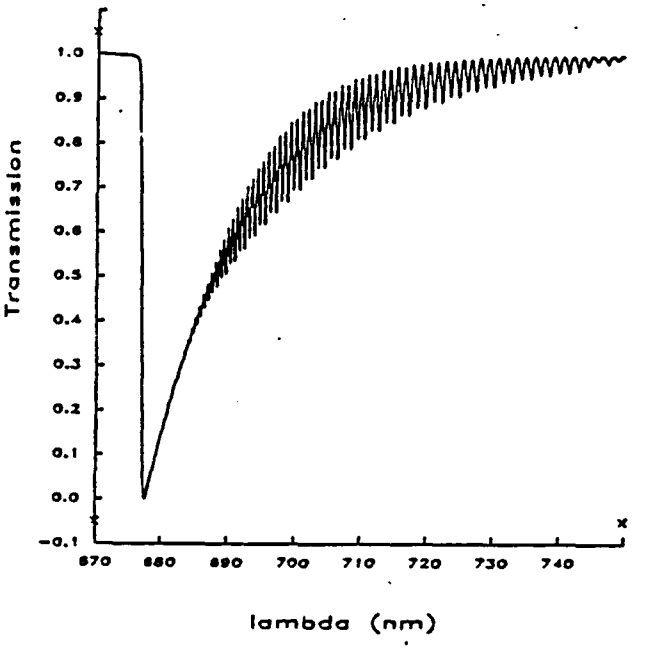

Figure 3. Calculated rotational structure in the X → A ($v''=0 \rightarrow v'=3$) band of Li_2 obtained employing Voigt lineshapes, a Lorentzian width of ≈ 1 cm^{-1}, and a a Gaussian width of ≈ 0.6 nm, corresponding to instrumental reolution.

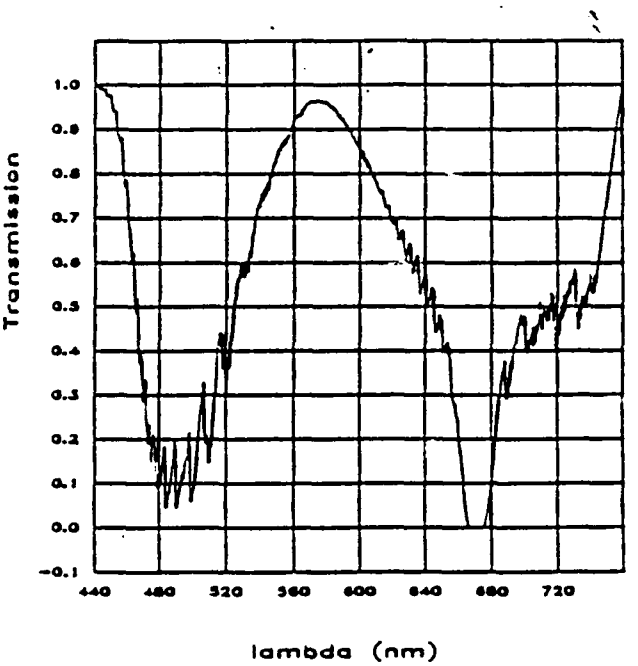

Figure 4. Calculated Li/Li_2 transmission spectrum obtained employing the development described in the text under conditions corresponding to the measured data of Figure 1.

CHEMISTRY OF A BURNING SURFACE

AFOSR-89-0521

Principal Investigator: Thomas B. Brill

Department of Chemistry
University of Delaware
Newark, DE 19716

SUMMARY/OVERVIEW

The absence of a chemical description of the burning surface of a rocket propellant is being addressed by experimental simulations using high-rate thermolysis of thin films. This simulation is validated by the accurate correlation of the regression rate calculated for the film and the burn-rate of the bulk material. The evolved gas products are identified and are the initial reactants for the flame zone. These details are required for advanced models of propellant combustion that predict the burn-rate, stability, and the effect of compositional differences on the combustion behavior.

TECHNICAL DISCUSSION

Relatively clean-burning, high-energy rocket propellants are likely to be in great demand in Air Force systems of the future. Economic realities dictate that extensive large-scale testing in the development of propellant components will not be as available as in the past. In place of many tests, guidance by theoretical and practical modelling will be emphasized. However, reliable predictive models require detailed, microscale chemical and physical parameters as input. In particular, details about the chemical reactions at the burning surface of a propellant are needed to relate the formulation of the propellant to its macroscale combustion characteristics. These details are not attainable during the actual combustion process because no diagnostics exist to determine the non-equilibrium, heterogeneous microchemistry at the burning surface. However, as is done in our research program, many of the requisite details can be established by experimental simulation of the burning surface.

The burning surface can be imagined to be a thin film of material 20-100 μM thick in which a phase change occurs driven by chemical reactions and heat transfer. In effect, it is a thin-film reaction zone that regresses through the condensed phase on one side and releases gas products on the other side. An instantaneous simulation of this reaction zone is a thin film of material experiencing a heating rate of 100-2000 °C/sec at a pressure $\geq$ 1 atm.

Two spectroscopic techniques have been developed in our laboratory to study the chemistry of a rapidly heated thin film: Simultaneous Mass and Temperature Change/FTIR spectroscopy (SMATCH/FTIR)[1] and T-jump/FTIR spectroscopy.[2] Arrhenius constants computed from the mass and temperature data of SMATCH/FTIR and applied in the pyrolysis law enable a linear regression rate, $\dot{r}$, to be calculated at 1 atm.[3-5] These values of $\dot{r}$ are compared in Table 1 to those obtained for the bulk combustion measured with a strand burner. The remarkable similarity of the microscale and macroscale regression rates strongly suggests that chemical conditions in the thin film are representative of those of the burning surface during combustion of the bulk material. The gas products evolved from the thin film by SMATCH/FTIR are

measured several mm above the surface by rapid-scan FTIR spectroscopy. We have long recognized that it would be advantageous to be able to measure the gases evolved during isothermal conditions rather than non-isothermally as in SMATCH/FTIR. To this end the T-jump/FTIR technique was developed.[2]

Table 1: Comparison of the linear burn rate calculated from microscale SMATCH/FTIR and macroscale strand-burner measurements/made in other laboratories.

	$\dot{r}$, mm/sec	
Compound	SMATCH/FTIR	Strand Burner
HMX	0.37	0.5
RDX	0.38	0.3
DNNC	0.27	0.3
13% N NC	0.3	0.4
GAP	1.35	1.7
HTPB	0.21	0.19

By T-jump/FTIR, a thin film of sample (ca. 22 μg) is heated on a Pt ribbon filament at 2000 °C/sec to a preselected temperature and then held isothermally at that temperature while the gas products are detected. The thermal response of the sample as sensed by the resistance change of the Pt filament is recorded simultaneously. When heated in this way, many of the interfering "cooking" processes that complicate slower heating rate and some non-isothermal techniques are minimized. The gas products coupled with the corresponding thermal changes indicate a great deal about the chemistry of the thin film (a simulated burning surface) and define the gases that initiate the first stage of the flame zone.

Details of the chemical decomposition mechanism of HMX,[6] RDX,[6] and organoazide polymers (AMMO, BAMO and GAP)[2] have now been established up to the burning surface temperature. As an illustration of the capability of the T-jump/FTIR method, preliminary data for a new potential ingredient ammonium dinitramide (ADN), $NH_4[N(NO_2)_2]$, is summarized below.[7]

The gas product concentration data and Pt filament control voltage data are shown in Figure 1 for ADN heated at 2000 °C/sec to 260 °C and then held at 260 °C under 1 atm of Ar. ADN melts at about 1 sec causing an endothermic deflection. At about 2.3 sec HNO_3, NH_3, N_2O, H_2O, and NO_2 appear simultaneously accompanied by very strong heat release. Litzinger[8] also observed these products and quantified N_2 and H_2O from a laser-pyrolyzed ADN sample by the use of a mass spectrometer with a quartz microprobe. Merging these data of Litzinger with those shown in Figure 1 produces a concentration ratio of $6N_2O:6H_2O:3NO_2:3N_2:1NO:1NH_3$ after the exotherm. NH_4NO_3 aerosol (AN) is observed as a white smoke in both the laser pyrolysis and IR studies. The IR spectrum confirms AN. The challenge is to reconcile the gas product concentrations after the exotherm (2.7-3 sec) with a reaction scheme.

The data suggest that ADN decomposes under combustion conditions by Scheme 1. A lesser channel leading to $HNO_3 + NH_3 + N_2O$, which is mildly exothermic (Branch A) initially occurs. The major decomposition channel is Branch B [reactions (1)-(8)] summarized by (9). Reactions (1) and (2) yield NH_3 and NO_2 which react exothermically by reaction (11). Reaction (11) is the dominant source of heat. Reaction (13) reproduces the approximate product

ratios (high in NH_3 and H_2O, and low in N_2O) that are found experimentally after the exotherm at 2.7-3.0 sec., as well as gives AN, which is the white smoke. Thus, Scheme 1 is based on plausible reactions of ADN, gives the approximate observed product ratios, and is highly exothermic. At this stage the detailed reactions are not proven to occur exactly as written. However, the key exothermic reactions leading to the ignition of ADN is identified to be $NH_3 + NO_2$. The corresponding initial major exothermic reaction in HMX is $CH_2O + NO_2$[6]. Scheme 1 is also consistent for ADN at 300 °C, which is close to the burning surface temperature of 300-310 °C for ADN.[8] Development of the sub-global reaction mechanisms as described above for ADN is continuing for other energetic materials as future work. The goal is to provide the probable chemical steps in the surface reaction zone that control the burn-rates of important classes of energetic materials. These data are key to the chemical component of advanced combustion models.

---

1. M. D. Timkin, J. K. Chen and T. B. Brill, Appl. Spectrosc. 44, 701 (1990).
2. T. B. Brill, P. J. Brush, K. J. James, J. E. Shepherd, and K. J. Pfeiffer, Appl. Spectrosc. in press.
3. J. K. Chen and T. B. Brill, Combust. Flame, 85, 479 (1991).
4. J. K. Chen and T. B. Brill, Combust. Flame, 87, 157 (1991).
5. J. K. Chen and T. B. Brill, Combust. Flame 87, 217 (1991).
6. T. B. Brill and P. J. Brush, Phil. Trans. R. Soc., London, A, in press.
7. D. G. Patil and T. B. Brill, to be published.
8. T. Litzinger, Penn State, personal communication, 1992.

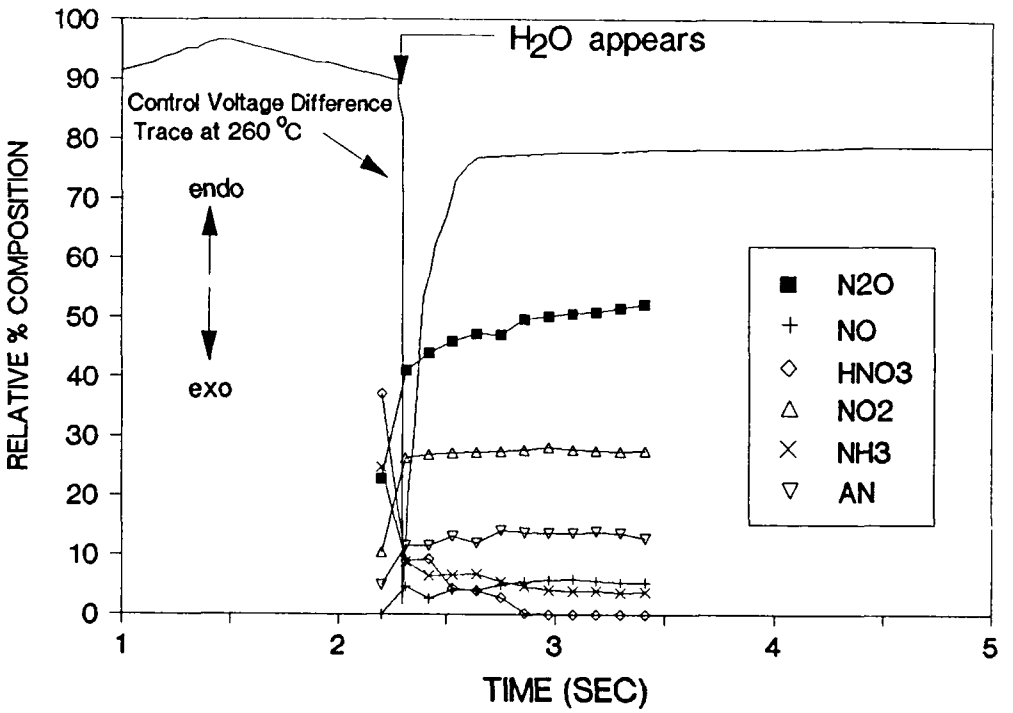

Figure 1. T-jump/FTIR data for ADN heated at 2000 °C/sec to 260 °C and held isothermally at 260 °C. The gas products and the thermal response of the sample are recorded simultaneously. Scheme 1 explains the chemistry.

SCHEME 1: THE PROPOSED REACTIONS THAT ARE RESPONSIBLE FOR THE GASES RELEASED BY ADN AT THE BURNING SURFACE.

		Approx. ΔH_{rxn}, Kcal
Branch A:	$3[ADN \longrightarrow NH_3 + HNO_3 + N_2O]$	-9
Branch B:	(1) $9[ADN \longrightarrow NH_3 + HN(NO_2)_2]$	
	(2) $9[HN(NO_2)_2 \longrightarrow NO_2 + HNNO_2]$	
	(3) $6[HNNO_2 \longrightarrow N_2O + OH]$	
	(4) $2[HNNO_2 + OH \longrightarrow 2NO + H_2O]$	
	(5) $HNNO_2 + NO \longrightarrow NO_2 + HNNO$	
	(6) $HNNO + OH \longrightarrow N_2O + H_2O$	
	(7) $3[NH_3 + OH \longrightarrow H_2O + NH_2]$	
	(8) $3[NH_2 + NO \longrightarrow N_2 + H_2O]$	
Sum of (1-8)	(9) $9ADN \longrightarrow 6NH_3 + 7N_2O + 10NO_2 + 9H_2O + 3N_2$	-49
Sum of branches A & B	(10) $12ADN \longrightarrow 9NH_3 + 10N_2O + 10NO_2 + 9H_2O + 3N_2 + 3HNO_3$	-58
	(11) $4NH_3 + 4NO_2 \longrightarrow 3N_2 + 2NO + 6H_2O$	-309
Sum of reactions (10+11)	(12) $12ADN \longrightarrow 5NH_3 + 10N_2O + 6NO_2 + 15H_2O + 2NO + 6N_2 + 3HNO_3$	-367
Occurs in gas phase away from surface so (13) is not included in ΔH_{rxn}	(13) $2NH_3 + 2HNO_3 \longrightarrow 2NH_4NO_3$ (aerosol)	
Approximate gas phase stoichiometry (12+13)	(14) $12ADN \longrightarrow 3NH_3 + 10N_2O + 6NO_2 + 15H_2O + 2NO + 6N_2 + HNO_3 + 2NH_4NO_3$	-367

STRUCTURE AND CHEMICAL KINETICS OF FLAMES SUPPORTED BY NITROGEN OXIDES

AFOSR Grant Contract No. 90-0121

Melvyn C. Branch
Center for Combustion Research
Mechanical Engineering Department
University of Colorado
Boulder, Colorado 80309-0427

SUMMARY/OVERVIEW:

In previous research we have investigated the structure of flames of CH_4, CH_2O, C_2H_2, CO and H_2 with N_2O, NO_2 and O_2. The flames studied with NO_x as oxidizer represent the first detailed measurements and flame modeling for stable and unstable species for these mixtures. The flames with O_2 as oxidizer were undertaken to help clarify the differences between the well known oxidation with O_2 and the less well defined oxidation with NO_x. The flame chemistry has been represented by an overall elementary reaction mechanism consisting of 260 reactions in order to derive a complete reaction set capable of describing all the flame data for fuel/NO_x flames. The comparison between the calculated flame structure and the experimental flame structure for stable species was found to be very good for fuel/N_2O flames and good for fuel/NO_2 flames. The concentration profiles for radical species were found to be generally well represented qualitatively but not well represented quantitatively. It was concluded that, despite some remaining difficulties with the reaction mechanism, it appeared to be reliable in describing the overall combustion behavior of a wide range of fuel and oxidizer mixtures.

TECHNICAL DISCUSSION:

The purpose of this report is to summarize the current status of studies we have undertaken of model gas phase flames associated with the combustion of nitramine based solid rocket propellants. These studies consist of measurements of the structure of stable and unstable species concentration profiles and temperature in laminar, premixed, flat flames of fuel/NO_x mixtures at low pressure. The experimental measurements are then compared to calculations of the concentration profiles using a one dimensional flame code which models the transport processes and chemistry of the flame. A comparison between modeling and experiment for a C_2H_2/NO_2 flame is given in Figure 1 as an example. The results of these investigations can be represented by the schematic in Figure 2 showing the oxidation in the presence of N_2O (top of figure) and with NO_2 (bottom of figure).

The most important reactions of the oxidizer (N_2O or NO_2) are with H atoms and, to a lesser extent, with CO. Reaction of either oxidizer with H is a chain propagating reaction, in contrast with the chain branching reaction of H with O_2 which is of equal importance in fuel oxidation by O_2. In addition, the reaction of NO_2 with H is slower than N_2O with H. Finally, the reaction of N_2O with CO can be significant both in consumption of CO and formation of CO_2. This situation is again in contrast with the oxidation chemistry of systems by O_2 in which the conversion of CO to CO_2 is almost entirely by reaction of CO with OH. The difference between the use of N_2O or NO_2 as oxidizer is that the former produces primarily N_2 while the latter produces NO. The subsequent slow reduction of NO to N_2, even when it is

thermodynamically favored, accounts for the most striking difference between the two oxidizers. The most important effects of the oxidizer, therefore, are that the nitrogen oxides are less effective chain carriers and lead to slower reaction rates compared to O_2.

The oxidation reactions of CH_4 in the presence of NO_2 is generally similar to the oxidation by O_2. Chain propagating and branching reactions lead to the formation of H, O and OH and these species progressively abstract hydrogen and partially oxidize CH_3 to CH_2O. The CH_2O is then converted largely to CO through the intermediate HCO. Subsequent oxidation of CO to CO_2 is by reaction with NO_x or OH as mentioned above. If the fuel is CH_2O instead of CH_4, the latter stages of this chain become dominant. If the fuel is C_2H_2 instead of CH_4, then reactions of CH_2 become more important and CH_2O becomes less important. Rate constants for the reactions involved in the hydrocarbon chemistry derived from previous studies are generally successful in the description of the transformation of CH_4 to CO.

The third major aspect of fuel/NO_x flame chemistry is the interaction of H, C and N containing species as shown in the lower portion of Figure 1 (a) and (b). Reaction of CH_i species with NO to form HCN and subsequent reaction of HCN, CN or NCO with NO lead to the conversion of NO to N_2. This process is obviously of most importance when NO_2 or NO is the oxidizer rather than when N_2O is oxidizer, since in the latter case N_2 is formed directly. This scheme also shows the essential features of the oxidation process in the case where HCN is formed as a fuel during the decomposition of the energetic solid.

PUBLICATIONS:

1. M.C. Branch, A. Alfarayedhi, M. Sadeqi and P.J. Van Tiggelen, "Measurements of the Structure of Laminar Premixed Flames of $CH_4/NO_2/O_2$ and $CH_2O/NO_2/O_2$ Mixtures," *Combustion and Flame, 83*, pp. 228-239, 1991.

2. M.B. Habeebullah, F.N. Alasfour and M.C. Branch, "Structure and Kinetics of CH_4/N_2O Flames," *23rd Symposium (International) on Combustion,* The Combustion Institute, Pittsburgh, pp. 371-378, 1991.

3. H. Dindi, H.M. Tsai and M.C. Branch, "Combustion Mechanisms of Carbon Monoxide-Nitrous Oxide Flames," *Combustion and Flame, 87*, pp. 13-20, 1991.

4. J. Vandooren, M.C. Branch and P.J.Van Tiggelen, "Comparisons of the Structure of Stoichiometric CH_4-N_2O-Ar and CH_4-O_2-Ar Flames by Molecular Beam Sampling and Mass Spectrometric Analysis," *Combustion and Flame*, in press.

5. M.C. Branch, "Structure and Chemical Kinetics of Flames Supported by Nitrogen Oxides," *4th International Seminar on Flame Structure,* International Union of Pure and Applied Chemistry, Oxford, in press.

6. J.V. Volponi and M.C. Branch, "Flame Structure of C_2H_2-O_2-Ar and C_2H_2-NO_2-Ar Laminar Premixed Flames," Paper No. 91-88, *Western States Section/Combustion Institute*, October 1991. Also, *24th Symposium (International) on Combustion,* in press.

7. J.V. Volponi and M.C. Branch, "Flame Structure of H_2O-NO_2Ar Laminar Premixed Flames," Paper No. WSS/CI 90-02, *Western States Section/Combustion Institute,* October 1990. Also, *Combustion and Flame,* under review.

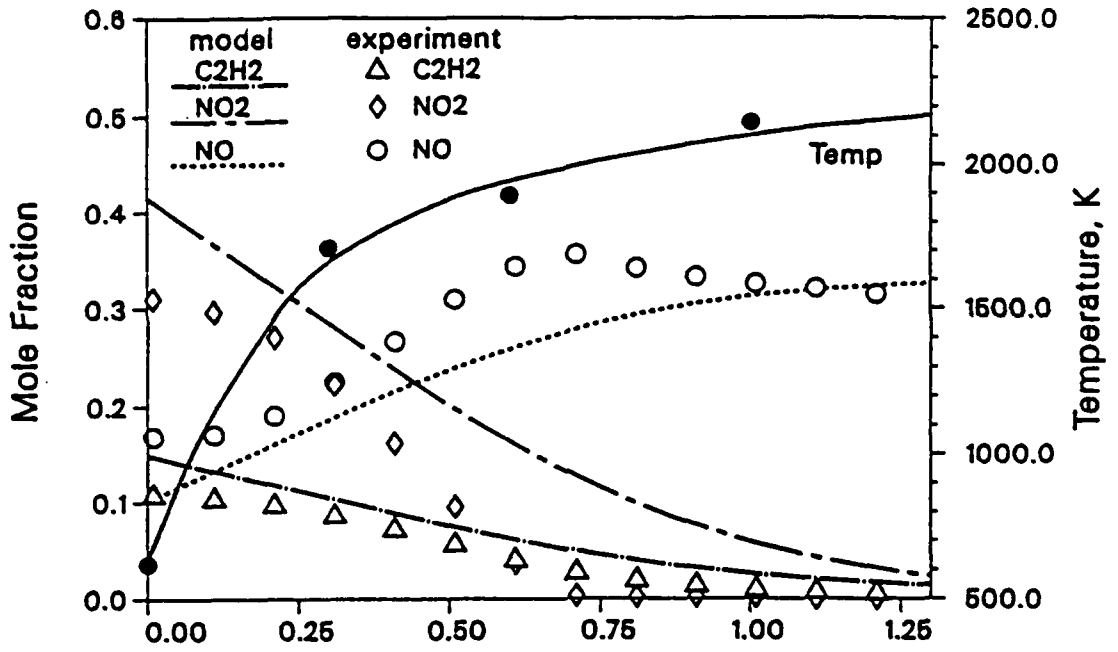

(a)

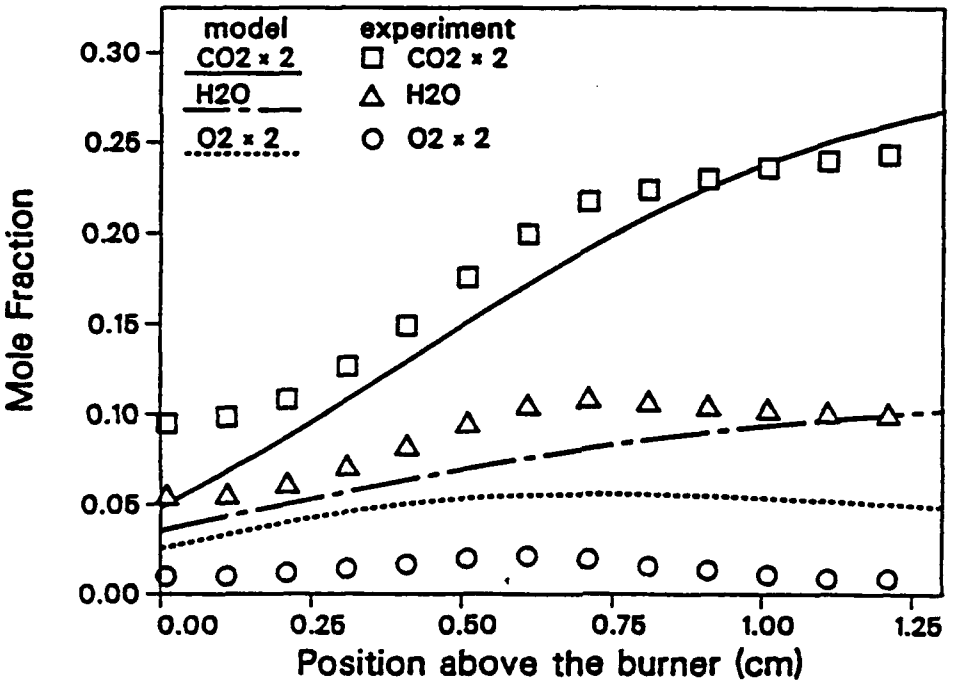

(b)

Figure 1 (a) and (b). Measured (symbols) and calculated (lines) profiles of composition of stable species in the 25 torr, C_2H_2-NO_2-Ar laminar premixed flame. Model calculated X_{H2O} is corrected for radical recombination reactions in the sampling probe by adding X_{OH} to the X_{H2O}. Experimentally measured temperature points are plotted with the fit to the data shown with the solid line. Reactant mole fractions are $X_{C2H2} = 0.201$, $X_{NO2} = 0.548$, $X_{Ar} = 0.251$ and the total reactant gas flow rate is 4.01 slm.

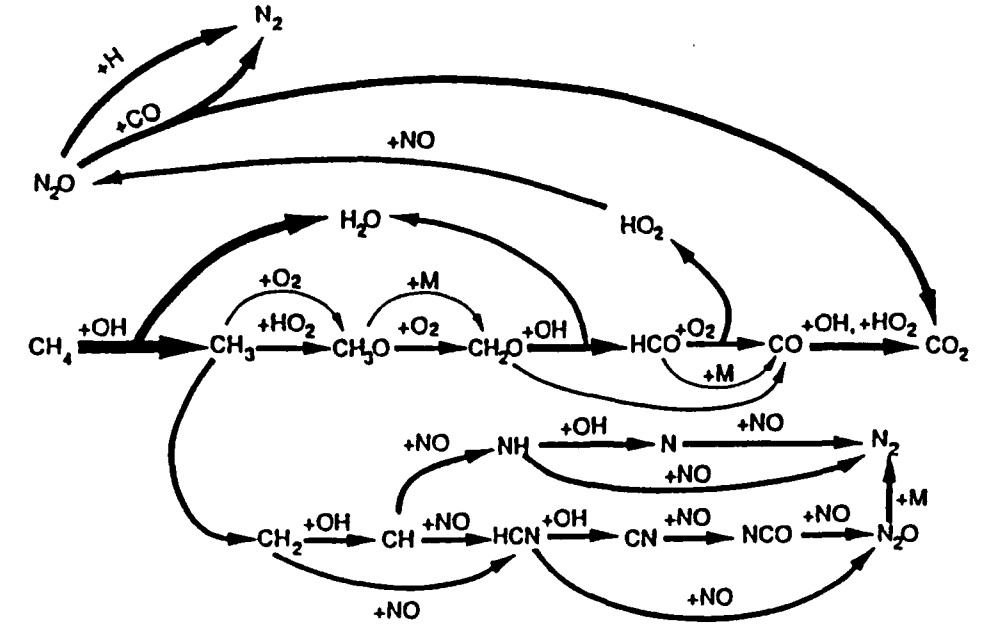

(a)

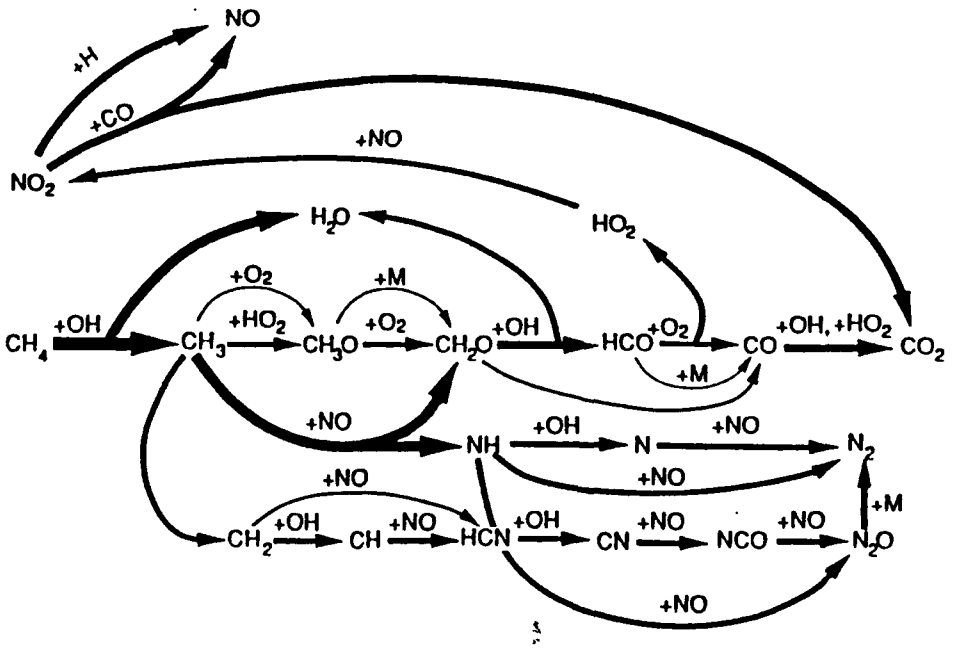

(b)

Figure 2. Schematic representation of the reaction of CH_4, CH_2O, C_2H_2, H_2 or HCN with a) N_2O and b) NO_2.

FUNDAMENTALS OF ACOUSTIC INSTABILITIES IN LIQUID-PROPELLANT ROCKETS
(AFOSR Grant No. 91-0310)

Principal Investigator: F. A. Williams

Department of Applied Mechanics and Engineering Sciences
University of California San Diego, La Jolla, CA 92093-0310

Summary/Overview

This research concerns the mechanisms by which flow, mixing and combustion process are coupled to acoustic fields in liquid-propellant rocket motors. The approach is primarily analytical, with use made of asymptotic methods. Nonhomogeneities in the flow field are taken into account, and attention is focused on both subcritical and supercritical conditions for vaporization, with real chemistry treated through the development of reduced chemical-kinetic mechanisms. Hydrogen-oxygen systems are being considered first and storables later. Dispersion relations are derived and amplification mechanisms analyzed.

Technical Discussion

This research was focused first on questions concerning the formulation of equations for describing acoustic instabilities in liquid-propellant rocket motors. In particular, complications associated with two-phase flow and with turbulence were addressed. The usual approximations for identifying acoustic modes, namely hypothesizing a chamber without flow and with a single, uniform sound speed, were questioned, and conservation equations were derived for use in testing the accuracies of these approximations [1]. It was found that various circumstances conspire to make these approximations better than might initially be thought. One contributing factor is that the reciprocal of the square of the frozen sound speed in the multiphase system involves a sum of terms from individual phases weighted by the square of the volume fraction of the phase, so that the gas phase, which typically has the largest volume fraction and the smallest sound speed, strongly dominates the frozen speed. Another factor is that frequencies of interest are high enough that the frozen speed is more relevant than any equilibrium speed. A third factor is that the wavelength generally is long compared with any scale of inhomogeneity within the chamber, so that a homogenized description, formed by taking averages of state variables, becomes appropriate. Since acoustic

convective effects scale with the Mach number and mean pressure changes with its square, a simple acoustic-mode description emerges as being quite accurate at low Mach numbers [1]. A tentative approach for taking two-phase flow into account in formulating the problem of acoustic instability was suggested [2].

This approach has now been extended to include effects of turbulence as well [1]. The method of smooth perturbation for a quasistationary random medium was employed for this purpose. The analysis results in a system of equations that is equivalent to a wave equation for mean acoustic amplitudes, augmented by a complicated source term. The corresponding Helmholtz equation (with a source) was derived for monochromatic waves. Source terms in these equations were identified as arising from molecular transport, from peculiar velocities of different phases, from phase changes and from homogeneous chemical reactions. The averaging needed for evaluating the source terms in the mean wave equation was shown to involve integrals extending over the turbulent correlation length derived from the Green's function for the source-free acoustic field [1].

This approach of smooth perturbation was used to identify the dispersion relation for monochromatic wave propagation in free space. If k_o is the (real, unperturbed) wave number based on the frequency and the frozen sound speed and $\mathbf{k}$ is the complex wave number whose imaginary part describes amplification, then

$$k^2 = k_o^2 + ik_o^2 a - ik_o \mathbf{b} \cdot \mathbf{k} + k_o^4 c,$$

where a, $\mathbf{b}$ and c are calculated from appropriate averages of source terms. Through specialization to transverse acoustic modes in cylindrical chambers, an analogous formulation involving temporal rather than spatial growth was derived, resulting in the generalized dispersion relation

$$k^2 = k_o^2 + ik_o^2 a - ik_o \mathbf{b} \cdot \mathbf{k} + k_o^4 c/(1 - k^2/k_o^2),$$

in which the resonance effect appears in the last term. The resonance enhances the influence of the term involving c which includes the pressure and velocity responses of the rate of chemical heat release through their effects on temperature variations under the influence of the turbulent flow [1].

The formulation provides a framework within which effects of specific amplification mechanisms can be analyzed. Potentially significant processes leading to amplification were identified [2], including atomization responses, counterflow diffusion-flame responses, droplet-burning responses, spray-combustion responses with time-dependent feedback between vaporization and combustion, and supercritical mixing responses, possibly including finite-rate chemistry in the reaction zone. Investigations have now begun in analysis of the counterflow diffusion-flame and droplet-burning responses for hydrogen-oxygen systems, to be included in the recently developed formulation [1]. These analyses are first using one-step activation-energy asymptotics for the chemistry but are planned to next address a recently developed two-step mechanism for hydrogen diffusion flames.

In related work that was completed during this period, compressibility effects in rotational, inviscid flows in cylindrical geometries were analyzed on the basis of the Euler equations [3]. The effects of rotationality on choking and the interaction between turbulence

and compressibility effects were considered. Although this work has some bearing on liquid-propellant rockets, it is more relevant to nozzleless solid-propellant rockets. The analysis defines a base flow, on top of which acoustic-instability oscillations can now be imposed. Rather than pursuing this line of study further, analyses based on the equations identified above currently are being performed.

References

1. J.S. Kim, "A Formulation for Transverse Acoustic Instability in Liquid-Propellant Rocket Motors," to be submitted, 1992.

2. F.A. Williams, "Fundamentals of Acoustic Instabilities in Liquid-Propellant Rockets," 1991 AFOSR Contractor's Meeting, pp. 128-132.

3. G. Balakrishnan, A. Liñán and F.A. Williams, "Rotational Inviscid Flow in Laterally Burning Solid-Propellant Rocket Motors," Journal of Propulsion and Power, to appear, 1992.

Appendix: Rotational Flow in Solid-Propellant Rocket Motors

A theoretical analysis to determine the effects of mass addition on the inviscid but rotational and incompressible flow field in a porous duct with the injection rate dependent on the the local pressure was performed for large ratios of length to duct diameter. The configuration considered is shown in Figure 1. The axial coordinate, x, runs from 0 to l along the center of the duct, and the radial coordinate, denoted by r, varies from 0 to a. Assuming $a/l \equiv \varepsilon$ to be a small parameter, the conservation equation can be reduced to a simplified set of Euler equations which can be transformed to an integral equation.

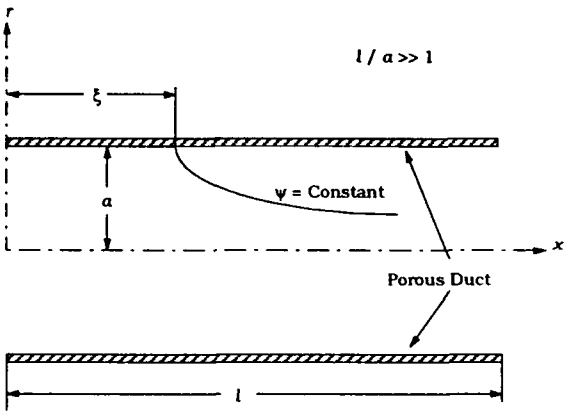

Figure 1: Schematic diagram of inviscid, rotational flow through a porous duct with wall injection.

If $m_w = Kp^n$ is the burning-rate law for the propellant, $P = p(x)/p_0$ is the nondimensional pressure, where p_0 is the dimensional pressure at $x = 0$, and X is the nondimensional strained axial coordinate defined by,

$$X = \sqrt{\frac{\gamma - 1}{\gamma}} \frac{p_0^{n-1} K}{a} \int_0^x \sqrt{2 c_p T_w(x')} dx'. \tag{1}$$

the integral equation can be solved for various values of γ and n and the results are plotted in Fig. 2. Also depicted on Fig. 2 are the results obtained for an irrotational, quasi-one-dimensional flow. The pressure ratio P_c at the choking is about 20% smaller for the rotational theory; the two theories agree in predicting that P_c is independent of n. The range of variation of the choking distance is seen in Fig. 2 to be somewhat greater for the rotational flow, which generally exhibits slightly earlier choking, except as n approaches unity, where the quasi-one-dimensional theory predicts choking very slightly sooner at the higher values of γ. Furthermore, it was shown that compressibility effects become important before steady erosive effects become important in solid-propellant rocket motors.

An idealized basis for comparison of nozzleless rockets is the vacuum throat specific impulse, which for both rotational and irrotational flow can be shown to be $I_{sp} = p_0 A/\dot{m}$, where $\dot{m}$ is the total mass flow rate. A choice must be made of what parameters to hold constant in making the comparisons, and it is reasonable to require the radius a and the length l of the two motors to be the same. With choked motors the rotationality produces an improvement in the specific impulse, R in the range of 3% to 4%. Calculations for $0 \leq n \leq 1$ show a negligible influence of n on R. A somewhat larger corresponding improvement applies in the absence of choking; for small values of $1 - P$ it can readily be shown that $R = 8/\pi^2 \approx 0.81$, which produces an I_{sp} increase of more than 20%.

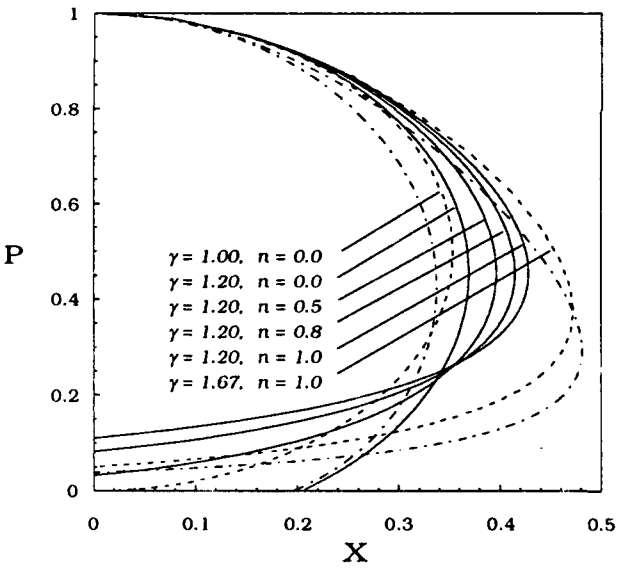

Figure 2: Variation of the pressure ratio with the nondimensional distance for the quasi-one-dimensional theory, for $\gamma = 1.2$ and various values of n (solid curves), and for limiting cases of $\gamma = 1, n = 0$ and of $\gamma = \frac{5}{3}, n = 1$ (dashed curves), with the corresponding limiting curves of the present theory shown as chain curves.

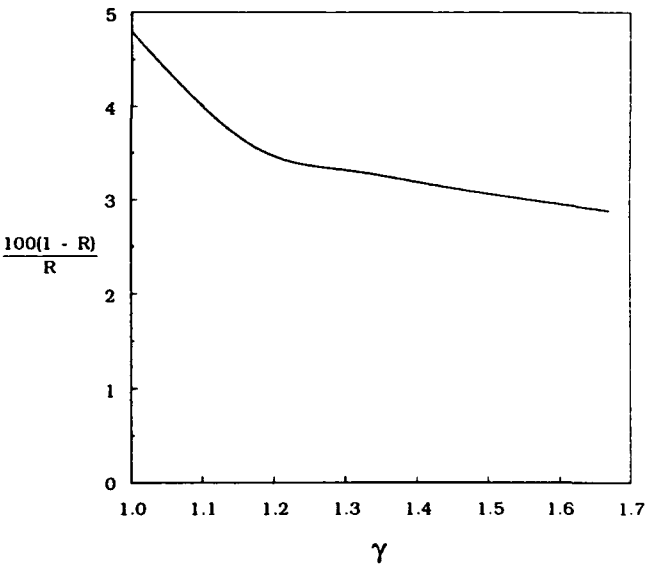

Figure 3: The percentage improvement in the vacuum throat specific impulse produced by rotationality as a function of the ratio of specific heats.

ACOUSTIC WAVES IN COMPLICATED GEOMETRIES AND THEIR INTERACTIONS WITH LIQUID-PROPELLANT DROPLET COMBUSTION

(AFOSR Contract No. 91-0171)

Vigor Yang
Department of Mechanical Engineering and
Propulsion Research Engineering Center
The Pennsylvania State University
University Park, PA 16802

SUMMARY/OVERVIEW

A focused theoretical program is being conducted to investigate acoustic wave characteristics in liquid-propellant rocket engines with injector-face baffles. The work primarily addresses the combustion stability behavior of a complicated geometry and the damping mechanisms of baffles - how does the baffle work in various environments; and what are the physical processes responsible for suppressing unsteady motions in a baffled combustor? In addition, the dynamic responses of liquid-propellant droplet combustion to ambient flow oscillations in the baffle region are examined in detail. A major goal of this research is to establish a unified framework for treating combustion instabilities in baffled liquid-propellant rocket engines.

TECHNICAL DISCUSSION

1. Relevance

Injector-face baffles provide significant stabilizing effects on pressure oscillations in liquid-propellant rocket engines, and have been widely used since 1954. Three mechanisms have been suggested with regard to the suppression of transverse modes of instabilities. These are (1) modification of acoustic properties in combustion chambers, (2) restriction of unsteady motions between baffle blades, thus protecting the sensitive mechanisms for instabilities, and (3) damping of oscillations by vortex shedding, flow separation, and viscous dissipation near baffle tips. Because of the complex nature of the flowfield in the baffle region, the effects of baffles on wave motions have never been understood quantitatively. The most important and least understood aspect of baffle design is how to ensure that baffles will eliminate instability. At present, no well-defined criteria exist for selection of baffle configurations that will lead to stable operation of an engine. Most designs in use today are based on experience with similar combustor configurations, propellant combinations, and operating conditions, thereby making development of a new system a costly trial-and-error process. For example, the development of F-1 engines for the Saturn-V launch vehicles required 15 baffle design iterations and 3,000 tests before a stable configuration was obtained.

2. Research Objectives

The primary purpose of this research is to develop a comprehensive theoretical analysis within which multi-dimensional acoustic waves in a baffled combustor and

their mutual coupling with liquid-propellant combustion can be treated properly. The work involves the following two tasks:

1. investigation of acoustic wave characteristics in baffled combustion chambers, including mean-flow/acoustics interactions; and
2. study of dynamic responses of liquid-propellant droplet vaporization and combustion to ambient flow oscillations in the near field of baffles.

3. Acoustic Waves in Baffled Combustors

Because of the geometrical discontinuities associated with baffle blades, the unsteady motions in the baffle compartments and the main chamber are best treated separately and then linked together at the interface, as shown in Fig. 1. The acoustic field in each region can be formulated using the general analysis constructed by the principal investigator. Briefly stated, a wave equation governing the flow oscillations is first derived from the conservation equations for a two-phase mixture, with expansion of the dependent variables in two small parameters measuring the Mach number of the mean flow and the amplitude of the unsteady motion. The wave equation can be written in the form

$$\frac{1}{\bar{a}^2}\frac{\partial^2 p'}{\partial t^2} - \nabla^2 p' = -h.$$

The function h contains all influences of droplet vaporization and combustion, mean flow/acoustics coupling, and two-phase interaction. It can be correctly modeled as a distribution of time-varying mass, momentum, and energy perturbations to the acoustic field. Boundary conditions are found by taking the scalar product of the outward normal vector with the perturbed momentum equation, and then applying appropriate acoustic admittance functions along the surface of the chamber. The next step lies in expressing the unsteady motions as a synthesis of modes described by the eigenfunctions of the wave equation. Finally, with appropriate matching of the acoustic pressure and velocity fields at the interface between the baffle compartments and the main chamber, a transcendental equation is obtained for the complex wave number characterizing the oscillatory flow in the entire chamber.

The major advantage of this approach is the provision of an analytical framework for studying mechanisms proposed as the stabilizing effects of baffles. Furthermore, it alleviates the computational burden associated with conventional numerical techniques, and consequently produces more sweeping results in a more efficient manner. Specific processes under investigation include:

- acoustic fields in entire chambers, including distributions of acoustic pressure, velocity, and energy;
- viscous dissipation of acoustic energy along baffle blades; and
- interactions between mean flow and oscillatory fields, including vortex generation and flow separation.

Calculations have been conducted to study the oscillatory flowfields in both two-dimensional and three-dimensional baffled combustion chambers. Figure 2 presents the acoustic pressure contours of the first and second transverse modes. The unsteady motions are basically longitudinal in the baffle compartments and transit to transverse

waves in the main chamber. As a result of the geometric constraints set by the baffle blades, rapid variations of the acoustic velocity take place near the baffle tips. The resulted vortices are convected downstream and subsequently modifies the mean flowfield. Figure 3 shows the frequencies of the first transverse mode. The frequency decreases progressively with increased baffle length. However, increasing the number of baffle blades causes only a slight decrease of the frequency.

4. Dynamic Responses of Liquid-Propellant Droplet Vaporization and Combustion

The second part of the present research is to examine the sensitivities of propellant droplet vaporization and combustion to ambient flow oscillations in a complicated wave environment. Both pressure- and velocity-coupled responses are considered. The study is based on the time-dependent supercritical droplet combustion model developed by the principal investigator. Specifically, the acoustic wave analysis developed in the first part of this project provides a realistic oscillatory flow condition in the chamber, which is then incorporated into the droplet model to calculate droplet responses. Results obtained are used as a source term in the wave equation to determine the mutual coupling between acoustic waves and droplet combustion responses in a baffled combustor.

The analysis of droplet vaporization and combustion treats the complete conservation equations of mass, momentum, energy, and species concentration for both droplet and ambient gases at Reynolds numbers of practical interest, with full account taken of variable properties and vapor-liquid interfacial thermodynamics. The model accommodates various important high-pressure phenomena, including ambient gas solubility, thermodynamic nonideality, property variation, transient diffusion, etc. Because of its completeness, the analysis enables a systematic examination of the droplet vaporization and combustion characteristics in a high-pressure environment. In particular, the underlying mechanisms of droplet vaporization, ignition, and combustion at near- and super-critical conditions, including the transition from the subcritical to supercritical state, are addressed. Figure 4 presents the instantaneous mass of a n-pentane droplet reacted with air at various pressures. The droplet gasification rate increases progressively with pressure. However, the data for the overall burnout time (as shown in Fig. 5) exhibits a considerable change in the combustion mechanism at the critical pressure. The ambient gas pressure exerts significant control of the droplet gasification and burning processes through its influences on the fluid transport, gas/liquid interface thermodynamics, and chemical reactions.

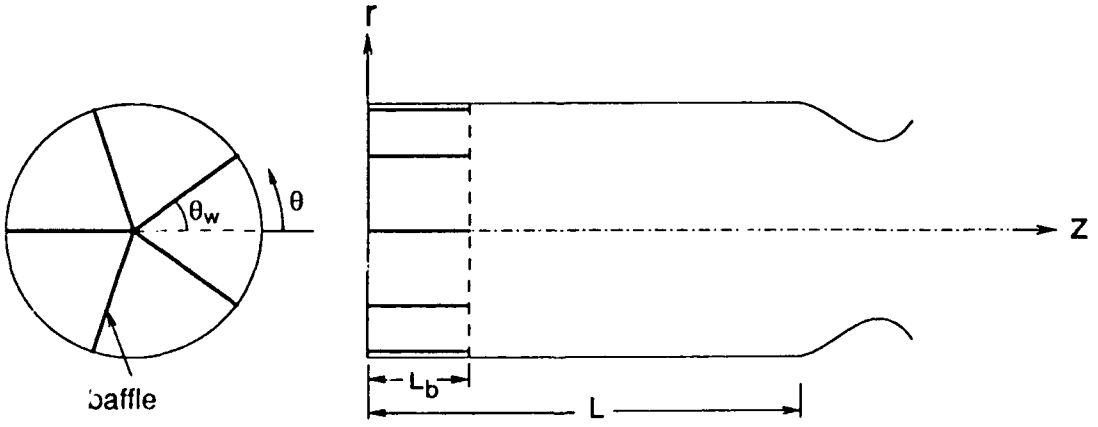

Fig. 1 Schematic of a Baffled Combustor.

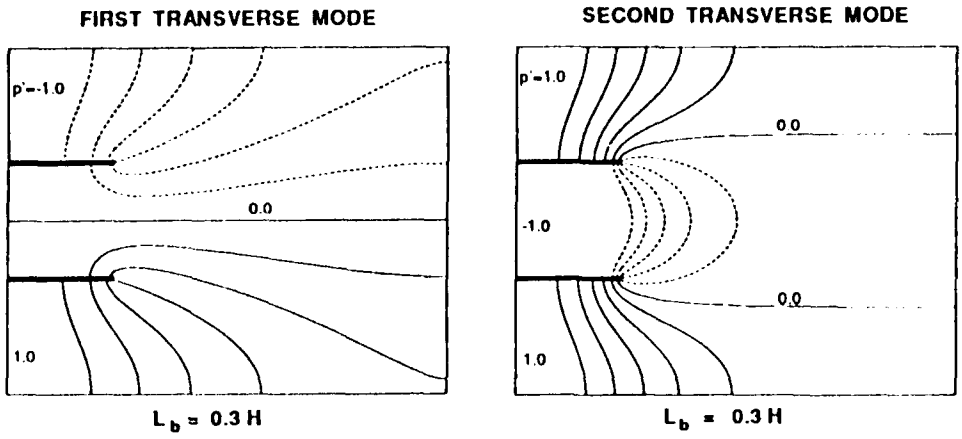

Fig. 2 Acoustic Pressure Contours in Baffled Combustion Chambers.

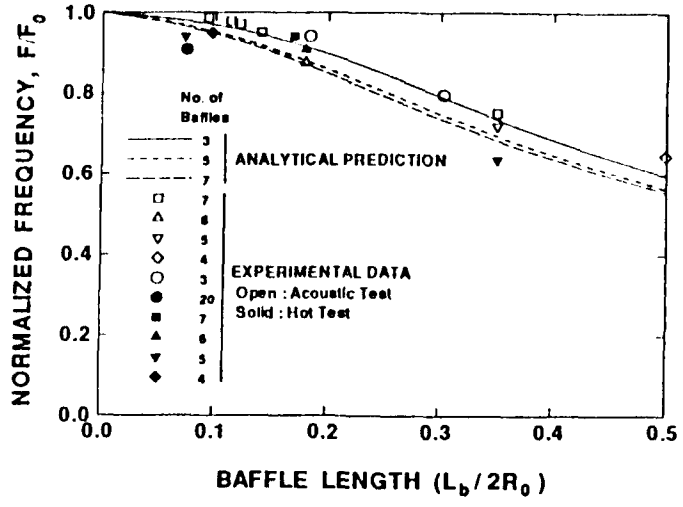

Fig. 3 Effect of Baffle Blades on the Frequency of the First Tangential Mode.

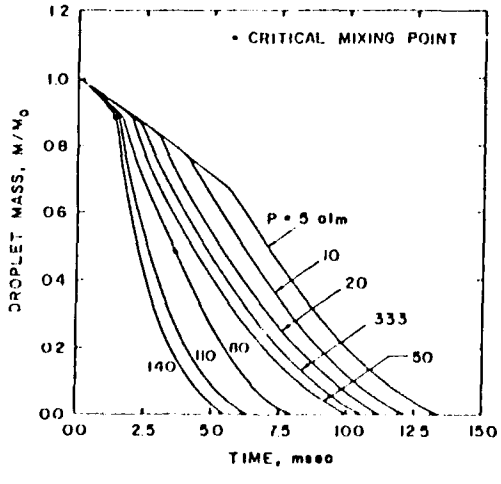

Fig. 4 Time Variations of Fuel Droplet Mass at Various Pressures.

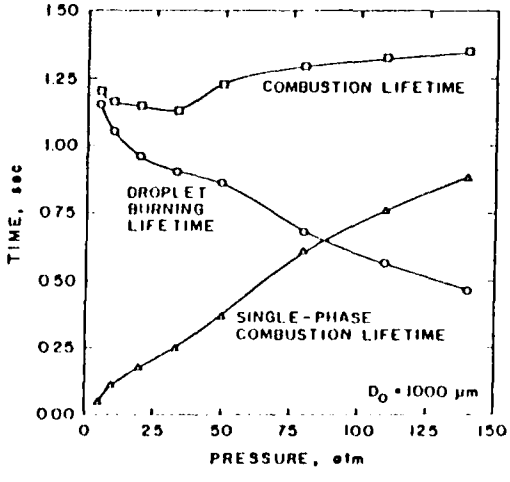

Fig. 5 Effect of Pressure on Milestone Times Associated with Droplet Gasification and Burning Processes.

DYNAMIC ATOMIZATION IN LIQUID ROCKET ENGINES

AFOSR Grant Contract No. AFOSR-90-0121

Principal Investigators: J. W. Daily and S. Mahalingam

Center for Combustion Research
Department of Mechanical Engineering,
University of Colorado at Boulder
Boulder, Colorado 80309-0427

SUMMARY/OVERVIEW

A study of the effect of acoustic perturbations on the atomization characteristics of a coaxial gas/liquid rocket engine injector is being carried out. A pair of compression drivers are used to excite a transverse acoustic field in a combustion chamber and its effect on the atomization behavior is observed. Ethanol and oxygen enriched air are used for hot flow studies and water and air are used for cold flow studies. Depending on the operating conditions, imposed transverse acoustic excitation at a field strength of 157 dB increases the spray angle by as much as 37% for cold flow cases. For hot flow cases at fixed operating conditions, addition of transverse excitation increases the combustion chamber pressure by as much as 20%. This study will elucidate fundamental physical mechanisms affecting the dynamic behavior of propellant atomization in an oscillatory environment.

TECHNICAL DISCUSSION

The long term objective of our research is to develop predictive models that will help rocket designers build high performance, stable liquid rocket engines. Combustion instability in liquid rocket engines is manifested as large amplitude combustion chamber pressure and velocity oscillations. These oscillations result in undesired vibrations, enhanced heat transfer and can ultimately lead to mission failure. Presently, rocket engine manufacturers rely heavily on empirical and actual test data in design stage of rocket engines. This approach is clearly expensive and unreliable.

The focus of our study is to understand the dynamics of atomizationin in an oscillatory environment. Numerous studies have shown that atomization plays an important role in determining both susceptibility to combustion instability and overall combustion performance of the engine. It is well known, for example, that finer atomization, while leading to increased combustion efficiency, also leads to an increase in the occurrence of combustion instability. It has also been shown that acoustic perturbations can dramatically alter atomization behavior. A typical scenario leading to combustion instability can be as follows: an initial chamber acoustic disturbance induces fluctuation in the atomization rate. This results in variation of propellant droplet size distribution, which affects vaporization, mixing, and reaction rates, inducing fluctuations in the overall combustion rate. If the perturbation in the rate of volumetric expansion occurs with proper phase, as described by Rayleigh's criterion, amplification of the initial disturbance can occur, leading to combustion instability.

The sensitivity of atomization to acoustic disturbances has previously been established. A detailed survey may be found in Huynh et al. (1992). Miesse (1955), Reba and Brosilow (1960), and Torda and Schmidt (1964) have shown that high acoustic amplification can produce strong modulation of liquid streams. Buffum and Williams (1967) in cold flow, and Heidmann (1965) in hot flow, both showed a strong correlation between the transverse acoustic field and jet behavior. Ingebo (1966) studied the behavior of liquid jet atomization perturbed by longitudinal acoustic waves and found that under resonant conditions, atomization and vaporization rates are significantly enhanced. However, the experiments cited have not dealt with realistic rocket injector operating

conditions. Furthermore, virtually all existing empirical information regarding injector combustion instability response has been obtained by inference from analysis of time dependent pressure data. To date, no direct measurements of the atomization response of a rocket injector have been carried out under realistic conditions. Our goal is to make such measurements in an environment similar to that of real engines.

EXPERIMENTAL CONSIDERATIONS

Important parameters in the atomization process include injector geometry, propellant velocities, densities and viscosities, the liquid phase surface tension, and heat of combustion. Depending on the number of parameters chosen as being significant, between six to ten similarity parameters arise from dimensional analysis. The most important of these are the Weber number based on the ratio of gas-liquid phase relative kinetic energy to liquid surface energy, the liquid jet Reynolds number, ratios of liquid to gas viscosity and density and normalized heat release.

Because of present experimental constraints, we have chosen to work with simulants to the important large engine propellants. If we chose to work with realistic geometry and propellant velocities, then the important similarity variables become the Reynolds number, the Weber number, the ratios of liquid to gas viscosity and density, and the normalized combustion heat release. The heat release can be varied independently by varying diluent concentrations in the simulant streams. A combination of water and air mixed with refrigerant was chosen for cold flow testing. To simulate LOX/Hydrogen hot flow, ethanol and oxygen enriched air have been selected. The major dilemma in selecting simulants for LOX/Hydrogen is in maintaining a large value of the gas phase density.

The experiments are carried out in a rectangular combustion chamber designed for controlled application of transverse acoustic disturbances. The combustion chamber has a square cross section of 5 cm by 5 cm and its length can be varied from 28 cm to 43 cm by moving the exit nozzle location. The injector used in the results reported here has a 1 mm inner diameter center post with a 4 mm wide annulus. The post recess can be varied over a range of 0-4 mm, but was zero for the results reported here. For details of the experimental design, Huynh et al. (1992) may be consulted.

RESULTS

Preliminary flow visualization results have been obtained for a limited set of cold and hot flow operating conditions. Initial observations were made without excitation to benchmark our apparatus and to verify that the injector characteristics are consistent with previous experience. The results showed, not surprisingly, that atomization behavior changes drastically with coflowing gas velocity, while being relatively insensitive to liquid jet velocity.

At a liquid velocity of 15 m/sec, the Reynolds number is 1.69×10^4 and the Weber number is 3.4. As the coaxial gas flow is initiated, the Weber number first decreases as the gas velocity approaches the liquid jet velocity, then increases to 1575 as the gas velocity is increased to its maximum value of 310 m/sec. At high gas phase velocities, greater than 200 m/sec, the liquid jet becomes completely atomized within one jet diameter. Visual observation of the spray indicates that as the gas velocity increases, droplet size decreases. Pressure measurements at the injector location indicate that the acoustic drivers can produce pressure amplitudes of approximately 157 dB and when the speakers are operated 180 degrees out of phase, the transverse velocity perturbation is about 4 m/sec. For cold flow studies, imposing a transverse velocity perturbation results in dramatic changes in the atomization characteristics, with the visual spray angle increasing by as much as 37%.

Hot flow studies with chamber pressures up to three atmospheres indicates that transverse acoustic excitation increases the combustion chamber operating pressure by as much as 20%. Pressure measurements were made at excitation frequencies of 100, 3000, and 4360 Hz , which are at transverse resonant frequencies of the chamber. The chamber pressure increase during excitation was relatively insensitive to the frequency. Schlieren images of hot case studies shows the presence of coherent vortices within the coaxial gas phase flow field shear layers. The

growth of vortices as they move downstream can be seen in Figure 1 (hot case, Chamber pressure: 2 atmospheres, ethanol velocity: 15.5 m/s, gas phase oxidizer velocity: 140 m/s, excitation frequency 3000 Hz.) .

FUTURE WORK

For the immediate future we will be focusing on bringing the combustor facility to full operational status and finishing development of our laser scattering and extinction instrument. (Higher chamber pressures are especially desirable both to increase the gas phase density and thus Weber number, and to increase the amplitude of the applied acoustic field through better coupling.) We will then make detailed diagnostic measurements while varying the important parameters systematically over a wide range of operating conditions. Parameters to be varied include velocities, heat release, chamber pressure, and injector geometry including post recess. Measurements will include chamber pressure, CH radical emission from the combustion chamber to detect combustion efficiency changes, laser scattering and extinction measurements, and flow visualization. We will utilize the data obtained to elucidate fundamental physical mechanicsms that show the coupling between atomization and combustion instability.

In the longer range future we will be making phase locked laser Doppler velocity measurements of both gas and liquid phase velocities. We will also make phase locked droplet size measurements using the Phase Doppler approach. These measurements will allow us to directly quantify the dynamic effect of acoustic fields on droplet size and velocity distributions.

CONCLUSIONS

Preliminary observations of the results of acoustic perturbation on an atomizing coaxial liquid/gas rocket injector have been made. Cold flow results show that varying the velocity of the liquid jet does not have a pronounced effect on atomization behavior. Gas phase velocity variation does have a pronounced effect on atomization. Increasing the gas phase velocity reduces the droplet size and increases the spray angle. Direct visual observation of cold tests indicate that a transverse acoustic excitation of 157 dB increases the spray angle by as much as 37%. In hot flow, transverse acoustic excitation resulted in increases of combustion chamber pressure by as much as 20%. Visualization observations reveal that the gas phase coaxial flow mixing layers are forced into coherence.

ACKNOWLEDGEMENTS

This work is partially supported by the Air Force Office of Scientific Research and the Air Force Philips Laboratory, AFOSR Grant Number AFOSR-90-0121.

REFERENCES

Buffum, F.G., and Williams, F.A., "The Response of a Turbulent Jet to Transverse Acoustic Fields," Proceedings of the 1967 Heat Transfer and Fluid Mechanics Institute, P.A. Libby, D.B. Olfe and C.W. Van Atta, Eds., Stanford University Press, 1967, pp. 247-276.

Heidmann, M.F., "Oxygen-Jet Behavior During Combustion Instability in a Two-Dimensional Combustor," NASA TN D-2725, 1965.

Heidmann, M.F., and Groegneweg, J.F., "Analysis of the Dynamic Response of Liquid Jet Atomization to Acoustic Oscillations," NASA TN D-5339, 1969.

Huynh, C., Ghafourian, A., Mahalingam, S., and Daily, J.W., "Combustion Design for Atomization study in Liquid Rocket Engine," AIAA 92-0465, 1992.

Ingebo, R.D., "Atomization of Ethanol Jets in a Combustor With Oscillatory Combustion-Gas Flow," NASA TN D-3513, 1966.

Miesse, C.C., "Correlation of Experimental Data on the Disintegration of Liquid Jets," Ind. Eng. Chem., Vol. 47, No. 9, 1955, pp. 1690-1701.

Torda, T.P. and Schmidt, L.A., "One-Dimensional Unsteady Aerothermochemical Analysis of Combustion Instability in Liquid Rocket Engines," Pyrodynamics, Vol. 1, Gordon and Breach, Science Publishers Ltd., 1964, pp. 9-111.

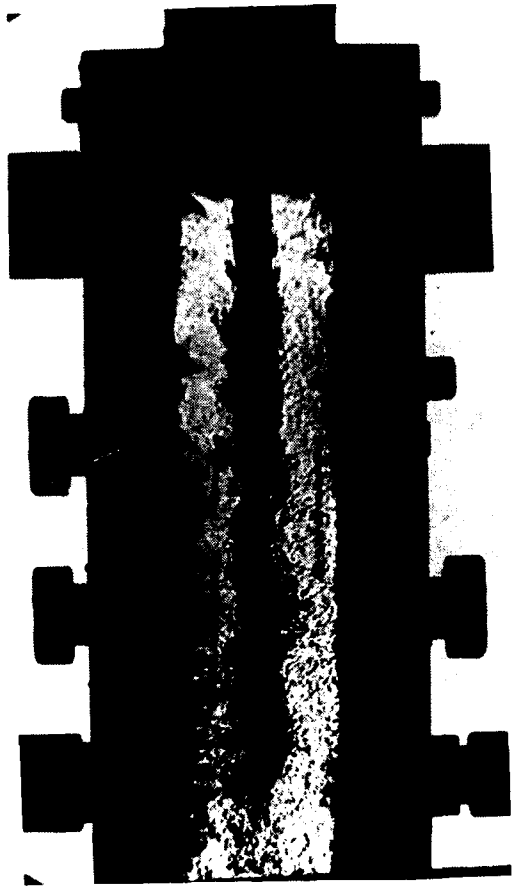

Figure 1: Schlieren image of a hot run, chamber pressure = 2 atmospheres, ethanol velocity = 15.5 m/s, gas phase oxidizer velocity = 140 m/s, excitation frequency = 3000 Hz.

COMBUSTION INSTABILITY PHENOMENON OF IMPORTANCE TO LIQUID PROPELLANT ROCKET ENGINES

AFOSR Grant No. 91-0336

Principal Investigators: W. E. Anderson and R. J. Santoro

Propulsion Engineering Research Center
and
Department of Mechanical Engineering
The Pennsylvania State University
University Park, PA 16802

SUMMARY/OVERVIEW:

A research program has been underway at the Propulsion Engineering Research Center to determine the role that fundamental physical mechanisms of impinging jet injector systems play in initiating or sustaining combustion instability. The impinging jet injector system was chosen for study because it is commonly used for storable propellants and even has potential advantages over the coaxial injector system for LOX/H_2 propellant systems. The experiments to date have concentrated on parametric measurements of atomization length and width, and drop size distribution with non-intrusive optical diagnostic techniques. These measurements are compared with results obtained from an analytic effort that extends linear stability theory to the case of an impinging injector system. The comparisons indicate that simple analytic models based on linear stability theory fail to predict the correct parametric trends and suggest the need for models that treat the dynamics at the impingement point. Currently, an optically accessible chamber is being fabricated that will extend the scope of the present experiments to include higher pressure environments and also facilitate the study of the effects of forced oscillatory motion on the atomization characteristics of impinging injectors. Concurrently, the analytic effort is concentrating on identifying CFD-based approaches that can be used to model the atomization phenomenon. Successful completion of this program will lead to more physics-oriented injector design analysis approaches which can be incorporated into comprehensive methodologies for future liquid rocket engine design.

TECHNICAL DISCUSSION:

Combustion instability in liquid rocket engines has often led to catastrophic consequences. The mechanism(s) that initiate and energize this phenomenon have escaped clear understanding despite nearly four decades of research. Potential mechanisms that have been postulated as possible sources for combustion instability are the principal component processes of liquid rocket engine combustion, namely injection, atomization, vaporization, mixing and kinetics.[1] Currently, not a single predictive capability exists that can predict the engine configuration parameters and operating conditions necessary to thwart the occurrence of combustion instability. Due to the lack of a validated predictive analysis tool, rocket engine designers have fallen back on empirically-derived guidelines to design injectors. This design procedure has succeeded satisfactorily for shear coaxial injector elements using the LOX/H_2 propellant combination up to the point that stable injector configurations can virtually be assured over the common range of operational conditions. However, for impinging jet injectors, the current design methodology system is not that well developed.

The current research program emphasizes understanding the physical processes that control the stability characteristics of the impinging jet injector system and uses a proven empirical correlation, which relates injector design and operational parameters to the frequency bounds of combustion instability as guidance in defining the pertinent experiments. The empirical correlation that is used is the previously unpublished Hewitt Stability Correlation developed at Aerojet Propulsion Division which is illustrated in Fig. 1. This correlation was originally developed for storable propellant combinations using like-on-like injector elements, and later found capable of predicting trends for triplet injectors and LOX/hydrocarbon propellants as well. The correlation indicates that the maximum sustainable instability frequency is dependent on the ratio of orifice diameter to injection velocity of the less volatile propellant. It should be recognized that by itself it does not predict a preferred frequency.

The performance of the correlation for a representative range of injector/combustor combinations using LOX/RP-1 propellant and like-on-like impinging injector elements[2] is indicated in the figure: the 100 cm (39 in.) diameter F-1 (5U, PFRT, and Qual); the 53 cm (21 in.) diameter H-1; a 20 cm (7.8 in.) diameter injector used in an Air Force combustion instability technology program (-0100); a 14 cm (5.4 in.) diameter injector used in a Lewis Research Center technology program (LeRC Pavli); and 9 cm (3.5 in.) and 14 cm (5.8 in.) diameter injectors used in a Lewis Research Heavy hydrocarbon technology program (HHC H-1 Derivative and HHC Canted Fan, respectively). The data reflects a high frequency cutoff point for these injectors; frequency at stable points correspond to calculations of the lowest stable acoustic mode, and frequencies at unstable points correspond to the highest observed frequency. For example, the 5-U was the early F-1 baseline injector, which was unstable at 750 Hz. Modifications to this injector eventually resulted in the marginally stable PFRT injector and the stable dual injector. These data, along with a much more extensive set of storable data, indicate that the Hewitt Stability Correlation is generally able to predict instability modes for impinging injectors over a wide range of frequencies. Furthermore, the functionality of the correlation suggests that certain physical processes play a role, which will be explored next.

The characteristic frequencies of liquid jet breakup, drop shattering, droplet thermal inertia and vapor diffusion are compared with the Hewitt Stability correlating parameter in Fig. 2. It is seen that jet breakup and droplet shattering exhibit relatively similar trends to the correlation, and that diffusion and thermal inertia frequencies are noticeably different from the correlation. It should be noted that frequencies estimated for smaller drops in the distribution would tend to decrease the difference observed in the thermal inertia case, but it would still have a slightly different slope.

In order to develop comparative data on combustion instability mechanisms important in impinging jet injectors, a series of experiments involving water jets has recently been completed. The objective of these studies was to spatially and temporally characterize the spray structure resulting from the impinging jets and compare those results with previous work wherever possible. There have been only two definitive experimental works on impinging injector systems.[3,4] Heidmann et al.[3] undertook an extensive study of impinging jets to characterize the effects of orifice diameter, jet velocity, impingement angle, pre-impingement length, and liquid properties on the structure of the resulting spray. The second study by Dombrowski and Hooper[4] studied the disintegration of the sheet formed by both laminar and turbulent impinging water jets. In the present research efforts, the spray characteristics of two impinging water jets issuing into a quiescent environment were experimentally evaluated.[5] Specifically, a Phase Doppler Particle Analyzer (PDPA) was used to measure the size and velocity of drops at various discrete points downstream of the impingement point for a range of flow conditions comparable to those used by Heidmann et al.[3] Additionally, multiple instantaneous images of the spray field at the same flow conditions were also taken and the length and width of the intact sheet resulting from the impingement of the two water jets were measured. When possible, measurements of the separation distance between clearly defined wave-like structures were also made from the spray images. These measurements were compared with predictions from a linear-stability based model for the atomization phenomenon. The analytical model[6] used is based on the aerodynamic amplification of infinitesimal disturbances on the surface of the liquid sheet formed downstream of the impingement point. Breakup length for the impinging injector system is predicted on a semi-empirical basis that relates the ratio of final to initial disturbance amplitude.[6] At this breakup point, the sheet is envisioned to form ligaments which further atomize into spherical drops by a surface tension controlled mechanism.

A typical image of the spray resulting from the impingement of two water jets is shown in Fig. 3. The structure of the spray and the behavior as velocity and impingement angle are varied, is very similar to that observed by Heidmann et al.[3] and Dombrowski and Hooper.[4] The breakup length of the sheet, measured from multiple digitized images of the spray for different velocities, is shown in Fig. 4 for three different impingement angles. The breakup length is observed to increase with increasing jet velocity and decreasing impingement angle. For the breakup length, seventeen spray realizations were measured and the bars indicated in the figure represent the $\pm$ root mean square associated with the spray measurement condition. The trends observed for breakup length are similar to the results of Heidmann et al.,[3] as is also the observation that the breakup length approaches an asymptote as the jet velocity increases to 18.5 m/s.

The corresponding analytic predictions of the breakup length obtained from the linear stability-based model are also shown in Fig. 4. The model predictions of breakup length variation with velocity do not agree with either the current results or those reported by Heidmann et al.[3] The inability of the theory to predict the observed trends with respect to breakup length is consistent with the results of Dombrowski and Hooper[4] who found impact wave effects controlled sheet breakup for high velocity, turbulent impinging jet conditions. They also argued that breakup length should decrease with increasing jet velocity for both aerodynamic instability and

impact wave mechanisms. However, no explicit theory or data verifying that argument has been presented for the impact wave mechanism.

Arithmetic mean drop size (D_{10}) measurements, made with the PDPA are compared with model predictions in Fig. 5 as a function of jet velocity and impingement angle. Qualitatively, there is agreement between the theoretical predictions and experimental measurements; both prediction and measurement indicate that drop size decreases significantly with increased velocity and impingement angle. It should be noted that the measurements using the PDPA instrument yield a mean value for the drop size distribution, whereas the theory effectively assumes that a monodispersed spray is formed. Consequently, the lack of quantitative agreement between the measurements and predictions is not surprising. The general similarity between the trends in jet velocity and impingement angle is considered noteworthy. The observed trends with respect to drop size are also in agreement with the results of Dombrowski and Hooper,[4] who reported Sauter mean diameters.

To summarize, the experiments on impinging jet systems in a quiescent environment yielded the following results. Linear stability-based analysis of liquid sheet atomization does not account for the observed magnitude of the sheet breakup length nor its behavior with increased jet velocity. Drop size predictions derived from the analysis reproduced the observed trend of decreasing drop size with increasing jet velocity and increasing impingement angle. Furthermore, the quantitative predictions of drop size were within a factor of two of the measured value with the difference attributed, in part, to the fact that the model is restricted to a monodispersed drop size. These comparisons suggest that to unravel the atomization phenomenon of impinging jet injectors, the fluid dynamic processes at the impact point have to be understood; disregarding this fact and treating the problem with linear stability theory is simply not correct.

The comprehensive data set on impinging jet injector systems in a quiescent environment provides a basis for comparison with future results obtained in pressurized environments. A rectangular chamber with extensive optical access is currently being fabricated with the purpose of obtaining impinging jet injector data under pressurized conditions and for testing the stable/unstable regions as predicted by the empirically based Hewitt correlation. The chamber measures 102 mm x 254 mm x 306 mm and is equipped with windows on three sides to provide optical access for laser-based diagnostic techniques. The chamber is designed to withstand pressures up to 100 psi. Both a high-intensity acoustic driver[7] and a rotating gear mechanism will be used to induce oscillatory motion in the chamber along the 254 mm width dimension.

The frequency characteristics of the chamber are shown in Fig. 6. Currently, the plan is to excite the resonant modes up to the third longitudinal mode of the chamber in both nitrogen and helium environments to obtain an oscillating pressure frequency range between 700 and 6000 Hz. This frequency span coupled with a modular design will allow the placement of the impinging jet fan both normal and parallel to the oscillating pressure field. Additionally, the injector can be placed such that the fan is either at a pressure or velocity node. This feature allows the study of the effects of pressure or velocity coupling on the impinging jet spray in an independent manner. The Hewitt correlation relating the operational characteristics of the injector with design elements is also plotted in Fig. 6 for two injector orifice diameters. The stable and unstable regions, predicted by the correlation, are marked in the figure. Thus, by varying the velocity of the jets for a given injector configuration and by measuring the spray characteristics in both stable and unstable regions, insight into the physical processes that govern the Hewitt correlation will be gained.

REFERENCES

1. Harrje, D. T. and Reardon, F. H., *Liquid Propellant Rocket Combustion Instability*, NASA SP-194, 1972.
2. Anderson, W. E., Ryan, H. M., Santoro, R. J., "Combustion Instability Phenomena of Importance to Liquid Bi-Propellant Rocket Engines," *Twenty-Eighth JANNAF Combustion Meeting*, San Antonio, TX, 1991.
3. Heidmann, M. F., Priem, R. J. and Humphrey, J. C., "A Study of Sprays Formed by Two Impinging Jets," NASA Technical Note 3835, March 1957.
4. Dombrowski, N. and Hooper, P.C., "A Study of the Sprays Formed by Impinging Jets in Laminar and Turbulent Flow," *J. Fluid Mechanics*, Vol. 18, Part 3, 1963, pp. 392-400.
5. Anderson, W. E., Ryan, H. M., Pal, S. and Santoro, R. J., "Fundamental Studies of Impinging Liquid Jets," AIAA Paper No. 92-0458, *30th Aerospace Sciences Meeting*, Reno, NE, January, 1992.
6. Dombrowski, N. and Johns, W. R., "The Aerodynamic Instability and Disintegration of Viscous Liquid Sheets," *Chem. Eng. Science*, Vol. 18, 1963, pp. 203-214.
7. Hoover, D. V., Ryan, H. M., Pal, S., Merkle, C. L., Jacobs, H. R. and Santoro, R. J., "Pressure Oscillation Effects on Jet Breakup," in *Heat and Mass Transfer in Spray Systems*, HTD-Vol. 187, C. Presser and A. K. Gupta (eds.), ASME, NY, 1991, pp. 27-36.

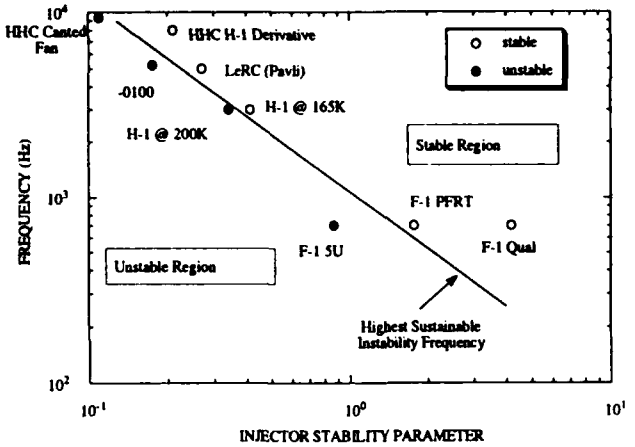

Fig. 1. Maximum instability frequency predicted by Hewitt correlation and comparison with stability behavior of various rocket chambers.

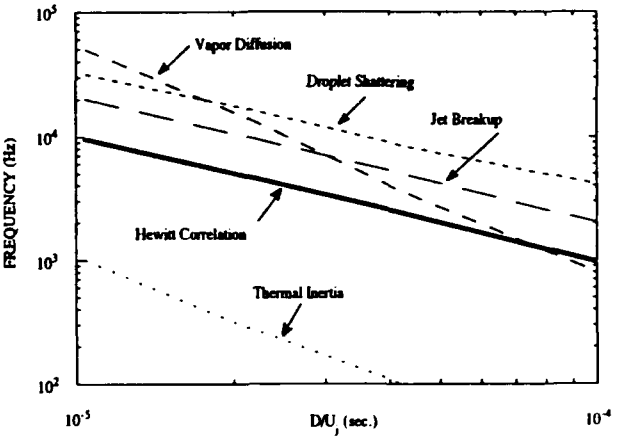

Fig. 2. Comparison of characteristic combustion process frequencies with instability frequency predicted by Hewitt correlation.

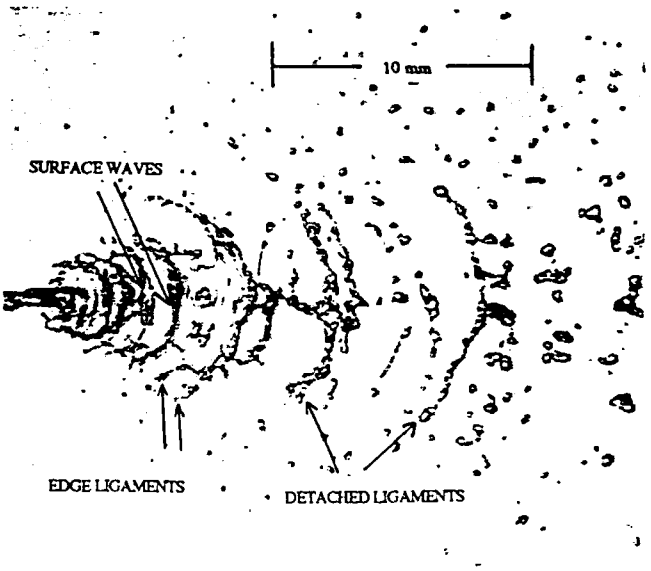

Fig. 3. A typical sheet formed by two impinging water jets issuing from 0.64 mm diameter, L/D=80 glass tubes.

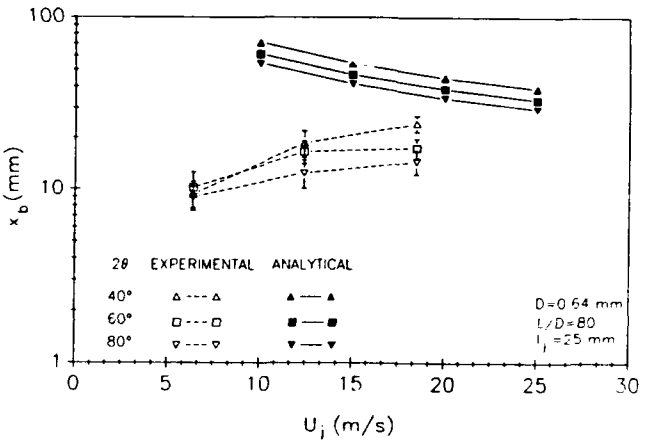

Fig. 4. Measured and predicted sheet breakup length, x_b, plotted as a function of velocity, U_j, for two impinging water jets.

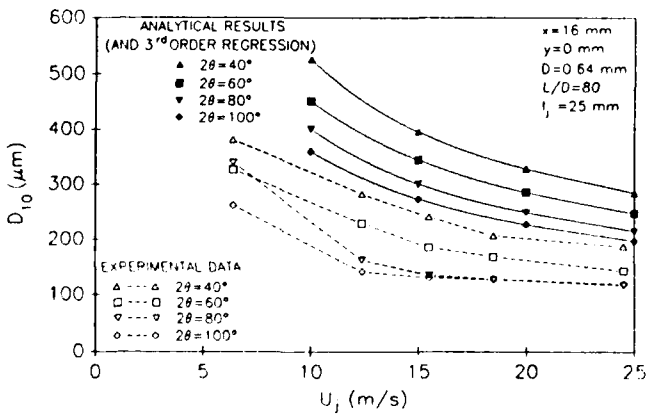

Fig. 5. Measured and predicted arithmetic mean diameter, D_{10}, plotted as a function of jet velocity, U_j.

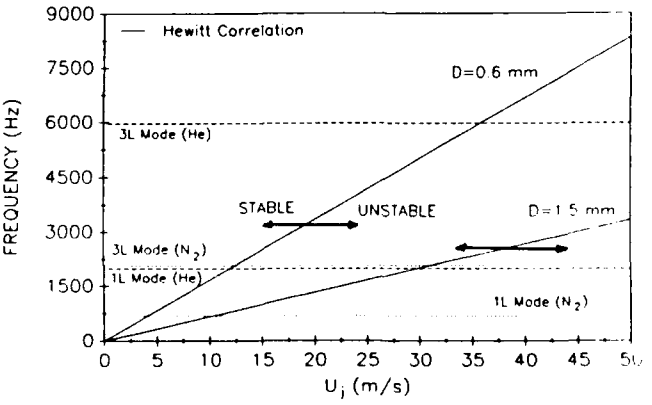

Fig. 6. Stable and unstable frequency limits as calculated by the Hewitt correlation superimposed onto the usable frequency domain of the test chamber.

A COLLABORATIVE RESEARCH PROGRAM BETWEEN ONERA AND THE PENNSYLVANIA STATE UNIVERSITY ON LIQUID ROCKET MOTOR COMBUSTION STABILITY USING COAXIAL INJECTORS

AFOSR Grant No. F49620-92-J-0042

Michael M. Micci

Aerospace Engineering Department &
Propulsion Engineering Research Center
The Pennsylvania State University
University Park, PA 16802

SUMMARY/OVERVIEW:

Although the hydrogen temperature ramping technique has been used for decades to determine the stability characteristics of cryogenic hydrogen/oxygen coaxial liquid rocket motor injectors, there is no knowledge of the effect of the injector velocity ratio on the atomization characteristics of coaxial injectors. This program will provide the first quantitative measurements of droplet size and velocity distributions and atomization zone lengths as a function of the injector velocity ratio. It will also be the first experimental examination of the recirculation region at the base of the injector LOX post. Due to the ability to use liquid oxygen at pressures occurring in actual liquid rocket motors, a level of similitude not obtained before in laboratory experiments will be achieved. This program will provide the experimental database from which modeling of the atomization process for coaxial injectors can be initiated.

TECHNICAL DISCUSSION:

Although stable operating regimes for cryogenic coaxial injectors have been experimentally determined, there is no knowledge of the spray characteristics (i.e. droplet size and velocity distribution) corresponding to stable operation or the physical processes which produce the atomization patterns that result in stable or unstable operation. The current engineering method for determining the stable operating regime of a cryogenic coaxial injector is the "hydrogen temperature ramping" method. One or more injectors are placed in a combustion chamber and hot fired while the temperature of the gaseous hydrogen being injected is slowly reduced until a spontaneous instability occurs. The physical significance of the hydrogen temperature ramping technique comes from the atomization process occurring in coaxial injectors where the high velocity outer gaseous hydrogen flow strips droplets from the lower velocity inner liquid oxygen flow. Experiments at ONERA using water as the liquid oxygen simulant have shown that a higher relative velocity between the two flows, one gaseous and the other liquid, results in smaller droplets and complete atomization closer to the injector exit[1]. Lowering the gaseous hydrogen temperature increases its density, thus lowering its injection velocity relative to the liquid oxygen in order to maintain the same mass flow and therefore the same fuel-to-oxygen ratio. Wanhainen et al have shown that it is not the hydrogen temperature itself causing the transition to instability but the ratio of the gas to

---

[1] Vingert, L., "Coaxial Injector Spray Characterization for the Ariane 5 Vulcain Engine", 6th Annual Conference "Liquid Atomization and Spray Systems - Europe", July 4-6, 1990.

liquid injection velocities[2] (Fig. 1). From this one might infer that the instability arises because of an increase in the liquid oxygen drop sizes along with an extension in the length of the atomization zone. A primary purpose of the proposed experiments is to identify what effect the velocity ratio has on atomization to provide a better understanding of this common stability rating technique. A more practical disadvantage to the hydrogen temperature ramping technique is that the occurrence of the spontaneous instability can lead to the destruction of the test motor within seconds.

Another proposed explanation for the emergence of unstable operation in the hydrogen temperature ramping test is that a recirculation region acting as a flameholder exists downstream of the LOX post tip. Below a minimum relative velocity between the liquid oxygen and gaseous hydrogen, the recirculation region becomes too weak to act as a flameholder and the combustion zone moves away from the injector face to a location where it can interact more strongly with the chamber acoustic modes. Liang and Schumann have examined this idea with an experimental and computational investigation of gaseous oxygen and hydrogen coaxial injectors[3]. They examined several injectors designed to produce recirculation regions of different sizes but found that all injectors tested showed the combustion region anchored to the base of the injector.

In order to provide information leading to the determination and modelling of the relevant unstable mechanism or mechanisms, the following experimental program is planned. The atomization behavior of coaxial injectors in terms of droplet size and velocity distributions and atomization zone lengths under steady conditions will be characterized as a function of decreasing injector velocity ratio using a planar laser imaging system and a Phase Doppler Particle Analyzer. The planar laser imaging will be used to examine the dense spray region as near to the injector as possible and to determine the atomization zone length while the Phase Doppler Particle Analyzer will measure the droplet size and velocity distributions further downstream (Fig. 2). The planar laser imaging system will allow the determination of the length of the central liquid core, the initial droplet sizes stripped from the central core and any intrinsic oscillations occurring in the near injector region. Liquid oxygen will be used for the liquid due to the lack of an accurate simulant with all of its physical properties and because the capability is currently available at Penn State, however both helium and nitrogen can be used for the outer annular gas down to temperatures of 77 K (the boiling temperature of the liquid nitrogen to be used in the heat exchanger system). The possibility will be examined to conduct final testing with gaseous hydrogen. Coaxial injectors of different designs in terms of flow area ratios, LOX post tip land width and liquid flow recess distance and (therefore different stability characteristics) will be examined in terms of the effects of decreasing injector velocity ratio. The liquid oxygen flow capability of the Penn State facility is 1.0 lbm/s (0.45 kg/s) and will allow a half size injector to be tested. Initial experiments will be at atmospheric pressure with the pressure systematically increased to 1500 psia (100 bars) because the chamber pressure affects the injected gas density and velocity. These experiments will establish an experimental data base from which efforts at modeling the atomization process can be initiated.

The process of flameholding at the base of the injector will be examined in cold flow experiments by planar laser imaging in the recess region of the injector. The use of fiber optic probes to introduce the planar laser beam and to receive the resulting images will be evaluated. The possibility of making fiber optic LDV measurements will be examined although there exist no

---

[2]Wanhainen, J. P., Parish, H. C. and Conrad, E. W., Effect of Propellant Injection Temperature on Screech in 20,000-Pound Hydrogen-Oxygen Rocket Engine, NASA TN D-3373, April 1966.

[3]Liang, P.-Y., and Schumann, M.D., "A Numerical Investigation of the Flame-Holding Mechanism Downstream of a Coaxial Injector Element", Proceedings of the 24th JANNAF Combustion Meeting, CPIA Publication 476, Vol. 3, Oct. 5-9, 1987, pp. 599-610.

commercially available LDV fiber optic probes which are small enough for use in a subscale coaxial injector. However, the use of a miniature diode laser LDV system under development at Penn State is being evaluated. Both liquid oxygen and LOX simulants will be used for the core liquid and helium or nitrogen (and possibly hydrogen) for the annular gas flow.

Simultaneously with the cryogenic research conducted at Penn State, ONERA will continue their research with both cryogenic and storable propellant coaxial injectors. ONERA has scheduled to begin in 1992 both cold flow and combusting liquid oxygen/gaseous hydrogen experiments at low pressures (up to 10 bars). Planned are Phase Doppler Particle Analyzer experiments with half scale coaxial injectors (due to a limited LOX flow capability of 0.2 kg/s) which can be compared with the Penn State. Their numerical modelling efforts are aimed at validating their current 2D code and ultimately developing a 3D code.

Work to date on the program has consisted of the design of a liquid nitrogen cooled heat exchanger to lower the temperature of the injected gas, either hydrogen or helium, from ambient down to 80K and construction has begun. The design of the initial test injector is being finalized in coordination with Santoro et al at Penn State and with ONERA in order to generate complementary data. Initial PDPA measurements will begin using ambient temperature gas while awaiting the completion of the heat exchanger.

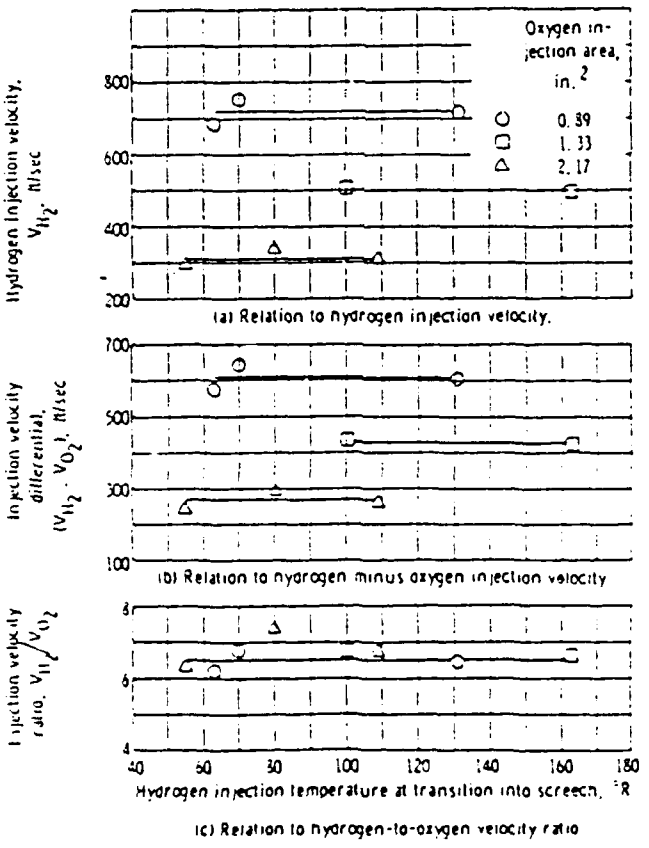

Fig. 1 Stability limits as a function of injector velocity, velocity differential and velocity ratio showing that all injectors tested suffered instability at the same velocity ratio (Ref. 2).

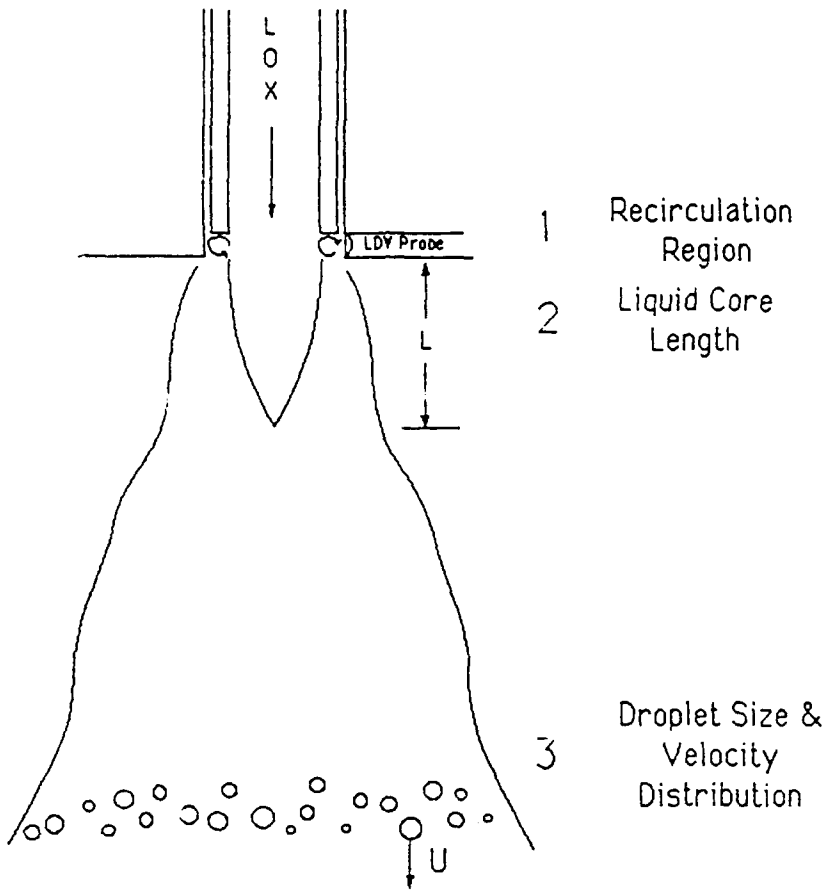

Fig. 2 Schematic of coaxial injector showing the three regions to be characterized as a function of velocity ratio.

DROPLET COLLISION IN LIQUID PROPELLANT COMBUSTION

(AFOSR Grant No. 89-0293)

Principal Investigator: Chung K. Law

Princeton University
Princeton, NJ 08544

SUMMARY/OVERVIEW:

Droplet collision is an essential process in spray combustion, intimately influencing the spray characteristics in the dense spray region. In the present program the dynamics of droplet collision and coalescence are investigated, with emphasis on the influence of the environment pressure, the environment vapor concentration, the droplet size, and the asymmetry of the colliding droplets on the outcome of collision. The study aims to gain fundamental understanding on the mechanisms governing the phenomena of permanent coalescence, rebounding, and coalescence and then separation with and without generation of satellite droplets. Specific issues of interest include the characteristics and thickness of the inter-droplet gas film, the definition of the gas-liquid interface, the extent of energy dissipation and thereby collision inelasticity, the relative influences of head-on versus shearing motion in governing droplet splitting, and the effects of the rheological properties of the liquid such as its surface tension and viscosity coefficient.

TECHNICAL DISCUSSIONS

Recent studies on spray combustion have emphasized the importance of the processes occurring within the dense spray region immediately downstream of the spray injector. Here the droplet ensemble is created and its properties serve as the initial conditions for the subsequent development and combustion of the spray. Because of the dense nature of the droplet concentration in this region, it is reasonable to expect that droplet collision is a frequent event, especially for impinging-type injectors. Depending on the velocity and configuration of the impaction, as well as the rheological properties of the fluid, such a collision can lead to various outcomes, such as bouncing, coalescence, and spattering. Thus, the initial spray statistics in terms of the number density, size and velocity of the droplets can be significantly affected by droplet collision.

Previous studies on droplet collision have mostly employed water as the medium of investigation because of meteorological interests. These works typically show results like Fig. 1, indicating that coalescence is favoured for small values of the collision Weber number, *We*, and impact parameter, *B*.

In the present investigation we have performed an extensive and systematic study of the collision of droplets of water and hydrocarbons, and have found that the collisional dynamics and outcome for the hydrocarbon droplets can be significantly different from those for the water droplets in the parametric range studied. Of particular interest is the observation that the transition between droplet separation and coalescence for hydrocarbons is far from being monotonic, and so the physical phenomena involved are substantially richer than previously recognized.

A crucial requirement of the present experiment is the generation of spatially and temporally stable droplets over extended periods of time. To meet the requirement of temporal stability, we adopted the ink-jet printing technique in which a stable stream of droplets of uniform and controllable size and spacing is generated by using a piezoelectric crystal coupled to a glass nozzle. Thus, droplet collision can be effected by directing one droplet stream against another with the use of a three-dimensional positioner. Extensive experiments were performed for

distilled water, heptane, decane, dodecane, tetradecane, and hexadecane. The droplet radii were about 150 μm while the collision Weber numbers ranged approximately up to 100.

The collisional outcome of hydrocarbon droplets can be approximately classified into five regimes, I to V, as shown in Fig. 2 Figures 3 and 4, respectively, show the photographic images of representative collision sequences for the head-on and off-centre collisions.

We first discuss the head-on and near-head-on situations of Fig. 2. In Regime I the Weber number is not large. Thus, the droplets suffer only a moderate amount of deformation upon "contact". Disappearance of the interface, however, occurs readily.

In regime II the collision is sufficiently energetic that substantial droplet deformation occurs. A distinct interface, however, always exists between the droplets, as evidenced by the presence of cusps at the edge of the interface. Thus, merging does not occur in this regime, and the droplets subsequently bounce off.

A further increase in the collision energy results in permanent coalescence, in Regime III, and is characterized by the total deformation of the merged droplet to the shape of a dimpled disc. Finally, in Regime IV, the collision energy is so high that the surface energy of the coalesced mass is not sufficient to contain the liquid in a closed surface. Thus, after the initial coalescence, contraction of the deformed droplet causes it to split. The outward velocity of the two receding fragments can cause instability of the ligament connecting them, resulting in the formation of one or more satellite droplets. The number of satellite droplets appears to increase with increasing collision energy.

It is significant to point out again that while permanent coalescence always results for the head-on collision of water droplets as long as We is not too large(Fig. 1), for the hydrocarbon droplets, with increasing collision energy, we have the phenomena of permanent coalescence, bouncing, permanent coalescence again, and coalescence followed by separation accompanied by the possible production of satellite droplets. These differences in the behaviour of water and hydrocarbons are obviously consequences of the differences in their material properties, especially the surface tension as represented by the Weber-number correlation.

For off-centre collisions in Regimes I to IV, the behaviour is qualitatively similar to the corresponding head-on situations except that a rotational motion is now imparted to the droplets in contact. Regime V, however, has some distinctive characteristics. Here collision is grazing and highly energetic. Thus, shearing action dominates and there is very little rotational motion. Satellite droplets are produced at higher collision energies and, hence, Weber numbers.

The above results have been analyzed phenomenologically. Specifically, it was shown that the collision event is inelastic, and that criteria governing the various transition boundaries were postulated. The details can be found in the publication "An Experimental Investigation on the Collision Behaviour of Hydrocarbon Droplets", by Y.J. Jiang, A. Umemura and C.K. Law, *J. Fluid Mech.*, vol. 234, pp. 171-190 (1992).

Additional experiments have also been performed under elevated pressures. Preliminary results show that with increasing pressure the behaviour of water droplets gradually resembles that of hydrocarbon droplets under atmospheric pressure. These very interesting results are being further studied.

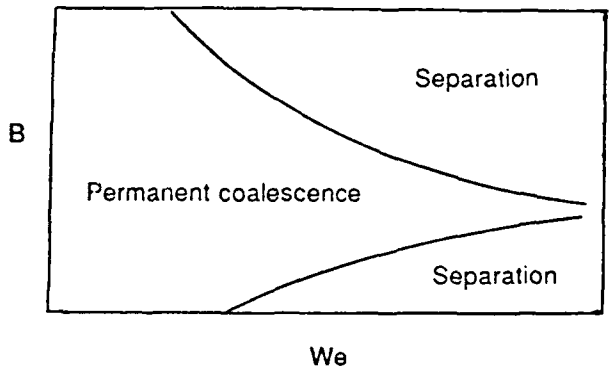

Figure 1. The transition boundaries for coalescence and separation for water droplet collision.

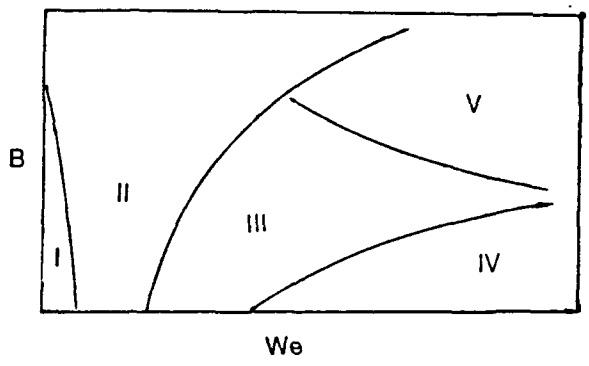

Figure 2 The transition boundaries for coalescence, bouning and separation for hydrocarbon droplet collision.

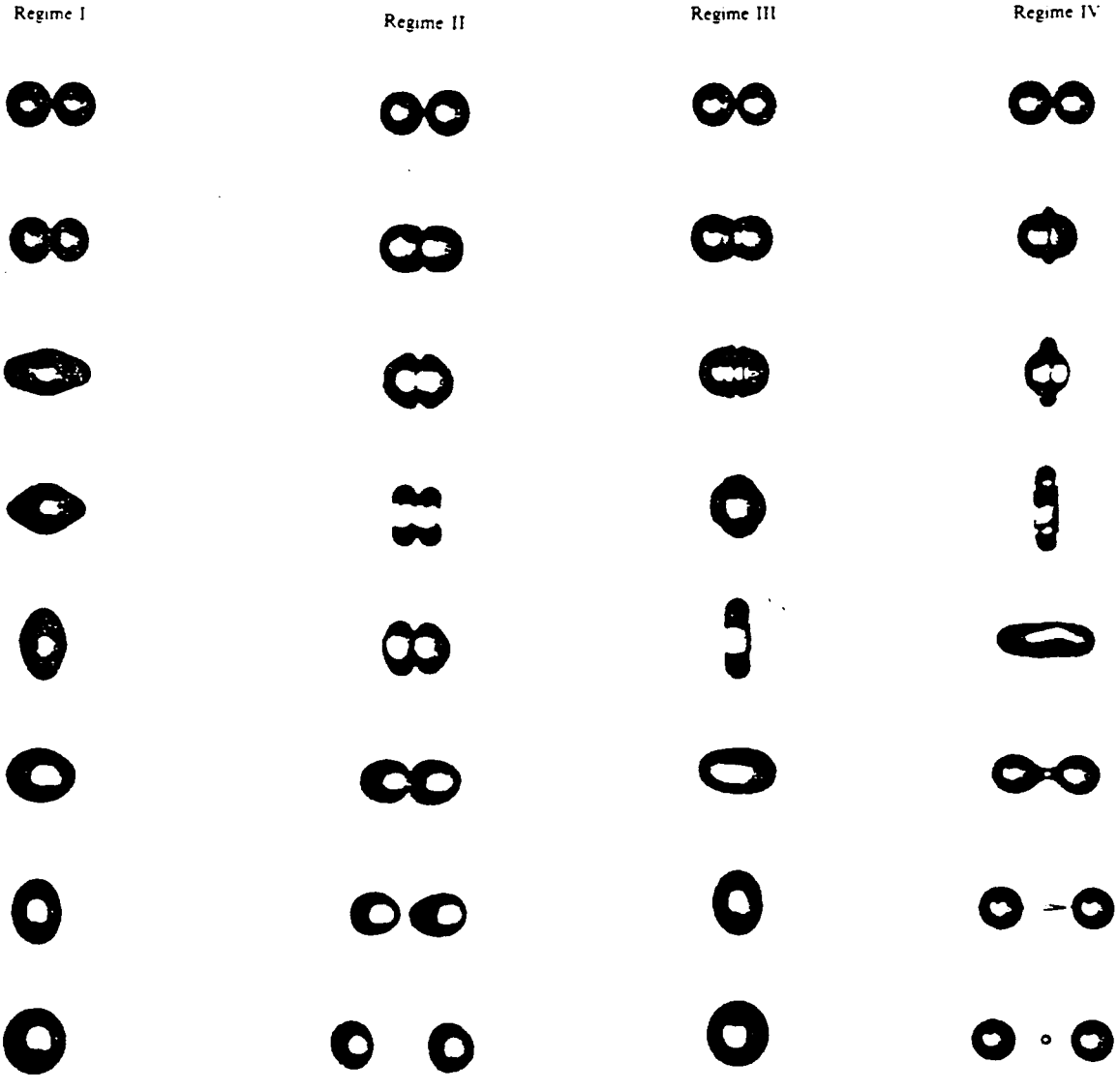

Figure 3. Photographs showing representive head-on collision sequences in Regimes I-IV.

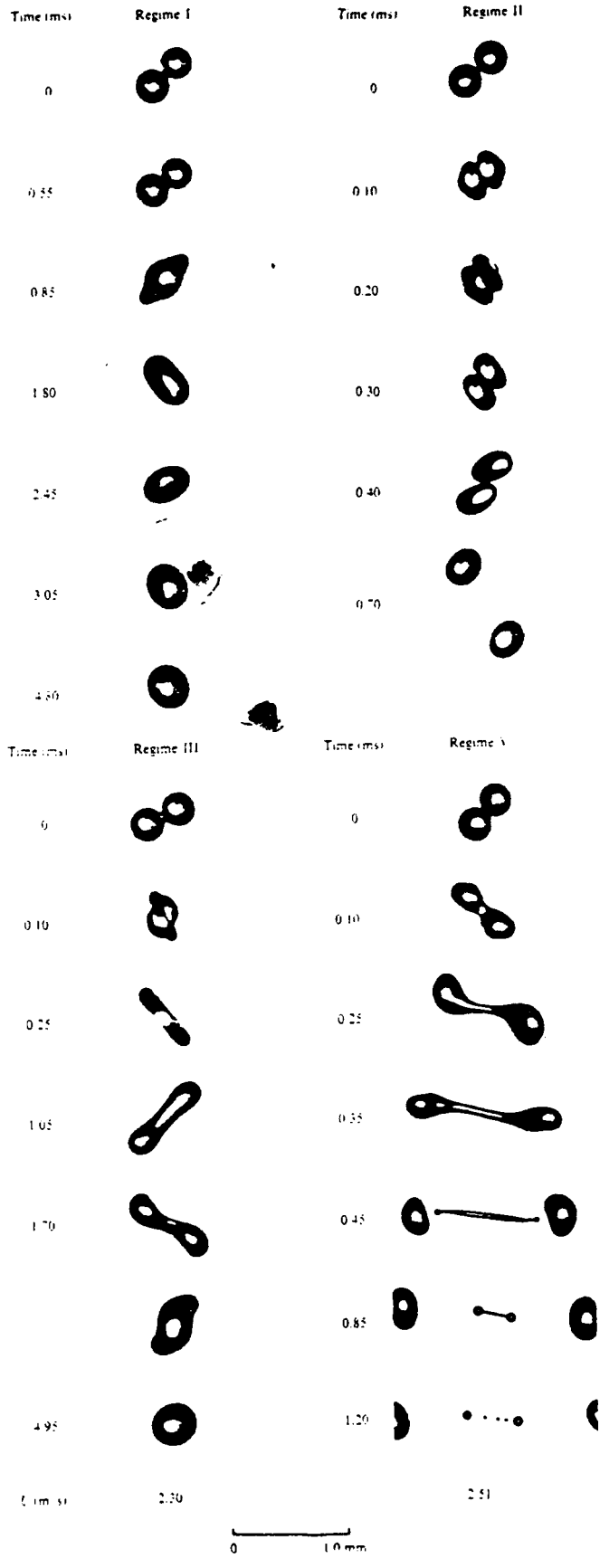

Figure 4. Photographs showing representive off-center collision sequences in Regimes I,II,III and V.

DISTRIBUTED COMBUSTION IN SOLID PROPELLANTS

(AFOSR Grant No: AFOSR-91-0152)

Investigators: M.W. Beckstead, and M. Queiroz

Chemical Engineering Department
Brigham Young University
Provo, Utah

Objective: Identify and develop a quantitative understanding of the mechanism of distributed combustion.

Overview: The current work aims at developing an experimental and analytical basis for determining the mechanisms of distributed combustion. A Rijke burner, constructed at BYU, has been initially characterized. In the burner, particles entrained in the flammable gases are ignited by the flame. Comparisons of the preliminary results from the experimental and analytical efforts are promising. This burner will continue to be used to study particle combustion in both oscillatory and steady flow. Work is beginning on a high pressure system to allow measuring the burning rate of aluminum at pressures up to 30 atm.

BACKGROUND

Acoustic damping mechanisms within a solid propellant rocket are particle, nozzle, structural and wall damping. The predominant driving mechanisms are normally considered to be pressure and velocity coupled driving. A third driving mechanism considered is distributed combustion, but the theoretical foundation for this phenomenon is not well established. The current work is aimed at developing both an experimental and analytical basis for understanding those mechanisms that contribute to distributed combustion.

Distributed combustion is a mechanism of interest since most particles currently used as additives (i.e. aluminum, ZrC, graphite flake, etc.) can also be oxidized, and therefore, will ignite and burn. As combustion occurs, the energy released can affect the acoustics as a positive or a negative contribution to the acoustic wave. There appear to be two predominant physical mechanisms that contribute to this acoustic interaction. The first is the amount of energy released, and the second is the rate of the combustion reaction (which is proportional to particle size). Studying different additives and different particle sizes should help in identifying the relative importance of the different mechanisms.

A Rijke burner has been developed at BYU and preliminarily tested as an experimental apparatus to identify the mechanisms of distributed combustion. Qualitative results show promise when compared to numerical predictions. Future quantitative results will be enhanced by use of a PCSV laser system, recently acquired by BYU. The Particle Counter Sizer Velocimeter (PCSV) is a laser diagnostic for combustion systems with the potential of real-time, simultaneous measurement of particle size, absolute concentration, and particle velocity. PCSV performance has been demonstrated in diverse applications such as pulverized coal combustion, coal-water slurry atomization studies, and liquid sprays.

MEASUREMENT OF DISTRIBUTED COMBUSTION

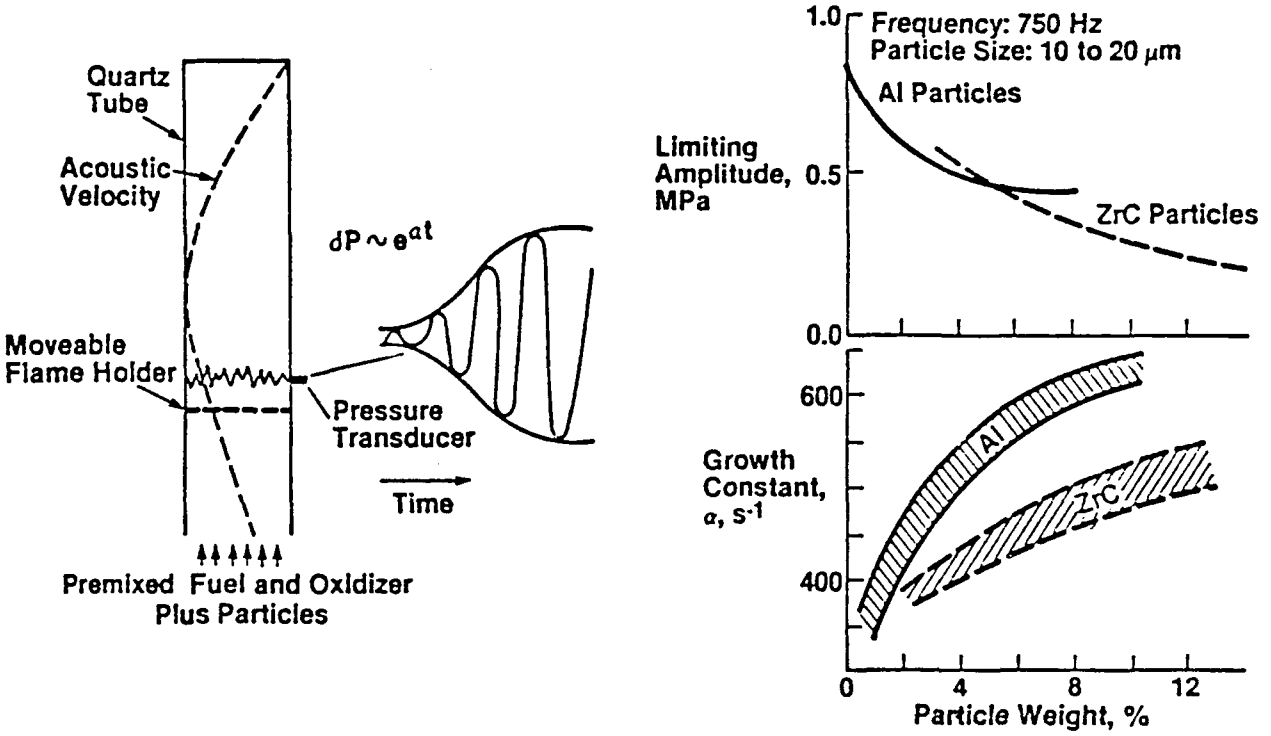

CURRENT PROGRESS

The Rijke burner has provided reasonable qualitative results showing that aluminum particles interact with the acoustic environment at more than twice the level that ZrC does. To make the transition from qualitative trends to quantitative data, several steps have been undertaken. Feeding a known, consistent rate of particles has proven difficult. A fluidized, drop-tube feeder has been developed and is currently being refined to alleviate this source of uncertainty. Flame flashbacks have hampered previous work, so the gas delivery system and burner have been improved to allow greater operating control and range. Lastly the PCSV laser system has been upgraded to the highest capability now available. These efforts should provide data that will prove useful in obtaining quantitative data.

The mathematical model of the Rijke burner was previously developed at BYU by Raun which predicts the frequencies and acoustic growth rates in the Rijke burner both with and without particle combustion. However, quantitative agreement between the model and experimental work has been difficult to attain. This difficulty is believed to be due to the over-simplified descriptions of the interaction of the flame and aluminum combustion with the acoustics. Therefore, an effort to improve these aspects of the mathematical model is currently underway.

This improvement began by replacing the original flame model with a more complex one derived by McIntosh. The McIntosh flame model is based on the unsteady conservation equations and uses activation energy asymptotics in deriving the flame-acoustic interaction. During the past year the McIntosh flame submodel has been coupled with the Rijke model, and verification has been done by using past experimental data from the Rijke burner, obtained by Finlinson. In his work, Finlinson studied growth rate as a function of burner length and inlet gas properties.

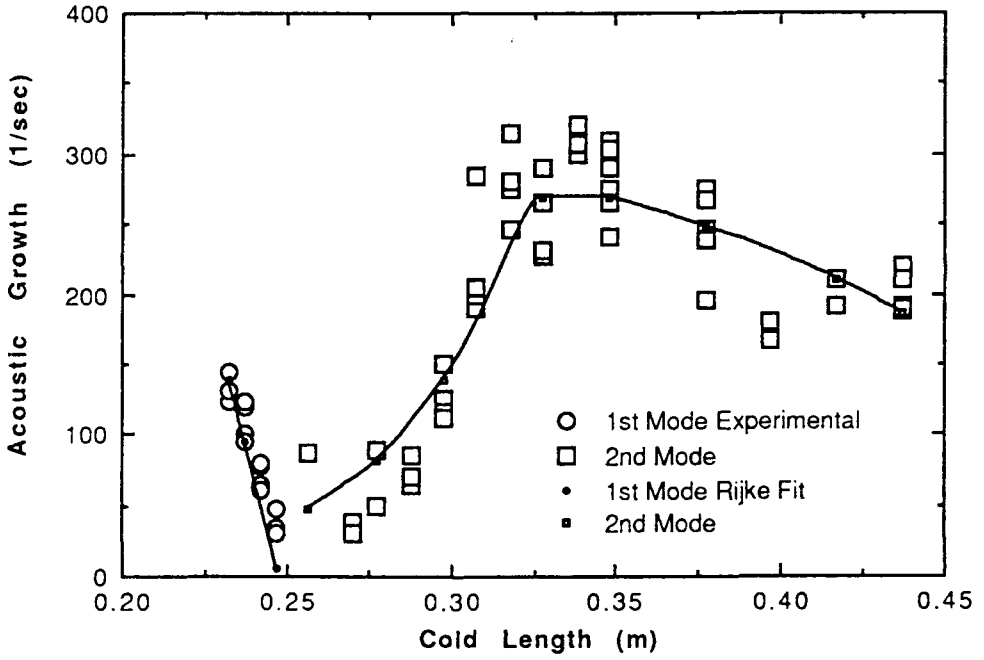

Comparison of Rijke model and Experimentally determined Acoustic Growth for Varying Cold Section Length.

In comparing the Rijke model with Finlinson's work, experimental data has been fit within 10% error for both acoustic growth rate and frequency for all test cases. The complex trends shown by Finlinson's data were followed, indicating a certain degree of fundamental correctness of the model, as shown in the figure. In addition, the temperature and flame holder impedance which were adjusted to fit the experimental data were found to follow reasonable trends. Due to its fundamental nature and ability to follow experiment trends, this flame model is felt to be a significant improvement in the overall predictive capabilities of the Rijke model.

FUTURE WORK

To identify and develop a quantitative understanding of the effects of distributed combustion on an acoustic wave, this study will continue to develop the Rijke burner as an apparatus. Three sizes and types of size-classified particles will be studied to focus on fundamental mechanisms. The baseline test condition is aluminum because it is known to burn vigorously. Zirconium carbide will be tested as a less reactive particle. An inert particle, such as Al_2O_3 or SiO_2, will also be studied. Preliminary data with Al_2O_3 Indicate that the Al_2O_3 may not be inert, but may be catalyzing the flame. If a truly inert particle cannot be found, particles showing both small and large catalytic effects will be used.

Each of the particles to be studied will be tested at baseline conditions, but the aluminum will be tested at a variety of conditions, varying frequency, concentration, temperature, and O/F ratio. Most testing will be done at relatively dilute levels (~1 to 5% additive) in order to minimize particle cloud effects. Data to be obtained will consist of precombustion particle size distributions, gas flow rates, particle flow rates, acoustic pressure amplitudes (at 2 or more locations), and particle combustion tracking (using the PCSV).

Data analysis will include acoustic growth rate measurements, acoustic mode shape reconstruction, particle combustion times, viscous particle damping calculations, etc.

The Rijke model is also being modified to include metal particle ignition delay and combustion. The vapor phase metal combustion model of Law has been selected as an appropriate, state of the art model, with an analytical instead of numerical solution. The aluminum combustion model has been modified to include radiation and convection heat transfer effects, to allow for multiple oxidizers, and to provide for the effects of oxide migration to the metal particle surface. Preliminary comparison between the model and aluminum combustion experimental data has shown reasonably good agreement. Using simple perturbation theory, the metal particle combustion model will be extended to describe the effects of an acoustic wave coupling with the metal particle reaction rate.

Work has been initiated to obtian particle combustion data at pressures up to 30 atm. An existing high pressure facility at BYU is being made available for testing. A modified particle ignition system is being design, and will be constructed to allow the steady state measurement of burning particles to be obtained. Test variables will include pressure, particle size and oxidizing atmosphere.

OSCILLATORY INTERNAL FLOW FIELD STUDIES

Contract F49620-90-c-0032

Principal Investigators: R. S. Brown and C. W. Shaeffer

United Technologies/Chemical Systems Division
P.O. Box 49028
San Jose, CA. 95161-9028

SUMMARY/OVERVIEW: Experimental studies are being conducted to measure the structure of oscillatory waves in the presence of rotational mean flows which characterize the internal flow fields of solid propellant rocket motors. Prior experiments indicated these waves motions deviated significantly from the irrotational behavior associated with classical acoustic waves. These deviations result from the effects of mean and oscillatory gas evolution from the chamber side walls and extend across the outer 33% to 40% of the chamber. Thus, 50% of the chamber volume deviates from the behavior assumed in the standard combustion stability analyses and may account from the significant deviations from predicted and observed motor stability behavior.

Experiments are being conducted in a cold-flow apparatus which simulates the internal flow field of a cylindrical port rocket motor. Results to date confirm that large deviations are generated in wave amplitude and phase from classical acoustic waves. These deviations extend downstream from the head-end at least 4.2 diameters, the limit of the current data. More tests are planned to evaluate the wave behavior further downstream. Viscous forces appear to have little effect since the wave characteristics are roughly independent of the mean chamber pressure. Surface Mach No. however, has a significant effect on the radial distribution of the deviations, as might be expected from the radial momentum equation. The mean velocity profiles also show no effect of mean pressure or surface Mach No. Further analysis of these data suggests the radial variation of oscillatory pressure have be important, even at the low frequencies of the fundamental longitudinal mode. These results agree qualitatively with the analytical results from Professor G. A. Flandro's studies at the Georgia Institute of Technology.

Combining the results of these two studies provides strong evidence that major deficiencies in the current analysis methods for combustion stability result from the assumption of irrotational mean and oscillatory flows. These deficiencies have a major influence on the damping predicted from flow turning and particle damping. They also show that interpreting velocity coupling on the basis of core wave motions is totally inappropriate.

Additional tests are planned to investigate the axial variation of these deviations, the magnitude of the radial variation of oscillatory pressure, the role of interactions between the wave motions and the mean flow turbulence, and propellant grain geometry. The composite results of these experimental and analytical studies will then provide a technically sound and realistic basis for correcting several deficiencies in combustion stability prediction methods.

TECHNICAL DISCUSSION: Measurements of the mean flow velocity, turbulence, and wave behavior are the essential aspect of this recent research. To obtain these data, the cold flow apparatus shown schematically in Figure 1 was constructed. Nitrogen flows through porous cylindrical bronze tubes to simulate the gas evolution by the propellant combustion and generated a realistic internal flow field. Considerable care was taken to ensure the surface Mach number is constant over the entire simulated burning surface. A flow distribution tube equalizes the flow circumferentially around the 10 cm. dia. porous tube. This basic technique has been used successfully in a number of programs to investigate the steady and oscillatory properties of the flow. Flow oscillations are generated by a rotating valve at the aft-end. A specially designed aft-end section was fabricated to mount a fixed diameter sonic exhaust nozzle on the centerline and to minimize the radial distortion of the velocity oscillations entering the port from the rotating valve. A variable speed drive electric motor connected to the rotating valve controls the frequency of the acoustic oscillations. The hole/slot geometry in the rotating valve produced nearly pure sine wave oscillations; 91% at the driving frequency, 4.5% at the third harmonic, and 4.5% at the higher odd harmonics.

The axial and radial components of the oscillatory velocity vector are being measured using a specially designed split-film anemometer. Measurements have been obtained to determine with fine spacial resolution, to define the radial profiles at several axial stations, and to evaluate the effects of surface Mach nos., and operational pressure (to vary the kinematic viscosity). Figure 2 shows the radial profile of the axial mean velocity component agrees very closely with the rotational inviscid cosine profile and demonstrates the mean flow profile is independent of mean pressure (kinematic viscosity) and surface Mach No., hence is independent of surface Reynolds No.

Figure 3 shows the typical behavior of the axial oscillatory velocity component at a surface Mach No. of 0.00103 during one wave cycle at L/D = 4.22. Time zero indicates the time of maximum head-end oscillatory pressure. The "floor" of this plot also shows the contours of wave magnitude as a function of radial position and time during one cycle. Note that the axial velocity maximum near the wall leads (shown as lagging by almost one cycle) the centerline maximum. Since the admittance of the porous wall causes the surface radial to lag the local oscillatory pressure, this behavior strongly suggests the oscillatory pressure and the wall leads the core pressure.

The future research on this program can be divided into two areas, near-term topics and longer-term topics. In the near term, additional radial profile data will be obtained at additional axial stations, specifically at L/D = 5.42. Additional data will also be obtained at L/D = 1.8 to remove some uncertainties in the existing results. These data will then be analyzed in concert with previously obtained data at L/D = 1.8, 3.04 and 4.22 to determine the axial behavior of the rotational flow structures. These results will also be compared to the analytical results currently being computed by Dr. G. A. Flandro of the University of Tennessee Space Institute. The objective of these near-term studies is to define the controlling forces on the oscillatory flow, to relate the rotational flow effects to flow turning and particle damping contributions to combustion stability, and to define the near wall oscillatory velocity which then oscillates the propellant combustion zone (commonly called velocity coupling).

In the longer term, additional cold flow tests will be conducted to investigate the interaction between the wave motions and the mean flow turbulence (which has a significantly different length scale than pipe flow turbulence). These interactions are very important in defining the combustion stability behavior of aft-end regions in many rocket motors.

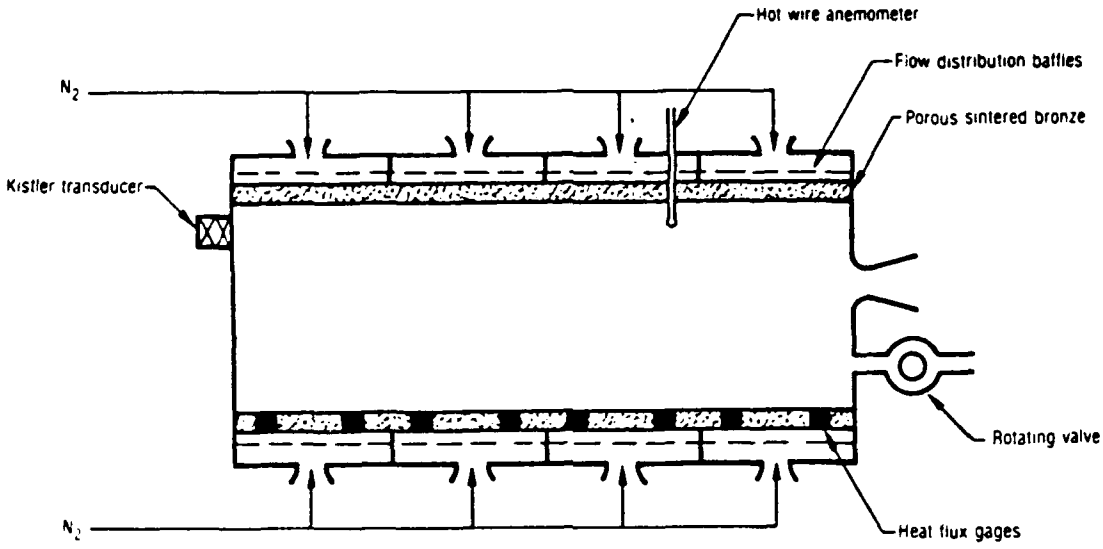

Figure 1. Cold-flow Apparatus

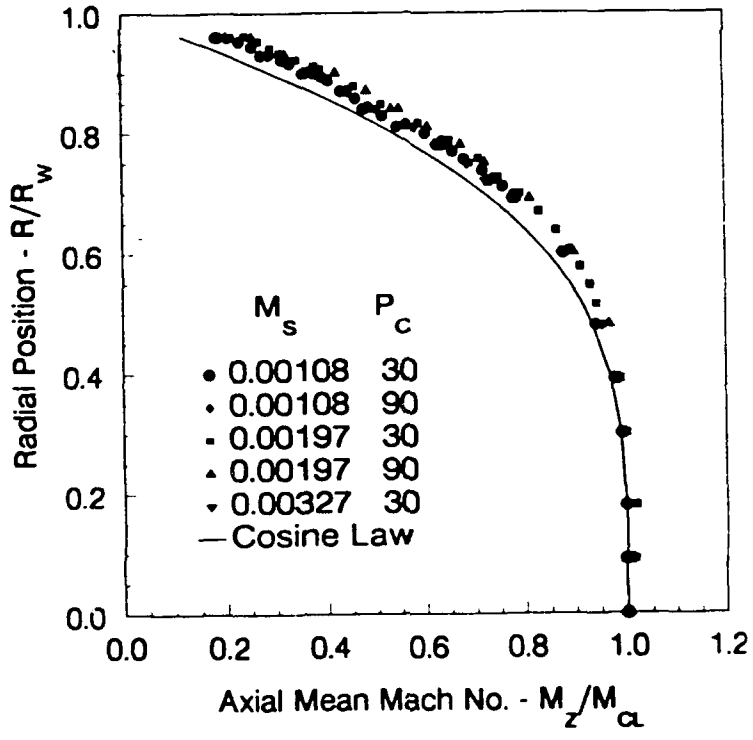

Figure 2. Mean Velocity Profile

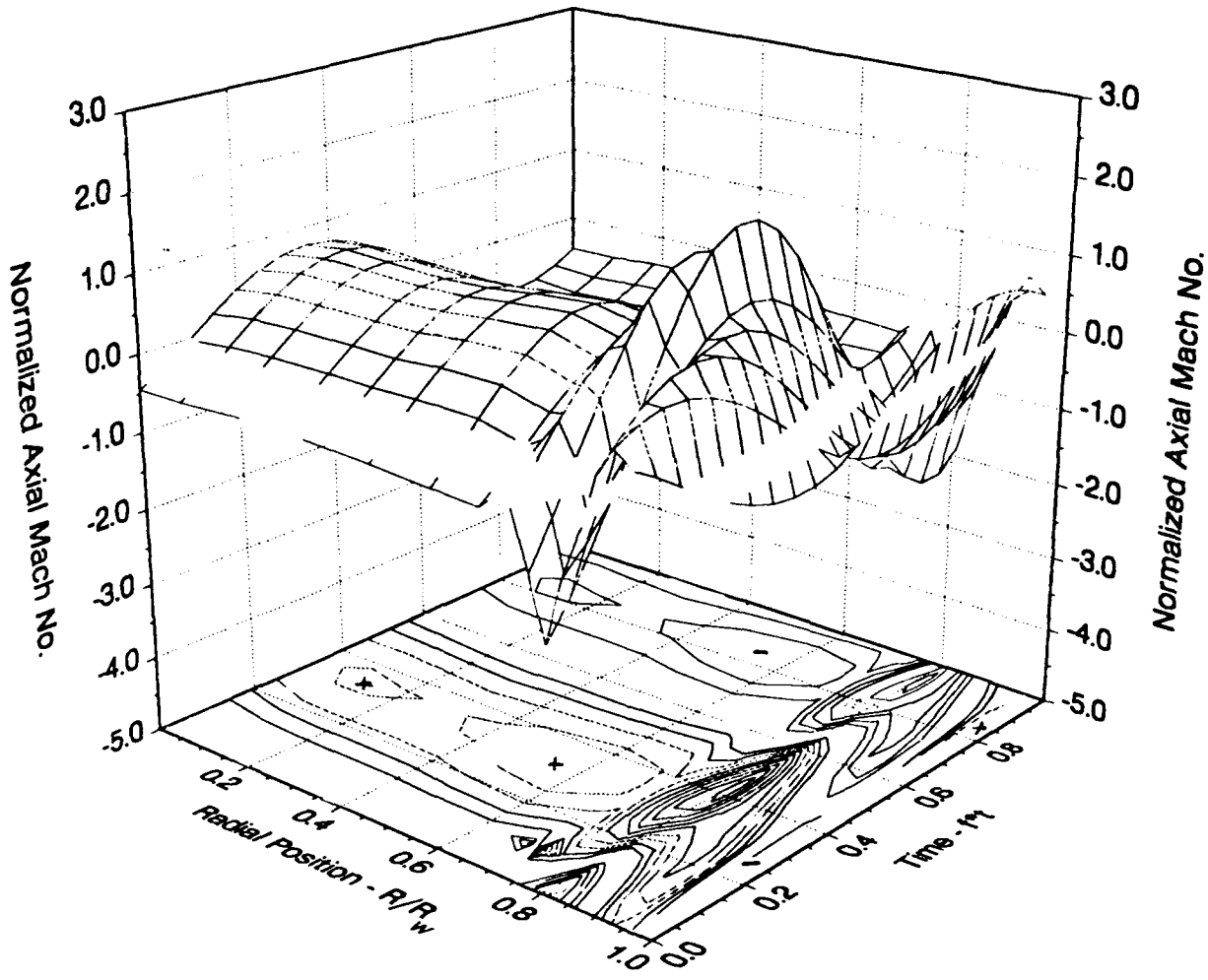

Figure 3. Axial Velocity Variation with Radius

NONLINEAR ACOUSTIC PROCESSES IN SOLID ROCKET ENGINES

(AFOSR Grant No. 89-0023)

Principal Investigator: **David R. Kassoy**

Mechanical Engineering Department/Center for Combustion Research
University of Colorado, Boulder, CO 80309-0427

SUMMARY:

Linear and weakly nonlinear acoustic analyses are employed to study the evolution of disturbances driven by explicit boundary forcing in models of solid rocket engine chambers. Transient sidewall mass addition, mimicing propellant burning, is shown to create surprisingly complex wave phenomena arising from wave reflections in a semi-confined geometry. In a second study, we show the consequences of using different eigenfunction representations in a weakly nonlinear stability analysis, on the long-time solution behavior.

AUTHORS: **David R. Kassoy, Meng Wang,** and **Qing Zhao**

TECHNICAL DISCUSSION

1. Acoustic Wave Modes Generated by Transient Sidewall Mass Addition

Sidewall mass addition is used to mimic the gasification of a burning solid propellant in a model of a rocket engine chamber. Velocity injection along the sidewalls of an open ended rectangle induces a low Mach number internal shear flow. A positive transient component of the injected mass, superimposed on a steady distribution of the same magnitude, is the source of acoustic wave disturbances in a basically steady, inviscid rotational background flow. Reflection processes alone in the semi-confined, open ended rectangle create distinct axial, oblique and transverse wave patterns. Specific harmonic mass transient frequencies are associated with rapid amplification of certain wave mode amplitudes. The primary objectives of this study are to show that complex, identifiable wave patterns are created by relatively simple boundary disturbances, and that boundary driven disturbances can be the source of large acoustic instabilities.

Rational perturbation methods are used to derive a mathematical model which describes a low Mach number compressible flow, in which viscous effects are weak. When the wall injection rate is steady, the equations describe an inviscid, rotational flow where the wall acts as a source of vorticity and the no-slip condition is satisfied.

The acoustic waves are created by initiating an additional transient component of mass addition, $\widehat{V}_w(x,t)$, at $t = 0^+$. In general the acoustic pressure field is $O(M)$ relative to the $O(1)$ spatially homogeneous field pressure, and the $O(M^2)$ pressure variation associated with the steady injection. On the acoustic time scale of the rectangle, the acoustic pressure $\widehat{P}_0(x,y,t)$ is described by a classical membrane equation with boundary conditions that represent the effects of transient wall mass addition.

Explicit results are obtained for the case $\widehat{V}_w \sim [1-\cos(\omega t)]\cos(\pi x/2)$. For most values of ω the solution is written as a benign superposition of a quasi-steady bulk response to the driving frequency, along with an axial wave pair and an infinite set of oblique wave pairs. However, when

ω is equal to certain eigenvalue numbers, modal resonance occurs and one finds explicit modes with linear amplitude growth with time.

Table 1 contains results for a system where the acoustic time $t'_A = 10^{-3}$s and the aspect ratio (length to width) $\delta = 5$, so that dimensional frequencies can be considered. When $\omega' = 125$ Hz the response is bounded and is composed almost entirely of a purely axial mode and the y-independent part of the quasi-steady solution. Beats are observed when $\omega' \approx 242$ Hz, the response arising primarily from the same modes as in the previously discussed case. Linear monotonic amplitude amplification is seen in Fig. 1 for the purely axial mode when $\omega' \approx 250$ Hz.

When $\omega' \approx 5000$ Hz, a linearly amplifying oblique mode is found in Fig. 2 at $y = 0.1$. The periodic modulation is due to the interference of the purely axial wave. Quite elongated beats, whose initial growth portion resembles the amplifying wave pattern in Fig. 2, are observed at the slightly lower frequency $\omega' \approx 4992$ Hz. The beats arise from an interaction of the first oblique mode with the second mode in the quasi-steady solution.

The results demonstrate that relatively simple boundary driven disturbances can produce a complex acoustic wave response in a semi-confined geometry. At or near the resonant driving frequencies explicit modal amplification occurs. Even in the case of beats, amplitudes can become large enough during the growth phase to render the perturbation approximation invalid. Clearly one must resort to a weakly nonlinear theory to describe acoustic evolution on a longer time.

Higher order linear acoustic theory shows that in addition to modal amplification arising from boundary driving, other sources of instability include quadratic and cubic acoustic wave interactions and refraction of the basic acoustics by the shear flow. The latter effect creates yet more wave complexity of the type described by Wang & Kassoy (1992a,b).

The results described are limited by a simplified boundary condition at the open end of the geometry (a pressure node) and by the lack of feedback between the transient wall injection and the pressure field, which could be described by a wall admittance function of some type. The pressure node boundary condition is of some importance because it implies that no work is done at the exit boundary. As a result the acoustic energy evolution in the cavity depends only upon the work done on the injection surfaces.

2. Role of Eigenfunctions in Weakly Nonlinear Acoustic Resonance

Traditional studies of acoustic instability in solid rocket engines are based upon the concept of normal mode expansion (e.g. Culick 1990; Price & Flandro 1991). The acoustic wave field is represented for mathematical convenience and simplicity in terms of the superposition of eigenfunctions for a closed chamber with rigid walls. These eigenfunctions do not accommodate transient mass transport associated with propellant gasification, or velocity disturbance at the nozzle entrance. The consequences of employing the wrong eigenfunctions in a higher order weakly nonlinear stability calculation, on the predicted solution behavior are unknown.

We use a simple model problem to investigate the impact of eigenfunction choice on the stability properties of flow in a tube, driven by an oscillatory piston at one end. The piston displacement is assumed small relative to the tube length, and the characteristic piston Mach number $\epsilon \ll 1$. The condition at the other end of the tube is either closed (velocity node) or perfectly open (pressure node), and in each case the appropriate eigenfunctions are used.

A systematic perturbation procedure is employed to solve an initial-boundary value problem based on the Euler equations. When the wave field is confined by a closed endwall, the linear asymptotic solution at the resonant frequency $\omega = \nu\pi$ (ν = integer) suggests that a limiting velocity amplitude $u \sim \epsilon^{1/2}$ is reached as $t \sim \epsilon^{-1/2}$. A two-timescale expansion based on the fast acoustic time t and the slow growth time $\tau = \epsilon^{1/2}t$ is employed to obtain uniformly valid solutions,

Table 1. Acoustic Response Properties for Several Forcing Frequencies

ω	ω' (Hz)	Properties	Primary Response
$\pi/4$	125	stable	axial + y-independent quasi-steady modes
$\pi/2 - 0.05$	242	beats	(same)
$\pi/2$	250	axial amplification	linear growth
$5\pi \approx \Omega_{10}/2$	2500	stable	axial + smaller high frequency modes
$\Omega_{10} - 0.05$	4992	beats	first oblique mode + quasi-steady mode with axial wave modulation
Ω_{10}	5000	oblique amplification	linear growth of first oblique mode + axial wave modulation

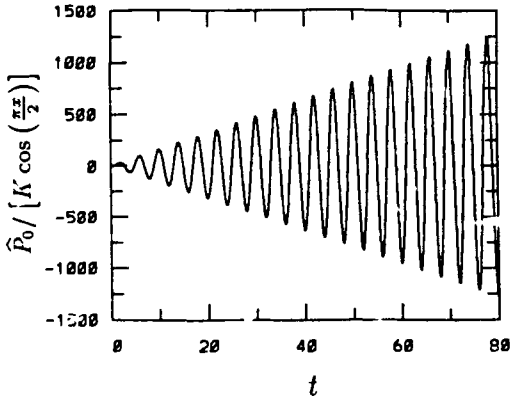

Figure 1: Resonant response of the normalized acoustic pressure for $\omega' \approx 250$ Hz, driven by transient sidewall mass injection.

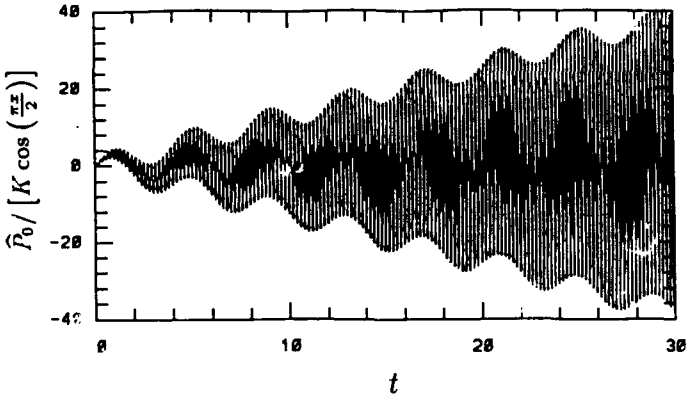

Figure 2: Resonant response of the normalized acoustic pressure at $y = 0.1$ for $\omega' \approx 5000$ Hz, driven by transient sidewall mass injection.

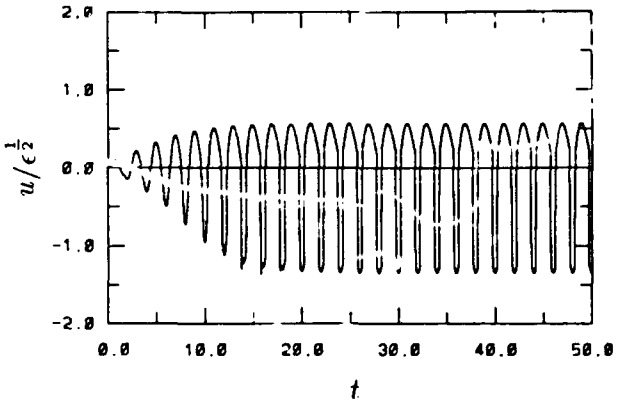

Figure 3: Nonlinear velocity response in a closed tube at $x = 1/4$, driven by an oscillatory piston; $\omega = \pi$ and $\epsilon = 0.01$.

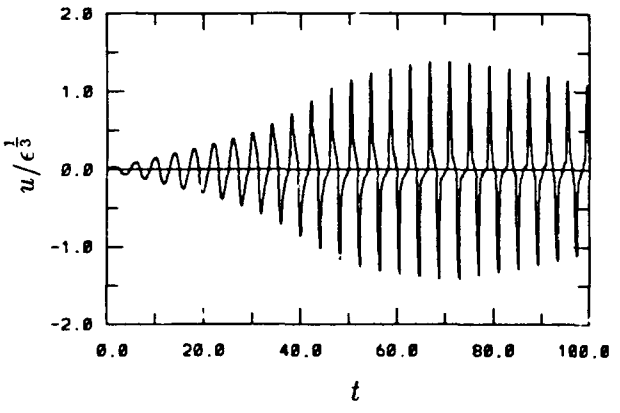

Figure 4: Nonlinear velocity response in an open-ended tube at $x = 1/4$, driven by an oscillatory piston; $\omega = \pi, 2$ and $\epsilon = 0.008$.

expressed in terms of summations of standing wave modes with slowly varying amplitudes. The τ-dependent Fourier coefficients are governed by an infinite system of coupled, first order ordinary differential equations. Due to the cumulative nature of the quadratic mode-coupling, wavefronts steepen to form shocks when $\tau = O(1)$. The internal dissipation associated with the shocks damps the growth of the amplifying wave field and a limit cycle is approached.

In an open tube (pressure node in the exit) the νth mode becomes resonant if the driving frequency $\omega = (\nu - 1/2)\pi$. The correct slow time used to carry out the multiple-scale analysis is $\tau = \epsilon^{2/3}t$, and the limiting amplitudes of the velocity and acoustic pressure are of $O(\epsilon^{1/3})$, considerably larger than that for the closed tube case. This arises because the mode coupling terms in the secular equations are cubic, the system is less prone to shock formation, and as a result energy dissipation effects are small. The wave amplification is ultimately limited by the corresponding frequency and phase shift relative to the piston motion, which renders the boundary work input by the piston zero or even negative.

Truncated versions of the coupled system can be integrated on a computer for both the open and closed resonant tubes. Results using a small number of modes are shown to be capable of describing the initial linear growth and evolution to the maximum amplitude. Subsequently, the solutions deteriorate due to poor convergence of the finite Fourier sums associated with the formation of shock or steep fronted waves. A computational solution is also developed, based on the MacCormack scheme, to complement the perturbation-based solutions and to carry out the calculations to longer time. The two types of solutions compare well.

Figs. 3 and 4 depict the time variations of the acoustic velocity at the axial location $x = 1/4$ in a resonant tube with closed and open end at $x = 1$, respectively. The oscillatory piston velocity is $U_p = \epsilon \sin(\omega t)$. In Fig. 3 $\epsilon = 0.01$ and $\omega = \pi$, the lowest resonant frequency for the closed system. The velocity curve shows clearly the initial linear growth leading to the appearance of a weak shock and the limit cycle behavior. In an open tube the first resonance occurs at $\omega = \pi/2$. The velocity response, depicted in Fig. 4 for $\epsilon = 0.008$, also shows the development of steep wavefronts whose properties are currently being investigated. The amplitude of oscillation reaches a maximum and then decreases, forming a beat-like pattern. It is likely that this pattern repeats for numerous times with decreasing amplitude variations and eventually settles down to a constant amplitude, limit cycle oscillation.

In summary, this study demonstrates the drastic influence of the boundary acoustic properties on the time-evolution and limiting amplitudes of the confined wave field. Due to the cumulative nature of the quadratic nonlinearity, normal mode approximation always leads to the quick formation of shock waves. This may generate erroneous results and overpredict damping mechanisms. More exact representations of system eigenfunctions in rocket engine chamber models should be explored in the future.

REFERENCES

Culick, F.E.C. (1990) AIAA–90–3927, 13th Aeroacoustics Conference.

Price, E.W. & Flandro, G.A. (1991) *Combustion Instability in Solid Propellant Rockets*, book manuscript in preparation.

Wang, M. & Kassoy, D.R. (1992a) *J. Fluid Mech.* **238**, 509–536 (in press).

Wang, M. & Kassoy, D.R. (1992b) *AIAA Journal*, in press.

FLAME DRIVING AND FLOW TURNING LOSSES IN SOLID ROCKETS

(AFOSR Grant/Contract No. 91-0160)

Principle Investigators: B. T. Zinn and B. R. Daniel

School of Aerospace Engineering
Georgia Institute of Technology
Atlanta, GA 30332

Summary/Overview:

The goal of this research program is to investigate the driving and damping of axial instabilities in solid propellant rocket motors due to gas phase solid propellant combustion and flow turning. This program began with an investigation of the responses of premixed and diffusion flames, stabilized on the side wall of a duct, to an imposed axial acoustic field. The current phase of this study is concerned with developing a greater understanding of the processes that control the flow turning loss and the role of this loss in the damping of combustion instabilities in solid rocket motors. This investigation consists of three parts: a theoretical study, a numerical simulation, and an experimental investigation. First, a theoretical approach that could be used to correlate the experimental data was developed. Next, a numerical simulation was developed to determine the behavior of the various terms that appear in the developed theoretical stability prediction equation. In the experimental phase, the response of an imposed acoustic field in a duct to mass injection from the sidewall was investigated. The mean and acoustic velocities as well as the acoustic pressure oscillations were measured throughout a control volume in the region where the flow turning loss was expected to occur. The measured data were then used to evaluate the terms of the acoustic stability equation. The behavior of the measured flow turning loss was found to agree with model predictions. Current efforts are directed toward incorporating non-isentropic effects into the developed theoretical model, in order to account for the effect of axial temperature gradients encountered in hot flow experiments.

Technical Discussion:

The occurrence of combustion instabilities is determined by the relative magnitudes of the driving and damping mechanisms within the combustor that add and remove energy from the oscillations, respectively. In order to eliminate or reduce the severity of acoustic oscillations resulting from combustion instabilities in solid rocket motors, the mechanisms by which energy is added to and removed from these oscillations must be identified and understood. It is generally accepted that the response of the combustion process of the solid propellent to the presence of acoustic oscillations provides the energy necessary to initiate and maintain

instabilities in rocket motors. Other factors, such as nozzle damping, viscous dissipation and flow turning, tend to remove energy from the oscillations and thus stabilize the system. In previous phases of this program, the mechanisms by which the gas phase combustion processes contribute to the driving of axial acoustic instabilities were investigated. The current program is concerned with the development of an understanding of the flow turning loss mechanism and the appropriateness of using a one dimensional linear approach to analyze the acoustic stability of solid rocket motors.

A theoretical investigation of the flow turning loss was initiated during the previous reporting period in an effort to develop a practical method for experimental verification. The primary result of this analysis was the confirmation that the classical flow turning loss term is indeed a part of the one dimensional acoustic stability equation. As a secondary result, the analysis confirmed Van Moorhem's[1] conclusion that the flow turning loss is not absent from the three dimensional analysis as suggested by Culick[2], but that the "classical flow turning" term can only be isolated after cross sectional averaging. The inability to isolate the flow turning term in a three dimensional stability equation suggests that developing an understanding of the details of the mechanisms that give rise to this term may be very difficult. Next, a new theoretical approach that could be used to determine the flow turning loss from experimental data was developed. In this approach, each of the dependent variables in the governing equations was expressed as a function of a time averaged and a fluctuating component. The acoustic stability equation developed in this analysis lends itself more readily to the verification of experimental results due to the way in which the terms have been defined.

In an effort to determine the behavior of the various terms that appear in the derived acoustic stability equation, the experimental setup used in the flow turning investigation was modeled numerically. This simulation involved the derivation and numerical solution of the mass and momentum conservation equations that describe the experimental setup and the test conditions. In this analysis, the flow was assumed to be isentropic with perturbations that are harmonic in time. The two dimensional forms of the equations were averaged over the cross-section of the duct and then integrated along the axis of the experimental setup. The solutions were then substituted into the developed acoustic stability equation to determine the values of the terms that affect the stability of the system and to determine whether the numerical solution satisfies the stability equation.

The experimental study was conducted in the setup shown schematically in Fig. 1. The setup is designed to simulate flow phenomena near the walls of a solid propellant rocket motor experiencing an axial acoustic instability. It consists of a 2.5 meter long, 3.75 x 7.5 cm^2 duct with a burner mounted on the bottom wall. The burner used in this study is a multi-diffusion flame burner (MDFB) that was developed earlier under this program to simulate gas phase solid propellant flames. The MDFB consists of a matrix of hypodermic tubes supply an oxidizer flow,

---

[1] Van Moorhem, W. K., "Theoretical Basis of the Flow Turning Effect in Combustion Stability," Final Report, AFOSR Grant No. 78-3654, March 1980.

[2] Culick, F. E. C., "Stability of Three-Dimensional Motions in a Combustion Chamber," *Combustion Science and Technology*, Vol. 10, 1975.

simulating the flow of combustion products from burning ammonium perchlorate particles. Fuel is supplied through the spaces between the tubes, which simulates the flow of pyrolysis products from the fuel binder. In cold flow experiments, room temperature air is injected through the burner. To date, only cold flow experiments have been performed due to the present inability of the theory to account for axial temperature gradients in the duct. Two acoustic drivers mounted on opposing duct walls just upstream of the exit plane are used to excite a standing acoustic wave in the duct that simulates an axial instability in a rocket motor. Axial flow is injected at the upstream end of the duct through a movable porous plate injector. The location of the MDFB relative to the standing acoustic wave can be varied by translation of the axial flow injector. Quartz windows in the side walls adjacent to the burner allow for flow visualization and optical diagnostics.

A complete investigation of the cold flow behavior has been performed. For each set of test conditions, the mean and acoustic velocities as well as the acoustic pressure oscillations were mapped in a control volume in the region where the flow turning loss was expected to occur. The measured data were then used to evaluate the terms of the acoustic stability equation developed earlier under this program. Experiments were performed to determine the effects of the frequency and amplitude of the oscillation, the magnitude of the injection and core flow Mach numbers, and the location of the burner relative to the standing axial acoustic wave upon the magnitude of the flow turning loss in the investigated control volume. The measured flow turning losses were observed to be in agreement with the developed model and Culick's predictions.

The numerical simulation was modified to aid in the interpretation of experimental results. The conditions used for the initial numerical simulations were idealized in order to simplify the interpretation of the results. The actual conditions encountered in the experimental investigation are rather complex, and difficult to approximate in a numerical simulation. Therefore, the numerical simulation was modified to use experimentally determined (i.e., measured) boundary conditions. The calculated and measured values of the flow turning loss for a typical test configuration are shown in Fig. 2. Excellent agreement between the measured and calculated values was obtained.

The results of the cold flow tests indicate that current one dimensional linear stability analysis techniques based upon Culick's work correctly predict the flow turning losses in solid rocket motors. Furthermore, this research suggests that, with exceptions, the effects of the terms of the acoustic stability equation that are proportional to the Mach number upon the stability of solid rocket motors will be minor in comparison to the effects of the Mach number independent terms. The objective of the next phase of this project is to include non-isentropic effects in the model that predicts the flow turning loss. This model will be necessary for correlating data measured in following hot flow studies where large temperature gradients are expected to occur. This investigation is expected to produce a stability equation that will differ from those predicted by earlier studies. It is also hoped that the results of this investigation will explain the results of hot flow tests performed previously under this program, which differed significantly from those measured in the cold flow tests.

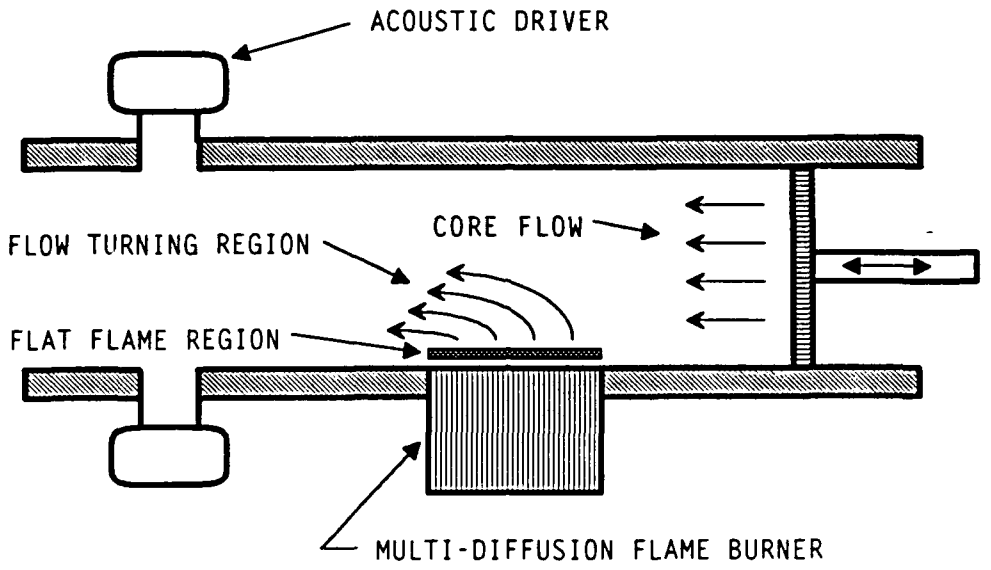

Figure 1. A schematic of the experimetal setup utilized in the investigation of flow turning losses.

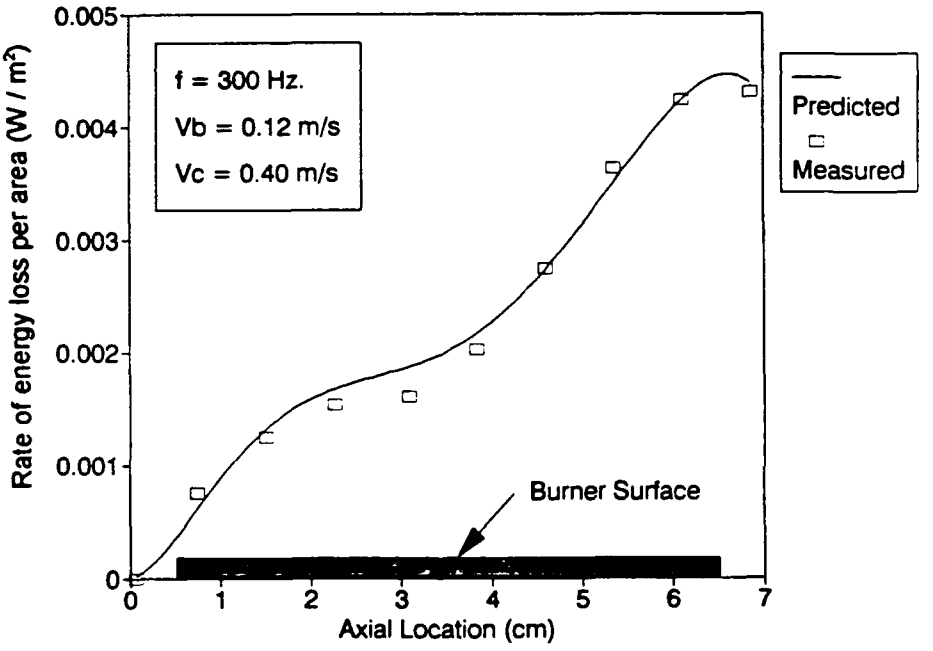

$$\text{FLOW TURNING LOSS} = \left\langle \frac{1}{H} \int_0^x \left(\left\langle u'^2 \right\rangle_y [\overline{m}_b]_0^H \right) dx \right\rangle_t$$

Figure 2. Comparison of measured and predicted values of the flow turning loss for a typical experimental configuration.

Combustion and Plume Studies

D. H. Campbell, I. Wysong, G. L. Vaghjiani, and D. P. Weaver
Phillips Laboratory
Rocket Propulsion Directorate
Edwards AFB, Ca. 93532-5000

In this program, research is performed in the areas of rocket exhaust plume physics and rocket propellant combustion. Both experimental measurements and theoretical computational investigations are carried out. Laser diagnostic techniques are used in both areas to map the properties, such as temperature and density, of gases in various combusting and non-combusting environments. Chemical kinetic measurements are also carried out to determine the specific reaction pathways and kinetic rates for specific reactions of interest. Results of these investigations are used to help in the design of future rocket propellants and to further our understanding of the chemical and collisional processes in rocket exhaust plumes that give rise to emissions in the infrared, visible and ultraviolet spectral regions so that better predictions of these emissions can be used in designing SDI detector systems. Typical results obtained in several of the research areas are detailed below.

During the last year both theoretical and experimental studies have been carried out to investigate the characteristics of the flowfield structure in rapidly expanding high altitude plumes. The Direct Simulation Monte Carlo (DSMC) computational method has been used to investigate the interaction of the plume expansion with a hypersonic atmospheric freestream at altitudes in the 90-150 km range. Traditional scaling laws based on the plume Knudsen number or other distance scales in plume-freestream interactions in the transitional flow regime (densities at which the flow is between the continuum regime and the free molecular regime) have been shown to have limited ability to predict the spatial distribution of density and temperature in these flows. Significant non-equilibrium between the plume and freestream gas components of these flows has also been found. These results indicate that detailed modeling of the type used in these studies will be necessary for accurate prediction of the structure of these flows.

Experimental studies were conducted during the last year in order to test and verify DSMC flowfield predictions. Laser-induced fluorescence (LIF) of nitric oxide has been developed as a diagnostic technique. LIF measurements, after being properly corrected for quenching effects and rotational partition function, yield number density and rotational temperature at a given point in the flowfield and have excellent sensitivity (10^{12} cm^{-3}) and spatial resolution. Results for the temperature and number density along the symmetry axis of a vacuum plume expansion show good agreement with predicted values. Attempts to measure the rarefied, high-angle region of the flowfield were frustrated by background gas interference due to limited pumping capacity for the LIF-NO measurements. Therefore, a pulsed jet orifice was installed and used as a nozzle source. Results from the high-angle region of the pulsed jet flowfield show good agreement with calculations (Figure 1). Experimental studies on argon and nitrogen expansion using the electron beam fluorescence technique have also been conducted.

Construction of a second-generation, higher flux atomic oxygen source flow was started. This new continuous source is housed in a cryogenically-pumped cell that can provide a flowfield simulation of the plume/freestream interaction. Initial work with the new source has demonstrated at least an order of magnitude increase in oxygen flux and a

much reduced energy spread. Initial collisional studies have demonstrated excitation with both nitrogen and oxygen species.

A discharge-flow/flash-photolysis apparatus to study elementary gas phase reactions important in the oxidation of hydrazine was constructed and tested out. Test reactions, $OH + H_2O_2 \rightarrow H_2O + HO_2$, and $H + CH_3SH \rightarrow H_2 + CH_3S$ were studied in this new apparatus. The measured reaction rate coefficients at 298 K were in excellent agreement with the recommended values in the literature. The apparatus has a high detection sensitivity for OH, H and O radicals whose chemistry with hydrazine propellants will be investigated in this work. Specific work on hydrazine includes the measurement of the ultraviolet absorption cross sections at 298 K in the wavelength range from 200 to 285 nm (see Figure 2). Further, the quantum yield of $H(^2S)$ production during 248 and 222 nm photodissociation has been measured. This was found for 248 nm photolysis of N_2H_4 to be 0.82, +/- 0.10. Additionally, a Burke-Schumann diffusion flame chamber has also been constructed and test emission spectra of $CH_4 + O_2$ flames are currently being collected using a two dimensional ccd-detector. A high-pressure/high-vacuum gas handling system has been constructed for making appropriate gas mixtures to be used in this work.

Our continuing propellant combustion studies involve the use of laser-induced fluorescence (LIF) and emission spectroscopies for the characterization of species and temperature in premixed, laminar, flat-flames of $CH_4/NO_2/O_2$, $CH_4/NO/O_2$ and CH_4/N_2O at 55 Torr. Relative concentration profiles were obtained for the following species: OH, CH, NO, NH, NO_2, and CN. Temperatures were measured by rotational analysis of OH radical LIF excitation spectra and yield a peak temperature of ≈2400 K. Chemical kinetic modeling of a 252 reaction, 54 species mechanism was performed using the Sandia Chemkin-II/Premix flame codes in order to obtain mechanistic information. In addition to such mechanistic information, flame laser diagnostic experiments can be used to pinpoint specific elementary reactions in the nitrogen chemistry mechanism that require further study. We have set up a new experiment that permits us to directly measure the rate constants for reactions whose kinetic parameters are found to be lacking in accuracy. This experiment is a two laser photolysis/laser-induced fluorescence (LIF) system. The first laser, a KrF excimer at 248 nm, is used to photolyze a precursor species, such as H_2O_2, to generate a radical species, in this case OH. The second laser, at a varying time delay, is used to probe the relative concentration of the radical by LIF. A cell was constructed out of quartz and allows rates to be measured from room temperature to 1000 K. Initial experiments have involved measurements of the termolecular reaction, OH + NO + M -> HONO + M. This reaction has been implicated in the lack of agreement seen in the above flame experiments for the absolute concentration of OH radicals. These data were taken as a function of temperature, pressure, and third-body species. Temperatures from 300 to 430 K were employed. Pressures from 50 to 400 Torr and argon, SF_6, and N_2 bath gases were used. These data provide the most complete measurements of this termolecular reaction to date.

Vacuum expansion of NO - Measured plume number density compared with DSMC computational results

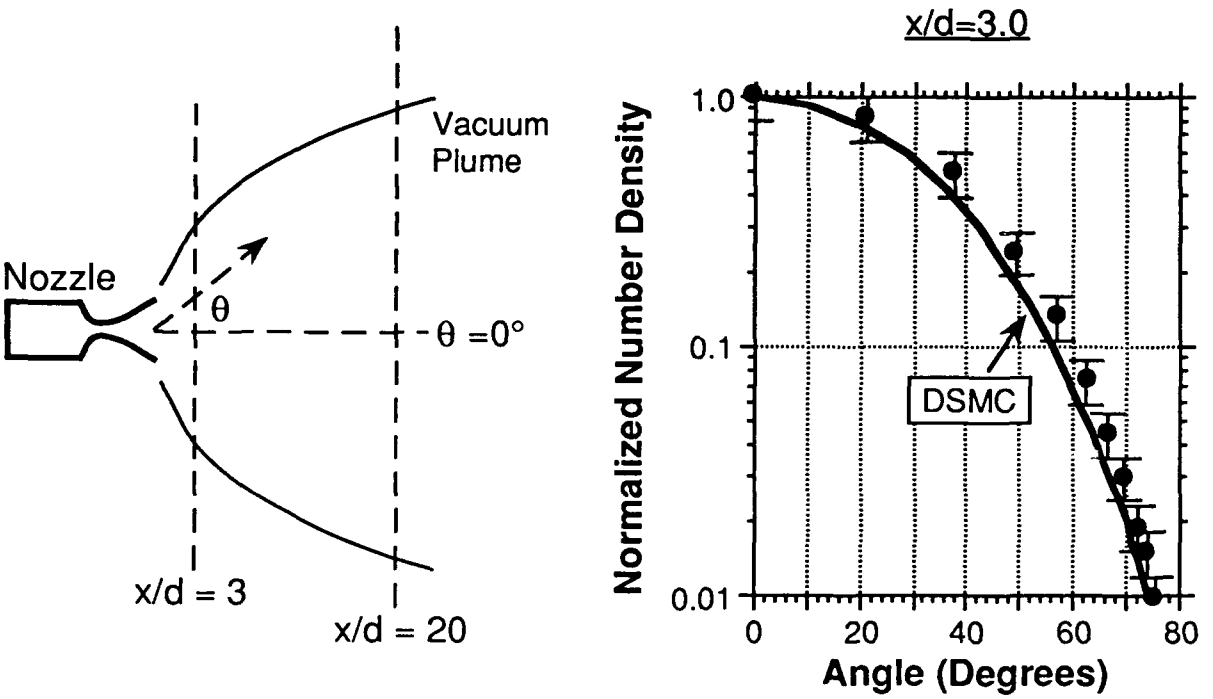

Results - DSMC accurately predicts high angle vacuum expansion flowfields

Research Significance - An accurate, validated flowfield computation for high radiant flows allows investigation of rarefaction influences on nonequilibrium

AF Significance - Verified DSMC technique can be used to examine breakdown limits in transition flow regime for continuum codes - Influence of phenomenological models can be quantified

Figure 1: Rarefaction influences on plume expansion flowfields - off axis number density comparison.

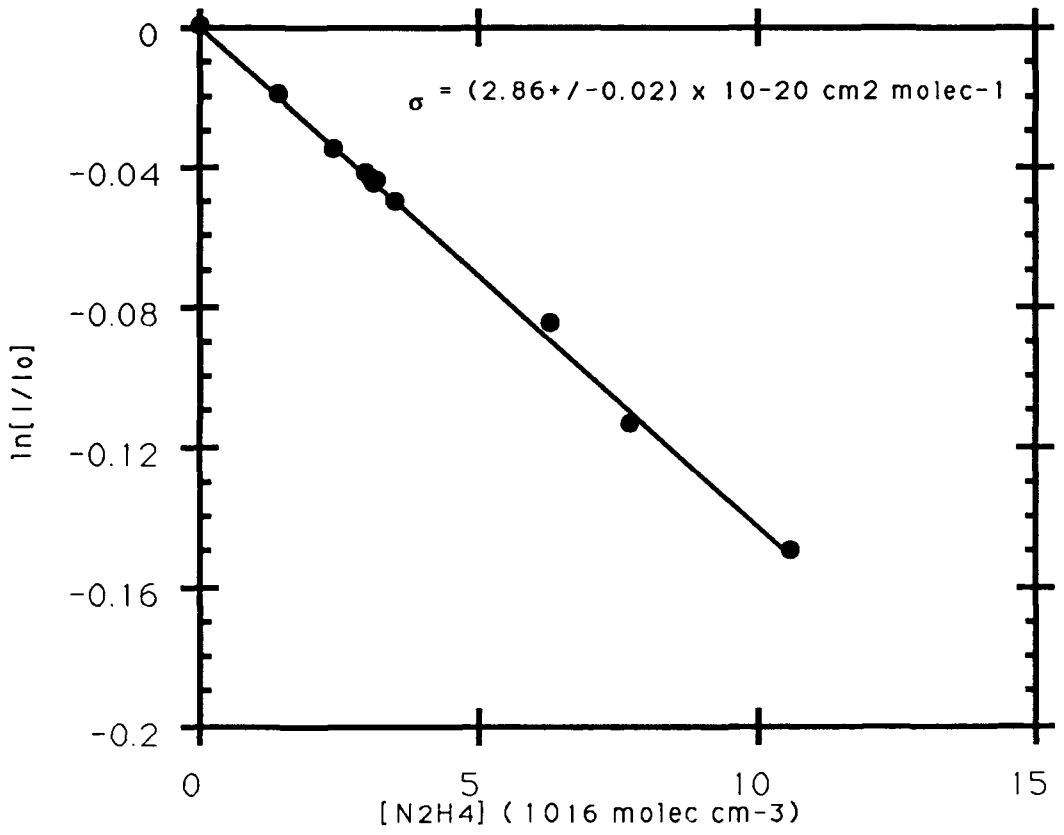

Figure 2: Hydrazine absorption cross section at 253.69 nm from measured absorption intensities.

PARTICLE DISPERSION IN TURBULENT SPRAYS

AFOSR Grant No. 89-0392

Principal investigators: I.M. Kennedy and W. Kollmann

MAME Department, University of California at Davis, CA 95616

SUMMARY:

Highly accurate finite-difference methods were developed for the simulation of the flow fields in turbulent round jets. The dynamics of particles released at the nozzle center were calculated numerically and their statistical properties compared to measurements. Measurements have been made of the Lagrangean auto-correlation over a wide range of Stokes number. In addition, the dispersion of vapourizing droplets in a heated jet has been studied.

TECHNICAL DISCUSSION

I. Numerical simulations.

The computational part of the project was concentrated on the simulation of Lagrangean particle dynamics in turbulent round jets. The simulation of turbulent flow fields in round jets was based on finite-difference methods, which offer the flexibility necessary for the treatment of non-periodic jet flows emitting from nozzles and the consideration of a variety of exit conditions. Furthermore, the influence of disturbances created at the jet pipe exit on the flow development can be studied.

Solution method.

Mass and momentum balances are set up in cylindrical coordinates for the primitive variables velocity and pressure. Stretching transformations are applied to the axial and radial directions to concentrate the grid points in the regions of interest. The discretization of the Navier-Stokes equations requires finite-difference approximations for time and space derivatives. Several versions offering different levels of accuracy were developed. The time derivatives were discretized using the three-point backward Adams-Bashfort scheme, which is second order accurate, and a third order accurate Runge-Kutta scheme. The convective terms in the momentum balances were discretized using a fully windward biased scheme and compact (Hermitian) differencing. The present compact scheme is fourth order accurate and can be extended to even higher accuracy without difficulty. The solution procedure consists of explicit solution of the momentum balances coupled with an PSOR algorithm for the pressure and velocity corrections to enforce mass balance. The time step was automatically adjusted in accordance with stability analysis.

The boundary conditions for velocity were set up to reflect the experimental conditions at the entrance section and zero normal derivative at the exit section. The axis $r = 0$ is

not a real boundary but requires conditions to ensure the smooth variation of the velocity components as the axis is crossed. The boundary conditions for the pressure and the pressure correction were zero normal derivative at entrance and exit sections and zero value at the outer boundary.

Fig.1 Iso-enstrophy surface in a round jet.

The initial conditions were set up as the inviscid solution consisting of the entrance profile for the axial velocity component extended through the whole flow field and the radial and circumferential components set to zero. The initial pressure and pressure correction were set to zero. In addition to the inviscid solution disturbances were introduced at the entrance section. These disturbances were chosen satisfying mass balance and having a known energy spectrum. Only two modes were selected for the results to be presented.

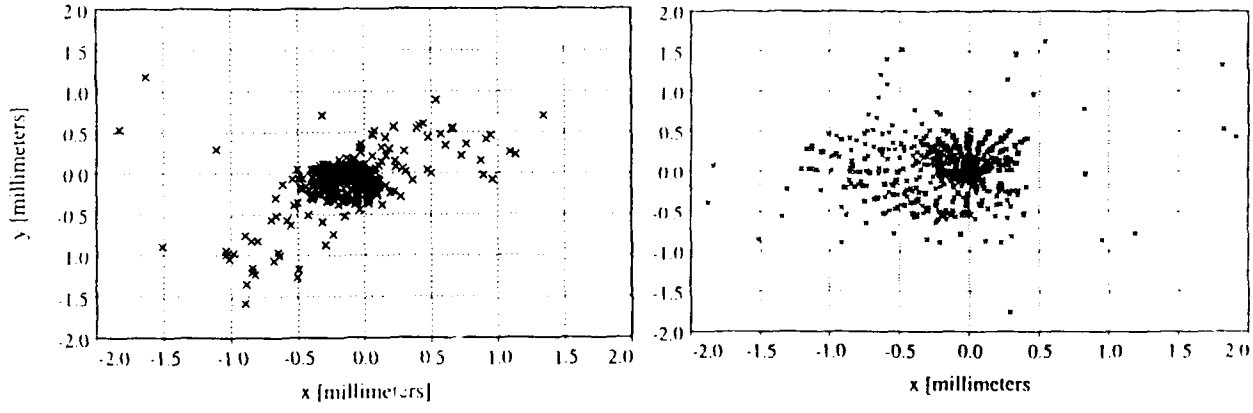

Fig.2 Scatter plots for fluid points (right graph) and hexadecane particles (left graph).

Particle dynamics.

Fluid particles (fluid material points) and solid particles were considered. The Lagrangean position field for fluid material points requires integration of the kinematic relation between velocity and position. This was carried out using the second order accurate trapezoidal method coupled with second order Bezier splines for the interpolation of velocity in three dimensions. The calculation of the pathlines of the solid particles requires the solution of the approximate momentum balance for the particles taking into account drag force and

buoyancy terms.

Selected results.

The simulation of the flow in round jets at a Reynolds number $Re = 15000$ based on the entrance conditions is illustrated in Fig.1 showing an iso-enstrophy surface. Vorticity shows a rich variety of structures which can be classified as braided and helical in the larger scale range and random in the small scale range. The particles are transported by these structures and two scatter plots for fluid (right graph) and solid particles (left graph) are shown in Fig.2 at $x/D = 10$. The solid particles show significantly less dispersion than the fluid material points. Detailed evaluation and comparison with the measurements will be presented for several axial stations up to $x/D = 40$.

II. Experiments.

The theoretical description of particle dispersion relies upon an understanding of the autocorrelation function for particle velocity. There exists experimental evidence for autocorrelation functions for particles with a range of inertia in grid generated turbulence, but there is no corresponding information available on Lagrangian particle autocorrelations for turbulent shear flows such as the round jet. The information that the autocorrelation can yield is doubly important because it provides information on Lagrangian time scales in a shear flow. Time scales are important in applying stochastic simulations of particle dispersion. A novel experimental method has been employed in our experiments to obtain these data.

Two co-planar laser sheets are formed with a beam splitter and a right angle prism. As a particle passes through the sheets, two spikes are observed with the photodetector. The signals are digitized and the timing information permits the velocity to be measured. The two sheets are directed back through the flow with a retroreflector; movement of the retroreflector in a direction that is normal to the beams allows us to vary the spacing of the two pairs of laser sheets. The minimum separation is approximately 12 mm and the greatest separation is about 68 mm.

Measurements of particle velocities have been obtained in the air jet that we have used for all our tests. The nozzle diameter is 7 mm and the Reynolds number based on this diameter is 15.000. Droplets of hexadecane were used. In room temperature air, they can be considered as non-vaporizing over the duration of their residence time in the jet. The droplet diameters ranged from 35 μm to 160 μm. The mean velocity profiles are shown in Fig. 3 along with stochastic simulations.

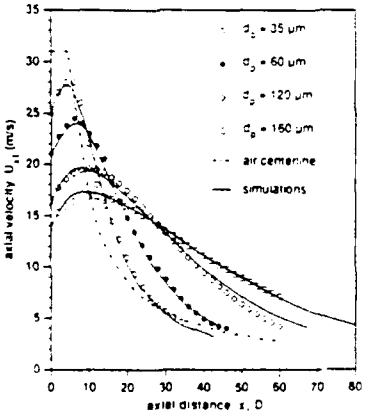

Fig.3 Mean droplet velocities.

Initially, the droplets lagged behind the air flow as they left the nozzle; the mean centerline

axial velocity of the air is shown as the dashed line in the figure. The 35 μm droplets quickly equilibrated with the air flow and they behaved like fluid particles in terms of the mean velocities. The larger particles exhibited quite substantial velocity slip compared to the surrounding air flow. The stochastic simulations did a reasonable job of predicting the mean particle velocities.

The data have been analyzed to yield the Lagrangian autocorrelation functions by sorting through the full data sets to extract data at a given time of flight from the nozzle. At a given time of flight we then find the correlation of particle axial velocity as a function of time increment. The results for 50 μm droplets are shown in Fig. 4 for times of flight of 14 and 20 ms. The autocorrelations for these droplets are approximately exponential.

Vaporizing droplets of pentane have been studied in an isothermal room temperature jet of air and in a heated turbulent air jet. In the latter case, the jet was heated to 60°C. In the isothermal case, the droplets experienced only unsteadiness in the velocity field while in the heated jet they also experienced unsteadiness in temperature. Hexadecane droplets were also used under both conditions to offer a wide range in volatilities at these temperatures. A slide impaction method was used to measure the droplet diameters. The results for the particle dispersion are shown in Fig. 5.

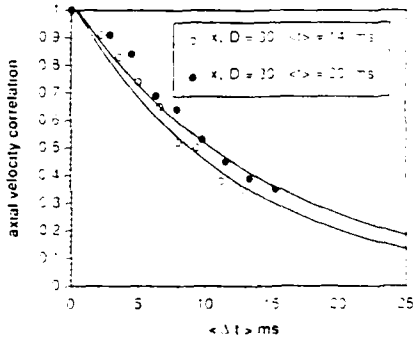

Fig.4 Lagrangean velocity auto-correlation function for 50μm Hexadecane droplets.

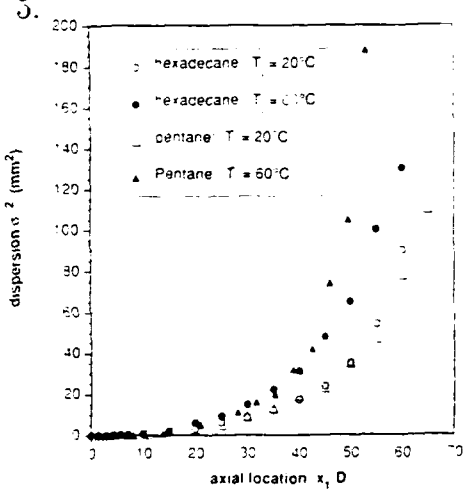

Fig.5 Dispersion of 115μm hexadecane and pentane droplets.

It appears that the effect of raising the jet temperature is to increase the rate of particle dispersion. Much of the increase in dispersion can be attributed to the decreasing size of the droplets as they vaporize. Measurements of the droplet diameters for pentane indicated that they decreased from 115 μm at the nozzle exit to about 80 μm at 60 nozzle diameters downstream in the isothermal air jet and to about 45 μm in the heated air jet. The d^2 law was found to be completely inadequate in predicting the droplet size. In addition, the stochastic simulation with a "thin-skin assumption" for droplet conduction yielded unsatisfactory results as well. Our results suggest that the stochastic simulations do a reasonable job of predicting particle velocities but the mass and heat transfer aspects may need further attention, particularly in terms of correlations of mass and heat transfer for turbulent flows.

DROP/GAS INTERACTIONS IN DENSE SPRAYS

(AFOSR Grant No. 89-0516)

Principal Investigator: G.M. Faeth

218 Aerospace Engineering Building
The University of Michigan
Ann Arbor, Michigan 48109-2140

SUMMARY/OVERVIEW

Secondary drop breakup and turbulence modulation (the turbulence field generated by drops) are being studied. Work on secondary drop breakup has yielded information on the regimes, dynamics and outcomes of drop deformation and breakup, using pulsed holography and phenomenalogical theories. An interesting feature of these results is that both deformation and breakup are inhibited by liquid viscous forces at the high Ohnesorge numbers reached by drops as they approach their thermodynamic critical point during high pressure combustion. Work on turbulence modulation has shown that drop-generated turbulence differs from conventional turbulence and has provided a means of estimating the properties of this flow based on a stochastic theory for randomly-arriving particle wakes. Motivated by this finding, current work is concentrating on the properties of low Reynolds number wakes (typical of conditions in sprays) in nonturbulent and turbulent environments.

TECHNICAL DISCUSSION

Introduction. Past work on the structure of dense sprays in this laboratory has highlighted the importance secondary breakup and turbulence modulation (Faeth, 1990; Ruff et al. 1989, 1991, 1992; Wu et al. 1991, 1992); current work concerning these processes is discussed in the following:

Secondary Breakup. Studies of liquid atomization have shown that drops produced by primary breakup generally are unstable to near-limit secondary breakup (Ruff et al. 1991, 1992; Wu et al. 1991, 1992). Thus, this phase of the investigation is studying secondary breakup. The following discussion of the research is brief, see Hsiang and Faeth (1992) for more details.

The breakup of individual drops is observed within a windowed shock tube. Flash cinematography is used to observe overall behavior; pulsed holography is used to resolve the outcome of breakup; and phenomenalogical theories are used to help interpret the measurements.

The deformation and breakup regime map of Fig. 1 has been developed to help organize the problem. This involves identifying various regimes in terms of the Weber and Ohnesorge numbers, We and Oh. The boundaries of the three well known breakup regimes (shear, multimode and bag breakup) have been identified, along with several new deformation regimes. Large Oh inhibits all forms of deformation and breakup; such conditions are reached as drops approach their thermodynamic critical point during high pressure spray combustion. This implies that earlier hypotheses that drops shatter near their thermodynamic critical point (Faeth 1990) should be reexamined.

Various characteristics of breakup and deformation have been measured and analyzed: time of maximum deformation and initiation of breakup, breakup times, maximum and minimum drop dimensions, drop drag coefficients during breakup, etc, see Hsiang and Faeth (1992). Drop size distributions after secondary breakup satisfied Simmons (1977) universal root normal distribution with the ratio of the mass median (MMD) to the Sauter mean (SMD) diameter equal to 1.2; therefore, drop size distributions can be represented by the SMD alone. SMD after secondary breakup are plotted in terms of a phenomenalogical theory of shear breakup in Fig. 2 (ρ = density, u_0 = initial relative velocity, σ = surface tension, μ = viscosity, d = initial drop diameter, and the subscripts G and L denote gas and liquid properties). Remarkably, a single correlation is effective for all three breakup regimes.

The breakup regime criteria marked in Fig. 2 suggest that drops are unstable to subsequent breakup if relative velocities are unchanged. Subsequent breakup is not observed, however, in part because relative velocities decrease, but mostly because rates of drop acceleration decrease, over the period when breakup occurs. This has provided a unified treatment of drop stability to breakup for processes as disparate as breakup for both step and gradual changes of relative velocities as well as the termination of shear breakup (which leaves a large drop-forming drop). Current work is pursuing this issue through measurements and analysis of drop size and velocity correlations after secondary breakup.

Turbulence Modulation. Turbulence modulation controls turbulence properties in dense sprays (Faeth 1990, Ruff et al. 1991, 1992). Parthasarathy and Faeth (1990) and Mizukami et al. 1991) have measured this flow and found a stochastic approach (based on random arrival of wakes), analogous to theories of noise (Rice 1954), that explains many of its features. Definitive evaluation of the theory was not possible, however, due to lack of information about drop wakes at the low Reynolds numbers (less than 1000) of interest for sprays. Thus, present work involves measurements of low Reynolds number sphere wake properties in both nonturbulent and turbulent environments.

Results for nonturbulent environments are reported by Wu and Faeth (1992). It was found that the wakes remained turbulent down to wake Reynolds numbers, $Re_w \approx 10$. This behavior is illustrated in Fig. 3, which is a plot of mean streamwise velocities, $\bar{u}$, as a function of radial distance r, in similarity coordinates for turbulent wakes, see Wu and Faeth (1992) for other notation. Remarkably, mean velocities at low Re_w satisfy the same scaling as the highly turbulent wakes of Chevray (1968): this confirms behavior suggested by turbulence modulation measurements (Mizukami et al. 1992). The decay of the turbulent wake, and its eventual transition to a laminar wake, can be seen from the plot of turbulence intensity along the axis as a function of Re_w in Fig. 4. For $Re_w > 70$, the turbulence intensity is roughly 85%, similar to strongly turbulent wakes. As laminar wake conditions are approached, however, the turbulence intensity becomes proportional to $Re_w^{7/4}$, which is consistent with theoretical scaling proposed for the final decay period of turbulent axisymmetric wakes (Phillips 1956). At $Re_w < 10$, measured mean velocities satisfy laminar wake similarity theory in spite of the continued slow decay of turbulent-like fluctuations; an explanation of this behavior is that unconnected turbulent spots are decaying so that mixing is dominated by laminar processes (Wu and Faeth 1992).

At present, low Reynolds number wakes in a turbulent environment are being studied. Initial findings are that large ambient turbulent intensities yield laminar-like scaling of mean velocities but with a high effective turbulent viscosity, while low ambient turbulence intensities yield scaling similar to quiescent environments. This work is continuing in order to provide a rational closure for the stochastic turbulence modulation theory.

REFERENCES

Chevray, R. (1968) J. Basic Engr. 90, 275-284.

Faeth, G.M. (1990) Twenty-Third Symposium (International) on Combustion, The Combustion Institute, Pittsburgh, 1345-1352.

Hsiang, L.-P. and Faeth, G.M. (1992) Int. J. Multiphase Flow, in press.

Mizukami, M., Parthasarathy, R.N. and Faeth, G.M. (1992) Int. J. Multiphase Flow, in press.

Parthasarathy, R.N. and Faeth, G.M. (1990) J. Fluid Mech. 220, 485-537.

Phillips, O.M. (1956) Proc. Cambridge Phil. Soc. 52, 135-151.

Rice, S.O. (1954) in Noise and Stochastic Processes (N. Wax, ed.) Dover Publications, New York, 133.

Ruff, G.A., Sagar, A.D. and Faeth, G.M. (1989) AIAA J. 27, 901-908.

Ruff, G.A., Bernal, L.P. and Faeth, G.M. (1991) J. Prop. Power 7, 221-230.

Ruff, G.A., Wu, P.-K., Bernal, L.P. and Faeth, G.M. (1992) J. Prop. and Power 8, 280-289.

Simmons, H.C. (1977) J. Engr. Power 99, 309-319.

Wu, J.S. and Faeth, G.M. (1992) AIAA J., submitted.

Wu, P.-K., Ruff, G.A. and Faeth, G.M. (1991) Atom. Sprays 1, 421-440.

Wu, P.-K., Tseng, L.-K. and Faeth, G.M. (1992) Atom. Sprays, in press.

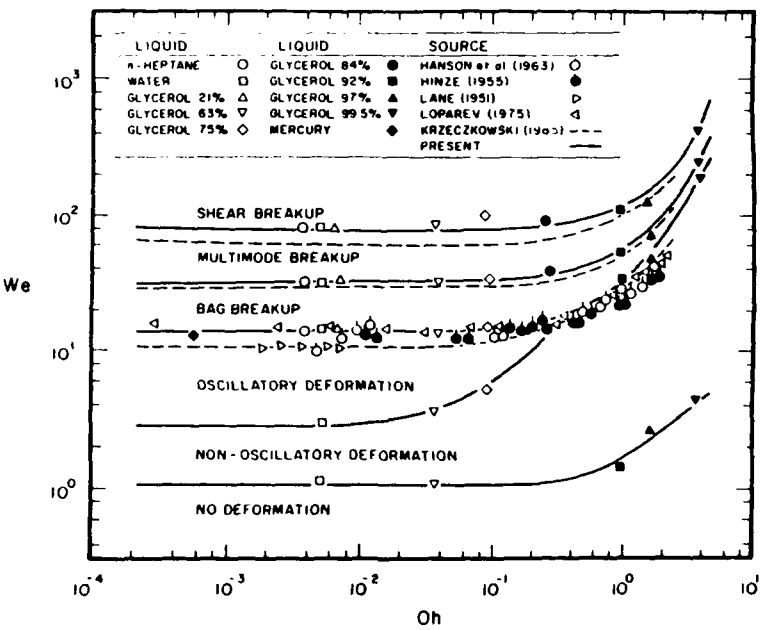

Fig. 1 Drop deformation and breakup regime map.

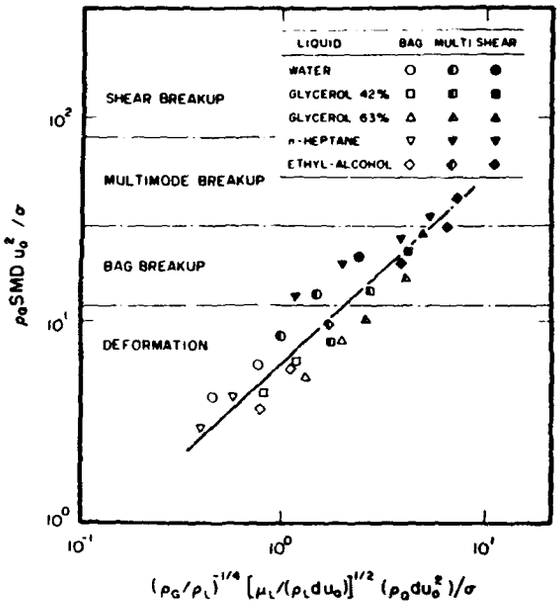

Fig. 2 Correlation of SMD after secondary breakup.

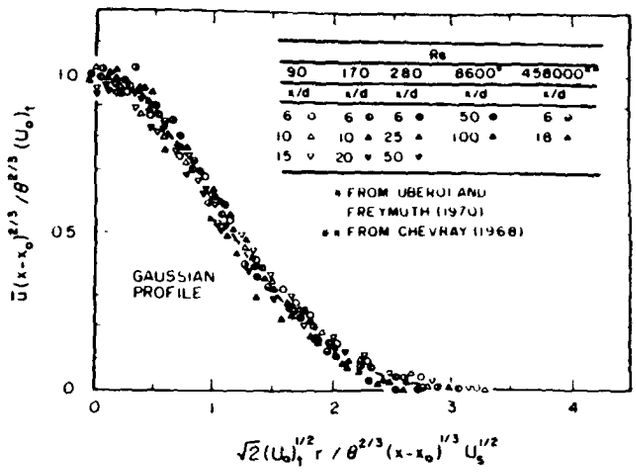

Fig. 3 Mean streamwise velocities in the turbulent wake region.

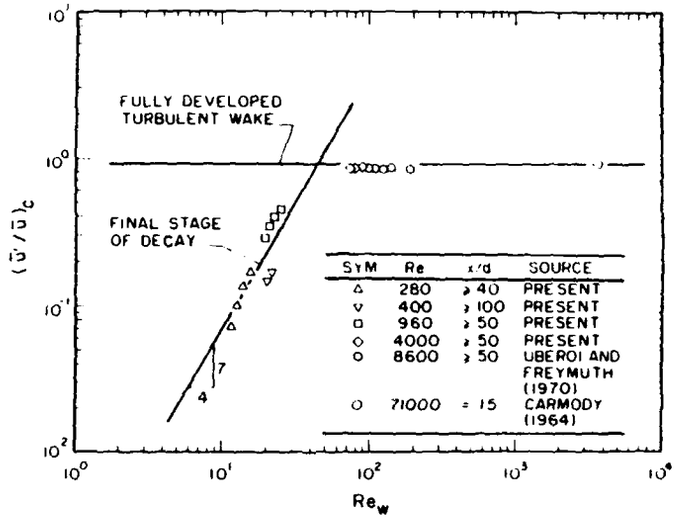

Fig. 4 Streamwise turbulence intensities along the axis as a function of wake Reynolds number.

TRANSVERSE LIQUID JET IN HIGH-SPEED CROSSFLOW

AFOSR TASK 2308BW

Nejad, A. S.
Aero Propulsion and Power Directorate
Wright-Patterson AFB, Ohio 45433-6523

SUMMARY/OVERVIEW

A laser sheet imaging technique was applied to acquire images of liquid jet in high-speed crossflow. Jet penetration height and trajectories were compared with the empirical formulations of Wotel et al., Chelko, Hojnacki, and Baranovsky and Schetz. Some of the formulations predicted the maximum penetration height adequately but failed to match the spray profile (jet trajectory) satisfactorily. Yet, an accurate description of the initial jet profile is crucial for modeling purposes. Here, an attempt was made to provide an explanation as to why the current models fail to match the spray profile. Analysis of the acquired images confirmed that the jet undergoes transition from a liquid core to a ligament region and finally into a droplet region. A composite empirical formula for jet penetration, which takes the multiple-zone behavior of the jet into account is presented in this study. A double pulsed imaging technique, similar to particle image velocimetry (PIV), was used to measure droplet and spray fragment velocities throughout the spray field. The results showed substantial droplet-freestream velocity slip even at far downstream locations. This suggests the possibility of prolonged secondary atomization, enhanced evaporation due to transport mechanisms, and intense droplet generated freestream turbulence.

TECHNICAL DISCUSSION

A fuel injection tunnel was specifically designed and constructed for flow visualization and optical diagnostics. The test facility consisted of a cylindrical settling chamber followed by a transition section 127 mm wide, 76.2 mm in height, and 762 mm in length. A series of flow straighteners (honeycomb section and screens) were implemented in the transition section to provide a uniform two dimensional flow. The test section had the same dimensions as the transition section. The top wall and the two side walls were equipped with optical quality quartz windows for optical access. High pressure, high capacity pumps were used to provide continuous air supply. The air handling system was capable of providing 13.6 Kg/sec flow rate at 51 atmospheres. The air flow rate was measured by an orifice flowmeter located upstream of the flow control valve. A two dimensional variable area sonic nozzle was locate downstream of the test section, which allowed precise control of the Mach number in the test section.

Temperature and pressure measurements, at various locations, were made for detailed flow monitoring and controlling. A micro-computer based data acquisition system was used to calculate, record, and monitor all pertinent flow parameters such as test section Mach number, static and stagnation pressures, air mass flow rate, injectant mass flow rate, static and stagnation temperatures, etc. The tunnel design proved to be versatile and offered the opportunity of varying the flow velocity (Mach Number) and freestream density independently and over a wide range. The variable area sonic nozzle was connected to the laboratory exhaust system, capable of maintaining 0.25 atmosphere back pressure. For all conditions tested in this study the measured total temperature was 300 °K. Freestream Mach number was set at 0.4 corresponding to a freestream velocity of 135 m/sec.

The fuel injection system consisted of a pressurized fuel reservoir, a flow control valve, a positive displacement flowmeter, and a number of interchangeable simple round orifice injectors. The fuel reservoir was pressurized with nitrogen to 27 atmospheres. A fast acting pressure regulator was used to maintain constant reservoir pressure for steady fuel flow during the runs. Injectors were flush mounted in the lower test section wall. In order to further reduce fuel flow disturbances and unsteadiness the fuel line was terminated into a one inch diameter plenum chamber just upstream of the injector.

The 532 nm green line of a double pulsed Quanta-Ray DCR-3 ND:YAG laser was used as the light source. The pulse duration was 8 nsec, which was sufficiently short to freeze the flow and act as an optical shutter. A thin (1 mm thick) laser sheet light was formed by a combination of conventional and cylindrical lens system. The sheet light was longitudinally oriented and passed through the top wall test section window to illuminate the spray at the plane of symmetry. The scattered light (Mie Scattering from the particles and spray fragments) was collected at right angles by an intensified two-dimensional CCD camera, Princeton Instrument Model 576S/B. The 384x578 pixel density of the CCD camera combined with the optical arrangement resulted in a 200 μm/pixel spatial resolution (coarsest resolution) which allowed observation of a 76.8x115.6 mm area of interest.

Each image acquired by the CCD camera was sent to a 486-PC through a controller unit for preliminary analysis and display. For each pixel, the light intensity resolution was up to 14 bits. Thus, each raw image data set contained ~440 KBytes of information. For each flow condition a set consisting of ten individual images was acquired. The images were then sent to a Macintosh IIfx computer for further analysis through data conversion by a custom software developed in this study. These images were averaged and used to determine the jet penetration by outlining the spray plume boundary and to obtain time averaged behavior of the jet. A computer program was written to recognize and identify the trajectory of the spray plume based on the assumption that the jet boundary had at least 10% of maximum field intensity, similar to the definition for boundary layer height. The upper part of this contour line is considered to be the penetration height, H. Approximately 400 data points were obtained to describe the upper jet contour, which typically extended to 70 jet diameters downstream of the injector orifice and reached its maximum penetration height. The present sheet lighting technique together with the ability of digitizing the images have markedly improved the accuracy of the measurements for determining jet trajectory over the methods used in previous studies. To account for the multi-zone behavior of the transverse jet, the following functional form

composed of three exponential terms with length scales corresponding to the three spray regions is proposed. This new form matched the jet trajectory extremely well, see Figure 1.

$$\frac{H}{d} = 9.91\ (\bar{q})^{0.44}\left(1 - \exp\left(\frac{-x/d}{13.1}\right)\right)\left(1 + 1.67\ \exp\left(\frac{-x/d}{4.77}\right)\right)\left(1 + 1.06\ \exp\left(\frac{-x/d}{0.86}\right)\right)$$

q = Jet to freestream dynamic pressure ratio
d = Injector diameter
x = Streamwise distance from injector orifice
H = Penetration height

Here, the first term has the longest characteristic length (13.1 injector diameters) and represents the far field droplet region. The second term with a characteristic length of 4.77 represents the ligament or the transition region. The third term, which represents the near field or the liquid column has the shortest characteristic length scale, 0.86 injector diameter.

Droplet image velocimetry (DIV) is a powerful technique for velocity measurement in the transition and dense spray regions where most other techniques have theoretical limitations and fail to extract useful information. Double pulsed images, 14 μsec separation time, were acquired to study the dynamic behavior of the jet. Figure 2 is a typical double pulsed image of a 1.8x1.2 cm section of the spray plume at approximately 50 jet diameters downstream of the injector orifice for freestream Mach number of 0.2 and jet-to-freestream dynamic pressure ratio of 21. By using a similar, but much simpler, technique employed in PIV systems many droplet pairs were matched and connected with straight lines, i.e., velocity vectors are shown. As expected, at 50 injector diameters downstream of the orifice, droplets nearly reached their maximum penetration height and showed very little subsequent transverse displacement, however, there was a large velocity slip between the droplets and the freestream. The average droplet velocity was roughly 35 to 40 m/sec as compared to nearly 70 m/sec freestream velocity. As expected, double pulsed images of the spray at the near injector field revealed droplet and spray fragment velocities to be nearly identical to the calculated jet velocity at the injector orifice. Future research efforts will explore the effects of surface tension and viscosity, freestream Mach number, and injector geometry on penetration and spray atomization.

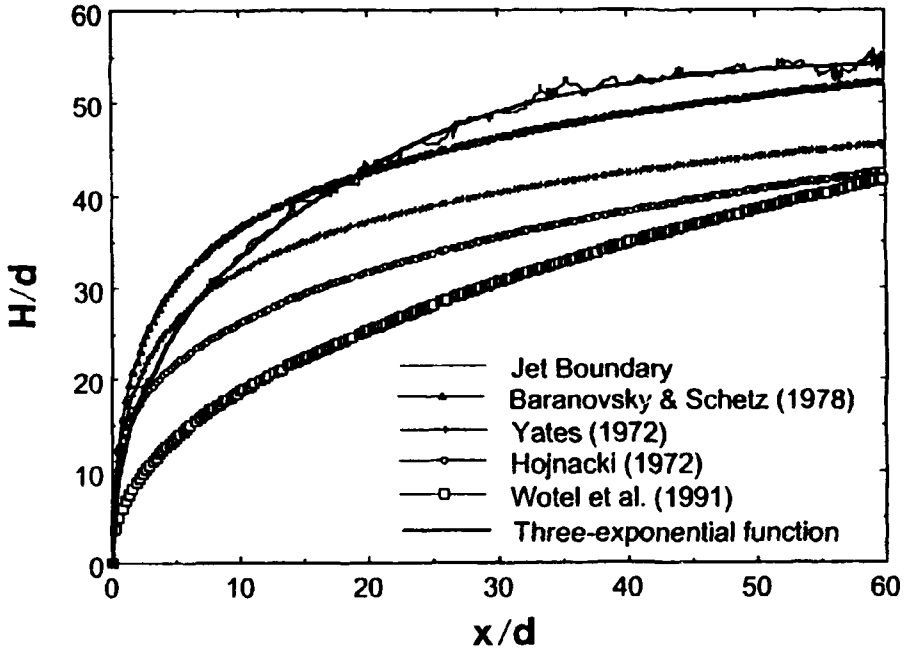

Figure 1. Calculated Vs. Measured Penetration Height as a Function of $\bar{q}$ and streamwise distance x/d

Figure 2. Double Pulsed Image of Spray Field
M = 0.2, d = 0.762 mm, $\bar{q}$ = 21

TECHNIQUE FOR VISUALIZING VAPORLINES EMANATING FROM WATER DROPLETS

AFOSR Contract No. 2308S705

Principal Investigators: Dr T. A. Jackson and Dr W. M. Roquemore

Fuels and Lubrication Division
Aero Propulsion and Power Directorate
Wright Laboratory
WPAFB OH 45433-6563

SUMMARY/OVERVIEW

This AFOSR sponsored program focuses on both gaseous and two-phase combustion. The gaseous combustion research is managed by Dr W. M. Roquemore and the two-phase combustion is managed by Dr T. A. Jackson. The two-phase combustion research program is quite extensive and involves the study of everything from single droplet evaporation to complex swirling spray flames. This abstract describes a new visualization technique that was developed as part of the two-phase combustion research program in cooperation with Dr A. S. Nejad (Task 2308S1) of the Advanced Propulsion Division. This visualization technique is used to investigate the convective transport of vapor from evaporating droplets in gaseous flows. Specifically, water droplets serve as point sources of vapor that react with $TiCl_4$ to form micrometer-sized seed particles that mark the convective transport of water vapor in two-dimensional vortical flows. This technique provides a tool by which complex two-phase flows can be investigated and will lead to a better understanding of droplet, vapor, and gaseous vortex interactions.

Author: 1Lt R. D. Hancock

TECHNICAL DISCUSSION

This abstract describes a novel visualization technique in which water droplets, vapor from these droplets, and their interaction with the carrier gas can be observed simultaneously as they interact with one another in two-phase flows.[1] Specifically, water droplets are injected into a $TiCl_4$-laden gaseous flow where they evaporate. The water vapor reacts spontaneously and quickly with the $TiCl_4$ vapor to form micrometer-sized TiO_2 particles. The particles are small enough to accelerate rapidly to the velocity of the carrier gas but are too large to diffuse readily. Thus, they are convected along the path that the water vapor follows as it leaves the droplets. The instantaneous locus of the TiO_2 particles is defined as a vaporline and can be visualized by using Mie scattering and laser sheet lighting. Although the technique for visualizing vaporlines is relatively simple, the physics needed to interpret them in terms of the droplet, vapor, and fluid interactions can be complicated. This abstract provides some insights into the physics needed to understand and interpret vaporlines.

This visualization technique is demonstrated in a two-dimensional, laminar shear-layer flow experiment shown schematically in Fig. 1. The splitter plate divides the 12.7-cm-square duct into two equal areas. Dry air is used in both air streams. Typical gas velocities are limited to ~1.3 and 0.5 m/s based on air supply limitations. The higher speed air is passed over a liquid $TiCl_4$ bath to collect the $TiCl_4$ vapor as is done for the reactive Mie scattering technique that is used to visualize diffusion flames.[2] Droplets are injected through a slot in the Plexiglas duct into the low-speed flow channel that is dry and void of $TiCl_4$. The droplets, typically from within a 40-80-μm-diameter range, have sufficient momentum to cross the shear layer into the high-speed, $TiCl_4$-laden side of the flow field. Micrometer-sized TiO_2 particles are formed as the water vapor mixes with the $TiCl_4$. The flow field is illuminated by the 532-nm light output of a frequency-doubled Nd:YAG laser. Water droplets and the TiO_2 particles are the only scatters in the flow field and they can be easily distinguished by their 50-to-1, or greater, diameter ratio. Water droplet injection is controlled by using a droplet-on-demand generator that is driven by a piezoelectric crystal transducer that operates in the frequency range from 1 to 4000 Hz.[3] Vortex formation is controlled by acoustically driving the low-speed air stream near its natural vortex shedding frequency of 20 Hz. The location of the water droplets and the entertainment of the water vapor into the individual vortices of the shear layer, as marked by TiO_2 particles, are recorded by using a digitizing camera and photographs. The curve identified by the location of the TiO_2 particles at the instant of visualization is referred to as a vaporline.

The new fluid dynamic term, vaporline, is used to refer to the line marked by the TiO_2 particles because standard fluid dynamic terms are not applicable. A vaporline contains some characteristics that are associated with a particle trajectory and a streakline.

To understand this, one must think in terms of the space and time histories of the droplet and water vapor and how they are acted on by the flow field. A water droplet is too dense to follow the gaseous flow field. Its motion is described by a particle trajectory, which is the path that a particle traverses in the flow field as a function of time.[4] Water vapor is being emitted from the droplet as it moves along its trajectory. The water vapor mixes with the $TiCl_4$ and spontaneously forms TiO_2 seed particles. This occurs near the droplet and in the convective vapor trail that originates from the droplet. Each micrometer-sized TiO_2 particle is sufficiently small to follow the fluid motion and is convected along a unique particle (fluid element) trajectory that is determined by the fluid velocities at the location and time that it is formed. The convective vaporline is defined as the locus of all the TiO_2 particles at the instant in time when the flow is visualized by firing the laser. The vaporline is believed to mark the location of the water vapor when no molecular diffusion takes place. It looks something like a streakline, defined by the instantaneous locus of all fluid particles that have passed through a particular fixed point of the flow field.[4] However, there is a fundamental difference between a vaporline and a streakline. The water droplet, which serves as the source of seed, is not fixed at some location in the flow but is influenced by the fluid motion and is moving as some velocity different from the gaseous flow itself. Therefore, each convective vaporline contains an evolutionary history of the evaporation and convective transport of the water vapor from each droplet.

The physics associated with the time and spatial development of the vaporlines is better understood by referring to Fig. 2. The flow field schematic illustrates a specific case in which each droplet is introduced into a driven laminar flow at the same frequency and phase angle, relative to the vortex generation, as the previous droplet. Therefore, this schematic is an instantaneous snapshot of the flow that allows one to follow the development of vaporlines at a given flow phase angle and separated by 360° phase increments. The thick solid curve represents the interface of the high and low streams and is a streakline that originated at the tip of the splitter plate. The dashed curves represent the particle trajectories that specific water droplets and specific TiO_2 particles would follow in moving from one phase angle to the same phase angle a period later. The thin solid curves represent the vaporlines from each droplet. The open circles indicate the locations of the first TiO_2 seed particles that were formed when each water droplet first passed through the shear layer and into the $TiCl_4$-laden side of the flow. The head (water droplet) and tail (first TiO_2 particle formed) of each vaporline are given the same number. A continuous line of seed particles exists between each identically numbered droplet and seed particle. This line of seed, or vaporline, grows and stretches relative to the gaseous velocity as it moves downstream. It should be noted that the convective vaporline remains fairly thin and well defined over a long distance for the two-dimensional gaseous flows investigated. This occurs largely because these flows are laminar and well behaved. If the flow were turbulent, the vaporline would become three-dimensional and only a broken line would appear in a two-dimensional visualization.

This experiment was modeled by L. P. Chin of Northwestern University to simulate the formation of vaporlines from droplets in a 2-D shear layer. This was done using the MAC (Marker And Cell) method, which is a numerical method originally developed by Welch et al.[5] and later modified by Hirt and Cook[6], allowing one to solve the pressure field more readily. To visualize the streaklines and vaporlines, massless markers (particles) convected by the velocity field were introduced. These markers have no influence on the velocity and pressure fields.

The vaporlines from droplets observed in the experiments can be produced numerically by tracing a number of massless particles emitted from the droplets while the droplets are traveling through the simulated flow fields. To obtain the particle velocities in the discretized flow field numerically, an accurate second order interpolation scheme from Chan et al.[7] was used. Artificial disturbances (1% at 20 Hz) were introduced along inflow velocity profiles in order to trigger the vortical shedding process. This numerical code was performed by the Cray Y-MP/48 super-computer. As illustrated in Fig. 3, the agreement between the experiment and computation is excellent.

In conclusion, this visualization technique allows the unique opportunity to diagnose complex gaseous flows with carefully positioned point sources of seed. These point sources of seed, or water droplets, have been injected into a $TiCl_4$-laden gaseous flow, and the convective transport of mass away from an evaporating droplet has been observed. This technique has been used to observe droplet, vapor, and vortex interactions in a driven two-dimensional shear-layer flow. While the flow investigated herein is laminar and relatively uncomplicated, this visualization technique has the potential to be applied to other more complex flows.

REFERENCES

1. R. D. Hancock, T. A. Jackson, and A. S. Nejad, App. Opt. **31**, No. 9, 1163-1166 (1992).
2. L.-D. Chen and W. M. Roquemore, Combust. Flame **66**, 81-86 (1986).
3. G. L. Switzer, Rev. Sci. Instrum. **62**, 2765-2771 (1991).
4. W. Merzkirch, *Flow Visualization* (Academic, New York, 1987).
5. J. E. Welch, F. H. Harlow, J. P. Shannon, and B. J. Daly, Los Alamos Scientific Lab., Report LA - 3425 (1966).
6. C. W. Hirt and J. L. Cook, J. Comput. Phys. **10**, 324 (1972).
7. R. K. C. Chan, R. L. Street, and T. Strelkoff, Tech. Report No. 104, Department of Civil Engineering, Stanford University, Stanford CA (1969).

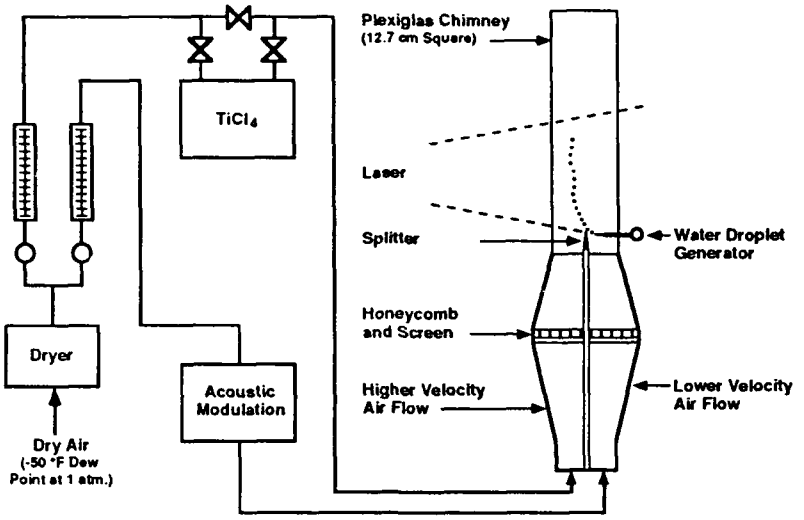

Fig. 1. Schematic representation of the experimental setup

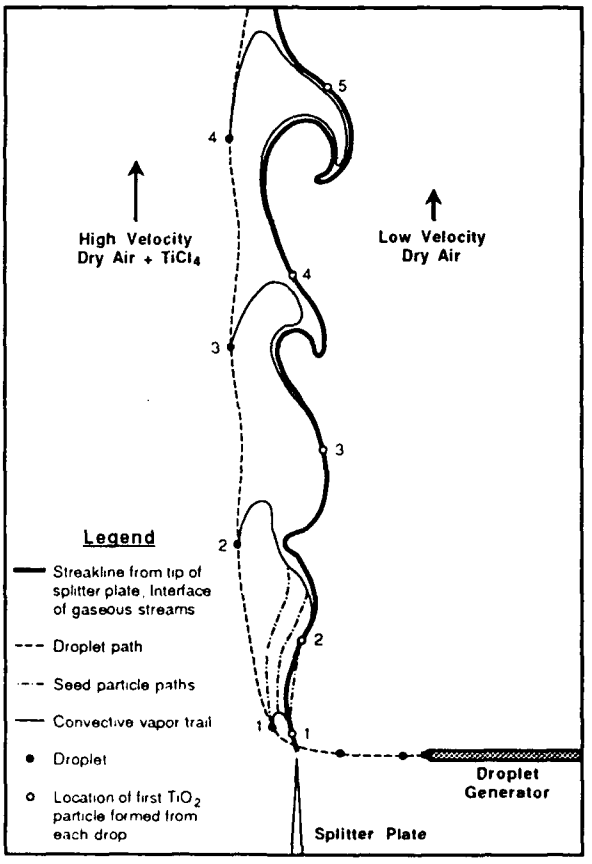

Fig. 2. Schematic representation of the two-dimensional shear-layer flow with droplet injection and vaporline development

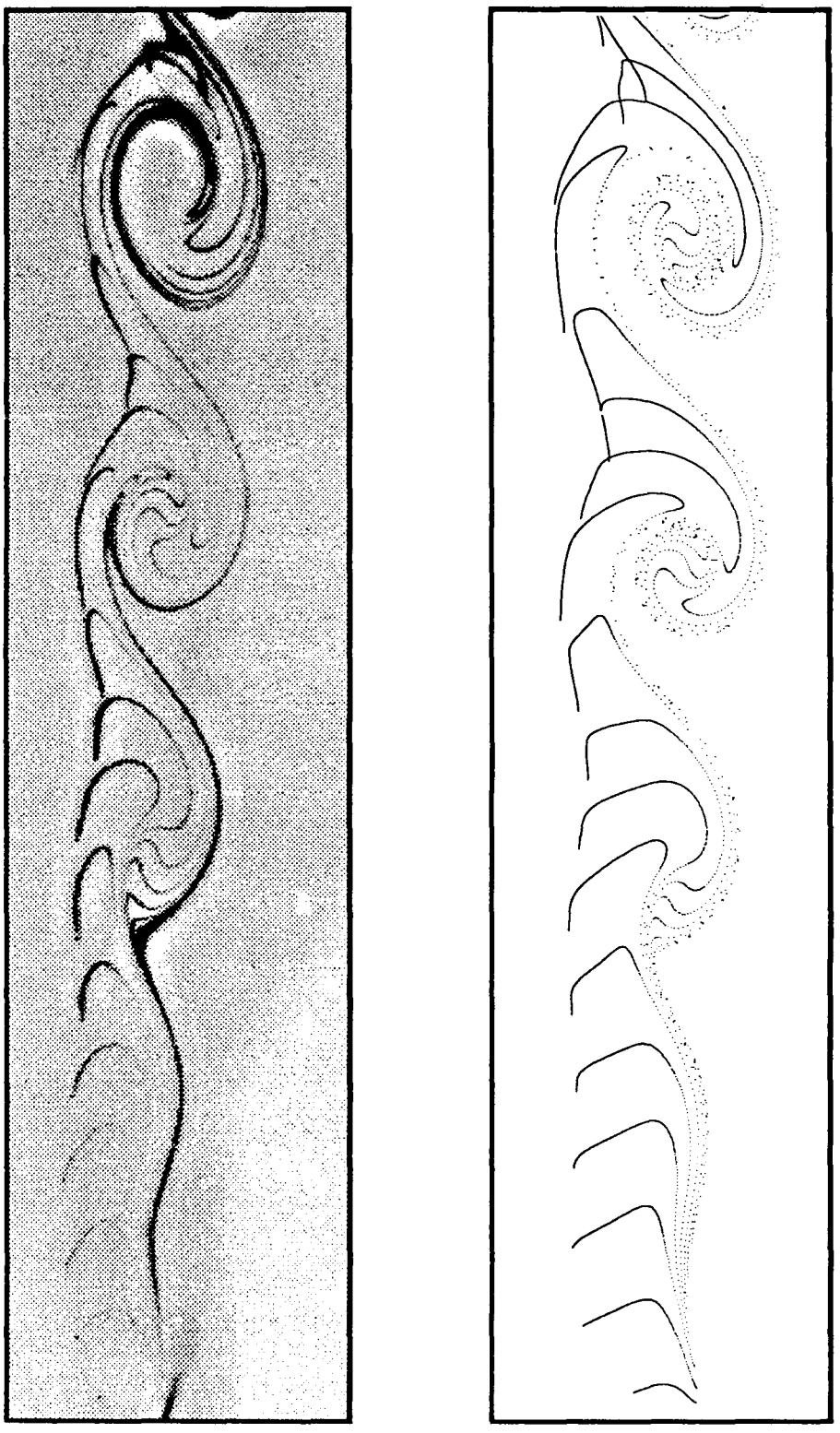

Fig. 3. Experimental and computed vaporlines in a two-dimensional shear layer. Velocities of 0.70 m/s on left and 0.35 m/s on right with a 20 Hz drive and droplet diameters of 60μm. Each image is 3 x 12 cm.

FUNDAMENTAL STUDIES OF DROPLET INTERACTIONS IN DENSE SPRAYS

AFOSR Grant/Contract No. 90-0064

PRINCIPAL INVESTIGATOR:

W.A. Sirignano

Department of Mechanical and Aerospace Engineering
University of California
Irvine, CA 92717

SUMMARY/OVERVIEW:

The research addresses interaction amongst droplets in a dense spray via a fluid dynamical computational approach. Flow fields, transport details, and droplet lift, drag, torque, trajectories, and vaporization rates are determined. In one task, three-dimensional interactions of fuel droplets are considered. In another task, vaporizing liquid oxygen droplets are studied including axisymmetric interactions amongst fuel and oxygen drolpets.

AUTHORS

C.H. Chiang
S.E. Elghobashi
I. Kim
W.A. Sirignano

TECHNICAL DISCUSSION

1. Three-Dimensional Interactions of Droplets

Recently, Kim *et al.* [1] investigated three-dimensional flow interactions with two identical spherical droplets which were *held fixed relative to each other* in the transverse direction against the uniform stream at Reynolds number O(100); they also studied two identical solid spheres in the same situation. They determined the effects of three-dimensional interactions on the lift, moment, and drag coefficients as a function of the dimensionless distance between the two spheres and Reynolds number and also discovered interesting near-wake flow patterns as the gap between the two spheres decreased. The computations show that for a given Reynolds number, the two spheres are repelled as the spacing becomes of the order of the diameter. On the other hand, they are attracted weakly at intermediate separation distances.

In the present study, we have extended the work of Kim *et al.* [1] and studied the droplets interaction in a more realistic situation where two identical droplets are injected and then move side-by-side into initially quiescent fluid medium. The droplets will be decelerating due to the drag and changing their direction of motion due to the lift. By placing the origin of a noninertial reference frame at the center of mass of the two droplets, the Navier-Stokes equations to be solved include a noninertial term, which will be evaluated from Newton's second law for the droplet motion. Here,

we present results for two identical droplets injected in the incompressible fluid medium, initially separated by a distance $d_o = 2$ and 9 with initial angle $\alpha_o = 0$ and initial Reynolds number 100.

Figure 1 shows the trajectory of one droplet for $d_o = 2$, where the numbers on the curve denote the dimensionless time, d_t denotes instantaneous dimensionless distance between droplet centers to droplet diameter, and l_t denotes instantaneous dimensionless position in y direction. Since the final location of a single droplet at $t = 250$ in the case of no drag and lift forces would be $(d_t, l_t) = (2, 250)$, the figure indicates that the two droplets are repelling each other via aerodynamic forces as well as decelerating. Figure 1 also shows the trajectory of one droplet for $d_o = 9$. The final location of a single droplet at $t = 250$ in the case of no drag and lift forces would be $(d_t, l_t) = (9, 250)$; therefore, Figure 1 identifies that the two droplets are weakly attracting each other as well as decelerating.

Figure 2 shows the lift coefficients of the droplet for $d_o = 2$ and 9 as a function of instantaneous Reynolds number, where the repelling force is taken as positive. The lift coefficient for $d_o = 2$ is positive during the time period $0 \leq t \leq 250$, and becomes gradually smaller in time because the distance between the droplets is increasing and their directions of motion are changing due to the repelling force. On the other hand, the lift coefficient for $d_o = 9$ is negative during that time period but slowly goes towards zero. The figure also shows that rapid change occurs initially due to the impulsive start of the droplets and the quasi-steady state occurs when $t \geq 30$.

Figure 3 shows the moment coefficients of the droplet for $d_o = 2$ and 9 as a function of instantaneous Reynolds number, where the counter-clockwise direction is taken as positive. The moment coefficient for $d_o = 2$ is positive initially and gets gradually smaller and changes its sign from positive to negative at $t = 150$. On the other hand, the moment coefficient for $d_o = 9$ is negative during the time period $0 \leq t \leq 250$ but slowly approaches zero.

Figure 4 shows the drag coefficients of the droplet for $d_o = 2$ and 9 as a function of instantaneous Reynolds number. The drag coefficient for $d_o = 2$ is higher than that for $d_o = 9$. At earlier times, the difference is greater but becomes gradually smaller as time passes because the droplets for $d_o = 2$ are repelling each other and the distance between them is increasing, and so the drag becomes gradually smaller. The drag coefficient for $d_o = 9$ is almost identical to that for a single droplet (and slightly higher that for a single droplet when $t \geq 30$).

2. Vaporization of LOX droplets

Vaporization of LOX droplets in convective hydrogen environment over a wide range of pressure has been investigated.. Current emphasis is placed on the understanding of supercritical LOX vaporization where many complex transport phenomena, such as the vanishing of the gas/liquid interface, diffusion of gas vapor into droplet, and real gas effects, become very important in determining the droplet vaporization rate.

Several modifications associated with physical behavior have been conducted to extend the previous low pressure LOX droplet vaporizing model to deal with the ambient pressure in the range from the near-critical region to the supercritical region. They are summarized below.

1. A comprehensive calculation of variations of thermophysical properties with respect to temperature for each species component is performed. The high pressure correction, mixing rules to evaluate the thermodynamic properties, and the quantum gas behavior of hydrogen vapor are considered.

2. The real gas effect at high pressure case is taken into account by incorporating a compressibility factor in the gas-phase equation of state. A modified Redlich-Kwong equation of state with

the mixing rules of Chueh and Prausnitz are employed. Since the swelling effect of the LOX vaporization is significant, a primitive variable approach is formulated to analyze the internal motion and thermal and mass transport within the droplet.

3. The solubility of the fuel vapor in the liquid phase has been considered by a multicomponent formulation. The principle of equal temperature, pressure, and fugacity of both phases for phase equilibria is used to compute the surface mass fraction of species for gas and liquid.

4. A new technique has been under testing to locate the gas/liquid interface and compute the regression rate due to vaporization as well as phase change across the critical surface, with continuous density and temperature gradients at the surface.

A calculation is performed to study vaporization behavior before the droplet reaches the critical mixing state. The changes of properties at the interface occur very rapidly during the droplet vaporization. Diffusion length scales are reduced at the elevated pressure. The transport rates are faster than those in the low pressure case, hence the droplet lifetime is shorter. As a result, a very small time step is mandatory to ensure accuracy. Figure (5) indicates that radius increases with time due to the swelling effect of droplet as well as the condensation of vapor. The reduced enthalpy of vaporization also contributes to the fast vaporization of the droplet. The enthalpy of vaporization shown in Figure (6) is significantly reduced from the conventional "latent heat". A remarkable condensation of gas-phase vapor occurred at the early droplet lifetime. The vaporization takes control as the surface temperature increases.

Figure (5) also presents the variations of compressibility factors (averaged around the azimuthal direction) for gas and liquid phases at the interface. When the two compressibilities are equal, the critical mixing state is reached. The apparent trend of two phases merging into one continuous phase is shown. Since the critical mixing state highly depends on temperature and mass fraction, the droplet surface at different locations will reach the critical mixing state at different times. The diffusivity for liquid phase is, in general, two orders-of-magnitude less than that of the gas phase, as a result, most of the diffusing vapors are concentrated in the boundary-layer region at the interface.

References

1. Kim, I., Elghobashi S. & Sirignano, W. A. 1991 Three-dimensional flow over two side-by-side spheres. submitted to *J. Fluid Mech.* also see AIAA Preprint 91-0073.

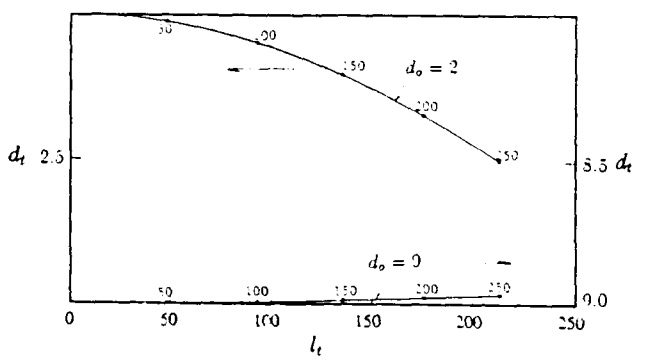

Figure 1. Trajectory of one droplet for $d_o = 2$ and 9, where the numbers on the curves denote the dimensionless time.

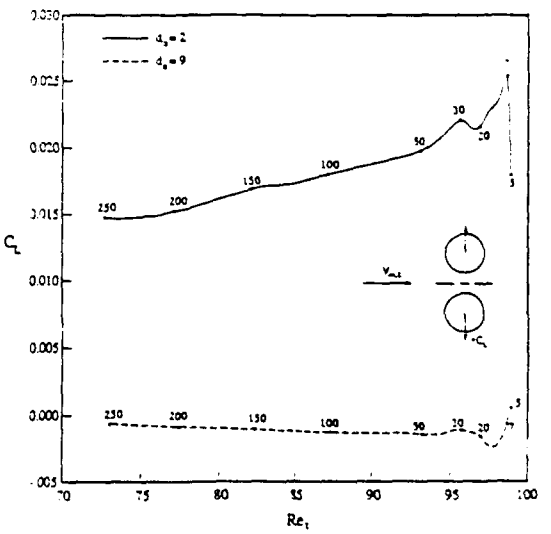

Figure 2. Lift coefficients as a function of instantaneous Reynolds number for $d_o = 2$ and 9

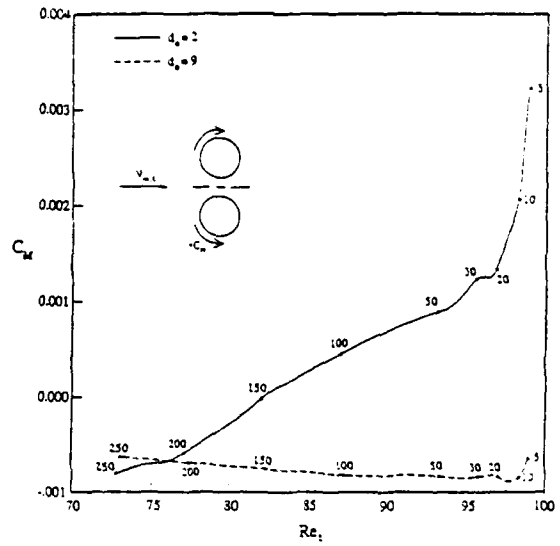

Figure 3 Moment coefficients as a function of instantaneous Reynolds number for $d_o = 2$ and 9.

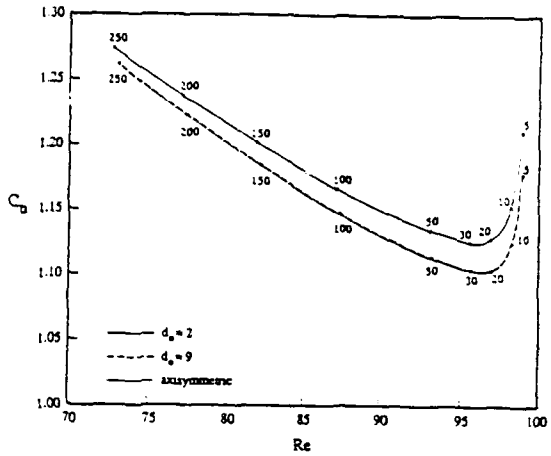

Figure 4. Drag coefficients as a function of instantaneous Reynolds number for $d_o = 2$ and 9.

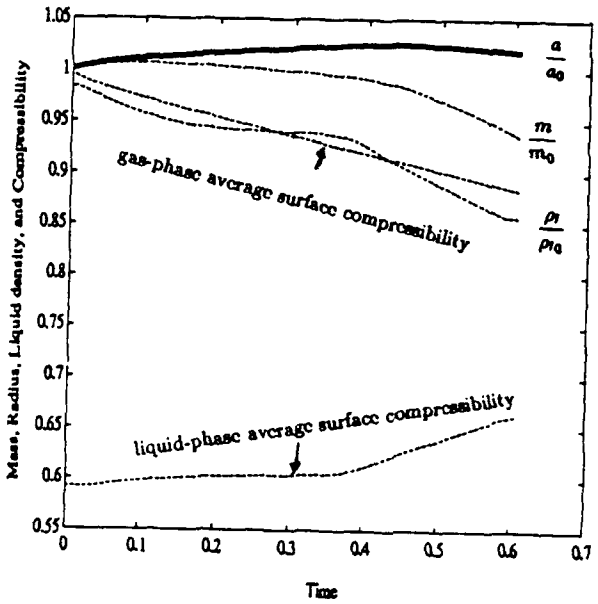

Figure 5 Time variations of droplet radius, mass, density, and surface compressibilities.

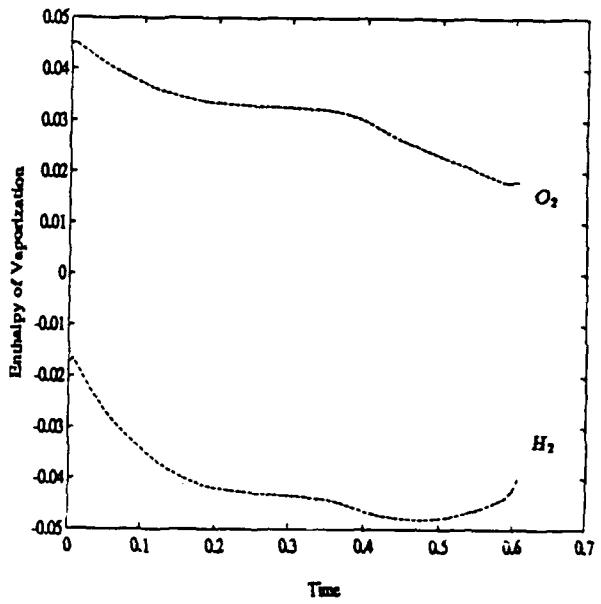

Figure 6 Time variations of enthalpy of vaporization for two components.

NUMERICAL ANALYSIS OF A TIME DEPENDENT TWO-PHASE NON-REACTING FLOW

(AFOSR Grant/Contract No. F49620-92-J-0231)

Principal Investigator: Suresh K. Aggarwal
Address: Department of Mechanical Engineering
University of Illinois at Chicago
Chicago, Illinois 60680

SUMMARY

The objective of this research is to study the dispersion and vaporization behavior of droplets in turbulent shear flows dominated by large vortical structures. The two-phase flow algorithm is based on a large eddy simulation for the gas phase and a Lagrangian approach for the liquid phase. The work completed so far includes: (i) the simulation of the dynamics of large vortical structures and the droplet dispersion in unforced and forced planar shear layer; and (ii) the study of droplet dispersion behavior in a transitional jet flow. The research currently in progress is focussing on the dispersion of evaporating droplets in heated shear flows, and the effects of droplets on the dynamics of large vortical structures.

INTRODUCTION

Particle-laden turbulent flows occur in numerous technological applications. The traditional approach for modelling these flows is based on the assumption that the turbulence is isotropic and statistical in nature. Numerous recent studies, however, indicate that the turbulent flows are dominated by large-scale coherent vortical structures. This has raised a number of important questions regarding the role of large-scale structures in determining the entrainment, mixing, and spray processes. Further interest in the study of large scale structures stems from the fact that by manipulating these structures, one may be able to control and enhance the performance of systems whose dynamics is strongly influenced by these structures.

The objective of this research is to study the dispersion and vaporization behavior of droplets in transitional shear layers dominated by large vortical structures. The results obtained so far and the work currently in progress are summarized in the following sections.

Numerical Simulation of Unforced and forced Shear Layer

In order to understand the dynamics of large scale vortical structures, a detailed simulation of a planar shear layer has been completed. The shear layer is formed by two coflowing streams downstream of a splitter plate. A large eddy simulation model is employed to predict the shear layer rollup due to the Kelvin- Helmholtz instability, and the interaction of vortices downstream. The spectral analysis of the axial velocity history recorded at several streamwise locations in the shear layer yields the fundamental mode and its subharmonics frequencies. The streamwise evolution of these frequencies clearly reveals the locations of shear layer rollup and vortex

interactions, which are further confirmed by the vorticity plots. A parametric study is performed to examine the effects of velocity ratio, inflow velocity profile, mean flow velocity, and initial momentum thickness on the dynamics of the shear layer. The results indicate that the Strouhal number of the fundamental mode remains approximately a constant, in the range of 0.0225-0.0269, somewhat lower than that predicted by the linear stability theory, but well within the range of experimental measurements. The effect of external forcing on the rollup, vortex pairing, and shear layer growth are also investigated. The results are described in Publications No. 2 and 6.

Droplet Dispersion in Unforced Planar Shear Layer

The objective here is to study the droplet dynamics and dispersion behavior in a temporally and spatially developing planar shear layer. Since the focus is on the droplet dynamics and dispersion behavior, the vaporization process is not considered in this study. From the observations of the droplet motion through the vortical structures, we are able to capture the centrifugal mechanism responsible for the enhanced dispersion of intermediate size droplets compared to the carrier fluid particles. One typical result is given in Fig. 1, which shows the snapshot of carrier fluid particles and the 10 micron droplets. It is clearly seen that the dispersion of 10 micron droplets exceeds that of carrier fluid particles. The dispersion function is calculated as a function of the Stokes number and other important parameters. Another important observation is that the droplet dispersion is asymmetric. The droplets injected in the fast stream exhibit greater dispersion compared to those injected in the slow stream. The asymmetric dispersion behavior is related to the process of asymmetric entrainment in the shear layer, observed in previous experimental and numerical investigations. Detailed results are discussed in Publications No. 3-4.

Effect of External Forcing on Droplet Dispersion

The objectives of this study is to investigate the effects of external forcing on droplet dispersion. The forcing is provided by superimposing a periodic, monochromatic fluctuating velocity on the axial velocity at the inflow boundary. The important observations are that the forcing can enhance the dispersion of droplets, and that the optimum forcing frequency is the first subharmonic mode of the shear layer. The gain in dispersion due to forcing is greater for the intermediate size droplets compared to that for the carrier fluid particles. This implies that the centrifugal mechanisms for enhanced dispersion can be strengthened by external forcing. It is also observed that forcing at the fundamental mode increases droplet dispersion in the initial part of the shear layer, but decreases it farther downstream. These results are quite consistent with the experimental observations regarding the effect of forcing frequency on the spreading rate of the shear layer. Further details are given in Publications No. 5.

Droplet Dispersion in a Transitional Free Jet

In this study, the dynamics and dispersion of droplets in a transitional, subsonic, free jet is considered. Again, a large eddy simulation model based on the Flux Corrected Transport (FCT) algorithm is employed for the carrier fluid. Results obtained so far again identify a droplet size range, where the droplets exhibit greater dispersion than the carrier fluid particles. See Fig. 2.

Results also indicate that the optimum droplet size for the maximum dispersion depends on the time and the location of injection. In addition, a detailed graphical representation of the large scale structures and the motion of droplets in these structures clearly reveals the centrifugal mechanism, responsible for the enhanced droplet dispersion. The details are discussed in Publication No. 7.

Research in Progress

The current activities include the continuation of the research efforts summarized above. In addition, the efforts are underway to consider the dispersion of evaporating droplets and the effect of dispersed phase on the dynamics of large vortical structures. For the evaporating case, an heated free jet and a differentially heated planar shear layer are considered. In addition to the explicit FCT algorithm, another gas-phase algorithm based on the implicit formulation is being used. For low-speed flows, being used in the experimental studies at the Wright Laboratory, the implicit algorithm may be more efficient. In the current funding period, it is expected that the appropriate droplet vaporization models will be incorporated, and some preliminary results on the dispersion behavior of evaporating droplets will be obtained. In addition, the effect of droplet dynamics and vaporization on the large vortical structures will be studied.

List of Publications

1. J.B. Yapo," Numerical Simulation of Instabilities in Planar Free Shear Layers by the Flux Corrected Transport Method", M.S. Thesis, Department of Mechanical Engineering, University of Illinois at Chicago, 1990.

2. L. Kung," Numerical Simulation of Forced and Unforced Shear Layers", M.S. Thesis, Department of Mechanical Engineering, University of Illinois at Chicago, 1992.

3. S.K. Aggarwal, G. Chen, J.B. Yapo, F.F.Grinstein, and K. Kailasnath," Numerical Simulations of Particle Dynamics in Planar Shear Layer", Paper AIAA-92-0109, 30th Aerospace Sciences Meeting, Reno, Nevada, Jan. 6-9, 1992.

4. S.K. Aggarwal, G. Chen, J.B. Yapo, F.F.Grinstein, and K. Kailasanath," Numerical Simulations of Particle Dynamics in Planar Shear Layer", Physics of Fluids (under review)

5. S.K. Aggarwal and Y. Xiao, " Droplet Dispersion in a Perturbed Transitional Shear Layer", Central States Section Meeting, The Combustion Institute, Columbus, April 1992. Also submitted to AIAA Journal.

6. L. Kung and S.K. Aggarwal, "A Parametric Study of Forced and Unforced Shear Layers," to be submitted to AIAA Journal.

7. S.K. Aggarwal, J. Uttupan, F.F.Grinstein, and K. Kailasnath," Droplet Dispersion in a Transitional Free Jet", Submitted to 31th Aerospace Sciences Meeting, Reno, Nevada, 1993. Also to be submitted to Physics of Fluids.

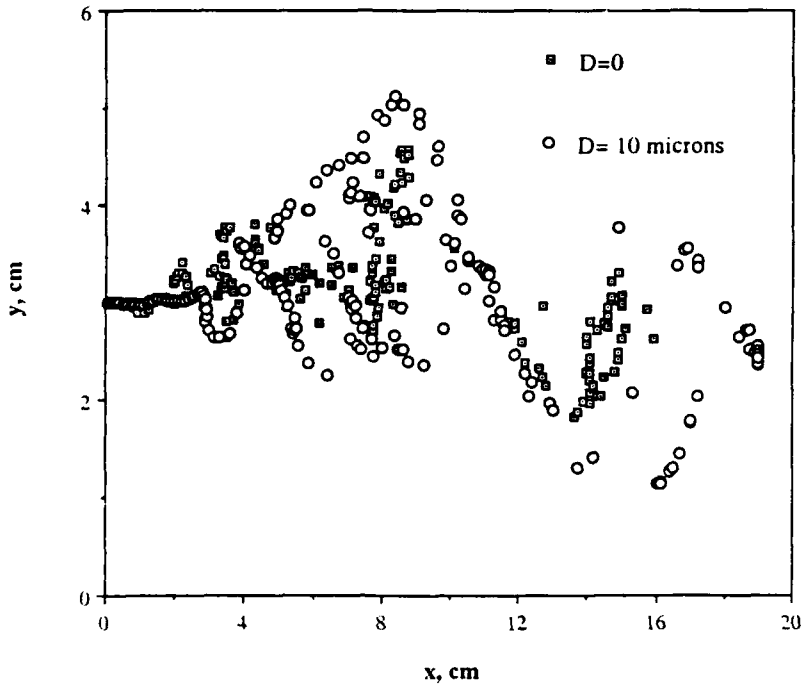

Figure 1 Snapshot of droplet (10 micron diameter) and carrier fluid particle positions in a planar shear layer formed by two coflowing streams past a splitter plate located at y=3.0 cm.

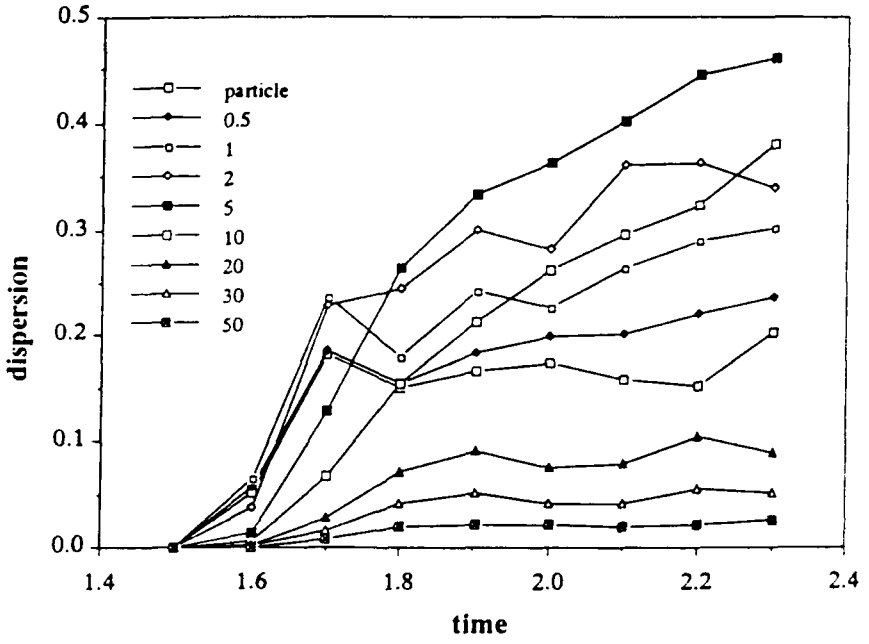

Figure 2 Droplet dispersion function versus time (ms) for a transitional free jet flow. The dispersion function is shown for the carrier fluid particles and for the droplets of diameters=0.5, 1, 2, 5, 10, 20, 30, 50 microns.

ATOMIZATION OF VISCOUS LIQUID SHEETS

AFOSR Grant No. F49620-92-J-0194

Principal Investigator: E. A. Ibrahim

Mechanical Engineering Department
Tuskegee University
Tuskegee, Alabama 36088

SUMMARY

The problem under consideration is that of predicting the characteristics of the spray produced by the atomization of liquid-fuel sheets such as in gas-burners nozzles. Use is made of the nonlinear instability theory to develop a simple but physically sound model of the atomization process. The results of the numerical solution of the model include the fuel-drop size and velocity. Predictions of the mean drop size and velocity may be used to eliminate the need of experimental measurements in the computation of the drop size and velocity distributions using the maximum entropy principle. A good understanding of the fundamental mechanism that govern atomization would enhance our ability to perform a controlled design of the combustion processes that take place in gas-turbine combustors.

TECHNICAL DISCUSSION

In many spray applications, liquid issues from an orifice in the form of a thin liquid sheet such as in swirl nozzles (hollow cone) in gas burners or by a fan spray nozzle. Most of the important features of sheet breakup processes in hollow cone sprays may be reasonably understood by studying the stability of a moving thin liquid sheet of constant thickness (Squire, 1953, Taylor, 1959). Crapper et al. (1973) advanced experimental evidence that the growth of instability waves on liquid sheets takes place spatially (exponentially growing with distance from nozzle) not temporally (exponentially growing with time).

We investigate the atomization of a viscous liquid sheet using the nonlinear spatial instability theory. The emphasis is on the predictions of the size and velocity of the drops that result from the sheet disintegration. The two basic modes of perturbations, namely, symmetrical and antisymmetrical instability waves, that the sheet may experience are studied. According to Li and Tankin (1991) the symmetrical perturbations control the instability process for

small Weber numbers, while antisymmetrical perturbations dominate for large Weber numbers. With regard to perturbation velocity, the basic difference between the two modes is that, in symmetrical waves, the perturbation component of velocity parallel with the sheet surface is large compared with that at right angles to it, while the opposite is true for antisymmetrical waves (Taylor, 1959). The theoretical treatment of the problem considered is carried out as follows.

1. Symmetrical Waves

Since the sheets is thin, the pressure and the perturbation velocity parallel with the sheet surface are considered constant across the sheet thickness. The only momentum equation that needs to be considered is the one in the direction parallel to the sheet velocity. The difference between the liquid pressure and the surrounding gas pressure is due to surface tension. The gas pressure is determined from the velocity potential of the gas motions produced by the wavy sheet. The displacement of the sheet surface is defined in terms of the velocity potential. The resulting partial differential equations with appropriate boundary and initial conditions are solved simultaneously using a TVD (Total Variation Diminishing) numerical scheme to yield the variation of the sheet thickness and velocity with time and distance along the sheet.

2. Antisymmetrical Waves

In this case, the perturbation velocity may be assumed constant throughout the sheet thickness. The pressure variation across the sheet thickness is approximately linear (Taylor, 1959). Under these conditions the only equation of motion that is needed is the one in the direction normal to the unperturbed liquid sheet. The kinematic condition at the liquid surface is used to relate the perturbation of the liquid sheet surface to the normal component of perturbation velocity. The liquid and gas pressures are determined in a way similar to that for the symmetrical waves. A finite-difference technique is used to solve the resulting system of partial differential equations subject to the appropriate boundary and initial conditions.

The breakup of the sheet in the symmetrical mode takes place when the thickness of the perturbed sheet equals half the wavelength of the dominant (fastest growing) instability waves. The diameter of the drops formed by sheet breakup in this regime is equal to the sheet thickness.

In case of antisymmetrical waves, the sheet breakup is assumed to take place when the sheet surface perturbation grows to exp(12) times its initial amplitude (Dombrowski and Hooper, 1962). This condition allows for estimation of the sheet breakup length.

According to the commonly accepted model of Dombrowski and Johns (1963), for the sheet disintegration process, the sheet will be torn transversely into ligaments. These ligaments quickly contract into cylindrical segments through the action of surface tension. The cylinders then continue moving broadside and undergo an unsymmetrical type of breakup process in the second phase of sheet disintegration. It is clear from this model that the drops are formed due to that second phase. To determine the size of these drops the theory advanced by Weihs and Frankel (1982) in their study of stability of a liquid cylinder in cross flow could be used, with the appropriate parameters from the present theoretical results. The mean velocity of the drops at the instant of sheet breakup matches that of the perturbation.

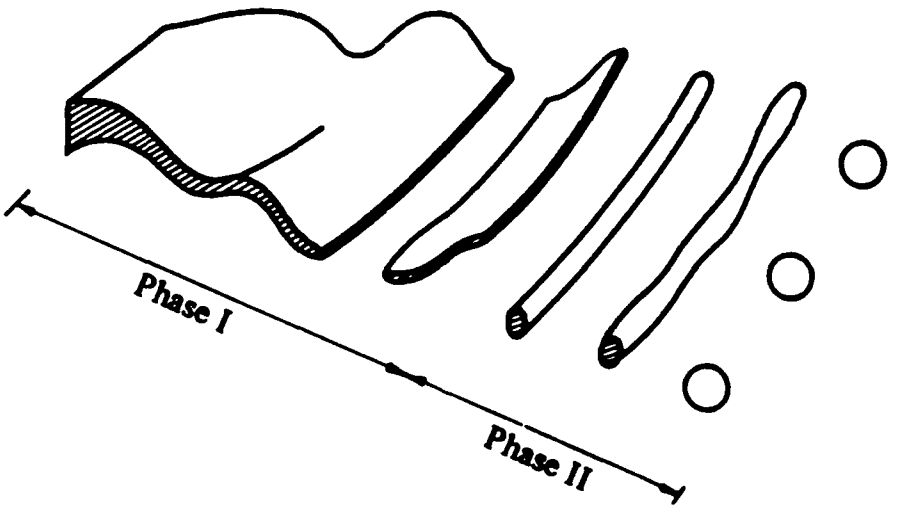

The Dombrowski and Johns (1963) model for liquid-sheet breakup and atomization

The maximum entropy formalism has been used by Tankin and co-workers (1991) to predict the droplet size and velocity distributions in sprays, provided that the mean droplet size and velocity are measured. The present theory could serve as a more convenient and affordable means of computing these parameters. This is evident given the large number of experimental conditions that need to be varied if the mean diameter and velocity are determined experimentally.

Crapper and Dombrowski (1984) found that the drop size may be affected by both nozzle amplitude and frequency. Since these factors may depend on natural frequencies in the apparatus, drop sizes in industrial applications could well be different from those given by the same nozzle in a laboratory test. This finding favors a theoretical approach to estimations of mean drop size which may then be incorporated in the maximum entropy formalism to yield purely theoretical predictions of drop size distribution.

REFERENCES

Chin, L. P., LaRo[illegible] P. G., Tankin, R. S., Jackson, T., Stutrud, J., and Switzer [illegible], 1991, Phys. Fluids A, 3, pp. 1897-1906.

Crapper, G. D , Dombrowski, N., Jepson, W. P., and Pyott, G. A. D., 1973, J. Fluid Mech., 57, pp. 671-672.

Crapper, G. D., and Dombrowski, N., 1984, Int. J. Multiphase Flow, 10, pp. 209-224.

Dombrowski, N., and Johns, W. R., 1963, Chem. Engng. Sci., 18, pp. 203-214.

Dombrowski, N., and Hooper, P., 1962, Chem. Engng. Sci., 17, pp. 291-305.

Li, X., and Tankin, R. S., 1991, J. Fluid Mech., 226, pp. 425-443.

Li, X., Chin, L. P., Tankin, R. S., Jackson, T., Stutrud, J., and Switzer, G., 1991, Combust. Flame, 86, pp. 73-89.

Squire, H. B., 1953, Brit. J. Appl. Phys., 4, pp. 167-169.

Taylor, G. I., 1959, Proc. Roy. Soc. A, 253, pp. 289-321.

Weihs, D., and Frankel, I., 1982, J. Fluid Mech., 116, pp. 393-409.

ADVANCED DIAGNOSTICS FOR REACTING FLOWS

AFOSR90-89-0067

Principal Investigator: Ronald K. Hanson

High Temperature Gasdynamics Laboratory
Mechanical Engineering Department
Stanford University, Stanford, CA

SUMMARY/OVERVIEW

This research is directed toward innovation of advanced diagnostic techniques applicable to combustion gases and plasmas, with some emphasis on high speed flows. The primary flowfield parameters of interest are species concentrations, temperature, pressure, mass density, electron density, and velocity, and quantities derivable from these parameters such as mass flux and thrust (calculable from mass density and velocity). Principal techniques under study include spectrally-resolved absorption and fluorescence, using wavelength-modulated cw ring dye laser and cw semiconductor diode laser sources, and planar laser-induced fluorescence (PLIF), using tunable pulsed laser sources (excimer-pumped dye and narrow-linewidth excimer). New plasma diagnostic techniques based on degenerate four-wave mising are also under study.

TECHNICAL DISCUSSION

In the following paragraphs we highlight primary activities of the past year.

Plasma Diagnostics

Recent research has involved two activities: (1) a new effort aimed at exploring degenerate four-wave-mixing (DFWM) as a plasma diagnostic; and (2) an ongoing program to apply tunable semiconductor diode lasers for line-of-sight absorption and single-point LIF measurements of plasma properties. The latter study has utilized a home-built RF-powered plasma torch (1 kW) which provides a convenient bench-top plasma source with good optical access. The torch operates at atmospheric pressure on argon, providing temperatures up to 9000 K and electron densities up to 10^{16}/cc, with the capability of adding trace levels of various additives of spectroscopic interest. Present work involves LIF studies of transitions from the 4s state of argon using tunable GaAlAs laser sources. In brief, spectrally resolved lineshapes are recorded, from which it is possible to infer: the kinetic gas temperature (Doppler linewidths), the population temperature of the quantum state being monitored, and the electron density (from the Stark shift or linewidth), all with mm spatial resolution. A sample data trace is shown in Fig. 1; see Ref. 1 for details. To our knowledge, these measurements represent the first diode-laser LIF measurements in plasmas. LIF offers important advantages over previous spectroscopic plasma diagnostics based on emission, since emission does not yield spatially resolved results.

PLIF Imaging in Shock Tube Flows

Shock tubes and tunnels provide a convenient means of studying nonequilibrium gasdynamic phenomena and of simulating conditions relevant to advanced air-breathing propulsion systems. During the past year we have continued development of our shock tube and tunnel facility, and have made good progress in efforts to establish PLIF imaging techniques for shock-heated flows. Published results include: PLIF imaging of OH in shock-ignited H_2-O_2-Ar mixtures, using a non-planar shock tube end wall to produce local nonuniformities in temperature and hence ignition times, see Ref. 2; a study of PLIF imaging of NO in vibrationally relaxing shock tube flows, e.g. normal shock waves and shock tube flow over blunt bodies, see

Ref. 3; and PLIF imaging of transverse jet mixing and combustion in supersonic, shock-heated flows, see Ref. 4. Initial results for PLIF imaging of velocity and temperature in a shock tunnel have also been presented (Ref. 5).

Shock Tube Studies of Combustion Kinetics

In addition to providing an attractive test environment for developing laser diagnostics, shock tubes are recognized as the facilities of choice for measurements of reaction rate coefficients at high temperatures. In the past year, we have continued efforts to develop and apply narrow-linewidth laser absorption techniques for the measurement of elementary reactions relevant to combustion and propulsion. Highlights include development of a new, more-sensitive laser absorption diagnostic for CH_3 at 216 nm, and completion of rae coefficient measurements for the reactions $CN + O \rightarrow CO + N$ and $CN + O_2 \rightarrow NCO + O$ (Ref. 6).

CW Ring Dye Laser Techniques

Tunable monochromatic laser sources provide opportunities for measurement concepts based on spectrally resolved absorption lineshapes. For example, cw ring dye lasers can be rapidly modulated in wavelength to record a pair of absorption lines, using either line-of-sight absorption or single-point LIF, allowing inference of gas temperature through the ratio of the signals for the two lines. The total static pressure can also be inferred, using the width of the recorded lines whenever collision-broadening is significant or the magnitude of the absorption (or fluorescence) signal when chemical composition is fixed. In addition, velocity can be inferred from the shift in spectral line position caused by the Doppler effect; in essence this is molecular velocimetry. Note that by a complete analysis of the spectra for each wavelength scan, one can infer all of these flowfield parameters simultaneously. Finally, with these quantities determined, it is feasible to infer other relevant flowfield parameters, such as mass flux or thrust, by appropriate combinations of the directly measured quantities.

An important accomplishement during the past year has been the extension of this method to perform spectrally-resolved, single-point LIF of NO in a supersonic jet. An example data trace acquired on the jet centerline at x/D = 0.75 during a single 200 microsecond scan of a pair of NO lines in the (0,0) band near 226.7 nm is shown in Fig. 2. A comparison of the measured and computed properties (see inset of Fig. 2) shows good agreement. See Ref. 7 for details.

Semiconductor Diode Laser Techniques

Tunable diode lasers offer the possibility of an economical, rugged and compact alternative to cw ring dye lasers for spectrally resolved absorption and fluorescence spectroscopy. Such lasers are presently available in several wavelength intervals at wavelengths generally in excess of 650 nm, although operation at shorter wavelengths is expected in the future. These lasers have significant potential advantages over ring dye lasers, including the possibility of high frequency modulation of laser wavelength through current modulation. At present we are pursuing two projects with these lasers, one aimed at detecting O_2 at 760 nm (the atmospheric band of oxygen) and the other at detecting H_2O near 1.35 microns. During the past year we have demonstrated the capability of monitoring spectrally resolved absorption lines of O_2 in supersonic flows produced in a shock tube. The scheme involves combining high-frequency (10 MHz) modulation with a high-speed (10 kHz) current ramp to repetitively tune the laser across one or more O_2 absorption lines. The data yield temperature, O_2 density, velocity and mass flux, all path-averaged over the width of the supersonic stream produced in a shock tube. A schematic of the experiment is shown in Fig. 3; a comparison between measured and calculated flow velocity is given in Fig. 4. Details may be found in refs. 10 and 11. It is clear that these lasers have great potential both for fundamental research and for packaged, user-friendly instruments, e.g. flight instrumentation.

Digital Camera For High-Speed Imaging

Continued progress has been made in the development of a high-speed digital camera for recording instantaneous 3-d images and fast 2-d image "movies." The basic concept involves modifying a commercial image converter camera (Imacon 790) to incorporate CCD detection. A tapered fiberoptic bundle is used to transfer the output plane image of the Imacon onto a high-resolution (400x1200 pixels), low-noise CCD array detector. This system is capable of recording at 10 million frames per second. Together with a high-energy, long-pulse dye laser source to provide "cw" flowfield illumination, this camera allows rapid recording of multiple PLIF images, constituting either an essentially instantaneous multiple-plane 3-d image data set or a multiple-image movie over a brief time interval (2 microseconds for the current pulsed dye laser); see Ref. 12 for recent results.

REFERENCES

1. D. S. Baer, H. A. Chang and R. K. Hanson, "Fluorescence Diagnostics for Atmospheric Pressure Plasmas Using Tunable Diode Lasers," submitted to JOSA B, Feb. 1992.

2. B. K. McMillin, M. P. Lee, P. H. Paul and R. K. Hanson, "Planar Laser-Induced Fluorescence Imaging of Shock-Induced Ignition," *Twenty-Third Symposium (International) on Combustion*, The Combustion Institute, 1909-1913 (1990).

3. B. K. McMillin, P. H. Paul and R. K. Hanson, "Planar Laser-Induced Fluorescence Imaging of Nitric Oxide in Shock Tube Flows with Vibrational Nonequilibrium," AIAA J. **30**, 436-443 (1992).

4. M. P. Lee, B. K. McMillin, J. L. Palmer and R. K. Hanson, "Two-Dimensional Imaging of Mixing and Combustion of Transverse Jets in Shock Tube Flows," J. Prop. and Power, in press.

5. J. L. Palmer, B. K. McMillin and R. K. Hanson, "Planar Laser-Induced Fluorescence Imaging of Velocity and Temperature in Shock Tunnel Free Jet Flow," paper AIAA-92-0762 at 30th Aerospace Sciences meeting, Reno, Jan. 1992.

6. D. F. Davidson, a. J. Dean, M. D. DiRosa and R. K. Hanson, "Shock Tube Measurements of the reactions of CN with O and O_2," I. J. Chem. Kin. **23**, 1035-1050 (1991).

7. M. D. DiRosa, A. Y. Chang and R. K. Hanson, "CW Dye Laser Technique for Simultaneous, Spatially-Resolved Measurements of Temperature, Pressure and Velocity of NO in an Underexpanded Free Jet," Applied Optics, submitted March 1992.

8. D. F. Davidson, A. Y. Chang, M. D. DiRosa and R. K. Hanson, "CW Laser Absorption Techniques for Gasdynamic Measurements in Supersonic Flows," Applied Optics **30**, 2598-2608 (1991).

9. A. Y. Chang, M. D. DiRosa, D. F. Davidson and R. K. Hanson, "Rapid-Tuning CW Laser Technique for Measurements of Gas Velocity, Temperature, Pressure, Density and Mass Flux Using NO," Applied Optics **20**, 3011- 3022 (1991).

10. L. C. Philippe and R. K. Hanson, "Laser Absorption Mass Flux Sensor for High-speed Airflows," Opt. Lett. **16**, 2002-2004 (1991).

11. L. C. Philippe and R. K. Hanson, "Sensitive Diode-Laser Absorption Technique for Aerodynamic Measurements," paper AIAA-92-0139 at 30th Aerospace Sciences Meeting, Reno, Jan. 1992.

12. B. J. Patrie, J. M. Seitzman and R. K. Hanson, "Planar Imaging at High Framing Rates: System Characterization and Measurements," paper AIAA-92-0584 at 30th Aerospace Sciences Meeting, Reno, Jan. 1992.

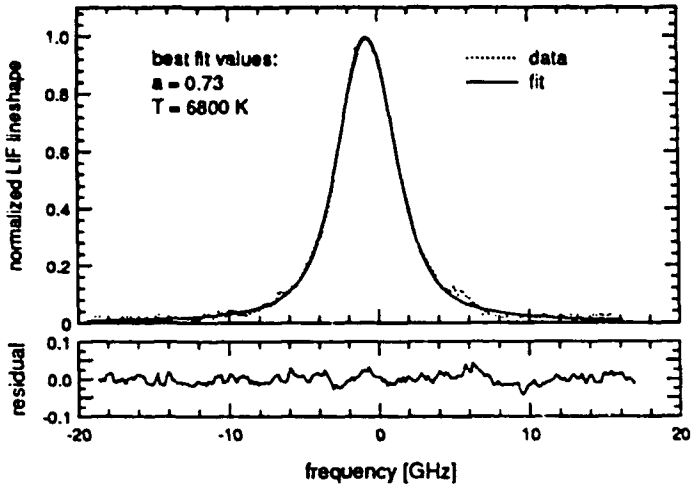

Fig. 1. LIF lineshape and best-fit Voigt profile of an excitation scan of the $4s^3P_1 - 4p^3D_1$ transition (8104 Å) in an argon plasma. The residual shows the difference between the data and the best-fit Voigt profile. The inferred value of N_e (from a = .73) is 3×10^{15}/cc.

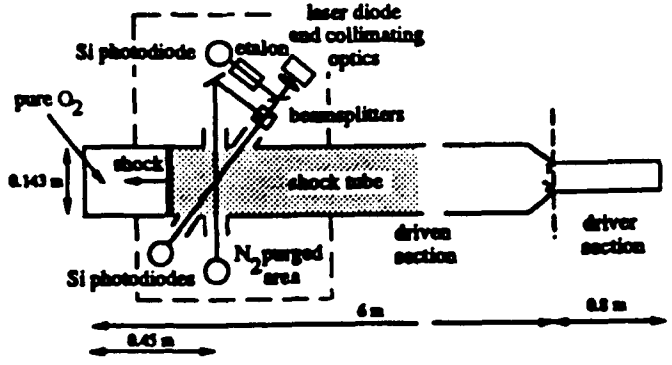

Fig. 3. Optical arrangement for velocity measurements in a shock tube using spectrally-resolved diode laser absorption.

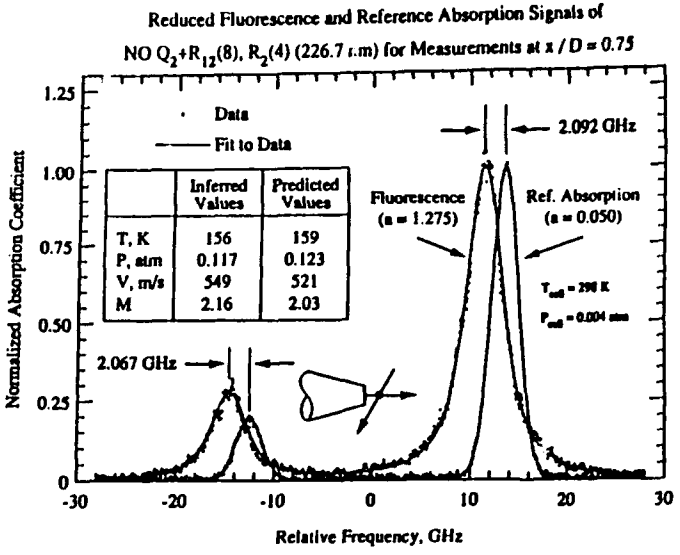

Fig. 2. Single-sweep single-point LIF data of NO in a free jet.

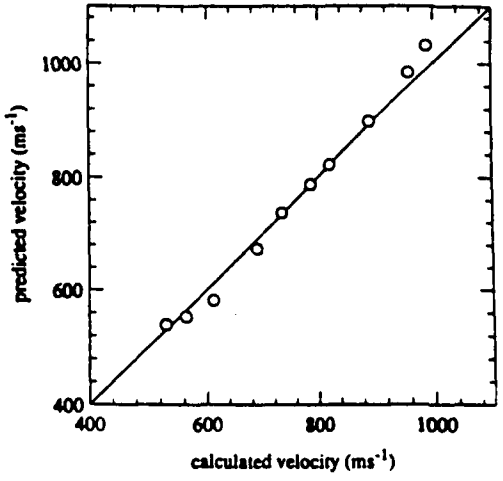

Fig. 4. Comparison of diode laser velocity measurements using the RQ(13,14) line with the predictions of shock wave theory.

NOVEL NONLINEAR LASER DIAGNOSTIC TECHNIQUES

(AROSR Contract No. F-49620-90-C-0044)

Principal Investigators: David L. Huestis, Gregory W. Faris, and Jay B. Jeffries

SRI International
Molecular Physics Laboratory
Menlo Park, CA 94025

SUMMARY/OVERVIEW:

Task 1: UV and VUV Generation and Detection Techniques

We are developing techniques for the extension of laser-based diagnostics into the vuv for detection of atomic ions and for other detection techniques requiring high powers in the vuv. We report the demonstration of two-photon-excited fluorescence at much shorter wavelengths than has previously been achieved; atomic neon is excited using 133 nm radiation produced by two-photon-resonant four-wave difference-frequency generation.

Task 2: Laser-Excited Amplified Spontaneous Emission (ASE)

Detection of atoms in reacting gas flows by ASE is attractive because the ASE signal is collimated along the excitation laser beam. Thus, ASE measurements are possible with minimal optical access compared to fluorescence techniques. The spectral bandwidth of the ASE signal contains information about the temperature and velocity of the gas; however, research is required to understand other contributions to the ASE bandwidth. During the second year of the research we have: 1) quantified laser-induced fluorescence measurements of atomic hydrogen in a variety of low-pressure flames and compared these linear measurements with simultaneous ASE measurements, 2) measured the bandwidth of the H atom ASE at 1200 and 1800 K, 3) obtained simultaneous O atom ASE and LIF signals, and 4) assembled a model and calculated the intensity variation from laser excited gain on a diode seed laser.

TECHNICAL DISCUSSION

Task 1: UV and VUV Generation and Detection Techniques
by Gregory W. Faris and Mark J. Dyer

We are pursuing the detection of hard to detect species such as atomic ions which require two-photon excitation with vacuum ultraviolet light. Through generation of higher power radiation in the vacuum ultraviolet, techniques commonly used in the near ultraviolet such as multiphoton ionization, two-photon-excited fluorescence, amplified spontaneous emission, and planar laser-induced fluorescence may be applied to other species for better understanding of chemical dynamics, plasma kinetics, and basic spectroscopy.

A year ago we reported on the generation of high power vuv radiation using two-photon-resonant difference-frequency mixing using an ArF excimer laser and a frequency-doubled dye laser.[1,2] The ArF laser can reach two-photon resonances in krypton, H_2, and HD. Mixing with the dye laser radiation results in tunable vuv radiation with energy equal to the difference between the two-photon resonance and the dye photon energy, corresponding to a tuning range between

110 and 180 nm. This same approach was also demonstrated by a second group last year.[3] Prior to these two demonstrations using ArF excimer lasers, a frequency-doubled dye laser has been used as the fixed-frequency laser for this four-wave-mixing process.[3,4] The advantages of using an ArF excimer laser for this mixing are the significantly higher powers available from the ArF laser and the shorter wavelength of the ArF laser, which allows reaching shorter vuv wavelengths as well as improved phasematching leading to higher powers. To date, we have obtained up to 20 microjoules at 133 nm using this technique. This is adequate for nonlinear optical diagnostic techniques such as two-photon-excited fluorescence.

In the past year we have applied this radiation to two experiments to examine feasibility of multiphoton techniques at short vuv wavelengths. By performing multiphoton excitation on noble gases we can examine basic questions concerning sensitivity and technological complications without the additional experimental difficulty of the production of atomic ions. We have investigated two systems; 1+1 resonantly-enhanced multiphoton ionization (REMPI) of atomic xenon and two-photon excited fluorescence of atomic neon.

We have used two photons at 147 nm to perform 1+1 REMPI through the $5p^5 6s[3/2,1]$ state of xenon. The 147-nm radiation was produced through mixing in krypton. Because vuv radiation can readily ionize many molecular species, background ion signals are a major consideration for vuv REMPI. With energies of only 3 microjoules we have obtained signal-to-noise ratios of > 50 for the ion signal, indicating that this approach can give useful signals. A power dependence of the ion signal from xenon is shown in Figure 1. From the figure, it is apparent that the signal follows the expected square dependence on the vuv power. Because the signal relies on detection of ions, 1+1 REMPI is not very well suited to detection in plasmas. However, 1+1 REMPI might be performed in plasmas in conjunction with optogalvanic detection. In addition 1+1 REMPI with vuv radiation is useful when high sensitivity measurements are required, such as for resonant ionization mass spectroscopy of trace species; when two-photon techniques lead to photodissociation or other production or destruction mechanisms that can cause detection errors; and it can serve as a calibration procedure for two-photon excitation.

For the demonstration of two-photon excited fluorescence at shorter wavelengths in the vuv, we have chosen neon, which, with the first two-photon resonance corresponding to ~133 nm, is the second most difficult neutral atom to excite after helium. The conversion efficiency for mixing in krypton drops significantly between 147 nm and 133 nm. We have used mixing in H_2 to produce the 133-nm radiation. The unwanted amplified spontaneous emission (ASE) produced when performing mixing in H_2[1,2,6] is weaker in the region of 133 nm than near 147 nm. We have been able to avoid difficulties from this ASE through separation of the four-wave-mixing radiation with a MgF_2 prism.

Production of 133-nm light is much more difficult than for the 147-nm light due to buildup of a vapor contaminant that strongly absorbs the vuv. We have not entirely solved this problem, but have been able to observe the two-photon resonant fluorescence on excitation of the $2p^5 3p[3/2,2]$ state of neon from the ground state. Fluorescence is detected using a photomultiplier and a 700-nm short pass filter. An excitation spectrum for this transition is shown in Figure 2 for a pressure of 100 torr of neon. The signal is fairly weak currently, on the level a few photons per shot, but the system has not been optimized. These initial measurements on two-photon-excited fluorescence in neon indicate the feasibility of two-photon-excited fluorescence in atomic ions through excitation with radiation produced by two-photon-resonant difference-frequency mixing. This is but one of many interesting diagnostic techniques possible with high power vuv radiation.

Task 2: Laser Excited Amplified Spontaneous Emission
by Jay B. Jeffries, Dwayne E. Heard, and Michael S. Brown

Atoms are excited by multiphoton laser excitation in flames, plasmas and reacting flows and are detected by fluorescence and ionization techniques. Two photon selection rules produce atoms excited to states which do not have an allowed transition to the ground state but instead radiate to an intermediate level. In light atoms like hydrogen and oxygen these intermediate states

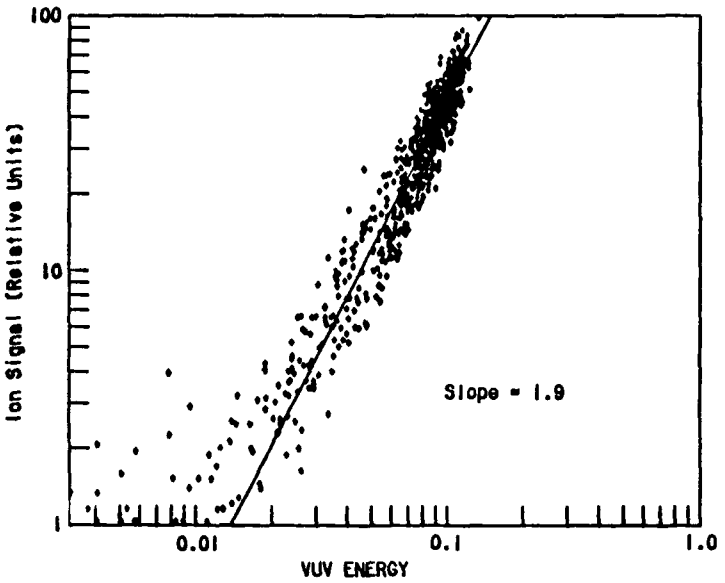

Fig. 1. Power dependence for ion signal from 1+1 REMPI in xenon.

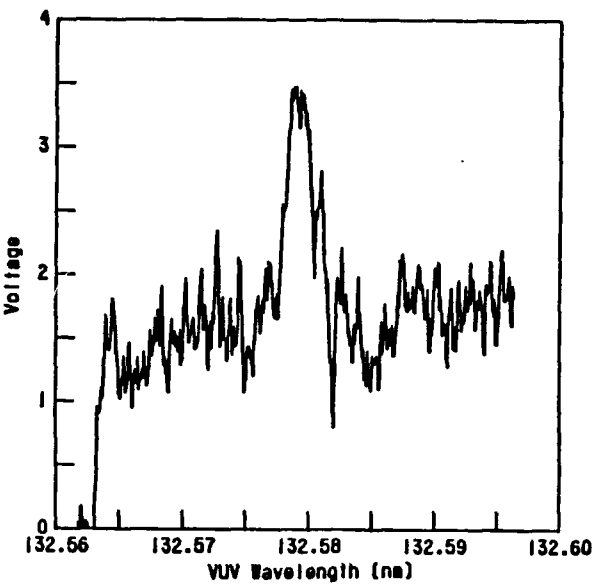

Fig. 2. Two-photon-excited fluorescence signal in neon using 133-nm radiation.

are more than 10 eV above the ground state. Thus at combustion temperatures, there is little thermal population in these intermediate states. As soon as a significant number of the ground state atoms are two-photon excited, there is a population inversion between the excited and intermediate states and spontaneous emission along the excitation laser direction can experience gain. Such gain produces amplified spontaneous emission (ASE) directed forward and backward along the laser beam.

During the past year we have studied two photon excited ASE of atomic hydrogen and oxygen in a variety of flames. Two photons near 205 nm excite the 3S and 3D states of hydrogen which subsequently radiate Balmer α near 656nm to the 2P state; two photons near 226 nm excite oxygen to the 3p ^{3}P state which subsequently radiates near 845 nm to the 3s ^{3}S state. Low-pressure flames provide stable sources of large concentrations of hot atoms; using flame conditions identical to those used previously in our laboratory to study OH[7], HCO[8], and NO[9], we have gas temperature measurements and model predictions of the gas composition.

Simultaneous H atom LIF and ASE are observed in all the flames studied. Using our model predictions of the major species concentrations, we corrected the LIF signals for collisional quenching using the data of Meier et al.[10] We found a serious discrepancy between our model prediction and the measured H atom concentration. We discovered that our low-pressure flames were not well described by a 1-D fluid model and that radial transport must be included. Radial transport increases the diameter of the flame and reduces the average gas flow velocity. This increases the reaction time and produces a flame closer to the burner surface than predicted by a 1-D model. Corrections to our fluid flow model have significantly improved the agreement between measurement and prediction for all the radical intermediate species previously measured in the laboratory for the flames below 10 Torr.

Measurements of the Balmer α ASE bandwidth from atomic hydrogen were demonstrated last year. The ASE signal is diverged through an etalon and the interference fringes imaged on a 2-D camera. We have made careful measurements of the bandwidth in 1200 K H_2/O_2 flames at 25 Torr and 1800 K CH_4/O_2 flames at 25 Torr. The velocity distributions of the atomic hydrogen in the two flames are significantly different. However, we find that the ASE bandwidth does not reflect this difference. The excited 3S and 3D states of atomic hydrogen are nearly degenerate and are within the Doppler width of the two-photon transition. However, the splittings can provide a significant contribution to the Balmer α bandwidth compared to the Doppler width. We believe that laser induced state mixing and excitation of only a fraction of the initial distribution of atomic hydrogen contributes to the ASE bandwidth observed.

Atomic oxygen appears to be a better candidate for determination of whether gas temperature can be determined from ASE bandwidth measurements. The difference in mass reduces the Doppler widths. We can selectively excite either the entire ground state velocity distribution or a narrow slice of the velocity distribution by varying the bandwidth of the excitation light by using our dye laser with or without an etalon. We excite only one of the lower state fine structure components. We have observed simultaneous ASE and LIF in the low-pressure H_2/O_2 flame from atomic oxygen, and bandwidth measurements are underway. We believe that these experiments will unravel the broadening mechanisms of the ASE.

Direct measurement of the atomic inversion via gain measurements has been theoretically investigated. Here a cw diode laser tuned to the wavelength of the atomic fluorescence is co-propogated with the two-photon excitation laser. When the pulsed excitation laser produces excited states, the light from the cw laser will be amplified. The amount of amplification is a direct measure of the gain. The two-photon excitation cross section for atomic oxygen is known;[11] thus, the gain measurement gives a direct measure of atom concentration. To understand how much gain to expect, we have developed a time dependent computer model of the ASE signal from atomic oxygen. The model includes loss from the excited state from collisional quenching, energy transfer from the triplet to quintet manifold, photo-ionization, fluorescence, and ASE. We consider the linear excitation regime to eliminate Rabi flopping and other complicating processes. For the oxygen concentration in our low-pressure flame, we predict that a 4 mJ, 10 ns excitation pump will stimulate a 5% power gain in a 10 mW cw single-mode diode laser at 845nm. The temporal profile of the gain follows that of the excitation pulse with less than 1 ns delay. The diode laser requirements are thus quite modest and a laser is being purchased.

REFERENCES

1. G. W. Faris, J. B. Jeffries, and D. L. Huestis, Annual Technical Report AFOSR Contract No. F49620-90-C-0044, SRI International, Menlo Park, CA (June 1991).
2. G. W. Faris and M. J. Dyer, in Short Wavelength Coherent Radiation: Generation and Applications, P. H. Buckbaum and N. M. Ceglio, Eds. (Optical Society of America, Washington, DC, 1991) pp. 58-61.
3. C. E. M. Strauss and D. J. Funk, Opt. Lett. **16** 1192 (1991).
4. G. Hilber, A. Lago, and R. Wallenstein, J. Opt. Soc. Am. B 4, 1753 (1978).
5. J. P. Marangos et al., J. Opt. Soc. Am B 7, 1254 (1990).
6. H. Pummer et al. Phys. Rev. A **28**, 795 (1983).
7. K. Kohse-Höinghaus, J. B. Jeffries, R. A. Copeland, G. P. Smith, and D. R. Crosley, 22d Symposium (International) on Combustion, The Combustion Institute, Pittsburgh, PA, 1989, p 1857.
8. J. B. Jeffries, D. R. Crosley, I. J. Wysong, G. P. Smith, 23d Symposium (International) on Combustion, Combustion Institute, Pittsburgh, PA, 1990, p. 1847.
9. D. E. Heard, J. B. Jeffries, G. P. Smith, and D. R. Crosley, Combustion and Flame, (1991) in press.
10. U. Meier, K. Kohse-Hönghaus, and Th. Just, Chem. Phys. Lett., **126**, 567 (1986).
11. D. J. Bamford, M. J. Dyer, and W. K. Bischel, Phys. Rev. **A36**, 3497 (1987).

RAPID CONCENTRATION MEASUREMENTS BY PICOSECOND TIME-RESOLVED LASER-INDUCED FLUORESCENCE

AFOSR Grant No. AFOSR-91-0365

Galen B. King
Normand M. Laurendeau

Flame Diagnostics Laboratory
School of Mechanical Engineering
Purdue University
West Lafayette, IN 47907

SUMMARY/OVERVIEW:

This research is concerned with the development of a laser-based diagnostic technique for the measurement of species concentrations in turbulent flames called picosecond time-resolved laser-induced fluorescence (PITLIF). Current diagnostic techniques have the capability to measure probability distribution functions (PDF's), but in many cases they lack the temporal resolution needed to measure power spectral densities (PSD's). The PITLIF instrument employs a high repetition rate mode-locked laser which gives it the temporal resolution and power necessary to rapidly obtain PSD's in addition to PDF's. The specific objective of this project is to develop the PITLIF instrument and to demonstrate its viability for obtaining PDF's and PSD's of concentration in turbulent flames.

TECHNICAL DISCUSSION:

Turbulent flames are characterized by random fluctuations in flow variables such as velocity or concentration.[1] These fluctuations must be described statistically using PDF's and PSD's. Laser Doppler velocimetry (LDV) can be used to measure PDF's and PSD's of velocity in a turbulent flame.[2] Laser-induced fluorescence (LIF) is commonly employed for measurement of minor species concentrations.[3] Typically, CW or Q-switched laser systems are employed for LIF measurements of PDF's, but these systems lack the power and temporal resolution necessary to measure PSD's of concentration in turbulent flames. Both the PDF and the PSD must be known to completely describe the random fluctuations in concentration. We report here on initial investigations with picosecond time-resolved laser-induced fluorescence (PITLIF), a new diagnostic technique which has the potential to rapidly and simultaneously measure both PDF's and PSD's of concentration in a turbulent flame.

A block diagram of the PITLIF instrument is shown in Figure 1. The laser system consists of a broadband dye laser synchronously pumped by a mode-locked frequency-doubled Nd:YAG laser. The laser system delivers a series of mode-locked laser pulses approximately 50 ps FWHM

---

[1] J. O. Hinze, *Turbulence*, McGraw Hill, New York (1975).

[2] J. O. Keller, J. L. Ellzey, R. W. Pitz, I. G. Shepherd and J. W. Daily, "The structure and dynamics of reacting plane mixing layers", *Experiments in Fluids*. **6**, 33 (1988).

[3] M. C. Drake and R. W. Pitz, "Comparison of turbulent diffusion flame measurements of OH by planar fluorescence and saturated fluorescence", *Experiments in Fluids*. **3**, 283 (1985).

at a repetition rate of 82 MHz. The laser system irradiates a region of the flame, and through interaction with atoms or molecules in the flame, light is absorbed and spontaneously emitted. The detector, a photomultiplier tube, measures some of this emitted light. The output of the detector is fed into two parallel data acquisition channels. The low-bandwidth acquisition system uses a low-pass filter to filter out individual laser pulses and records the integrated fluorescence signal which provides a measure of the low frequency (<10 kHz) fluctuations in the LIF signal. The low-bandwidth system can be used alone to measure concentration fluctuations in systems where the variation in quenching is small. The high-bandwidth acquisition system (0-2 GHz) has the temporal resolution necessary to record each laser pulse, and thus can be used to measure the lifetime of the decay for the excited state. From this measurement of lifetime, we can determine the magnitude of the quenching rate coefficient. Thus, when the high-bandwidth system is used in conjunction with the low-bandwidth system, the PITLIF instrument can be used to measure concentration fluctuations in systems where the variation in quenching is large. In either case, the result is a temporal record of concentration fluctuations which can be used for on-the-fly generation of the PDF and the PSD.

Initial investigations with the PITLIF instrument have focussed on the development of the low-bandwidth system. We have elected to study atomic sodium seeded into a $H_2/O_2/Ar$ diffusion flame. The burner is a concentric tube diffusion burner in which hydrogen flows through a circular tube, and an oxygen/argon mixture flows through a surrounding annulus. Sodium is seeded into the oxygen/argon mixture using an atomizer. The flame is a laminar diffusion flame, and the fluctuations in sodium are caused primarily by the atomization process. Using this simple flame, we are able to demonstrate the utility of the technique for systems where concentration fluctuations are caused by turbulent mixing in the flame.

To characterize the frequency response of the low-bandwidth system, an acoustic oscillator was constructed to perturb the flame at a known frequency. The acoustic oscillator consists of an audio speaker enclosed in a chamber which is connected to the hydrogen supply line. The speaker is driven by a function generator. The acoustic oscillator produces compressions and rarefactions in the hydrogen gas which perturbs the combustion process sufficiently to produce a measurable variation in sodium concentration. Figure 2 shows the power spectrum of the concentration fluctuations with the acoustic oscillator operating at 200 Hz. The power spectrum has been normalized to a value of unity at the low frequency point. To minimize noise introduced by the fast Fourier transformation process, 16 individual FFT's were averaged to produce this PSD. Each FFT was obtained from a data record of 2048 points acquired at a 16 kHz rate. The spike due to the acoustic oscillator can clearly be resolved above the background. Using this technique we have been able to demonstrate that frequencies from 20 to 900 Hz can be resolved with minimal averaging. The system is currently limited to < 1 kHz by the passband of the lock-in amplifier used in the low-bandwidth system, but the frequency response can easily be extended to 10 kHz with simple modifications to the detection system.

Figure 3 shows an example of the type of data which can be collected using the low-bandwidth system. Figure 3(a) shows a temporal record of the concentration fluctuations in which 2048 data points were collected at a 2 kHz acquisition rate. Data were collected 1 cm above the center of the burner, and the values are normalized to a mean value of unity. Figure 3(b) shows a probability distribution function for the temporal record shown in Figure 3(a). The probability is plotted versus the number of standard deviations from the mean; each bin is 1/3 of a standard deviation. Figure 3(c) shows the power spectral density for the concentration fluctuations obtained by taking the fast Fourier transform of the temporal record in Figure 3(a).

We have demonstrated that the low-bandwidth system can be used to study fluctuating concentration in systems where the variation in quenching is small. We have also shown that we can generate PDF's and PSD's of these concentration fluctuations. Future work will focus on the development of the high-bandwidth system which will allow the PITLIF instrument to be applied to systems where the variation in quenching is large.

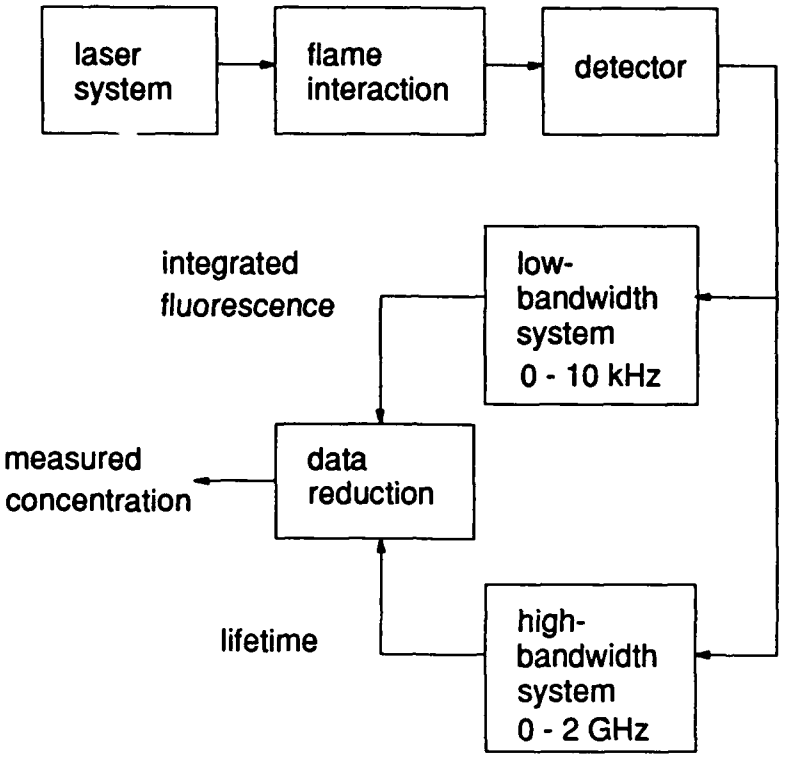

Figure 1. Block diagram of the PITLIF instrument

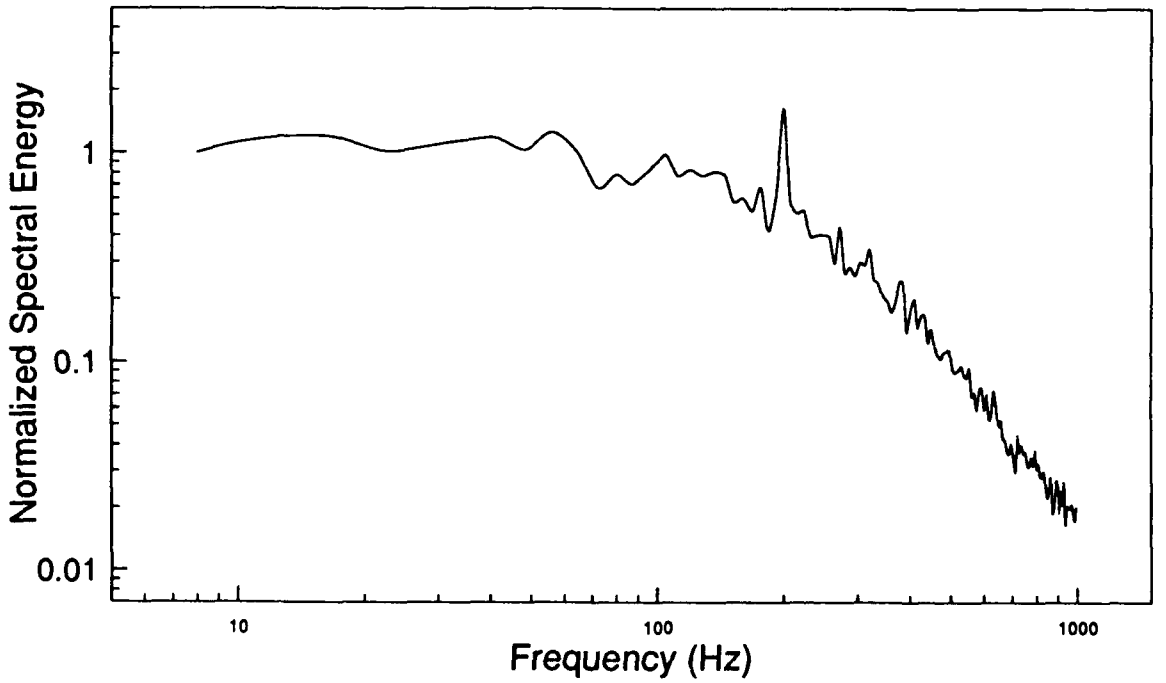

Figure 2. Power spectrum of the concentration fluctuations with the acoustic oscillator operating at 200 Hz. The spike due to the acoustic oscillator can clearly be resolved above the level of the background.

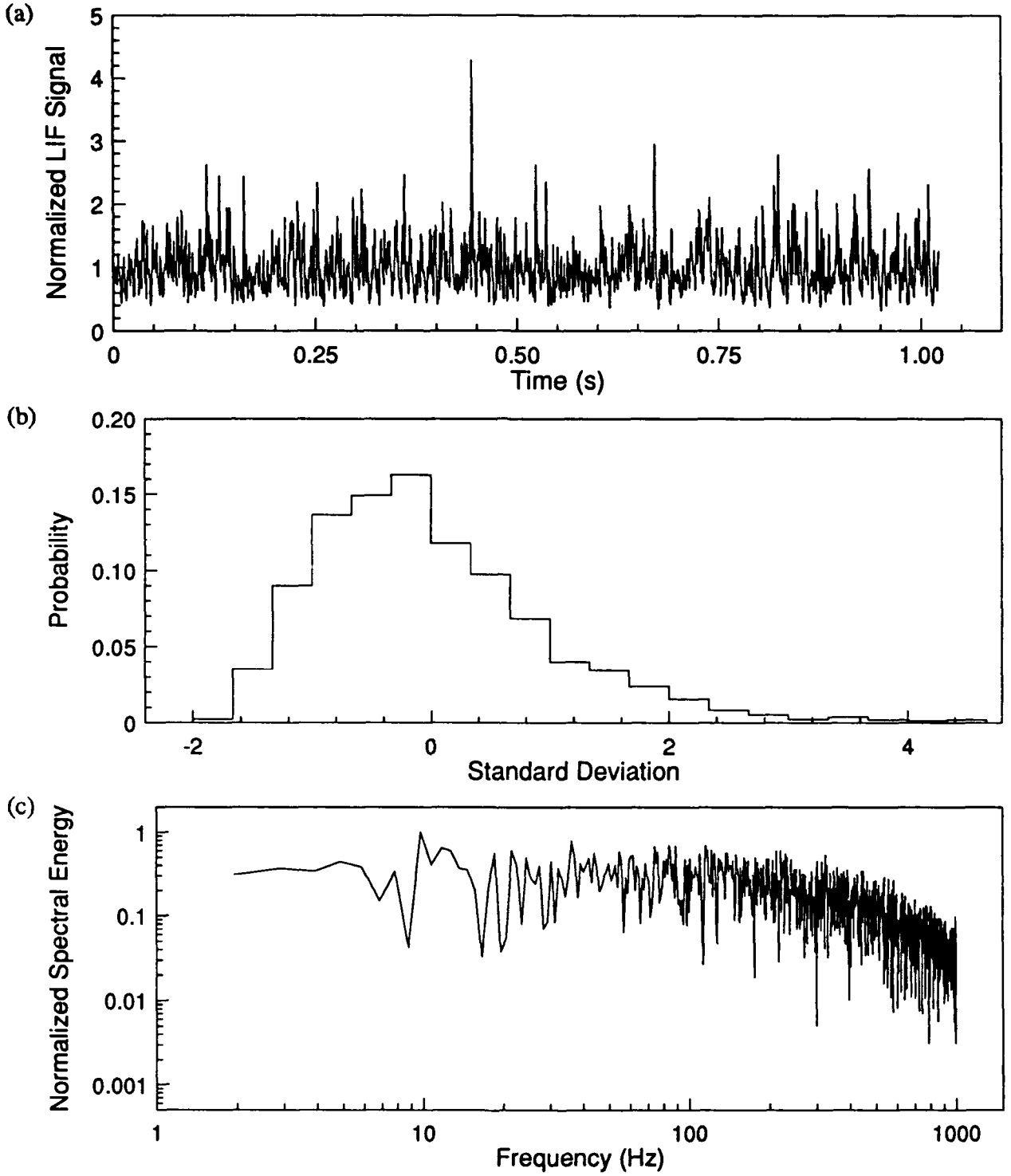

Figure 3. A temporal record of the concentration fluctuations is shown in (a) where the LIF signal is normalized to a mean value of one. The probability distribution function for (a) is shown in (b) where probability is plotted versus number of standard deviations from the mean; the bin sizes are 1/3 of a standard deviation. The power spectral density of the concentration fluctuations is shown in (c) where spectral energy is normalized to a maximum value of one.

ENERGY CONVERSION DEVICE DIAGNOSTICS

Principal Investigator: B. N. Ganguly

Wright Laboratory
Wright-Patterson AFB, OH 45433-6563

SUMMARY/OVERVIEW: Spectroscopic methods are developed for the measurements of electric field profiles, space-charge density and electrical conductivity of plumes subjected to electrical stress. Combustion kinetics modificatons caused by applied external voltages are investigated by measuring gas temperature, velocity and chemi-excited radical profiles changes.

TECHNICAL DISCUSSION: The characterization of basic plasma parameters of flames and plumes, such as electric field and ion density have, so far, relied primarily on the electrostatic probe measurement[1]. The validity of the electrostatic probe measurements would be questionable in turbulent flames where temperature and gas density fluctuations lead to corresponding variations in electron and ion energies, densities, and mobilities. Some of these effects, in turn, will cause a nonlinear fluctuation of the probe characteristics that may severely limit the accuracy of the probe measurements.

The Rydberg state Stark spectroscopic technique has been shown to be an excellent diagnostic tool for plasma parameters measurement in low pressure glow discharges.[2,3] We report the application of the Rydberg state Stark spectroscopic method for spatially resolved electric field measurement in an atmospheric pressure, cesium-seeded, flame.

A schematic of the experimental setup is shown in fig. 1. The flame is seeded with cesium by atomizing a dilute CsOH solution into the air line of the premixed burner. An external electric field is applied across copper electrodes placed on both sides of the flame. The Stark spectra of n=19 and 20 Rydberg states measured at 2 mm, 3.5 mm, and 4.5 mm from the cathode surface, with 780 volt applied voltage, are shown in fig. 2.

The electric field values are estimated from the Stark energy splittings of $nP_{3/2}$ and $nD_{5/2}$ spectral lines by fitting the measured energy splittings with the electric field dependent calculated Stark energy levels. The Stark perturbation calculation is performed by following the procedure developed by Zimmerman et. al.[4] for the case of $m_j=1/2$, corresponding to the Π polarization, using j-basis which takes into account the nondegenerate j states for each value of l.

The electric field profiles in the flame, obtained with 780 volts and 380 volts applied voltage, are shown in fig. 3. The electric field values at each position are obtained from both n=19 and n=20 energy splittings of $P_{3/2}$ and $D_{5/2}$ spectral lines and the mean electric field values for each measurement location are plotted in fig 3. The electric field values lower than 450 v/cm could not be measured because the $P_{3/2}$ and $D_{5/2}$ lines become unresolved due to the line broadening.

The measured electric field gradients are 2800 v/cm^2 for 780 volts and 2400 v/cm^2 for 380 volts; using Poisson's equation the corresponding net space-charge densities at the flame edge are $1.5x10^9/cm^3$ and $1.3x10^9/cm^3$.

The measured electric field profile in an atmospheric pressure flame appears to be similar to the low pressure glow discharges[2,3] although the physical processes responsible for this spatial variation of the electrical field are quite different.

The absolute electrical conductivity of the flame, at the flame edge, can be estimated from the electric field and the current density measurements. Under the measured flame conditions, the electrical conductivity values ranged between $6x10^{-9}$ mhos/cm at 0.5 mm from the cathode and up to $22x10^{-9}$ mhos/cm at 6 mm form the cathode surface.

REFERENCES

1. C. S. MacLatchy, Combust. and Flame 36, 171, (1979).

2. D. K. Doughty, S. Salih, and J. E. Lawler, Phys. Lett. 103A, 41, (1984); D. K. Doughty, E. A. Den Hartog and J. E. Lawler, Phys. Rev. Lett. 58, 2668, (1987).

3. B. N. Ganguly and A. Garscadden, Phys. Rev. A 32, 2544, (1985); B. N. Ganguly, B. L. Preppernau, J. R. Shoemaker and A. Garscadden, J. Appl. Phys. 61, 2778 (1987).

4. M. L. Zimmerman, M. G. Littman, M. M. Kash, D. Kleppner, Phys. Rev. A 20, 2251, (1979).

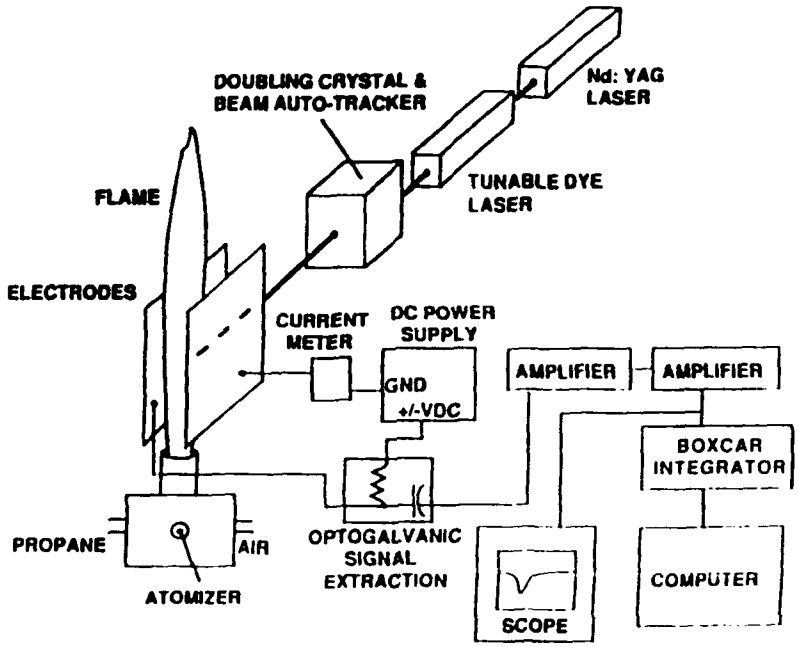

Figure 1: A schematic of the experimental set-up.

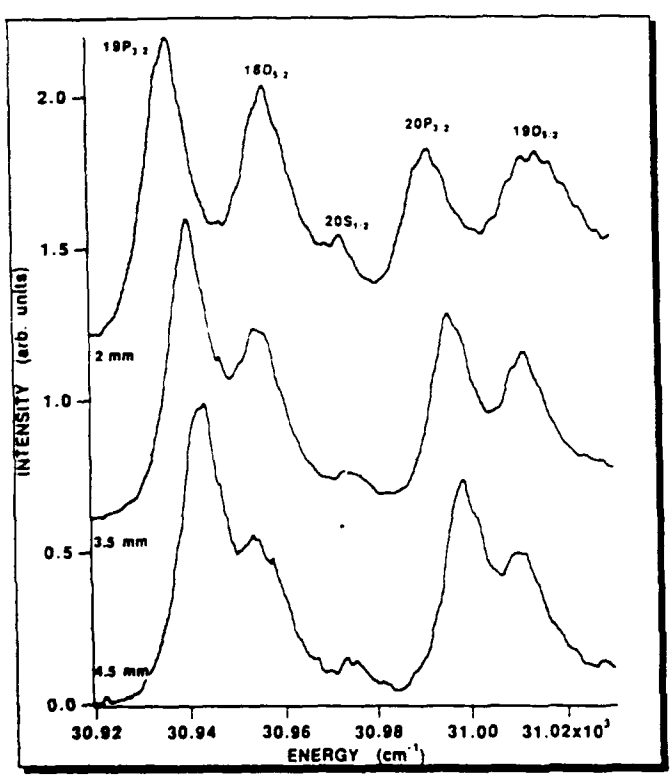

Figure 2: Rydberg state Stark spectra of cesium in atmospheric pressure propane-air flame.

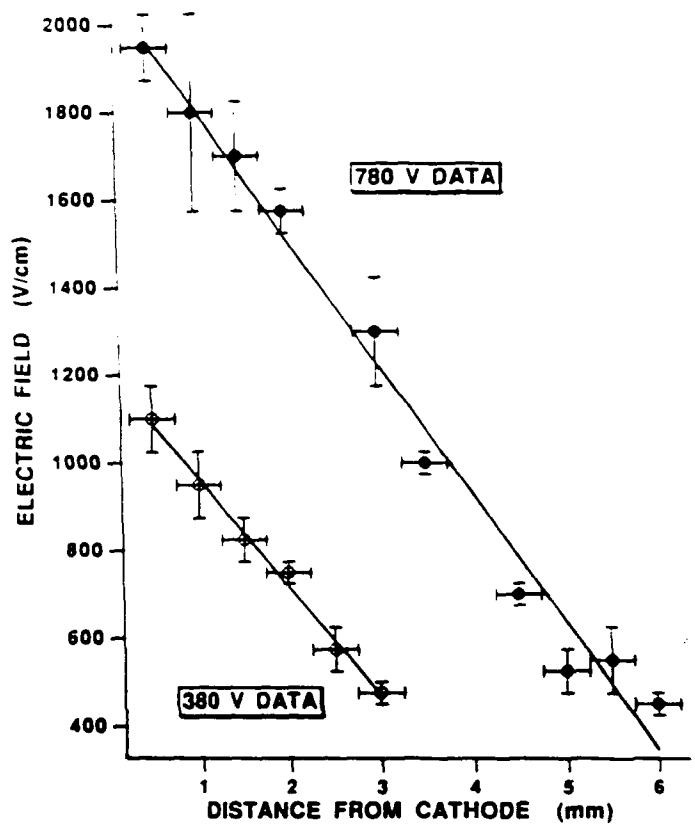

Figure 3: Electric field profiles in the cesium seeded atmospheric pressure propane-air flame.

TWO DIMENSIONAL COHERENT ANTI-STOKES RAMAN SCATTERING WITH APPLICATION TO THE HYDROGEN ARCJET

EDWARD J. BEITING (PRINCIPAL INVESTIGATOR)

The Aerospace Corporation
P. O. Box 92957
Los Angeles , CA 90009

SUMMARY/OVERVIEW

This is an experimental program to extend the utility of coherent anti-Stokes Raman spectroscopy (CARS) as a diagnostic of flows and plasmas. Pump and Stokes radiation focused into a sheet produces a line of anti-Stokes radiation in the cross section of a flow. The anti-Stokes radiation detected with a multichannel array provides one angle of projection data. A cross section of an asymmetrical region is calculated from projection data taken at several angles using tomographic algorithms. Only one projection is required to reconstruct the cross section of a cylindrically symmetric flow. This technique allows the measurement of field maps of internal state distributions (temperatures) and number densities. Currently, CARS is restricted to collecting data sequentially at single points in space. This year methods of attaining constant pulse-to-pulse, point-to-point ratios of signal and reference channels were explored. The principal components of the a 1-KW hydrogen arcjet thruster were brought into operation.

TECHNICAL DISCUSSION

METHOD

In the CARS process, three fields $E_1(\omega_1)$, $E_2(\omega_2)$, and $E_3(\omega_3)$ impinge on a medium and mix through the third order nonlinear susceptibility χ_{ijkl} to generate a fourth wave $E_4(\omega_4)$ at a frequency ω_4. If we assume the input fields are plane monochromatic waves propagating in the z direction with aligned polarizations, and the medium has no spatial symmetry, then χ_{ijkl} can be written as a scalar and the solution of Maxwell's equations with a nonlinear polarization source term yields

$$\frac{\partial^2 E_4}{\partial z^2} + 2ik_3\frac{\partial E_4}{\partial z} = -4\pi\left(\frac{\omega_4}{c}\right)^2 \chi(\omega_1,\omega_2,\omega_3)E_1 E_2^* E_3 \exp(i\Delta kz) \qquad (1)$$

where $\Delta k = 2k_1 - k_2 - k_3$ and $k \equiv n\omega/c$. Assuming a solution of the form $E_4(z) = E_4^0(z)\exp(ik_4 z)$ and noting $\Delta k << 2k_3$ for phasematched geometries, the spatial variation of E_4^0 is small and the second derivative can be ignored. Accordingly, the spatial variation of the amplitude of the CARS field can be written

$$\frac{dE_4^0}{dz} = K(\omega_4)\chi(\omega_1,\omega_2,\omega_3)E_1 E_2^* E_3 \exp(i\Delta kz) \qquad (2)$$

where $K(\omega_4)$ is a known function of ω_4. This expression can be simplified further using the following assumptions which are valid for most experimental implementations of CARS: $\Delta k = 0$ (phasematched waves); the amplitudes of E_1, E_2, and E_3 are independent of z over the region they coherently interact; $E_1(\omega_1) = E_3(\omega_3)$; and $\omega_1 = \omega_3$. Then Eq. (2) becomes

$$E_4^0(\omega_4) = K(\omega_4)E_1^2E_2^* \int \chi(\omega_1,\omega_2)dz. \tag{3}$$

The susceptibility can be expressed as a sum of the nonresonant part, χ_{nr}, and a resonant part with real and imaginary components, *i.e.* $\chi_j = \chi_{nr} + \chi_j^r + \chi_j^i$. If the lasers are focused into a thin sheet with a transverse coordinate x and ω_2 is tuned away from all resonances then the signal that results is due primarily to the interaction of the waves with the nonresonant susceptibility. Noting $I_4(\omega_4) = \frac{n_4 c}{8\pi}|E_4^0(\omega_4)|^2$, a projection in terms of the molecular density can be written:

$$P(x) \equiv [\tilde{I}_4(\omega_4)]^{\frac{1}{2}} = \int \chi_{nr}(x,z)dz = \tilde{\chi}_{nr} \int n(x,z)dz \tag{4}$$

where $\tilde{\chi}_{nr}$ is a knowm constant and $n(z)$ is the number density of the gas. A reconstruction from this projection yields a map of the density directly. If ω_2 is tuned to a strong isolated resonance then

$$P(x) \equiv [\tilde{I}_4(\omega_4)]^{\frac{1}{2}} = \int \chi_j^i(x,z)dz. \tag{5}$$

Since $\chi_j^i \propto n(x,z)\Delta_j(x,z)$ one can obtain a spatial map of Δ_j, the population difference between the two states in the Raman resonance j. In thermal equilibrium this defines a temperature. Under nonequilibrium conditions, measuring $\Delta v = 1$ transitions for a line from each vibrational level starting with $v = 0$ allows spatial maps of the population of the vibrational energy levels to be constructed.

PROGRESS

The experimental program is advancing on two fronts. The first is the development of a technique to obtain single pulse projections. The second is an effort to acquire CARS projection data point-by-point across the plume of a hydrogen arcjet thruster. If both efforts are successful, then acquisition of single pulse projections in the arcjet will be undertaken.

The current configuration of the instrument designed to capture single pulse CARS projections is shown in Figure 1. Important changes were made in this setup during the past year. All of these changes were implemented in order to obtain a constant pulse-to-pulse, point-to-point ratios of detected counts in the signal and reference channels. The feasibility of the technique depends on being able to obtain predictable projections when large shot-to-shot variations of the lasers' mode structures, frequencies, and phases take place. The reference channel must exactly duplicate these variations and is used to normalize the signal channel.

Experimentally it was found that channel-to-channel, shot-to-shot variations in the signal-to-reference ratios consistently varied between 10% and 50% when single longitudinal mode pump-radiation was used. These large variations occurred even when the CARS images in both reference and signal legs appeared to be identical in both spatial dimensions. In the summary submitted to FY91 contractor's meeting, I reported that these large variations in the signal-to-reference ratios were eliminated by using broadband pump radiation. Upon further investigation, this was discovered to be incorrect. The seemingly constant ratios were an artifact of an improper background subtraction method. To investigate this problem and to calibrate the projections, two identical rectangular flow channels were built to be used as reference and calibration channels.

Because recent studies show that ratioing techniques used in CARS are sensitive to saturation effects [1], optical components were obtained that split both the pump and Stokes

intensities evenly between the signal and reference channels. The beamsplitter and turning mirror used to create this channel are precision components designed so as to not introduce any phase distortions and interference effects to either beam. A matching compensation plate was inserted in the reference channel to account for chromatic aberration. The identical hydrogen flows were placed at the center of the beam waists in both channels. These efforts did not materially improve the stability of the ratios and it was concluded that saturation effects are not the principal source of the instability.

Although theoretically the ratio of the signal and reference channels should be constant regardless of the composition of the individual pump and Stokes beams, in practice it has been difficult to accurately reference CARS signals if both lasers are not single mode [2]. The conventional method of obtaining single-mode narrow-band pulsed tunable radiation is to pulse amplify the output of a ring dye laser. Space and monetary considerations preclude using this method, so several alternatives were explored. A variant of a recently introduced design for a modeless laser was constructed [3]. However, reasonably narrowband operation could not be achieved without highly specialized optical components that were not readily available. Pulse amplifying the output of newly available visible diode laser was viewed as a quick solution because driver and temperature controllers were available within the company. Two Toshiba diode lasers were acquired and tested. This was not an acceptable solution because tandem Faraday isolators are required between the diodes and pulsed amplifier and a large enough pool of the Toshiba diodes are not yet available in this country to allow wavelength selection.

The current approach is the construction of a scanning single mode dye oscillator based on a grazing incidence design [4]. This design is mechanically demanding, but a recent modification has relaxed the physical tolerances [5]. At this writing, initial testing of the cavity has been completed using components on hand, but a better dye cell and mechanical components are needed for reliable single mode operation. The components are being acquired. The final amplifier will use a Bethune cell [6] to assure a stable transverse mode.

Work is underway to acquire time-averaged projections from a cylindrically symmetric, stabilized arcjet thruster. A large vacuum chamber has been modified to house the arcjet and accommodate the diagnostics (see Figure 2). The pump and Stokes beams are overlapped for collinear phasematching within the vacuum chamber to avoid nonresonant CARS signal generation in the atmosphere. The overlapped beams pass through a lens whose focal length is long compared to the diameter of the diameter of the plume. In order that the signal is generated only within the plume, the exhaust from the arcjet is captured by a diffuser pumped with two roots blowers in parallel. Two diffusion pumps with a total capacity of 16,000 liters/sec evacuate the chamber. The ambient number density of H_2 in the chamber must be below one-tenth the H_2 density in the plume. An XYZ translator allows projections to be acquired one point at a time at a series of positions along the thrust axis of the plume. Initial measurements will be time averaged in the stabilized arcjet, obviating the need for referencing. At this writing, all pumping systems are operating. The vacuum chamber has been leak tested. A 1-KW arcjet and power unit have been built and have undergone initial testing in the chamber. These tests indicate that the diffuser must be cooled and water coils are being added to the system. The XYZ translator will be integrated into the computerized data acquisition system when delivered.

References: [1] M. Pealat and M. Lefebvre, Appl. Phys. B **53**, 23-29 (1991). [2] Personal communications with D. A. Greenhaugh, R. Farrow, and G. Rosasco. [3] P. Ewart, Opt. Commun. **55**, 124-126 (1985). [4] M. G. Littman, Appl. Opt. **23**, 4465-4468 (1984). [5] T. D. Raymond, P. Esherick, A. V. Smith, Opt. Lett. **14**, 1116-1118 (1989). [6] D. S. Bethune, Appl. Opt. **20**, 1897-1899 (1981).

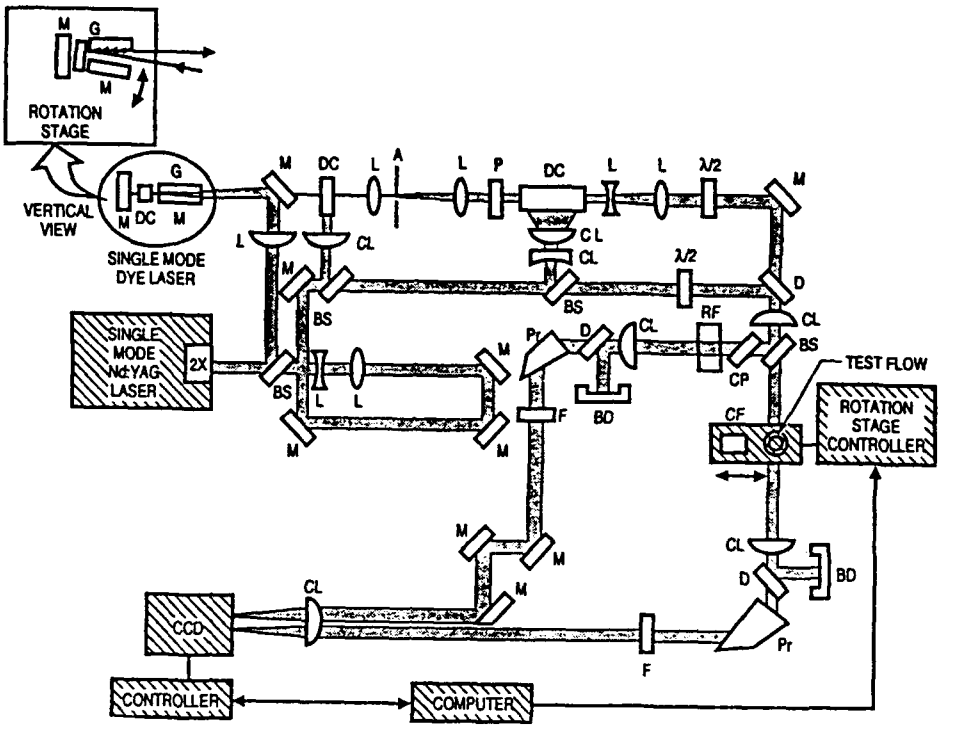

Figure 1. Experimental configuration used to study CATCARS concept. CODE: A, aperture; BD, beam dump; BS, beam splitter; CL, cylindrical lens; CT, cylindrical telescope; D, dichroic mirror; DC, dye cell; IR, image rotator; G, diffraction grating; L, spherical lens; M, mirror; P, polarizer; Pr, prism; 2X, doubler; $\lambda/2$, half wave plate.

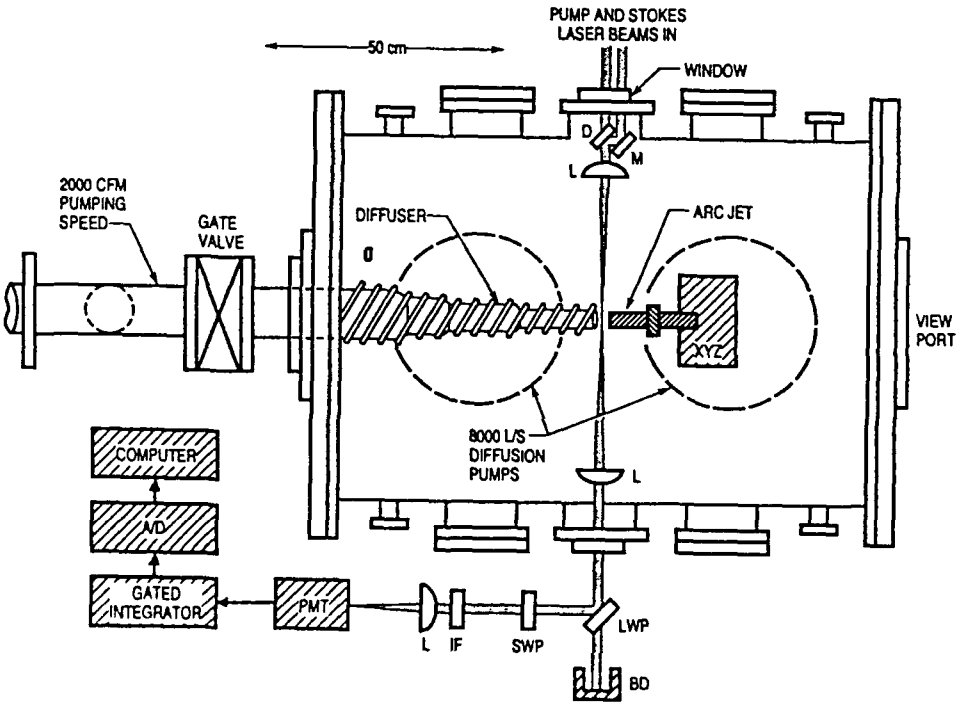

Figure 2. Diagram of arcjet thruster diagnostic facility.

INVESTIGATION OF THE APPLICATIONS OF LASER-INDUCED FLUORESCENCE TO FUEL SPRAY AND SINGLE DROPLET VAPORIZATION

ARO Contract No. DAAL03-91-G-0033

Principal Investigator: Lynn A. Melton
Research Collaborator: Michael Winter*

Department of Chemistry
University of Texas At Dallas
Richardson, TX 75083-0688

SUMMARY/OVERVIEW:

A series of laser diagnostic techniques has been developed to measure heat and mass transfer associated with individual droplets characteristic of a spray. Techniques under development and/or available now include exciplex-fluorescence thermometry, "droplet slicing" and flow-pattern imaging, correction for refraction effects by droplet surfaces, measurement of the temperature field within droplets, and production of monodisperse droplets at high pressures. Also under development and recently demonstrated are apparatus and techniques for lifetime imaging, which holds the potential for imaging of the equivalence ratio. New results describe refinements to droplet slicing for unambiguously determining the presence of internal circulation, and further interpretation of exciplex fluorescence thermometry.

TECHNICAL DISCUSSION:

At UTD, two projects involving the optics of droplets have been pursued in the last year: (1) interpretation of exciplex fluorescence thermometry (EFT) results for optically-thin droplets and (2) inverse ray tracing (IRT) methods for computing the true spatial distributions when necessarily distorted images are obtained in "droplet slicing" experiments.

---

*United Technologies Research Center, East Hartford, CT 06108

Hanlon and Melton[1] have used exciplex-fluorecence thermometry to infer the temperature of 280 micron hexadecane droplets falling into a hot, quiescent, nitrogen ambient. The droplets were optically thin, and the OMA detection system collected fluorescence from the entire droplet. In brief, their plots of inferred temperature versus time show a slow rise in temperature, a sudden jump of 80-100 C, and finally a continued slow rise. Since they collected fluorescence from the entire droplet, the refraction effects of the droplet, which affect both the distribution of fluorescing molecules within the droplet and the efficiency of collection of the emission, caused systematic errors in the interpretation of the integrated intensities. The current analysis shows that the apparent jump in temperature is a result of the shape of the EFT calibration curve and that the shape of the inferred temperature curve can be used to estimate directly the gas-to-liquid heat transfer coefficient. In addition, other potential systematic errors in the interpretation of EFT data have been identified and, in some cases, procedures have been developed to render them negligible.

In "droplet slicing" experiments, the image is significantly distorted, with the central portion being expanded linearly and the outer portions being compressed near the droplet edge. Algorithms for the removal of these distortions have been developed. Recovery of the central portions of the image is straightforward, but accurate recovery of the outer portions is difficult. Initial attempts at data analysis proved unstable analyzing noisy data. Least squares fitting of functional forms, such as polynomials, appears to have controlled the instability problem, and actual recovery of "droplet slicing" images is now underway.

At UTRC, measurement of internal circulation using laser-induced oxygen-quenched fluorescence are being pursued under known initial conditions. A schematic of the experimental apparatus is shown in Fig.1. Decane doped with naphthalene is used to form droplets from either a droplet-on-demand generator, an aerodynamic droplet generator, or levitated droplets formed from melting solids, which fall a short distance in a chamber filled with a carefully controlled shear flow of nitrogen and a variable amount of oxygen. A thin sheet of ultra-violet light from the fourth harmonic of a Nd:YAG laser illuminates single droplets. Sheet thickness has been significantly reduced by careful selection of a uniform portion of the initial laser beam waist. A Questar QM100, long working distance microscope, with uv quartz optics is used to provide high quality images even through the thick windows characteristic of high pressure test vessels. The microscope produces a highly-magnified image of the naphthalene fluorescence which is recorded digitally using an intensified two-dimensional CCD detector interfaced to a laboratory computer. Use of an off-the-shelf low $f^{\#}$ microscope is particularly useful to allow careful quantification of the imaging modulation transfer function which is used for ray tracing corrections on droplet

slicing image data. Since oxygen is a strong fluorescence quencher, any liquid volume element which has been exposed to it by surface contact or diffusion will suffer a reduction in fluorescence intensity. Convection from the surface due to internal circulation as well as diffusion cause image regions to appear dark. Figure 2 shows uncorected data from a 450 μm droplet which has fallen a short distance into a uniform upward Oxygen flow. Oxygen-free experiments provide a baseline case for comparison.

Variation of droplet initial internal flow patterns, and varied shear flow conditions are being used to examine shear-induced internal circulation. The process of ejecting a droplet through the nozzle of a droplet generator may induce internal circulation in the same direction as that caused by aerodynamic forces. An alternate scheme has been developed in order to determine unambiguously the source of the internal circulation. If the droplets are ejected into an electrostatic trap, they can be held there long enough for any fluid motions due to the droplet formation process to damp out. The droplet will then be released and will accelerate due to gravitational forces into the test section which will contain either a controlled gas environment for isothermal experiments, or a heated ambient for temperature measurements. By supporting the droplet long enough to assure quiescent initial conditions, accurate data can be collected on shear-induced internal circulation unambiguously. Another approach to introduce internal circulation of the opposite sense has been formulated. An aerodynamic droplet generator[2] can be used to produce monodisperse droplets in the core of an axisymmetric jet. A hypodermic needle is situated within the plenum with its end at the throat of the nozzle. The gas flow around the end of the needle strips off droplets at the Strouhal frequency of the jet and monodisperse droplets are produced at regular frequencies. Since the gas flow velocity is greater than the liquid velocity initially, the shear environment for the droplets is of opposite sense within the nozzle and potential core of the jet than when the droplet is in free fall. A droplet generator has been developed and has shown to produce extremely regular droplets at fixed time intervals. These measurements are currently proceeding in our laboratory.

1 T. R. Hanlon and L.A. Melton, "Exciplex Fluorescence Thermometry of Falling Hexadecane Droplets", Trans. ASME J. Heat Transfer, in press, (1992).

2 G. J. Green, F. Takahshi, D. E. Walsh, and F. L. Dryer, "Aerodynamic Device for Generating Mono-disperse Fuel Droplets", Rev. Sci. Instrum. 60 (4), April 1989.

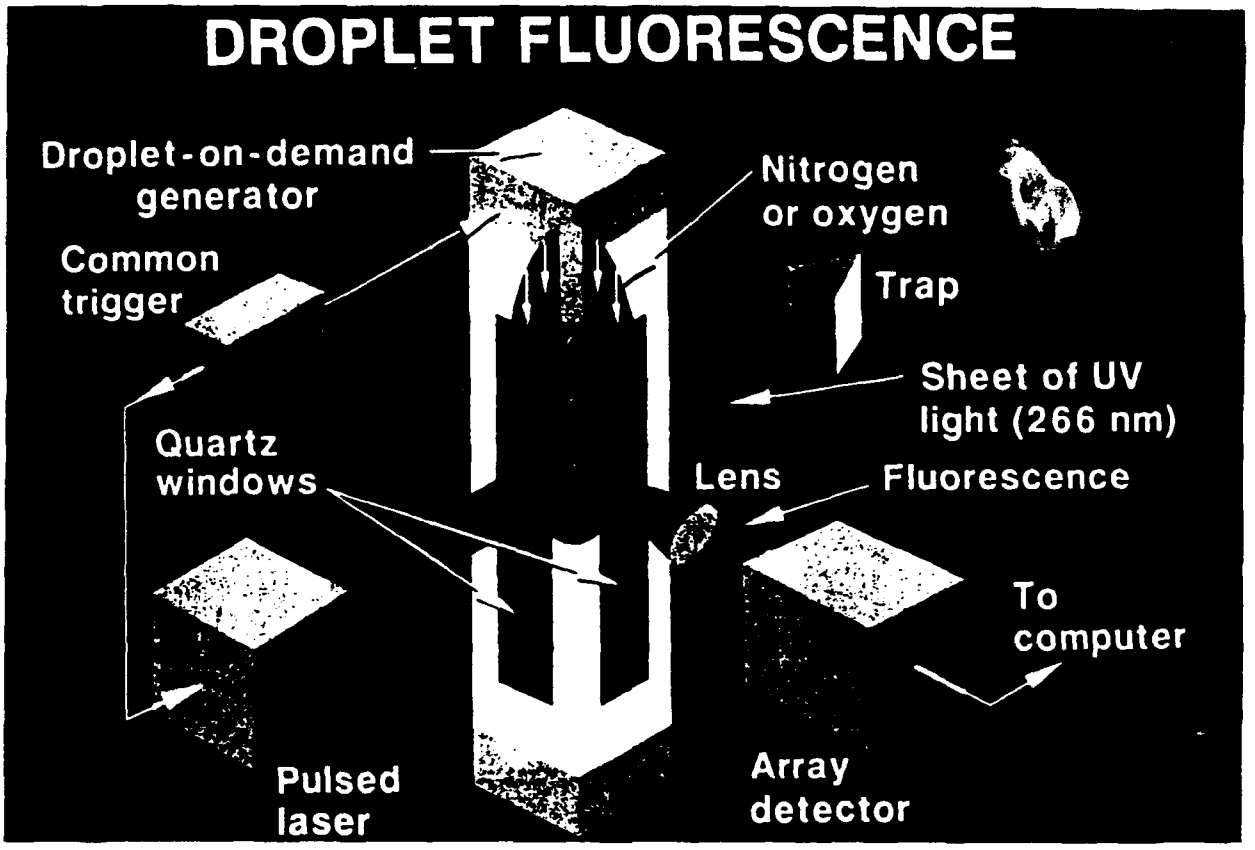

Figure 1. Schematic of the droplet slicing experimental setup.

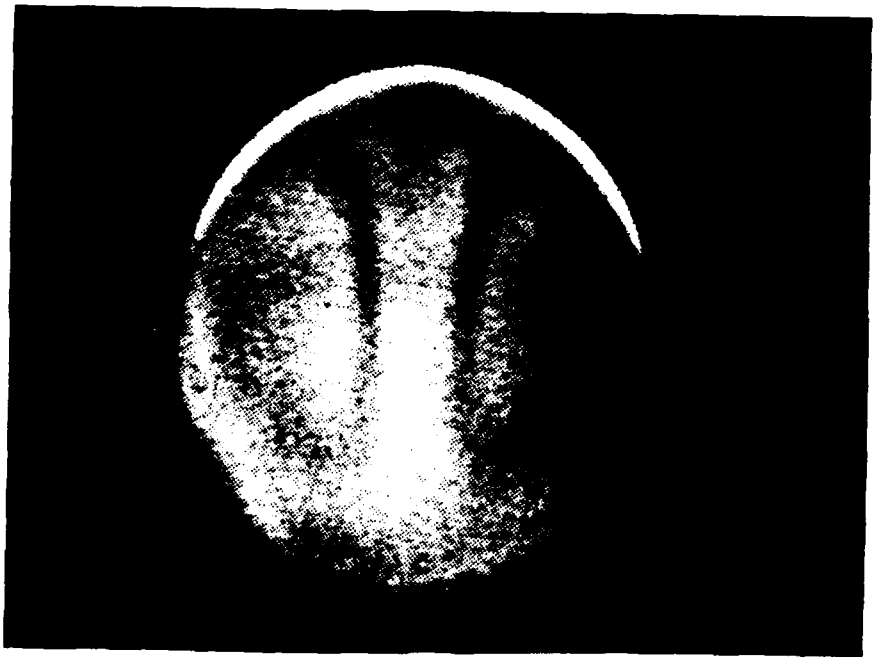

Figure 2. Internal circulation in a 450 μm droplet imaged by laser-induced fluorescence quenching by oxygen.

NONLINEAR SPECTROSCOPY OF MULTICOMPONENT DROPLETS

(AFOSR Grant No. 91-0150)

Co-Principal Investigator: Richard K. Chang

Yale University
Department of Applied Physics and Center for Laser Diagnostics
New Haven, Connecticut 06520-2157

SUMMARY/OVERVIEW

Nonintrusive in-situ optical diagnostics techniques have the potential of determining the chemical species and physical properties of multicomponent liquid droplets in a spray combustor. Our research is directed toward the understanding of nonlinear optical processes within individual droplets and the application of nonlinear optical techniques for chemical identification of multi-component fuel droplets and physical characterization of flowing droplets. The five main research results during the past year are: (1) development of a heuristic model for the nonlinear optical processes that are simultaneously occurring within the droplet;[1] (2) the relationship between phase matching of nonlinear waves in droplets and spatial overlaps of morphology-dependent resonances (MDR's);[2,3] (3) observation of stimulated anti-Stokes Raman scattering (SARS) from single droplets;[4] (4) the deteriorative effect of two-photon absorption on the stimulated Raman scattering (SRS) from droplets;[5] and (5) in a two-component fuel droplet, the observation of evaporation of one-component from the decrease of SRS intensity of that component.[6] The paper reporting on the frequency splitting of the SRS peaks because of inertial force induced shaped deformation of a flowing droplet has appeared in print.[7] An invitation to deliver a keynote address at a SPIE meeting provided the opportunity to summarize our recent understanding of nonlinear optical processes in droplets with single-mode excitation.[8]

TECHNICAL DISCUSSION

The spherical liquid-air interface of a droplet (with radius greater than the wavelength) gives rise to three unique features: (1) concentrates the input laser intensity within the droplet and, thus, the droplet experiences a much larger pump intensity; (2) enhances the fluorescence and Raman scattering efficiency as discrete wavelengths that satisfy the MDR's and, thus, increases the lasing and SRS gain coefficients; and (3) provides optical feedback for discrete wavelengths within the fluorescence and Raman gain profiles, and as a result, partially retains the radiation within the droplet for further amplification.

We have modified the standard one-dimensional nonlinear-wave equations to accommodate the growth and coupling of nonlinear waves in droplets. The heuristic model includes the following processes: radiation leakage; one-photon absorption; depletion of the input-laser intensity because of pumping the Brillouin waves and the first-order Stokes SRS; depletion of the stimulated Brillouin scattering because of pumping of the first-order Stokes SRS; conversion of the first-order Stokes SRS to the second-order Stokes SRS; and the quantum-electrodynamic enhancement of the Raman gain coefficient. The delay time and the correlated growth and decay of the nonlinear waves resulting from the numerical simulation compares favorably with those of the experimental observations.[1]

Experiments and calculations related to the third-harmonic generation (THG) and third-order sum frequency generation (TSFG) in droplets were completed. Among all the four-wave mixing processes, which include CARS, THG and TSFG are most simple nonlinear interactions. The connection between the phase-matching condition for plane waves in an extended medium and spatial overlap among MDR's in a droplet is made.[2,3] The observation of stimulated anti-Stokes Raman scattering (SARS) is related to THG, TSFG, and CARS. In fact, SARS and CARS involve the same physical process. However, for the SARS experiments there is only one pump beam (at the input-laser frequency) and the second beam (at the Stokes Raman frequency) is provided by the intense SRS generated within the droplet. Instead of the usual phase-matching considerations for the anti-Stokes wave, we need to further our understanding of the spatial overlap among the MDR's of the input-laser, Stokes Raman, and anti-Stokes Raman waves.[4]

In diesel fuel droplets it was reported that SRS is not observable because of one- and two-photon absorptions suppressed the SRS. Figure 1 shows the SRS spectra from a highly aromatic diesel fuel droplet that required the input-laser wavelength to be in the yellow ($\lambda = 565$ nm) in order to minimize the one-photon absorption in the green. Whereas the one-photon absorption can be minimized by selecting the input-laser to be in the yellow or red, two-photon absorption in the blue may not be avoidable. We selected a liquid (1-methylnaphthalene) that has known amounts of two-photon absorption. The effect of two-photon absorption on nonlinear processes in droplets needs further understanding.[5]

In order to demonstrate the capability of using SRS spectra to study differential evaporation of a fuel droplet, we selected a binary mixture of low- and high-vapor pressure liquids.[6] Figure 2 shows, as a function of the ambient temperature, the SRS spectra from droplets containing 3:7 volumetric mixture of pentane and 1-methylnaphthalene.

REFERENCES

1. A. Serpengüzel, G. Chen, R.K. Chang, and W.-F. Hsieh, "Heuristic Model for the Growth and Coupling of Nonlinear Processes in Droplets," JOSA B., (to be published).

2. David H. Leach, Richard K. Chang, William P. Acker, and Steven C. Hill, "Third Order Sum Frequency Generation in Droplets: Experimental Results,"(submitted to JOSA B).

3. Steven C. Hill, David H. Leach, and Richard K. Chang, "Third Order Sum Frequency Generation in Droplets: Model with Numerical Results for Third Harmonic Generation," (submitted to JOSA B).

4. D.H. Leach, R.K. Chang, and W.P. Acker, "Stimulated Anti-Stokes Raman Scattering in Microdroplets," Opt. Lett., (to be published).

5. R. K. Chang and Ali Serpengüzel, "Characteristics and Applications of Stimulated Raman Scattering in Microdroplets", in Proceedings of the XIII th International Conference on Raman Spectroscopy, 1992, Würzburg, Germany, (to be published).

6. Ali Serpengüzel, Richard K. Chang, William P. Acker, and Rodney L. Sung, "Laser Diagnostic Techniques for Characterizing Droplet Size, Composition, and Differential Evaporation in Fuel Sprays", (submitted to the 1992 FISITA Congress, to be held June 7-11, 1992 in London, England).

7. G. Chen, R.K. Chang, S.C. Hill, and P.W. Barber, "Frequency Splitting of Degenerate Spherical Cavity Mode: Stimulated Raman Scattering Spectrum of Deformed Droplets," Opt. Lett. 16, 1269 (1991).

8. R.K. Chang, G. Chen, S.C. Hill, and P.W. Barber, "Nonlinear Optical Processes in Droplets with Single-Mode Laser Excitation", in Proceedings of the SPIE Conference on Nonlinear Optics and Materials, Vol. 1497 (SPIE, Bellingham, Washington, 1991), p. 2.

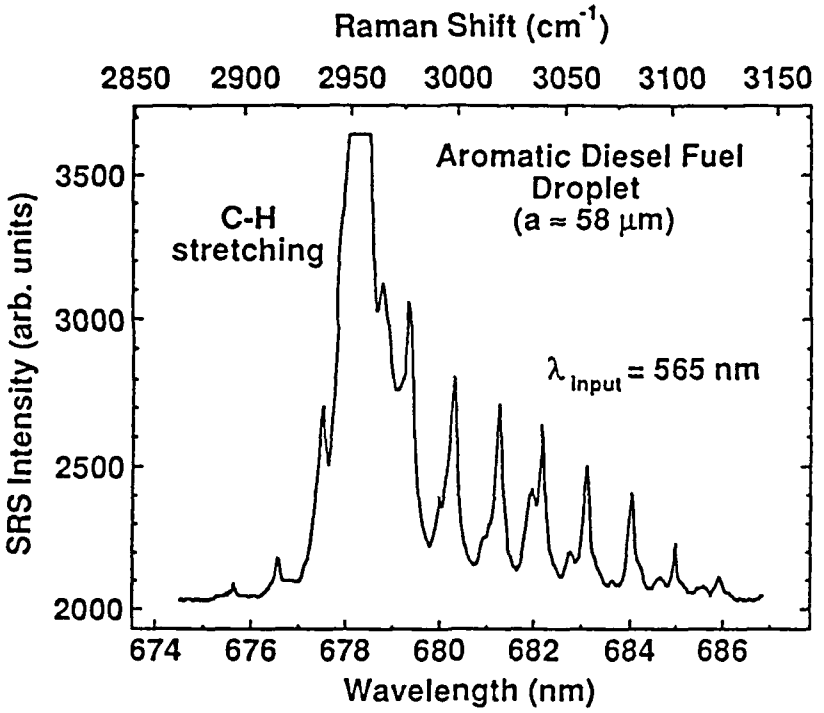

Figure 1. High-spectral resolution SRS spectra from a highly aromatic diesel fuel. The intense peak of the C-H stretching mode at 678.5 nm is truncated in order to emphasize the MDR-related peaks in the wings of the SRS spectra. From the MDR spectral spacing, accurate droplet sizing can be achieved.

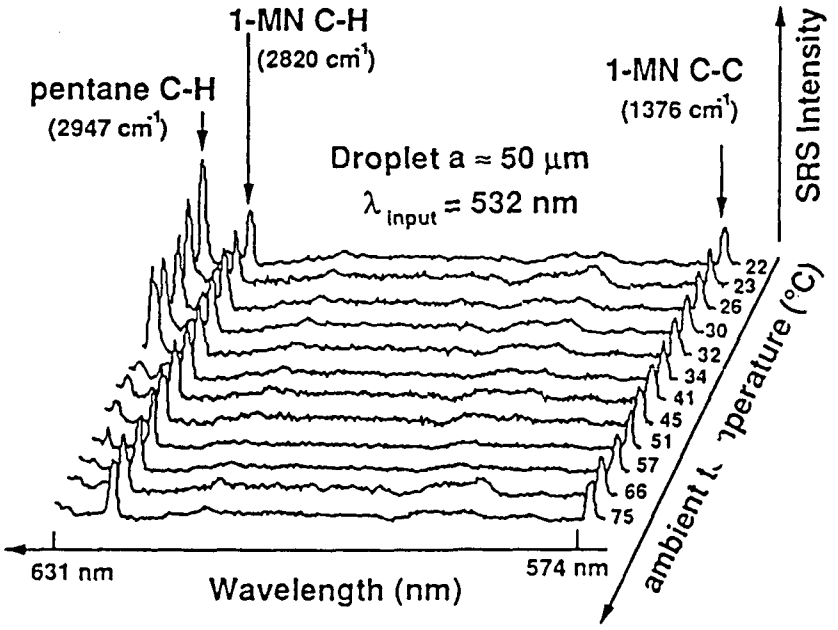

Figure 2. SRS spectra from droplets containing 3:7 volumetric mixture of pentane and 1-methly-naphthalene (1-MN). The SRS spectra are detected from the heated region downstream from the droplet generator. Each track indicates the surrounding gas temperature. The SRS intensity of the C-C ring breathing mode of 1-MN at 574 nm is normalized to a fixed value for all temperatures.

High Temperature Reaction Kinetics of Non-metal Oxides

(AFOSR Contract No. F49620-91-C-0057)

Principal Investigator: Allen Twarowski

Rockwell International Science Center
1049 Camino dos Rios
Thousand Oaks, CA 91360

SUMMARY/OVERVIEW:

Catalysis of heat-releasing H+OH recombination in the nozzle section of a SCRAM-jet could potentially increase the fuel efficiency and therefore the thrust of a hydrogen-fuelled air-breathing hypersonic aircraft. The oxides of phosphorus and boron are potential recombination catalysis, however, the reaction chemistry of phosphorus and boron combustion products (oxides and acids) is poorly understood at present. The objective of this research program is to determine the rate constants for reactions of phosphorus and boron combustion products in a high temperature gas. Recent experimental results from the combustion of hydrogen/phosphine fuel with oxygen are presented along with a plausible reaction set which describes the experimental findings.

TECHNICAL DISCUSSION

Hydrogen reacts with oxygen at high temperature to produce water vapor and a considerable amount of heat. In our combustion reactor, gas temperatures of 1500-2500°K are achieved at pressures of 300-750 Torr. At these temperatures the equilibrated combustion products consist of small but significant amounts of radicals such as OH and H. To probe the reaction chemistry of the combustion products, the equilibrated system is perturbed by laser photolysis of H_2O which substantially increases the pool of OH and H radicals. The return of the system to equilibrium is experimentally investigated by recording, as a function of time, the OH absorption of a frequency-doubled cw-dye laser probe beam producing 312 nm radiation. The OH absorption signal is recorded on a digital oscilloscope and transferred as a binary file to a computer for subsequent analysis.

Figure 1 shows the dramatic effect on the rate of recovery of the OH signal when PH_3 is added to the hydrogen fuel and burned with oxygen. Photolysis occurs at 0.1 ms on the graph and results in a very fast increase in OH density (the value plotted in Figure 1 is the change in OH density from the equilibrium level). When phosphine is not present in the hydrogen fuel stream, the OH signal is observed to relax back towards its equilibrium value at a slow rate and is represented by the black squares plotted in Figure 1. The rate at which OH returns to its equilibrium value is increased significantly by the addition of only 0.03% by volume phosphine in the hydrogen flow stream. Addition of larger flows of phosphine cause an even more dramatic increase in OH disappearance as demonstrated by the parametric series shown in Figure 1.

Reaction Model

The large change in the OH relaxation rate observed when phosphine is added to the hydrogen fuel suggests that phosphorus combustion products are participating in the H+OH recombination process probably by opening alternate channels for recombination to occur. To further analyze the experimental OH decay data a kinetic model was constructed. As a first step in constructing

the model, a list of phosphorus species which could potentially participate in the reaction chemistry was assembled. Table 1 lists these species along with their heats of formation at 0°K and entropies at 298.15°K. The thermodynamic quantities of a few of the listed species are reported in JANAF Tables and these values are included in Table 1. Phosphorus species which do not have a JANAF Table entry were estimated from quantum chemical calculations reported in the literature.

The heats of formation and entropies for the each phosphorus compound were used to calculate a set of coefficients for thermochemical polynomials. From the thermochemical polynomials the free energy of formation for each phosphorus compound was calculated given a typical gas temperature of 2150°K. Finally, the equilibrium densities of the selected phosphorus species were calculated given typical experimental conditions of 533 Torr and a rich fuel mixture with a phosphine fuel fraction of 0.008. Figure 2 shows a bar chart of the equilibrium densities of phosphorus containing species along with the major species of hydrogen/oxygen combustion for the experimental conditions given above. From Figure 2 it is clear that the equilibrium densities of many of the selected phosphorus species are too small to participate in reactions which could possibly cause the observed OH decay shown in Figure 1. Therefore, a smaller species list was chosen consisting of PO, PO_2, HOPO, $HOPO_2$, PO_3 and P_2O_3 from which a reaction set was assembled.

A reaction set was systematically assembled by writing a computer program to list all the bimolecular reactions (including recombination reactions) possible among the species set consisting of H_2O, H_2, O_2, H, OH, O, HO_2, PO, PO_2, HOPO, $HOPO_2$, PO_3 and P_2O_3. From this reaction set, those reactions which have a positive heat of reaction were excluded along with those reactions which did not have a phosphorus species participating as a reactant. Furthermore, those reactions which involved the breaking of more than one chemical bond were also eliminated. The final list of 40 phosphorus reactions is given in Table 2 along with 13 reactions which describe hydrogen / oxygen combustion.

Finally, the rate constants for the bimolecular reactions listed in Table 2 were estimated using standard procedures.[1] The unimolecular reactions were estimated using RRKM theory. The values of the reverse rate constants were calculated as needed from the equilibrium constants and the forward rate constants.

Sensitivity Analysis

A sensitivity analysis of the OH decay profile was performed using the reaction set listed in Table 2. Here, sensitivity is defined as the fractional change in the OH signal divided by the fractional change in the value of a particular reaction rate constant. The result of this analysis for each reaction listed in Table 2 is shown in Figure 3 for typical experimental conditions of 2300°K, 700 Torr, a rich fuel mixture and a phosphine fuel fraction of 0.01. The reaction numbers in Figure 3 follow those listed in Table 3. The reaction which shows the largest sensitivity of the OH time profile to a change in the value of the reaction rate constant is

$$HO + PO_2 \rightarrow HOPO_2. \qquad \text{(Rxn 21)}$$

Furthermore, an analysis of the net reaction rates of the entire reaction set given in Table 3 shows that the reactions with the largest net rate are reactions 21 and the reverse of reaction 25,

$$H + HOPO_2 \rightarrow H_2O + PO_2 \qquad \text{(-Rxn 25)}$$

These two reactions add to net recombination of H and OH to form water.

---

[1] S.W. Benson, "Thermochemical Kinetics", (Wiley, NY), 1976.

Data Analysis

The rate constant for reaction 21 was used as a parameter in a data fitting routine. In a series of experiments the phosphine flow rate was increased from 0 to 0.15 per cent of the hydrogen fuel flow rate. For each phosphine flow rate an H_2O photolysis experiment was performed and the OH decay was recorded. The data set in which no phosphine was added to the fuel was analyzed using a reaction set consisting of the first 13 reactions listed in Table 3 (the H_2/O_2 combustion set). In this analysis the initial amount of OH and H formed by photolysis, DelOH, was treated as a fitting parameter. The average value of DelOH from several sets of data was used in the subsequent analysis of the phosphine data in which the rate constant for reaction 21 was treated as a fitting parameter. Figure 4 shows the OH decay data along with the model calculation for one of the phosphine data sets. The mean of four measurements is $6.2 \times 10^{17} cm^6 mol^{-2} s^{-1}$ at 1970°K which is 50 per cent greater than the originally estimated value.

Table 1. Estimated heats of formation at O°K (Del Hf) and entropies at 298.15°K (S298) for phosphorus compounds.

Species	Del Hf	S298	Species	Del Hf	S298
HOPO2	-784	0.255	HPO	-75	0.216
P2O3	-655	0.311	PO	-23	0.212
HOPO	-524	0.241	PH3	31	0.210
PO3	-487	0.245	P4	66	0.280
PO2	-311	0.254	P2O	90	0.236
H2POH	-217	0.229	PH2	129	0.213
HPOH	-117	0.230	P2	145	0.218
P2O2	-96	0.291	PH	255	0.196
			P	316	0.163

Table 2. Reaction set used to analyzed OH decay data.

Rxn #	Reaction	Rxn	Reaction
1	H + H = H2	27	H2 + PO3 = H + HOPO2
2	O + O = O2	28	O2 + PO = O + PO2
3	H + O = OH	29	O2 + HOPO = O + HOPO2
4	H + OH = H2O	30	H + HOPO = H2 + PO2
5	H + O2 = HO2	31	H + PO3 = O + HOPO
6	H + O2 = OH + O	32	H + PO3 = OH + PO2
7	OH + H2 = H2O + H	33	H + P2O3 = PO + HOPO
8	OH + OH = O + H2O	34	O + PO3 = O2 + PO2
9	O + H2 = OH + H	35	O + P2O3 = PO + PO3
10	HO2 + H = OH + OH	36	O + P2O3 = PO2 + PO2
11	HO2 + H = H2 + O2	37	OH + PO = H + PO2
12	HO2 + O = O2 + OH	38	OH + PO2 = O + HOPO
13	HO2 + OH = H2O + O2	39	OH + HOPO = H2O + PO2
14	O2 + PO = PO3	40	OH + HOPO = H + HOPO2
15	H + PO2 = HOPO	41	OH + PO3 = O + HOPO2
16	H + PO3 = HOPO2	42	OH + P2O3 = PO + HOPO2
17	O + PO = PO2	43	OH + P2O3 = PO2 + HOPO
18	O + PO2 = PO3	44	HO2 + PO = O + HOPO
19	O + HOPO = HOPO2	45	HO2 + PO = OH + PO2
20	OH + PO = HOPO	46	HO2 + PO2 = O2 + HOPO
21	OH + PO2 = HOPO2	47	HO2 + PO2 = O + HOPO2
22	HO2 + PO = HOPO2	48	HO2 + PO2 = OH + PO3
23	PO + PO2 = P2O3	49	HO2 + HOPO = OH + HOPO2
24	H2O + PO = H + HOPO	50	HO2 + PO3 = O2 + HOPO2
25	H2O + PO2 = H + HOPO2	51	PO + HOPO2 = PO2 + HOPO
26	H2O + PO3 = OH + HOPO	52	PO + PO3 = PO2 + PO2
		53	HOPO + PO3 = PO2 + HOPO2

Figure 1. OH Relaxation Data

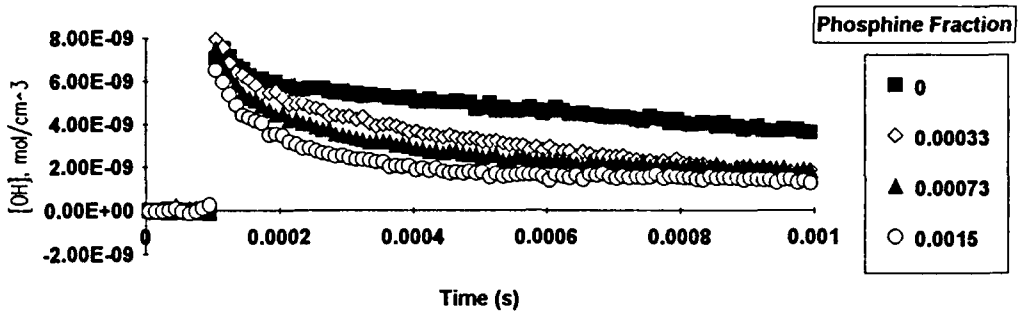

Figure 2. Equilibrium Densities of Combustion Products

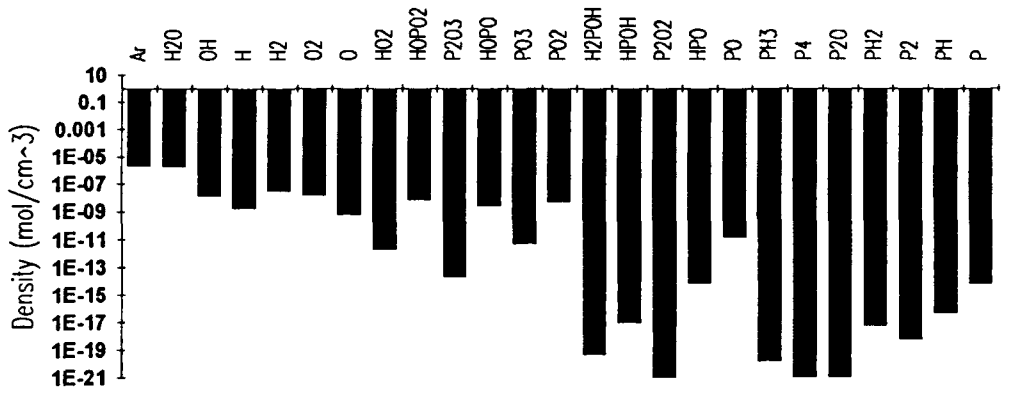

Figure 3. Sensitivity of Phosphorus Reactions.

Figure 4. Data and Model Results

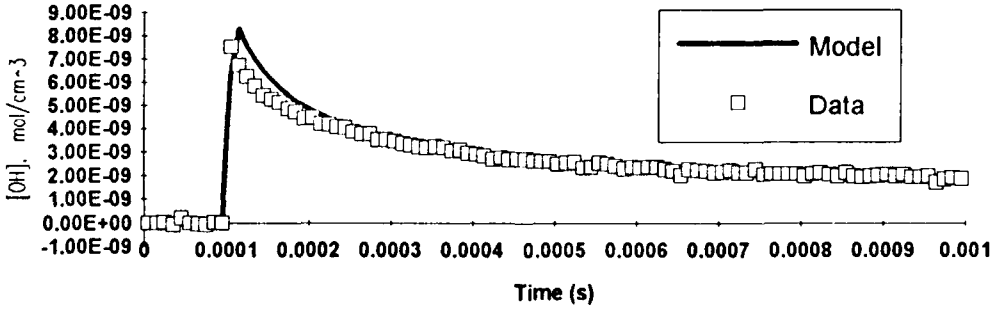

IGNITION AND MODIFICATION OF REACTION BY ENERGY ADDITION: KINETIC AND TRANSPORT PHENOMENA

AFOSR Contract No. F49620-90-C-0070

Principal Investigator(s): Francis Fendell and Mau-Song Chou

Center for Propulsion Technology and Fluid Mechanics
TRW Space & Technology Group, One Space Park, Redondo Beach, California

SUMMARY/OVERVIEW

High-speed air-breathing combustion systems necessitate the release of chemical energy during the relatively brief residence time of reactants within combustors of practical length: mixing, ignition, and chemical reaction must be achieved in a relatively short time. We address, from a fundamental chemical-kinetics and fluid-transport point of view, the use of laser irradiation (including photochemical ignition) and possibly of mixture-sensitizing additives, in order to alter chemical-reaction pathways to achieve rapid ignition and enhanced combustion rate. We also address the influence of mixture inhomogeneity, and departure from stoichiometry in fuel/air mixtures, on the processes of combustion-wave initiation, combustion-wave propagation, and completion of reaction. Chemical systems of particular interest include hydrogen/air and simple-hydrocarbon/air, sometimes with trace amounts of carefully selected sensitizers. We seek to identify optimal conditions [minimum input energy and power, minimal amount of sensitizer(s), etc.] for achieving ignition and burnup with currently available optical sources, both by laboratory experiments involving the irradiation of gaseous mixtures flowing faster than the adiabatic flame speed and by approximate analyses.

We have developed the concept of a supersonic combustor based on a nonintrusively stabilized oblique (conical) detonation wave. The conical wave is the resultant of the interaction of a train of spherical detonation waves, each initiated (in a very-fast-flowing gaseous fuel/air mixture) by energy deposition from a rapidly repeated pulsed laser. The proof-of-principle technology for such a supersonic combustor, in which relatively small entropy rise is incurred, is addressed by the above-discussed experiments and analyses.

TECHNICAL DISCUSSION

We have discussed nonintrusive energy deposition into a combustible mixture flowing very modestly faster than its adiabatic flame speed[1]. The stabilization of a deflagration may be achieved via a temporally continuous source (plane, line, or point) focused on a fixed site, which would be situated in the burned-gas region. However, a less-energy-demanding stabilization would be achieved by the initiation of a train of very closely spaced spherical deflagrations. Each spherical deflagration evolves from a transient, point-like, ignition-achieving deposition of energy at a fixed site in the flowing unburned mixture. The downwind interaction of the periodically initiated, individual spherical deflagrations results in a burned-gas region of roughly paraboloidal configuration, enveloped by unburned gas. The paraboloidal envelope (or "separatrix") is well approximated by the deflagration-wave locus for the above-discussed continuous point source.

The typical value for a laminar flame speed is highly subsonic, and very much less than the speed of the oncoming stream in many practical aerodynamic contexts. A very large number of energy-deposition sources, situated transverse to a stream of fast-flowing mixture, would be required to span that stream with flame within a modest distance downward of the plane containing the sources. Furthermore, while the intention might be to initiate nonintrusively the stabilization of deflagration wave that spans the stream, the inadvertent result might be the creation of a normal detonation wave, which incurs a large rise of entropy. Such a large entropy rise implies the unavailability of much energy to do useful work.

Therefore, for the objective of spanning a stream of supersonically flowing mixture with flame, attention is turned to the use of nonintrusive energy deposition at a fixed site in a combustor, not to initiate a deflagration, but rather to initiate a detonation[2]. For fuel-air mixtures of practical interest, as a high priority, we seek data on the minimum-deposition-energy, minimum-pulse-duration, and minimum-deposition-volume requirements for the direct (nonintrusive) initiation and propagation of a Chapman-Jouget (CJ) "spherical" detonation. The members of a train of such spherical detonation waves, each directly initiated by one of a train of pulses from a rapidly repeated pulsed laser, interact to form a nonintrusively stabilized conical (oblique) CJ detonation wave. The "corrugations" in the conical wave are smoothed as the temporal interval between pulses is reduced, but pulsing should not be so frequent that effectively the same "element" of mixture is irradiated more than once. Furthermore, a cellular structure is observed for all real detonations, so the conical wave in fact has finite thickness, but that property does not compromise any of this discussion.

Three significant advantages of the laser-initiated-oblique-detonation-wave combustor over an alternative design employing an intrusive conical body have been delineated[2]. Use of an intrusive body without a positive ignition device incurs additional friction drag, and may incur the large entropy increases associated with a normal detonation if the body becomes blunted or misaligned with respect to the flow. Further, in the rarefied flow at high altitudes for which such a combustor is likely to be utilized, the pressure of the (weakly) shocked gas may be sufficiently modest that chemical reaction rates are slow, ignition-delay times are significant, and the conversion of reactants to products may occur undesirably far downwind of the oblique shock.

If axial position $x = 0$ [or $x' \equiv (x - L) = - L$] is the site of energy deposition (Fig. 1) in a circular-pipe-type container of radius r_{pipe}, the conical-detonation-wave/container interaction occurs at downwind distance $x = L \equiv r_{pipe}/\tan \beta$, $\sin \beta \equiv u_{CJ}/u_o$, where, by design, the known CJ-detonation-wave speed for the mixture $u_{CJ} < u_o$, the (supersonic) speed of the oncoming mixture. For $x > L$, the flow is no longer selfsimilar; a (say, method-of-characteristics) solution of the steady isentropic supersonic flow in trial axisymmetric containers of cross-section $A(x)$, $A_x(x) > 0$, suggests a nozzle configuration for which, within a relatively short streamwise distance, the detonated mixture is uniformized for exhaust at ambient pressure[3]. If the combustor is enveloped with a streamlined sheath, a favorable thrust-to-drag ratio seems attainable (even after accounting for the decrement from ideal performance, owing to real-gas effects).[3]

Attention is turned to the nonintrusive direct initiation of a spherical detonation wave in a reactive mixture, then to the initiation of a train of such waves in a fast-flowing stream by a periodic energy source focused at a fixed site (Fig 2). First, we suggest[4] that previously reported values of the minimum (or "critical") energy required for direct initiation may be overestimates because they are based on the use of (1) a relatively slow mode of energy deposition, and/or (2) a strong initial blast wave that decays asymptotically to a CJ detonation. We suggest that a conservative value for the required energy E is given by

$$E = E_{CJ}[1 + (t/t_m)]^3, \quad t_m \equiv \lambda/u_{CJ}, \quad E_{CJ} \equiv \rho_o V_o q , \qquad (1)$$

where ρ_o is the initial density, $V_o = (4/3)\,\pi\lambda^3$, q is the exothermicity per mass of mixture, λ is the (empirically established) cell size, and t is the time interval of energy deposition. This result is predicated on the sufficiency of depositing, in a cell-sized volume, the energy chemically derivable from the (presumably) detonable mixture in that volume. In this sense, Eq. (1) is the extention to the direct initiation of a detonation of the empirical criterion for the ignition of a deflagration (specifically, the mass in a volume of dimension comparable to that of a propagating deflagration must be raised, from ambient to burned-gas temperature, for sustained burning to ensue). Of course, the temporal interval for energy deposition for ignition of a deflagration is limited by the diffusive time scale, whereas [Eq. (1)] the temporal interval for energy deposition for direct initiation of a detonation is limited by the much shorter wave-dispersion time scale. Indeed, Eq. (1) quantifies the advantage of rapid energy deposition, and recovers the empirically known power, as

well as energy, criteria for direct initiation. Second, we have considered[4] the entropy rise associated with the reflected shock waves formed in already-detonated mixture when neighboring spherical detonations interact, since the same reactive "blob" of mixture can be converted to product but once. This particular source of entropy rise is minimized if the time interval between pulses is minimized and if the ratio Λ ($\equiv u_o/u_{CJ}$) $\downarrow$ 1.

Experimentally, we have used an ArF laser at 193 nm on mixtures of C_2H_2/O_2 and of $H_2/O_2/C_2H_2$: the laser energy can be coupled efficiently into these mixtures owing to a strong resonant absorption by C_2H_2, which readily dissociates into reactive fragments. Thus, as a first step, we have investigated the direct initiation of detonation without the use of laser energy high enough to induce gas breakdown, a requirement for lasers at wavelengths not in resonance with the reactive mixture. "Planar" detonation waves were initiated in mixtures contained in a straight tube of 1.6-cm inner diameter and 1-m length, and spherical detonation waves were initiated in an open system above a 6-cm-diameter flat-flame burner. For stoichiometric C_2H_2/O_2 mixtures, the critical energy and the delay time for direct initiation decrease with increasing initial pressure over the range of 100-800 torr, in consistency with the literature. For stoichiometric C_2H_2/O_2 mixtures at atmospheric pressure, the critical energy for directly initiated spherical detonation is 181±15 mJ, on the basis of a limited number of tests--a value almost three times larger than the corresponding value for a planar detonation. However, the available excimer-laser energy ($\leq$ 375 mJ) typically was insufficient for direct initiation in the $H_2/O_2/C_2H_2$ system, and the use of more powerful lasers to induce gas breakdown appears necessary for direct initiation in mixtures of practical interest for propulsion.

Still to be addressed in detail are the nature and extent of modifications to the combustor concept owing to inevitably imperfect mixing of fuel added to a very-fast-flowing airstream. We have suggested[2] that (1) mixing with as little shock heating as possible seems desirable; (2) the relatively well-mixed portion of an inhomogeneous mixture may be reacted in the conical detonation wave; and (3) the inhomogeneity of the less-well-mixed portion may possibly be so "tailored" that diffusive burnup of the residual fuel occurs rapidly in the hot flow downwind of the conical detonation.

REFERENCES

[1]Fendell, F., Kung, E., and Sheffield, M., "Flame Configuration Associated with Localized Energy Addition to a Flowing Reactive Mixture," *Journal of Propulsion and Power*, Vol. 8, March-April 1992, pp. 464-471.

[2]Carrier, G., Fendell, F., McGregor, D., Cook, S., and Vazirani, M., "Laser-Initiated Conical Detonation Wave for Supersonic Combustion," *Journal of Propulsion and Power*, Vol. 8, March-April 1992, pp. 472-480.

[3]Fendell, F., Mitchell, J., McGregor, R., Magiawala, K., and Sheffield, M., "Laser-Initiated Conical Detonation Wave for Supersonic Combustion. II," AIAA Paper 92-0088, AIAA, Washington, DC, January 1992.

[4]Carrier, G., Chou, M.-S., and Fendell, F., "Laser-Initiated Conical Detonation Wave for Supersonic Combustion. III," AIAA Paper 92-3247, AIAA, Washington, DC, July 1992 (to be presented at the 28th Joint Propulsion Conference, Nashville, TN).

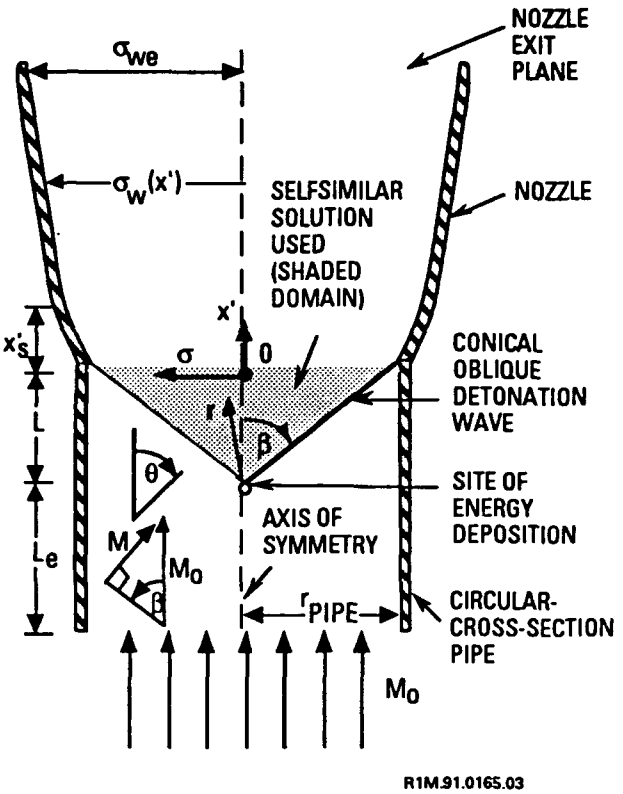

Fig. 1 Schematic (not to scale) of a supersonic combustor, where sin β = M/M_0, $M_0 = u_0/a_0$, $M = u_{CJ}/a_0$, a_0 being the sound speed of the cold mixture and $L = r_{pipe}/\tan \beta$. The pipe container is flared at the position of intersection with the nearly conical detonation wave, to avoid reflected shocks.

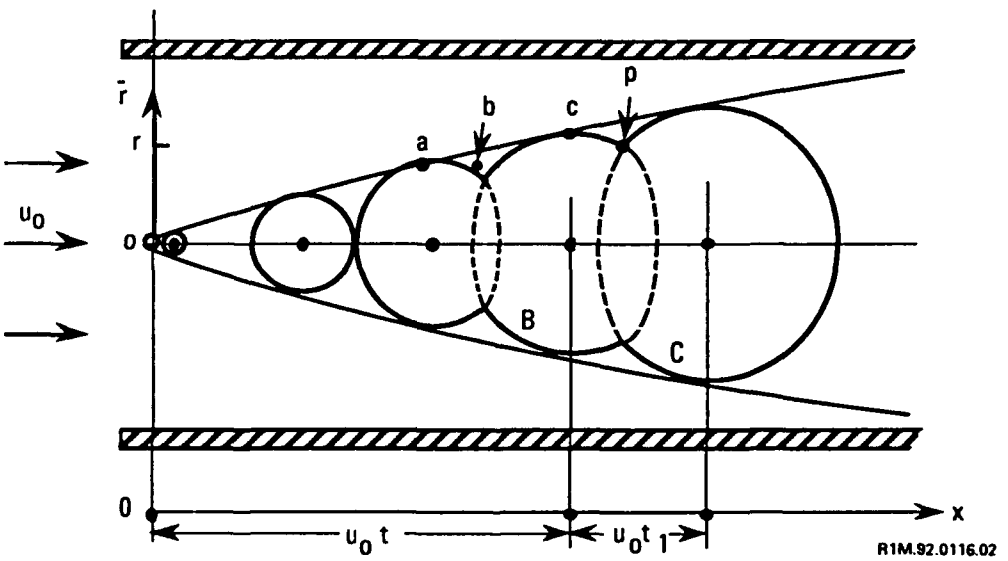

Fig. 2. A cone conceptually envelops a train of spherical detonations, each directly initiated by a pulse of energy, deposited at the origin ($\bar{r} = 0$, $x = 0$) with period t_1. The mixture flow speed u_0 exceeds the Chapman-Jouguet (CJ)-wave speed u_{CJ}. Dashed curves denote entropy-increasing reflected shocks from the interaction of neighboring spherical detonations.

TRANSPORT PHENOMENA AND INTERFACIAL KINETICS IN MULTIPHASE COMBUSTION SYSTEMS†

AFOSR Grant No. 91-0170

Principal Investigator: Daniel E. Rosner‡
High Temperature Chemical Reaction Engineering Laboratory
Department of Chemical Engineering, Yale University
New Haven, CT 06520-2159,USA

SUMMARY/OVERVIEW

The performance of ramjets burning slurry fuels (leading to oxide aerosols and liquid deposits), and gas turbine engines in dusty atmospheres depends upon the formation and transport of small particles, often in non-isothermal combustion gas boundary layers (BLs). Even airbreathing engines burning "clean" hydrocarbon fuels can experience *soot* formation/deposition problems (*e.g.*, combustor liner burnout, turbine blade erosion,...). Moreover, particle formation and transport are important in chemical reactors used to synthesize or process aerospace materials (turbine coatings, optical waveguides, ceramic precursor powders, ..). Accordingly, our research is directed toward providing chemical propulsion system and materials engineers with new techniques and quantitative information on important particle- and vapor-mass transport mechanisms and rates. An interactive experimental/theoretical approach is being used to gain understanding of performance-limiting chemical-, and mass/energy transfer-phenomena at or near interfaces. This includes the development and exploitation of seeded laboratory burners (Sections 1, 2), flow-reactors (Section 4), and new diagnostic techniques. Resulting experimental rate data, together with the predictions of asymptotic theories, are then used to propose and verify simple viewpoints and rational engineering correlations for future design/optimization.

TECHNICAL DISCUSSION

1. TRANSPORT OF AGGREGATED PARTICLES

The Brownian diffusion-, inertial-, and optical-properties of *aggregated* particles, as formed in sooting diffusion flames, are quite *sensitive* to size (*eg.* number N of "primary" particles) and morphology. In Fig. 1 (*eg.*) we summarize the orientation-averaged Brownian diffusivity of aggregates in the continuum limit. Of interest are methods for anticipating coagulation and deposition rates of *populations* of such particles, especially in non-isothermal flow systems. We predict that capture rates from "coagulation-aged" polydispersed aerosols of a particular morphology by the mechanisms of convective-diffusion and, especially, thermophoresis will be close to those calculated if all such particles had the mean particle volume ϕ_p/N_p. Correction factors (Fig.2) for convective-diffusion are found to be *ca.* 0.9 for a surprisingly wide range of gas-dynamic/environmental conditions, and particle morphologies.

The ability to reliably measure and predict the *thermophoretic* properties of isolated aggregated flame-generated particles (carbonaceous soot, Al_2O_3, ...) is important to many technologies, including chemical propulsion and refractory materials fabrication. We just completed a manuscript describing our measurements of the *thermophoretic diffusivity* of flame-generated submicron TiO_2(s) "soot" particles using a $TiCl_4$(g)-seeded low strain-rate counterflow laminar diffusion flame (CDF-) technique (Fig. 3, Gomez and Rosner, 1992)). Depending on the sharpness of the gas temperature and velocity gradients in such flames there are one or more *particle stagnation planes*.(PSPs, Fig.4). A knowledge of the relative positions of the gas and particle stagnation planes (shown (Fig.5) *vs.* flame stoichiometry), and the associated chemical environments, can be used to control the composition and morphology of flame-synthesized particles.These factors should also influence particle production and radiation from *turbulent* non-premixed "sooting" flames, as discussed further in Gomez and Rosner, 1992.

2. MULTIPHASE BOUNDARY LAYER THEORY: THERMOPHORESIS AND INERTIA

The results of Seeded micro-combustor experiments, and ancillary theoretical calculations on the interesting competition between particle *inertia* and particle *thermophoresis* for the case of laminar gaseous boundary layers on surfaces with streamwise curvature (eg.,turbine blades) are shown in

† AFOSR Contractors Meeting on Propulsion, La Jolla , CA 92037, 15-19 June 1992

‡ For research collaborators consult **REFERENCES**

Fig.6 (from Konstandopoulos and Rosner, 1992; Rosner *et. al.* 1991). The combined effects of thermophoretic- and inertial-particle drift toward a concave, "cold" target are seen to substantially augment local particle deposition rates, in excellent accord with the predictions of two-phase laminar boundary layer theory. On *convex* cooled surfaces (*eg.* the "suction" side of a GT blade) our prediction-correlation methods predict the *competing* effects of thermophoretically-augmented capture and inertial drift *away* from the target. Instructive results for the angular distribution of mass transfer to cooled cylinders and spheres are displayed in Fig. 7.

3. HEAT TRANSFER EFFECTS ON COAGULATION DYNAMICS

Our continuing studies of submicron particle motion in host-gas temperature gradients and radiation fields (see, *eg.*, Mackowski *et.al.*1992, Rosner, *et. al.*,1992, Mackowski, D.W.,1990) have demonstrated that even spherical particles thermally out of equilibrium with their local host gas will coagulate with particle-particle encounter rate constants quite different from their usual "isothermal" Brownian values (see, *eg.*, the "correction" factors of Fig.8 for unequal-sized carbonaceous particles in a black-body radiation environment with the stated temperatures). This leads to *unusual population dynamics*, including the strong tendency of radiatively *cooled* large particles to grow still larger by rapidly "scavenging" smaller ones. Localized radiative cooling can also thermophoretically concentrate the radiating particles, with interesting stability consequences (Mackowski *et.al.* 1992).

4. KINETICS AND MORPHOLOGY OF CVD-MATERIALS IN MULTI-PHASE ENVIRONMENTS

A small impinging jet (stagnation flow) reactor is being used to study the CVD-rates of refractory layers on inductively heated substrates, including those deliberately "pre-loaded" with porous particulate deposits. These measurements and associated "chemical vapor infiltration" theory will be useful to understand deposition rates and deposit microstructures that have been observed in particle-containing CVD environments. Analogous questions arise in anticipating the vapor scavenging ability of *suspended* aggregated particles, on which we are also working.

CONCLUSIONS, FUTURE RESEARCH

In our 1991-1992 OSR-sponsored Yale HTCRE Lab research (briefly described above, and in greater detail in the archival references cited and updated below) we have shown that new methods for rapidly measuring vapor- and particle-mass transfer rates , combined with advances in transport theory, provide useful means to identify and incorporate important, often previously neglected, transport phenomena in propulsion/materials engineering design/optimization calculations. We are now extending our work on the effects of these new "phoretic" phenomena, 'polydispersed' particle populations and the consequences of highly nonspherical particles (eg. aggregates).For this purpose an improved CDF burner is being constructed, with supplementary optical and thermophoretic sampling diagnostics.

REFERENCES

Castillo, J.L., Garcia-Ybarra, P., and Rosner, D.E.,"Morphological Instability of a Thermophoretically Growing Deposit", *J. Crystal Growth* **116**,105-126 (1992)

Gomez, A., and Rosner, D.E., "Thermophoretic Effects on Particles in Counterflow Laminar Diffusion Flames" *Combustion Science and Technology*; (submitted May, 1992)

Konstandopoulos, A.G., **Effects of Particle Inertia on Aerosol Transport and Deposit Growth Dynamics**, PhD Dissertation, Yale University, December 1991.

Konstandopoulos, A.G. and Rosner, D.E.,"Inertial Effects on Thermophoretic Transport of Small Particles to Walls With Streamwise Curvature---I. Experiment, II. Theory", Submitted to *Int. J. Heat Mass Transfer (1992)*

Mackowski,D.W., "Phoretic Behavior of Asymmetric Particles in Thermal Non-equilibrium with the Gas : Two-Sphere Aggregates", *J. Colloid and Interface Science* **140** (1), 138-1576(1990)

Mackowski, D.W., Tassopoulos, M. and Rosner, D.E.,"Effect of Radiative Heat Transfer on the Coagulation Dynamics of Combustion-Generated Particles" (to be submitted to *Aerosol Sci. Technol (AAAR)* (1992))

Rosner, D.E., **Transport Processes in Chemically Reacting Flow Systems**, Butterworth-Heinemann (Stoneham MA), 3d Printing 1990.

Rosner, D.E., Mackowski, D.W and Garcia-Ybarra, P., "Size and Structure-Insensitivity of the Thermophoretic Transport of Aggregated 'Soot' Particles in Gases", *Comb. Sci & Technology* **80** (1-3), 87-101 (1991)

Rosner, D.E., Konstandopoulos, A.G., Tassopoulos, M., and Mackowski, D.W, "Deposition Dynamics of Combustion-Generated Particles: Summary of Recent Studies of Particle Transport Mechanisms, Capture Rates, and Resulting Deposit Microstructure/Properties", *Proc. Engineering Foundation/ASME Conference*: **Inorganic Transformations and Ash Deposition During Combustion**, (1992), pp. 585-606

Rosner, D.E.and Tassopoulos, M.," Direct Solutions to the Canonical 'Inverse' Problem of Aerosol Sampling Theory: Coagulation and Size-dependent Wall Loss Corrections for Log-Normally Distributed Aerosols in Upstream Sampling Tubes", *J. Aerosol Sci.* 22 (7) 843-867 (1991)

Rosner, D.E., Mackowski, D.W, Tassopoulos,M., Castillo, J.L., and Garcia-Ybarra, P., "Effects of Heat Transfer on the Dynamics and Transport of Small Particles in Gases", *I/EC-Research.* 31 (3) 760-769(1992))

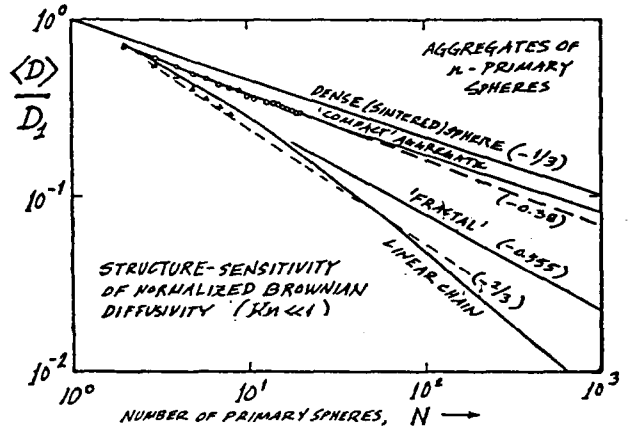

Fig.1. Predicted normalized orientation-averaged Brownian diffusivity of *aggregated* particles containing N-primary spheres in the near-continuum limit; Normalization: Brownian diffusion coefficient, D_1, of *primary sphere* in the same local environment (after Rosner *et.al.* 1991)

Aggregate Particle Morphology	Sc>>1 Convective-diffusion				Turbulent Eddy Impaction
	LBL		TBL		
	fm	c	fm	c	(c)
dense single spheres[d]	0.905	0.942	0.904	0.940	2.94
compact aggregates	?	0.936	?	0.934	2.62
fractal aggregates	0.925	0.922	0.933	0.921	1.79
linear chains[e]	0.914	0.918	0.919	0.917	1.47

a Thermophoretically-dominated deposition rate ratios (closer to unity) not reported here; present values are for negligible transport by non-convective mechanisms other than Brownian diffusion (numerical columns 1-4) or inertia (column 5)

b log-normal orientation averaged populations with $\sigma_g(fm)=2.46$ and $\sigma_g(c)=2.30$ (see,*e.g.* Rosner & Tassopoulos(1989))

d Reference case; sintered single spheres with abovementioned σ_g-values for PSD

e For continuum cases not strictly a power-law (Fig. 1), however, values stated are for approximate power-law representation for $\langle D_p(N)\rangle$

Fig. 2 Predicted values of $[-\dot{m}''_p/(-\dot{m}''_p(\bar{v}))]$ for isothermal deposition from coagulation-aged aggregated particle populations (after Rosner *et.al.*,1992)

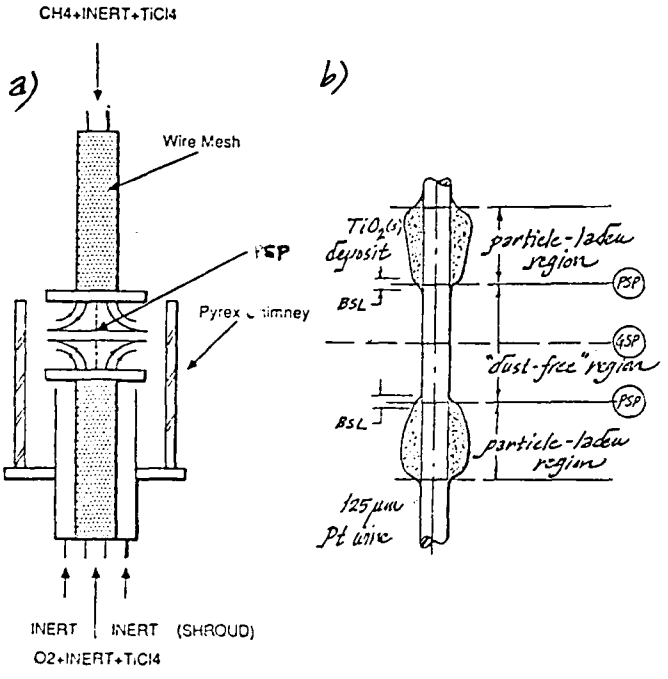

Fig.3 a). Axisymmetric counterflow diffusion flame (CDF) burner configuration used for experimental determination of particle thermophoretic diffusivity based on observed axial position of "particle stagnation planes" (PSPs); b) Appearance of axially mounted 125 μm diam. filament revealing existence of dust-free region straddling the flat diffusion flame (after Gomez and Rosner,1992)

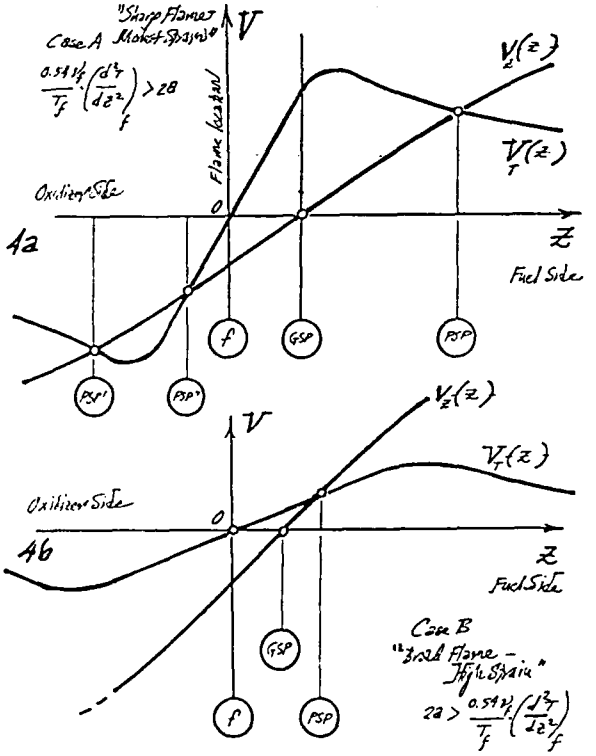

Fig.4 Axial gas velocity and particle thermophoretic velocity profiles in near-stoichiometric counterflow laminar diffusion flames; a) "Sharp flame-modest strain" case with *three* eligible particle stagnation planes (PSPs); b) Broad flame-high strain" case with *one* eligible particle stagnation plane (after Gomez and Rosner,1992)

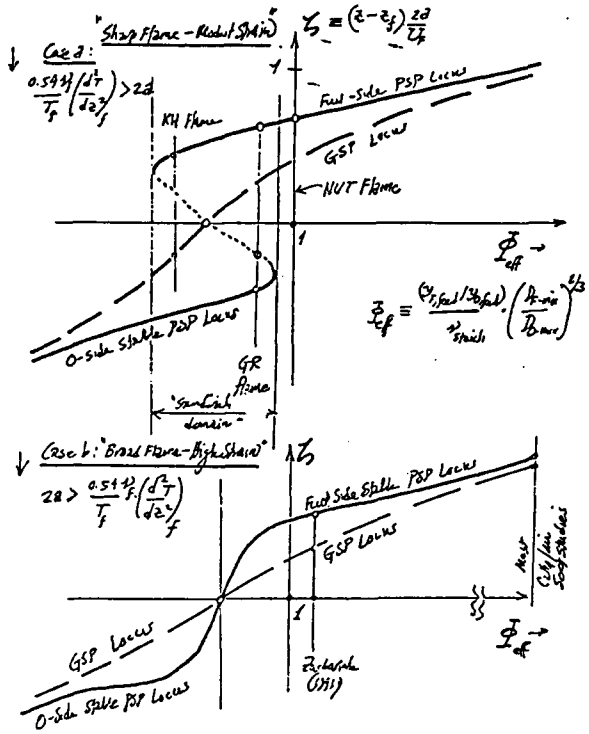

Fig.5 Locus of dimensionless axial positions of *particle stagnation plane*(s) (PSP) and *gas* stagnation plane (GSP) for laminar counterflow diffusion flames as a function of the effective fuel vapor equivalence ratio; Case a) ("Sharp flame-modest strain") (after Gomez and Rosner,1992)

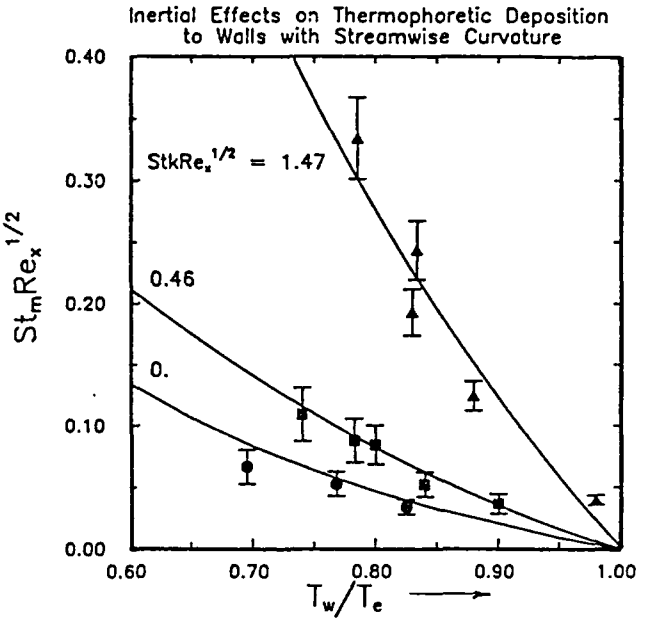

Fig.6 Experimental and theoretical dimensionless particle deposition rate coefficient $St_m Re_x^{1/2}$ *vs.* temperature ratio T_w/T_e and the relevant particle relaxation time parameter $StkRe_x^{1/2}$; laminar boundary layer flow, concave circular arc solid target (after Konstandopoulos and Rosner, 1992)

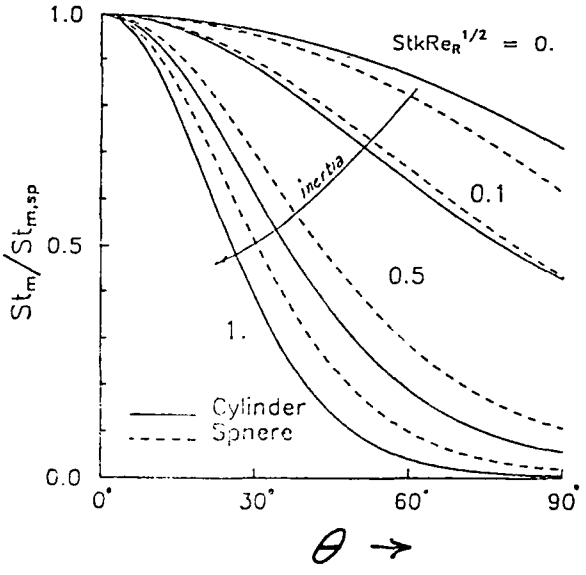

Fig. 7 Predicted inertial effects on thermophoretic-convective mass transfer rates to cooled convex objects at subcritical Stokes numbers; angular distribution of mass transfer coefficient for spheres and cylinders at high Reynolds numbers (Normalization: Stagnation point value at the prevailing Stk) (after Konstandopoulos(1991))

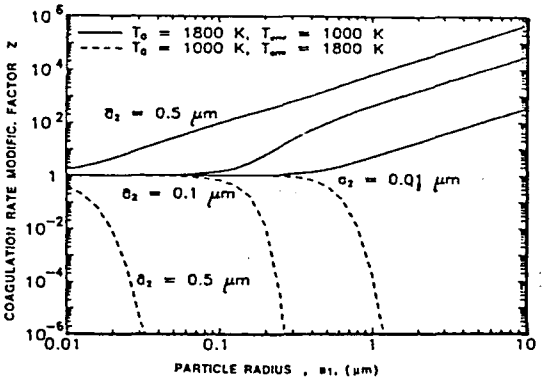

Fig. 8. Multiplicative "correction" to the Brownian (Smoluchowski isothermal) coagulation rate constant due to energy exchange to/from spherical particles of unequal radius (after Rosner *et.al.*,1992, Mackowski *et.al.* 1992)

MECHANISTIC MODELS FOR SOOT FORMATION

AFOSR Contract No. F49620-91-C-0056

Principal Investigators: M.B. Colket, III and R.J. Hall

United Technologies Research Center
East Hartford, CT 06108

SUMMARY/OVERVIEW

The overall objectives of this work are to (1) refine and update an existing soot formation model and (2) incorporate this soot model into a code describing a laminar, opposed jet diffusion flame. Pyrolysis data has been obtained from a single-pulse shock tube coupled to a GC/MSD analytical system. Many high molecular weight species have been identified and this information is being used to examine and compare PAH growth mechanisms. The soot model has been updated to include effects from particle ageing and a radiation model has been developed to treat radiation from flames with varying degrees of optical thickness.

TECHNICAL DISCUSSION

A. Ring Formation During Oxidative Pyrolysis Of Methane

As part of the effort to develop a model for soot production in an opposed jet diffusion flame, the reaction kinetics and mechanisms associated with ring formation during the oxidative pyrolysis of methane need to be established. Using data and a kinetic model from another program the amount of benzene produced during the oxidative pyrolysis of methane has been calculated. Several ring formation pathways were included in this model: $C_2H_x+C_4H_y$, $C_3H_x+C_3H_y$, and $C_5H_x+CH_3$. As shown in Fig. 1, the C_3H_3 recombination was found to be by far the dominant reaction pathway under high temperature, partial oxidation conditions. For these simulated single-pulse shock tube conditions, elapsed time is about 600 microseconds. The practical importance of this result is that (at least in preliminary diffusion flame calculations) only the kinetic processes associated with the C_3-mechanism need to be included in the otherwise complex model.

B. PAH Formation

Toluene (1% in a bath of argon) has been pyrolyzed in a single-pulse shock tube over the temperature range of about 1200 to 2000K and total pressures of 7 to 10 atmospheres. Products have been analyzed using a gas chromatograph coupled to a HP5971A mass spectrometric detector (MSD). Structural information has been obtained on species with molecular weights as high as 228 amu. Modeling, speculation on likely reaction processes and comparisons to literature have assisted in identifying most of these species. A total of over 100 individual peaks have been detected and the structure of more than 80 of these have been identified. Probable identifications have been made for most of the remaining trace species. Data is consistent with previous results[1] on toluene pyrolysis (which are shown in Fig. 2) and confirms the tentative identifications of product species. The recent results support the early results showing early formation of bibenzyl and fluorene. Bibenzyl is formed via benzyl radical recombination. A proposal has been made[1] for the early formation of fluorene involving addition of a benzyl radical to benzene. Many of the previously unidentified peaks produced at low temperatures are methyl-biphenyl species, intermediates in the proposed fluorene formation mechanism. These results as well as the identification of a cyclopentadienyl-benzyl species strongly support the formation of high molecular weight species via ring-ring combinations. In addition, several high molecular weight, closed ring species with methyl or acetylene side chains were

identified. Existence of these species also support growth pathways involving addition of methyl radicals to rings and addition of aromatic radicals to acetylene. Kinetic modeling will be performed and results compared to the experimental data in an attempt to determine the relative importance of these different pathways. Reactions associated with addition of acetylene to five-membered rings are discussed elsewhere[2].

C. Soot Ageing

The soot formation model[3,4] has been extended to include an active site decay (ageing) term which slows the rate of surface growth at longer times. Following the suggestion of Haynes, et. al[5]., the surface density of active sites, denoted by χ, is allowed to decay with time according to

$$\frac{\chi}{\chi_o} = \exp\left(- \int_o^t k_{age}(T(t')) \, dt' \right) \tag{1}$$

where the decay rate constant is

$$k_{age} = 7 \times 10^6 \exp\left(- \frac{20,000}{T} \right) \text{ sec}^{-1} \tag{2}$$

and the time origin is the onset of net particle growth. The time-dependent value of χ can then be used with any of the several models of surface growth[3,4]. Inclusion of this term has an important effect in the simulations of high temperature soot growth, as shown in Fig. 3 for the acetylene and propane flames simulated[3,4]. The "modified Frenklach" growth mechanism, which gave the best overall agreement in the earlier studies, was used here. For the acetylene flame, which is at the highest temperature, the predicted asymptotic growth behavior is now more consistent with experiment, as seen; although the absolute magnitude is decreased. The lower temperature propane flame experiences a less drastic ageing effect in the simulation at long times, but the agreement with experiment is seen to be much improved. The ageing term is not as significant for the simulations of the lower temperature ethylene flames previously described[3,4]. Overall, inclusion of this effect has improved the theory-experiment comparisons. A lower overall activation energy than that shown in Eqn. (2) above should provide an even better comparison to the data.

D. Species Conservation

In preparation for coupling the soot formation model with a counterflow diffusion flame solver, the species conservation equations for the sectional representation of the particle sizes have been derived. Because soot in flames corresponds to a large Knudsen number limit, the thermophoretic velocity will sensibly be independent of particle size. The diffusion coefficient for a size class is shown to be a mass-weighted mean value with an analytic expression derived from the intra-class density distribution function. In the large Knudsen number limit the problem of using sectional equations in a flame solver is much simplified.

E. Radiative Transfer

An objective of the current contract is to model radiative transfer effects in sooting counterflow flames. It was decided to approach the problem in an incremental fashion by first coupling gas band radiation alone to the counterflow solver. An expression for the radiant power density for gas band emission from H_2O, CO_2, and CO was derived based on wideband absorption models. The expression is derived from a solution to the radiative transfer equation for an infinite slab, and is distinguished from other work in this area in being valid for any degree of optical thickness. Generally the optically thin limit is valid for higher strain rates, but finite optical thickness effects

can become important at high pressure and very low strain rates. Nonadiabatic radiation loss from a flame will lower the peak temperatures, and can appreciably affect predicted NO_x levels, for example. The radiant power density, which is equivalent to the divergence of the net radiative flux, has been included in the energy equation of a widely used counterflow code[6]. Thus a completely self-consistent analysis of the temperature reduction due to radiation and its effect on flame chemistry has been made. Details of the radiative algorithm are given in Ref. 7, and radiative effects on predicted NO_x levels for conditions meant to simulate an aircraft gas turbine combustor have been described[8]. Sample calculations showing the effect of optical thickness on the local radiant power density are shown in Fig. 4 for a 10.5 atm counterflow flame in which the methane fuel temperature has been chosen so that the adiabatic flame temperature approximates that of jet fuel. The base case strain rate is 56 sec^{-1}, and the lower strain rate cases have been generated by stretching the base case coordinates, assuming that characteristic lengths scale as $(\text{strain rate})^{-0.5}$. All the cases in this figure employ the same converged temperature and species profiles from the adiabatic counterflow code for illustrative purposes. The non-adiabatic counterflow solver predicts that 1.75% of the total flame enthalpy release is converted to radiation at 56 sec^{-1}; at a strain rate of 20.5 sec^{-1}, it is predicted to rise to 4.5%. In sooting flames, the radiative losses are expected to rise significantly. Extension of the radiative model to include soot contributions will be a straightforward exercise. Professor M. Smooke is assisting with the modifications of the opposed jet laminar flame code.

REFERENCES

1. M. B. Colket, et. al., "The Determination of Rate-Limiting Steps During Soot Formation," Annual Report AFOSR Contract F49620-88-C-0051, April, 1989.

2. M. B. Colket and R. J. Hall, "A Soot Growth Mechanism Involving Five-Membered Rings," Presentation to the Eastern Section of the Combustion Institute, Ithaca, N.Y., Oct. 14-16, 1991.

3. M. B. Colket and R. J. Hall, "Description and Discussion of a Detailed Model for Soot Formation in Laminar, Premixed Flames," United Technologies Research Center, UTRC91-20, August, 1991. Also Appendix A in M. B. Colket, et. al., "The Determination of Rate-Limiting Steps During Soot Formation," Final Report AFOSR Contract F49620-88-C-0051, August, 1991.

4. M. B. Colket and R. J. Hall, "Successes and Uncertainties in Modeling Soot Formation in Laminar, Premixed Flames," presentation to the workshop on Mechanisms and Models of Soot Formation, Heidelberg, Germany, to be published in Springer Series of Chemical Physics, ed. H. Bockhorn, 1992.

5. B. T. Haynes, private communication, October, 1991.

6. M. D. Smooke, I. K. Puri, and K. Seshadri, "A Comparison Between Numerical Calculations and Experimental Measurements of the Structure of a Counterflow Diffusion Flame Burning Diluted Methane in Diluted Air," *Twenty-first Symposium (International) on Combustion*, The Combustion Institute, pp. 1783-1792, (1986).

7. R. J. Hall, "The Radiative Source Term for Plane-Parallel Layers of Reacting Combustion Gases," submitted to *JQSRT*, (1992).

8. A. Vranos and R. J. Hall, "Influence of Radiative Loss on NO_x Formation in Counterflow Diffusion Flames at High Pressure," to be submitted to *Combustion and Flame*, (1992).

Figure 1

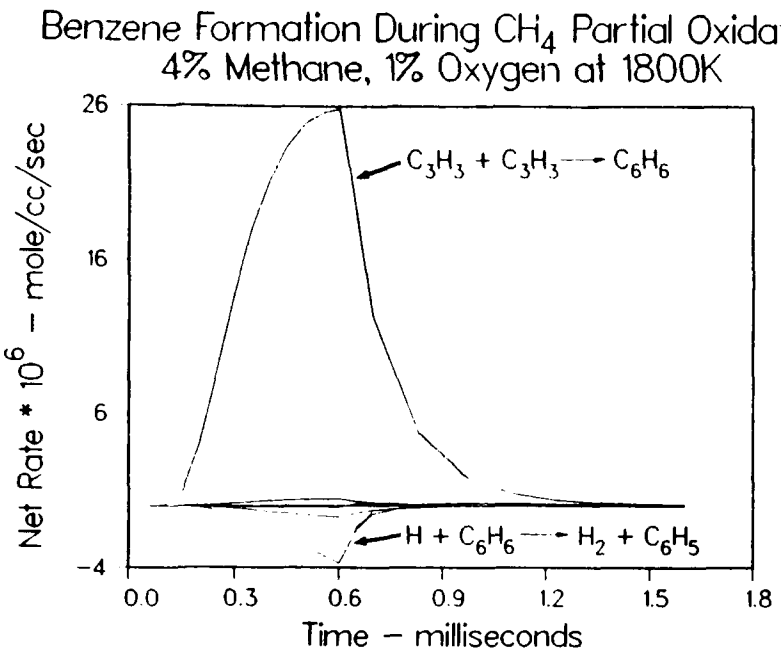

Figure 2

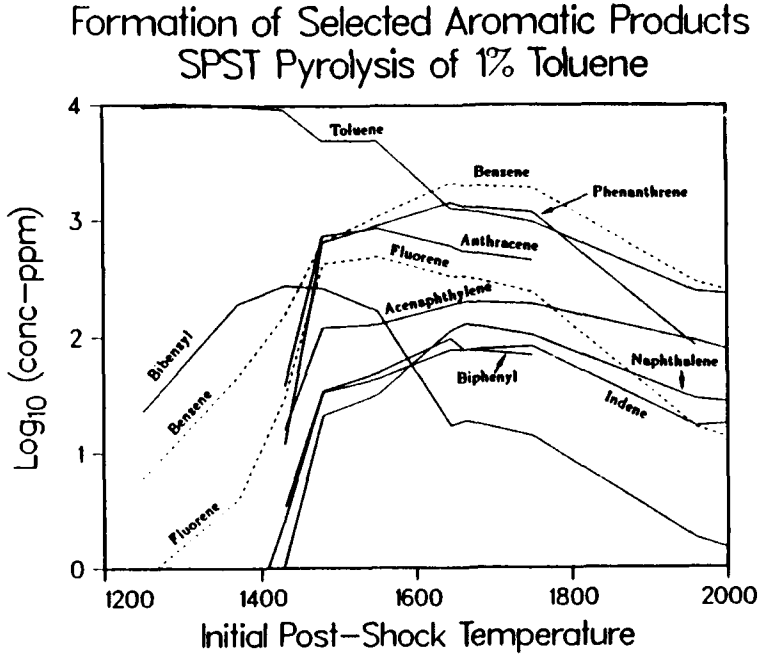

Figure 3

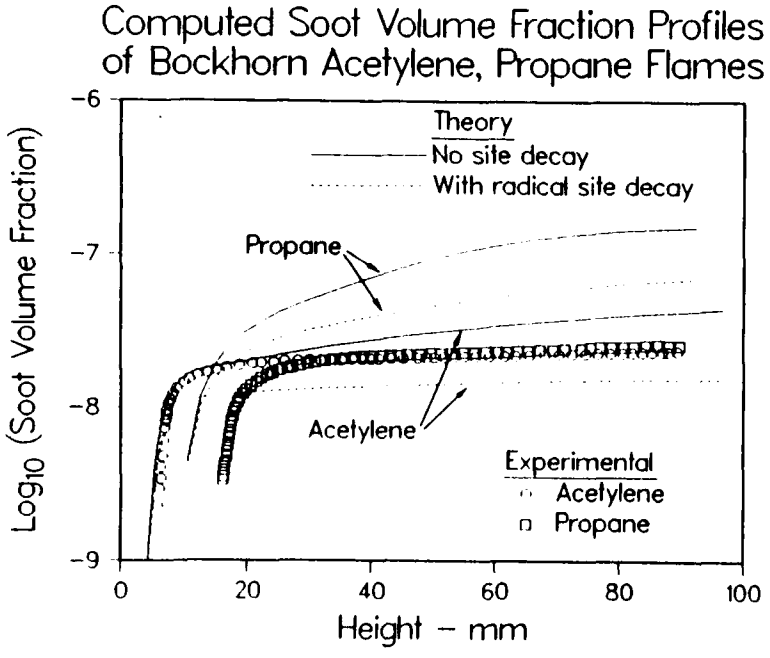

Figure 4

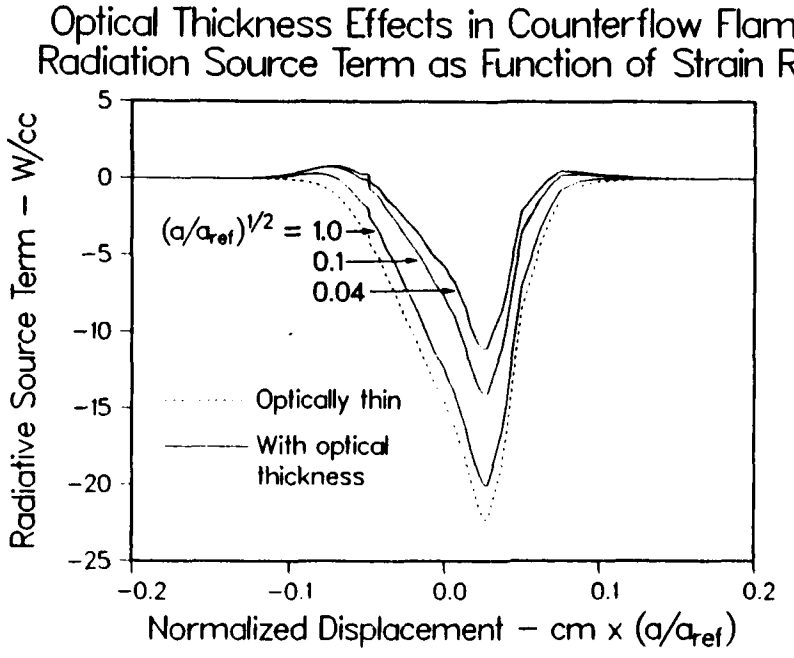

DETAILED STUDIES OF SOOT FORMATION IN LAMINAR DIFFUSION FLAMES FOR APPLICATION TO MODELING STUDIES

AFOSR Grant No. F49620-92-J-0161

Principal Investigator: Robert J. Santoro

Department of Mechanical Engineering
Propulsion Engineering Research Center
The Pennsylvania State University
University Park, PA 16802-2320

SUMMARY/OVERVIEW:

The primary objective of the present research program is to provide a fundamental understanding of the processes which control soot particle formation under conditions applicable to gas turbine engine operation. Current efforts emphasize laminar diffusion flames studies to elucidate fuel structure effects on particle precursor, inception and surface growth processes. Through extensive measurements of the gas and particle fields, direct comparison with detailed soot formation models can be undertaken to determine the controlling processes. Recently developed soot formation models based on premixed and diffusion flame studies have shown reasonable predictive capability. However, data for model validation remains limited and is a major deficiency in extending current understanding to practical problems. Studies during the current year have examined the relative importance of concentration and temperature variations as well as the operating pressure effects on soot production. These studies indicate that the temperature sensitivity of the soot formation processes generally dominates concentration variations, while increases in pressure result in a near first-order increase in the amount of soot formed.

TECHNICAL DISCUSSION

During the past year of the research program, efforts have focused on the completion of the study of the concentration and temperature effects on soot formation[1,2] as well as reexamining the role of operating pressure. Additional studies have also been conducted to investigate the effects of soot aggregates on the optical properties of soot particles[3,4]. In all cases these studies have been conducted in coannular laminar diffusion of flames burning in air. A laser scattering/extinction system was used to obtain data on the soot particle field.

Concentration and Temperature Effects

A detailed study has been made of the relative effects of concentration and temperature on soot formation in diluted laminar ethene/air diffusion flames[1,2]. Total integrated soot volume fraction measurements showed that in argon and nitrogen diluted flames with equal calculated adiabatic flame temperatures, the more diluted argon flames consistently displayed lower soot concentrations. However, in flames of equal dilution, argon flames consistently contained higher soot concentrations than the slightly cooler nitrogen diluted flames. Local temperature measurements showed that for nitrogen and argon diluted flames with equal calculated adiabatic flame temperature, argon diluted flames displayed lower temperatures in the region where soot is first formed. Mass spectrometric measurements of gas concentrations in diluted and undiluted methane/air diffusion flames were obtained and compared with a numerical flame model. These results indicated that the initial difference in fuel concentration in diluted and undiluted flames diminishes rapidly with height. Furthermore, laser light scattering measurements show that as inert diluent is added, soot inception is delayed and consequently less time is available for soot growth. Based on this extensive set of data, a quantitative assessment was made of the relative effects of temperature and concentration variations on soot formation indicating that for coflow diffusion flames, the role of temperature is more important than the reduction in fuel concentration when an inert diluent is added to the fuel flow. The analysis yielded an apparent activation energy of 94.5 $\pm$ 25.5 Kcal/mole for the temperature dependence, while the fuel concentration sensitivity expressed as $[X_o]^n$ where X_o is the initial fuel mole fraction, was given by $n = 0.3 \pm 0.18$.

Operating Pressure Effects on Soot Formation

In order to study the effect of operating pressure on soot formation, a series of ethene/air diffusion flames were studied over a pressure range from 0.1 to 0.5 MPa (1 to 5 atm). The ethene fuel flow rate was held constant at 2.8 cm^3/s, while an air flow rate of 950 cm^3/s provided overventilated conditions. Soot volume fraction measurements were obtained from a laser extinction technique using an argon ion laser operating at the 514.5 nm laser line. For most of the measurements, extinction measurements were made along the centerline, although a few radial profiles of the extinction due to soot particles were obtained to assess the effects of flame diameter changes on the total amount of soot formed. Four quantities related to the local soot volume fraction were determined. The first involved the integral of the soot volume fraction, f_v, along the laser path:

$$f_{v,cl} = \int_{-\infty}^{+\infty} f_v \, dx = -C(\lambda,m)\ln(I/I_o) \tag{1}$$

where $f_{v,cl}$ is the centerline integrated soot volume fraction, f_v is the local soot volume fraction, x lies along a laser path through the flame on a diameter, $C(\lambda,m)$ is a constant which can be determined from Rayleigh scattering theory to be 1.05×10^{-5} cm for $m = 1.57 - 0.56i$ at $\lambda = 514.5$ nm, and finally, I/I_o is the ratio of the transmitted laser to incident laser power. The average soot volume fraction, $f_{v,av}$, is defined as

$$f_{v,av} \equiv \frac{1}{d} \int_{-\infty}^{+\infty} f_v \, dx = -\frac{1}{d} C(\lambda,m)\ln(I/I_o) \tag{2}$$

where d is the measured soot zone diameter at a given flame height z and pressure p. The total integrated soot volume fraction, F_v, then becomes

$$F_v = \int_{-\infty}^{+\infty} \int_{-\infty}^{+\infty} f_v \, dxdy = \alpha \, f_{v,av} \frac{\pi}{4} d^2 = -\alpha \, C(\lambda,m)\ln(I/I_o) \frac{\pi}{4} d \tag{3}$$

Here, the correction factor, α, which is required due to the non-uniform radial distribution of soot volume fraction across the flame, was determined by comparing to the measured integrated volume fractions at several locations. The value $\alpha = 1.5$ was selected for the height $z \leq 25$ mm, where most soot particles are in the annular region.

Previous measurements have shown that the axial velocity in a buoyant diffusion flame increases with flame height, is independent of fuel flow rate, and can be calculated as $u_{max} = (2az)^{0.5}$, where a is 2500 cm^2/sec. Since the maximum velocity is nearly independent of pressure in a buoyant diffusion flame, the soot mass flux, $\dot{m}_s$, at a given height was approximated as

$$\dot{m}_s \simeq \rho_s F_v \, u_{max} \simeq -\rho_s C(\lambda,m)\ln(I/I_o) \frac{\pi}{4} d \, \alpha\sqrt{2az} \tag{4}$$

The soot yield, ϕ, at a given height, then becomes $\phi = \dot{m}_s/\dot{m}_{f,c}$, where $\dot{m}_{f,c}$ is the carbon mass flow rate in the fuel.

Figure 1 shows the measurements of $f_{v,cl}$ ($= -C(\lambda,m)\ln(I/I_o)$) versus flame height, z, at pressures from 0.1 to 0.5 MPa (1 to 5 atm). The height above the fuel tube is expressed in a nondimensionalized form, η, as

$$\eta = \ln\left[1+\frac{1}{S}\right] \frac{D}{Q} z \tag{5}$$

where S is the stoichiometric air-fuel ratio for ethene ($= 14.28$), and D is the gas diffusion coefficient (0.156 cm^2/s). The maximum value of $-C(\lambda,m)\ln(I/I_o)$ appears approximately at the same height for the pressure range tested in this study, and its pressure dependence, $(f_{v,cl})_{max} \propto p^{1.2\pm0.3}$, agrees with previously measured values [5].

Average soot volume fraction, $f_{v,av}$, and soot yield, ϕ, are plotted versus time in Figure 2. While both $f_{v,av}$ and ϕ increase with time and pressure, $f_{v,av}$ shows relatively stronger pressure dependence. Average soot volume fraction, $f_{v,av}$, increases with time and its rate, $df_{v,av}/dt$, increases with pressure at a given time. Soot yield, ϕ, also increases with time; however, soot yield rate, $d\phi/dt$, significantly increases with pressure

only during the early stage of soot formation and then becomes similar for all the cases. This observation indicates that the effect of pressure is more significant for the early stage of soot formation.

The difference between $f_{v,av}$ and ϕ implies that the flame size change at a given height should be considered to understand the role of pressure in soot production in laminar diffusion flames. From continuity $ud^2 \propto \dot{m}_{f,c}/p$ at a given z, and therefore, $d \propto p^{-0.5}$ for a constant fuel mass flow rate. The soot zone diameter dependence on pressure measured from direct photographs yielded $d \propto p^{-0.5 \pm 0.1}$, which agrees reasonably well with the above relation. Therefore, average soot volume fraction, $f_{v,av}$, the total integrated soot volume fraction, F_v, and soot yield, ϕ, at a given z using equations 1 through 4 are related as $\phi \propto F_v \propto p^{-1} f_{v,av}$.

Figure 3 shows $f_{v,av}$ and ϕ versus pressure at different times (heights). Generally, both $f_{v,av}$ and ϕ are reasonably well fit by an expression proportional to p^n. The exponent n decreases with time for both cases, which indicates that the pressure effect on soot production is more important at the early stage of soot formation, where soot formation is likely to be kinetically controlled. The exponents for ϕ and $f_{v,av}$ differ by approximately unity when compared at the same time (height). This result is consistent with the above discussion which indicated that $\phi \propto p^{-1} f_{v,av}$.

The pressure dependency of the maximum average soot volume fraction, $(f_{v,av})_{max}$, and soot yield, ϕ_{max}, are shown in Figure 4. In order to compare to the previous results of Flower and Bowman [5], $(f_{v,cl})_{max}$ is also shown in this figure. The maximum soot yield increases as $\sim p^n$, where $n = 0.7 \pm 0.3$ and moderately decreases with pressure, while $(f_{v,av})_{max} \propto p^{1.8 \pm 0.3}$. This difference of the exponents is again consistent with the above discussion of $\phi \propto F_v \propto p^{-1} f_{v,av}$. The present measurements indicate that $(f_{v,cl})_{max} \propto p^{1.2 \pm 0.3}$ which agrees with previous results obtained in an axisymmetric diffusion flame[5] while the observations that $(f_{v,av})_{max} \propto p^{1.8 \pm 0.3}$ and $\phi \propto p^{0.7 \pm 0.3}$ are similar to those observed from 2-D flames [6]. Thus, by considering the flame diameter changes with pressure, $d^2 \propto p^{-1}$, the pressure dependency of the maximum average soot volume fraction and the soot yield measured in this study are consistent with previously reported values in 2-D and axisymmetric diffusion flames[5,6]. These values are also similar to the premixed flame results where $f_{v,\infty} \propto p^{\sim 1}$. The fundamental reaction process of diffusion flames is different to that of premixed flames; however, the soot production process might be essentially the same and therefore the pressure effect on soot formation could be similar.

REFERENCES

1. Richardson, T. F. and Santoro, R. J., "Soot Formation in Coannular Diffusion Flames: The Effect of Fuel Dilution with Inert Species," submitted to *Combustion Science and Technology*.
2. Santoro, R. J. and Richardson, T. F., "Concentration and Temperature Effects on Soot Formation in Diffusion Flames," in *Mechanisms and Models of Soot Formation*, Springer Verlag (in press).
3. Dobbins, R. A., Santoro, R. J. and Semerjian, H. G., *The Twenty-Third Symposium (International) on Combustion*, The Combustion Institute, Pittsburgh, pp. 1524-1532 (1990).
4. Puri, R., Richardson, T. F., Santoro, R. J. and Dobbins, R. A., "Aerosol Dynamic Processes of Soot Aggregates in a Laminar Ethene Diffusion Flame," submitted to *Combustion and Flame*.
5. Flower, W. L. and Bowman, C. T., *Twenty-First Symposium (International) on Combustion*, The Combustion Institute, Pittsburgh, pp. 1115-1124 (1986).
6. Flower, W. L. and Bowman, C. T., *Twentieth Symposium (International) on Combustion*, The Combustion Institute, Pittsburgh, pp. 1035-1044 (1984).
7. Böhm, H., Hesse, D., Jander, H., Lüers, B., Pietscher, J., Wagner, H. Gg., and Weiss, M., *Twenty-Second Symposium (International) on Combustion*, The Combustion Institute, Pittsburgh, pp. 403-411 (1988).

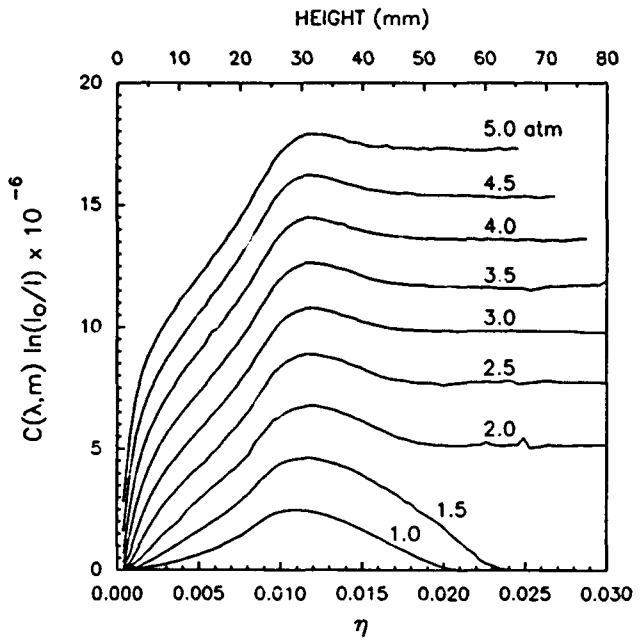

Figure 1. The integrated center line extinction as a function of axial location for operating pressures between 0.1 and 0.5 MPa (1 to 5 atm) in an ethene/air diffusion flame.

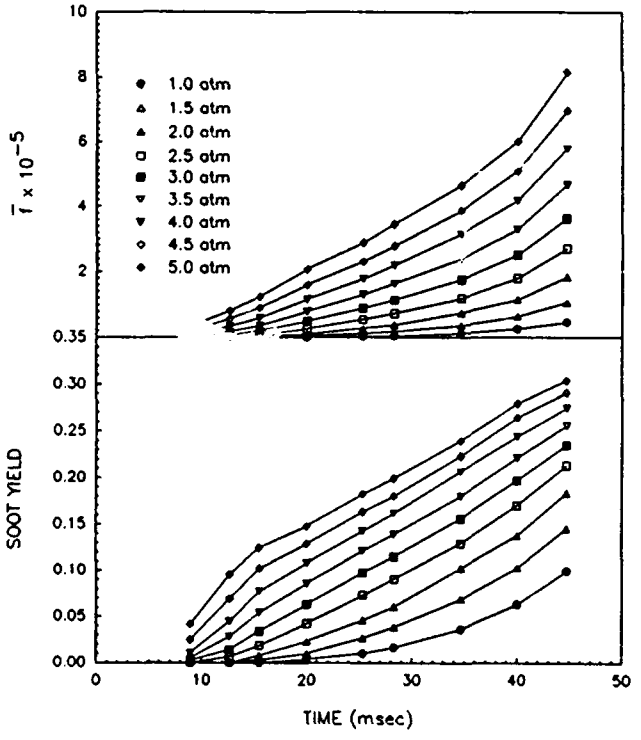

Figure 2. The average soot volume fraction, $f_{v,av}$, and soot yield, ϕ, as a function of time for operating pressures between 0.1 and 0.5 MPa (1 to 5 atm) in an ethene/air diffusion flame.

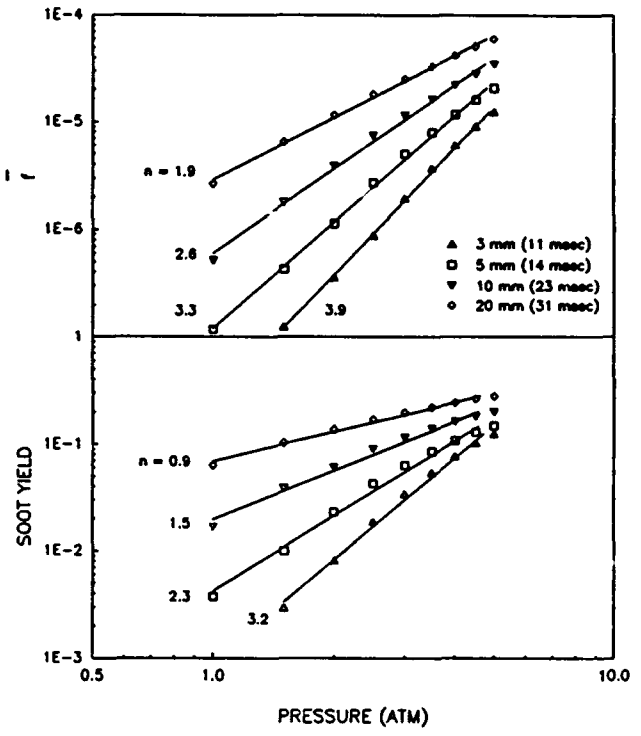

Figure 3. The average soot volume fraction. $f_{v,av}$, and soot yield, ϕ, as a fucntion of operating pressure for various heights (residence times) in an ethene/air diffusion flame. The values n indicate the pressure dependence expressed as p^n for each measurement height.

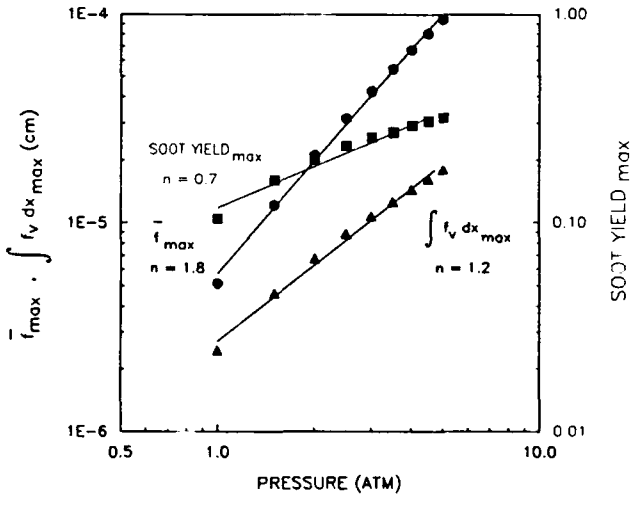

Figure 4. A comparison of the pressure dependency of the maximum average soot volume fraction, $(f_{v,av})_{max}$, the maximum soot yield, ϕ_{max} (soot $yield_{max}$), and the maximum centerline integrated volume fraction, $(f_{v,cl})_{max}$. The values n indicate the pressure dependence expressed as p^n for each maximum quantity.

MODELING STUDY TO EVALUATE THE IONIC MECHANISM OF SOOT FORMATION

(AFOSR Contract No. F49620-91-C-0021)

Principal Investigator: H.F. Calcote

AeroChem Research Laboratories, Inc.
P.O. Box 12, Princeton, New Jersey 08542

SUMMARY/OVERVIEW

An understanding of the mechanism of soot nucleation remains the major deficiency in our understanding of soot formation in flames. The ionic mechanism of soot nucleation is being evaluated by computer modeling to determine whether or not an ionic model can account for the experimental results. This requires development of thermodynamic properties of large ions, development of a detailed mechanism with appropriate rate constants, and examination of the theoretical basis of the Langevin theory of ion-molecule reactions when large ions at flame temperatures are involved. The mechanism will be evaluated on how well it agrees with experiment and how reasonable were the assumptions. Comparison is also made with other mechanisms proposed to account for soot formation.

TECHNICAL DISCUSSION

The ultimate driving force for any sequence of chemical reactions, such as must occur for soot formation, is thermodynamics. As water flows downhill, reactions proceed in the direction of a negative gradient in free energy. To compare this driving force for ions, free radicals, and neutral molecules, we compare the free energy of formation of these three components of the ionic and free radical mechanism of soot formation in Fig. 1 for a temperature of 2000 K. Several features are obvious. First, the driving force for ions is distinctly greater than for free radicals or neutral molecules. Second, the free energy per carbon atom of either a free radical, neutral molecule, or ion rapidly levels off as the compound becomes larger. Third, the ion and neutral species free energies of formation per carbon atom converge when the species contain about 30 carbon atoms, i.e., a molecular weight of about 350 to 400 u. It is interesting that kinetic analysis, see below, also indicates that the advantages of the ionic mechanism over free radical mechanisms fall off with increasing mass. In this same mass range, the concentration of neutrals and ions appear to approach each other.[1,2]

We have used the Langevin theory to calculate ion molecule reaction rate coefficients. This theory has repeatedly been shown to agree with experiments for small ions near room temperature, but has not been tested for large ions at flame temperatures. The theory assumes a point electric charge, which for large ions is questionable. Langevin theory for nonpolar molecules is independent of temperature. We have thus generalized the theory to include temperature and to account for ions of finite dimensions. Two cases were analyzed, a nonconducting and a conducting sphere.

Some results are shown in Fig. 2 for the ratio of the collision rate, calculated by the expanded theory, to the Langevin collision rate as a function of temperature for the conducting and nonconducting sphere cases. The neutral molecule is assumed to be acetylene. Curves are shown for ion diameters of 0.5, 1, and 2 nm, corresponding to molecular weights of approximately 60, 200 and 2,500 u, respectively. Figure 2 shows that: the collision rate is increased more for the conducting sphere than for the nonconducting sphere; the increase is greatest for larger ions; and the temperature effect is positive. The result is not what we had anticipated; we had anticipated a decrease in ion-molecular rate coefficient with

both increasing temperature and molecular size. These effects have not yet been included in our rate coefficients for ion-molecule reactions; they will not make a significant difference. The major contribution to the model is the demonstration that there are no large reductions required in the ion-molecule rate coefficients we have been using. The analysis does demonstrate (not clear in Fig. 2) that as the ion increases in size, for a fixed temperature, the expanded Langevin rate coefficient approaches that for a hard sphere collision. For the nonconducting sphere, this occurs at about mass 800 u; for the conducting sphere it approaches about two times the hard sphere diameter at about 2000 u.

In our previous use of the CHEMKIN flame code to model soot formation several problems were associated with using ions in the code: (1) ionic diffusion, usually treated as ambipolar diffusion could not be incorporated into the code so an artificial fit was employed; (2) nonArrhenius ion-molecule reaction rate coefficients could not be accommodated by the code; and (3) it was not possible to use some experimental ion and neutral profiles as input to the code, just as an experimental temperature is used. The third limitation was the most serious because the program calculated greater concentrations of small neutral species than were observed experimentally and thus calculated greater concentrations of initial ions than were observed experimentally. It also had to carry along a large number of neutral species which made no contribution to the ionic mechanism but exhausted computer memory. These problems limited our capability of evaluating the ionic mechanism without getting involved with the neutral mechanism, and of course the calculations gave greater ion concentrations than would have been obtained were the neutral concentrations consistent with experimental data. Modifications were thus made in the code to incorporate: (1) ion chemistry; (2) ambipolar diffusion of ions; (3) the ability to input neutral and ion profiles; and (4) the ability to employ a modified Arrhenius form for entering forward rate coefficients. We now run the code on a Silicon Graphics IRIS workstation.

A comparison between the calculated and experimental ion profiles for some odd carbon atom species is shown in Figs. 3 and 4. For this set of runs, the experimental profile of the propargyl ion and all of the neutral species involved in the ionic mechanism, e.g., acetylene, diacetylene and hydrogen, were input profiles just like the experimental temperature profile. One of the problems which has plagued us since the beginning has been that if we extrapolate the experimental data closer to the burner, and calculate closer to the burner than where experimental measurements were made, we observe very large peaks at within 0.5 cm above the burner. These have been traced to thermodynamic equilibria which is much more favorable to ion growth at low temperatures than at high temperatures. Entropy becomes very important as the temperature increases. For neutral reactions this equilibrium entropy effect is balanced to some extent by an increase in the rate coefficients with temperature; in ion-molecule reactions there is little temperature effect, see above. This presumably also explains experimental observations that sometimes a small ion peak is observed preceding the main peak; experimental measurements with mass spectrometer sampling probes are difficult to make close to the burner. The entropy effect may also explain the general observation that soot formation maximizes at a temperature between about 1400 and 1900 K.

The following people have participated in this program: Drs. R.J. Gill and C.H. Berman, AeroChem, and Prof. F. Egolfopoulos, University of Southern California.

REFERENCES

1. Calcote, H.F. and Keil, D.G., "The Role of Ions in Soot Formation," Pure & Appl. Chem. 62, 815-824 (1990).

2. Calcote, H.F. and Gill, R.G., "Comparison of the Ionic Mechanism of Soot Formation with a Free Radical Mechanism," to be published in Proceedings International Workshop, Mechanisms and Models of Soot Formation, Springer-Verlag.

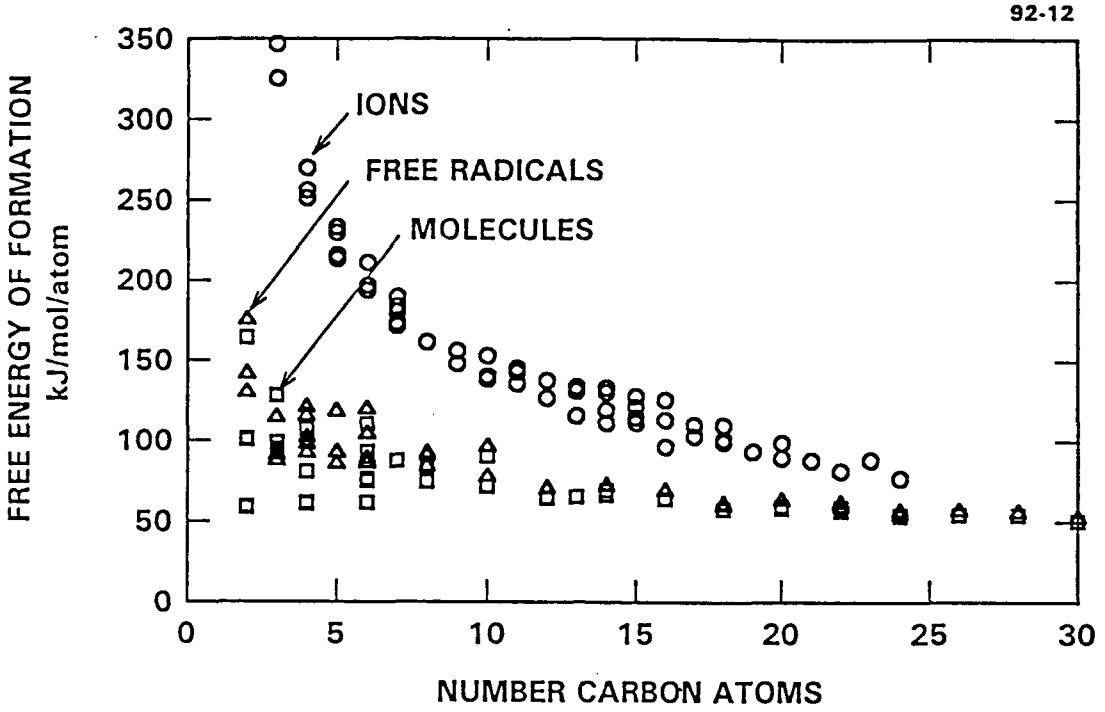

FIGURE 1 FREE ENERGY OF FORMATION PER CARBON ATOM FOR IONS, FREE RADICALS, AND MOLECULES AT 2000 K

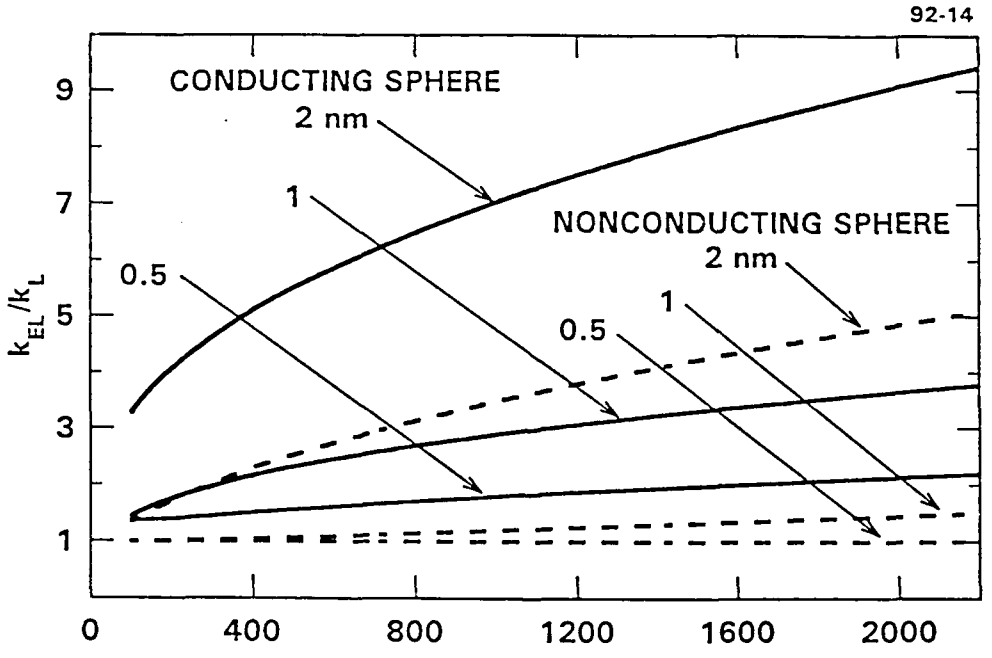

FIGURE 2 RATIO OF EXPANDED LANGEVIN TO LANGEVIN COLLISION RATE

Assumes acetylene as neutral reactant
and a single charge on sphere.
Diameter of sphere indicated in nm

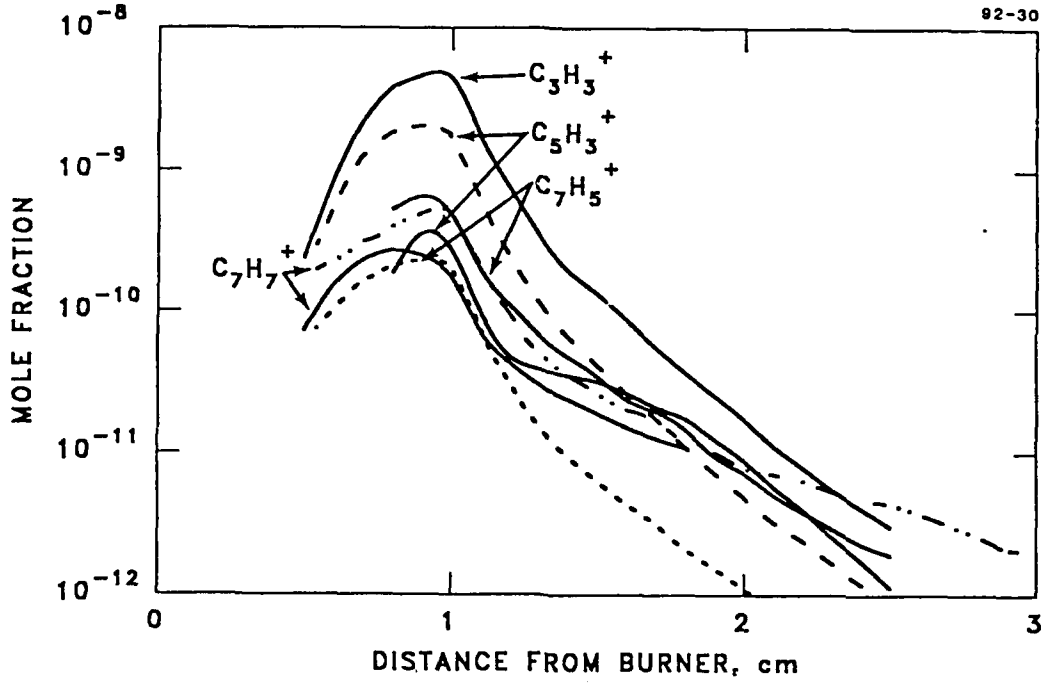

FIGURE 3 COMPARISON OF CALCULATED AND EXPERIMENTAL ION PROFILES IN AN ACETYLENE/OXYGEN SOOTING FLAME
ϕ = 3.0; P = 2.77 kPa
Solid lines experimental; others calculated

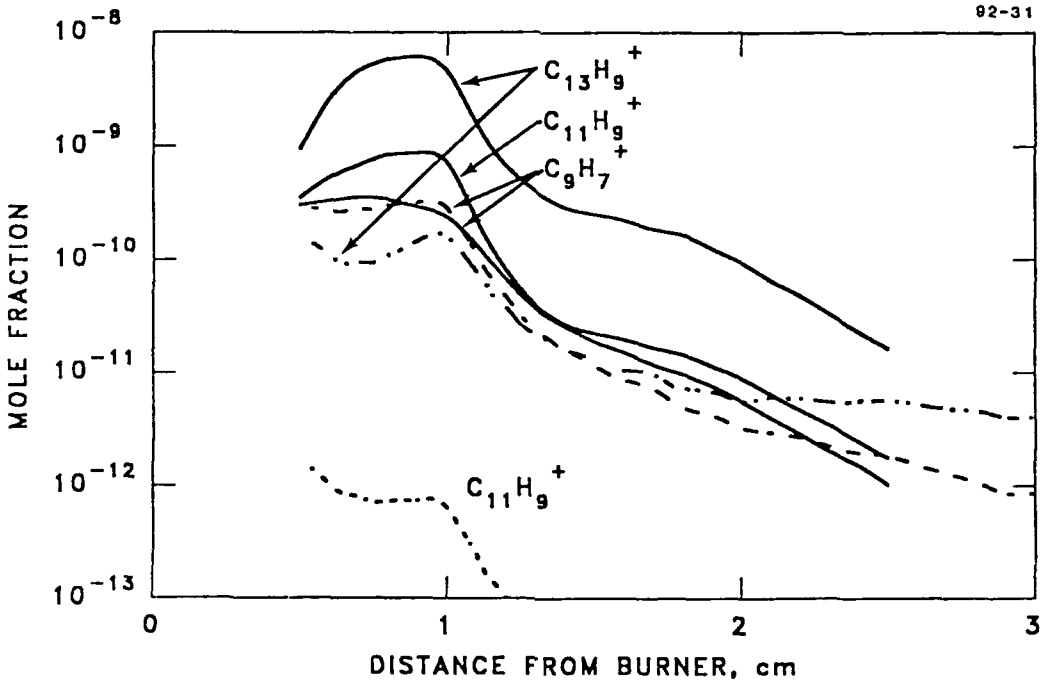

FIGURE 4 COMPARISON OF CALCULATED AND EXPERIMENTAL ION PROFILES IN AN ACETYLENE/OXYGEN SOOTING FLAME
ϕ = 3.0; P = 2.77 kPa
Solid lines experimental; others calculated

DEVELOPMENT OF PREDICTIVE REACTION MODELS OF SOOT FORMATION

(AFOSR Grant No. 91–0129)

Principal Investigator: M. Frenklach

Fuel Science Program
Department of Materials Science and Engineering
The Pennsylvania State University
University Park, PA 16802

SUMMARY/OVERVIEW:

The ultimate goal of this program is to develop a predictive reaction model for soot formation in hydrocarbon flames. The specific objectives of the current 3-year study are to extend the modeling efforts to computer simulation and analysis of more complex sooting phenomena, such as sooting limits in laminar premixed flames, soot formation in premixed flames of aromatic fuels, and soot formation in laminar diffusion flames, and to further refine the underlying reaction mechanism of soot formation. During the past year, progress has been made in the following areas: simulation of sooting limits of laminar premixed flames; further refinements and testing of the detailed reaction mechanism for the formation and growth of polycyclic aromatic hydrocarbons (PAHs); and quantum-chemical potential energy calculations for ion-molecule reactions.

TECHNICAL DISCUSSION

Detailed Simulation of Sooting Limits

Among principal experimental data available on soot formation in hydrocarbon combustion, critical equivalence ratios for soot appearance in laminar premixed flames,[1,2] ϕ_c, attract particular attention. Takahashi and Glassman[1] demonstrated that the values of ϕ_c for a wide range of fuels can be correlated by a remarkably simple relationship. It is of interest to see if this correlation can be predicted from first principles. Here we present the results of such efforts, using the recently developed reaction model for soot formation.[3]

The critical equivalence ratios in laminar premixed atmospheric ethane-, ethylene- and acetylene-oxygen-nitrogen flames were calculated at several maximum flame temperatures. For each of these temperatures a series of flame calculations was performed at different equivalence ratios. The maximum flame temperature in these calculations was kept constant by varying the amount of N_2 in the mixture. The calculations were performed in two stages. In the first stage, PAH formation up to coronene was simulated using a burner stabilized flame code[4] with a fixed temperature profile. This temperature profile was obtained from the equivalent free adiabatic flame calculated using small hydrocarbon chemistry (primarily C_1 to C_4). In the second stage, the computed profiles of H_2, H, C_2H_2, O_2, OH, H_2O and pyrene were used as

input for the simulation of soot particle nucleation and growth, accomplished with an in-house kinetic code.[3] The gas phase and surface reaction mechanisms used in both stages of the calculations were those presented in Ref. 3.

Experimentally,[1,2] the critical equivalence ratio for the appearance of soot was determined by observing the onset of yellow light emission in a flame. In our simulations, the critical equivalence ratio ϕ_c was determined from the computed luminous intensity flux emitted by the soot particles. The latter was calculated through the moments of the particle size distribution function.[5]

Figure 1 shows the computed luminous intensity flux as a function of the equivalence ratio at several heights above the burner for ethane flames with maximum temperature of 1640K. The same fluxes, but now each curve, at a given height and scaled to its maximum value, are plotted in Fig. 2. These scaled curves were used to determine the critical equivalence ratio corresponding to the maximum flame temperature. We assumed that the critical equivalence ratio is reached when the luminous flux undergoes a sudden rise illustrated in Fig. 2. The critical equivalence ratios determined in this manner for three fuels — ethane, ethylene and acetylene — are compared with the experimental data of Harris *et al.*[2] in Fig. 3. As can be seen in this figure, a reasonable agreement is achieved. The analysis of the factors determining the sooting limits is in progress.

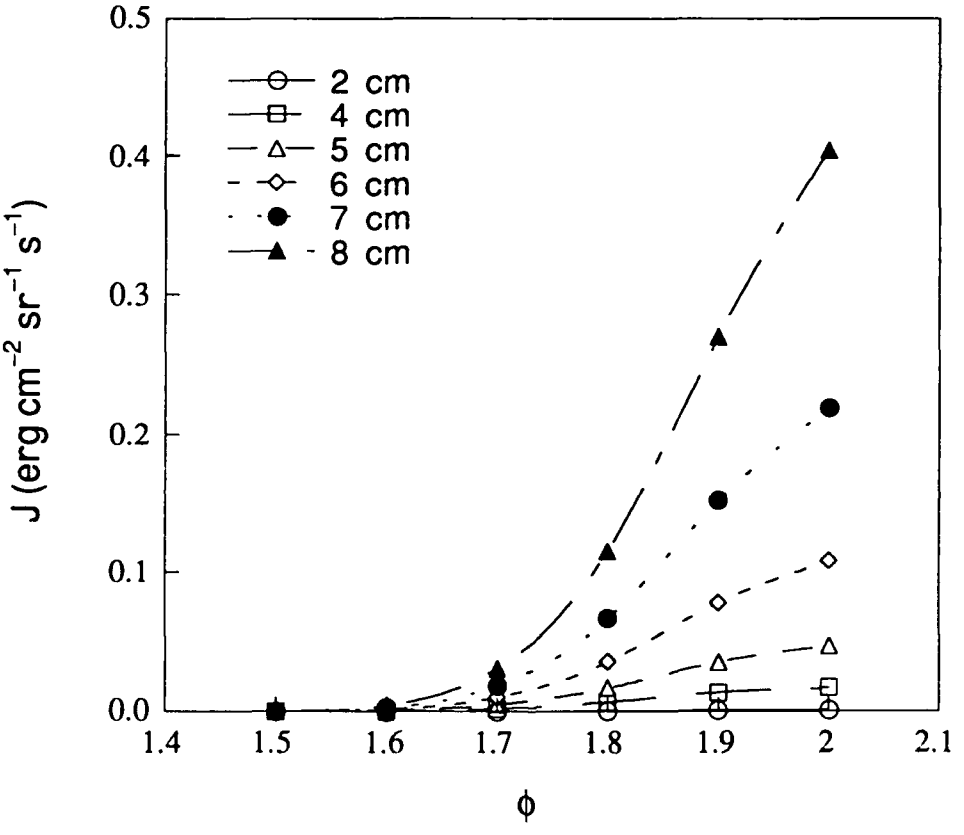

Figure 1. Computed luminous intensity flux for the C_2H_6-O_2-N_2 flames with T_{max} = 1640 K.

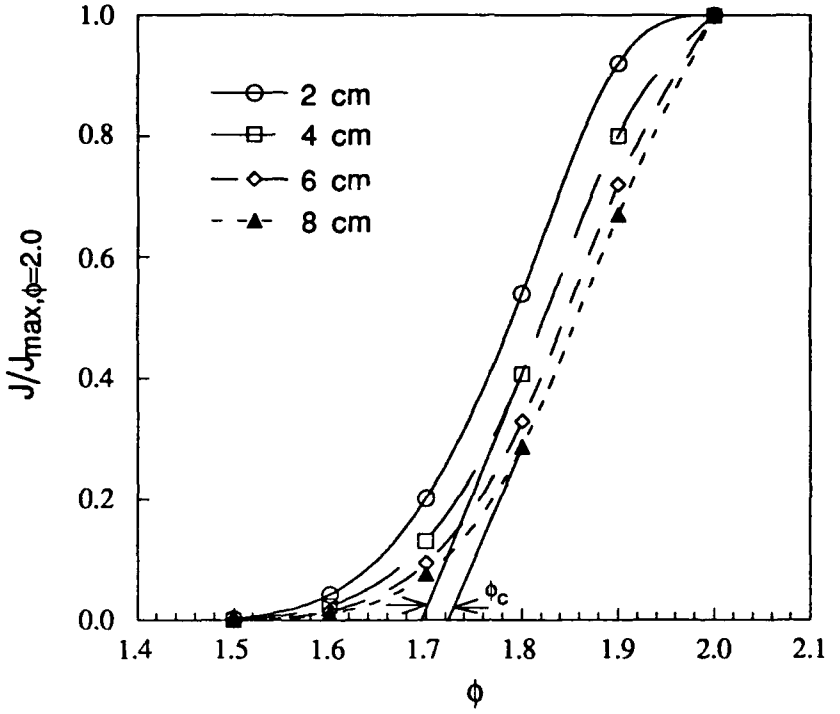

Figure 2. Relative luminous intensity flux for the C_2H_6-O_2-N_2 flames with T_{max} = 1640K.

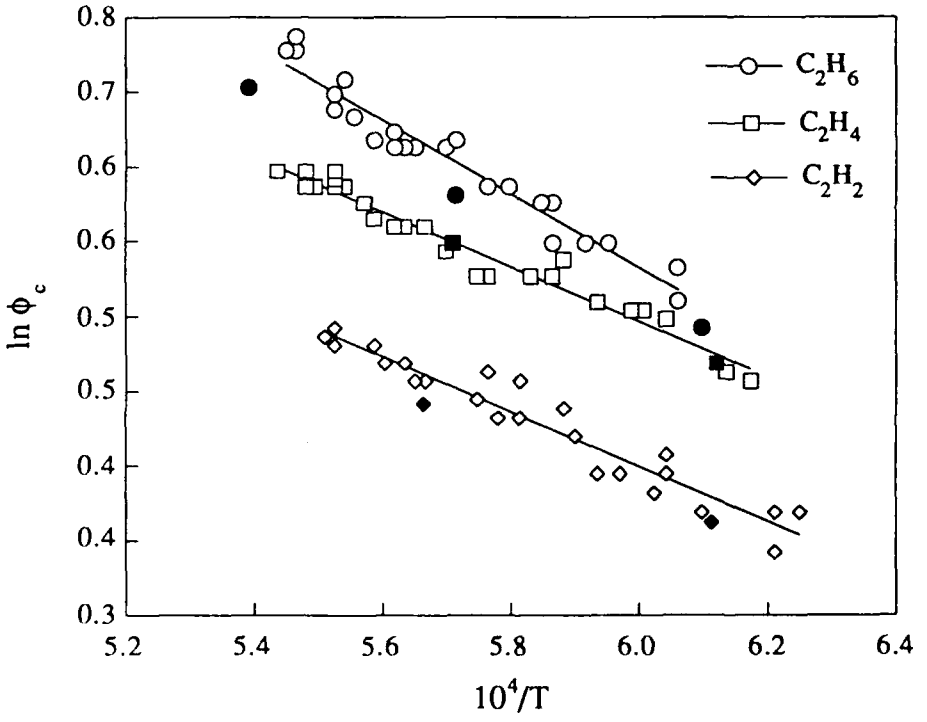

Figure 3. Comparison of the computed and experimentally determined[2] critical equivalence ratios of C_2H_6-O_2-N_2 flames.

We also examined the effect of the flame temperature on the flame sooting tendency. The results for a series of ethane flames having an equivalence ratio of 1.7 are shown in Fig. 4. The bell-shaped dependence of the luminous intensity flux on temperature seen in this figure is in accord with a similar bell-shaped dependence observed for the soot volume fraction in the experiments of Böhm *et al.*[6] for acetylene-, ethylene- and benzene-air flames.

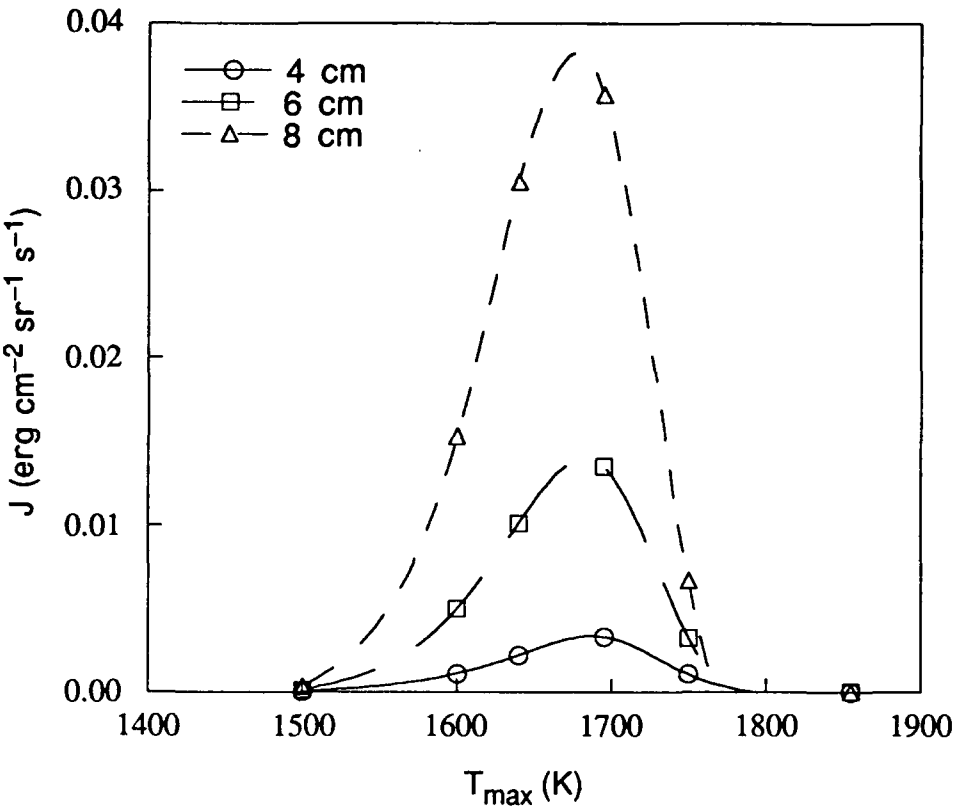

Figure 4. Computed luminous intensity flux as a function of maximum flame temperature for the C_2H_6-O_2-N_2 flames with $\phi = 1.7$.

Reaction Mechanism

Several computational runs were performed to test the role of the $C_3H_3 + C_3H_3 \rightarrow$ benzene reaction in the formation of the first aromatic ring under flame conditions. These tests indicated that the inclusion of the propargyl cyclization channel does not *always* increase the production rate of benzene, and when it does, its contribution is comparable to those of other cyclization channels. A more detailed analysis of the critical reactions for PAH formation and growth is in progress.

REFERENCES

1. Takahashi, F. and Glassman, I., *Combust. Sci. Technol.* **37**, 1 (1984).
2. Harris, M. M., King, G. B. and Laurendeau, N. M., *Combust. Flame* **64**, 99 (1986); **67**, 269 (1987).
3. Frenklach, M. and Wang. H., *Twenty-Third Symposium (International) on Combustion*, The Combustion Institute, Pittsburgh, 1991, p. 1559.
4. Kee, R. J., Grcar, J. F., Smooke, M. D., and Miller, J. A., Sandia Report No. SAND85-8240, 1985.
5. Frenklach, M. and Wang, H., to be published.
6. Böhm, H., Hesse, D., Jander, H., Lüers, B., Pietscher, J., Wagner, H. Gg. and Weiss, M. *Twenty-Second Symposium (International) on Combustion*, The Combustion Institute, Pittsburgh, 1989, p. 403.

FUELS COMBUSTION RESEARCH

(AFOSR GRANT 89-0034)

Principal Investigators: I. Glassman and K. Brezinsky

Department of Mechanical and Aerospace Engineering
Princeton University
Princeton, NJ 08544

SUMMARY/OVERVIEW

Because of the interest in high energy density fuels for air-breathing propulsion systems and the corresponding concern with respect to the sooting tendency of these fuels, estimates have been made of their relative sooting tendency based upon results obtained in the program. The first model and further results for the oxidation of the residual fuel component, 1-methyl naphthalene are presented. The model and results will permit combustion modeling of real JP fuels. Studies of the sub and supercritical fluids degradation kinetics of JP fuels at high temperature have been initiated in order to attack the feedline-injector fouling problem in very high compression ratio gas turbine engines.

TECHNICAL DISCUSSION

More extensive experiments on the oxidation of 1-methylnaphthalene have been performed in the Princeton turbulent flow reactor. These data extend those on this JP fuel component reported last year. Based on all the results obtained and detailed modeling, it is now possible to propose a reaction mechanism for this fuel. The major routes for consumption of the fuel are the abstraction of an H from the methyl sidechain to form the 1-naphthyl-methyl radical and displacement of the sidechain by an H atom to form a methyl radical and naphthalene. The major reaction paths for the 1-naphthyl-methyl radical lead to the formation of 1-napthaldehyde, which further reacts to form the 1-naphthyl radical. This portion of the complete mechanism is depicted in Fig. 1. The major reaction paths for naphthalene and the 1-naphthyl radical ultimately produce the 1-naphthoxy radical. The 1-naphthoxy radical decomposes to the indenyl radical, which further reacts to form the 1-phenyl-2-vinyl radical which leads to styrene, phenylacetylene and acetylene. This aspect of the mechanism is depicted in Figure 2. The mechanisms for these compounds produced in Figure 2 were reported in the earlier parts of the program. More extensive details are given in recent publications (1,2).

The major efforts with regard to the soot formation aspect of the program was directed at publishing the extensive results recently obtained in the program and concentrating on estimating the sooting tendency of the new high energy density hydrocarbon fuels for air-breathing propulsion systems. This direction was taken because a continuation student or post-doc was not found. Three papers (3-5) have been submitted for publication and all have been accepted. Because of the new interest in a class of high energy density fuels and the concern with their sooting tendency, consideration was given to estimating their relative tendency to soot. In making these estimates consideration must be given to the type of air-breathing propulsion system in which the fuels will be used and, more specifically, whether the combustion zone in these systems emulate either a pre-mixed or diffusion flame

configuration. Attention was focused on cubane (C_8H_8) and dihydrobenzvalene (DHBV, C_6H_8). If pre-mixed flame conditions are approached, then based on the analysis developed in the program DHBV would not soot to any great extent, no more than octene. Cubane would have a much greater sooting tendency, more like cumene, yet much less than 1-methylnaphthalene. These results are represented in Figure 3 in which the log of the critical sooting equivalence ratio y_C is plotted versus the number of C-C bonds in the fuel. The fundamental elements of this correlation is explained in Ref. 6. Because DHBU is thought to rapidly pyrolyze to benzene, then under diffusion flame conditions it would have the same relative sooting tendency of benzene. Little is known about the pyrolysis of cubane, but the possibility of undergoing a transformation to benzene exists. Thus it is as noted, that its sooting tendency would be like that of allene. These estimates are shown in Figure 4, in which the log of the reciprocal of the mass fuel flow rate at the diffusion flame smoke height is plotted as a function of the calculated adiabatic flame temperature (also, see Ref. 6).

The initial phase of a set of studies focusing on the thermal degradation of jet fuels at supercritical and near supercritical fluid conditions has been devoted to the design of a versatile fluid phase flow reactor and to a review of kinetic phenomena under supercritical conditions (7,8). A flow reactor with homogeneous radial species and temperature profiles that can be used to determine chemical changes occurring in both high temperature liquid and supercritical fluid phase hydrocarbon fuel components is required. In the gas phase 1-methyl naphthalene oxidation experiments described above, a reactor that relies on turbulent flow to achieve plug radial concentration and temperature profiles has been used. However, the Reynolds numbers required to achieve turbulent flow in a liquid reactor would lead either to a limited, and generally too short, range of residence times or to a large throughput of liquid. Consequently, a low Reynolds number reactor modeled after other supercritical fluid reactors and which meets the plug flow criteria of Cutler, et al. (9) is being constructed for these studies.

REFERENCES

1. Shaddix, C.R., Brezinsky, K., and Glassman, I., "Further Considerations of the High-Temperature Oxidation of 1-Methylnaphthalene", Eastern States Section/The Combustion Institute Meeting, Paper No. 68, Ithaca, NY, Oct. 1991.

2. Shaddix, C.R., Brezinsky, K., and Glassman, I., "Oxidation of 1-Methylnaphthalene", accepted for presentation and publication for 24th Symposium (Int'l.) on Combustion, 1992.

3. Sidebotham, G.W. and Glassman, I., "Effect of Oxygen Addition to a Near-Sooting Ethene Inverse Diffusion Flame", Comb. Sci. and Tech. 81, 1992, p. 207.

4. Sidebotham, G.W., Saito, K. and Glassman, I., "Pyrolysis Zone Structure of Allene, 1,3 Butadiene and Benzene Smoke Point Diffusion Flames", accepted for publication in special issue of Comb. Sci. and Tech., 1992.

5. Sidebotham, G.W. and Glassman, I., "Flame Temperature, Fuel Structure and Fuel Concentration Effects on Soot Formation in Inverse Diffusion Flames", accepted for publication in Combustion and Flame, 1992.

6. Glassman, I., "Soot Formation in Combustion Processes", 22nd Symp. (Int'l.) on Combustion, The Combustion Institute, Pittsburgh, 1988, p. 295.

7. Brezinsky, K., "Fuel Deposit Formation and Supercritical Fluids", presentation at Bolling Air Force Base, December 3, 1990.

8. Subramanian, B. and McHugh, M.A., "Reactions in Supercritical Fluids - A Review", Ind. Eng. Chem. Process. Des. Dev. 25, 1, 1986.

9. Cutler, A.H., Antal, M.J. and Jones, M., Ind. Eng. Chem. Res. 27, 691, 1988.

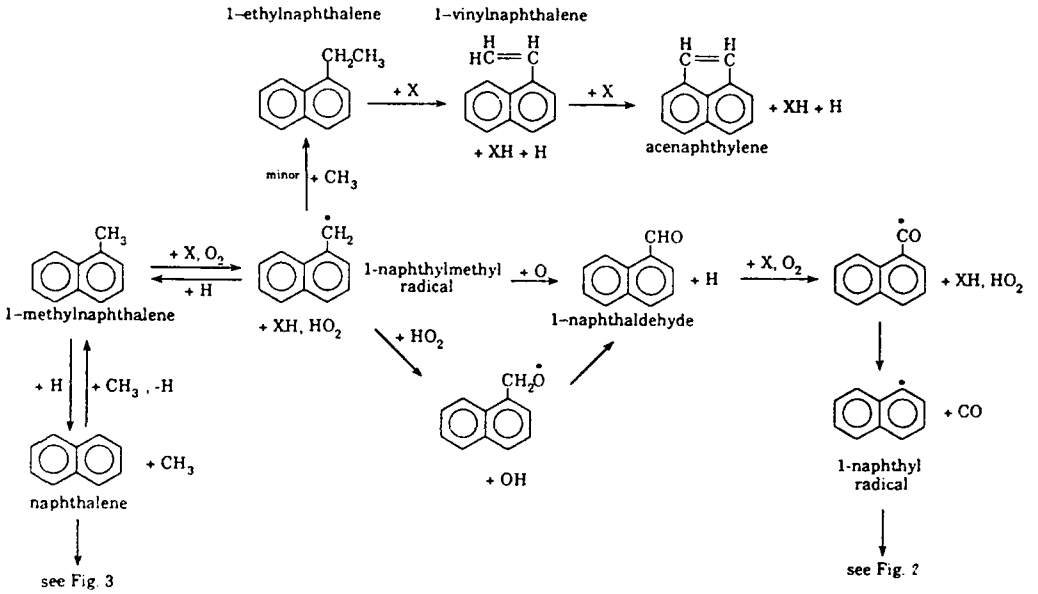

FIG. 1 Oxidation Mechanism of 1-Methylnaphthalene

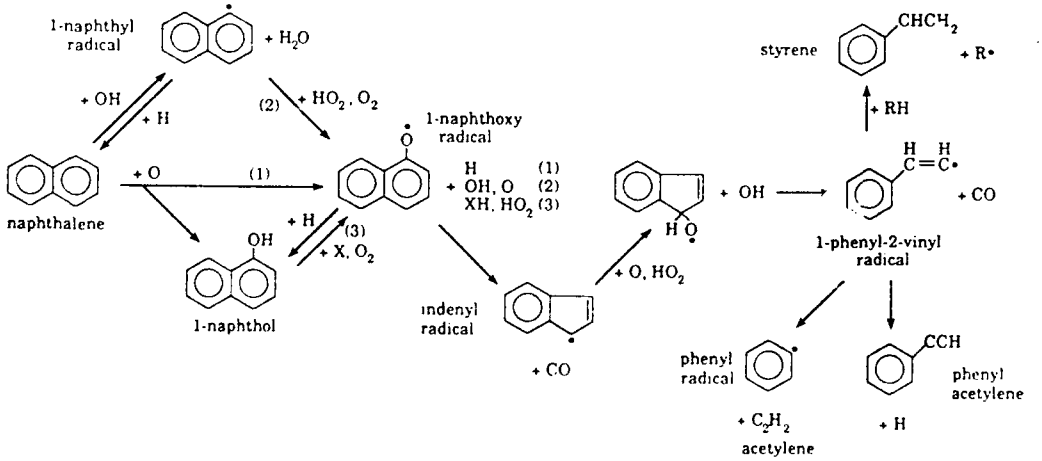

FIG. 2. Continuation of 1-Methylnaphthalene Mechanism

FIG. 3. Relative Sooting Tendency of Fuels Under Premixed Conditions - The Critical Sooting Equivalence Ratio as a Function of the Number of C-C Bonds in the Fuel

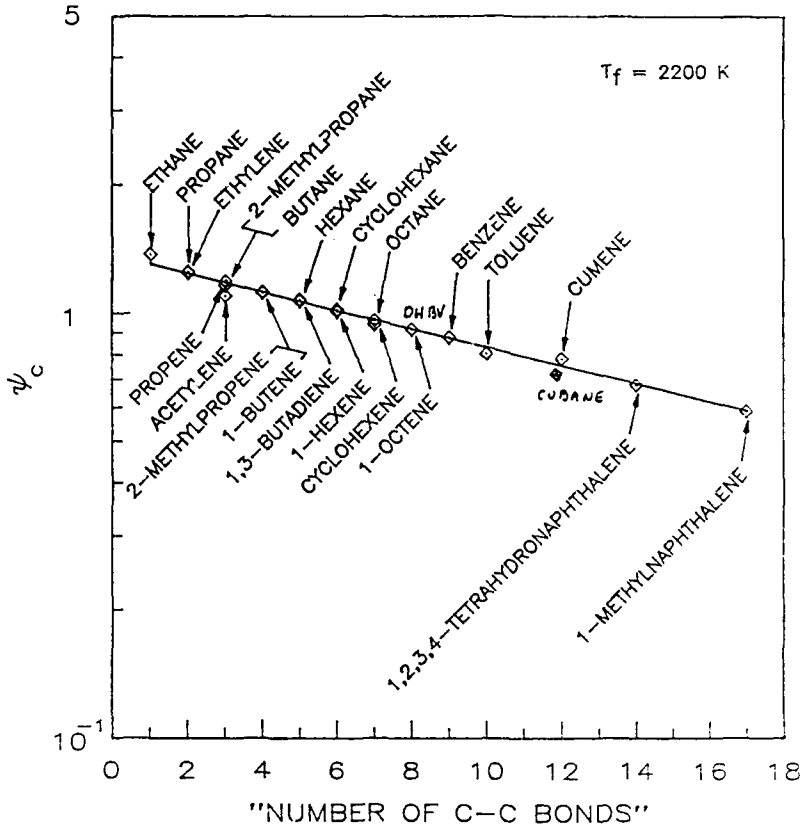

FIG. 4. Relative Sooting Tendency of Fuels Under Diffusion Flame Conditions - The Reciprocal of the Fuel Flow Mass Rate at the Smoke Point as a Function of the Calculated Adiabatic Flame Temperature

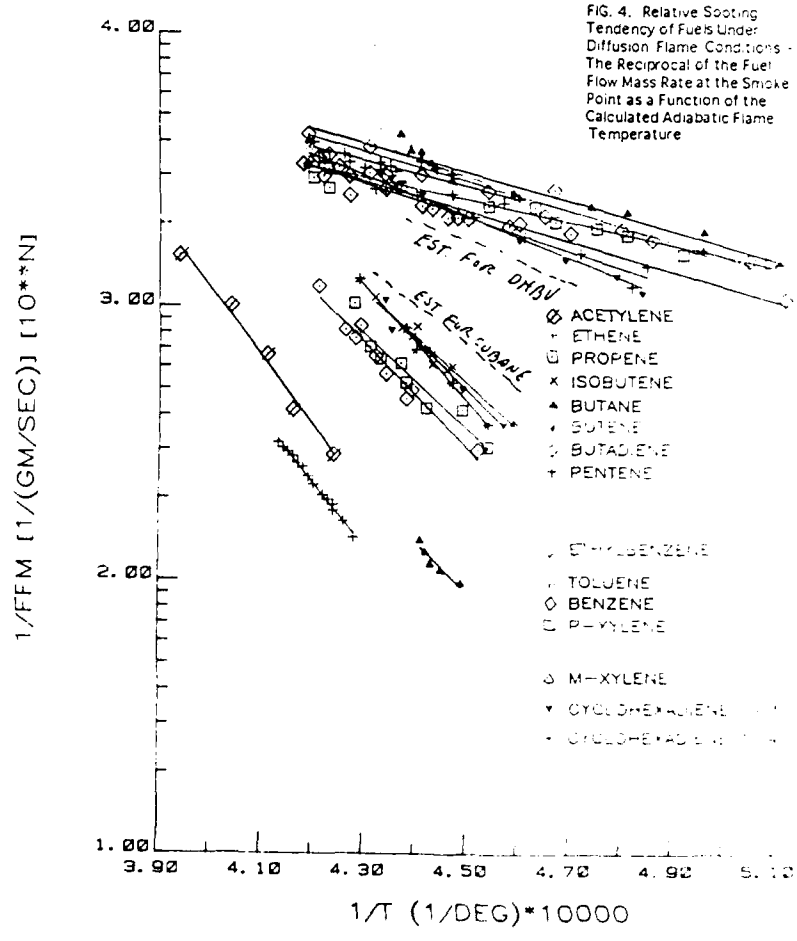

A STUDY OF MIXING AND COMBUSTION IN SUPERSONIC FLOWS

(AFOSR Contract No. 90-0151)

Principal Investigators: C. T. Bowman, R. K. Hanson, M. G. Mungal, and W. C. Reynolds

Department of Mechanical Engineering
Stanford University
Stanford, CA 94305-3032

SUMMARY/OVERVIEW:

An experimental and computational investigation of supersonic combustion flows is being conducted to gain a more fundamental understanding of mixing and chemical reaction in supersonic flows. The research effort comprises three interrelated elements: (1) an experimental study of mixing and combustion in a supersonic mixing layer; (2) development of laser-induced fluorescence techniques for time-resolved, two-dimensional imaging of species concentration, temperature and velocity; and (3) numerical simulations of compressible reacting flows.

TECHNICAL DISCUSSION:

Experiments on Mixing and Reaction in Supersonic Flow

The objective of this part of the program is to experimentally study mixing and chemical reaction in a compressible mixing layer. Current work is focussed on studying the effects of compressibility and heat release on the structure of a reacting mixing layer.

The experiments are performed in a large-scale flow facility which produces a plane mixing layer between a supersonic, high-temperature, oxidizing stream and a subsonic, ambient-temperature, hydrogen-containing stream. The high-temperature stream is produced by burning oxygen-enriched air and hydrogen in a vitiation heater and expanding the combustion products through a supersonic nozzle. Stagnation temperatures up to 2000 K have been achieved with oxygen mol fractions up to 21%. The subsonic stream is hydrogen diluted with nitrogen; the hydrogen mol fraction in this stream currently is limited to 20% to prevent flammable exhaust gas mixtures. The test section measures 10 cm by 6 cm in cross-section and 45 cm in length. For the results reported here, the high-speed stream Mach number is 1.35, and the low-speed stream Mach number is 0.3.

Much of the work this past year was dedicated to configuring the facility for reacting flow experiments with a great deal of emphasis placed on safety. The major facility modifications included: 1) fabricating a new cooled splitter tip for the desired range of convective Mach number, 2) installing a make-up oxygen system for the high-speed vitiated air stream, 3) installing a hydrogen system for the low-speed stream, 4) installing exhaust gas dilution and quench systems, 5) upgrading the computer control system to handle the additional control variables required for reacting flow experiments and to allow remote operation of the facility and 6) fabricating quartz test section windows to provide complete optical access to the test section for laser-based diagnostics and schlieren visualization. To prepare the facility for reacting flow studies, experiments were conducted to test the vitiation heater and the thermal protection of critical wind tunnel components. Schlieren and shadowgraph visualizations were used to verify the quality of flow in the test section and to measure the nonreacting mixing layer growth-rates. A typical nonreacting schlieren image is shown in Figure 1.

Initial reacting flow experiments mapped the ignition envelop of the mixing layer as a function of high-speed stream stagnation temperature and oxygen mol fraction and low-speed stream hydrogen mol fraction. Ignition of the mixing layer was verified using time-averaged

assumed $h_f \sim K^2$. We are currently investigating the specific forms of the Euler equations that result for ϕ.

REFERENCES

1. Nixon, D., Keefe, L. R., and Kuhn, G.: The Effects of Compressibility on a Supersonic Mixing Layer. AIAA Paper 90-0706, Jan. 1990.

2. Hermanson, J.C. and Dimotakis, P.E.: Effects of Heat Release in a Turbulent, Reacting Shear Layer. Journal of Fluid Mechanics **199**, 1989, pp. 333.

3. McMurty, P.A., Riley J.J. and Metcalfe, R.W.: Effects of Heat Release on the Large Scale Structure in Turbulent Mixing Layers. Journal of Fluid Mechanics **199**, 1989, p297.

4. Keller, J.O. and Daily J.W.: The Effects of a Highly Exothermic Chemical Reaction on a Two-dimensional Mixing Layer. AIAA Journal **23**, 1985, p1937.

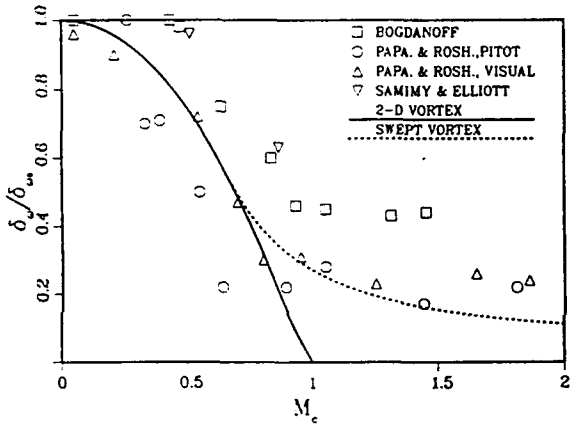

Figure 1.

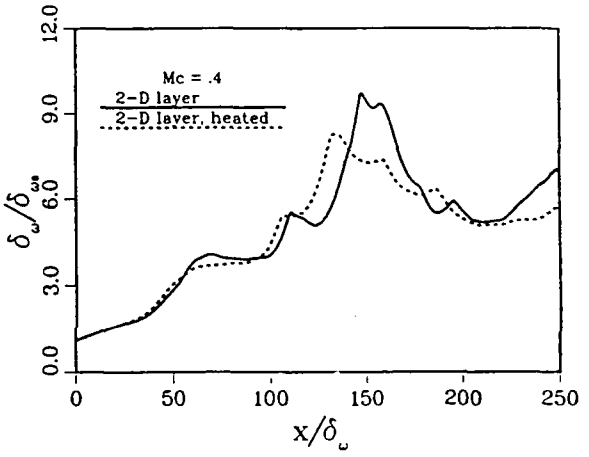

Figure 2.

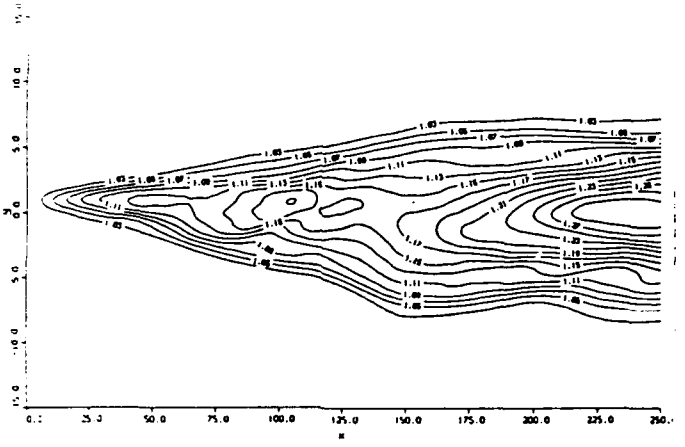

Figure 3.

wide range of Damköhler numbers. We plan to perform simulations at larger Reynolds-numbers (larger computational domain) to verify these conclusions.

• *Realistic Chemistry Scheme in DNS Studies.* As discussed above, SLFM was designed to account for the superequilibrium of radicals resulting in increased NO_x production. It follows that SLFM validity cannot be fully studied without a chemistry scheme that accounts for the radicals. We have built the partial-equilibrium model of hydrogen-air combustion (Chen and Kollmann, *Combustion and Flame, 79,* 75, 1990) into our DNS-code (Ref. 6). Preliminary results show tendencies similar to the behavior found in the laboratory.

• *Large Eddy Simulation (LES) of Reacting Turbulent Flows.* Direct simulation is, for the time being, a research tool; it cannot be directly applied to practical problems. The reason for this is that in DNS one resolves all the length and time scales. We pay the price for this "luxury" by being limited to relatively low Reynolds number values, simple geometries, and moderate (or infinite) reaction rates. LES is designed for practical applications. One simulates only the "engineering eddies" and accounts for the small scales by subgrid modeling (Lesieur, *Turbulence in Fluids,* 2nd Ed., Ch. XII, 1990). Due to the special importance of the small scales for the reactions, the application of LES in combustion studies is not a trivial task, although it is most desirable from a practical point of view (Jou and Riley, *AIAA J., 27,* 1543, 1989). We have worked out some fundamental ideas regarding this problem and started working in this important direction.

LIST OF PUBLICATIONS

(The papers on this list acknowledge the joint support from NSF and AFOSR under NSF Grant No. CTS-9021928.)

1. W.E. Mell, G. Kosály and J.J. Riley, "The length scale dependence of scalar mixing," *Phys. Fluids A 3,* 2474, 1991.

2. G. Kosály, "Frequency spectra of reactant fluctuations in turbulence," *Journal of Fluid Mechanics* (Submitted for publication, Nov. 1991. Editor's letter asking for revisions obtained Feb. 1992).

3. W.E. Mell, G. Kosály and J.J. Riley, "Investigation of laminar flamelet modeling via turbulent simulations," *Bull. Amer. Phys. Soc. 36,* 2641,1991.

4. W.E. Mell, G. Kosály and J.J. Riley, "Direct numerical investigation of turbulent reacting flows," Fourth Int'l Conference on Numerical Combustion, *Abstract Book,* pages 106-107, Dec.2-4,1991.

5. V. Nilsen, W.E. Mell and G. Kosály, "Investigation of the CMC model of turbulent reacting flows," UW-ME-TRR-92-1, Jan. 1992.

6. C.J. Montgomery, G. Kosály and J.J. Riley, "Analytic investigation of turbulent reacting flows," *Bull. Amer. Phys. Soc. 36,* 2679, 1991.

GK:km3
5/7/92

Development of Supersonic Flow Diagnostics

This research is aimed primarily at establishing Planar Laser-Induced Fluorescence (PLIF) techniques for imaging in supersonic flowfields. Successful methods will subsequently be applied in the supersonic mixing layer facility. Recent work has been in three areas: (1) development of a supersonic flow facility for diagnostics research; (2) code development for nonequilibrium underexpanded supersonic jets; and (3) investigation of PLIF imaging in low and high enthalpy supersonic jets.

With regard to facility development, our shock tunnel is now fully operational. This facility utilizes reflected shock wave heating in a pressure-driven shock tube to generate high stagnation enthalpies; expanded gas flows through a sonic nozzle located in the center of the end wall and into a dump tank. By varying the pressure ratio between the shock tube and dump tank, a wide range of flow velocities and Mach numbers can be created in the interior region of the barrel shock and Mach disc. This steady (for a few hundred microseconds) flow is highly reproducible and provides convenient optical access to a flow with a very wide range of flow conditions. Since the shock tube facility can be operated with a short turn-around-time (about 4 minutes), it is well-suited for research on hypersonic flow diagnostics.

In the area of code development, our method-of-characteristics (MOC) program is now fully operational for simple mixtures of diatomic and monatomic gases undergoing vibrational relaxation. The code is suitable for gases which remain vibrationally equilibrated, freeze (vibrationally) at an intermediate point in the flow, or expand with a constant gamma. Good agreement is found between calculations with this code and prior calculations where available. The code is required to establish the flowfield properties against which the PLIF measurements can be compared.

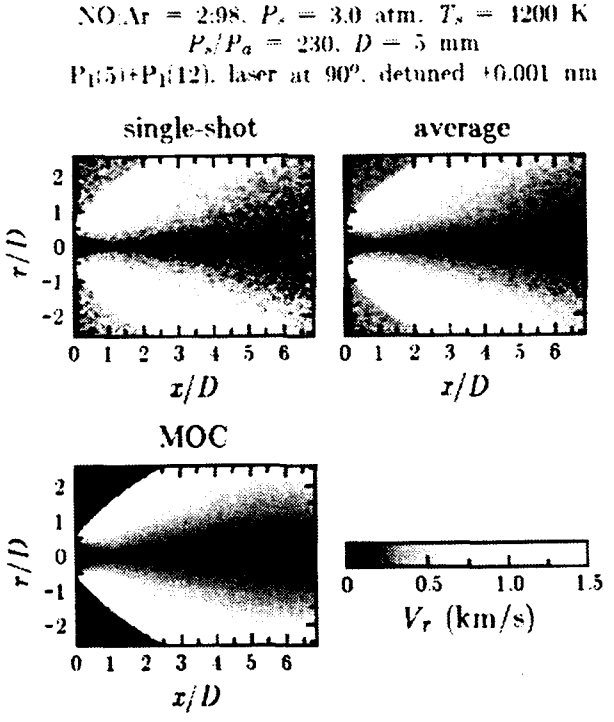

Figure 3. Planar laser-induced fluorescence and method of characteristics images of radial velocity.

Work with PLIF imaging has been conducted in two facilities, the shock tunnel described above and a continuous, low stagnation enthalpy, supersonic jet. The latter facility has allowed a detailed study of temperature imaging in NO, including consideration of saturation effects, spectral convolution of laser and absorption lineshapes, and quenching effects. Details of that

DEVELOPMENT AND ASSESSMENT OF TURBULENCE-CHEMISTRY MODELS IN HIGHLY STRAINED NON-PREMIXED FLAMES

AFOSR Contract No. F-49620-91-C-0072

Principal Investigator: Sanjay M. Correa

General Electric Research Center

Schenectady, New York 12301

OBJECTIVES AND PRIOR RESULTS

Turbulence-chemistry interactions are not solely of academic interest: demands on combustion models are increasing the need for advanced understanding. For example, (i) flameout and relight are related to interactions with chain-branching reactions, (ii) hydrogen burnout in supersonic combustors is related to interactions with recombination reactions, and (iii) emissions of NO_x, CO, smoke, and other observables are related to non-equilibrium among species such as oxyhydrogen radicals and C_xH_y.

The disparity in chemical time-scales complicates the nature of the interactions with turbulence [1,2]. Thus there simultaneously exist (i) relatively weak interactions which are characterized by order-of-unity Damkohler numbers for radical recombination reactions and large Damkohler numbers for chain-branching reactions; this regime exhibits superequilibrium radical levels, which affect NO formation and burnout of CO, and (ii) strong interactions, where even ignition reactions may have order-of-unity Damkohler numbers leading to a question of localized turbulence-induced extinction and eventually to blowoff.

The objective here is to develop and assess sub-models for turbulence-chemistry interactions by comparing predictions with data on turbulent flames. Experiments with laser-based spectroscopic data on critical quantities are favored. Critical quantities are minor species such as OH, which are very sensitive to interactions between turbulence and chemistry; major species and temperature; joint minor-major species; and velocity and turbulence fields.

The framework provided by the joint velocity-composition pdf transport model will be emphasized here [3]. Predictions have been compared with Raman and OH-LIF data from turbulent jet "diffusion" flames [4]. An important aspect of this phase of the work is extension from jet flames to bluff-body stabilized flames. The reasons for and the difficulties associated with this extension are discussed in Ref. 5. The available database includes (i) the axisymmetric bluff-body stabilized burner studied in a previous phase of the present study [5]; (ii) the axisymmetric "Reverse Flow Reactor", which uses flow recirculation to stabilize the flame above jet-blowoff conditions [6]; and (iii) Raman imaging in an axisymmetric bluff-body stabilized flame [7].

PROGRESS IN THE PAST YEAR

I. PDF modeling of Bluff-Body Stabilized Flame:

A Monte Carlo pdf/finite-volume mean flow model has been developed. Predictions have been compared with Raman data on the non-premixed axisymmetric bluff-body stabilized 27.5% CO/ 32.3% H_2/ 40.2% N_2 - air flame studied in the preceding phase [5]. Note that Raman data on a N_2-diluted CH_4 flame are also available. The approach combines the accuracy of the joint velocity-composition pdf model [3] with the geometric flexibility of pressure-corrected finite-volume methods for mean flow in curvilinear coordinates. Details and further references are supplied in Ref. 8. Standard limitations such as (i) assumption of pdf shape, (ii) statistical independence of scalars, and (iii) gradient diffusion, are removed.

The bottom half of Fig. 1 shows the bluff-body burner in the wind-tunnel. The top half of Fig. 1 shows the computed mean velocity field in the vicinity of the jet exit: the off-axis stagnation zone and the region of high shear at $x/d \leq 10$ are evident ("d" $\equiv$ jet exit diameter).

dimensional flame with detailed chemistry and diffusive properties, allowing for radiative heat loss form the major species, and to generate the characteristic extinction turning points. At the same time, the relative efficiencies of the key termination versus branching reactions will be assessed through the concept of the flammability exponent, especially near and at the state of the turning point. The kinetic data base used is that of a C_1 mechanism of 18 species and 74 reactions. The flame is assumed to be optically thin and radiation from CO_2, H_2O, CO and CH_4 are included. The flame code of Kee was modified to include the pseudo arc-length continuation technique of Keller.

Figure 1 shows the laminar flame speed and the maximum flame temperature as functions of the equivalence ratio for lean methane/air flames with and without radiative heat loss. Compared to the adiabatic flame, the nonadiabatic flame exhibits a turning point. It may be noted that this is the first time that a turning point behavior is obtained for the numerically simulated laminar flame with detailed description of chemistry, diffusive transport, and radiative heat loss. It is further seen that, at the turning point, the flammability limit is 0.493, the flame speed is 2.3 cm/s, and the maximum flame temperature is 1375K. The flammability limit is well within the range of the empirically determined lean flammability limit of methane/air mixtures, while the flame speed and flame temperatures are also very close to those predicted from asymptotic theories when referenced to the respective adiabatic values, which are well established.

We have also studied the flammability limit of a fairly different system, namely the rich hydrogen/air flames, shown in Fig. 2. The extinction point is again exhibited, and close agreement between calculated and asymptotic flammability characteristics also exist. The calculated flammability limit also agrees well with the experimental values in the literature.

In order to assess the influence of chain mechanisms on the flammability limits, Figs. 3 and 4 show the calculated flammability exponents for the methane/air and hydrogen/air flames, respectively, with and without radiative heat loss. The controlling branching and termination reactions for both flames were found to be those involving the H and O_2 species. It is significant to note that, for the methane case with radiative heat loss, the equivalence ratio of 0.502 at the critical chain termination state of $\alpha=1$ is just slightly higher than the corresponding value of 0.497 at the critical heat loss state of the turning point. for hydrogen/air mixtures, the corresponding values at the rich flammability limits are 10.1 and 10.4, respectively.

The above results provide a unified interpretation of flammability limits by recognizing that the influence of heat loss and chain termination on flame propagation become critical almost simultaneously. As such, flammability limits determined through the turning point extinction criterion are almost identical to those determined through the unity flammability exponent criterion. The result id entirely physically reasonable by considering the following. As the flammability limit is approached, the adiabatic flame temperature is reduced due to the change in stoichiometry. This weakens the temperature-sensitive two-body branching reaction but usually has a much smaller influence on the termination reactions, especially when it involves three bodies. Therefore, a state will be reached at which the termination reaction becomes overwhelmingly strong, as indicated by $\alpha=1$, and consequently causes a rapid slow down of the overall reaction rate and, thereby, the overall heat release rate. This, in turn, makes the influence of heat loss relatively severe and, therefore, simultaneously results in the extinction turning point.

This work is reported in Publication No. 1.

2. Reduced Mechanism for Methane Oxidation

In an effort to describe the effects of chemical reaction on combustion phenomena with greater realism than the one-step reaction frequently used in theoretical analyses, various reduced mechanisms based on steady-state and partial equilibrium concepts have been developed. Most of these mechanisms consist of four steps. In this study on methane oxidation we compared calculated results on the species and temperature profiles, as well as the extinction strain rates from a representative four-step mechanism, against those obtained with the detailed mechanism. Such a comparison was not satisfactory. The comparison, however, was greatly improved by relaxing the steady-state assumption for the CH_3 radical. A five-step mechanism was consequently proposed, and the agreement was significantly improved. This result is expected to be of particular relevance to phenomena that are strongly dependent on accurate descriptions of the CH_3 such as the formation of prompt NO_x and fuel rich combustion.

This work is reported in Publication No. 2.

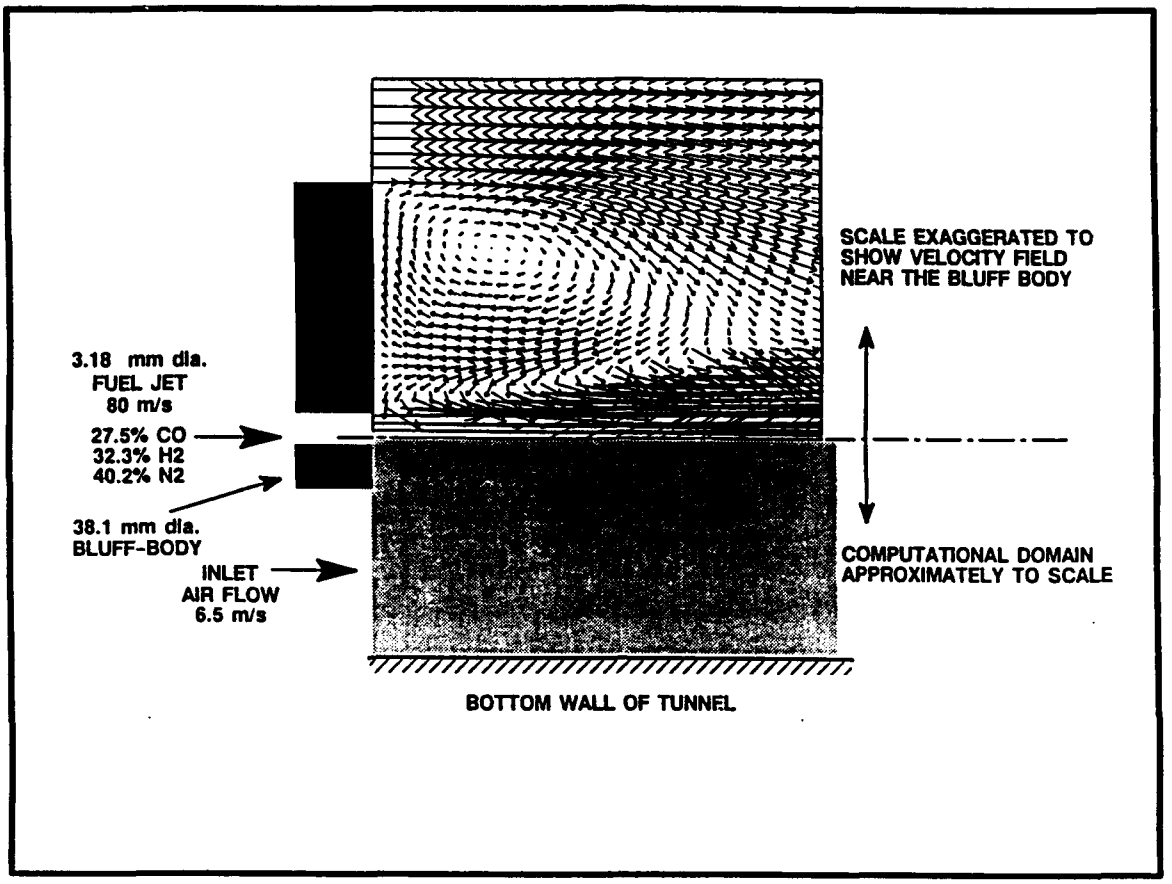

Figure 1. Burner conditions and near-field velocity.

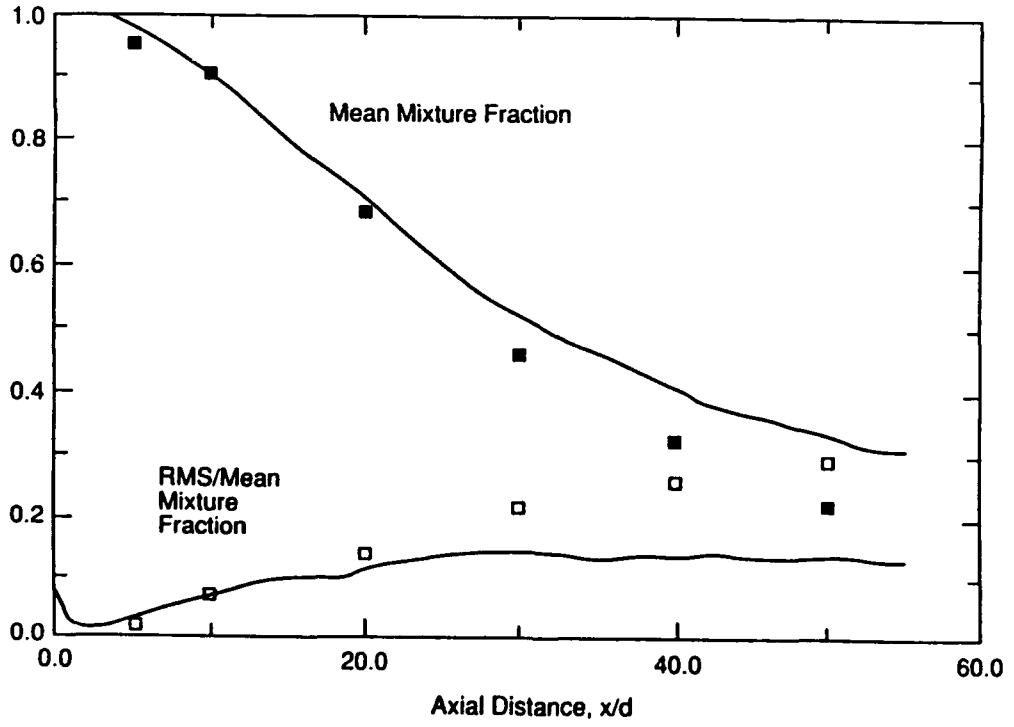

Figure 2. Comparisons along centerline.

Research has also been initiated on the responses and chemical kinetics of high pressure flames and on the response of stretched flames in unsteady flows. These new research directions are expected to be relevant to high-pressure chemical and flame kinetics, to the modeling of turbulent flames through the concept of steady and unsteady laminar flamelets, and to the general understanding of the various extinction phenomena.

MAJOR PUBLICATIONS

1. "A Unified Chain-Thermal Theory of Fundamental Flammability Limits", by C.K. Law and F.N. Egolfopoulos, to appear in *Proc. of Twenty-Fourth Symposium (International) on Combustion*, 1993.
2. "Reduced Kinetic Mechanisms for Counterflow Methane-Air Diffusion Flames", by H. Chelliah, K. Seshadri and C.K. Law, to appear in *Reduced Kinetic Mechanisms for Application in Combustion,* (Ed.: B. Rogg and N. Peters), Springer-Verlag.
3. "A Compilation of Experimental Data on Laminar Burning Velocities", by C.K. Law, to appear in *Reduced Kinetic Mechanisms for Application in Combustion,* (Ed.: B. Rogg and N. Peters), Springer-Verlag.
4. "On Adiabatic Stabilization of Inverted Flames", by C.J. Sung, C.K. Law and A. Umemura, to appear in *Proc. of Twenty-Fourth Symposium (International) on Combustion*, 1993.
5. "Mechanisms of Flame Stabilization in Subsonic and Supersonic Flows", by C.K. Law, *Major Research Topics in Combustion* (Eds.: M.Y. Hussaini, A. Kumar and R.G. Voigt), Springer-Verlag, New York, pp. 201-236 (1992). ** Invited Position Paper**

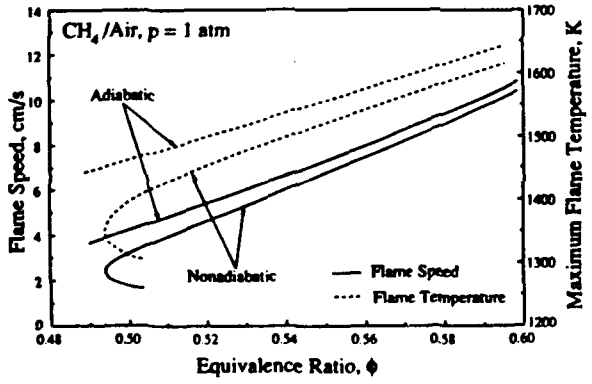

Figure 1

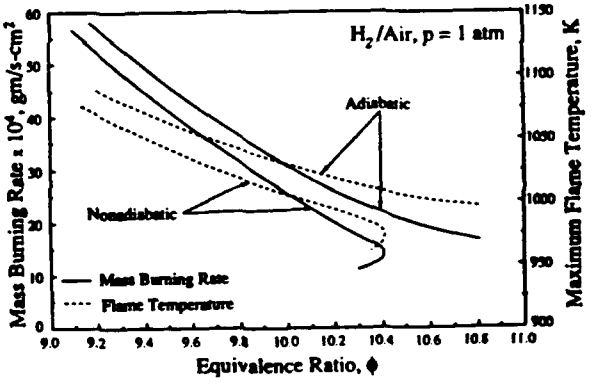

Figure 2

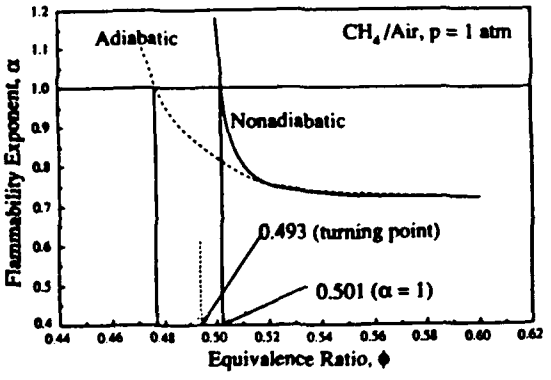

Figure 3

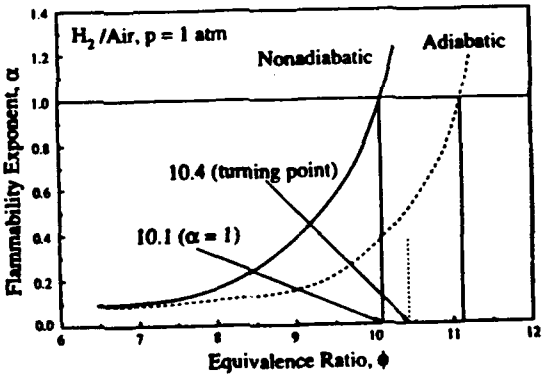

Figure 4

HIGH RESOLUTION MEASUREMENTS OF MIXING AND REACTION PROCESSES IN TURBULENT FLOWS

AFOSR Grant No. 89-0541

Werner J.A. Dahm

Gas Dynamics Laboratories
Department of Aerospace Engineering
The University of Michigan
Ann Arbor, MI 48109-2140

Summary/Overview

This research program is focused on an experimental investigation into the fine scale structure of combustion reactions in turbulent flows, with the following three major objectives: *(i)* to develop and implement new, high-resolution, multi-dimensional, quantitative, imaging capabilities for obtaining direct experimental measurements of the small scale structure associated with the mixing and chemical reaction processes in turbulent flows, *(ii)* to use these new measurement techniques to experimentally investigate the essential physical characteristics of the structure of mixing and chemical reactions in turbulent flows, and *(iii)* to incorporate results from these new measurements into an improved understanding of the molecular mixing, chemical reaction, and local extinction processes in reacting turbulent flows. Collectively, results from this program are providing new insights into the mixing and combustion processes in turbulent reacting flows of interest for practical air-breathing propulsion systems.

Technical Discussion

A correct understanding of the physical processes by which molecular mixing and nonequilibrium chemical reactions occur in turbulent shear flows is central to the development of techniques for enhancing the rates of mixing and combustion in advanced airbreathing propulsion systems. This program is yielding new insights into the structure of reacting turbulent flows at the molecular diffusion and chemical reaction scales of the flow. The approach is based on direct experimental measurements of the fully space- and time-varying small scale structure of conserved scalar fields $\zeta(\mathbf{x},t)$ in nonreacting turbulent flows (see Refs. 1 and 2), and the relation between these and the physical structure of the corresponding chemical species concentration fields $Y_i(\mathbf{x},t)$ and the associated chemical reaction rate fields $w_i(\mathbf{x},t)$ in reacting turbulent flows. The investigation being undertaken consists of four primary tasks. The first is conducting an extensive series of four-dimensional spatio-temporal conserved scalar imaging measurements of the type developed during our previous grant period to allow a detailed study of several quantitative aspects of the $Sc \gg 1$ molecular mixing process in turbulent shear flows. These include the geometric scaling properties associated with the interleaving of strained molecular diffusion

MODELING OF NEUTRALS

The predominant neutral effluent source around spacecraft is the operation of various thrusters. The SSF is for example equipped with 25 and 55 lbf chemical monopropellant hydrazine thrusters, whereas the Shuttle Orbiter, with its 25 and 870 lbf bipropellant thrusters is a contamination source during docking maneuvers at the SSF. Electric propulsion thrusters, to be flown on future satellites, transfer vehicles, space platforms, and inter-planetary spacecraft, will emit plasmas ionized to various degrees.

Our modeling approach is to first model the neutral effluents with direct simulation Monte Carlo (DSMC) methods. The input to the DSMC code is the thruster flow densities, velocities, and temperatures along a startline which is the line where the continuum flowfield transitions to rarefied flow. The continuum part of the flow is calculated with the Method of Characteristics. The DSMC simulations, provide the self-induced neutral distribution (density, velocity, temperature) anywhere in the rarefied part of the flow. Figure 1 shows the results for a 25 lbf monopropellant thruster to be flown on SSF; the geometry is shown in Figure 2. The thrusters, which will operate along and across the 160 V solar arrays during the SSF build-up phase, can be seen to generate neutral densities along the arrays which are as high as $3x10^{19}$ m^{-3}, which is about four orders of magnitude greater than the nominal ambient neutral density of 10^{15} m^{-3}. These results were for a thermal accommodation coefficient of one; reducing the coefficient to zero, i. e., specular reflection, reduced the density along the array by a factor of two. The local densities were insensitive to the day/night variations in the array temperature (199-333 K).

MODELING OF IONS

Once the initial neutral flowfield has been established, we include relevant ionization mechanisms to determine the local plasma density. The predominant ionization mechanisms include charge exchange with the ambient O^+, critical velocity ionization (CVI), and photo-ionization. A set of fluid continuity equations for all neutral and ion species were established, and the set of equations were numerically solved with a flux solver to first order in space and time. The ion-molecule reaction rates are shown in Table 1 for both mono and bipropellant thruster flowfields. Numerically determined CVI rates for the species N_2 and CO_2 were provided by *Biasca* at MIT [Ref. 4]; these rates are a product of 1-D implicit particle in cell (PIC) simulations, assuming a constant density, infinite background of neutrals, and realistic mass ratios for the ions and electrons. The rates are a function of neutral and electron densities, as well as neutral velocities. The critical ionization velocities for CO_2 and N_2 are 7.7 and 10.2 km/s, respectively.

The SSF orbital velocity with respect to the ionospheric plasma is about 7.7 km/s, and the thruster effluents have exit velocities as high as 3 km/s. Hence, if the thrusters are directed into the platform wake, the neutral effluents will have velocities as low as 7.7 - 3 = 4.7 km/s relative to the ambient; too low for CVI to occur. When the thrusters are operating into the ram, however, relative velocities as high as 7.7 + 3 = 10.7 km/s will occur; sufficient to trigger CVI.

We solved a 2-D set of ion and neutral continuity equations of the form

$$dn/dt + df/dx + df/dy = 0$$

using the donor-cell method, where n denotes density and f denotes the 2-D flux. The initial neutral densities and velocities were provided by the DSMC runs. New ions formed through ion-molecule reactions and CVI were assumed to travel at their initial neutral velocities, i. e., no collisional momentum change was included. Magnetic effects were omitted; that is acceptable at the array dimensions (5-10 m), since the ion gyro radii range from 20 to 100 m. The ambient O^+ density was initially set to 10^6 cm^{-3} everywhere, and the flux solver was advanced at time steps on the order 10^{-6} s, which is well within the Courant stability

dimensional Rayleigh scattering measurements suitable for applying this formulation to directly study the non-equilibrium structure of reacting turbulent flows. Results obtained in the full equilibrium limit (e.g. Figs. 3 and 4) have already given several new insights into the nature of combustion reactions in turbulent flows (see Ref. 5).

References

1. Dahm, W.J.A., Southerland, K.B. & Buch, K.A. (1991) "Direct, high-resolution, four-dimensional measurements of the fine scale structure of Sc » 1 molecular mixing in turbulent flows," *Physics of Fluids A* **3**, 1115-1127.

2. Dahm, W.J.A., Southerland, K.B. & Buch, K.A. (1991) "Four-dimensional laser induced fluorescence measurements of conserved scalar mixing in turbulent flows," to appear in *Applications of Laser Techniques to Fluid Mechanics*, R. Adrian, Ed. Springer Verlag, Berlin.

3. Southerland, K.B., Porter, J.R., Dahm, W.J.A. & Buch, K.A. (1991) "An experimental study of the molecular mixing process in an axisymmetric laminar vortex ring," *Physics of Fluids A* **3**, 1385-1392.

4. Dahm, W.J.A. and Buch, K.A. (1991) Fine structure characteristics of large Schmidt number molecular mixing in turbulent flows, *Chemical Reactions and Physical Processes in Turbulent Liquids*, J. Hunt, Ed., Cambridge University Press, in press.

5. Buch, K.A., Dahm, W.J.A., Dibble, R.W. and Barlow, R.S. (1992) "Structure of equilibrium reaction rate fields in turbulent jet diffusion flames," to be presented at *Twenty-fourth International Symposium on Combustion*, Sydney, Australia, July 5–9, 1992.

6. Dahm, W.J.A., Su, L.K., & Southerland, K.S. (1992) A scalar imaging velocimetry technique for fully-resolved four-dimensional vector velocity field measurements in turbulent flows," to appear in *Physics of Fluids* A.

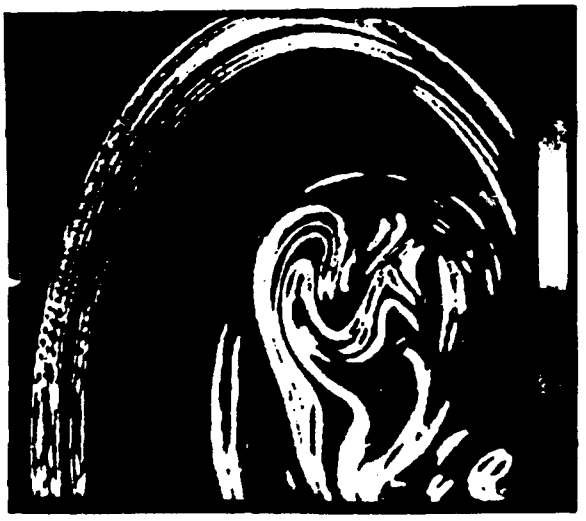

Fig. 1. Large Schmidt number scalar dissipation rate field $log_e \nabla\zeta \cdot \nabla\zeta(\mathbf{x},t)$ obtained in the self-similar far field of a nonreacting turbulent jet at $Re_\delta \approx 6{,}000$.

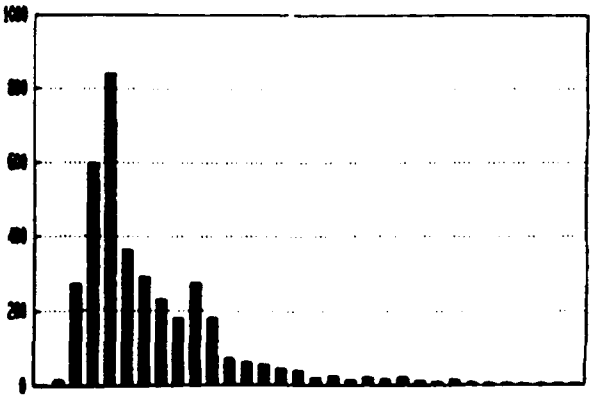

Fig. 2. Typical distribution of the scalar dissipation layer separations obtained from fully-resolved four-dimensional imaging measurements as in Fig. 1.

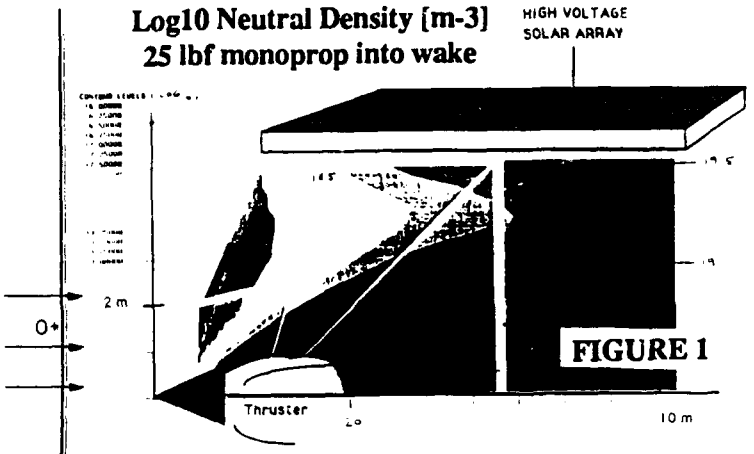

FIGURE 1

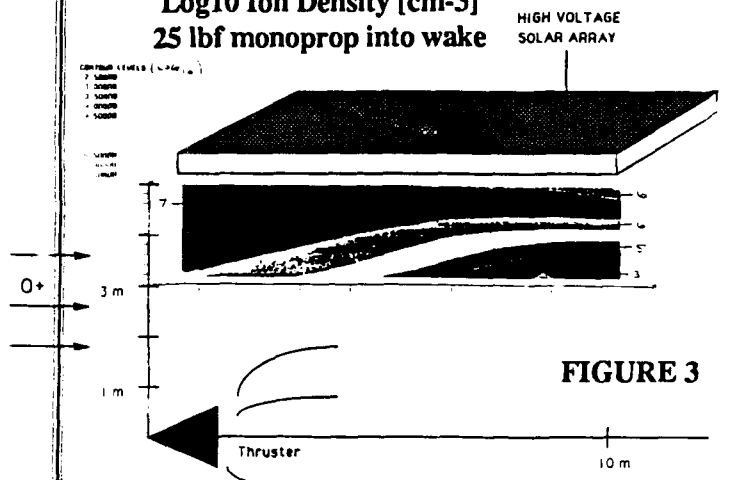

FIGURE 3

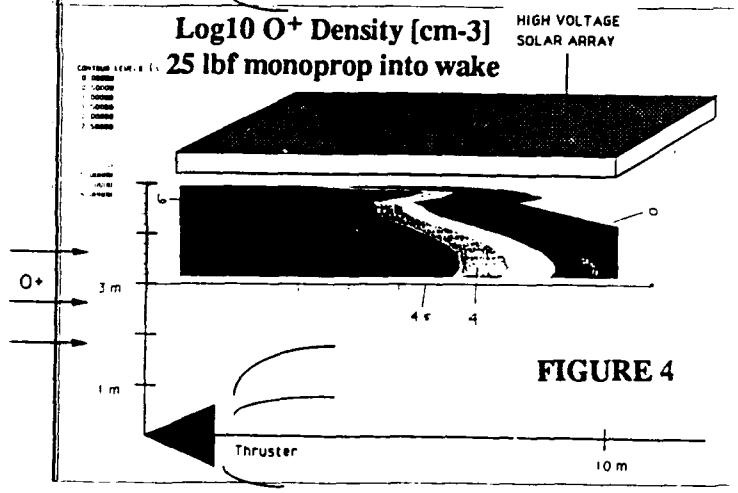

FIGURE 4

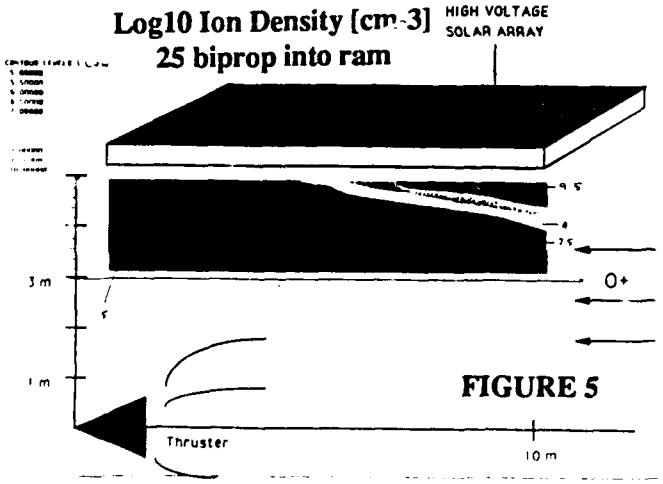

FIGURE 5

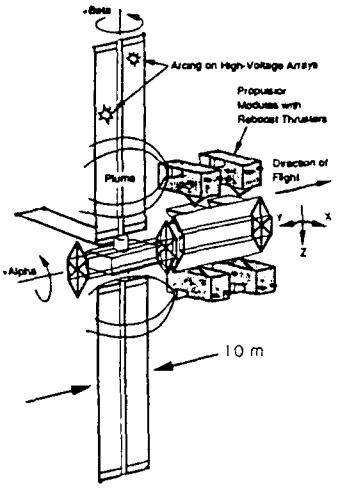

FIGURE 2 SSF Arrow Mode Configuration

TABLE 1
Reaction Rates

Reactions in monoprop SSF thrusters
[Mole fractions: 0.48 H_2, 0.29 N_2, 0.22 NH_3]

$O^+ + H_2 \rightarrow OH^+ + H$	$k=1.7 \times 10^{-9}$ cm^3/s	Bernhardt, 1987 [Ref. 4]
$OH^+ + e^- \rightarrow O^* + H$	$k=7.5 \times 10^{-8} (300/T_e)^{0.5}$	"
$OH^+ + H_2 \rightarrow H_2O^+ + H$	$k=1.5 \times 10^{-9}$	"
$H_2O^+ + e^- \rightarrow OH^* + H$	$k=6.5 \times 10^{-7} (300/T_e)^{0.5}$	"
$O^+ + N_2 \rightarrow NO^+ + N$	$k=3. \times 10^{-10}$ (at 5 eV)	Caledonia et al., 1987 [Ref. 5]
$NO^+ + e^- \rightarrow N + O$	$k=4.2 \times 10^{-7} (T_e/300)^{-0.85}(0.22)$ (at 2.75 eV)	Rees, 1989 [Ref. 7]
$O^+ + NH_3 \rightarrow NH_3^+$	$k=1.2 \times 10^{-9}$	Ikezoe et al., 1987, [Ref. 7]
$NH_3^+ + e^- \rightarrow NH_3$	$k=1. \times 10^{-7}$	

Additional reactions for the biprop thrusters (Shuttle type)
[Mole fractions: 0.31 N_2, 0.20 H_2, 0.32 H_2O, 0.11 CO, 0.06 CO_2]

$O^+ + H_2O \rightarrow O + H_2O^+$	$k=6 \times 10^{-10}$ (at 5 eV)	Caledonia et al., 1987 [Ref. 5]
$H_2O + H_2O^+ \rightarrow H_3O^+ + OH$	$k=1.67 \times 10^{-9}$	Bernhardt, 1987 [Ref. 4]
$H_3O^+ + e^- \rightarrow$ Neutrals	$k=6.3 \times 10^{-7} (300/T_e)^{0.5}$	"
$O^+ + CO_2 \rightarrow O_2^+ + CO$	$k=0.$ (at 5 eV)	Caledonia et al., 1987 [Ref. 5]
$O^+ + CO_2 \rightarrow CO_2^+ + O$	$k=6 \times 10^{-10}$	"
$CO_2^+ + e^- \rightarrow CO^* + O^*$	$k=3.8 \times 10^{-7}$ (at 5 eV)	Bernhardt et al., 1991, [Ref. 8]
$O^+ + CO \rightarrow CO^+ + O$	$k=6 \times 10^{-11}$ (at 5 eV)	Caledonia et al., 1987, [Ref. 5]

CHEMICAL REACTIONS in TURBULENT MIXING FLOWS

AFOSR Grant 90-0304

P. E. Dimotakis,* J. E. Broadwell,** and A. Leonard†

Graduate Aeronautical Laboratories
California Institute of Technology, Pasadena, CA 91125

Summary/Overview

The purpose of this research is to conduct fundamental investigations of turbulent mixing, chemical reaction, and combustion processes, in turbulent, subsonic, and supersonic free shear flows. The program is comprised of an experimental effort, an analytical and modeling effort, a computational effort, and a diagnostics development and data-acquisition effort, the latter as dictated by specific needs of our experiments. Our approach is to carry out a series of detailed theoretical and experimental studies primarily in two, well-defined, fundamentally important turbulent flow fields: free shear layers and axisymmetric jets. To elucidate molecular transport effects, experiments and theory concern themselves with both liquids and gases. The computational studies are, at present, focused at fundamental issues pertaining to the computational simulation of compressible flows with strong fronts.

Technical discussion

A review of turbulent, free-shear layer mixing and combustion, originally presented as an invited paper at the 1989 *AIAA Aerospace Sciences Meeting*. has been updated and covers much of the recent work in supersonic shear layers and shear layer combustion. It was published as a separate chapter in Vol. 137 of the *Progress Series in Astronautics and Aeronautics* (copies available on request).[1]

We were substantially delayed in our experimental, Supersonic Shear Layer effort by earthquake damage last June to the high pressure, hydrogen reactant tank seal. The attendant issues of safety dictated a very careful repair and redesign to minimize the possibility of such mishaps in the future. Since that period, we have begun to address the question of how best to differentiate between Reynolds number and compressibility effects. The current set of experiments involves runs that are identical as regards compressibility. Using helium, or argon, which have different kinematic viscocities, as the diluent gas in both high- and low-speed streams, at

---

* Professor, Aeronautics & Applied Physics.

** Visiting Associate, Aeronautics.

† Professor, Aeronautics.

temperature is higher behind the reactive shock than behind the shock-deflagration structure near the wall. Because of the difference in velocities, a slip line can be observed between the two regions.

This basic structure of oblique detonations has been observed in a wide range of hydrogen-oxygen-nitrogen mixtures from 2:1:0 to 2:1:7 and for a range of wedge angles from 23 to 35 degrees. As the amount of nitrogen dilution decreases, the amount of energy released increases. This results in a higher temperature, greater speed of sound, and lower Mach number in the products of combustion. As a consequence, the reactive shock above the induction region becomes stronger and the shock angle increases accordingly. When the amount of dilution is further decreased to zero, the shock angle is too large for the overall configuration to be stable and the entire structure moves upstream continuously. A similar effect is observed when the wedge angle is increased while keeping the mixture proportions constant.

Stability of Oblique Detonations

The simulations described above demonstrate that an oblique detonation can be stabilized on a wedge. We then investigated the stability of such detonation structures and whether disturbances would significantly change the structures. The results of one such computation performed to answer this question are shown in Figure 3. In this simulation, a burning pocket is artifically introduced as a disturbance into the flow field originally computed for a stable detonation in a hydrogen-air mixture. This pocket is convected downstream and eventually merges with the original detonation structure, creating a larger and stronger detonation. However, the changes in the structure caused by the disturbance are eventually convected out of the computational domain and the original flow field is recovered, indicating that the detonation structure is stable to such a perturbation.

The large number of simulations performed indicate that the detonation structure is stable except when the flow behind the structure is choked. For every flow configuration, there exists a maximum amount of heat that can released without choking the flow. When the energy released exceeds this value, the heated flow will no longer be able to pass through the area behind the shock and, therefore, the shock-detonation structure is driven upstream to create a larger area to accomodate the heated flow. If a sufficiently large area of outflow cannot be generated, the entire structure will be driven out of the computational domain in a simulation or out of the test apparatus in an experiment.

Effects of Viscosity

Since the boundary layer is very thin in the supersonic flows in ram accelerators, very high computational resolution is required to conduct direct numerical simulations to study the effects of boundary layers. Therefore, models such as the Baldwin-Lomax model are usually used to represent a turbulent boundary layer. Since these models are usually calibrated in a different flow regime, it is important to closely examine the results predicted using such models. Figure 4b shows a simulation using the Baldwin-Lomax model and Figure 4c shows results from a simulation without any explicit turbulence models. Although the overall detonation structure is the same in the two cases, the simulations using the Baldwin-Lomax model show a significantly shorter induction delay and much earlier establishment of the overall detonation structure. However, the simulation without any explicit turbulence models show results much closer to the inviscid simulations. This disrepancy is currently being studied in greater detail.

PUBLICATIONS AND PRESENTATIONS

Publications

Numerical Simulations of Detonation Transmission, E.S. Oran, D.A. Jones, and M. Sichel, *Proc. Roy. Soc. Lond.*, A 436, 267–297, 1992.

Numerical Simulation of Layered Detonations, D.A. Jones, M. Sichel, R. Guirguis, and E.S. Oran, in *Dynamics of Detonations and Explosions: Detonations*, eds. A.L. Kuhl, J.-C. Leyer, A.A. Borisov, and W.A. Sirignano, *Progress in Aeronautics and Astronautics*, vol. 133, pp. 202–220, AIAA, Washington, 1991.

Structure of Reaction Waves behind Oblique Shocks, C. Li, K. Kailasanath, and E.S. Oran, submitted to *Prog. Aero. Astro., Proceedings of the 13th International Colloquium on the Dynamics of Explosions and Reactive Systems*, 1991.

We have also conducted a detailed study of the conserved scalar spectrum. Classical theories of turbulence offer predictions through the range of scales and provide the basis for much of the present modeling on turbulent mixing. Our measurements represent the highest resolution and signal-to-noise ratio measurements of laboratory, liquid jet scalar spectra, over this range of Reynolds numbers, to date and cast serious doubt on the validity of some classical assumptions and models. A paper discussing these results, extending the discussion in Ref. 4, has been submitted for publication.[6]

Other important conclusions can also be gleaned from this part of our effort, with counterparts to the gas-phase effort. By way of example, we have discovered that far-field turbulent jet mixing is *very* sensitive to the initial conditions. We have also confirmed this behavior in our gas-phase experiments with substantial changes in flame length as a result of minor changes to the jet flow geometry, that could rightfully have been assumed to be inconsequential.

Our liquid-phase jet investigations have also addressed the proposed fractal behavior of iso-scalar interfaces in fully-developed turbulent flows.[7,8] In response to a first publication on this topic,[9] we were invited to contribute a discussion to *Nonlinear Science Today*.[10] These publications, in which we have argued that power-law fractal descriptions are not applicable, at least in the case of fully-developed turbulent jets, as well as a series of invited lectures and seminars on the subject, are responsible for some controversy in the Fluid Mechanics Community.

Work presently in progress in liquid-phase turbulent jets is focused on the quantitative study of far field, conserved scalar interface geometry. Two-dimensional, high resolution (1024×1024), high dynamic range ($\sim 60\,\mathrm{dB}$), digital planar images of the concentration field of a turbulent jet, across the full turbulent flow field normal to the jet axis, have been obtained using laser-induced fluorescence techniques, and a cryogenically-cooled CCD focal plane array, whose output is digitized to 14 bits per pixel. The planar laser illumination is created by sweeping a CW (Argon Ion) laser beam with a custom-built, phase-locked mirror system. This results in only a small variation in illumination intensity across the field of view, which is subsequently corrected for by appropriate calibration and normalization of the image data. Preliminary experiments have been performed at a jet Reynolds number of $Re \simeq 1.3 \times 10^4$.

The work on the Two-Stage Lagrangian model has continued, in collaboration with A. Lutz of Sandia, with an emphasis on improved quantitative predictions of NO_x production in hydrocarbon flames. In the past, the mixing rate provided to the model had been inferred from the dependence of flame length on the stoichiometric mixture ratio. For a cold jet, the recent data by Dowling and Dimotakis provide the necessary information.[11] For combusting jets, the temperature profiles measured by Becker and Yamazaki,[12] combined with an energy-conservation analysis, yield the required rate. The newly-computed results are in good agreement with recent data from $CO - H_2$ and CH_4 flames.

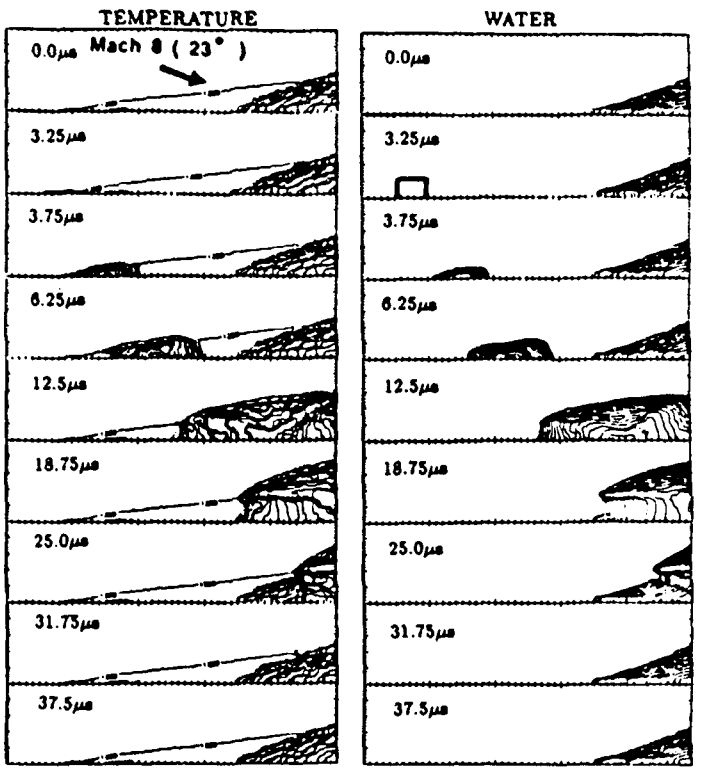

Fig. 3. Development of a disturbance on an oblique detonation structure.

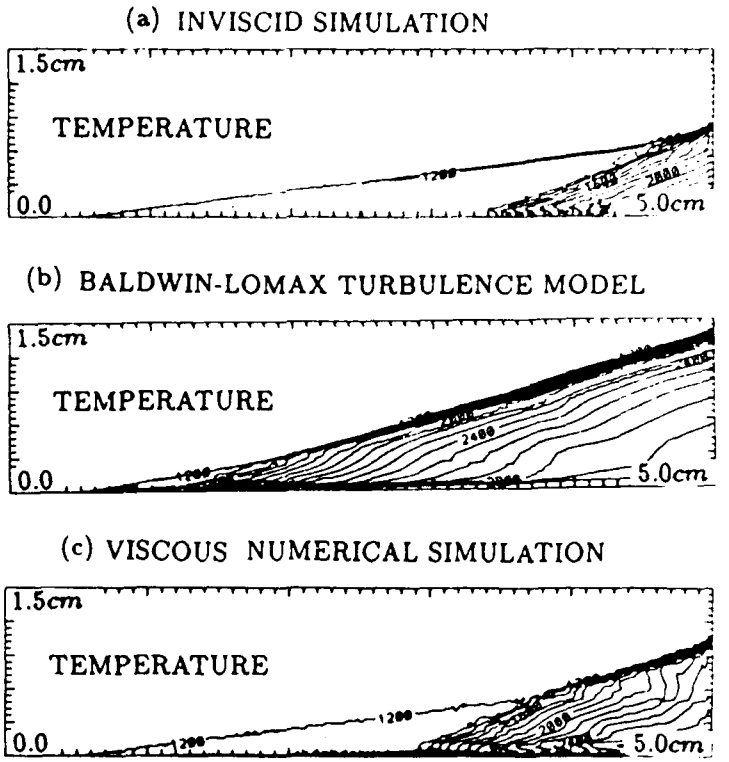

Fig. 4. The oblique detonation structure predicted using different numerical models.

References

[1] Dimotakis, P. E., "Turbulent Free Shear Layer Mixing and Combustion," *High Speed Flight Propulsion Systems*, in *Progress in Astronautics and Aeronautics* **137**, Ch. 5, 265–340 (1991).

[2] Gilbrech, R. J., *An Experimental Investigation of Chemically-Reacting, Gas-Phase Turbulent Jets*, Ph.D. thesis, California Institute of Technology (1991).

[3] Gilbrech, R. J., and Dimotakis, P. E., "Product Formation in Chemically-Reacting Turbulent Jets," *AIAA* 30th *Aerospace Sciences Meeting*, AIAA Paper 92-0581 (1992).

[4] Miller, P. L., *Mixing in High Schmidt Number Turbulent Jets*, Ph.D. thesis, California Institute of Technology (1991).

[5] Miller, P. L., and Dimotakis, P. E., "Reynolds number dependence of scalar fluctuations in a high Schmidt number turbulent jet," *Phys. Fluids A* **3**, 1156–1163 (1991).

[6] Miller, P. L., and Dimotakis, P. E., "Log-normal behavior of scalar power spectra in high Schmidt number turbulent jets," submitted to *Phys. Fluids A* (1991).

[7] Mandelbrot, B. B., *The Fractal Geometry of Nature* (W. H. Freeman & Co., New York, 1982).

[8] Sreenivasan, K. R., "Fractals and Multifractals in Fluid Turbulence," *Ann. Rev. Fluid Mech.* **23**, 539–600 (1991).

[9] Miller, P. L., and Dimotakis, P. E., "Stochastic geometric properties of scalar interfaces in turbulent jets," *Phys. Fluids A* **3**(1), 168–177 (1991).

[10] Dimotakis, P. E., "Fractals, dimensional analysis and similarity, and turbulence," *Nonlinear Sci. Today* #2/91, pp. 1, 27–31 (1991).

[11] Dowling, D. R., and Dimotakis, P. E., "Similarity of the concentration field of gas-phase turbulent jets," *J. Fluid Mech.* **218**, 109–141 (1990).

[12] Becker, H. A., and Yamazaki, S., "Entrainment, Momentum and Temperature in Vertical Free Turbulent Difusion Flames," *Comb. and Flame* **33**, 123–149 (1978).

in use—provides valuable information on the microstructure of the composition field that is responsible for molecular diffusion. One virtue of this approach is that it can reconcile flamelet and nonflamelet notions in both premixed and diffusion flames (Pope 1990). For the joint pdf of composition and its gradient contains the same information as the joint pdf of mixture fraction and its dissipation rate, that is the cornerstone of flamelet models of diffusion flames (Peters 1984). Similarly, this joint pdf contains full information on the surface-to-volume ratio, which is used in flamelet models for premixed combustion.

Mapping closure is a *formalism* rather than a *model.* Thus, if the formalism is successfully applied to one problem, then it can readily be extended to all problems of the same type. The principal closure problem is connected with the molecular diffusion term. If the formalism can be developed for a simple diffusion problem, then it can be extended to others. The simplest diffusion problem is the unsteady heat conduction equation with no velocity field and no source term. Thus the initial objective of this aspect of the research is to develop a mapping closure for the 2D heat conduction equation with random initial conditions.

Advances on this topic have been hard won, and are not reported here.

PARTICLE IMPLEMENTATION

Consider a single scalar $\phi(\mathbf{x}, t)$ in homogeneous turbulence. In a particle method, the pdf of ϕ is represented by an ensemble of N particles, the n-th having the scalar value $\phi^{(n)}(t)$. The role of a mixing model is to specify how $\phi^{(n)}(t)$ evolves in time.

For this problem, the mapping closure yields a fascinating particle method (Pope 1991). Let the particles be ordered so that

$$\phi^{(1)}(t) \le \phi^{(2)}(t) \le \ldots \le \phi^{(N)}(t). \tag{1}$$

Then (according to the mapping closure) the particles evolve by a coupled set of ode's

$$\frac{d}{dt}\phi^{(n)}(t) = B_{n+\frac{1}{2}}[\phi^{(n+1)} - \phi^{(n)}] + B_{n-\frac{1}{2}}[\phi^{(n-1)} - \phi^{(n)}], \tag{2}$$

where (for large N) the positive coefficients are

$$B_{n+\frac{1}{2}} = N^2 A\left(\frac{n+\frac{1}{2}}{N}\right), \tag{3}$$

and A is a known function. (The coefficients $B_{\frac{1}{2}}$ and $B_{N+\frac{1}{2}}$ are zero, so $\phi^{(0)}$ and $\phi^{(N+1)}$ can remain undefined.) A simple interpretation of Eq. (2) is that $\phi^{(n)}(t)$ is drawn to its two neighbors at a rate proportional to its separation from them.

How can this particle method be extended to the case of multiple scalars? With there being σ scalars, the n-th particle has the properties $\phi^{(n)}(t) = \phi_1^{(n)}, \phi_2^{(n)}, \ldots, \phi_\sigma^{(n)}$. But there is no simple and unique extension of the concept of "ordering" to a σ-dimensional space.

We are developing a model (applicable to any number of scalars) based on Euclidean minimum spanning trees (EMST). This is now sketched for the two-scalar case, in which each particle $\{\phi_1^{(n)}(t), \phi_2^{(n)}(t)\}$ can be viewed as a point on the plane: Figure 1 shows an ensemble of N=256 such points. Corresponding to any set of points there is an EMST. By

COMBUSTION KINETICS OF HEDMs AND METALLIC FUELS

AFOSR Grant No. F49620-92-J-0172

Principal Investigator: Arthur Fontijn
Research Collaborators: Peter M. Futerko, David P. Belyung

High-Temperature Reaction Kinetics Laboratory
The Isermann Department of Chemical Engineering
Rensselaer Polytechnic Institute
Troy, NY 12180-3590

SUMMARY

The use of new advanced solid rocket propellant constituents, such as, e.g., boron as a HEDM and ammonium nitrate as replacement for halogen-containing oxidants, requires knowledge of their combustion characteristics. The present program will provide critical kinetic data to allow modeling of such combustion. Our HTFFR (High-Temperature Fast-Flow Reactor) and Metals-HTP (High-Temperature Photochemistry) facilities are uniquely suited to provide such data over very wide temperature ranges, within the limits 300-1900 K. In this work we will investigate reactions of B, BO and BO_2 with O_2, CO, CO_2, H_2O and NO_x and such AlO reactions with some of these oxidants as may be helpful to elucidate the kinetics of the boron species reactions. Major goals are to establish correlations between the pre-exponentials as well as the activation barriers of the reactions and to investigate the fundamental reasons for any trends thus established to allow predictions for further reactions.

TECHNICAL DISCUSSION

The present program has just started and there are no results to report as yet. However, the work will at least initially be conducted along similar lines as our recently completed AFOSR work on reactions occurring in the combustion of metallized propellants containing ammonium perchlorate. Since major advances were made in that study we discuss those here, which also illustrates the sort of results to be anticipated from the new work.

Rate coefficients were obtained for the following individual reactions: Al + N_2O; AlO + Cl_2; AlO + HCl; AlO + CH_4; AlCl + CO_2; AlCl + N_2O; AlCl + N_2O; AlCl + HCl; BCl + CO_2; BCl + N_2O; BCl + SO_2. The results have been summarized in a recent overview article.[1] As illustrated in Fig. 1 for the BCl + SO_2 reaction, curved Arrhenius plots are usually obtained when rate coefficients of exothermic reactions are considered over wide temperature ranges.[2] For such plots the term "activation energy" merely signifies the local slope of the plot at a given temperature. If we wish to compare the temperature dependence of reactions, a more useful approach is to use the expression

$$k(T) = AT^n \exp(-E/RT) \qquad (1)$$

We have found for series of exothermic homologous reactions that, by fixing n, simple correlations exist between the "activation barriers" E and the sums of the σ-π,

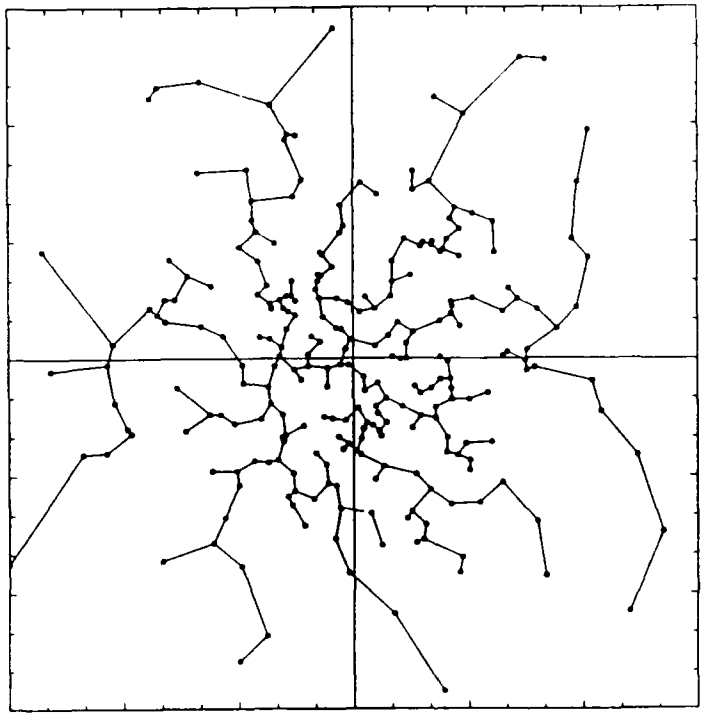

Fig. 1: Euclidean Minimum Spanning Tree For 256 Points in the Plane (i.e. a two-dimensional composition space)

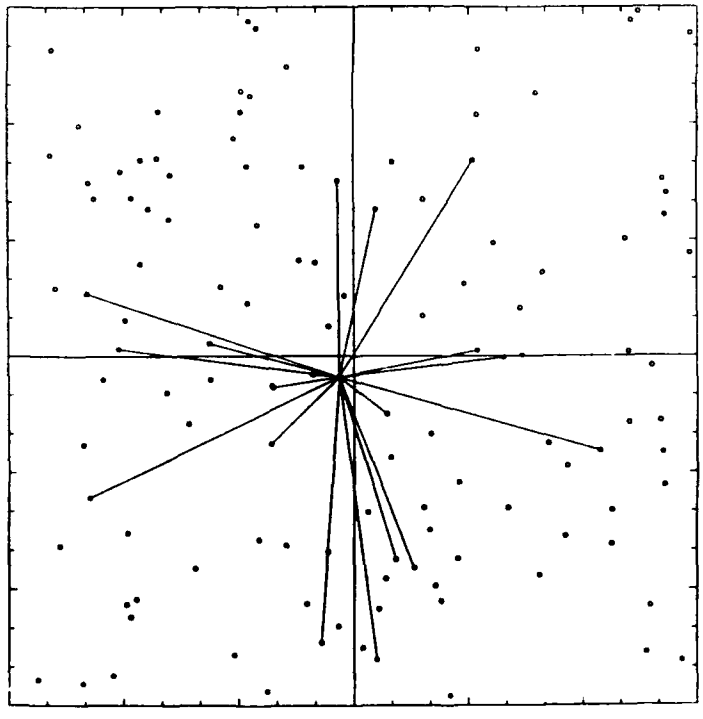

Fig. 2: Edges incident on a single point from 10 EMST's formed from sub-ensembles.

5. P.M. Futerko, D.P. Belyung, and A. Fontijn, "Activation Barriers for Series of Exothermic Homologous Reactions. Comparison of Measurements to Theory for Reactions of Boron Group Atoms with Oxygen Oxidants", J. Chem. Phys., in preparation.

6. D.P. Belyung and A. Fontijn, "Gas-Phase H-atom Abstraction from Hydrocarbons by Metal Oxides. The AlO + CH_4 Reaction from 590-1380 K", J. Phys. Chem., in preparation.

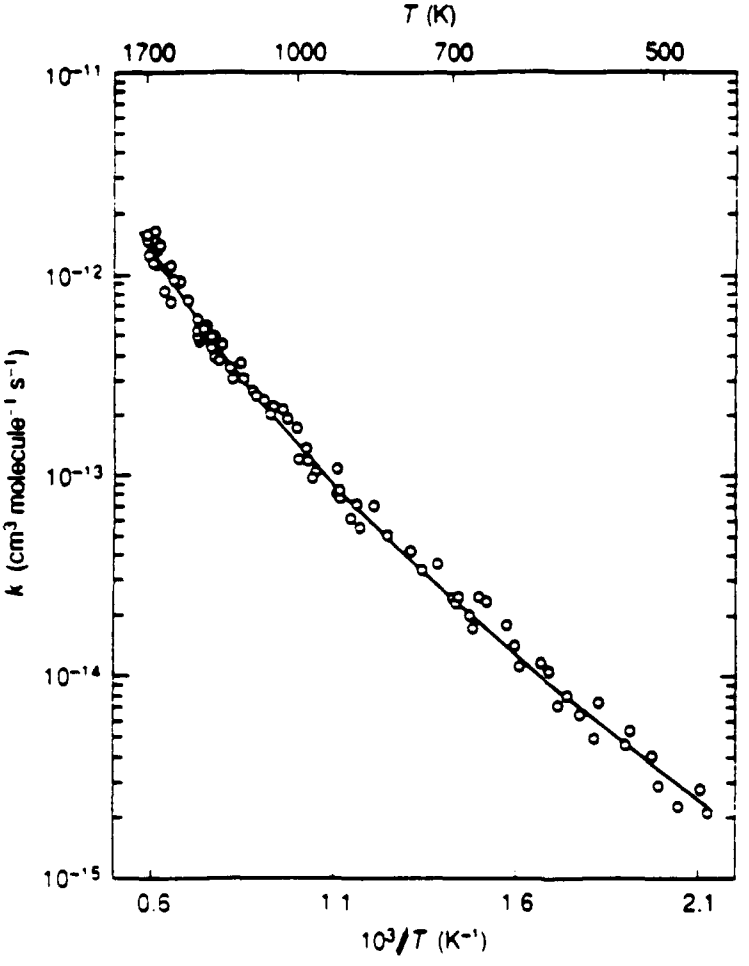

Figure 1. Arrhenius plot of the rate coefficient data of the BCl + SO_2 reaction from 460 to 1690 K. The solid line corresponds to the best-fit expression.

VORTEX SIMULATION OF TURBULENT COMBUSTION
(AFOSR Grant No. 89-0491

Principal Investigator: Ahmed F. Ghoniem

Department of Mechanical Engineering
Massachusetts Institute of Technology
Cambridge, MA 02139

SUMMARY/OVERVIEW

The objectives of this work are to develop an accurate and efficient numerical methodology for the simulation of the flowfield, mixing and burning rate in high Reynolds number shear flow, and the application of these methods to study flow combustion interactions in these flows. The methodology is based on a set of Lagrangian, grid-free schemes for the transport of vorticity and scalar gradients along particle trajectories. This endows the method with the necessary qualities of low numerical diffusion and spatial and temporal adaptivity. The reaction zones are represented by one or a number of transport elements distributed between the two reacting streams, depending on the Damkohler number and resolution level. During this year, we focused on investigating the effect of the initial conditions on the three-dimensional structure of the mixing layer, the effect of heat release on the evolution of the large-scale structures and the overall growth of the layer, and the effect of periodic strain on the burning rate, extinction and re-ignition in a thin strained flame.

TECHNICAL REPORT

During the 1991-92 academic year, we pursued three projects to study: (1) the effect of the initial vorticity and density profiles on the formation of streamwise vorticity in the shear layer; (2) the effect of heat release on the roll-up and growth of the spatially developing reacting shear layer; and (3) the effect of periodic strain on the burning rate and extinction in a thin diffusion flame. Results of these studies have been documented and accepted for publication in the open literature. In the following, we summarize the most important results in each project and discuss its current status.

Questions regarding the experimentally observed uneven spacing of the streamwise vorticity rods which form due to the evolution of the three-dimensional instabilities prompted our study of the role of the initial conditions in establishing these flows [1,2]. Vortex simulations of a doubly periodic shear layer separating two streams of different densities were performed. Two cases, in which the initial vorticity layer was either symmetric or asymmetric, were analyzed in detail. In both cases, it was found that the layer rolls up into streamwise cores which deform along their spanwise axes leading to the formation of thin vorticity layers stretching between neighboring cores into vortex rods. These rods wrap around individual cores in the shape of twisted hairpin vortices which stretch between neighboring vortex cores.

The numerical results indicate that both instability modes, the translative instability which causes the deformation of the cores along the spanwise direction, and the "Corcos" instability, which leads to the roll up of the vortex sheets between the core into rods, grow simultaneously energized by the extensional strain generated by the cores. While neither the density gradients across the layer nor the shape of the initial vorticity profile seem to affect this series of events in any substantial way, only the density gradients across the layer was able to affect the layer dynamics. This occurs as a result of the baroclinic vorticity term in the governing equation. Disturbing the symmetry of vorticity in the large eddies induces a motion in the direction of the heavy stream while the eddy itself penetrates further into the light stream. It was thus concluded that the observed even separation of the streamwsie rods is a sequence of the pairing dynamics [3]. In future work, the effect of heat release on this instability will be investigated.

A sequence of flame structure measurements (40 mm x 40 mm) for increasing U_θ/S_L is shown in Figure 2, where the unburned gas is colored white and the burned gas is colored black. The ratio of the vortex flame to laminar flame areas and the average positive and negative curvature calculated from such images for each of the test conditions studied are given in Table 1. Note that these results are obtained by averaging over from 10 to 30 individual flame structure measurements for each test condition.

Flame Curvature Measurements

A typical flame curvature distribution is shown in Figure 3. Over the range of U_θ/S_L, δ_V/δ_L and Le conditions studied, the flame curvature distribution was found to be unchanged and to exhibit positive mean curvature. This latter fact is consistent with the frequent appearance of cusp-like structures in the vortex flames. It is interesting to note, however, that in previous measurements, the curvature distributions of turbulent flames have been shown to have zero mean curvature. This suggests that vortex spacing and the dynamic response of the flame front are important factors, and that if one wants to describe turbulence-flame interactions based on the interaction of individual vortices with flame fronts, such effects must be accounted for. In addition, the curvature distributions of turbulent flames have been shown experimentally to broaden with increasing u'/S_L; however, the fact that this was not observed in the vortex flame is due to the limited range of U_θ/S_L studied to date.

Flame Area Measurements and the Minimum Scale of Flame Wrinkling

The flame area increase due to the flame-vortex interaction is given in Table 1 for each test condition. Over the range of conditions studied, the flame area was found to increase with increasing U_θ/S_L and with decreasing Lewis number, i.e., as the flame becomes more unstable. As indicated in Table 1, there are conditions under which the vortices produce no observable wrinkling of the flame front. Figure 4 is a plot of the ratio of the vortex flame to laminar flame areas versus U_θ/S_L for different vortex diameters (δ_v/δ_L). Although the data is sparse, it is clear that the area production decreases with decreasing U_θ/S_L for a given vortex size; and that the minimum vortex size required to wrinkle the flame front decreases with increasing U_θ/S_L.

Flame-Vortex Modeling

Figure 5 shows calculated flame contours for the case of an array of four vortices where the direction of rotation of the individual vortices is rearranged. Analyses of such flame contours show that the mean flame curvature scales more strongly with vortex size than with vortex velocity, and tends to be of the order of $(2r_m)^{-1}$ for U_θ/S_L = 0.25 - 1.0, where r_m is the characteristic vortex radius. The decrease in tangential vortex spacing increases the coupling of actions of adjacent vortices that leads to an increase in flame area and changes in the flame curvature and stretch statistics, while normal vortex spacing has less effect. Also, for interactions with a single isolated vortex, the maximum flame stretch that occurs during the interaction can be estimated by $K^* = U_\theta/r_m + S_L/2r_m$, which includes the flame curvature contribution, while the mean flame stretch has a maximum that asymptotes to approximately 20% of K^* when U_θ/S_L is increased to 2 and beyond. Maximum flame stretch generated by a single vortex and vortex arrays are nearly the same, while the actual flame stretch pdf's differ significantly due to the additional flame curvature and strain caused by vortex arrays.

REFERENCES:
(1) Knio, O.M. and Ghoniem, A.F. "Three-dimensional vortex simulation of roll-up and entrainment in a shear layer," J. Comput. Phys., 97, Nov 1991, pp. 172-223.

(2) Knio, O.M. and Ghoniem, A.F. " Vortex simulation of a three-dimensional reacting shear layer with infinite reaction rate," AIAA Journal, Jan 1992, pp. 105-116.

(3) Knio, O.M. and Ghoniem, A.F. "The three-dimensional structure of periodic vorticity layers under non-symmetric conditions," tp appear in the Journal of Fluid Mechanics.

(4) Soteriou, M., Knio, O.M., Ghoniem, A.F. and Cetegen, B. "Simulation of flow-combustion interactions in a spatially developing mixing layer," AIAA-92-0081.

(5) Soteriou, M., Knio, O.M., Ghoniem, A.F. and Cetegen, B. "Effect of steady and periodic strain on unsteady flamelet combustion," accepted for presentation at the 24th Symposium (International) on Combustion, Sidney, Australia, July 1992.

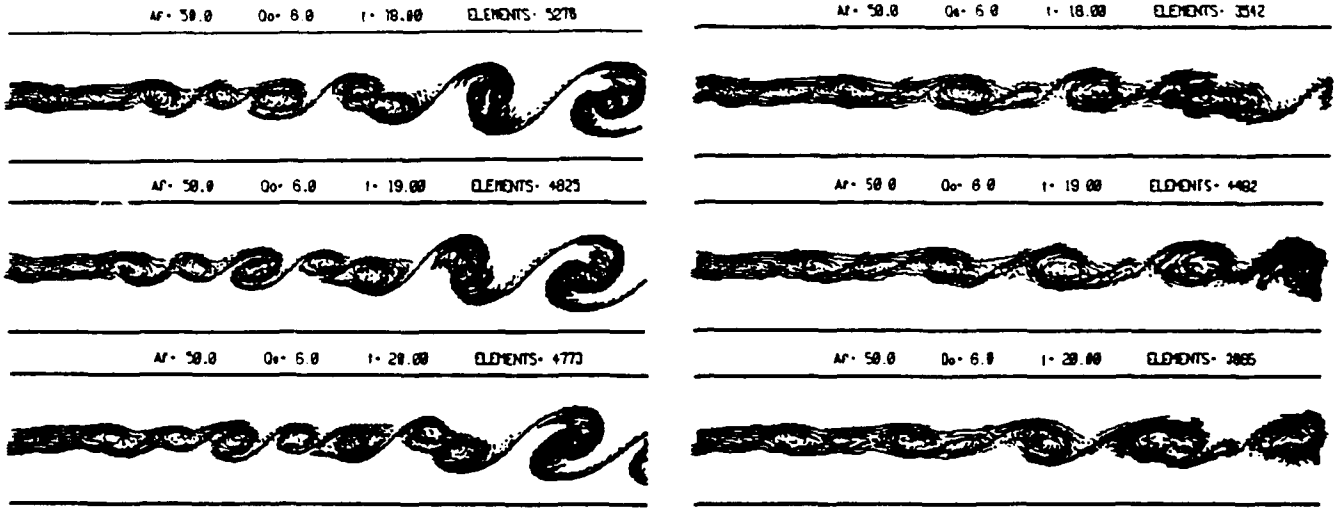

Figure 1. The location and velocity vectors of the vortex elements of the uniform-density (left) and variable-density (right) reacting shear layers, both with $A_f = 50$ and $Q = 6$.

Figure 2. Two-Dimensional Flame Structure Images

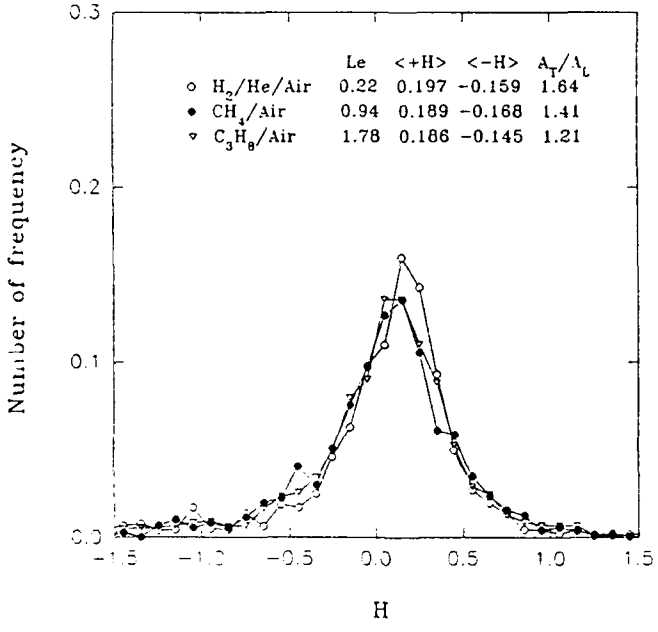

Figure 3. Flame Curvature Distribution

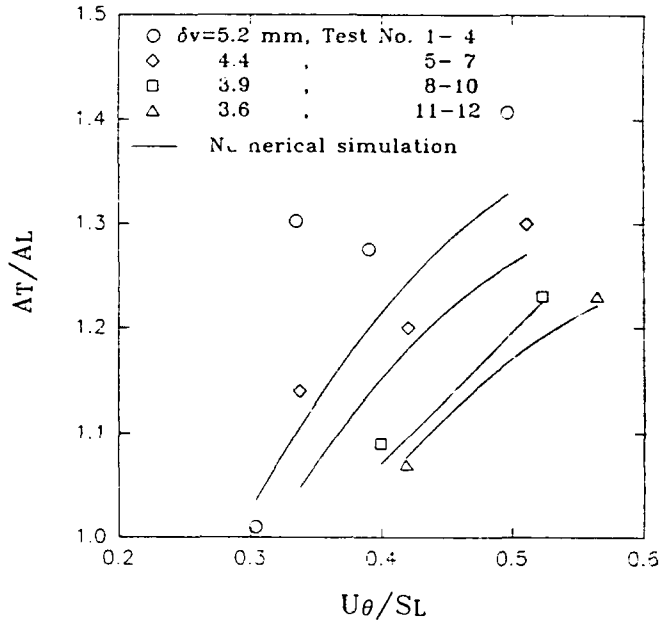

Figure 4. Flame Area Ratio vs. U_θ/S_L

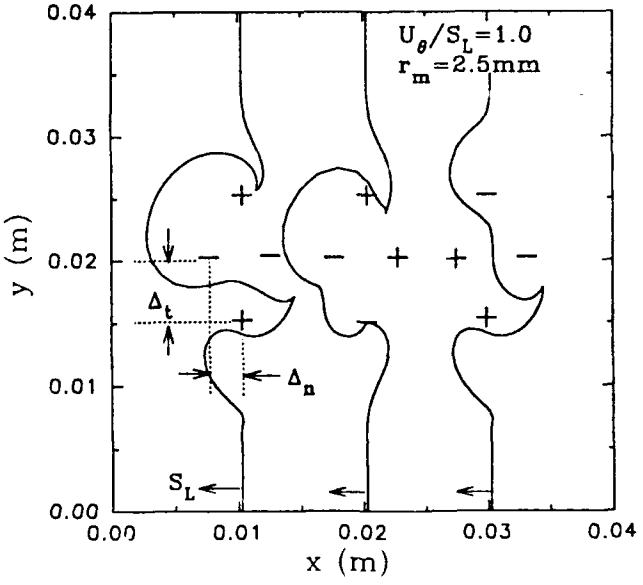

Figure 5. Calculated Flame Contours

CONTROLLING COMBUSTION AND MAXIMIZING HEAT RELEASE IN A REACTING COMPRESSIBLE FREE SHEAR LAYER

AFOSR Contract No. F49620-91-C-0020

Principal Investigators: David Nixon, Laurence Keefe

Nielsen Engineering & Research, Inc.
510 Clyde Avenue
Mountain View, CA 94043-2287

SUMMARY

The objective of the work is to study the interaction between heat release and mixing in compressible shear layers by analysis and computation, with an eye to finding flow configurations that maximize the heat release per unit distance in the streamwise direction. A previous nonreacting theory has been extended to include the effects of weak heat release and entropy generation. The preliminary conclusion is that heat release and/or entropy generation can *increase* the mixing rate of a shear layer over its nonreacting value, provided the profile of heat release is asymmetric, and the profile of entropy generation is symmetric across the layer. In addition, the original 2-D nonreacting theory has been made 3-D by inclusion of the effects of vortex sweep or obliquity. In this form it is capable of making analytic predictions of mixing behavior across a wide range of Mach numbers in both plane mixing layers and round jets, and is found to give the correct behavior in both flows. The numerical work has consisted in the addition of heat release and simple chemistry to the existing three-dimensional Navier-Stokes simulation capability. A variational approach to maximizing heat release has been pursued in the context of the weak heat release extension of the original 2-D theory. The search for a plausible nonlinear functional connecting the flow and the heat release is underway.

EXTENSIONS TO THE THEORY

In the past year one objective has been to clarify and extend the theoretical structure of the mixing problem. The theoretical basis originally proposed for studying the heat release problem assumed irrotational flow with weak heat release, $h_f(x,y)$. This produces a new field equation for the flow perturbation potential to be used in calculating the entrainment velocity of a bound vortex in a uniform free stream. This equation has the form:

$$\left[1 - M_c^2\right]\phi_{xx} + \phi_{yy} = \frac{(\gamma-1)\,(h_f)_x}{a_c^2} \qquad (1)$$

Since then the analysis has been extended to include the effects of weak entropy generation - thus relaxing the irrotationality assumption. The resulting governing equation for the perturbation potential and stream function are

A new area of interest is the changing requirements for the utilization of hydrocarbon fuels in propulsion systems. Future systems will require fuels to absorb substantial thermal energy, raising fuel temperatures to supercritical thermodynamic conditions. Understanding and controlling fuel properties at these conditions will be crucial for avoiding thermal degradation and for subsequent processes within the combustor. Environmental concerns and the availability of petroleum supplies also will contribute to future propulsion system design and operational needs.

The purpose of this abstract has been to communicate AFOSR perceptions of research trends to the university and industrial research communities. However, communication from those communities back to AFOSR also is desirable and essential for creating new research opportunities. Therefore, all proposals and inquiries for fundamental research are encouraged even if the content does not fall within the areas of emphasis described herein. Comments and criticisms of current AFOSR programs also are welcome.

the contrary. Although mixing rate increases due to heating asymmetry have not yet been found in the parameter study, neither have noticeable decreases in mixing been detected. Figures 2 and 3 display the spreading rates and temperature contours of an M_c=.4 layer with and without heating. Normalized temperature contours ($T-T_\infty/T_\infty$) are shown only for the heated layer, since at the same contour resolution the unheated layer has no perceptible variation. The parameter values for the heat release are D=.002, b=1., σ=2. and c=.02. For these conditions the heat is released completely within the layer and the time averaged temperature rise of the fluid within the turbulent part of the flow reaches a centerline peak more than 30% greater than its unheated value. Yet the spreading rate, measured by the vorticity thickness δ_ω, is essentially unaffected. This case has not yet been analyzed in detail, but it indicates, along with the strong heat release cases reported in Reference 4, that there can be heat release scenarios without decreased mixing.

VARIATIONAL APPROACH TO HEAT RELEASE MAXIMIZATION

The desire is to maximize the volumetric heat release H

$$H = \int_{x=x_o}^{x_o+L} \int_{y=-\infty}^{\infty} h_f(\phi,\ \phi_x,\ \phi_y,\ \phi_{xx},\ \phi_{xy}\ldots?)\,dydx \qquad (5)$$

subject to the constraint that the velocity field satisfy Equation 1. The key here is to find plausible models to link the specific heat release h_f to the local velocity field (ϕ, ϕ_x, ϕ_y....). At this stage the research centers on functionals dependent upon streamline length and/or some positive definite function of the streamline curvature. These two quantities provide a characterization of the length and wrinkledness of interfaces between reactants, and the expectation is that the longer and more convoluted this interface the greater the total product formation and heat release. The variational problem involves finding a flow configuration that balances streamline convolution against the diffusive or averaging character of the potential flow constraint.

The first problem to be dealt with is the description of the streamline length and curvature in terms of the potential ϕ. By writing the formal expressions for arclength and curvature of the streamfunction $\psi(x,y)$ in terms of u and v and then substituting the appropriate expressions in terms of the potential ϕ, one obtains the length element as

$$S = \left[\ 1 + \left(\ \phi_y\ /\ \phi_x\ \right)^2\ \right]^{1/2} \qquad (6)$$

and the curvature K as

$$K = \frac{\phi_{xy}\ /\ \phi_x \left[\ 1 - \left(\ \phi_y\ /\ \phi_x\right)^2\ \right]}{\left[\ 1 + \left(\ \phi_y\ /\ \phi_x\right)^2\ \right]^{3/2}} \qquad (7)$$

Since the streamline length is a positive definite quantity a possible relation between it and heat release can be reasonably assumed. The curvature, on the other hand, may be negative, and thus the heat release can be connected to it only through some positive valued function of K. The magnitude of K is an obvious choice, but leads to analytical difficulties in obtainir g the appropriate Euler equation for the variational problem. Instead, it has been

INVESTIGATION OF THE LAMINAR FLAMELET MODEL OF TURBULENT DIFFUSION FLAMES

(AFOSR Grant/Contract No. NSF CTS-9021928)

Principal Investigator(s): George Kosály, James J. Riley

The Department of Mechanical Engineering, FU-10
The University of Washington
Seattle, WA 98195

SUMMARY OVERVIEW:

Our main target is the investigation of closure methods for reacting turbulent flow theory via direct numerical simulation and theoretical analysis. In order to judge the quality of our simulation the simulated results are tested against laboratory data. The researcher will help understanding the limitations of the different closure models, most importantly, the flame conditions that make the laminar flamelet approach applicable.

TECHNICAL DISCUSSION:

Our main target is the investigation of closure methods for reacting turbulent flow theory via direct numerical simulations (DNS) and theoretical analysis. Besides pursuing our main goal we have also performed further research on related topics. We list the subjects of our research and discuss the results briefly. (Reference numbers refer to the list of publications at the end of this document. The publications listed acknowledge support by NSF and AFOSR under NSF Grant No. CTS-9021928.)

• *Length Scale Dependence of Scalar Mixing.* In studies of turbulent reacting flow the scalar dissipation is often modeled as universal, i.e., independent of the initial conditions. Recently, Eswaran and Pope *(Phys. Fluids, 31,* 506, 1988) performed simulations in forced turbulence and found this universal behavior. The result, however, contradicts the laboratory findings of Warhaft and Lumley *(JFM, 88,* 659, 1978). Our investigations (Ref. 1) clearly show that the Eswaran-Pope result is due to the forcing of the turbulence, and should not be expected to hold in the decaying turbulence investigated in the laboratory.

• *Frequency Spectra of Reactant Fluctuations in Turbulent Flows.* Bilger et al. *(JFM,* to be published, 1992) measured auto-and cross-spectra of reactant fluctuations in a mixing layer. The coherence and the phase-shift versus frequency graphs show a characteristic structure that the authors could not explain. We have used the equilibrium and the frozen chemistry limits to explain the structure from first principles (Ref. 2).

• *Investigation of the Validity of the Stationary Laminar Flamelet Model (SLFM) and the Conditional Moment Closure (CMC) of Reacting Turbulent Flows.* The Stationary Laminar Flamelet Model was suggested by Peters as a valid model to account for radical superequilibrium *(Progr. Energ. Comb. Sci. 10,* 319, 1984). The model has been seriously challenged by Bilger *(Symp. Intl. Combustion, 22nd,* 475, 1989). The Conditional Moment Closure (CMC) has been independently suggested by Bilger *(Phys. Fluids,* to be published,1992) and Klimenko *(JFM,* submitted, 1992). We have performed preliminary simulations in homogeneous, decaying turbulence with a simple chemistry scheme (Refs. 3,4,5). The results indicate that SLFM does not represent substantial improvement over the equilibrium approach. However, CMC does an excellent job in a

Air Force Basic Research

Aerospace Sciences

Diagnostics Of Reacting Flow

Research Area	Trend	Decrease	Increase
Gas-Phase Measurements			Degenerate Four-Wave Mixing
Plasmas			Degenerate Four-Wave Mixing
Particle/Droplet Measurements			Supercritical Behavior - FY94 Init

CHEMICAL KINETIC AND AERODYNAMIC STRUCTURES OF FLAMES

(AFOSR Grant No. 89-0293)

Principal Investigator: Chung K. Law

Princeton University
Princeton, NJ 08544

SUMMARY/OVERVIEW:

The objective of the present program is to study the structure of laminar premixed and nonpremixed flames through (a) non-intrusive experimental determination in reduced and elevated pressure environments, (b) computational simulation using detailed flame and kinetic codes, and (c) asymptotic analysis for the reduced mechanisms. During the reporting period (1) a unified chain-thermal theory on the phenomena of flammability limits was formulated; (2) a five-step reduced mechanism was proposed for methane oxidation; (3) a compilation of the experimental laminar flame speed data as a centralized source of reference was performed; (4) the possibility of adiabatic flame stabilization due to flame stretch was demonstrated; (5) a review article on supersonic flame stabilization was published.

TECHNICAL DISCUSSIONS

1. A Unified Chain-Thermal Theory of Fundamental Flammability Limits

Although the term flammability limits has been extensively used to describe the failure of a flame to propagate in mixtures beyond a certain concentration, a clear and unique fundamental definition, which would also allow for its unambiguous theoretical and experimental determination, has yet to be identified. The configuration that is most suitable for the identification of such system-independent phenomena is the state at which the steady, one-dimensional, planar premixed flame in the doubly-infinite domain fails to propagate, as originally adopted by Spalding in his attempt to define such a limit. By introducing a volumetric heat loss rate into the energy equation, and by assuming a on-step overall reaction as well as conventional constant transport properties, subsequent analytical solutions yield an extinction state in terms of a "turning point" response of the mass burning rate to increasing heat loss, indicating the incipient loss of balance between heat loss and chemical heat generation. It is further shown that the ratio of the limit flame speed to the adiabatic flame speed is $e^{-1/2} = 0.61$.

The loss theory is inherently incapable of explaining the chemical kinetic dependence of the flammability limits, in terms of the frequently-present chain branching and termination mechanisms, on such system parameters as pressure, stoichiometry, and fuel type. In last year's report a chain-based approach was proposed, in which it was argued that competition between branching and termination reactions must be important to the weakly reactive flames close to the flammability limits. Thus, by numerically simulating the one-dimensional flame propagation with detailed chemistry and transport properties, but without radiative heat loss, a normalized sensitivity coefficient of the termination reaction to variations in the branching reaction can be calculated. This coefficient α, termed the flammability exponent, was found to assume a value close to unity in the vicinity of the experimentally-observed flammability limits of a great variety of mixtures.

It is clear that the heat loss theory of Spalding and our chain branching-termination criterion are based on completely different concepts and approaches, and that neither one is complete. These two concepts have since been unified. The approach towards such a unified treatment, with quantitative accuracy, is to numerically simulate the freely-propagating, one-

state. Figure 2 shows the peak temperature as a function of the strain rate, according to predictions of full and two-step chemistry. It is seen that the two-step chemistry give higher maximum temperatures, by as much as 200 K at the lower rates of strain, yet the extinction strain rates are nearly identical. Corresponding curves for three- and four-step mechanism lie between those plotted, giving a continual increase in temperature with reduction in mechanism [1]. Figure 3 gives the extinction strain rate predicted by full and two-step chemistry over a wide range of pressure. The effect of dilution on extinction strain rate, gives by the two-step approximation, and by the full chemistry, is shown in Fig. 4. A small deterioration of the agreement is seen at higher dilutions, signaling the onset of failure of two-step mechanism at low temperatures.

Figure 5 gives the representative temperature profiles as a function of the mixture fraction Z based on the element H. It is seen that the higher temperatures associated with the two-step approximation are restricted mainly to the region of maximum temperature. At higher rates of strain (near extinction) the temperature differences exist over a somewhat broader range of mixture fraction, but a narrower range of the physical coordinate y. Also shown in Fig. 5 for the higher rate of strain are the profiles of the scalar dissipation rate $\chi = [2\lambda/\rho c_p]\,(dZ/dx)^2$; the differences in predictions for full and two-step chemistry are less than the width of the line. The largest discrepancy between the predictions of full chemistry and reduced mechanisms occur in the radical concentrations as can be seen in Fig. 6.

A two-step chemical scheme for hydrogen-air diffusion flame retains all the essential features of the flame and is the minimum number of steps needed for satisfactory descriptions of these flames [4]. An asymptotic analysis that involved the two-step reduced mechanism was developed and the results from the analysis are shown in Table 1. Reasonable agreement was found for extinction strain rates, but there are large discrepancies in radical-concentration predictions, as expected. Future work is intended to address influences of chemistry on the asymptotic structure of hydrogen-air diffusion flames. Effects of boundary conditions on extinction strain rates have to be investigated. Numerical simulation of flame structures with one-step chemistry, and ignition characteristics of hydrogen-air mixtures also have to be performed.

Feed Conditions	Z_{H_m}		Reduced Temperature		Normalized H Concentration		$a\,(s^{-1})$	
	Asy.	Num.	Asy.	Num.	Asy.	Num.	Asy.	Num.
Undiluted ($P = 1atm$)	0.3638	0.03528	0.4069	0.4720	0.2266	0.1263	7006	8140
Diluted ($P = 1atm$) (75% Mole Frac. H_2)	0.3378	0.1564	0.4073	0.4997	0.2164	0.0895	5264	6940
Diluted ($P = 1atm$) (50% Mole Frac. H_2)	0.3498	0.2944	0.4263	0.5541	0.2144	0.0545	3422	4850
Undiluted ($P = 10atm$)	0.3782	0.03613	0.4759	0.6555	0.1959	0.1218	269,000	118,650

Table 1: Results from Asymptotic Analysis

Nonpremixed Flames in Stagnating Turbulence

The greatest advances in combustion are obtained when a close coordinate among theory, computation and experiment can be effected. Unfortunately this synergism is seldom achieved for a variety of reasons. Thus there exists at present considerable interests in flames in stagnating turbulence since they provide a means for realizing such coordination. They are relatively easy to establish in the laboratory, provide ready access for instrumentation and are free of wall and other contaminating effects. Moreover, the entire range of chemical behavior from near equilibrium to extinction can be studied by altering the mean rate of strain imposed on the flame, i. e. by changing the rate of flow from the exit of the jets. Thus the problems of ignition and extinction, so important in high-speed combustion, can be examined experimentally. From the theoretical point of view these flames are described by ordinary differential equations with a resultant enormous simplification.

The initial experiments and theory of these flames relate either to a single turbulent reactant stream

3. Compilation of Laminar Flame Speed Data

A useful approach in improving or validating a certain chemical kinetic mechanism is to compare the calculated results with the experimental data. The comparison can be conducted either at the global level of the bulk flame responses, such as the laminar flame speed, or at the detailed level, which also includes the temperature and species profiles across the flame. Because of the difficulty in experimentally obtaining the various profiles, much of the comparisons have only involved the flame speed.

Early comparisons were complicated by the scatter and uncertain accuracy of the experimental data. The most serious source of error was probably caused by the coupled effects of stretch and preferential diffusion, which can lead to systematic shifts in the measured flame speed depending on the specific experimental methodology and even mixture stoichiometry. Unaware of such experimental and phenomenological subtleties, some kinetic mechanisms have been either incorrectly "validated" or unjustifiably "calibrated".

Recognizing the importance of stretch, a counterflow flame technique was developed with support from the present program and nearly stretch-free flame speed data of mixtures of hydrogen, methane, the C_2-hydrocarbons, and propane have been determined with extensive variations in stoichiometry and pressure. Upon request from many of our colleagues, these data have been consolidated and re-plotted in a uniform format.

The compilation is reported in Publication No. 3.

4. Adiabatic Flame Stabilization

The mechanism with which a Bunsen flame is stabilized at the burner rim is generally considered to be well established. The concept of stabilization is based on the existence of a dynamic balance between the local flow velocity and flame velocity at a certain point on the flame surface, and the ability of the flame to adjust its flame velocity, and thereby the location of stabilization, through heat loss to the rim. Blowoff occurs when such a balance cannot be achieved everywhere over the flame surface. This mechanism has also served as the fundamental concept in flame stabilization through heat loss to the stabilization body in other practical situations.

However, recent studies on the dynamics of stretched flames have shown that, in addition to heat loss, the flame speed can also be modified by flow nonuniformity, flame curvature, and mixture preferential diffusion. It is, therefore, of interest to explore the possibility that flame stabilization can be achieved in the absence of heat loss due to these additional mechanisms. The configuration adopted for investigation is the inverted flame because of its symmetry. By measuring the temperature distribution in the stabilization region, we conclusively demonstrated that the flame can indeed be stabilized in the absence of heat loss. We subsequently formulated a theory that satisfactorily describes the stabilization of this adiabatic flame through the combined influence of flow nonuniformity and flame curvature.

It may be emphasized that the concept and methodology developed in this study will be useful in further studies of flame stabilization in combustors, as well as the quenching of laminar flamelets constituting turbulent flames.

This work is reported in Publication No. 4.

5. Mechanisms of Flame Stabilization in Subsonic and Supersonic Flows

This is an invited review paper discussing current understanding on the fundamental physico-chemical mechanisms governing the structure and stabilization of premixed and nonpremixed flames in subsonic and supersonic laminar and turbulent flows, with emphasis on possible applications in supersonic propulsion. Specific topics discussed include the design concepts of supersonic engine operation and fuel injection, the ignition of combustibles in homogeneous and diffusive media, the extinction of premixed and nonpremixed flames through reactant leakage, heat loss and aerodynamic stretching, the stabilization and liftoff of burner-stabilized and jet flames. Research topics of potential importance to supersonic combustion are suggested.

This review is designated as Publication No. 5.

6. Studies on High-Pressure and Unsteady Flame Phenomena

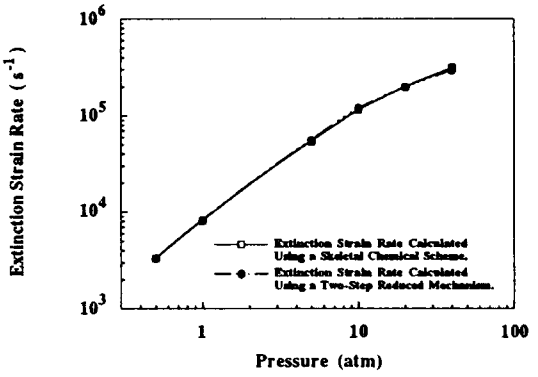

Figure 3: The dependence of the air side extinction strain rate on the pressure for axisymmetric counterflow mixing of hydrogen with air with $T_{-\infty} = T_{\infty} = 300K$ calculated using full chemistry and two-step chemistry.

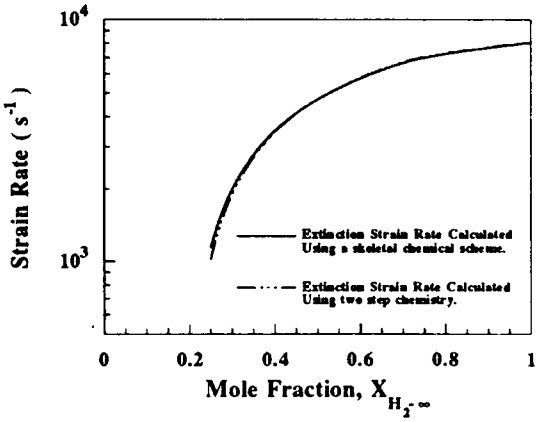

Figure 4: The dependence of the air-side extinction strain rate on the hydrogen mole fraction in the fuel stream for axisymmetric counterflow mixing of hydrogen-nitrogen mixtures with air at $T_{-\infty} = T_{\infty} = 300K, p = 1$ atm.

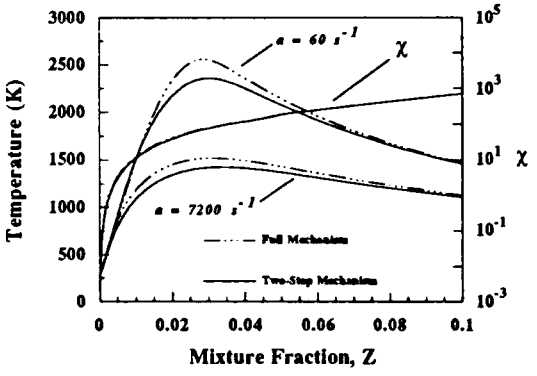

Figure 5: The variation of the temperature with the mixture fraction for full and two-step chemistry with $T_{-\infty} = T_{\infty} = 300K, p = 1$ atm, at two strain rates, and the variation of scalar dissipation at the higher strain rate.

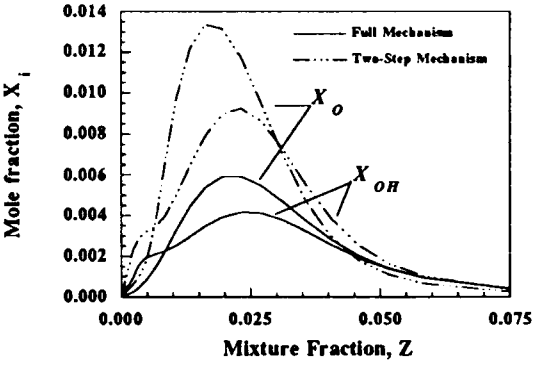

Figure 6: The variations of the O-atom and OH-radical mole fractions with the mixture fraction for full and two-step chemistry with $T_{-\infty} = T_{\infty} = 300K, p = 1$ atm and $a = 7200\ s^{-1}$.

SPACECRAFT INTERACTION WITH AMBIENT AND SELF-GENERATED PLASMA / NEUTRAL ENVIRONMENT

AFOSR Grant Contract No. F49620-90-C-0051DEF

Principal Investigator: Torkil S. Mogstad

McDonnell Douglas Space Systems Company
5301 Bolsa Ave., Huntington Beach, CA 92647

SUMMARY

Exposed high-voltage power systems in space may undergo electrical breakdown and arcing at certain conditions. Arcing, followed by sputtering of surface materials and in some cases subsequent redeposition on sensitive surfaces (e. g., arrays, radiators, sensors), reduces both operational efficiency and lifetime of space systems. A physical model of the microscopic arcing process has been developed at MIT under a related AFOSR grant. This model, combined with the local neutral/plasma parameters, allows predictions to be made concerning arcing voltage thresholds and arcing rates. The research reported on here focuses on developing theoretical and computational models of the self-induced neutral/plasma environment at high-voltage surfaces. The models have been used to predict the environments around existing high-voltage power space systems, but can also be used to predict the environments around future systems. By understanding and predicting detrimental arcing, space systems can be designed and built for higher operational efficiencies and lifetimes.

INTRODUCTION

Effluents released from spacecraft thruster operations will generate a self-induced neutral/plasma environment that may affect spacecraft operations. From space and ground testing it is known that electrically biased surfaces break down and arc at a certain voltage threshold. Arcing thresholds and frequencies are functions of the local neutral/plasma environment and there is a need to predict the self-induced environment in the vicinity of high-voltage surfaces.

For negatively biased solar cell interconnects, it is observed that below a critical voltage, arc discharges occur on the solar array. Negative voltage thresholds ranging from 200 to several 100 V have been observed in ground-based tests [Ref. 1]. The flight data from the PIX I and II space experiments shows arcing occurring at -700 V [Ref. 2]. Recent ground testing of Space Station Freedom (SSF) anodized aluminum samples have demonstrated arcing at around -100 V.

The 75 kW needed for SSF will be supplied at high voltage and low current to minimize resistive losses and the mass of cabling and harnesses. The SSF solar arrays will be operating at 160 volts; this is significantly higher than the voltage drops on currently used arrays, which range from 28 to 75 V. Future space power systems are expected to operate at even greater voltage drops.

A microscopic arcing mechanism has been proposed by *Cho and Hastings* [Ref. 3]. Their theory indicates that the arcing threshold voltage depends on the local neutral density, but is independent of the local plasma density. If, however, arcing is triggered, the arc rate will be sensitive to the local plasma density. This is our motivation for modeling the local neutral/plasma environment around the space system.

Plasma Properties in the Thruster Exhaust Field

The plasmas being ejected from arc and MPD arc devices have been categorized in a number of research studies. In 1985, an MPD arc thruster was operated at AFAL and diagnosed with Langmuir probes developed by the principal investigator; results indicated Te = 2eV at 25 cm, while Ne = 4.48 x 10^{15} at 20 cm and Ne = 1.9 x 10^{15} at 30 cm.

The new diagnostics will be applied to a 1/4-scale arc and MPD arc thruster which generates plasmas with Te=.5-2.0 eV and Ne=10^{13}-10^{15}cm^{-3} between source and field separation in the exhaust flow.The magnitudes of plasma properties are critical when utilizing a successful, new diagnostic system.

PROPOSED RESEARCH STUDIES

The effort to study plasmas thursters with new diagnostics can involve three different diagnostic measurements with the CO_2 laser based system: (1) multi-beam interferometry to map electron density; (2) electron density fluctuation studies; and (3) Faraday-rotation measurements of local B-field. Each of these has its own inherent difficulty; i.e., this is not an application of off-the-shelf type techniques, but the application of relatively recently demonstrated techniques which will require careful experimental design to match the plasma and unique optical and electronic components to produce the desired results. The first effort, with a preponderent percentage of the work being carried by a graduate student researcher, has concentrated on the simpler interferometer technique in order to provide a base for other work and to optimize research output. Accordingly, while the other techniques (2 and 3) are receiving careful and complete evaluation with respect to experiment design, emphasis has been directed to accomplishing measurements with the multi-beam interferometer.

condition. The electron density is set equal to the total ion density at each time step. This assumes that electrons are available to neutralize the local plasma at all times. For the SSF solar array case, we were concerned with ionization on time scales on the order of the effluent propagation time passed the arrays. For thruster exit velocities on the order of 3 km/s, and array dimensions of 10 m, it takes the neutral effluents about 3 milliseconds to blow past the array; that is also the time extent of the continuity equation flux solver. Ionization occurring later on, will not influence the local environment and the arcing characteristics at the array surface.

Figure 3 shows the modeled total ion distribution along the solar array for a 25 lbf monoprop thruster operating into the wake. The array is located about 5 m off the thruster axis, and extends about 10 m downstream of the thruster exit plane. Total ion densities along the array are as high as $3x10^7$ cm^{-3}, which is 13 times the initial ambient O^+ density. The relatively slow neutral effluents (3 km/s) lose electrons via charge exchange to the faster O^+ (7.7 km/s), thus generating a local plasma of ionized effluents. Figure 4 shows how the O^+, entering from the left, has been depleted downstream of the thruster exit plane through ion-molecule reactions.

In order to simulate CVI, we have also simulated a Shuttle 25 lbf biprop thruster firing across the arrays, but this time into the ram. Effluent velocities with respect to the ambient plasma are now as high as 10.7 km/s; subsequently, both CO_2 and N_2 experience CVI. The results, which are shown in Figure 5, indicate that ion densities along the array reach levels of 10^{10} cm^{-3}, which is a four order of magnitude increase over the initial ambient O^+ density. For this run we assumed that there was an infinite supply of electrons to keep the plasma overall charge neutral; since this is not strictly true, we suspect that the induced ion density is lower than the 10^{10} cm^{-3}. We are currently modifying our models to correctly model the electron distribution.

IMPACTS ON ARCING

According to the arcing mechanism proposed by *Cho and Hastings* [Ref. 3], the arc rate is linearly proportional to the local ion density at negative voltages below approximately -400 V. This indicates that any arcing on the SSF solar arrays (-160 V) will be insensitive to ion density. If, however, the arrays were operating at more negative voltages, the arc rate would increase about one order of magnitude during operation of the 25 lbf monopropellant thrusters. The thruster induced neutral density build-up along the SSF arrays (-160 V) is not likely to trigger arcing. For arrays operating at more negative voltages, the increased neutral density may trigger arcing.

REFERENCES

1. Hastings, D. E., G. Weyl, and D. Kaufman, "Threshold Voltage for Arcing on Negatively Biased Solar Arrays", *J. Spacecraft, 27,* 539, 1990.

2. Grier, N. T., and N. J. Stevens, Plasma Interaction Experiment (PIX) Flight Results, Spacecraft Charging Technology - 1978, NASA Conference Publication 2071, AFGL-TR-79-0082, p. 295.

3. Cho, M., and D. E. Hastings, Dielectric Charging Processes and Arcing Rates at High Voltage Solar Array, AIAA-Paper 91-0605, Presented at 29th Aerospace Sciences Meeting, Jan. 1991, Reno, NV.

4. R. Biasca, MIT (currently Phillips Lab/Hanscom AFB), private communication.

Where P_o is incident power, r_e is electron radius, λ_o is incident wavelength, $\tilde{N}$ is defined by $\tilde{N}$ cos (kZ-wt) and L_v is the length of the scattering volume. CO_2 lasers with 10-100 W can be used, and that application is intended here following electron density determinations by interferometry. Also, FIR lasers generating 119 μm at 10-100 mW output power levels have been sufficient to perform scattering measurements from electron density fluctuations with good signal-to-noise ratios. One critical element in this type of measurement is a low-noise fundamental mode mixer. Fluctuation measurements over a range of frequencies have been made with plasmas similar to those expected in MPD exhaust flows.

Faraday Rotation Measurements of B field - Polarimetry

The determination of local, unperturbed magnetic field is quite difficult; all experimenters use physical loops placed in the plasma. This disturbs the medium, cools the plasma, and alters the current conduction path; a nonintrusive technique is quite valuable. Through Maxwells' equation, the local current density can also be determined. The basic principle of this measurement is that the plane of polarization of a laser beam will be rotated proportional to B,

as $$\theta\ (deg) = 1.5 \times 10^{-12} \lambda_o^2 \int_o^l NeB_{11}\,(kG)\,dl$$

Clearly, a large λ_o will allow significant Θ to be generated even though B_{11} (the component of B along propagation) will be small. Specifically with Ne $\simeq 10^{15}$ cm^{-3} and $\ell \simeq 10$ cm, the θ with CO_2 radiation would be very difficult to measure. However, using 118.8 μm will produce a rotation of greater than 1 degree. It can be seen that the signal involves the product, Ne B_{11}, so the results from the CO_2 measurement of Ne(r) will be critical to accurate determination of B_{11}(r) profiles.

NUMERICAL STUDIES FOR THE RAM ACCELERATOR

AFOSR-MIPR-92-0017

Elaine S. Oran, Chiping Li, K. Kailasanath, and Jay P. Boris

Laboratory for Computational Physics, Code 4400
Naval Research Laboratory, Washington, DC 20375

SUMMARY/OVERVIEW

Time-dependent, multidimensional Euler and Navier-Stokes reactive-flow simulations have been performed to help resolve basic issues in the development of the ram accelerator. Studies of the past year have focused on obtaining a comprehensive understanding of the structure and stability of oblique detonations generated by supersonic flows over wedge-shaped projectiles. The simulations show that the multidimensional detonation structure consists of the following elements: (1) a nonreactive, oblique shock, (2) an induction zone, (3) a set of deflagration waves, and (4) a "reactive shock" in which the shock front is closely coupled with the energy release. This structure is stable and resilient to disturbances in the flow for a wide range of flow and mixture conditions. Parameter regimes investigated include a range of wedge angles, mixture ratios, and viscosities. The conditions under which the overall detonation structure becomes unstable have also been identified. The limitations of several global approaches to including viscous effects and their effect on the overall detonation structure are now being investigated.

TECHNICAL DISCUSSION

In the ram accelerator, a projectile which resembles the center-body of a ramjet travels through a premixed fuel-air mixture. When the projectile travels at supersonic speeds, oblique shocks are formed which may ignite the mixture and lead to oblique detonations. Because of the very rapid conversion of chemical energy to high pressures, detonations present an interesting alternative to usual forms of energy conversion in such propulsion systems. However, in order to maximize performance, the oblique detonation must be generated and stablized at appropriate locations in the system. Therefore, successful development of such systems depends on knowledge of the structure of these detonation waves and understanding the related physical and chemical processes.

The problems of achieving detonation stability on a projectile are complex and nonlinear. Whereas many aspects of the steady-state problem may be addressed by theoretical analyses and thermodynamic considerations, the fundamental multidimensional time-dependent structure of the complex reactive flow must be addressed computationally. Our approach in this project has been to consider both the fundamental numerical and physical issues related to modeling these flows and then to use simulations to study the detailed structure of oblique detonation waves and investigate the role of relevant factors such as viscosity and the amount of energy release on the stability of the detonation.

The basic configuration is supersonic flow of a premixed fuel-air mixture over a wedge, as shown in Figure 1. The large number of simulations we have performed can be classified into investigations of the basic structure of oblique detonations, structures in different mixtures; effects of shock strength, stability of the detonations, and effects of viscosity.

Basic Structure of Oblique Detonations

The simulations show a basic multidimensional detonation structure whose essential configuration is independent of the flow and mixture conditions, although, depending on mixture conditions, the scale of the structure may change by several orders of magnitude. A schematic of this basic structure, Figure 2, shows the following elements: (1) a nonreactive, oblique shock, (2) an induction zone, (3) a set of deflagration waves, and (4) a "reactive shock" in which the shock front is closely coupled with the energy release. This reactive shock is significantly steeper than the original, nonreactive oblique shock in front of the induction zone near the wall. The larger angle of the reactive shock accommodates the change in the flow direction as well as the rapid heat release. Also, the velocity is lower and the

experiments discussed here the "cylinder" was a vertically directed laminar jet of helium which was injected into the 25 cm square test section of a 43-cm shock tube. The interaction between a 1-cm diameter helium jet and shock waves with Mach numbers in the range 1.05 to 2.0 were studied and the concentration field generated by shock impingement on the jet has been observed by use of a Rayleigh scattering technique. In each experiment, the distortion of the helium cylinder was recorded by a cooled CCD camera. The size of the jets, the exposure time of the laser pulse and the density of the pixel array allowed the diffusion process to be resolved in time and space. Thus, the Rayleigh scattering technique has allowed us for the first time to make quantitative measurements of the mixing process.

This study has been carried out by Dr. John Budzinski in experiments in which the primary experimental parameter was the Mach number of the incident shock. In addition, the influence of the passage of a second shock over the developing light gas structure, and the effects of the initial density ratio and pressure have been investigated.

For applications to propulsion systems, the mixing rate between the light and heavier air is the critical factor. The degree of mixing can be described in terms of a parameter which is the total mass of light gas which is in regions in which its concentration is higher than some target value. The value of this parameter normalized by its initial value, gives a parameter called m which is a convenient measure of the mass of unmixed light gas. For hydrogen-air combustion, the stoichiometric fuel-air ratio gives a mole fraction for hydrogen of about 30% and this was taken as one target value in our study. The rate of mixing is characterized by describing the decrease of m with time. Finally, these results can be applied to real systems when scaling laws for the time scale measured in the shock tube experiments can be described as a function of the parameters of the system such as the Mach number of the shock, the speed of sound in the chamber and the size of the original hydrogen jet.

Budzinski has found that the value of m can be reduced from 1.0 at the start of the interaction to values of 0.5 within a few milliseconds for interactions with a single shock with Mach numbers in the 1.1 to 1.5 range. Qualitative data are also available for Mach 2.0 shocks, but the Rayleigh scattering technique could not be successfully applied here because of pressure limitations fixed by the structure of the test section.

A time scale parameter has been developed which correlates the time dependence of the parameter m. This scaling law is based on the experimental results and the computations of Dr. J. Yang which were also carried out under this program. This time scaling process also correlates the time required for the vortical structures, formed by the interaction of the shock with the light gas, to develop toward a steady state. Thus, this scaling model can be used to determine the times required for the structures to develop and the mixing to occur for the conditions expected in a combustion chamber in which heat is added in a supersonic flow, such as the combustion chamber for the NASP engine. Fortunately, our estimates show that the time required for the shock enhancement process to occur is much less than the expected residence times of gas within such combustion chambers.

The results obtained by Budzinski are available now as a PhD thesis and several papers are in preparation.

The computational results of Yang are being used now to aid our analysis of the experimental data used to predict mixing. Given the fact that only numerical diffusion is present in the Euler codes used by Yang, we are interested in making a determination of the degree to which they can be used to predict the results of the experiments. The time scaling model mentioned above is one result of this ongoing effort.

Wind Tunnel Experiments: Studies are being carried out in a Mach 2.6 flow to investigate the mixing produced by shear forces when a hydrogen jet embedded in an air stream passes through a shock wave. The effects of the shear on the shock-induced mixing process are not modeled in the shock-tube

Oblique Detonations in Ram-Accelerators, C. Li, K. Kailasanath, and E.S. Oran, to appear, Proceedings of the *28th JANNAF Combustion Meeting*, CPIA, 1991.

Stability of Oblique Detonations in Ram Accelerators, C. Li, K. Kailasanath, and E.S. Oran, AIAA Paper 92-0089, American Institute of Aeronautics and Astronautics, Washington, DC, 1992.

Detonation Structures behind Oblique Shocks, C. Li, K. Kailasanath, and E.S. Oran, submitted to *Physics of Fluids*, March, 1992.

Effects of Boundary Layers on Oblique Detonation Structures, C. Li, K. Kailasanath, and E.S. Oran, submitted to the AIAA 31st Aerosapce Sciences Meeting, Reno, NV, January, 1993.

Additional Presentations

A Uniform Algorithm for Boundary and Interior Points and its Application to Supersonic Flow Simulations, C. Li, E.S. Oran, and J.P. Boris, Conference on Parallel Computational Fluid Dynamics, Indianapolis, May, 1990.

The Microscopic and Macroscopic Physics of Detonations, E.S. Oran, invited presentation, University of Washington, Applied Mathematics Colloqium, Seattle, WA, March 1992.

Microcopic and Macroscipic Physics in Detonations, E.S. Oran, invited presentation, Los Alamos National Laboratory, Los Alamos, NM, April, 1992.

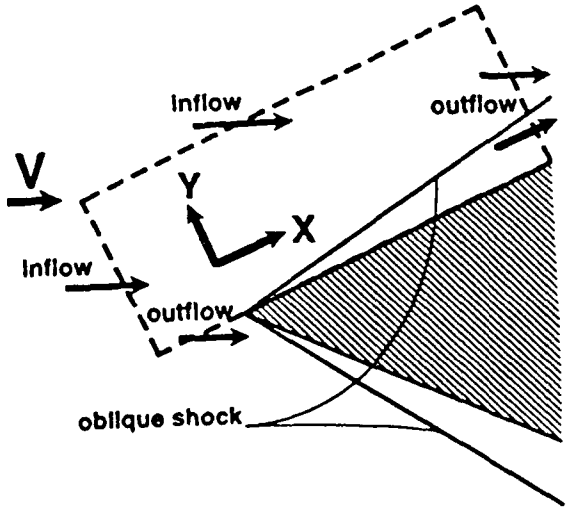

Fig. 1. The Computational Domain

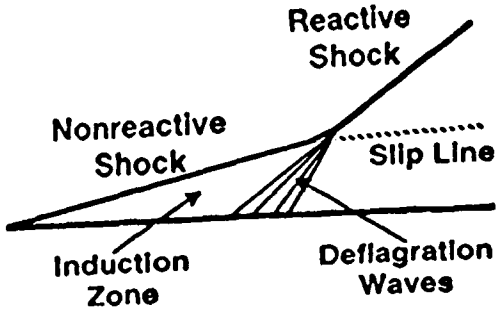

Fig. 2. The Basic Structure of Oblique Detonations

We are now examining data sets obtained with 36 operating conditions which include inlet velocities of 21, 30, and 35 m/s; fuel air ratios fraction of stoichiometric of 1.0, 1.2 and 1.4; combustion chamber depths of 2.5, 5.0 and 10 cm; and several mixtures of methane and hydrogen as fuel. Each data set includes shadowgraph movies at 5,000 Hz, video movies of chemiluminescence at 3,000 Hz, and velocity, pressure and temperature data obtained at about 12,500 Hz.

Data obtained with these techniques are being analyzed now to find the downstream motion and rate of growth of the vortex, the delay time between vortex shedding and the ignition of the vortex fluid, and the time required for completion of the combustion of the body of the vortex as a function of the initial velocity and pressure perturbations, the mean flow speed, and the fuel-air ratios.

Results obtained prior to the acquisition of the video movies of the chemiluminescence are reported in Zsak et al (1991). The data suggest that stretching of the interface between the hot products and the combustible mixture by the rapid growth of the vortex may inhibit combustion at the interface.

PAPERS:

Budzinski, J. M., "Planar Rayleigh Scattering Measurements of Shock-Enhanced Mixing," California Institute of Technology PhD Thesis, June 1992.

Budzinski, J. M., Marble, F. E., Zukoski, E. E., "Planar Rayleigh Scattering Measurements of Shock-Enhanced Mixing," Presentation at the 28th Joint Propulsion Conference sponsored by the AIAA/SAE/ASME/ASEE.

Jacobs, J. W., "The Dynamics of Shock Accelerated Light and Heavy Gas Cylinders," submitted to the *Physics of Fluids*.

Jacobs, J. W., "Shock Induced Mixing of a Light Gas Cylinder," *J. Fluid Mech.*, 234, 629-649, 1992.

Yang, J., Kubota, T. and Zukoski, E. E., "An Analytical and Computational Investigation of Shock-Induced Vortical Flows," AIAA Paper 92-0316, presented at the 30th Aerospace Sciences Meeting and Exhibit, Reno, NV, Jan., 1992.

Zsak, T. W., Kendrick, D., Sterling, J. D. and Zukoski, E. E., "An Investigation of Reacting Vortex Structures AssociatedWith Pulse Combustion," Proceedings of The International Symposium on Pulsating Combustion, Vol. 1, August 5-8, 1991, Monterey, CA.

MAPPING CLOSURES FOR TURBULENT COMBUSTION

AFOSR 91-0184

Principal Investigator: S.B. Pope

Cornell University
Ithaca, NY 14853

SUMMARY

An important process in turbulent combustion is mixing (coupled with reaction) which occurs dominantly on the smallest scales. In statistical models of turbulent combustion, convection and reaction can be treated without approximation, while mixing must be modelled. Research is being performed to extend the applicability of Mapping Closures to address this problem. Progress has been made on two topics: extension of the particle implementation of the mapping closure to multiple composition; and, the computational implementation of the mapping closure for a composition and its gradient.

INTRODUCTION

A simple way to understand the theoretical problem of turbulent combustion is to consider how (at a given point) the fluid composition changes with time. There are three processes that cause this change: convection, reaction, and molecular diffusion. In pdf methods the first two of these processes are treated exactly, while the third—molecular diffusion—has to be modelled. Many other theoretical and experimental studies lead to the same conclusion: the major current issue in turbulent combustion is to understand and model the effects of molecular diffusion.

A most promising recent advance is the development of *mapping closures* (Chen et al. 1989, Kraichnan 1990, Pope 1991, Gao 1991). This is a new formalism that yields "constant-free" pdf closures. In its initial application to the marginal pdf of a scalar (Pope 1991) the accuracy of the mapping closure has been remarkable.

For simple test cases, analytic solutions to the mapping-closure equations can be obtained. But for application to inhomogeneous flows of practical importance, the closure needs to be implemented as a particle method. For a single scalar, a particle-implementation has been developed by Pope (1991). The first topic reported (in the next section) is an attempt to extend this to multiple scalars.

The first contribution that has been made is an attempt to extend this to multiple scalars. This topic is described more fully in the next section.

The second topic that has been addressed concerns the joint pdf of composition and its gradient. The addition of the composition gradient—compared to pdf methods currently

Dr Clifford Bedford
SRI International
Chemistry Laboratory
Menlo Park CA 94025
(415)859-4449

Dr S J Bennett
Adv Technology Projects Div
Morton Thiokol, Inc, Wasatch
Box 524
Brigham City UT 84302
(801)863-2980

Dr Greg Berry
Argonne National Laboratory
9700 South Cass Avenue
Argonne IL 60439
(312)972-6160

Dr Oscar Biblarz
Department of Aeronautics
Naval Post Graduate School
Monterey CA 93943-5100
(408)646-2972
AV878-2972

Mr Robert Biggers
OLAC PL/XRX
Stop 24
Edwards AFB CA 93523-5000
(805)275-5241
AV525-5341

Dr S Binkley
Combustion Research Facility
Sandia National Laboratories
Livermore CA 94551-0969

Dr Mitat Birkan
AFOSR/NA
Bolling AFB DC 20332-6448
(202)767-4938
AV297-4938

Dr Fred Blomshield
Code 3892,Propulsion
Research Branch
Naval Weapons Center
China Lake CA 93555
(619)939-3650
AV437-3650

Dr Arthur Bracut
ARDC
LCWSL
Dover NJ 07801
(201)724-3788
AV880-3788

Dr Mel Branch
Mechanical Engineering Dept
University of Colorado
Boulder CO 80309-0427
(303)492-6318
(303)492-7151

Dr John Brandenburg
Mission Research Corporation
8560 Cinderbed Road
Suite 700
Newington VA 22122
(703)339-6500

Dr Thomas Brill
University of Delaware
Department of Chemistry
Newark DE 19716
(302)451-6079

Dr Robert Brown
United Technologies Corp
Chemical Systems Division
P. O. Box 49028
San Jose CA 95161-9028
(408)778-4680

Dr James Bryant
Naval Weapons Center
China Lake CA 93555-6001
(619)939-7206
AV437-7206

definition, this is the set of edges joining the points, such that all points are connected, with the $N-1$ edges chosen (out of the N^2 possibilities) so that their total length is minimal. By this construction, one or more neighbors are identified for each particle, and hence evolution equations analogous to Eq. (2) can be constructed.

In testing this basic model, a deficiency was uncovered that has led to the development of a refinement. In the basic model, as mixing proceeds, it is found that the particles tend to cluster in strands in composition space. In the refined model, on each time step Δt, the particles are randomly divided into $N^{1/2}$ sub-ensembles of $N^{1/2}$ particles each. Then the EMST is formed for each sub-ensemble, and the mixing proceeds (for the time Δt) as before.

It is readily shown that as Δt tends to zero, the above method converges to a deterministic model in which each particle shares an edge with *many* neighbors (not just the 1-3 typical of the basic method). As an illustration, for the same particle properties used in Figure 1, Figure 2 shows the edges incident on a particular particle from 10 EMST's.

Although testing is far from complete, it appears that the qualitative performance of the model is satisfactory in all respects. It is hoped that it can be analyzed to determine a more precise connection with mapping closures.

Future work includes the testing of the model against DNS data for turbulent reactive flows, and its use in conjunction with PDF methods to calculate the properties of turbulent flames.

REFERENCES

Chen, H., Chen S., and Kraichnan, R.H. (1989) Phys. Rev. Lett., **63**, 2657.

Gao, F. (1991) Phys. Fluids A, **3**, 511.

Kraichnan, R.H. (1990) Phys. Rev. Lett., **65**, 575.

Peters, N. (1984) Prog. Energy Combust. Sci., **10**, 319.

Pope, S.B. (1990) Twenty-third Symp. (Int'l.) on Combust., The Combustion Institute, p. 591.

Pope, S.B. (1991) Theoretical and Computational Fluid Dynamics, **2**, 255.

Dr Fan-Bill Cheung
Penn State University
208 Mechanical Engineering
University Park PA 16802
(814)863-4281
FAX 865-3389

Dr Peck Cho
Dept. of Mechanical Engg.
College of Engineering
Michigan Technological Univ.
Houghton MI 49931

Dr Won-Ho Choe
214 Nuclear Engineering Lab
University of Illinois
103 South Goodwin Avenue
Urbana IL 61801
(217)333-2821

Dr Chan K Choi
Purdue University
School of Nuclear Engrg
West Lafayette IN 47907
(317)494-6789

Dr Edgar Choueiri
Department of Mechanical And
Aerospace Engineering
Princeton University
Princeton NJ 08544-5263
(609)452-5221

Dr Karl Christe
Rocketdyne Division
Rockwell International
6633 Canoga Ave
Canoga Park CA 91304
(818)710-3268

Dr T J Chung
University of Alabama
Huntsville AL 35801
(205)895-6394

Dr George Clark
Aerojet Tactical Systems
PO Box 13400
Building 0525
Sacramento CA 95813
(916)988-6919

Dr William Clark
Naval Weapons Center
Code 3895
China Lake CA 93555-6001

Dr Ronald Cohen
The Aerospace Corporation
PO Box 92957
Mail Stop M5-754
Los Angeles CA 90009
(213)336-5946

Dr Norman Cohen
Aerospace Corporation
PO Box 92957
M/S 747
Los Angeles CA 90045
(213)648-7427

Dr Norman Cohen
Professional Services
141 Channing St
Redlands CA 92373
(714)792-8807

Dr Cliff Coon
Lawrence Livermore National
Laboratories
Livermore CA 94550
(415)422-6311

Mr Robert Corley
OLAC PL/DYC
Stop 24
Edwards AFB CA 93523-5000
(805)275-5353
AV525-5353

A STUDY OF MIXING AND COMBUSTION IN THE PRESENCE OF A STRONG STREAMWISE VORTICITY

(AFOSR Grant No. F49620-92-J-0224)

M. Samimy and L. A. Kennedy

Department of Mechanical Engineering
The Ohio State University
Columbus, Ohio 43210

SUMMARY/OVERVIEW

Under this AFSOR grant, which is just getting started, we will be investigating the effect of passively generated streamwise vortices on the mixing process in a model combustor. Initially noncombusting but eventually combusting flow experiments will be conducted. Streamwise vortices of different strength will be generated and various diagnostics from planar filtered Rayleigh/Mie scattering to laser velocimetry techniques will be utilized to explore the nature of these vortices and their effect on the mixing process.

TECHNICAL DISCUSSION

Mixing is an important phenomena in all combustion systems from coal fired boilers, to furnaces, to gas turbine engines. How quickly and how well a fuel and oxidant can be mixed will have a major influence on the combustion efficiency, heat release rate, pollutant formation, combustor size and other pertinent parameters. It is widely accepted that the vorticity dynamics greatly impact mixing process. The streamwise vortices passively generated in flows, in addition to spanwise vortices or vortex rings, have been found to mix fluid streams quickly and efficiently. One of the devices that is used to produce streamwise vortices is called a lobed mixer. Many studies have shown that a lobed mixer used as a mixer nozzle in a gas turbine engine efficiently mixes the hot and cold fluid streams and can even produce additional thrust.

The research effort under this AFOSR grant is designed to study the detailed mixing mechanisms of an axisymmetric lobed mixer. The emphasis will be on the influence of the streamwise vortices on the flow through a concentric geometry with the streamwise generated using the inner tube. Various flow visualization techniques and quantitative turbulence measurements will be utilized. The work is divided into noncombusting and combusting tests. The noncombusting tests will be performed at the Ohio State University, while the combusting tests are planned to be performed at Wright Research and Development Center, Wright-Paterson Air Force Base.

Dr John Fischer
Code 3853
Naval Weapons Center
China Lake CA 93555-6001
(619)939-1641
AV437-1641

Dr J E Flanagan
Rocketdyne
6633 Canoga
Canoga Park CA 91304
(818)710-2466

Dr Gary Flandro
School of Aerospace Engg.
Georgia Institute of Tech.
Atlanta GA 30332-0420
(404)853-9160

Dr James Fong
Aerojet Tech Systems
P O Box 13222
Sacramento CA 95813

Dr Arthur Fontijn
Chemical & Environmental
Engineering Department
Rensselaer Polytechnic Inst.
Troy NY 12180-3590
(518)276-6508

Dr Milt Frankel
Rocketdyne
6633 Canoga Avenue
Canoga Park CA 91304
(818)710-4803
(818)710-5088

Dr R A Frederick
Sverdrup Technology, Inc
Mail Stop 900
Arnold AFB TN 37389-9998
(615)454-3130

Dr Sheilah Fultz
Naval Weapons Center
China Lake CA 93555-6001
(619)939-7521
AV437-7521

Dr Eugene Gerber
Univ of Dayton Research
Institute
KL465
Dayton OH 45419
(513)229-3221

Dr Robert Ghirardelli
U.S. Army Research Office
P.O. Box 12211
Research Triangle Pk NC 27709-2211
(919)549-0641
AV935-3331

Dr David Golden
SRI International
333 Ravenswood Avenue
Menlo Park CA 94025-3696
(415)859-0811

Dr B B Goshgarian
OLAC PL/MKPB
Stop 24
Edwards AFB CA 93523-5000
(805)275-5183
AV525-5183

Dr William Graham
Morton Thiokol, Inc
Huntsville Division
Huntsville AL 35807-7501
(205)882-8397

Dr Alten Grandt
Department of Aeronautics
and Astronautics
Purdue University
West Lafayette IN 47907

TURBULENCE-FLAME INTERACTIONS

(AFOSR Grant No. AFOSR-90-0025)

Principal Investigator: D. A. Santavicca

Department of Mechanical Engineering
Propulsion Engineering Research Center
Penn State University
University Park, PA 16802

SUMMARY/OVERVIEW:

Turbulence-flame interactions in the reaction sheet regime can be viewed as the interaction between vortices in the turbulent flow and the flame front. With this phenomenological description in mind, the objective of this study is to investigate the interaction between individual vortices and laminar flame fronts. Experiments are conducted where PIV is used to characterize the velocity field and planar laser induced fluorescence is used to characterize the flame structure. In addition, a model based on a kinematical relationship between flame propagation and vortex motion is employed. This study is intended to address a number of important fundamental issues regarding flame-turbulence interactions including the effect of vortex size and strength on flame area production, flame curvature, and the minimum scale of flame wrinkling, as well as the relationship between the local flame curvature and strain and the local flame structure and speed. Also of interest is the temporal evolution of the flame structure, particularly as it relates to the vortex spacing.

TECHNICAL DISCUSSION

Experiments are conducted in a laminar flow system which is illustrated schematically in Figure 1, where a Karman vortex street is generated by a rod located upstream of a rod-stabilized, laminar, V-flame. The flame and vortex parameters are varied by changing the diameter of the vortex rod, the mean flow velocity, the fuel and the diluent. The test conditions studied to date are given in Table 1, where δ_v is the vortex diameter, δ_L is the laminar flame thickness, U_θ is the maximum vortex velocity, S_L is the laminar flame speed, a is the vortex spacing, Da is defined as $(\delta_V/U_\theta)/(\delta_L/S_L)$, N refers to no wrinkling, W refers to wrinkled, P refers to pocket formation, $<-H>$ is the average negative curvature, $<+H>$ is the average positive curvature, and A_T/A_L is the ratio of the vortex flame to laminar flame areas. Note that the actual vortex parameters are determined from two-dimensional velocimetry measurements made using particle image velocimetry (PIV). The PIV measurements also allow determination of the strain along the flame front during the flame-vortex interaction. The flame geometry is determined from two-dimensional OH fluorescence measurements. Since the OH fluorescence signal strength clearly demarcates the unburned and burned gases, these measurements define the flame interface, from which the flame area and the local flame curvature are calculated. In addition, the profile of the OH fluorescence signal strength through the flame front, which approximately follows the temperature profile, is used to determine the local flame thickness.

Premixed flame fronts interacting with vortices are also investigated numerically using a kinematical relationship between the flame propagation and vortex tangential velocity. Use of Lagrangian grid points allows convenient calculations of both flame coordinates and flame stretch.

Dr Donald Jassowski
Aerojet Technical Systems Co
PO Box 13222
Sacramento CA 95813
(916)355-2849

Dr S M Jeng
University of Tennessee
Space Institute
Tullahoma TN 37388

Dr Robert Jensen
Rockwell/Rocketdyne Division
6633 Canoga Ave
Canoga Park CA 91303
(818)718-3730
FAX 718-3600

Dr M W Johnson
Head of Neutron Inst. Division
Rutherford Appleton Laboratory
Science Department
Chilton, Didcot, Oxon UK OX11 OQX
0235-21900
0235-44-5720F

Dr Abraham Kadish
Earth and Space Sciences Div.
Atmospheric Sciences Group
Mail Stop D466, LANL
Los Alamos NM 87545

Dr Jordin Kare
Building 197, Room 1020
Lawrence Livermore Nat'l Lab
P O Box 808
Livermore CA 94550
(415)423-8300

Dr David Kassoy
Dept of Mechanical Engineering
University of Colorado at
Boulder, Campus Box 427
Boulder CO 80309
(303)492-2991
(303)492-7694

Dr Myron Kaufman
Department of Chemistry
Emory University
Atlanta GA 30322
(404)727-6619

Dr Dennis Keefer
University of Tennessee
Space Institute
Tullahoma TN 37388
(615)455-0631

Dr Arnold A Kelly
Department of Mechanical and
Aerospace Engineering
Princeton University
Princeton NJ 08544-5263
(206)452-5221

Dr Philip Kessel
OLAC PL/LSCF
Edwards AFB CA 93523-5000

Dr Sue Kim
California State University
6000 J Street
Sacramento CA 95819
(916)454-6712

Dr David King
Mail Stop 125-224
Jet Propulsion Laboratory
4800 Oak Grove Drive
Pasadena CA 91103
(818)354-3315

Mr Mark Kleim
NASA Lewis Research Center
21000 Brookpark Rd
MS 510-219
Cleveland OH 44135

TABLE 1

Case No	Mixture	Le	δ_V/δ_L	U_θ/S_L	Da	Regime	$<-H>$	$<+H>$	A_T/A_L
1	CH_4/Air	.94	17.3	0.61	28	N	-0.086	0.079	1.01
2	CH_4/Air	.94	17.3	0.67	25	W	-0.144	0.176	1.31
3	CH_4/Air	.94	17.5	0.78	22	W	-0.118	0.160	1.28
4	CH_4/Air	.94	17.9	0.99	18	P	-0.128	0.166	1.44
5	CH_4/Air	.94	16.6	0.68	24	W	-0.177	0.194	1.14
6	CH_4/Air	.94	16.6	0.84	20	W	-0.155	0.185	1.20
7	CH_4/Air	.94	16.7	1.02	16	W	-0.138	0.159	1.30
8	CH_4/Air	.94	17.0	1.35	13	P	-0.126	0.174	1.51
9	CH_4/Air	.94	16.0	0.80	20	W	-0.175	0.168	1.09
10	CH_4/Air	.94	16.0	1.05	15	W	-0.181	0.177	1.23
11	CH_4/Air	.94	15.8	1.30	12	W	-0.141	0.177	1.38
12	CH_4/Air	.94	17.0	0.84	20	W	-0.173	0.108	1.07
13	CH_4/Air	.94	17.0	1.13	15	W	-0.173	0.192	1.23
14	C_3H_8/Air	1.78	15.8	1.30	12	W	-0.145	0.186	1.11
15	H_2/He/Air	0.22	15.8	1.30	?	W	-0.159	0.197	1.64

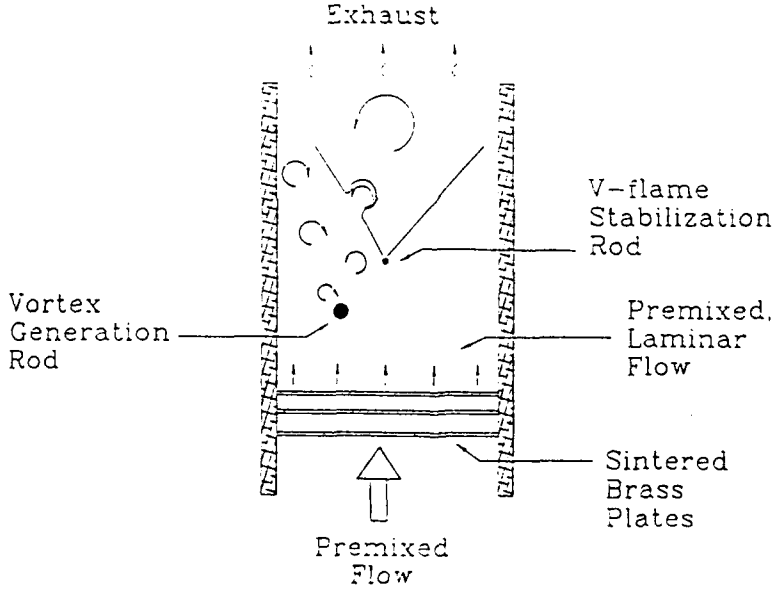

Figure 1. Schematic Drawing of Flame-Vortex Experiment

Dr G Lengelle'
Office National D'Etudes et de
Recherches Aerospatiales
29,Ave de la Division Lecherc
France

Mr Jay Levine
OLAC PL/LSCF
Edwards AFB CA 93523-5000
(805)275-5366
AV 525-5366

Dr P Y Liang
Advanced Combustion Devices
Rocketdyne Div, Rockwell Int.
6633 Canoga Avenue
Canoga Park CA 91303

Lt Col R Lisowski
EOARD
Box 14
FPO NY 09510-0200
71-402-4505
AV235-4505

Dr George Lo
Lockheed Palo Alto Research
Laboratory
3251 Hanover St, 8204-93-50
Palo Alto CA 94304
(415)424-2514

Dr Geoffrey Main
School of Mechanical Engrg
Georgia Institute of
Technology
Atlanta GA 30332-0420
(404)894-3242
(404)951-8058

Dr David Mann
Army Research Office
P.O. Box 12211
Research Triangle Pk NC 27709-2211
(919)549-4249
AV832-4249

Prof Alan Marchand
Dept of Chemistry
North Texas State Univ
NTSU Station, Box 13767
Denton TX 76203-5068
(817)565-3823

Dr Stephen Margolis
Combustion Research Facility
Sandia National Laboratories
Livermore CA 94551-0969

Lt Col Charles Martin
Nuclear Weapons Development
The Pentagon
Room 5D543
Washington DC 20330-5040
(202)693-6303
AV244-6303

Dr Manuel Martinez-Sanchez
Aeronautics and Astronautics
Massachusetts Inst of Tech
Building 37-401
Cambridge MA 02139
(617)253-5613

Dr Peter Mattern
Combustion Sciences
Sandia National Laboratories
Livermore CA 94551-0969

Dr Jyotirmoy Mazumder
Department of Mechanical and
Industrial Engineering
University of Illinois
Urbana IL 61801
(217)333-1964

Dr John McKee
McDonnell Douglas Astronautics
5301 Bolsa Avenue
Huntington Beach CA 92647
(714)896-1133

AFOSR SPONSORED RESEARCH IN AIRBREATHING COMBUSTION

PROGRAM MANAGER: JULIAN M. TISHKOFF

AFOSR/NA
BOLLING AFB DC 20332-6448

SUMMARY/OVERVIEW: The Air Force Office of Scientific Research (AFOSR) program in airbreathing combustion currently is focused on seven areas of study: supersonic combustion, reacting flow, soot, sprays, kinetics, ram accelerators, and supercritical fuel behavior. An assessment of major research needs in each of these areas is presented.

TECHNICAL DISCUSSION

AFOSR is the single manager for Air Force basic research, including efforts based on external proposals and in-house work at Air Force laboratories. Airbreathing combustion is assigned to the AFOSR Directorate of Aerospace Sciences along with programs in rocket propulsion, diagnostics in reacting media, and fluid and solid mechanics.

Interests of the AFOSR airbreathing combustion task are given in the SUMMARY section above. Many achievements can be cited for these interests, yet imposing fundamental research challenges remain. The objective of the program is publications in the refereed scientific literature describing significant new understanding of multiphase turbulent reacting flow. Incremental improvements to existing scientific approaches, hardware development and computer codes fall outside the scope of this objective.

Decisions on support for research proposals are based on scientific opportunities and technology needs. Current AFOSR perceptions of scientific opportunities appear in Figure 1, and areas of emphasis are indicated by arrows with positive slopes.

Two major emphases define the main thrusts of current and near term future research activity: supersonic combustion to support hypersonic airbreathing propulsion technology and issues affecting the future utilization of hydrocarbon fuels. Starting in 1987 new research efforts were directed at novel means for achieving ignition, combustion enhancement, and low-loss flameholding in supersonic combustion. 1989 saw new research in interactive control of fluid transport processes. These opportunities reflect a generic interest in interdisciplinary efforts between researchers in control theory and fluid transport behavior. For hypersonic propulsion a particular focus of interactive flow control is the investigation of means to overcome the suppression of mixing which high Mach number flows experience in relation to subsonic flows.

Dr S N B Murthy
Dept of Mechanical Engineering
Purdue University
West Lafayette IN 47907
(317)494-1509
(317)494-5639

Dr Jeffery Muss
Aerojet Techsystems
P.O. Box 13222
Sacramento CA 95813
(916)355-3663

Dr Subhash Narang
Chemistry Laboratory
SRI International
333 Ravenswood Avenue
Menlo Park CA 94025-3696

Dr Vittorio Nardi
Stevens Institute of
Technology
Castile Point Station
Hoboken NJ 07030
(201)420-5938

Dr Thong Nguyen
Aerojet Techsystems
P.O. Box 13222
Sacramento CA 95813
(916)355-3664

Dr Jim Nichols
OLAC PL/RKLB
Edwards AFB CA 93523-5000
(805)275-5249
AV 525-5249

Dr Gary Nickerson
Software&Engineering Assoc.
1000 E. William St., Suite 200
Carson City NV 89701
(702)882-1966

Dr Arnold Nielsen
Naval Weapons Center
China Lake CA 93555-6001
(619)939-1614
AV437-1614

Mr Randy Nishiyama
R/E/WPS
US Dept of Commerce
NOAA, 325 Broadway
Boulder CO 80303-3328

Col James Nunn
OLAC PL/CC
Edwards AFB CA 93523-5000

Dr Douglas Olson
AeroChem Research Laboratories
Inc.
P. O. Box 12
Princeton NJ 08542
(609)921-7070

Dr Tae-Woo Park
OLAC PL/TODP
Stop 24
Edwards AFB CA 93523-5000
(805)275-5196
AV525-5196

Col Arthur Pavel
AFOSR/CD
Bolling AFB DC 20332-6448
(202)767-5018
AV297-5018

Ms Dorothy Pecker
The John Hopkins Univ/APL
John Hopkins Rd
Laurel MD 20707

Air Force Basic Research

Aerospace Sciences

Airbreathing Combustion

Research Area	Trend	Decrease	Increase
Supersonic Combustion	→		
Reacting Flow	→		
Soot	→		Comprehensive Growth Modeling
Sprays	↗		Supercritical Behavior - FY94 Init
Kinetics	→		Lumping And Reduction Methods
Ram Accelerators	→		New Air Force Laboratory Task
Supercritical Fuel Behavior	↗		FY93 And FY94 Initiatives

Mr Wayne Roe
OLAC PL/XRX
Stop 24
Edwards AFB CA 93523-5000
(805)275-5206
AV525-5206

Dr David Rosen
Physical Sciences Inc.
Dascomb Research Park
Andover MA 01810
(617)475-9030

Dr S D Rosenberg
P O Box 13222
Sacramento CA 95813
(916)355-2609

Dr Thomas Rosfjord
United Technologies Res.Ctr.
Silver Lane
East Hartford CT 06108
(203)727-7418

Dr David Ross
Director,Physical Organic Chem
SRI International
333 Ravenswood Avenue
Menlo Park CA 94025-3696
(415)859-2430

Dr J Reece Roth
Dept of Elec and Comp Engrg
316 Ferris Hall
The University of Tennessee
Knoxville TN 37996-2100
(615)974-4446

Dr Gabriel Roy
ONR Code 1132P
800 North Quincy Street
Arlington VA 22217
(202)696-4405

Dr Kevin Rudolph
Martin Marietta Corporation
Mail Stop S8071
PO Box 179
Denver CO 80201
(303)977-3681

Lt James Rymarcsuk
OLAC PL/RKLB
Edwards AFB CA 93523-5000
(805)275-5542
AV 525-5542

Dr Mark Salita
Morton Thiokol/Wasatch Div
MS 280B
PO Box 524
Brigham City UT 84302
(801)863-2163

Dr Michael Salkind
President
Ohio Aerospace Institute
2001 Aerospace Parkway
Brookpark OH 44142
(216)891-2100

Dr Robert Santoro
Penn State University
Mechanical Engineering Dept
208 Mechanical Engineering
University Park PA 16801
(814)863-1285
FAX 865-3389

Dr Robert Schmitt
Chemistry Lab
SRI International
333 Ravenswood Avenue
Menlo Park CA 94025-3696
(415)859-5579

Dr Keith Schofield
Quantum Institute
University of California,
Santa Barbara
Santa Barbara CA 93106

AFOSR SPONSORED RESEARCH IN DIAGNOSTICS IN REACTING MEDIA

PROGRAM MANAGER: JULIAN M. TISHKOFF

AFOSR/NA
BOLLING AFB DC 20332-6448

SUMMARY/OVERVIEW: The Air Force Office of Scientific Research (AFOSR) program in diagnostics in reacting media currently is focused on three areas of study: gas-phase measurements, plasmas, and particle/droplet measurements. An assessment of major research needs in each of these areas is presented.

TECHNICAL DISCUSSION

AFOSR is the single manager for Air Force basic research, including efforts based on external proposals and in-house work at Air Force laboratories. The diagnostics of reacting flows task is assigned to the AFOSR Directorate of Aerospace Sciences along with programs in rocket propulsion, airbreathing combustion, and fluid and solid mechanics.

Interests of the AFOSR diagnostics in reacting media subarea are given in the SUMMARY section above. This program, now in its tenth year, has produced many "first-ever" laser-based measurements. The instrumentation with which these measurements were made is becoming commonly available for laboratory and bench test utilization. Measurements range from microscopic to macroscopic scales with relevance to: plasma acceleration; combustion aerothermochemistry; the behavior and synthesis of advanced energetic materials; characterization of exhaust plume formation and radiation; and dynamic control of propulsion, weapon and power generation systems.

Decisions on support for research proposals are based on scientific opportunities and technology needs. Current AFOSR perceptions of scientific opportunities appear in Figure 1. As indicated by the orientation of the arrows in Figure 1, the task areas with the greatest growth potential are plasmas and measurements in supercritical fluids.

The purpose of this abstract has been to communicate AFOSR perceptions of research trends to the university and industrial research communities. However, communication from those communities back to AFOSR also is desirable and essential for creating new research opportunities. Therefore, all proposals and inquiries for fundamental research are encouraged even if the content does not fall within the areas of emphasis described herein. Comments and criticisms of current AFOSR programs also are welcome.

Dr Douglas Talley
OLAC PL/RKFT
Edwards AFB CA 93523-5000
(805)275-6174
AV525-6174

Mr Robert L Talley
Viritay Technologoies, Inc
4845 Millersport Highway
East Amherst NY 14051
(716)689-0177

Dr Mostafa Talukder
OLAC PL/LKLR
Edwards AFB CA 93523-5000
(805)275-5416
AV525-5416

Dr James Tien
Case Western Reserve
University
Glennan Building, Room 415
Cleveland OH 44106
(216)368-4581

Prof William Trogler
Department of Chemistry
University of California, San
Diego
La Jolla CA 92093-0310
(619)452-6175

Dr Wing Tsang
National Institute of Standard
and Technology
Chemical Kinetics Division
Gaithersburg MD 20899
(301)975-3507

Dr Peter Turchi
Aero/Astro Engineering
328 CAE Building
Ohio State University
Columbus OH 43210
(614)292-2691

Mr Gary Vogt
OLAC PL/DYCR
Stop 24
Edwards AFB CA 93523-5000
(805)275-5258
AV525-5258

Dr Robert Vondra
PO Box 596
Wrightwood CA 92397
(619)249-3451

Dr Nzoo Vu
Naval Weapons Center
China Lake CA 93555-6001
(916)939-7392
AV437-7392

Dr Francois Vuillot
Office National D'Etudes et de
resherches Aerospatiales
29,Ave de la Division Lecherc
Chatillon-sous-Bagneux France

Dr R H Woodrow Waesche
Atlantic Research Corporation
7511 Wellington Road
Gainesville VA 22065

Dr Richard Walker
Aerojet Techsystems
P.O. Box 13222
Sacramento CA 95813
(916)355-2694

Dr Peter Wayner
Dept of Chemical and
Environmental Engineering
Rensselaer Polytechnic Inst
Troy NY 12180-3590
(518)276-6199

THEORIES OF TURBULENT COMBUSTION IN HIGH SPEED FLOWS

(AFOSR Grant No. 89-0310)

Principal Investigators: P. A. Libby and F. A. Williams

Department of Applied Mechanics and Engineering Sciences
University of California San Diego, La Jolla, CA 92093-0310

Summary/Overview

The objective of this research is to improve understanding of the chemical kinetic and fluid dynamics of turbulent combustion in high speed flows. At present emphasis is being placed on the extinction and ignition characteristics of laminar and turbulent flames in the hydrogen-air system, the one preferred for supersonic combustion.

Technical Discussion

In early work on this project estimates were made of the combustion regime likely to apply in scramjet operations. Although combustion under a wide range of conditions can be envisaged in such operations as a consequence of a relatively wide altitude, flight-speed corridor and of the variety of possible engine configurations, the reaction-sheet regime was identified to be of applied as well as fundamental interest. Attention was thus focused on flamelets in the hydrogen-air system, and two separate studies presently underway are reported here, both involving flames in counterflowing configurations but one directed towards laminar flamelets and the other turbulent.

Laminar Flamelets

The structure of hydrogen-air flames in counterflowing configurations was calculated for a range of pressures from 0.5 to 40 atmospheres, for a range of initial temperatures from 300 K to 1200 K and for a range of rates of strain on the oxidizer side of the flame from 5×10^{-4} s^{-1} to extinction. The full conservation equations with detailed chemical kinetics were numerically integrated [1]. The results of such complete calculations provide the basis for assessing various approximate treatments of these flames.

An example of such an assessment is provided by Fig. 1 which shows several calculations of the equilibrium constant based on partial pressures for the reaction $H_2 + \frac{1}{2}O_2 \rightleftharpoons H_2O$ at a rate of strain of 60 s^{-1}, a value sufficiently low as to encourage use of the frequently employed assumption of chemical equilibrium [2]. One determination employs the calculated temperature distribution and the tabulated values of $K_p(T)$ while the other two use the calculated concentrations in terms of partial pressures of the participating species on each side of the reaction zone. The implication of the significant difference between the first and the other two determinations is that even for such low rate of strain the equilibrium approximation is not very satisfactory.

A second utilization of the complete calculations relates to the assessment of various reduced mechanisms for the treatment of hydrogen oxidation since in the calculation of multidimensional laminar flames and in turbulent flames with even simple geometries it is computationally desirable to reduce the number of species which must be taken into account [3]. A four-step mechanism was obtained by imposing a steady-state approximations for HO_2 and H_2O_2. A three-step mechanism results from introduction of a steady state approximation for O, and finally a two-step mechanism is obtained if OH is similarly assumed to be in steady

impinging on a solid surface or to two identical reactant streams flowing counter to one another (cf. [5] for the pertinent references to these experiments and for the first theoretical treatment of this latter case.) However, flames involving a turbulent air stream flowing counter to a hydrocarbon stream are being studied experimentally at the Imperial College and it is planned that in due course hydrogen-air flames in stagnating turbulence will be studied.

A present effort relates to the theory of nonpremixed flames in stagnating turbulence. The k–ϵ theory was applied for the description of the fluid mechanical behavior and, as part of initial effort, chemical equilibrium was assumed. Comparison will be made with the available data from Imperial College, the theory assessed and modified as appropriate and then applied to the hydrogen-air system. Follow-on studies will concern chemical-kinetic effects based on the laminar flamelet calculations discussed earlier.

Reference [6] gives the final page numbers of a study of compressibility effects discussed in the previous summary.

References

[1] G. Balakrishnan. *Studies of Hydrogen-Air Diffusion Flames and of Compressibility Effects, Related to High Speed Propulsion.* PhD Thesis, University of California San Diego, to appear, September 1992.

[2] E. Gutheil, G. Balakrishnan, and F. A. Williams. Structure and extinction of hydrogen-air diffusion flames. In N. Peters and B. Rogg, editors, *Reduced Kinetic Mechanisms for Application in Combustion Systems*, Springer Verlag, Berlin, 1992, to appear, Germany.

[3] E Gutheil and F. A. Williams. A numerical and asymptotic investigation of structures and extinction of hydrogen-air diffusion flames at pressures and temperatures of high-speed combustion. In *Twenty-Third Symposium (International) on Combustion*, pages 513–521, Pittsburgh, PA, 1990. The Combustion Institute.

[4] G. Balakrishnan, C. Treviño, and F. Mauss. Asymptotic structure of hydrogen-air diffusion flames. submitted to *Combustion and Flame*, 1992.

[5] K. N. C. Bray, M. Champion, and P. A. Libby. Premixed flames in stagnating turbulence: Part I. the general formulation for counterflowing streams and gradient models for turbulent transport. *Combustion and Flame*, 84:391–410, 1991.

[6] G. Balakrishnan, A. Liñán, and F.A. Williams. Compressibility effects in thin channels with injection. *AIAA Journal*, 29(12):2149–2154, December 1991.

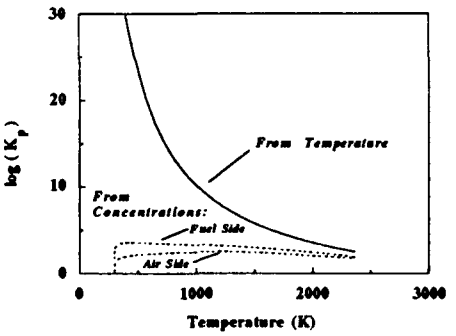

Figure 1: The equilibrium constant for partial pressures, K_p, for $H_2 + \frac{1}{2}O_2 \rightleftharpoons H_2O$, evaluated from the temperature and from the computed profiles of partial pressures with the full mechanism, for a = 60 s^{-1}, p = 1 atm, $T_{-\infty} = T_{\infty} = 300K$.

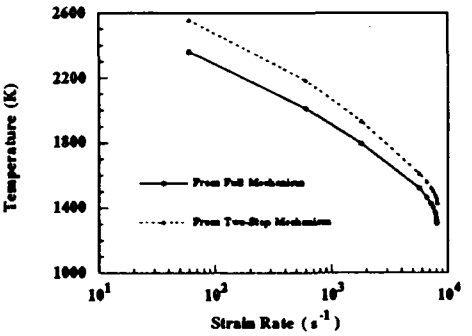

Figure 2: The dependence of the maximum temperature on the strain rate for axisymmetric flow with $T_{-\infty} = T_{\infty} = 300K, p$ = 1 atm, as obtained with full chemistry and with the two-step mechanism.

Dr Gary Borman
University of Wisconsin
Engine Research Lab, ME Dept
1500 Johnson Drive, Rm 119 ERB
Madison WI 53706
(608)263-1616
FAX:262-6707

Dr Kevin Bowcutt
Rockwell International
Mail Code NA40
12214 Lakewood Boulevard
Downey CA 90241
(213)420-0317

Dr C T Bowman
Department of Mechanical Engineering
Stanford University
Stanford CA 94305-3032
(415)723-1745

Dr K N C Bray
University of Cambridge
Department of Engineering
Trumpington Street
Cambridge CB2 1PZ, England UK
0223 332744
0223 337733

Dr Robert Breidenthal
Department of Aeronautics and Astronautics
University of Washington, FS10
Seattle WA 98195
(206)685-1098

Dr Kenneth Brezinsky
Department of Mechanical and Aerospace Engineering
Princeton University
Princeton NJ 08544-5263
(609)258-5225

Dr J E Broadwell
Graduate Aeronautical Labs
California Institute of Technology
Pasadena CA 91125

Dr Garry Brown
Department of Mechanical and Aerospace Engineering
Princeton University
Princeton NJ 08544-5263

Dr R C Brown
Aerodyne Research, Inc.
45 Manning Road
Manning Park Research Center
Billerica MA 01821-3976
(508)663-9500
FAX:663-4918

Lt Col Larry Burggraf
AFOSR/NC
Bolling AFB DC 20332-6448
(202)767-4960
AV297-4960

Dr Dennis Bushnell
NASA Langley Research Center
Mail Stop 168
Hampton VA 23665
(804)864-4546

Dr Ron Butler
WL/POSF
Wright-Patterson AFB OH 45433-6563

Dr T D Butler
Group T-3
Los Alamos National Laboratory
Los Alamos NM 87545
(505)667-4156

Dr H F Calcote
AeroChem Research Laboratories Inc.
P. O. Box 12
Princeton NJ 08542
(609)921-7070

LASER DIAGNOSTICS FOR PLASMA THRUSTERS USING A CW CO_2 RADIATION SOURCE

(AFOSR Grant No. 89-0297)

Principal Investigator: Dr. Thomas M. York

Professor
Aeronautical and Astronautical
Engineering Department
328 Bolz Hall., 2036 Neil Avenue
The Ohio State University
Columbus, Ohio 43210
(614-292-2691)

SUMMARY/OVERVIEW:

This research involves new diagnostic studies of plasma thrusters. These devices generate ionized gases which are accelerated by thermal and electromagnetic mechanisms. The research effort will develop new, high resolution diagnostic techniques that will determine electron densities, electron density fluctuations indicative of anomalous transport, and local magnetic fields. A 65 Watt carbon dioxide laser, which allows more sensitive measurements with its long wavelength, will be used. The laser can be coupled to a Far Infrared Laser System capable of generating beams with tens of milliwatt power levels, and will allow diagnostic studies that have not yet been used for thruster plasma diagnosis.

TECHNICAL DISCUSSION:

Description and Capabilities of Laser Source

The laser system that is the heart of the diagnostic arrangements is a CO_2 source (Model 570, Apollo Lasers, Chatsworth, CA). This is a tunable system with an output of 30 Watts minimum at 50 or more wavelengths, TEM_{∞}. It is capable of 65 W output CW or 200 W pulsed. This laser can also be used to pump an FIR laser (Model 122, Apollo Lasers, Chatsworth, CA). Using methanol, this can operate between 70 μm and 500 μm; at 118.8 μm, power levels on the order of 100 mW CW or 200 mW pulsed are available; beam diameter is 10 mm. These wavelengths and power levels are appropriate for diagnosing the plasmas of interest in the exhaust of plasma thruster, as will be discussed below. Along with the laser, modulating and mixing components in the optical train, as well as detectors at the various wavelengths, are critical.

Dr Clayton Crowe
Department of Mechanical Engineering
Washington State University
Pullman WA 99164-2920
(509)335-3214

Dr E T Curran
WL/CA-P
Wright-Patterson AFB OH 45433-6563
(513)255-2246
AV785-2246

Dr Eli Dabora
Mechanical Engineering Dept
University of Connecticut
Box U-139 ME
Storrs CT 06268
(203)486-2415
(203)486-2189

Dr Werner Dahm
Department of Aerospace Engineering
The University of Michigan
Ann Arbor MI 48109-2140
(313)764-4318

Dr Sanford M Dash
Science Applications International Corporation
501 Office Ctr Dr, Suite 420
Fort Washington PA 19034-3211
(215)542-1200
FAX:542-8567

Dr Ron Davis
Chemical Science and Techn Lab
Building 221, Room B312
National Inst of Stds & Tech
Gaithersburg MD 20899

Lt Col Larry Davis
HQ AFSC/XTR
Andrews AFB DC 20334
(301)981-7882

Dr George Deiwert
NASA Ames Research Center
MS 230-2
Moffett Field CA 94035
(415)604-6198

Dr R W Dibble
Department of Mechanical Eng
6159 Etcheverry Hall
University of California
Berkeley CA 94720
(415)642-4901
FAX -6163

Dr Paul Dimotakis
Graduate Aeronautical Labs
California Institute of Technology
Pasadena CA 91125
(818)356-4456

Mr Lee Dodge
Southwest Research Institute
P O Drawer 28510
San Antonio TX 78284
(512)684-5111
Ext 3251

Dr David Dolling
Department of Aerospace Engrg and Engineering Mechanics
University of Texas at Austin
Austin TX 78712
(512)471-4470
(512)471-7593

Capt Randy Drabczuk
WL/MNSH
Eglin AFB FL 32542-5434
AV872-0360
(904)882-0360

Dr Michael Drake
Physical Chemistry Department
General Motors Research Labs
Twelve Mile and Mound Roads
Warren MI 48090-9055

Multi-beam Interferometer

This technique generally utilizes a Mach-Zender configuration. A measurement of phase shift (ϕ) allows determination of electron density, as:

$$\phi = 2.82 \times 10^{-13} \lambda_o \int_{z1}^{z2} Ne(Z)\, dZ \qquad \text{(cgs units)}$$

where λ_o is the laser wavelength and Z is the path variable through the plasma. In the above, measurement of ϕ indicates the integrated line density, $N_e dz$.

Clearly, one can see the enhanced sensitivity of CO_2 radiation at 10μm, compared to red light at 0.6973 μm. The unfolding of an axisymetric profile of Ne requires a large number (2-5) of interferometer channels. Successful applications of this technique with CO_2 lasers have produced time histories of profiles of Ne(r) over a period of 20 ms with Ne $\approx 10^{15}$ cm^{-3} and $\ell \approx 10$ cm. Considerable care is being exercised in detector selection. The use of a Bragg cell to modulate the beam has proven successful and that technique is being applied here. An advantage of large λ_o is that the sensitivity to mechanical vibration decreases; specifically, when $\lambda_o > 4 \times 10^8 [\Delta e / r_o n_o]$ where Δe is vibration induced path change and r_o is plasma radius. However, care will have to be taken with the beam deflection ($\propto$) due to gradients, as $\propto \sim M_o \lambda_o^2$, and this could cause problems in location of detector windows.

Measurement of Electron Density Fluctuations

This technique is based upon the principles of Thomson scattering -scattering from free elections and ions. The ability to measure fluctuations, which are extremely important because they generate anomalous transport, is related to a number of factors. The characteristic parameter for Thomson Scattering is $\propto = 1/k\lambda_D = \lambda_o/4\pi\lambda_D \mathrm{Sin}(\Theta_s/2)$ where λ_D is the Debye length and Θ_s is the scattering angle. The range, $\propto << 1$, defines normal Thomson Scattering for Te, Ne. When $\propto >> 1$ plasma waves and thermal ion fluctuations may be studied and ion temperature determined.

Wave scattering can result in large enhancements in the scattered power, well above those achieved with thermal motion, as scattered power

is $$P_s = 1/4 P_o r_e^2 \lambda_o^2 (\bar{N})^2 L_v$$

Dr David Fyfe
Laboratory for Computational Physics
Naval Research Laboratory
Washington DC 20375
(202)767-6583
AV297-6583

Dr Alon Gany
Department of Aeronautical Eng
Technion-Israel Institute of Technology
32000 Haifa, ISRAEL
04-292308

Dr Ahmed Ghoniem
Department of Mechanical Engineering
MIT
Cambridge MA 02139
(617)253-2295
FAX:253-5981

Mr R Giffen
General Electric Company
Aircraft Engine Group
Neumann Way
Cincinnati OH 45215

Dr P Givi
Department of Mechanical and Aerospace Engineering
State University of New York
Buffalo NY 14260

Dr Irvin Glassman
Department of Mechanical and Aerospace Engineering
Princeton University
Princeton NJ 08544-5263
(609)258-5199
(813)442-1118

Dr A D Gosman
Department of Mechanical Engrg
Imperial College of Science and Technology
London WS7 2BX UK

Dr Frederick Gouldin
Department of Mechanical and Aerospace Engineering
Cornell University
Ithaca NY 14853-1301
(607)255-5280

Dr F Grinstein
Laboratory for Computational Physics
Naval Research Laboratory
Washington DC 20375

Dr Ephraim Gutmark
Research Department
Code 3892
Naval Weapons Center
China Lake CA 93555-6001
(619)939-3745
AV437-3745

Dr Howard Hanley
Chem & Sci Tech Lab
National Inst of Stds & Tech
325 Broadway
Boulder CO 80303-3328
(303)497-3320

Dr Robert Hansen
Office of Naval Research
Code 1215
800 North Quincy Street
Arlington VA 22217-5000
(202)696-4715

Dr Stephen Harris
Physical Chemistry Department
General Motors Research Labs
30500 Mound Road
Warren MI 48090-9055
(313)986-1305

Dr James Hermanson
Propulsion Technology
United Technologies Research Center
East Hartford CT 06108

SHOCK-INDUCED MIXING AND COMBUSTION IN A VORTEX

AFOSR Grant Nos. 89-0413 and 90-0188

Principal Investigator:

E. E. Zukoski

California Institute of Technology
Pasadena, California 91125

SUMMARY/OVERVIEW:

Experimental studies are being made of a novel technique to enhance the mixing and combustion in a supersonic flow between a jet of hydrogen and a coflowing stream of air. This technique, called shock-induced mixing , uses impinging oblique shocks to produce streamwise vorticity at the interface between a coflowing light gas jet immersed in an air stream. The vorticity produced in this interaction causes rapid distortion of the interface and greatly enhances the rate of mixing between the light gas and air. Experimental studies of this process have been carried out in several facilities. Experiments performed in the GALCIT 17 Inch Shock Tube, used a two dimensional transient flow to model the interaction without the additional mixing caused by the shear produced by velocity differences between the hydrogen and air stream. In related wind tunnel experiments, the influence of both shear and shock enhancement is being investigated. Combustion in a vortex, of the type produced by the shock-induced mixing process, is being studied experimentally in a dump burner in which combustion is initiated in vortices formed in the mixing layer between a premixed flow of fuel and air, and the hot products of combustion contained in a recirculation zone produced by a rearward-facing step.

TECHNICAL DISCUSSION

1. SHOCK-INDUCED MIXING INVESTIGATION

During the past year we have completed the experimental study of shock-induced mixing of a helium jet with shock Mach numbers in the range 1.05 to 2.0 and are continuing the study of shock enhanced mixing when shear induced mixing is present and the study of combustion in a vortex. Under the support of another grant we have been able to apply the results of this AFOSR supported work to carry out tests in the new T-5 Free Piston Shock Tunnel at Caltech. These tests allow us to investigate the effects of the shock-induced mixing process on the mixing and combustion of high temperature hydrogen jets injected into a Mach 5 air flow with an enthalpy corresponding to Mach 17.

Shock-Tube Experiments: The experimental investigation of shock induced mixing was carried out in the shock tube because we showed that a two-dimensional transient flow, which is easy to produce in the shock tube, gives an excellent picture of many of the features of the three-dimensional interaction between a steady oblique shock and the flow of a hydrogen jet embedded in air. The shock tube allows us to study these features in a particularly efficient manner.

Experimental work in the shock tube has concentrated on understanding the mixing produced by the passage of a shock over a cylinder of helium whose axis is parallel to the shock front. In the

Dr Lawrence A Kennedy
Department of Mechanical Engineering
The Ohio State University
Columbus OH 43210-1107
(614)292-5782

Dr Ian Kennedy
Mechanical Engineering Dept
University of California, Davis
Davis CA 95616
(916)752-2796

Dr James Kezerle
Gas Research Institute
8600 West Bryn Mawr Avenue
Chicago IL 60631
(312)399-8331

Dr Merrill K King
National Science Foundation
Chemical and Process Eng. Div.
1800 G Street, N. W.
Washington DC 20550
(202)357-9606

Dr Galen King
Department of Mechanical Engineering
Purdue University
West Lafayette IN 47907
(317)494-2713

Mr R Kirby
Garrett Turbine Engine Company
111 South 34th Street
P. O. Box 5217
Phoenix 85010

Dr William H Kirchhoff
Division of Chemical Sciences
Office of Basic Energy Science
Department of Energy
Washington DC 20585

Dr Charles Kolb
Aerodyne Research, Inc.
45 Manning Road
Manning Park Research Center
Billerica MA 01821-3976
(508)663-9500
FAX:663-4918

Dr Wolfgange Kollmann
Mechanical Engineering Dept
University of California, Davis
Davis CA 95616
(916)752-1452

Mr William E Koop
HQ AFMC(P)/STTA
Wright-Patterson AFB OH 45433

Dr George Kosaly
Department of Mechanical Engineering
University of Washington
Seattle WA 98195
(206)543-6933
FAX:685-8047

Dr C R Krishna
Department of Nuclear Energy
Brookhaven National Laboratory
Upton NY 11973

Mr David Kruczynski
Attn SLCBR-IBA
Interior Ballistics Division
Ballistic Research Laboratory
Aberdeen Proving Gnd MD 21005-5066
(410)278-6202
AV298-6202

Dr Kenneth Kuo
Department of Mechanical Engineering
Pennsylvania State University
University Park PA 16802
(814)865-6741
FAX:863-3203

experiments and they may be important in real systems in which substantial differences between the velocities of hydrogen and air can be present.

Dr. L. Hill and K. Moore have completed the construction of a Mach 2.6, continuous-flow wind tunnel, with a cross-section of 6.25 by 6 cm and a total pressure of one atmosphere. In this facility, we are studying experimentally the modification to the shock-induced mixing process that is provided by shear which is generated by velocity differences at the interface between the helium jet and the air stream. In the experiments, parallel flows of air and a helium jet will pass through an oblique shock and the resulting mixing processes will be measured with the Mie scattering technique Scattering of a laser light sheet by ice particles formed by condensation in the wind-tunnel nozzle will be the primary experimental technique. The wind tunnel and associated instrumentation has been completed and preliminary experiments have been successfully carried out. The laser used in the shock tube experiments has now been made available for this work.

Recently, we have been able to test the injection concept, with hot hydrogen as the injectant, and the resulting combustion of hydrogen injectant in the new T-5 Free Piston Shock Tunnel at Caltech. These tests, funded by NASA, allow us to investigate the effects of the shock-induced mixing process on the mixing and combustion of high temperature hydrogen jets injected into a Mach 5 air flow with the enthalpy corresponding to a Mach 17 flight speed.

2. COMBUSTION IN A VORTEX

In a practical application, the enhanced mixing technique described above involves the generation of longitudinal vortices in the mixing layer between coflowing hydrogen jets and the ambient air stream. Because combustion will occur at the interface between the hydrogen jets and air as the vortices roll up and hence we have been interested in studying combustion in a vortex.

The flow being studied is that produced by vortices shed from a rearward-facing step which forms the lower wall of a two-dimensional combustion chamber and which acts as a flame holder for a premixed flow of fuel and air which passes over the step. Combustion occurs in the mixing layer formed downstream of the step between the unburnt fuel-air flow, which separates from the lip of the step, and the products of combustion which recirculate behind the step. For certain sets of values for the gas speed and fuel-air ratio, a combustion instability develops which produces vortex shedding from the lip of the step at frequencies which range between 180 to 530 Hz. Given the complexity of the ducting, several modes can be excited at the same time.

T. Zsak and D. Kendrick are studying the combustion within these vortices with a variety of experimental techniques with the primary aim of determining the influence of a number of parameters on the motion of the vortices, the ignition process and ignition time delay for the vortex, and the time required for the complete combustion of the fuel-air mixture within the vortices.

During the past year we have been able to make use of a high speed, enhanced video camera which allows us to measure the chemiluminescence produced by the combustion process. These measurements, and the measurements of velocity, pressure and temperature discussed in earlier reports, now allow us to determine the parameters described above. In the past, we relied on individual photographs of the flow to determine the intensity of the chemiluminescence; with the high speed, enhanced video camera, we can now get a much better understanding of the combustion process.

The enhanced video camera allows photographs to be taken of a 30 cm length of the combustion chamber in which most of the combustion occurs and to obtain photographs with a time exposure of 10 microseconds and with a frequency of about 3,000 Hz. This frequency gives us 15 photographs per cycle of a 200 Hz shedding process which is enough to allow us to develop an excellent understanding of the combustion process.

Dr Wilbert Lick
Department of Mechanical and
Environmental Engineering
University of California
Santa Barbara CA 93106

Dr Hans Liepmann
Graduate Aeronautical Labs
California Institute of
Technology
Pasadena CA 91125
(818)356-4535

Dr F E Lytle
Department of Chemistry
Purdue University
West Lafayette IN 47907
(317)494-5261

Dr Andrej Macek
National Institute of
Standards and Technology
Physics Building, B-312
Gaithersburg MD 20899
(301)975-2610

Dr James Madson
McDonnell Douglas Research Lab
McDonnell Douglas Corporation
PO Box 516
St Louis MO 63166-0516

Dr Edward Mahefkey
WL/POOC-5
Wright-Patterson AFB OH 45433-6563
(513)255-6241
AV785-6241

Mr Nick Makris
SA-ALC/SFT
Kelly AFB TX 78241-5000
AV945-8212
FAX:945-9964

Dr Oscar Manley
US Department of Energy
Office of Energy Research
1000 Independence Avenue, SW
Washington DC 20585
(202)353-5822

Dr David Mann
U. S. Army Research Office
Engineering Sciences Division
P. O. Box 12211
Research Triangle Pk NC 27709-2211
(919)549-4249
AV832-4249

Dr Nagi Mansour
Computational Fluid Mechanics
Branch, RFT 202A-1
NASA Ames Research Center
Moffett Field CA 94035
(415)604-6420

Dr Frank Marble
Engrg. and Appl. Sci. Dept.
California Institute of
Technology
Pasadena CA 91125
(818)356-4784

Dr John Marek
NASA Lewis Research Center
21000 Brookpark Road
Cleveland OH 44135-3127

Mr C R Martel
WL/PO
Wright-Patterson AFB OH 45433-6563
(513)255-7431
AV785-7431

Dr Bruce Masson
PL/ARDF
Kirtland AFB NM 87117-6008
(505)844-0208
AV244-0208

ROCKET PROPULSION

Invitees

Dr George Adams
USA-BRL
AMXBR-I8D
Aberdeen Proving Gnd MD 21005-5006
(410)278-6168
(410)278-6783

Dr Horst Adolph
Synthesis and Formulations Br
Naval Surface Weapons Center
10901 New Hampshire Avenue
Silver Spring MD 20903-5000

Dr William E Anderson
Department of Mechanical
Engineering
Pennsylvania State University
University Park PA 16802
(814)863-6289

Mr W C Andrepont
P. O. Box 431
858 W. Jackman
Suite 111
Lancaster CA 93534
(805)942-5098

Lt John Andreshak
OLAC PL/LKLR
Stop 24
Edwards AFB CA 93523-5000
(805)275-5194
AV525-5194

Mr Chris Andrews
OLAC PL/LSVE
Edwards AFB CA 93523-5000
(805)275-5766
AV 525-5766

Dr Ron Atkins
Naval Weapons Center
China Lake CA 93555-6001
(619)939-1630
AV437-1630

Dr William Bailey
AFIT/ENP
Wright-Patterson AFB OH 45433-6583
(513)255-4498
AV785-4498

Dr Joseph Baum
SAIC
1710 Goodridge Drive
P.O. Box 1303,
McLean VA 22102
(703)827-4952

Maj Douglas Beason
Director, Advanced Weapons
and Survivability
Philips Laboratory
Kirtland AFB NM 87117
(505)844-3672
AV244-3672

Dr Roger Becker
KL-462
Research Institute
University of Dayton
Dayton OH 45469
(513)229-3938

Mr Charles Beckman
OLAC PL/MKPA
Stop 24
Edwards AFB CA 93523-5000
(805)275-5487
AV525-5487

Dr Merrill Beckstead
Dept of Chemical Engineering
Brigham Young University
Provo UT 84602
(801)378-6239

Dr Robert Beddini
Univ of Illinois
AAE Department
104 South Mathews Avenue
Urbana IL 61801-2997
(217)333-4239

Dr Arje Nachman
AFOSR/NM
Bolling AFB DC 20332-6448
(202)767-5028
AV297-5028

Dr ABdollah Nejad
WL/POPT
Wright-Patterson AFB OH 45433-6563
(513)255-9991
AV785-9991

Dr Herbert Nelson
Code 6110, Chemistry Division
Naval Research Laboratory
Washington DC 20375
(202)767-3686

Dr G B Northam
NASA Langley Research Center
MS 168
Hampton VA 23665-5225
(804)864-6248

Dr R C Oldenborg
Chemistry Division
Los Alamos National Laboratory
Los Alamos NM 87545
(505)667-2096
(505)667-3758

Dr A K Oppenheim
Department of Mechanical
Engineering
University of California
Berkeley CA 94720
(415)642-0211

Dr Elaine Oran
Laboratory for Computational
Physics
Naval Research Laboratory
Washington DC 20375
(202)767-2960

Dr Simon Ostrach
Case Western Reserve Univ
Department of Mechanical and
Aerospace Engineering
Cleveland OH 44106

Dr Richard Peterson
Department of Mechanical
Engineering
Oregon State University
Corvallis OR 97331-6001
(503)754-2567

Dr W M Pitts
National Institute of
Standards and Technology
Center for Fire Research
Gaithersburg MD 20899
(301)975-6486

Dr Robert Pitz
Department of Mechanical and
Materials Engineering
Vanderbilt University
Nashville TN 37235
(615)322-0209

Dr S B Pope
Department of Mechanical and
Aerospace Engineering
Cornell University
Ithaca NY 14853-1301
(607)255-4314

Dr C L Proctor II
Department of Mechanical
Engineering
University of Florida
Gainesville FL 32611
(904)392-7555

Dr Herschel Rabitz
Department of Chemistry
Princeton University
Princeton NJ 08544-1009
(609)258-3917
FAX:258-6746

Dr Rodney Burton
Dept. of Aero. And Astro. Engg
University Of Illinois-UC
101 Transportation Building
Urbana IL 61801-2997
(217)333-2651

Mr David Byers
NASA Lewis Research Center
MS 500-219
21000 Brookpark Road
Cleveland OH 44135-3127
(216)433-2447

Dr George Caledonia
Physical Sciences Inc
20 New England Business Center
Andover MA 01810
(617)475-9030

Dr David Campbell
OLAC PL/DYC
Stop 24
Edwards AFB CA 93523-5000

Dr Robert Carrol
Pratt & Whitney
P.O. Box 109600
West Palm Beach FL 33410-9600
(407)796-2889

Dr Robert Cassel
Naval Sea Systems Command
Code 62D
Washington DC 20362
(202)692-8635

Dr Robert Cattolica
Sandia National Laboratories
Division 9351
Livermore CA 94551-0969

Dr Leonard Caveny
OSD/SDIO/IST
Pentagon
Washington DC 20301-7100
(703)693-1687

Dr Yunus Ali Cengel
University of Nevada-Reno
Dept of Mechanical Engg
Reno NV 89557-0030

Dr May Chan
Naval Weapons Center
China Lake CA 93555-6001
(619)939-7519
AV437-7519

Dr C I Chang
AFOSR/NA
Bolling AFB DC 20332-6448
(202)767-4987
FAX:767-4988

Dr Franklin Chang-Diaz
Lyndon B Johnson Space Center
Code CB
Houston TX 77058
(713)483-2714

Dr Robert Chapman
OLAC PL/LKLR
Stop 24
Edwards AFB CA 93523-5000
(805)275-5416
AV525-5416

Dr Malcolm Chase
Center for Chemical Physics
National Inst of Stds & Tech
Building 222, Room A158
Gaithersburg MD 20899
(301)975-2526

Dr John Ross
Department of Chemistry
Stanford University
Stanford CA 94305-3032
(415)723-9203

Dr Gabriel Roy
Office of Naval Research
Mechanics Division, Code 1132
800 North Quincy Street
Arlington VA 22217-5000
(202)696-4405

Mr Kurt Sacksteder
NASA Lewis Research Center
MS 500-217
21000 Brookpark Road
Cleveland OH 44135
(216)433-2857

Dr Leonidas Sakell
AFOSR/NA
Bolling AFB DC 20332-6448
(202)767-4935
AV297-4935

Dr Mohammad Samimy
Ohio State University
Mechanical Engineering Dept
206 West 18th Street
Columbus OH 43210-1107
(614)422-6988

Dr G S Samuelsen
Department of Mechanical
Engineering
University of California
Irvine CA 92717
(714)856-5468

Mr John Sanborn
Garrett Turbine Engine Company
111 South 34th Street
P. O. Box 5217
Phoenix AZ 85010
(602)231-2588

Dr Billy Sanders
University of California
Davis CA 95616

Dr Joseph Sangiovanni
United Technologies Research
Center
Silver Lane
East Hartford CT 06108
(203)727-7328

Dr Lakshmi Sankar
School of Aerospace Engrg
Georgia Institute of
Technology
Atlanta GA 30332
(404)894-3014

Dr Domenic Santavicca
Department of Mechanical
Engineering
Pennsylvania State University
University Park PA 16802
(814)863-1863

Dr R J Santoro
Department of Mechanical
Engineering
Pennsylvania State University
University Park PA 16801
(814)863-1285

Mr William Scallion
NASA Langley Research Center
Mail Stop 408
Hampton VA 23665
(804)864-5235

Dr Klaus Schadow
Naval Weapons Center
Code 3892
China Lake CA 93555-6001
(619)939-6532
AV437-6532

Dr George Cox
United Technologies
Pratt-Whitney
P.O. Box 109600
West Palm Beach FL 33410-9600
(407)796-2887
FAX 796-5825

Dr F E C Culick
Engrg and Appl Sci Dept
California Institute of
Technology
Pasadena CA 91125
(818)356-4470

Dr C L Dailey
TRW Space and Technology Group
Applied Technology Division
One Space Park
Redondo Beach CA 90278
(213)536-1874

Dr John Daily
University of Colorado
Engineering Center ME 1-13
Campus Box 427
Boulder CO 80309-0427
(303)492-7110

Dr B R Daniel
School of Aerospace Rngrg
Georgia Institute of
Technology
Atlanta GA 30332

Dr William Deininger
Jet Propulsion Laboratory
California Inst. of Technology
4800 Oak Grove Drive
Pasadena CA 91109
(818)354-7765

Mr S T Demetriades
STD Research Corp
P.O. Box C
Arcadia CA 91006
(818)357-2311

Dr Gregory Dobbs
United Technologies Res. Ctr.
MS 129-90 Silver Lane
East Hartford CT 06108
(203)727-7145
FAX 727-7669

Dr Joel Dubow
Materials Science
Univ of Utah
2008B Mechanical Engrg Bldg
Salt Lake City UT 84112
(801)581-8388

Dr John Eisch
Department of Chemistry
State University of New York
Binghamton NY 13901
(607)798-3994

Dr William Escher
NASA Headquarters
Code RP
Washington DC 20546
(202)453-9111

Dr James Fang
Rockwell/Rocketdyne Division
6633 Canoga Park
Canoga Park CA 91303
(818)718-3728
FAX 718-3600

Mrs Karen Farner
OLAC PL/RKLB
Edwards AFB CA 93523-5000
(805)275-5198
AV525-5198

Dr Allan Ferrenberg
Manager, Advanced Comb. Device
Rocketdyne Div, Rockwell Int.
Mail Stop IR06,6633 Canoga Ave
Canoga Park CA 91303
(818)718-3713

Dr Anthony Strawa
NASA Ames Research Center
MS 230-2
Moffett Field CA 94035
(415)604-3437

Dr F D Stull
WL/POPS
Wright-Patterson AFB OH 45433-6563
(513)255-5210
AV785-5210

Dr B Sturtevant
Engrg and Appl Sci Dept
California Institute of
Technology
Pasadena CA 91125

Dr G Sullins
Applied Physics Laboratory
Johns Hopkins University
Johns Hopkins Road
Laurel MD 20707-6099
(301)953-5000

Dr Dexter Sutterfield
National Institute for
Petroleum and Energy Research
Post Office Box 2128
Bartlesville OK 74005
(918)337-4251

Dr Larry Talbot
Department of Mechanical
Engineering
University of California
Berkeley CA 94720
(415)642-6780

Dr Christopher Tam
Department of Mathematics
Florida State University
Tallahasee FL 32306-3027
(904)644-2455

S Richard Tankin
Mechanical Engineering Dept
Northwestern University
Evanston IL 60208-3111
(708)491-3532

Dr Julian Tishkoff
AFOSR/NA
Bolling AFB DC 20332-6448
(202)767-0465
AV297-0465

Dr T Y Toong
Department of Mechanical
Engineering
MIT
Cambridge MA 02139
(617)253-3358

Dr Michael Trenary
Department of Chemistry
The University of Illinois
Chicago IL 60680

Dr Timothy Troutt
Department of Mechanical
Engineering
Washington State University
Pullman WA 99164-2920

Dr Allen Twarowski
Rockwell International Sci Ctr
1049 Camino dos Rios
P O Box 1085
Thousand Oaks CA 91360
(805)373-4576

Dr C J Ultee
United Technologies Research
Center
Silver Lane
East Hartford CT 06108

Dr Ashwani K Gupta
Director, Combustion Lab.
The University of Maryland
Dept. of Mechanical Engrg.
College Park MD 20742
(301)454-8865

Mr Eugene Haberman
OLAC PL/MK
Stop 24
Edwards AFB CA 93523-5000
(805)275-5420
AV525-5420

Dr V E Haloulakos
Advanced Propulsion
McDonnell Douglas
5301 Bolsa Avenue
Huntington Beach CA 92647
(714)896-3456

Dr Elmer Hansen
Department of Mechanical
Engineering
University of Florida
Gainesville FL 32611
(904)392-0802

Lt Col George Haritos
AFOSR/NA
Bolling AFB DC 20332-6448
(202)767-4987
FAX:767-0466

Dr Kenneth Harstad
Jet Propulsion Laboratory
4800 Oak Grove Drive
Pasadena CA 91109

Dr David Hastings
Department of Aeronautics
and Astronautics
Massachusetts Inst of Tech
Cambridge MA 02139

Ms Sharon Hasty
John Hopkins Univ/APL
CPIA
John Hopkins Road
Laurel MD 20707
(301)992-7306

Dr Donald Hautman
United Technologies Res. Ctr.
Silver Lane
East Hartford CT 06108
(203)727-7424

Dr Helmut Hellwig
AFOSR/CC
Bolling AFB DC 20332-6448
(202)767-5017
AV297-5017

Dr Alan Hersh
Hersh Acoustical Engineering
9545 Cozycroft Avenue
Chatsworth CA 91311
(818)998-8311
FAX 341-0978

Dr Rich Hollins
Naval Weapons Center
China Lake CA 93555-6001
(619)939-1650
AV437-1650

Dr H R Jacobs
Mechanical Engg Bldg, 208
Penn State University
University Park PA 16802
(814)863-2519
FAX 865-3389

Dr J I Jagoda
Aerospace Engineering Dept
Georgia Institute of
Technology
Atlanta GA 30329
(404)894-3060

Dr E E Zukoski
Engrg. and Appl. Sci. Dept.
California Institute of
Technology
Pasadena CA 91125
(818)356-4785

Dr Kenneth Kolouko
Morton Thiokol
Wasatch Division
P.O. Box 524
Brigham City UT 84302
(801)863-4220

Dr James Komar
Atlantic Research Corp
5390 Cherokee Avenue
Alexandria VA 23312
(703)642-4473

Dr Herman Krier
Dept of Mechanical and
Industrial Engineering
University of Illinois
Urbana IL 61801
(217)333-0529

Prof M Kristiansen
P.W. Horn Professor
Dept of Electrical Engg,MS3102
Texas Tech University
Lubbock TX 79409-4439
(806)792-3007

Dr Warren Krueger
167 Alvana Street, NW16-160
Massachusetts Institute of
Technology
Cambridge MA 02139
(617)253-0236

Dr Al Kudlach
OLAC PL/RKLA
Edwards AFB CA 93523-5000
(805)275-5248
AV 525-5248

Dr Paul Kuentzmann
Office National D'Etudes et de
rechersches Aerospatiales
29,Ave. de la Division Leclerc
Chatillon-sous-Bagneux France

Dr Kenneth Kuo
Penn State University
208 Mechanical Engineering
University Park PA 16802
(814)863-6741
FAX 863-3203

Dr William Larson
OLAC PL/LSVF
Edwards AFB CA 93523-5000
(805)275-5657
AV525-5657

Dr C K Law
Department of Mechanical and
Aerospace Engineering
Princeton University
Princeton NJ 08544-5263
(609)258-5271

Dr Miller Layton
OLAC PL/LKLR
Stop 24
Edwards AFB CA 93523-5000

Dr Joel Lebowitz
Rutgers-The State University
Department of Mathematics
Hill Center-Busch Campus
New Brunswick NJ 08903
(201)932-3117

Mr Edward Lee
Special Projects Leader
P.O. Box 808,L-368
LLNL-University of California
Livermore CA 94550
(415)422-1316

Dr Ja H Lee
NASA Langley Research Center
M/S493
Hampton VA 23665
(804)864-4332

Dr Larry Goss
Research Applications Division
Systems Research Labs, Inc.
2800 Indian Ripple Road
Dayton OH 45440-3696
(513)252-2706

Dr Ronald Hanson
Department of Mechanical
Engineering
Stanford University
Stanford CA 94305-3032
(415)723-1745

Dr D L Hartley
Combustion Sciences
Sandia National Laboratories
Livermore CA 94551-0969

Dr L Hesselink
Department of Aeronautics and
Astronautics
Stanford University
Stanford CA 94305-3032
(415)723-3466

Dr E D Hirleman
Department of Mechanical and
Aerospace Engineering
Arizona State University
Tempe AZ 85287
(602)965-3895
FAX:965-1384

Dr Donald Holve
Insitec
28 Bobbie Court
Danville CA 94526
(415)837-1330

Dr David Huestis
SRI International
333 Ravenswood Avenue
Menlo Park CA 94025
(415)859-3464

Dr Thomas Ishii
Department of Electrical
Engineering
Marquette University
Milwaukee WI 53233
(414)288-6998
FAX:288-7082

Dr Jay Jeffries
SRI International
333 Ravenswood Avenue
Menlo Park CA 94025
(415)859-6431

Dr Roman Kuc
Department of Electrical
Engineering
Yale University
New Haven CT 06520
(203)432-4891

Dr Marshall Long
Department of Mechanical
Engineering
Yale University
New Haven CT 06520
(203)432-4229

Dr Bruce MacDonald
Research Applications Division
Systems Research Labs, Inc.
2800 Indian Ripple Road
Dayton OH 45440-3696
(513)252-2706

Dr T E Parker
Physical Sciences
20 New England Business Center
Andover MA 01810
(508)689-3232

Dr Timothy Parr
Naval Weapons Center
Code 3893
China Lake CA 93555
(619)939-2521

Dr John McVey
Rasor Associates, Inc
253 Humboldt Court
Sunnyvale CA 94086
(408)734-1622

Dr Franklin Mead
OLAC PL/LKVE
Edwards AFB CA 93523-5000
(805)275-5540
AV525-5540

Dr Carl Melius
Sandia National Laboratories
Livermore CA 94551-0969
(415)294-2650

Dr Charles Merkle
205 ME
Pennsylvania State University
University Park PA 16802
(814)863-1501
FAX 865-3389

Dr Claude Merrill
OLAC PL/MKPL
Stop 24
Edwards AFB CA 93523-5000
(805)275-5169
AV525-5169

Dr Michael Micci
233 Hammond Building
Pennsylvania State University
University Park Pa 16802
(814)863-0043

Dr George Miley
University of Illinois
103 South Goodwin Avenue
214 Nuclear Engineering Lab
Urbana IL 61801
(217)333-3772

Dr Richard Miller
Office of Naval Research
Mechanics Division, Code 432
800 North Quincy Street
Arlington VA 22217-5000
(202)696-4403

Dr Charles Mitchell
Dept. of Mechanical Engineerin
Colorado State University
Fort Collins CO 80523
(303)491-6654

Mr T S Mogstad
McDonnell Douglas Astr.Co-West
Design And Tech. Center
Huntington Beach CA 92647
(714)896-3437

Dr Robert Moriarty
University of Illinois
(Chicago Circle)
Department of Chemistry
Chicago IL 60680
(312)996-2364

Dr Marlow Moser
OLAC PL/DYCC
Stop 24
Edwards AFB CA 93523-5000
(805)275-5442
AV525-5442

Dr Kenneth Moses
Fusion Physics and Technology
3547 Voyager Street, Suite 104
Torrance CA 90503-1667
(213)542-3800

Dr Philip Muntz
Dept. of Aerospace Engineering
University of Southern
California
Los Angeles CA 90089

Dr Don Penn
OLAC PL/RKLB
Edwards AFB CA 93523-5000
(805)275-5316
AV525-5316

Dr Jerry Pieper
Aerojet Techsystems
P.O. Box 13222
Sacramento CA 95813
(916)355-3087

Dr Robert Poeschel
Plasma Physics Department
Hughes Research Laboratories
3011 Malibu Canyon Road
Malibu CA 90265
(213)317-5443

Dr Dimos Poulikakos
University of Illinois
(Chicago Circle)
Dept. of Mechanical Engg.
Chicago IL 60680
(312)996-5239

Dr Edward Price
School of Aerospace Engrg
Georgia Institute of
Technology
Atlanta GA 30332-0420
(404)894-3063

Dr Richard Priem
Priem Consultants
13533 Mohawk Trail
Cleveland OH 44130
(216)845-1083

Dr Andrej Przekwas
CFD Research Corporation
3313 Bob Wallace Ave,Suite 205
Huntsville AL 35805
(205)536-6576

Dr Lawrence Quinn
OLAC PL/DYC
Edwards AFB CA 93523-5000
(805)275-5353
AV 525-5353

Dr Frederick Reardon
Cal State U.-Sacramento
Dept of Mechanical Engineering
6000 J Street
Sacramento CA 95616
(916)278-6727

Dr Russell Reed
Naval Weapons Center
China Lake CA 93555-6001
(619)939-7296
AV437-7296

Dr Robert Rhein
Research Chemist
Code 3244
Naval Weapons Center
China Lake CA 93555-6001
(619)939-7392
AV 437-7310

Dr J W Rich
Department of Mechanical
Engineering
The Ohio State University
Columbus OH 43210-1194
(614)292-6309

Dr Frank Roberto
OLAC PL/MKP
Stop 24
Edwards AFB CA 93523-5000
(805)275-5430
AV525-5430

Dr Stephen Rodgers
OLAC PL/LKLR
Stop 24
Edwards AFB CA 93523-5000
(805)275-5416
AV525-5416

photographic images of OH emission. At a high-speed stagnation temperature of 1900 K, the mixing layer ignited for oxygen mol fractions above 12% and hydrogen mol fractions above 5%. A composite OH emission image is shown in Figure 2. Ignition occurs a few centimeters downstream of the splitter tip. Some residual OH emission from the vitiated-air stream is visible at the furthest upstream position.

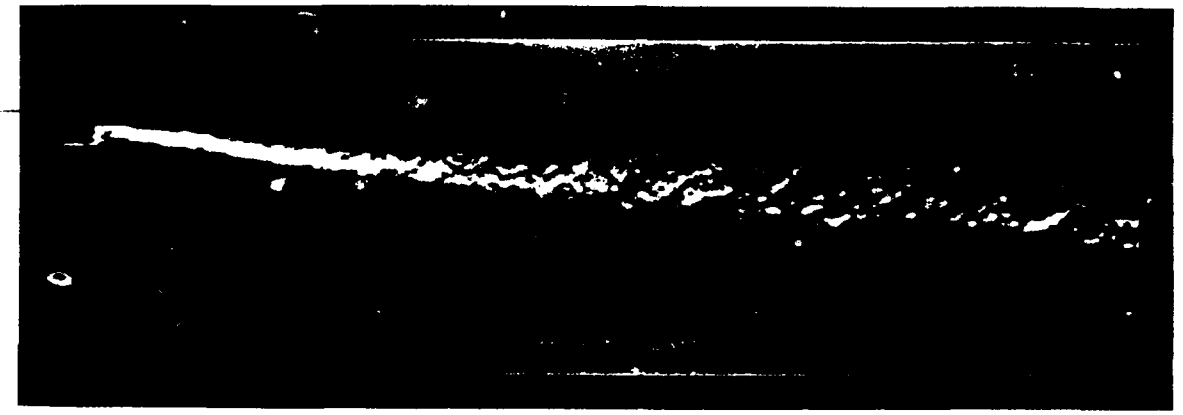

Figure 1. Schlieren image of nonreacting mixing layer. Top stream: T_0 = 1900 K and M = 1.35; bottom stream: T_0 = 300 K and M = 0.3. M_c = 0.88 and P_{static} = 12 psi. Splitter tip is located at the left-hand side of the image.

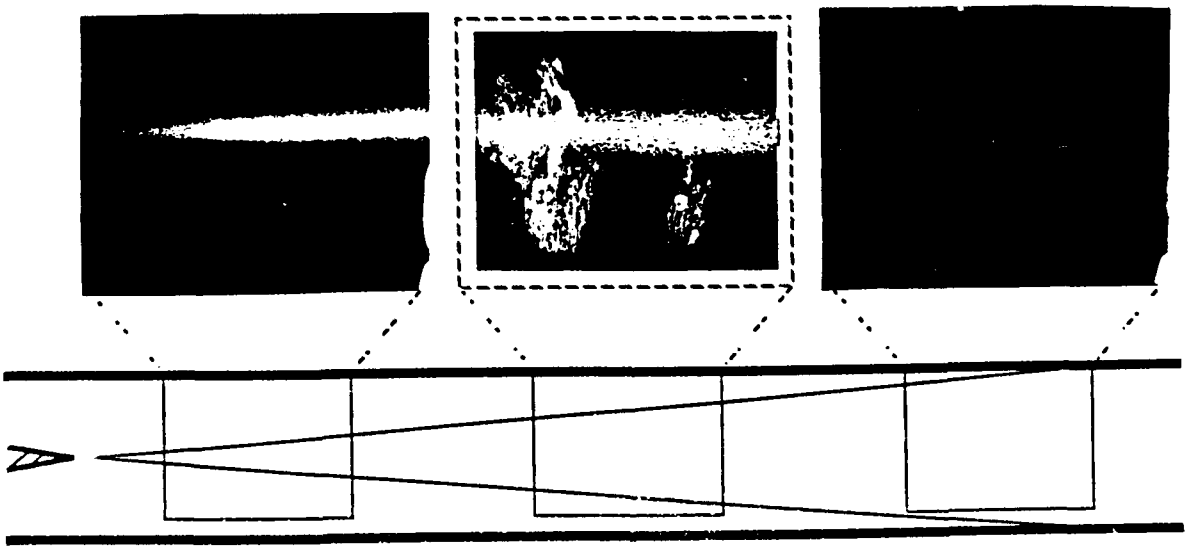

Figure 2. Composite ultraviolet emission image of reacting mixing layer. Top stream: T_0 = 1900 K, M = 1.35 and X_{02} = 0.16, bottom stream: T_0 = 300 K, M = 0.3 and X_{H2} = 0.06. M_c = 0.88 and P_{static} = 12 psi.

Current experiments are focussed on studying the effects of compressibility and heat release on the structure of the reacting mixing layer. The compressibility of the mixing layer is controlled by the high-speed stream temperature and Mach number; the heat release is controlled by the oxygen and hydrogen mol fractions. Planar laser-induced fluorescence measurements of OH are being used to determine the structure of the reacting mixing layer; OH marks the regions of the mixing layer where chemical reaction is occurring and where hot combustion products are present. The optical access of the test section allows planar visualizations in three orthoganal planes. These images will be compared to the time-averaged OH emission images and schlieren visualizations. Also, preparations are being made to seed the low-speed stream with acetone and simultaneously image the OH and acetone fluorescence. The acetone marks unmixed fuel in the mixing layer since it does not fluoresce at elevated temperatures. The simultaneous OH and acetone fluorescence images will be useful in determining the structure of the reacting mixing layer.

Dr Herbert Schrade
Institut Fur Raumfahrtantriabe
Universitat Stuttgart
Pfaffenwaldring 31
D-7000 Stuttgart GE
7116-852-383
or 375

Dr Gary Sega
Aerospace Corp
P.O. Box 92957
MS/747
Los Angeles CA 90004
(213)648-6501

Maj Scott Shackelford
F J Seiler Research Laboratory
United States Air Force Acad
Colorado Springs CO 80840
(719)472-2655

Dr Pam Sherretz
Naval Weapons Center
China Lake CA 93555-6001
(619)939-7392
AV437-7392

Dr R Shoureshi
School of Mechanical
Engineering
Purdue University
West Lafayette IN 47907
(317)494-5639

Prof Jean'ne Shreeve
Dept of Chemistry
University of Idaho
Moscow ID 83843
(208)885-6554

Dr Isaac F Silvera
Harvard University
Department of Physics
Cambridge MA 02138
(617)495-9075

Dr William Sirignano
College of Engineering
University of California
Irvine CA 92717
(714)856-6002

Ms Elizabeth Slimak
OLAC PL/LSCF
Edwards AFB CA 93523-5000

Lt Col LaRell Smith
EOARD/LRC
Box 14
FPO NY 09510-0200
AV235-4505

Dr Ronald Spores
OLAC PL/LSVE
Edwards AFB CA 93523-5000
(805)275-5766
AV 525-5766

Dr Warren Strahle
School of Aerospace Engrg
Georgia Institute of
Technology
Atlanta GA 30332
(404)894-3032

Dr William C Stwalley
The University of Iowa
Iowa Laser Facility
Chemistry and Physics
Iowa City IA 52242-1294
(319)335-1299

Dr V V Subramaniam
Department of Mechanical
Engineering
The Ohio State University
Columbus OH 43212-1194
(614)292-6096

work are available in a paper by Lee et al. (see Ref. list). Shock tunnel imaging has also emphasized NO, and has progressed to the point that quantitative single-shot imaging of both velocity and temperature (rotational/translational) has been achieved. A sample comparison of radial velocity data with MOC calculations is shown in Fig. 3. Two different algorithms have been used to relate the PLIF signal to the Doppler shift: one based on a simple linear model of laser lineshape, valid only for small shifts in frequency, and a more complex model suitable for larger shifts. Agreement with the MOC calculations is quite good. Modifications to the laser system and shock tunnel are now planned which will extend this work to single-shot imaging of two velocity components. See the paper by Palmer et al. for details. Application of these methods in the supersonic mixing layer will begin during the coming year.

Stability and Numerical Simulation

The computational phase of the program focuses on stability analyses (which reveal the key flow mechanisms and probable flow structures) and direct numerical simulations (which reveal the non-linear features of the flow). Together these have shown that the number of maxima of the mean profile of the density-mean vorticity product determines the number of instability modes. In reacting mixing layers, there are two such peaks, so the layer behaves as two independent colayers as shown in Fig. 4. The size of each colayer and its structural obliquity depend on the free-stream temperature ratio, the flame temperature, and the position of the flame inside the layer. At high speeds, the large-scale structures on the two sides of the layer evolve nearly independently from one another, and serve to mix fuel with product and oxidizer with product, but not fuel with oxidizer. The predicted result is a relatively flat flame, a structural feature of compressible reacting mixing layers that will be investigated in the laboratory experiments.

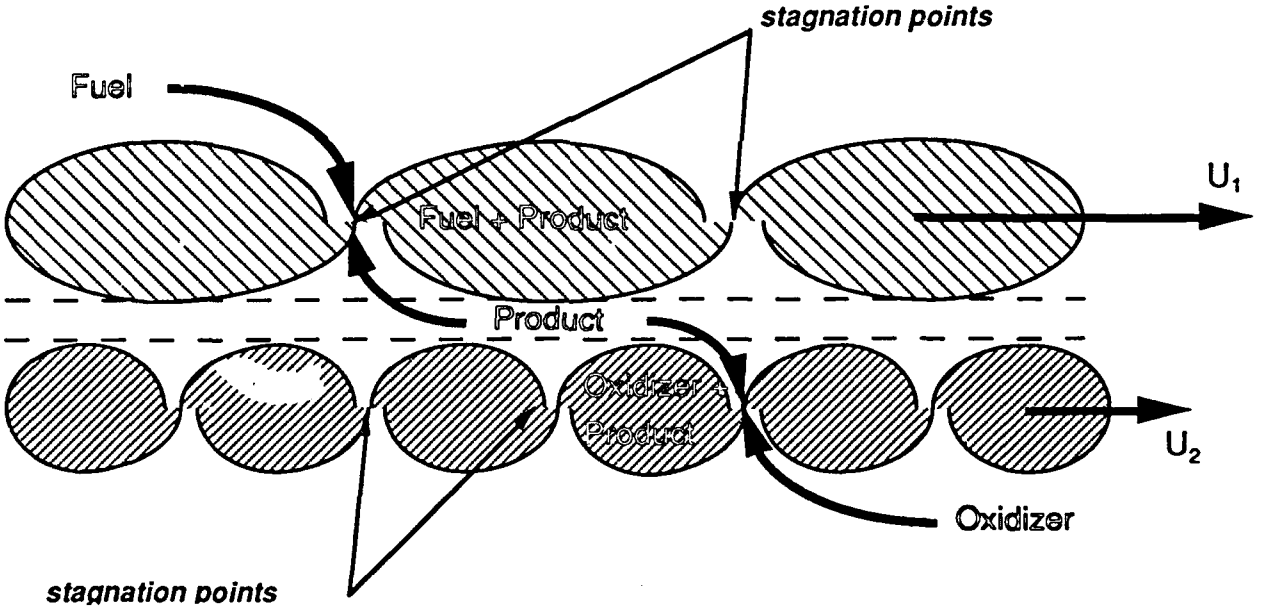

Figure 4. Direct numerical simulation results for the structure of a high-speed reacting mixing layer.

References

1. M. P. Lee, B. K. McMillin and R. K. Hanson: Temperature Measurements in Gases Using Planar Laser-Induced Fluorescence Imaging of NO, Applied Optics, submitted April 1992.

2. J. L. Palmer, B. K. McMillin and R. K. Hanson: Planar Laser-Induced Fluorescence Imaging of Velocity and Temperature in a Shock Tunnel, Paper AIAA 92-0762, AIAA 30th Aerospace Sciences Meeting, Reno, January 1992.

Dr David Weaver
OLAC PL/DYCR
Edwards AFB CA 93523-5000
(805)275-5657
AV525-5657

Dr Jim Weber
Rocketdyne Division
Rockwell International Corp.
6633 Canoga Ave
Canoga Park CA 91303
(818)710-5558

Dr Richard Weiss
OLAC PL/CA
Edwards AFB CA 93523-5000
(805)275-5622
AV525-5622

Dr Rodney Willer
Morton Thiokol Inc
Elkton Division
P.O. Box 241
Elkton MD 21921
(301)398-3000
(301)398-4440

Dr Forman A Williams
Center for Energy and
Combustion Research, 0411
University of California
La Jolla CA 92093-0411
(619)534-5492

Dr W S Williamson
Plasma Physics Department
Hughes Research Laboratories
3011 Malibu Canyon Road
Malibu CA 90265
(213)317-5443

Dr D O Woolery
Rocketdyne
6633 Canoga Avenue
Canoga Park CA 91304

Dr Ted Yang
Massachusetts Institute of
Technology
167 Albany Street
Cambridge MA 02139
(617)253-8453

Dr Vigor Yang
Department of Mechanical
Engineering
Pennsylvania State University
University Park PA 16802
(814)863-1502
FAX 865-3389

Dr Thomas York
AERO/ASTRO Engineering
328 CAE Building
Ohio State University
Columbus OH 43210
(614)292-2691

Dr Ben Zinn
School of Aerospace Engrg
Georgia Institute of
Technology
Atlanta GA 30332
(404)894-3033

Capt Joseph Zirrolli
FJSRL/NC
United States Air Force
Academy
Colorado Springs CO 80840
(303)472-2655

Mr Robert Zurawski
Program Manager
Propulsion Technology Programs
NASA HQA, OAST-MAIL CODE RP
Washington DC 20546
(202)453-2261

The velocity-composition joint pdf evolution equation is solved by an explicit Lagrangian Monte Carlo method. This joint pdf is iteratively adjusted in velocity sub-space to agree with the mean velocity fields given by the implicit finite-volume CFD procedure for the elliptic equations. By proper refinement of grid, "numerical diffusion" in the finite-volume mean flow calculation was eliminated [8]. Particle mixing occurs via deterministic relaxation to the mean, at a frequency obtained from the turbulence kinetic energy and dissipation rate equations. Thermochemical properties evolve according to the partial equilibrium model as described by two scalar variables, the mixture fraction and a reaction progress variable for the partially equilibrated oxyhydrogen radical pool. The mean density field obtained from the pdf calculation is passed back to the finite-volume sub-model and the hybrid algorithm is iterated to convergence.

Centerline profiles of the mean and rms of mixture fraction agree with the data except in the region beyond x/d=20, where the jet decay rates and turbulence levels are too low (Fig. 2). The agreement in the zone of high shear (x/d < 20) is within that expected of the partial equilibrium thermochemical model; comparisons on mean temperature (Fig. 3) and mean CO (Fig. 4) are shown here. Further comparisons are made in Ref. 8 with similar Raman profiles of mean major species, and mean and rms of mixture fraction.

II. Homogeneous Mixing Processes:

To concentrate computational power on interactions of turbulence with a "full" kinetic scheme, a hypothetical "partially-stirred reactor" is considered. The prototypical equation for a reactive quantity "ϕ" (e.g., mass fractions) in this spatially homogeneous but unmixed flow is:

$$\frac{d\phi^{(n)}}{dt} = -c_\phi \omega \left(\phi^{(n)} - \overline{\phi} \right) + \dot{w}^{(n)} \qquad (1)$$

Superscript (n) is the particle index. The first term is the deterministic relaxation-to-the-mean referred to above [3,8], but other models could be substituted. The second term is the total chemical rate term for quantity "ϕ" and can be arbitrarily complicated. A time-marching algorithm provides particle tracking solutions of Eq. (1). A steady-state ensemble is obtained from which scatter-plots and various correlations can be obtained. The limiting cases of very fast and very slow mixing are being reproduced for CO/H_2 fuels (18 species, 43 reactions). The code is being implemented on an Intel hypercube, as a prelude to full methane chemistry.

REFERENCES

[1] Correa, S.M.,"Relevance of Non-premixed Laminar Flames to Turbulent Combustion," in *Major Research Topics in Combustion,* Hussaini, M.Y., Kumar, A., and Voight, R.G., Eds., pp. 45-69, Springer-Verlag, 1992.

[2] Correa, S.M.,"A Review of NO_x Formation Under Gas-Turbine Combustion Conditions," in press, *Comb. Sci. and Tech.,* 1991.

[3] Pope, S.B., Twenty-Third (International) Symposium on Combustion, The Combustion Institute, Pittsburgh, PA, pp. 591-612, 1990.

[4] Pope, S.B. and Correa, S.M., Twenty-First (International) Symposium on Combustion, The Combustion Institute, Pittsburgh, PA, pp. 1341-1348, 1986.

[5] Correa, S.M. and Gulati, A.,"Measurements and Modeling of a Bluff-Body Stabilized Flame," in press, *Comb. and Flame,* 1992.

[6] Mansour, M.S., Bilger, R.W., and Dibble, R.W., Twenty-Second (International) Symposium on Combustion, The Combustion Institute, Pittsburgh, PA, pp. 711-719, 1989.

[7] Schefer, R.W., Namazian, M., and Kelly, J., Twenty-Second (International) Symposium on Combustion, The Combustion Institute, Pittsburgh, PA, pp. 833-842, 1989.

[8] Correa, S.M. and Pope, S.B.,"Comparison of a Hybrid Monte-Carlo PDF/Finite-Volume Mean Flow Model with Bluff-Body Raman Data," Twenty-Fourth (International) Symposium on Combustion, Sydney, Australia, July 5-10, 1992.

AIRBREATHING COMBUSTION

Invitees

Dr Suresh P Aggarwal
Mechanical Engineering Dept
University of Illinois
at Chicago
Chicago IL 60680
(312)996-2235

Dr Griffin Anderson
NASA Langley Research Center
M/S 168
Hampton VA 23665
(804)864-3772

Dr Scott Anderson
Department of Chemistry
State University of New York
Stony Brook NY 11794-3400
(516)632-7915

Dr K Annamalai
Mechanical Engineering Dept
Texas A&M University
College Station TX 77843-3123

Dr Kurt Annen
Aerodyne Research, Inc.
45 Manning Road
Manning Park Research Center
Billerica MA 01821-3976
(508)663-9500
FAX:663-4918

Dr Jad Batteh
Science Applications
International Corporation
1519 Johnson Ferry Rd #300
Marietta GA 30062
(404)973-8935
FAX:973-6971

Dr Simon Bauer
Department of Chemistry
Cornell University
Ithaca NY 14853-1301

Dr S L Baughcum
Spectra Technology
2755 Northrup Way
Bellevue WA 98004-1495
(206)828-3517

Dr Howard Baum
National Institute of
Standards and Technology
Center for Fire Research
Gaithersburg MD 20899
(301)975-6668

Dr John Bdzil
Los Alamos National Laboratory
Los Alamos NM 87545

Dr H L Beach
NASA Langley Research Center
MS 168
Hampton VA 23665-5225
(804)864-3772
(804)864-2658

Dr Josette Bellan
Applied Technologies Section
Jet Propulsion Laboratory
4800 Oak Grove Drive
Pasadena CA 91109
(818)354-6959

Dr Michael Berman
AFOSR/NC
Bolling AFB DC 20332-6448
(202)767-4963
DSN 297-4963

Dr Paul Bonczyk
United Technologies Research
Center
Silver Lane
East Hartford CT 06108
(203)727-7162

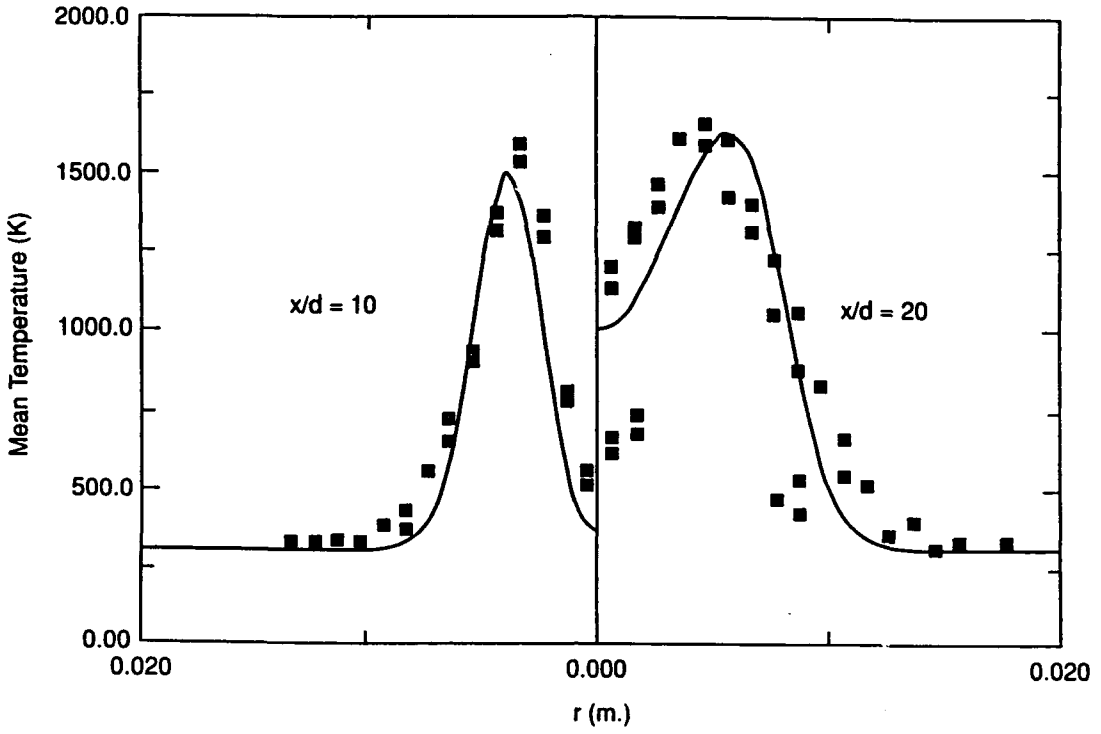

Figure 3. Comparisons of radial temperature profiles.

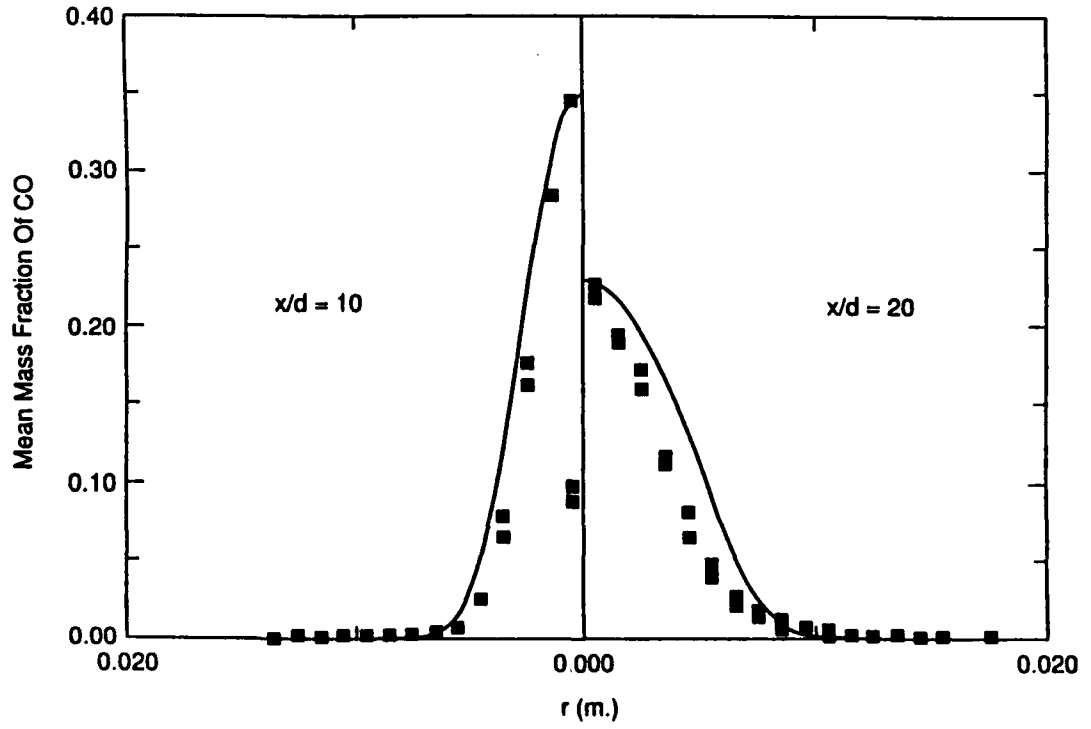

Figure 4. Comparisons of radial CO profiles.

Dr Graham Candler
Mars Mission Research Center
North Carolina State
University
Raleigh NC 27695-7921
(919)515-5941
FAX:515-5934

Dr Brian Cantwell
Department of
Mechanical Engineering
Stanford University
Stanford CA 94305-3032
(415)723-4825

Dr Tryfon Charalampopoulos
Mechanical Engineering Dept.
Louisiana State University
Baton Rouge LA 70803
(504)388-5792
(504)388-5799

Capt Wayne Chepren
HQ AFESC/RDV
Tyndall AFB FL 32403-6001
(904)283-4234
AV523-4234

Dr Norman Chigier
Department of Mechnanical
Engineering
Carnegie-Mellon University
Pittsburgh PA 15213-3890
(412)578-2498

Dr Robert Childs
Nielsen Engineering and
Research, Inc.
510 Clyde Avenue
Mountain View CA 94043-2287
(415)968-9457

Dr S Y Cho
Department of Mechanical and
Aerospace Engineering
Princeton University
Princeton NJ 08544-5263

Dr M-S Chou
Building R1, Room 1044
TRW Space and Technology Group
One Space Park
Redondo Beach CA 90278
(213)535-4321

Mr R.W. Claus
NASA Lewis Research Center
21000 Brookpark Road
Cleveland OH 44135-3127
(216)433-5869

Mr Steven Clouser
Research and Technology Group
Naval Air Propulsion Center
Trenton NJ 08628
(609)896-5752
AV442-7752

Dr M B Colket
United Technologies Research
Center
Silver Lane
East Hartford CT 06108
(203)727-7481

Mr Stephen Corda
Applied Physics Laboratory
Johns Hopkins University
Johns Hopkins Road
Laurel MD 20707-6099
(301)953-5000
Ext 4654

Dr S M Correa
General Electric - Corporate
Research and Development
P. O. Box 8
Schenectady NY 12301
(518)387-5853

Dr C Criner
Mach I, Inc
346 East Church Road
King of Prussia PA 19406
(803)292-3345

layers in turbulent flows (see Figs. 1 and 2) and their connection with various scaling analyses (e.g. see Ref. 4). The second task is extending our earlier fully-resolved, two-dimensional, planar laser Rayleigh imaging measurements (see Ref. 6) to four-dimensions to allow direct measurement of the $Sc = 1$ molecular mixing process in gaseous turbulent flows. Such data provide a fully-detailed description of the mixing process in gaseous turbulent flows comparable in many respects to the four-dimensional data we are obtaining for large Schmidt number molecular mixing. The third task is examining the equilibrium and nonequilibrium structure of the species concentration fields $Y_i(\mathbf{x},t)$ and reaction rate fields $w_i(\mathbf{x},t)$ in chemically reacting turbulent flows from the measured conserved scalar fields $\zeta(\mathbf{x},t)$, allowing a detailed examination of the structure of the chemical reaction processes in reacting turbulent flows (see Figs. 3 and 4). A final task is aimed at obtaining direct, fully-resolved, reacting flow imaging measurements of various species whose reaction rates span the range from fast to very slow reactions.

Our technical approach is centered on a new, geometry-independent, Lagrangian formulation for dealing with the nonequilibrium structure of chemically reacting turbulent flows in terms of the mixing of a conserved scalar field. Briefly, if the four-dimensional conserved scalar field $\zeta(\mathbf{x},t)$ and the corresponding instantaneous velocity field $\mathbf{u}(\mathbf{x},t)$ are simultaneously known, then it is possible to formulate the nonequilibrium chemical species concentration fields $Y_i(\mathbf{x},t)$ in terms of the scalar field as $Y_i(\mathbf{x},t) = f[\zeta(\mathbf{x},t), \dot{\zeta}(\mathbf{x},t), \ddot{\zeta}(\mathbf{x},t), \ldots]$, where the dots denote Lagrangian time derivatives, namely

$$\dot{\zeta}(t) = \left\{\frac{\partial}{\partial t} + \mathbf{u}\cdot\nabla\right\}\zeta(\mathbf{x},t)$$

and $\mathbf{u}(\mathbf{x},t)$ is the vector velocity field. As the extent of non-equilibrium decreases, the influence of higher Lagrangian derivative terms can be expected to become increasingly less significant. For example, for $Y_i(\mathbf{x},t) = f[\zeta(\mathbf{x},t), \dot{\zeta}(\mathbf{x},t)]$, the species reaction rate fields $w_i(\mathbf{x},t)$ can then be obtained as

$$\begin{aligned}\dot{w}_i(\mathbf{x},t) = -\frac{1}{ReSc}\Bigg\{&(\nabla\zeta\cdot\nabla\zeta)\left[\frac{\partial^2 Y_i}{\partial\zeta^2}\right]_{(\zeta,\dot{\zeta})}\\ &+(\nabla\zeta\cdot\nabla\dot{\zeta})\left[\frac{\partial^2 Y_i}{\partial\zeta\partial\dot{\zeta}}\right]_{(\zeta,\dot{\zeta})}\\ &+(\nabla\dot{\zeta}\cdot\nabla\dot{\zeta})\left[\frac{\partial^2 Y_i}{\partial\dot{\zeta}^2}\right]_{(\zeta,\dot{\zeta})}\\ &+(2\nabla\mathbf{u}:\nabla(\nabla\zeta)+\nabla^2\mathbf{u}\cdot\nabla\zeta)\left[\frac{\partial Y_i}{\partial\dot{\zeta}}\right]_{(\zeta,\dot{\zeta})}\Bigg\}\end{aligned}$$

The simultaneous conserved scalar and vector velocity field information required to practically apply this geometry-independent nonequilibrium formulation would, until recently, have seemed out of experimental reach. However, our work has shown (Refs. 3 and 6) that it is possible to extract the underlying vector velocity field $\mathbf{u}(\mathbf{x},t)$ from four-dimensional scalar field measurements. Our current work includes four-

Dr Frederick Dryer
Department of Mechanical and Aerospace Engineering
Princeton University
Princeton NJ 08544-5263
(609)258-5206

Dr C Dutton
Department of Mechanical and Industrial Engineering
University of Illinois
Urbana IL 61801

Dr Harry Dwyer
Department of Mechanical Engineering
University of California
Davis CA 95616

Dr Raymond Edelman
WC 70
Rocketdyne
6633 Canoga Avenue
Canoga Park CA 91304
(805)371-7196

Dr J T Edwards
WL/POSF
Wright-Patterson AFB OH 45433-6563
(513)476-7393
FAX:255-1125

Ms Charlotte Eigel
WL/POSF
Wright-Patterson AFB OH 45433-6563
(513)255-5106
AV785-5106

Dr Phillip Emmerman
Harry Diamond Laboratories
Attn. SLCHD-ST-RD
2800 Powder Mill Road
Adelphi MD 20783-1197
(301)394-3000

Mr Peter Erbland
National Aero-Space Plane JPO
ASD/NAF
Wright-Patterson AFB OH 45433-6503
(513)255-9757
AV785-255-9757

Dr K C Ernst
Pratt and Whitney Aircraft Group
Government Products Division
West Palm Beach FL 33402

Mr John Facey
Code RP
NASA
400 Maryland Avenue, SW
Washington DC 20546
(202)453-2854

Dr G M Faeth
Department of Aerospace Engineering
University of Michigan
Ann Arbor MI 48109-2140
(313)764-7202

Dr Francis Fendell
TRW Space and Technology Group
Building R1, Room 1022
One Space Park
Redondo Beach CA 90278
(213)812-0327

Dr Michael Frenklach
202 Academic Projects Building
The Pennsylvania State University
University Park PA 16802
(814)865-4392

Mr Jack Fultz
WL/POPR
Wright-Patterson AFB OH 45433-6563
(513)255-2175
AV785-2175

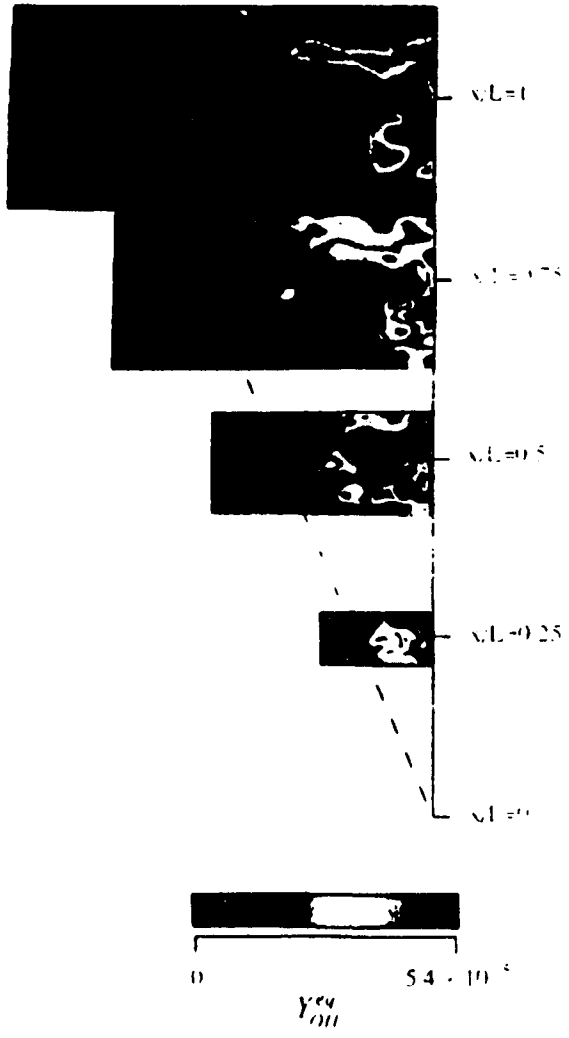

Fig. 3 Equilibrium OH mass fraction field $Y_{OH}(\mathbf{x},t)$ in a hydrogen-air jet diffusion flame deduced from fully-resolved planar Rayleigh imaging measurements of the conserved scalar field $\zeta(\mathbf{x},t)$ in a nonreacting turbulent jet at $Re_\delta \approx 14{,}000$.

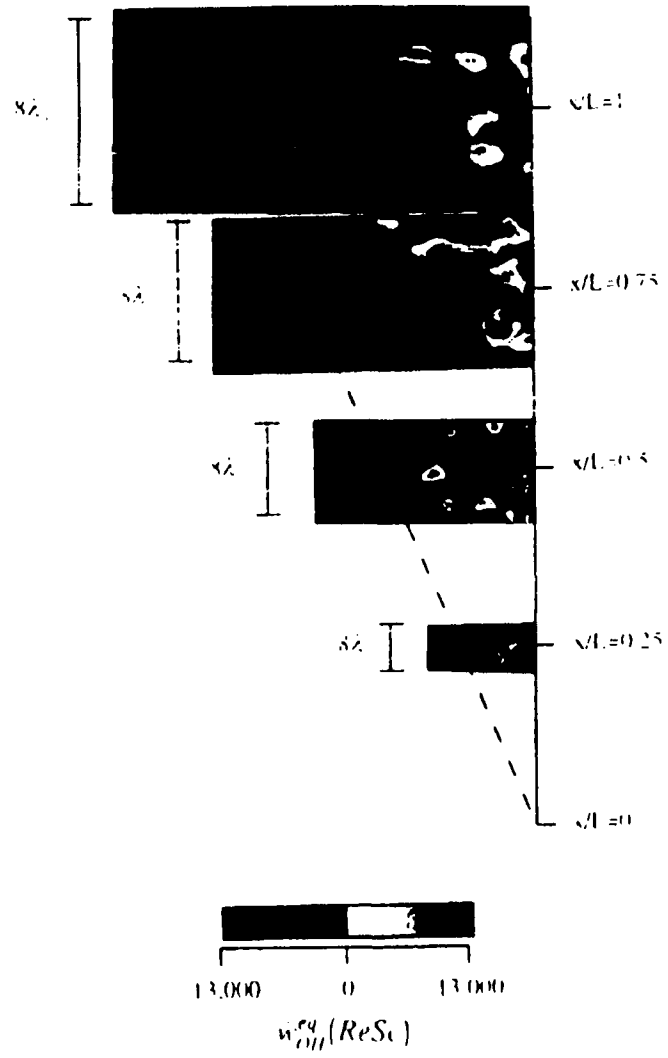

Fig. 4. Equilibrium OH reaction rate field $w_{OH}(\mathbf{x},t)$ in a hydrogen-air jet diffusion flame deduced from the same fully-resolved planar Rayleigh imaging measurement as in Fig. 3.

Mr Norman Hirsch
WL/POPR
Wright-Patterson AFB OH 45433-6563
(513)255-2175
AV785-2175

Dr David Hofeldt
125 Mechanical Engineering
111 Church Street, S E
University of Minnesota
Minneapolis MN 55455
(612)625-2045

Mr Robert Holland
United Technologies Chemical
Systems Division
P O Box 49028
San Jose CA 95161-9028
(408)224-7656

Dr M Y Hussain
ICASE, Mail Stop 132C
NASA Langley Research Center
Hampton VA 23665
(804)864-2175

Dr A K M F Hussain
Department of Mechanical
Engineering
University of Houston
Houston TX 77004
(713)749-4444

Dr Essam A Ibrahim
Department of Mechanical
Engineering
Tuskegee University
Tuskegee AL 36088
(205)727-8974

Dr T A Jackson
WL/POSF
Wright-Patterson AFB OH 45433-6563
(513)255-6462
AV785-6462

Mr Gordon Jensen
United Technologies Chemical
Systems Division
P O Box 49028
San Jose CA 95161-9028
(408)365-5552

Dr Sheridan Johnston
Combustion Sciences
Sandia National Laboratories
Livermore CA 94551-0969
(415)294-2138

Dr W-H Jou
M/S 7K-06
P. O. Box 3707
Seattle WA 98124-2207
(206)865-6102

Dr Ann Karagozian
Mechanical, Aerospace and
Nuclear Engineering Department
University of California, LA
Los Angeles CA 90024
(213)825-5653

Dr Laurence R Keefe
Nielsen Engineering and
Research, Inc.
510 Clyde Avenue
Mountain View CA 94043-2287
(415)968-9457
FAX:968-1410

Dr Arnold Kelly
Department of Mechanical and
Aerospace Engineering
Princeton University
Princeton NJ 08544-5263
(609)258-5221

Dr John Kelly
Altex Technologies Corporation
650 Nuttman Road
Suite 114
Santa Clara CA 95054
(408)980-8610

the same Mach numbers,‡ allows for an independent estimate of Reynolds number effects. The first of the supersonic, all helium diluent, reacting experiments has yielded an interesting surprise. The amount of chemiluminescence was substantially higher than had been experienced before, with colors, judged by eye at this point, possibly identifiable with overtone (anharmonic) emission from excited HF molecules. The emitted light is sufficiently intense to suggest that spectroscopic analysis should be undertaken. We plan to do this in the near future.

The last 12 months saw the completion and documentation of a large part of our work in turbulent reacting and non-reacting jets in the last 5 years, or so.♯ Specifically, the first part of the gas-phase, chemically reacting, turbulent-jet effort was completed and documented in the form of a Ph.D. thesis by R. Gilbrech (copies are available on request).[2] To summarize, this part of our effort focused on an experimental investigation of Reynolds number effects in turbulent jet mixing and combustion. Our gas-phase, chemically reacting jet experiments spanned jet Reynolds numbers in the range of $5 \times 10^3 \leq Re_{\text{gas}} \leq 1.5 \times 10^5$. The data indicate that the flame length L_f, can be expressed as a linear function of the stoichiometric ratio, ϕ, *i.e.*, $L_f/d^* \simeq A\,\phi + B$. where d^* is the momentum (source) diameter of the jet, as had traditionally been assumed, but that the dimensionless coefficients A and B must be accepted as Re-dependent. A first paper was presented at the 1992 *AIAA, Aerospace Sciences Meeting*, summarizing the experimental method and some of our results.[3] A by-product of this effort was the discovery of an interesting enhancement to molecular mixing, depending on the relative influence of buoyancy to momentum forces. We have undertaken a study of this behavior, which is important in the context of flow and mixing control, as part of a separate experimental effort currently in progress.

A separate part of our effort has focused on an experimental investigation of liquid-phase mixing in turbulent jets, over similar flow conditions covered in our gas-phase, chemically reacting jet experiments. A Ph.D. thesis by P. Miller, documenting parts of this effort, was also completed in the last 12 months (copies are available on request).[4] The difference in Schmidt number in the two sets of experiments, over almost the same range of Reynolds numbers, $3 \times 10^3 \leq Re_{\text{liq}} \leq 1.05 \times 10^5$, provides an invaluable comparison through the two sets of data with important clues on the fully-developed turbulent flow behavior at the small scales, where molecular mixing is taking place. In particular, our liquid-phase measurements of scalar fluctuations are in accord with the improvement in mixing-rate with increasing Reynolds number, found in our gas-phase measurements, even though the liquid-phase data do not exhibit a Re-independent regime to the highest Reynolds numbers that were investigated. These data corroborate results presented in a recent paper documenting an earlier set of measurements at lower Reynolds numbers ($Re \leq 2.4 \times 10^4$), and extend the range of validity of these conclusions.[5]

---

‡ $M_1 = 1.55, M_2 = 0.2$, plus high subsonic runs.

♯ The investigations of turbulent jet mixing are co-sponsored by the Gas Research Institute.

Dr Marshall Lapp
High Temperature Interfaces Division
Sandia National Laboratories
Livermore CA 94551-0969
(415)294-2435

Dr John Larue
Department of Mechanical Engineering
University of California
Irvine CA 92717

Dr A Laufer
Office of Energy Research
U. S. Department of Energy
1000 Independence Avenue, N.W.
Washington DC 20585
(202)903-5820

Dr N M Laurendeau
Department of Mechanical Engineering
Purdue University
West Lafayette IN 47907
(317)494-2713

Dr Moshe Lavid
ML Energia, Inc.
P. O. Box 1468
Princeton NJ 08540
(609)799-7970

Dr C K Law
Department of Mechanical and Aerospace Engineering
Princeton University
Princeton NJ 08544-5263
(609)258-5271
FAX:258-6109

Dr Stan Lawton
McDonnell Douglas Research Lab
McDonnell Douglas Corporation
PO Box 516
St Louis MO 63166-0516
(314)233-2547

Dr J Carl Leader
McDonnell Douglas Research Lab
McDonnell Douglas Corporation
PO Box 516
St Louis MO 63166-0516
(314)232-4687

Dr C C Lee
Environmental Protection Agency
Cincinnati OH 45268
(513)569-7520

Dr Spiro Lekoudis
Office of Naval Research
Mechanics Division, Code 432
800 North Quincy Street
Arlington VA 22217-5000
(202)696-4406

Dr Anthony Leonard
Graduate Aeronautical Labs
California Institute of Technology
Pasadena CA 91125
(818)356-4465

Dr R S Levine
National Institute of Standards and Technology
Center for Fire Research
Gaithersburg MD 20899
(301)921-3845

Dr Erwin Lezberg
NASA Lewis Research Center
21000 Brookpark Road
Cleveland OH 44135-3127
(216)433-5884

Dr Paul Libby
Center for Energy and Combustion Research, 0411
University of California
La Jolla CA 92093-0411
(619)534-3168

We are continuing our numerical simulation work on multidimensional, compressible flows. The mathematical and numerical simulation progress that has been made will be applied to compute flows that cannot be computed reliably with standard methods. Progress this last year has included the development of data structures for front-tracking purposes. They are an extremely useful tool for a variety of applications. In addition to the computation of reacting flows with detonation fronts, the front-tracking software can be used for flows with flame fronts or other physical interfaces of interest. Our scheme is sufficiently general to also allow the treatment of solid boundaries as fronts and thus compute flows on simple orthogonal grids, with bodies present in the flow, *whose boundaries need not conform with the grid coorainates*. The modification of the codes, as needed for each application, is straightforward.

In our diagnostics development effort, we have completed the fabrication and testing of many of the component parts of a new, parallel, high-speed digital data acquisition system. As presently implemented, it allows us the capability of four channels of 12-bit A/D conversion, at 20 MHz each. These can be staggered in time to yield 12-bit two-channel conversion at 40 MHz, or 12-bit single channel conversion at 80 MHz. At this writing, each pair of A/D channles is buffered by a high speed 32 MB on-board memory buffer. This system is being developed in anticipation of the very high data rate requirements dictated by the need to record spatially- and temporally-resolved image scalar data that arise in fully-developed turbulent flows, in turn detected by custom CCD focal plane arrays. Presently, the system is being used to acquire data, by digitizing contiguous frames of a high resolution (700 lines), color video camera, yielding high dynamic range ($\sim$ 60 dB) data from each color (RGB) output, at full video rates.

In a related part of this effort, we have made progress in our development of fast image correlation techniques for the purpose of extracting velocity field information from successive images, in a three-way collaboration with M. Gharib of UCSD and J. Janesick of the Imaging Group at the Jet Propulsion Laboratory. This effort is comprised of two parts. One, the development of custom CCD focal plane arrays capable of recording pairs of image closely spaced in time. At this writing, a low-noise (5 e/pixel) CCD array, exhibiting nearly perfect charge-transfer efficiency, capable of two images, as close as 400 ns apart, has been developed and bench-tested at JPL. The second part of this effort is focusing on the development of algorithmic procedures for image analysis. We hope to be in a position to apply these techniques to large range of velocities, ranging from low-speed, liquid-phase flows, to gas phase, supersonic flows in the future.

---

* Co-sponsored by a DARPA grant through the Office of Naval Research.

or s-p, promotion energies PE and the ionization potentials IP of the metallic species minus the electron affinities EA of the oxidants. (In other words, we have extended the Evans-Polanyi relationships.) This is shown in Fig. 2 for B and Al diatomic species reactions. In this case n has been taken to be 2.0, but values between 2 and 4 all give comparable correlations. Similarly, we get good agreement with this relationship for metal atom-N_2O reactions as shown in Fig. 3 (the EA term is left off here as only one oxidant is considered.) In this case n was taken as 0.5, but values between 0 and 1 give correlations nearly as good. Since n reflects the ratio of the partition functions of the activated complex over those of the reactants, different groups of reactants should, of course, require different values of n. Here the Al, AlCl and BCl data all are from the AFOSR work, the Cu + N_2O result came from our NSF-supported studies, and the other data from the literature.

These relationships have been explained in terms of resonance theory as applied to the transition state.[1,3-5] The theoretical activation barriers are semi-empirically calculated for each of the series shown in Fig. 3 by using an experimental barrier value for one member of the series, i.e., the Na, Cu and Al reactions with N_2O, respectively. For atom reactions with other oxidants the parameters can similarly be determined by selecting one member of each group of reactions, which again allows predicting the others. These same parameters for each oxidant for the metal atom reactions have been used for the calculations on the diatomics shown in Fig. 2.

This completed work was oriented to reactions of Al and B species in NH_4ClO_4-based propellant formulations. In the present work the emphasis shifts to their oxygen-equivalents, i.e., halogen-free propellant combinations are considered, with the two-fold goal to measure rate coefficients and establish and interpret correlations between these, to allow predictions for further reactions. We plan to study reactions of B, BO and BO_2 with O_2, CO, CO_2, H_2O and NO_x and some AlO reactions additional to those already studied[1,6] to provide a comparison. Additionally, we plan to observe oxide dimerization reactions, i.e., the first steps in condensation, and their competition with oxidation reactions.

References

1. A. Fontijn and P.M. Futerko, "Homogeneous Kinetics of Metal Species over Wide Temperature Ranges: Techniques, Measurements, and Correlations", in Gas-Phase Metal Reactions, A. Fontijn, Ed., Elsevier, Amsterdam, in press, 28 pages.

2. A. Fontijn and R. Zellner, "Influence of Temperature on Rate Coefficients of Bimolecular Reactions", in Reactions of Small Transient Species, A. Fontijn and M.A.A. Clyne, Eds., (Academic Press, London, 1983), Chap. 1.

3. P.M. Futerko and A. Fontijn, "Activation Barriers for Series of Exothermic Homologous Reactions. I. Metal Atom Reactions with N_2O", J. Chem. Phys. 95, 8065 (1991).

4. P.M. Futerko and A. Fontijn, "Activation Barriers for Series of Exothermic Homologous Reactions. Comparison of Measurements to Theory for AlCl and BCl Reactions with Oxygen Oxidants", J. Chem. Phys., in preparation.

Dr Saad Ragab
Engrg Sci & Mechanics Dept
Virginia Polytechnic Institute
and State University
Blacksburg VA 24061
(703)231-5950

Dr S R Ray
National Institute of
Standards and Technology
Center for Chemical Engrg
Gaithersburg MD 20899

Dr R G Rehm
National Institute of
Standards and Technology
Center for Fire Research
Gaithersburg MD 20899
(301)975-2704

Dr Rolf D Reitz
Mechanical Engineering Dept
University of Wisconsin
1500 Johnson Drive
Madison WI 53706
(608)262-0145
FAX:263-6717

Dr M Renksizbulut
Department of Mechanical
Engineering
University of Waterloo
Waterloo, Ontario CN N2L 3G1
(519)885-1211
Ext 3977

Dr David Reuss
Fluid Mechanics Department
General Motors Research Labs
30500 Mound Road
Warren MI 48090-9055
(313)986-0029

Dr William Reynolds
Department of Mechanical
Engineering
Stanford University
Stanford CA 94305-3032
(415)723-3840

Dr James Riley
Mechanical Engineering Dept
University of Washington
Seattle WA 98195
(206)543-5347

Dr Michael Roco
National Science Foundation
Chemical and Thermal Syst Div
1800 G Street, N W
Washington DC 20550
(202)357-9606

Dr U S Rohatgi
Department of Nuclear Energy
Brookhaven National Laboratory
Upton NY 11973
(516)282-2475

Dr Glenn Rolader
Science Applications
International Corporation
1247-B N Eglin Parkway
Shalimar FL 32579
AV872-0360
(904)882-0391

Dr W M Roquemore
WL/POSF
Wright-Patterson AFB OH 45433-6563
(513)255-6813
AV785-6813

Dr Anatol Roshko
Graduate Aeronautical Labs
California Institute of
Technology
Pasadena CA 91125
(818)356-4484

Dr Daniel Rosner
Department of Chemical
Engineering
Yale University
New Haven CT 06520
(203)432-4391

Dr John Schaefer
Energy and Environmental Div.
Acurex Corporation
555 Clyde Ave., P. O. Box 7555
Mountain View CA 94039

Dr W H Schofield
Aeronautical Research Labs
506 Lorimer St, Fishermen's Bn
Box 4331, P O
Melbourne, Victoria AUSTRALIA 3001

Dr Thomas A Seder
Rockwell International Sci Ctr
1049 Camino dos Rios
P O Box 1085
Thousand Oaks CA 91360
(805)373-4576

Dr D J Seery
United Technologies Research
Center
Silver Lane
East Hartford CT 06108

Dr Hratch Semerjian
National Institute of
Standards and Technology
Center for Chemical Engrg
Gaithersburg MD 20899
(301)975-2609

Dr K Seshadri
Center for Energy and
Combustion Research, 0411
University of California
La Jolla CA 92093-0411
(619)534-4876

Dr G S Settles
309 Mechanical Engrg Building
Pennsylvania State University
University Park PA 16802
(814)863-1504

Dr Robert Shaw
Division of Chemical and
Biological Sciences
U S Army Research Office
Research Triangle Park NC 27709-221
(919)549-0641

Mr Harold Simmons
Parker Hannifin Corporation
Gas Turbine Fuel Systems Div.
17325 Euclid Avenue
Cleveland OH 44143
(216)531-3000
Ext 2309

Dr Neeraj Sinha
Science Applications
International Corporation
501 Office Ctr Dr, Suite 420
Fort Washington PA 19034-3211
(215)542-1200
FAX:542-8567

Dr William Sirignano
School of Engineering
University of California
Irvine CA 92717
(714)856-6002

Dr Bernard Spielvogel
U S Army Research Office
P O Box 12211
Research Triangle Pk NC 27709-2211

Dr F Dee Stevenson
Office of Basic Energy Science
U. S. Department of Energy
1000 Independence Avenue, N W
Washington DC 20585

Dr David Stewart
Department of Theoretical and
Applied Mechanics
University of Illinois
Urbana IL 61801

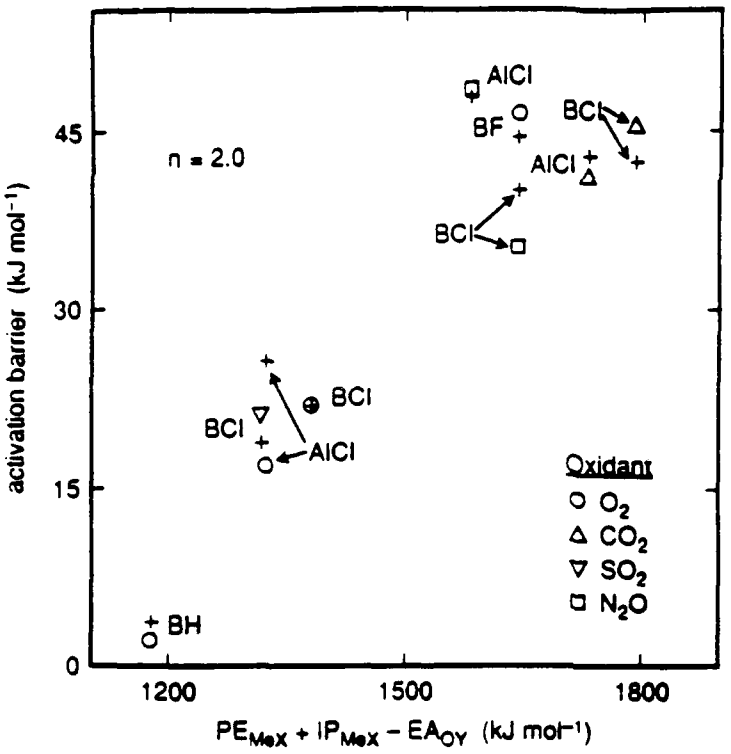

Figure 2. Plot of the experimental (open *symbols) and calculated* (plus signs) activation barriers of reactions between diatomic B and Al species, MeX, and oxygen species, OY, versus the sums of the σ-π promotion energies and ionization potentials of MeX minus the electron affinities of OY.

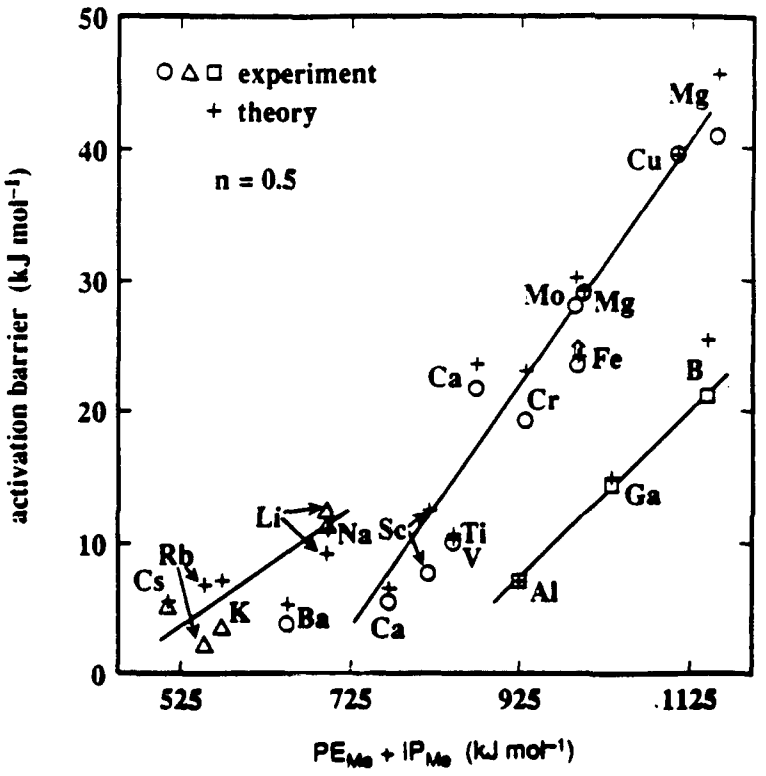

Figure 3. Plot of the experimental (open symbols) and calculated (plus signs) activation barriers for metal atom, Me, reactions with N_2O versus the sums of the s-p promotion energies and the ionization potentials of Me. The alkali metals (triangles) and boron group atoms (squares) are distinguished from the alkaline earth and transition metals (circles).

Dr A D Vakili
University of Tennessee
Space Institute
Tullahoma TN 37388

Dr S P Vanka
Department of Mechanical
and Industrial Engrg
University of Illinois
Urbana IL 61801

Dr Earl VanLandingham
National Aeronautics & Space
Administration, Code RB
400 Maryland Avenue, SW
Washington DC 20546
(202)453-2847

Dr P J Waltrup
Applied Physics Laboratory
Johns Hopkins University
Johns Hopkins Road
Laurel MD 20707-6099
(301)953-5000
Ext. 4186

Dr Charles Westbrook
Lawrence Livermore National
Laboratories
P. O. Box 808
Livermore CA 94550

Dr James Whitelaw
Department of Mechanical Engrg
Imperial College of Science
and Technology
London SW7 2BX UK

Dr Forman Williams
Center for Energy and
Combustion Research, 0411
University of California
La Jolla CA 92093-0411
(619)534-5492

Dr Michael Winter
Propulsion Science
United Technologies Research
Center
East Hartford CT 06108
(203)727-7805

Dr Bernard T Wolfson
Wolfson Associates
International
4797 Lake Valencia Blvd West
Palm Harbor FL 33563
(813)786-3007

Dr J M Wu
University of Tennessee
Space Institute
Tullahoma TN 37388

Dr Richard Yetter
Department of Mechanical and
Aerospace Engineering
Princeton University
Princeton NJ 08544-5263

Dr Shaye Yungster
Institute for Computational
Mechanics in Propulsion
NASA Lewis Research Ctr
Cleveland OH 44135
(216)433-6680

Dr Michael Zachariah
National Institute of
Standards and Technology
Center for Chemical Engrg
Gaithersburg MD 20899
(301)975-2063

Mr Fred Zarlingo
Code 3246
Naval Weapons Center
China Lake CA 93555-6001
(619)939-7395
AV437-7395

In the second project, the simulation of a spatially-developing, reacting shear layer using the transport element method was applied to study the effect of heat release on the development of large structures and the overall growth rate of the two dimensional part of the mixing zone [4]. Simulations were conducted at different enthalpy of reaction and Damkohler number, all under conditions of periodic forcing to ensure that the roll-up occurs within the computational domain. Results show that heat release, as expected, enlarges the size of the fundamental eddies, stretching their streamwise axis and reducing their cross stream axis. A comparison between a non-reacting and a reacting shear layer simulations showing the effect of heat release is depicted in figure 1. When forcing is applied at both the fundamental and subharmonic modes simultaneously, heat release increases/decreases the in-phase/out-of-phase eddy (the former is the eddy which forms when the two waves are in phase and the latter forms while the two waves are out of phase), and reduces the overall rate of growth of the layer.

The non-uniform acceleration of the eddies in the streamwise direction, which results from the difference between the amount of heat release within the eddies, modifies their relative locations from that of the case of uniform density. As a result the conventional process of pairing in which two similar eddies separated by a distance equal to their wavelength merge by spinning around the same center, is modified into that of a tearing/gulping process. In this process, the strain field produced by the larger of the two eddies tears the smaller eddy and engulfs its vorticity. Our results indicate that increasing the total heat release is more effective than increasing the rate of heat release in reducing the growth rate of the layer. Events which precede pairing, at low heat release rate, or tearing, at high heat release rate, are shown in terms of the distributions of the products mass fraction, reaction rate and vorticity in figure 2. The suppression of pairing, and the tearing/gulping processes that ensue instead, reduce the overall rate of mixing between the two streams, a fact that has been observed experimentally. We are currently exercising the model at higher rate of heat release, higher initial perturbations and different pressure gradients downstream the shear layer.

The third project which we worked on this year concerns the development and application of an unsteady, finite-rate kinetics, strained flat flame model. The model is developed as a vehicle to facilitate the implementation of multi-step kinetics, and preferential diffusion processes in large-scale turbulent combustion simulations [5]. As a first step, we applied the model to investigate the effect of unsteady strain on flamelet combustion. Results show that for a short-duration ignition source (such as a spark or an energy pulse), a steady positive strain enhances the burning rate while exponentially increasing the ignition delay time. Increasing the strain rate beyond a critical value, at which the kinetics rate can no longer balance the heat dissipation rate, leads to the sudden quenching of the reaction with no potential for re-ignition. The quenching strain is increased and the ignition delay is reduced when the ignition source is replaced by a long duration "pilot flame."

Results also indicate that, when the flow and chemical time scales are close, the burning rate depends on the strain history. An important example of strain history, which resembles that encountered in a turbulent flame, is the oscillating strain. We find that flamelet combustion exhibits strong sensitivity to oscillating strains. For large amplitude oscillations, whose value is a sensitive function of the frequency, the flame is quenched as the total strain exceeds the steady quenching strain, even though the mean value of the strain may be well below the quenching strain. Partial quenching and re-ignition may replace permanent quenching if the frequency of oscillations is increased. When compressive strains prevail, partial extinction is observed. Quenching, partial quenching, extinction and re-ignition result in large variation in the unsteady burning rate and in a mean burning rate which is smaller than the steady burning rate computed using the mean strain. The effects of the oscillating strain amplitude and frequency on the mean burning rate are shown in figure 3. We are currently extending this model at incorporate preferential diffusion and multi-step kinetics reactions.

DIAGNOSTICS IN REACTING MEDIA

Invitees

Mr Leonard Angello
Electric Power Research Institute
3412 Hillview Avenue
Palo Alto CA 94303
(415)855-2873

Dr William Bachalo
Aerometrics, Inc.
550 Del Rey Avenue
Unit A
Sunnyvale CA 94086
(408)738-6688

Dr Edward Beiting
Aerophysics Lab, Prop & Env Sc
The Aerospace Corporation
P O Box 92957, M5/754
Los Angeles CA 90009-2957
(213)336-7035

Dr William Bischel
Coherent, Inc.
3210 Porter Drive
Palo Alto CA 94304
(415)858-7639

Dr Richard Chang
Electrical Engineering Dept.
P. O. Box 2157, Yale Station
Yale University
New Haven CT 06520
(203)432-4272

Dr Wai K Cheng
Department of Mechanical Engineering
MIT
Cambridge MA 02139
(617)253-4531

Dr David Crosley
Molecular Physics Department
SRI International
333 Ravenswood Avenue
Menlo Park CA 94025-3696
(415)326-6200

Dr Gregory Dobbs
United Technologies Research Center - Mail Stop 90
Silver Lane
East Hartford CT 06108
(203)727-7145

Dr A C Eckbreth
United Technologies Research Center
Silver Lane
East Hartford CT 06108
(203)727-7269

Dr Thomas Ehlert
Department of Chemistry
Marquette University
Milwaukee WI 53233
(414)288-7066

Dr Gregory Faris
SRI International
333 Ravenswood Avenue
Menlo Park CA 94025
(415)859-4131

Dr Richard Field
U. S. Army Armament R&D Center
DRSMC-LCA-G(D)
Building 382-S
Dover NJ 07801
(201)724-5844
(201)724-5682

Dr Bish Ganguly
WL/POOC-3
Wright-Patterson AFB OH 45433-6563
(513)255-2923
AV785-2923

Dr Alan Garscadden
WL/POOC-3
Wright-Patterson AFB OH 45433-6563
(513)255-2923
AV785-2923

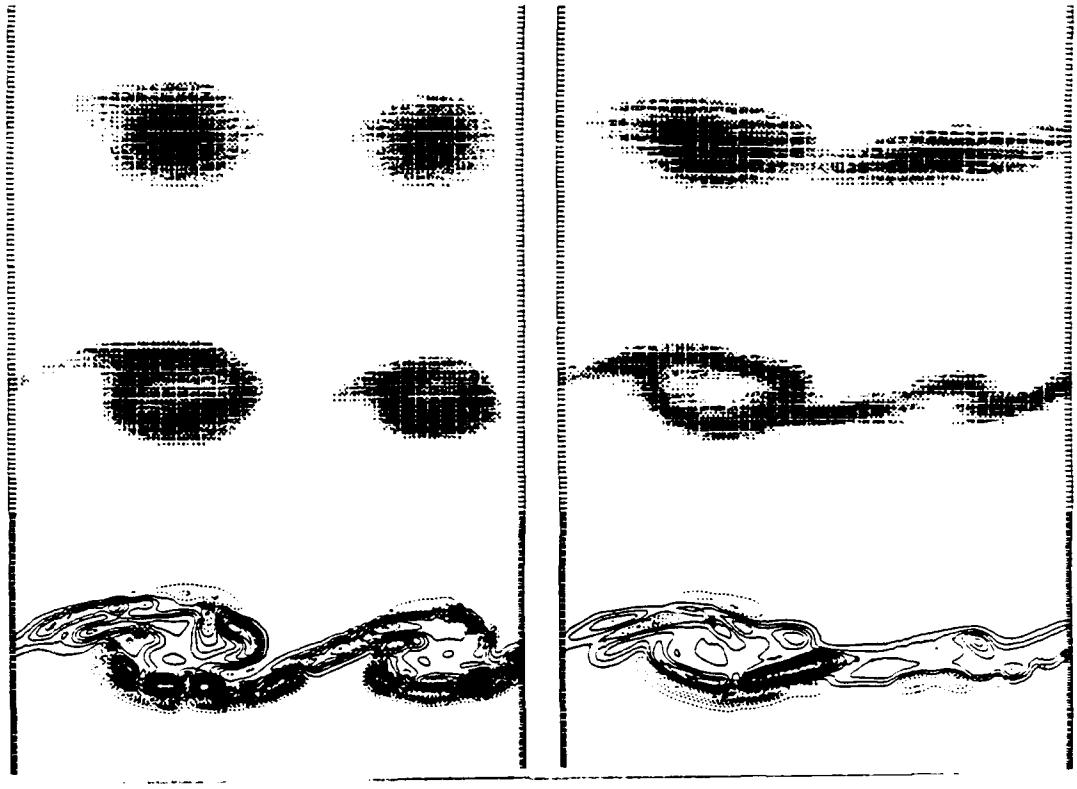

Figure 2. From top, the product mass-fraction, reaction rate and vorticity for the reacting shear layer at $A_f = 50$ and $Q = 4$ (left) and $Q = 6$ (right). The results are shown for $1.43 < x < 2.43$. In all cases $0.25 < y ,< 0.75$.

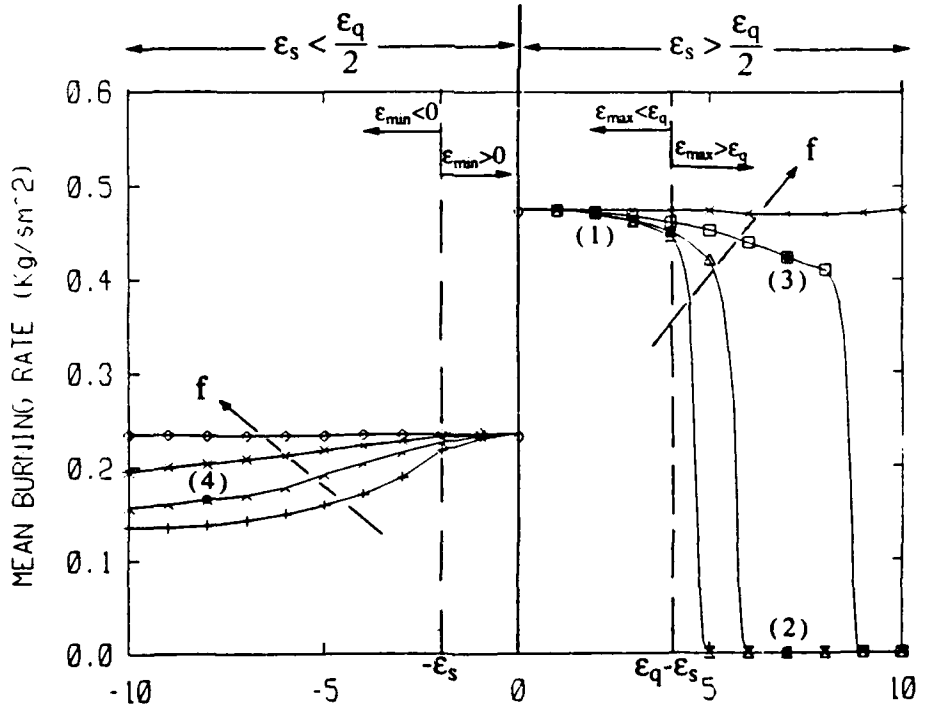

Figure 3. Effect of periodic strain amplitude on the mean burning rate in a pilot-ignited diffusion flame. The amplitude of the mean strain component and the frequency of the oscillating component are indicated. The horizontal axis shown is the strain oscillation amplitude in 10^{-4} 1/s.

Dr S S Penner
Center for Energy and
Combustion Research, 0411
University of California
La Jolla CA 92093-0411
(619)534-4284

Dr Emil Pfender
Department of Mechanical Engrg
125 Mechanical Engineering
The University of Minnesota
Minneapolis MN 55455

Dr John Renie
Department of Mechanical and
Industrial Engineering
University of Illinois
Urbana IL 61801
(217)333-6199

Dr Won B Roh
Department of Engrg Physics
Air Force Institute of
Teechnology
Wright-Patterson AFB OH 45433-6583

Dr Gregory Smith
Department of Chem Kinetics
SRI International
333 Ravenswood Avenue
Menlo Park CA 94025
(415)859-3496

Dr Alan Stanton
Southwest Sciences, Inc.
1570 Pacheco Street
Suite E-11
Santa Fe NM 87501
(505)984-1322

Dr James Trolinger
MetroLaser
18006 Skypark Circle
Suite 108
Irvine CA 92714-6428
(714)553-0688

Dr John Vanderhoff
Ballistic Research Laboratory
DRSMC-BLI(A)
Aberdeen Proving Ground MD 21005
(410)278-6642

Dr James Verdieck
Rockwell International
Rocketdyne Div, M/S FA26
6633 Canoga Avenue
Canoga Park CA 91303
(818)700-4709

Dr Joda Wormhoudt
Aerodyne Research, Inc.
45 Manning Road
Manning Park Research Center
Billerica MA 01821-3976
(508)663-9500
FAX:663-4918

$$\left[1 - M_c^2\right]\phi_{xx} + \phi_{yy} = \frac{(\gamma-1)(h_f)_x}{a_c^2} + M_c^2\,\psi_{xy} + \gamma M_c^2 \Gamma_{ox}$$

$$\psi_{xx} + \psi_{yy} = -\frac{\omega}{U_c} \qquad (2)$$

The integral solution of the first of these two sets of equations, subsequently differentiated to obtain the entrainment velocity, shows that that heat release can either increase or decrease mixing dependent upon the asymmetry or symmetry of the heat release profile across the layer. In a similar fashion the entrainment velocity calculated for the case with both heat release and vorticity generation can show either increased or decreased mixing dependent upon the symmetry or asymmetry of the vorticity generation profile across the layer.

In Reference 1 a 2-D theory was described that accurately predicts the decline in the mixing of a plane mixing layer up to a convective Mach number M_c of about .7. Since then the original theory has been made fully 3-D, and the assumption of no shocks embedded in a crude 3-D extension of the theory has become a conclusion rather than an hypothesis. This extension has been achieved by simple geometrical arguments generalizing the normalizing quantities in the original theory and allows vortices to become oblique. However, the angle of the vortices at a given value of M_c is a prediction of the extended analysis and is not assumed *a priori*. The new expression for the normalized mixing ratio is:

$$\frac{\dot{m}}{\dot{m}_i} = \left[\frac{1 - M_c^2\cos^2\theta}{1 - \frac{M_c^2\cos^2\theta}{2}}\right]^{3/2} \left\{\frac{\left[1 + \frac{\gamma(\gamma-1)}{2}M_c^2\right]\cos^2\theta}{\left[1 + \frac{\gamma(\gamma-1)}{2}M_c^2\cos^2\theta\right]}\right\} \qquad (3)$$

We theorize that the actual mixing ratio that occurs at any given convective Mach number is that which is maximum for all values of θ at that value of M_c. For $M_c \le .662$ the maximum occurs for 2-D structures, but beyond that M_c, the maximum occurs at $M_c \cos\theta = .662$. The resulting mixing ratio curve for $M_c \le 2.$ is shown in Figure 1 along with various experimental measurements. There the solid line is the 2-D result, and the dashed curve is the 3-D result beyond $M_c = .662$. Note that the swept vortex analysis predicts a finite mixing rate for large M_c and that this rate should be reached by $M_c = 3$.

NUMERICAL SIMULATIONS

After addition of an independently specifiable heat release term to the energy equation in our Navier-Stokes simulations, the effect of steady, but spatially varying, heating on a 2-D shear layer has been investigated. The heating profile is specified as a shifted Gaussian:

$$h_f(x,y) = D\,\frac{a^2}{\gamma-1}\,e^{-\sigma\left((y-b)/(1+cx)\right)^2}\Big/(1+cx) \qquad (4)$$

By varying D, b, σ and c the intensity, displacement and spreading rate of the heating profile can be adjusted in a parameter study. Because of the particular form chosen the total heat release per unit distance in the flow direction is constant, consistent with linear growth of a reacting shear layer. Previously reported experiment[2] and simulation[3] have left the general impression that heating reduces shear layer growth, although there is one report[4] to